

**RETRIEVAL OF  
TURBULENCE AND TURBULENCE PROPERTIES  
FROM RANDOMLY SAMPLED  
LASER-DOPPLER ANEMOMETRY DATA WITH NOISE**

**PROEFSCHRIFT**

ter verkrijging van de graad van doctor  
aan de Technische Universiteit Delft,  
op gezag van de Rector Magnificus prof. ir. K.F. Wakker  
in het openbaar te verdedigen ten overstaan van een commissie,  
door het College voor Promoties aangewezen,

op dinsdag 21 september 1999 te 10.30 uur

door

Hans Rudi Eduard VAN MAANEN

doctorandus in de natuurkunde,  
geboren te Arnhem

Dit proefschrift is goedgekeurd door de promotoren:

Prof. dr. ir. G. Ooms

en

Prof. Dr. C. Tropea

Samenstelling promotiecommissie:

Rector Magnificus

Voorzitter

Prof. dr. ir. G. Ooms

J.M. Burgerscentrum aan de Technische Universiteit Delft

Prof. Dr. C. Tropea

Universiteit Darmstadt (Duitsland)

Prof. dr. ir. H.E.A. van den Akker

Technische Universiteit Delft

Prof. dr. R.V.A. Oliemans

Technische Universiteit Delft

Ir. D. Passchier

Technische Universiteit Delft

Prof. dr. ir. F.T.M. Nieuwstadt

Technische Universiteit Delft

Prof. dr. ir. J.M.H. Fortuin, emeritus

Universiteit van Amsterdam

*Dit onderzoek is uitgevoerd bij het Koninklijke/Shell Laboratorium, Amsterdam (KSLA), sinds begin 1996 Shell Research and Technical Service Centre, Amsterdam (SRTCA) genaamd, ter ondersteuning van experimenteel onderzoek naar complexe stromingen.*

Copyright © 1999 by H.R.E. van Maanen, Muiden, Netherlands

All rights reserved. No part of this publication may be reproduced, stored in a retrieval system or transmitted in any form or by any means, electronic, mechanical, photocopying, recording or otherwise, without the prior written permission of Hans R.E. van Maanen, Muiden, Netherlands.

Publisher: Hans R.E. van Maanen  
Kalkovens 1  
1398 EK Muiden  
Netherlands  
Tel.: (+31) 294 27 00 94  
Fax.: (+31) 294 27 00 94

ISBN 90-9012847-6

Opgedragen aan *Ton Nieberg* †

# Retrieval of Turbulence and Turbulence Properties from Randomly sampled Laser-Doppler Anemometry Data with Noise

## Summary

Turbulence, the "chaotic" motion of fluids in flows, plays a dominant role in our lives, science and technology. It is a complicated problem of "classical" physics. Although major progress has been made in the investigation of turbulence, the governing Navier-Stokes equation has not been solved satisfactorily in general for turbulent flows and complete numerical simulation is not possible in all cases either. That is why often physical "models" are used, which, however, are not able to predict the turbulence (or its statistical properties) without experimental input data. In other problems experimental verification of the results, based on the model calculations, is required or desired. But measurement of turbulence is no sinecure either. *Only two* techniques for the measurement of turbulent velocity fluctuations have been developed which have a sufficiently high spatial and temporal resolution to cover the largest part of the size distribution of turbulent eddies: Hot-Wire Anemometry and Laser-Doppler Anemometry. The first uses vulnerable platinum wires (3 - 5  $\mu\text{m}$  in diameter) and can therefore only be used in clean gases. The technique is not suited for high turbulence intensities. The second technique, Laser-Doppler Anemometry, which offers a number of important advantages over Hot-Wire Anemometry, is basically more powerful, but it has a number of serious problems. The two most important problems - but certainly not the only ones - for our kind of measurements are the high noise level and the random sampling.

Every measurement has a noise contribution added to it, but in Laser-Doppler Anemometry this is a very serious problem: the level is -roughly speaking- two orders of magnitude higher than in Hot-Wire Anemometry. The second problem is caused by the requirement to use tracer particles, carried by the flow, to generate the measurement signal. As only a velocity measurement is obtained when such a tracer particle traverses the measurement volume, the information is not available "on call" but only when statistics allows so. As a result, the information about the (turbulent) flow velocity is fragmented and is only available at unpredictable moments. These two disadvantages hamper the interpretation of Laser-Doppler Anemometry data and limit its applicability.

To overcome these problems, first an inventory has been made as to the noise sources, which occur in the different parts of a Laser-Doppler Anemometer. Subsequently, it has been analyzed how these different noise sources translate into noise which obscures the information about the turbulence. This knowledge can then be used to optimise the Laser-Doppler Anemometer for the specific measurement problem. Secondly, it has been studied in which way the optimum estimators for the instantaneous velocity and the arrival time (of the tracer particle in the measurement volume) can be obtained from the photo detector signal. This can be improved, compared to the currently available techniques, but even if this would be realised, we will still have to live with (lots of) noise in Laser-Doppler Anemometry. And in order to get the best information about the turbulence, we will always have to take the noise contribution to the individual velocity estimates into account, *no matter which data-processing technique will be used*. In other words: data-processing techniques are required which use as a starting point that a significant part of the individual velocity estimates consists of noise. Hence, new algorithms have been developed which strive to separate the turbulence and the noise contributions to the measurement data as much as possible. One approach is aimed at obtaining statistical information about the turbulence, the other at arriving at a continuous record of the turbulent velocity fluctuations as if it were a Hot-Wire Anemometer.

The first approach can be used in virtually all cases (even when the information density, the data-rate, is low) by combining an attractive property of the statistics which govern the time between successive measurements, with a novel algorithm for the estimation of the auto correlation function. The properties of this novel estimator for the auto correlation function can be fully brought to fruition by the application of a "curve-fit" technique, which suppresses the statistical fluctuations significantly. This combination enables the estimation of the properties of the turbulent velocity fluctuations with a high

## *Retrieval of turbulence and turbulence properties from LDA data with noise*

accuracy down to 2 - 2.5 decades below the noise level by making use of a number of known properties of turbulence too. In this way, information is obtained about the turbulent eddies at frequencies which lay *above* the average data-rate. Application of this algorithm to different sets of data, both from simulated turbulence and from Hot-Wire Anemometry, showed that it is indeed possible to obtain accurate estimates at relative high frequencies and far below the noise level. Application to "real" measurement data from Laser-Doppler Anemometry also resulted in good estimators, which are in agreement with previous results.

The second approach, the so-called "velocity signal reconstruction technique", requires a high(er) data-rate than the first technique. The influence of the data-rate has been analyzed: it should be at least  $2\pi$  times the highest frequency of the turbulent velocity fluctuations of interest to enable velocity signal reconstruction, based on zero- and first-order interpolation. Higher-order based reconstructions require an even higher data-rate. The influence of the data-rate, however, is further reaching than the upper frequency limit only, as it is of prime importance for the *quality* of the end results obtained with this approach. But no matter how high the data-rate is, any velocity signal reconstruction has to "bridge" the gaps in time, caused by the random sampling. Assumptions sneak easily into such a reconstruction technique and therefore the danger is real that one is reconstructing one's own assumptions, which should be avoided at any price. Therefore we have required that all relevant information should be retrieved from the Laser-Doppler Anemometry data themselves and that assumptions should be avoided as much as possible in order to circumvent this pitfall. Except for the assumption that the accelerations should be finite<sup>1</sup>, we have succeeded, but the price we had to pay is a rather complicated data-processing scheme. This, however, can be done by computers during those parts of the day that they would have been idle and therefore we do not regard this as a serious drawback. Even if additional processing power would be required, the costs of this pale into insignificance compared to those of a Laser-Doppler Anemometry system.

The above described results have been obtained by using, whenever required, available knowledge about turbulence, in combination with knowledge of and insight into the measurement system. As a result, we have succeeded in finding methods which circumvent the -at first sight insurmountable- hurdles to reach the goal of retrieving more details of the turbulence from Laser-Doppler Anemometry data. The use of these data-processing techniques lifts Laser-Doppler Anemometry to a higher level and therefore Laser-Doppler Anemometry can become a more important measurement technique for the study of turbulence than before.

---

<sup>1</sup> This is a very reasonable assumption: as the forces are finite and we are talking about viscous fluids with mass, the accelerations should also be finite.

# Reconstructie van turbulentie en turbulente grootheden uit willekeurig bemonsterde Laser-Doppler Anemometrie meetgegevens met ruis.

## Samenvatting

Turbulentie, het complex van de "chaotische" wervelingen van gassen en vloeistoffen in stromingen, speelt een dominante rol in ons leven, de wetenschap en de techniek. Het is een gecompliceerd probleem van de "klassieke" natuurkunde. Hoewel er inmiddels belangrijke vooruitgang is geboekt in het onderzoek van turbulentie, is de beschrijvende Navier-Stokes vergelijking niet algemeen bevredigend opgelost voor turbulente stromingen en is volledige numerieke simulatie evenmin in alle gevallen mogelijk. Regelmatig worden daarom fysische modellen gebruikt, die niet in staat zijn om de turbulentie (of de statistische eigenschappen ervan) te voorspellen zonder gebruik te maken van experimentele gegevens. Voor andere problemen is experimentele verificatie van de resultaten, verkregen op basis van modelberekeningen, vereist of gewenst. Maar ook het meten aan turbulentie is geen sinecure. Er zijn *slechts twee* technieken voor het meten van de turbulente snelheidsfluctuaties ontwikkeld die een voldoende hoog ruimtelijk en temporeel oplossend vermogen hebben om het belangrijkste gedeelte van de grootteverdeling van turbulente wervels te bestrijken: Hittedraad Anemometrie en Laser-Doppler Anemometrie. De eerste maakt gebruik van kwetsbare platina draadjes van 3 - 5  $\mu\text{m}$  diameter en kan daarom alleen in schone gassen worden gebruikt. Daarenboven is de techniek niet geschikt voor hoge turbulentie intensiteiten. De tweede techniek, Laser-Doppler Anemometrie, die een aantal belangrijke voordelen biedt t.o.v. Hittedraad Anemometrie, is in principe krachtiger, maar heeft een aantal andere serieuze problemen. De twee, voor ons soort metingen, belangrijkste (maar zeker niet de enige) problemen zijn: het hoge ruisniveau en de willekeurige bemonstering.

Iedere meting is behept met ruis, maar in Laser-Doppler Anemometrie is het een zeer ernstig probleem: het ruisniveau is daar -grofweg- twee orden van grootte hoger dan in Hittedraad Anemometrie. Het tweede probleem wordt veroorzaakt door het gegeven dat de techniek gebruik maakt van "tracer" deeltjes, meegevoerd door de stroming. Omdat er alleen een snelheidsmeting kan plaatsvinden als zo'n tracer-deeltje het meetvolume doorkruist, is de informatie niet "op afroep" beschikbaar, maar slechts dan wanneer de statistiek het ons gunt. Het gevolg daarvan is dat de informatie over de (turbulente) stromingssnelheid gefragmenteerd is en alleen beschikbaar komt op onvoorspelbare momenten. Deze twee nadelen belemmeren de interpretatie van de meetgegevens van Laser-Doppler Anemometrie aanzienlijk en beperken daarmee de toepasbaarheid.

Om deze problemen te overwinnen is allereerst een inventarisatie gemaakt van de ruisbronnen die in de verschillende onderdelen van een Laser-Doppler Anemometer optreden en vervolgens is geanalyseerd hoe deze ruisbronnen zich vertalen in ruis die de informatie over de turbulentie maskeert. Deze kennis kan dan gebruikt worden om de Laser-Doppler Snelheidsmeter te optimaliseren voor het betreffende meetprobleem. Als tweede stap is nagegaan op welke manier de optimale schatters voor de momentane snelheid en aankomsttijd (van het tracer-deeltje in het meetvolume) kunnen worden verkregen uit het signaal van de fotodetector. Dit kan worden verbeterd in vergelijking met de thans beschikbare technieken, maar zelfs als dit wordt gerealiseerd zullen we nog altijd moeten leren leven met (veel) ruis in Laser-Doppler Anemometrie metingen. En teneinde de beste informatie over de turbulentie te verkrijgen zullen we daarom altijd rekening moeten houden met de ruisbijdrage in de snelheidsschatters, *welke verwerkingstechniek voor meetgegevens dan ook gebruikt wordt*. Met andere woorden: er zijn data-verwerkingstechnieken vereist die uitgaan van het gegeven dat ruis een wezenlijk bestanddeel van de individuele snelheidsschatters is. Om die reden zijn nieuwe algoritmen ontwikkeld die de bijdragen van turbulentie en ruis aan de meetresultaten zo goed mogelijk van elkaar scheiden. De ene benadering is gericht op het verkrijgen van statistische informatie over de turbulentie, de andere op het bewerkstelligen van een continue registratie van de turbulente snelheidsfluctuaties als bij een Hittedraad Anemometer.

## *Retrieval of turbulence and turbulence properties from LDA data with noise*

De eerste benadering kan in vrijwel alle gevallen worden gebruikt (ook als de informatiedichtheid, het aantal waarnemingen per seconde, laag is) door het combineren van een aantrekkelijke eigenschap van de statistiek die de tijdsintervallen tussen twee opeenvolgende metingen beheerst met een nieuw algoritme voor het schatten van de autocorrelatiefunctie. De eigenschappen van deze nieuwe schatter van de autocorrelatiefunctie kunnen ten volle worden benut door het toepassen van een "curve-fit" techniek, waardoor de statistische fluctuaties sterk worden onderdrukt. Deze combinatie maakt het mogelijk om de eigenschappen van de turbulente snelheidsfluctuaties tot 2 à 2,5 decade beneden het ruisniveau met een hoge nauwkeurigheid te schatten, mede door gebruik te maken van een aantal bekende eigenschappen van turbulentie. Ook blijkt dat het mogelijk is om gegevens te verkrijgen over de turbulentie bij wervel-frequenties die beduidend *boven* de gemiddelde bemonsteringsfrequentie liggen. Dat het mogelijk is om zo ver beneden het ruisniveau goede schatters te verkrijgen bij relatief hoge frequenties is aangetoond door het toepassen van dit algoritme op verschillende verzamelingen van gegevens, waarin zowel gesimuleerde turbulentie als Hittedraad Anemometrie meetgegevens zijn vertegenwoordigd. Toepassing op "echte" meetgegevens van Laser-Doppler Anemometrie resulteerde eveneens in goede schatters, die in overeenstemming zijn met eerdere resultaten.

De tweede benadering, de zg. "signaalreconstructietechniek" vereist een hoger aantal waarnemingen per seconde (bemonsteringsfrequentie) dan de eerste techniek. De invloed van de bemonsteringsfrequentie is geanalyseerd en het bleek dat deze tenminste  $2\pi$  maal de hoogste frequentie die van belang is in het gereconstrueerde signaal dient te zijn, zowel bij nulde- als eerste-orde interpolatie. Hogere orde interpolaties vereisen een nog hogere bemonsteringsfrequentie. De invloed van de bemonsteringsfrequentie is echter verderreikend dan alleen maar de begrenzing in de te reconstrueren frequentie. De bemonsteringsfrequentie blijkt ook van groot belang te zijn voor de *kwaliteit* van de resultaten die met deze techniek verkregen kan worden. Maar hoe hoog de bemonsteringsfrequentie ook is, de signaalreconstructietechniek moet, omdat er geen informatie over de stroming op ieder gewenst moment beschikbaar is door de willekeurige bemonstering, deze "informatie-gaten" overbruggen waarvoor een of andere techniek nodig is. Hierin sluipt gemakkelijk het gevaar dat men zijn eigen aannamen aan het reconstrueren is, hetwelk tegen elke prijs voorkomen dient te worden. Wij hebben derhalve als eis gesteld dat alle relevante informatie uit de Laser-Doppler Anemometrie gegevens zelf moet worden verkregen en dat veronderstellingen zoveel mogelijk vermeden dienen te worden. Met uitzondering van de aanname dat de versnellingen begrensd dienen te zijn<sup>1</sup>, zijn wij hierin geslaagd, maar de prijs die we hebben moeten betalen is een nogal gecompliceerd verwerkingsschema voor de meetgegevens. Dit kan echter door computers worden uitgevoerd gedurende die delen van de dag dat deze anders doelloos zouden blijven en daarom beschouwen wij dit niet als een ernstig nadeel. Zelfs al zou extra rekencapaciteit vereist zijn, dan nog vallen de kosten hiervan in het niet bij die van een Laser-Doppler Anemometrie meetsysteem.

Bovenbeschreven resultaten zijn gerealiseerd door waar nodig gebruik te maken van reeds beschikbare kennis van turbulentie en dit te combineren met kennis van en inzicht in het meetsysteem. Hierdoor zijn wij erin geslaagd om methoden te vinden die de -op het eerste gezicht onoverkomelijke- horden omzeilen teneinde het vooropgestelde doel te bereiken om meer details van de turbulentie uit Laser-Doppler Anemometrie data te verkrijgen. Door het gebruik van deze gegevensverwerkingstechnieken komen de meetresultaten van Laser-Doppler Anemometrie op een hoger plan te staan en de Laser-Doppler Anemometer kan daardoor een belangrijker meetinstrument worden voor experimenteel onderzoek van turbulentie dan voorheen.

---

<sup>1</sup> Dit is een heel acceptabele aanname, want omdat de krachten begrensd zijn en we het hebben over viskeuze gassen en vloeistoffen met massa, moeten de versnellingen eveneens begrensd zijn.

# Contents

<b>1. Introduction</b>	1
<b>2. Monte Carlo Simulations</b>	13
2.1 Introduction.	13
2.2 Generation of random numbers with different probability distributions.	13
2.3 Simulation of Doppler signals with narrow band noise.	15
2.4 Turbulence-like signals according to predefined power spectra.	16
2.5 Simulated LDA data-sets on the basis of simulated turbulence or HWA data.	17
Appendix: The turbulence power spectra used for the simulation of turbulence.	18
<b>3. Noise in Laser-Doppler Anemometry</b>	33
3.1 Introduction.	33
3.2 Inventory of the noise and its sources.	33
3.3 Noise in the Doppler signal.	38
3.4 Experimental results.	41
3.5 On the definition of the Signal-to-Noise Ratio of the Doppler signal.	41
3.6 Concluding remarks.	41
<b>4. Preliminary Diagnostic Testing of Experimental Data-Sets</b>	55
4.1 Introduction.	55
4.2 The Time Interval Distribution.	55
4.2.1 The theoretical Time Interval Distribution.	56
4.2.2 Practical Time Interval Distributions.	56
4.3 Causes of the deviations of the Time Interval Distribution.	57
4.3.1 The dead time of the processor.	57
4.3.2 Round-off errors in the data-file.	57
4.3.3 Round-off errors in the internal clock of the processor.	57
4.3.4 Arrival time estimation noise.	58
4.3.5 Velocity bias.	58
4.3.6 Bias caused by tracer particle concentration fluctuations.	58
4.3.7 Multiple validation.	59
4.4 The actual velocity trace.	60
4.5 The linear Velocity Probability Distribution.	60
4.6 The logarithmic Velocity Probability Distribution.	60
4.7 The Auto Correlation Function estimated using the novel slotting technique.	60
4.8 The number of products in the slotted Auto Correlation Function.	61
4.9 Concluding remarks.	61
<b>5. Application of the Wavelet Transform to Laser-Doppler Signal Processors</b>	79
5.1 Introduction.	79
5.2 The Signal-to-Noise Ratio of the Doppler signal revisited.	80
5.3 Wavelet Transformation.	81
5.4 Numerical simulation.	82
5.5 Results and discussion.	83
5.6 Proposal for a design of a Wavelet Transform Processor.	83
5.7 Concluding remarks.	85
<b>6. Data-rate requirement for velocity signal reconstruction</b>	93
6.1 Introduction.	93
6.2 Statement of the problem.	93
6.3 Noise level as a function of the data-rate.	95

## *Retrieval of turbulence and turbulence properties from LDA data with noise*

6.4 Filtering of periodic signals.	96
6.5 Concluding remarks.	98
<b>7. Velocity signal reconstruction I</b>	<b>113</b>
7.1 Introduction.	113
7.2 Zero-order (S&H) and first-order reconstruction.	114
7.3 Kalman velocity signal reconstruction.	115
7.3.1 Background.	115
7.3.2 Derivation of the First-Order Kalman Reconstruction Algorithm.	115
7.3.2.1 Assumptions.	115
7.3.2.2. The Turbulence Model.	116
7.3.2.3 Design of the Kalman Filter.	117
7.3.2.4 Determination of the Turbulence Model Parameters.	121
7.4 Results.	122
7.5 Concluding remarks.	123
<b>8. High interpolation rate pre-processing of LDA data</b>	<b>139</b>
8.1 Introduction.	139
8.2 The novel approach.	140
8.3 The minimised time-smear anti-aliasing filter.	140
8.3.1 Aliasing in periodically sampled data.	140
8.3.2 Possibilities for the digital filtering.	141
8.3.2.1 Filtering in frequency domain.	141
8.3.2.2 Filtering in time domain.	142
8.3.3 Filter selection.	142
8.4 Results.	143
8.5 Concluding remarks.	144
<b>9. The Cross-Covariance Technique</b>	<b>151</b>
9.1 Introduction.	151
9.2 Spectral estimates using the cross covariance technique.	151
9.3 Discussion.	153
9.4 Concluding remarks.	156
<b>10. The auto correlation estimation using the slotting technique</b>	<b>165</b>
10.1 Introduction.	165
10.2 The slotting technique.	165
10.3 Description of the ACF estimation with Local Normalisation.	167
10.4 Analysis of the properties of the ACF estimated with Local Normalisation.	167
10.5 Results.	168
10.6 Discussion.	169
10.7 Concluding remarks.	170
<b>11. Estimation of Turbulence Power Spectra by Curve-Fit to the Auto Correlation Function</b>	<b>179</b>
11.1 Introduction.	179
11.2 The curve-fit approach.	180
11.2.1 Requirements for the curve-fit approach.	180
11.2.2 Choices made for the spectrum description.	180
11.3 The curve-fit procedure.	181
11.4 Verification of the curve-fit algorithm.	183
11.4.1 Simulated velocity estimations.	184
11.4.2 Simulated velocity estimations with a noise contribution.	185
11.4.3 Hot-Wire Anemometry velocity estimations.	185
11.4.4 Measured LDA velocity estimates.	186
11.4.4.1 Pipe flow.	186
11.4.4.2 Mixing-layer flow.	186

## Contents

11.4.4.3 Mixing vessel flow.	186
11.4.4.4 Airfoil flow.	187
11.5. Discussion	189
11.6 Concluding remarks.	192
<b>12. Extended reconstruction of turbulent velocity fluctuations</b>	<b>235</b>
12.1 Introduction.	235
12.2 The Second-Order Kalman Reconstruction Filter.	236
12.2.1 Simulation & Results.	236
12.2.2 Analysis.	236
12.2.3 Discussion.	237
12.3 The extended reconstruction filter.	238
12.4 Results.	239
12.5 Concluding remarks and future work.	242
<b>13. Conclusions</b>	<b>265</b>
<b>Appendices</b>	<b>267</b>
Appendix A: Experimental evidence for the existence of velocity bias.	267
Appendix B: The slope of the Auto Correlation Function.	275
Appendix C: The Derivation of the Analytical Auto Correlation Function.	277
C.1 Introduction.	277
C.2 Theory.	277
C.3 Application of the theory.	278
C.4 Verification.	279
Appendix D: Derivation of the Second-Order Kalman Reconstruction Filter.	281
D.1 Introduction.	281
D.2 Improved turbulence model.	281
D.3 Design of the Second-Order Kalman Filter.	283
D.4 Determination of the Turbulence Model Parameters.	289
<b>References</b>	<b>291</b>
<b>List of Symbols</b>	<b>297</b>
<b>List of Abbreviations</b>	<b>300</b>
<b>Acknowledgments</b>	<b>301</b>
<b>Curriculum Vitae</b>	<b>303</b>

# Chapter 1

## Introduction

*Nor deem the irrevocable Past  
As wholly wasted, wholly vain,  
If, rising on its wrecks, at last  
To something nobler we attain.*  
Henry Wadsworth Longfellow

The governing equation of turbulent flow, the Navier-Stokes equation, is already known for more than a century (ref. 1 and 2). Although major progress has been made, it has, however, not been solved in general and for many interesting, practical cases no analytical solutions can be found. To overcome this problem, several different approaches have been developed:

- Reynolds averaged Navier-Stokes equation.
- Turbulence modelling.
- Large eddy simulation with sub-grid modelling.
- Direct numerical solution of the Navier-Stokes equation.

Except for the last approach, all these techniques are unable to solve the Navier-Stokes equation without either certain assumptions or experimental input. Direct numerical solution of the Navier-Stokes equation is basically possible, but it requires significant computer power because of the large range in both spatial and temporal scales in combination with the random-like character of turbulent flows. Therefore experimental data are still required in many cases for the improvement of the knowledge of turbulence in order to validate and calibrate the models. An important field in these experimental investigations requires measuring velocity fluctuations at a high spatial and temporal resolution. In accordance with common definitions, first stated for the Reynolds Averaged Navier-Stokes equation, the turbulent velocity fluctuations are defined in the following way:

$$\underline{u}(t) = \begin{pmatrix} u(t) \\ v(t) \\ w(t) \end{pmatrix} \quad [1.1]$$

in which  $\underline{u}(t)$  is the velocity vector and each component is separated as

$$u(t) = U + u'(t) \quad \text{m/s}$$

in which:

$$U = \text{average velocity} \quad \text{m/s}$$

$$u'(t) = \text{fluctuating part of the velocity (note that the average value of } u'(t) \text{ is zero)} \quad \text{m/s}$$

Similar separations are made for the  $v$  and  $w$  components of the velocity vector.

The scales, required for the spatial and temporal resolution, are determined by the properties of the flow and the fluid. These are usually expressed as the Kolmogoroff scales:

$$\eta_k = \left( \frac{\nu^3}{\epsilon} \right)^{1/4} \quad \tau_k = \left( \frac{\nu}{\epsilon} \right)^{1/2} \quad [1.2]$$

## Retrieval of turbulence and turbulence properties from LDA data with noise

in which:

$\eta_k$	=	Kolmogoroff length scale	m
$\nu$	=	kinematic viscosity	m <sup>2</sup> /s
$\varepsilon$	=	dissipation rate per unit mass	m <sup>2</sup> /s <sup>3</sup>
$\tau_k$	=	Kolmogoroff time scale	s

The Kolmogoroff length scale can be interpreted as -loosely speaking- the eddy size where the dissipation of the turbulent kinetic energy dominates the flow. The size of the eddies corresponding to the Kolmogoroff length scale is usually small (even in water flows the corresponding value is 50 - 100  $\mu\text{m}$ , the corresponding frequency at 1 m/s is 10 - 20 kHz). This gives an impression of the required resolutions of the measurement apparatus and at this moment only two techniques are available that approach the requirements for the resolution sufficiently close to enable detailed experiments. These techniques are Hot-Wire Anemometry and Laser-Doppler Anemometry.

Hot-Wire Anemometry (HWA) uses the heat loss from a small (length 250 - 1000  $\mu\text{m}$ , diameter 5  $\mu\text{m}$ ) wire, caused by the flow of the fluid. The technique is developed before the Second World War (e.g. ref. 3 - 6) and is still extensively used in gas flows. Its operation will not be discussed in detail here (see e.g. ref. 7 and 8), but it is simple to understand its major drawbacks:

- The sensors are vulnerable and thus the technique can only be used in "clean" fluids.
- The heat loss is mainly determined by the flow perpendicular to the wire, which means that two components are measured simultaneously.
- The heat loss is determined by the flow velocity *and* the temperature difference. Thus the fluid must be at a constant temperature.
- Flow reversal (the fluid moving from right to left) will lead to readings equivalent to the flow moving from left to right. This leads to problems in highly turbulent flows.
- The calibration curve is non-linear, thus requiring calibration facilities.

In spite of the above listed drawbacks, HWA has been -and still is- an essential tool for the development of the understanding of turbulence.

The study of turbulence in flows with a higher turbulence intensity and/or less favourable conditions, however, has become possible by the development of Laser-Doppler Anemometry (LDA). The basic principle is that two laser beams, derived from the same laser, are focused into the flow to be investigated. The focus is not a single point in space, but due to the wave properties of light a *volume*, which size is determined by the wavelength of the laser light, the diameter and the separation of the incoming beams and the focal length of the lens. This volume is usually called the measurement volume. Small (2 - 5  $\mu\text{m}$  diameter) tracer particles, carried by the flow, scatter the laser light towards a detector and because of the movement of the tracer particles, the laser light is Doppler shifted. As the incoming angle of the two laser beams is different, the Doppler shift differs. Therefore, light with different frequencies arrives at the detector, leading to (temporal) interference and corresponding intensity fluctuations. This causes an oscillating signal in the photodetector, which is usually referred to as the "Doppler signal". The frequency of this Doppler signal is proportional to the component of the velocity of the tracer particle, perpendicular to the bisectrix of the smallest angle between the beams in the plane of the beams, as can be seen from fig. 1.1. However, if the tracer particle would move from right to left it would result in the same frequency as when it would be moving from left to right, as only the *absolute value* of the frequency difference is important in reality. The use of a so-called "preshift" in which the two beams are given a predetermined frequency difference before they build up the measurement volume enables the measurement of "negative" velocities (from right to left) up to a certain value as is illustrated in fig. 1.2. This opens the possibility to apply LDA in highly turbulent flows, but this preshift has many other advantages as well, so it is a standard concept for modern LDA systems. The details of the technique have been described elsewhere (e.g. ref. 9) and will not be repeated here.



## *Retrieval of turbulence and turbulence properties from LDA data with noise*

limitations of signals that can be derived from randomly sampled data: whereas the highest frequency that can be reproduced by a periodically sampled signal is  $1/(2\delta t)$  or half the sampling frequency, with randomly sampled signals this is  $1/(2\pi \cdot t_0)$ , which is more than a factor of three lower<sup>2</sup>.

### Ad 3.

The amount of light, scattered by the tiny tracer particles, is small (ref. 15) and, as a consequence, the Doppler signal is accompanied by a certain amount of noise. Although there is no agreement on how to define the Signal to Noise ratio (SNR) of the Doppler signal (this will be discussed in more detail in the Chapters 3 and 5), the noise will result in a noise contribution to the individual velocity estimate. This is unavoidable and, in general, the noise level in LDA is significantly (20 - 40 times) higher than in HWA. This is a major obstacle in the application of LDA.

Over the years, different techniques for the processing of the randomly sampled LDA data have been developed (eg. ref. 16 - 44), but in general these have not been very successful because they usually suffer from the noise contribution to the individual velocity estimates and from large variances due to the random sampling. None of these has been able to come even close to the dynamic range of Hot-Wire Anemometry data. The noise problem has been recognised as a drawback of LDA (e.g. ref. 45 - 49), but it has not been sufficiently coped with, not even for average properties such as power spectra. The only exception is the cross correlation technique (ref. 50) which explicitly tries to eliminate the noise from turbulence power spectra. This technique will be extended in Chapter 9. The insufficient attention the noise to the individual velocity estimators has received, has been enhanced by the notion that modern processors are able to estimate the velocity with a high accuracy even if the Doppler signal has a low SNR, see ref. 51 - 58. This, however, is disputable, as will be demonstrated in Chapter 3. Although optimisation can improve the situation, not much has been published in this area. A few exceptions are e.g. ref. 59 -61.

An ideal situation would be if the velocity fluctuations could be reconstructed from the LDA data in order to obtain a continuous record as with Hot-Wire Anemometry. A few attempts have been made (e.g. ref. 62), but again because the noise contributions have not been taken into account, these have not been very successful, as will be discussed in Chapter 7. This was the situation when a special workshop in Veldhoven (1993, ref. 63) was devoted to this topic. There it showed that the data-processing of LDA data was not yet able to retrieve the properties of turbulence as was possible with HWA and that sometimes the results obtained with the modern systems were inferior to those published in the seventies (e.g. ref. 50, 64 - 66). In fig. 1.4 and 1.5 two turbulence power spectra are shown which have been measured using a simple 5 mW He-Ne laser with a rotating grating as preshift, photo diodes as detectors and a tracker as processor, similar to the equipment that has been used in ref. 50 and 64 - 66. Using modern equipment, the power spectrum, shown in fig. 1.6, has been obtained under similar flow conditions. Even though the modern equipment did use a powerful laser (800 mW), fiber optics for the light transmission and an advanced processor, the result is rather disappointing, but the causes were then completely unclear<sup>3</sup>.

I would like to point out that the work, reported in this thesis, is not aimed at the reduction of errors in e.g. the average velocity, which is a subject in itself (ref. 67), but at retrieving detailed information about the fluctuating part of the velocity, down to the small eddies as far as possible. To achieve this, the major drawbacks, as described above, need to be overcome. To that end, novel data-processing algorithms have been developed. However, testing of these algorithms on real (measured) signals is

---

<sup>2</sup> This will be shown in Chapter 6.

<sup>3</sup> This was enhanced by the fact that these problems occurred with all types of modern LDA systems, as a "round robin" test at our Laboratory showed. There were -of course- differences but none of these modern systems was able to reproduce the large dynamic range of the power spectra, measured with the older equipment.

## 1. Introduction

neither straightforward nor trivial, as -in general- the properties of these flows are unknown. Therefore, a different approach has been applied and the tools, required for the analysis of both the underlying problems and the data-processing algorithms, will be discussed in Chapter 2. The techniques applied rely mostly on Monte-Carlo simulations, because it is the only way to separate different error sources and to study their influence, because the input signal is known. As input signals both simulated "turbulence" signals and HWA data have been used to stay as closely to reality as possible. In Chapter 3, an inventory of the different noise sources in LDA will be presented. Also, some general remarks will be made about possibilities to optimise the system in order to reduce the noise contributions as much as possible.

In Chapter 4, preliminary diagnostic testing of experimental data-sets will be discussed, which is helpful in determining the quality of the LDA data and in guiding the optimisation of the experimental set-up. In Chapter 5 an optimised processing for Doppler signals will be presented, which gives more accurate estimators for the velocity and the arrival time, thus reducing the noise contributions to the experimental data further.

The most ideal situation is that the LDA data would allow complete reconstruction of the turbulent velocity fluctuations. The information would then be similar to HWA data and all the required information could be retrieved from the reconstructed signal. The major stumbling block to achieve this is the random sampling and in Chapter 6 the limitations, which are imposed by the limited data-rate, will be analyzed. This will set lower limits to the requirements of data-sets for turbulent velocity signal reconstruction. In Chapter 7, the first steps to reconstruct the turbulent velocity fluctuations will be made. The results will show that the approach has some shortcomings, like the inefficient use of information. This will be overcome in Chapter 8, where a "pre-processor" will be described, which uses the information in the data-set more optimal. The other shortcoming is the lack of an accurate estimator for the turbulence power spectrum. This estimator can be obtained using the cross-covariance technique, which will be described and analyzed in Chapter 9. Although it gives good results, its major drawback is that it required a doubling of the measurement chain, which cannot be realised in all cases. Therefore, alternative approaches are attractive.

The search for additional techniques to determine accurate estimators of the power spectrum is also important for those conditions that the data-rate is insufficient to apply reconstruction. A novel algorithm for the estimation of the auto correlation function for randomly sampled data, the slotting technique with Local Normalisation, enabled estimation of the power spectrum under these less favourable conditions. The algorithm for the estimation of the auto correlation function is described in Chapter 10, while the estimation of the power spectrum, based on the information contained in the auto correlation function, is presented in Chapter 11. It will show that it is possible to estimate the power spectrum *above* the frequency of the data-rate and *below* the noise level. These algorithms have been tested both on simulated and on experimental (HWA and LDA) data.

Once the power spectrum of the turbulent velocity fluctuations is accurately known, it is possible to determine the relative contributions of noise and turbulence to the reconstructed signal as resulted from the technique, described in Chapters 7 and 8. This information can subsequently be used to remove as much as possible of the noise, remaining in the reconstructed signal. The extended reconstruction filter will be described in Chapter 12 and it will be shown that the result is a signal with a close resemblance to the input signal, with the correct spectral properties and with the correct distribution of the accelerations.

The result of the data-processing, described in this thesis, is a signal that is comparable to HWA, provided that the data-rate is sufficiently high. Although the signal will always have some reminiscent noise contribution, it offers the possibility for detailed study of turbulence, maintaining all the advantages of LDA as described previously in this chapter.

*Retrieval of turbulence and turbulence properties from LDA data with noise*

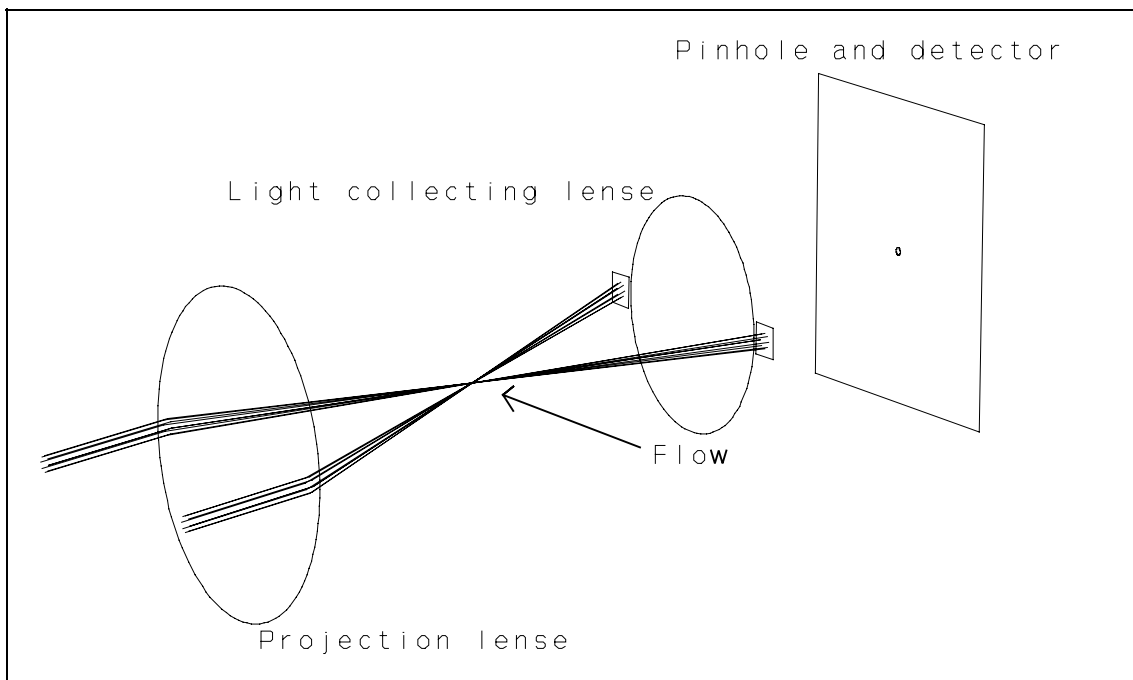


**Figure 1.1<sup>a</sup>:** Schematic drawing of an LDA system in the forward scatter mode. The intersection of the laser beams is the measurement volume.

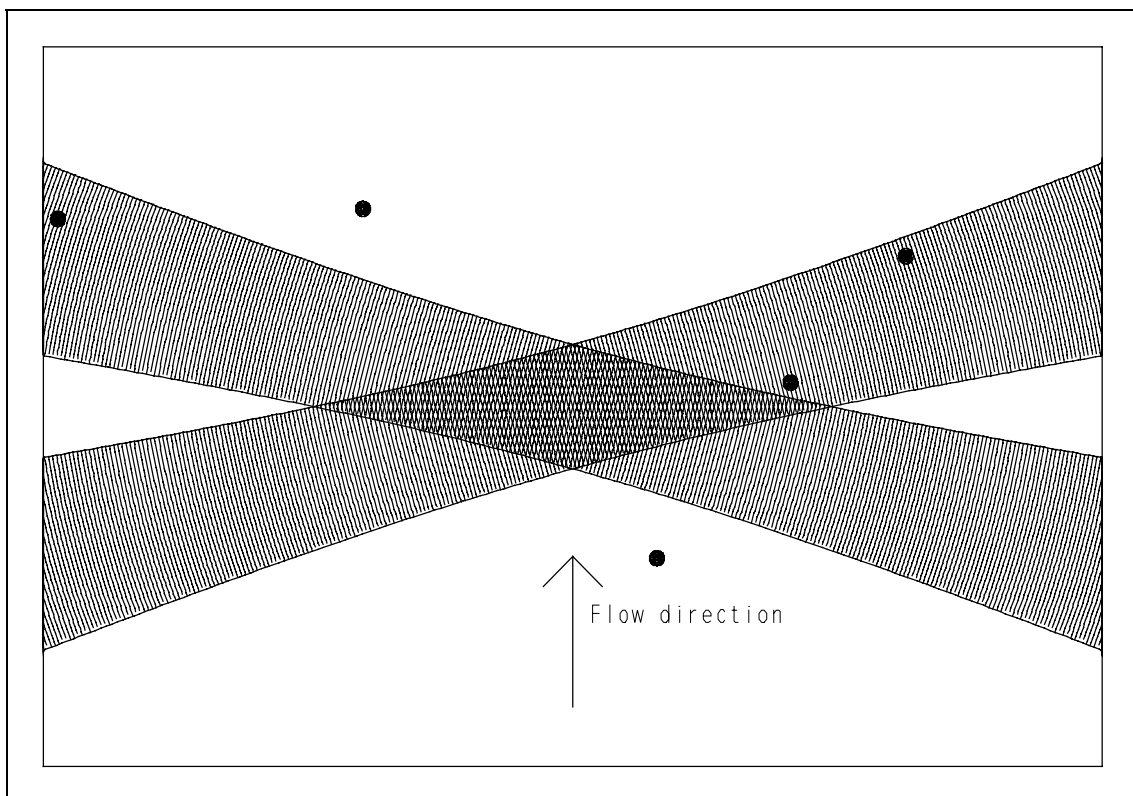


**Figure 1.1<sup>b</sup>:** In the simplest model, interference fringes in the measurement volume modulate the light intensity, received by the tracer particles.

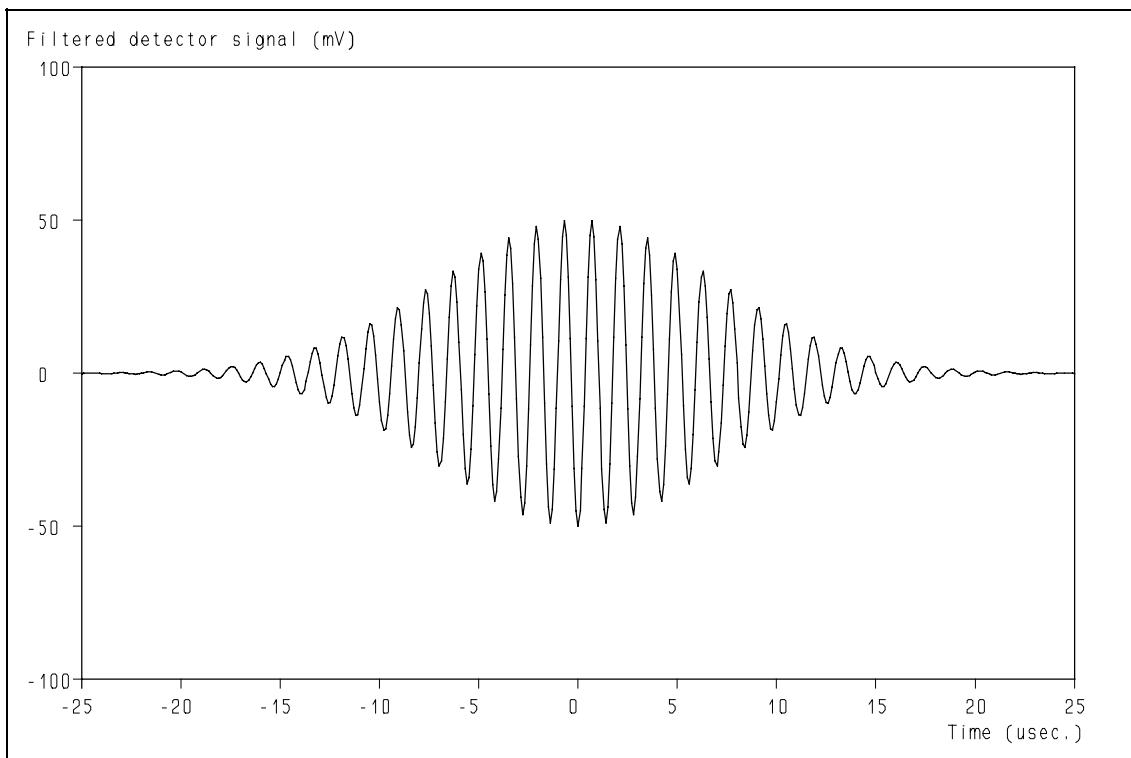


**Figure 1.1<sup>c</sup>:** After high-pass filtering the modulated light intensity, received by the photo detector, results in an oscillating signal. The frequency corresponds to the velocity of the tracer particle.

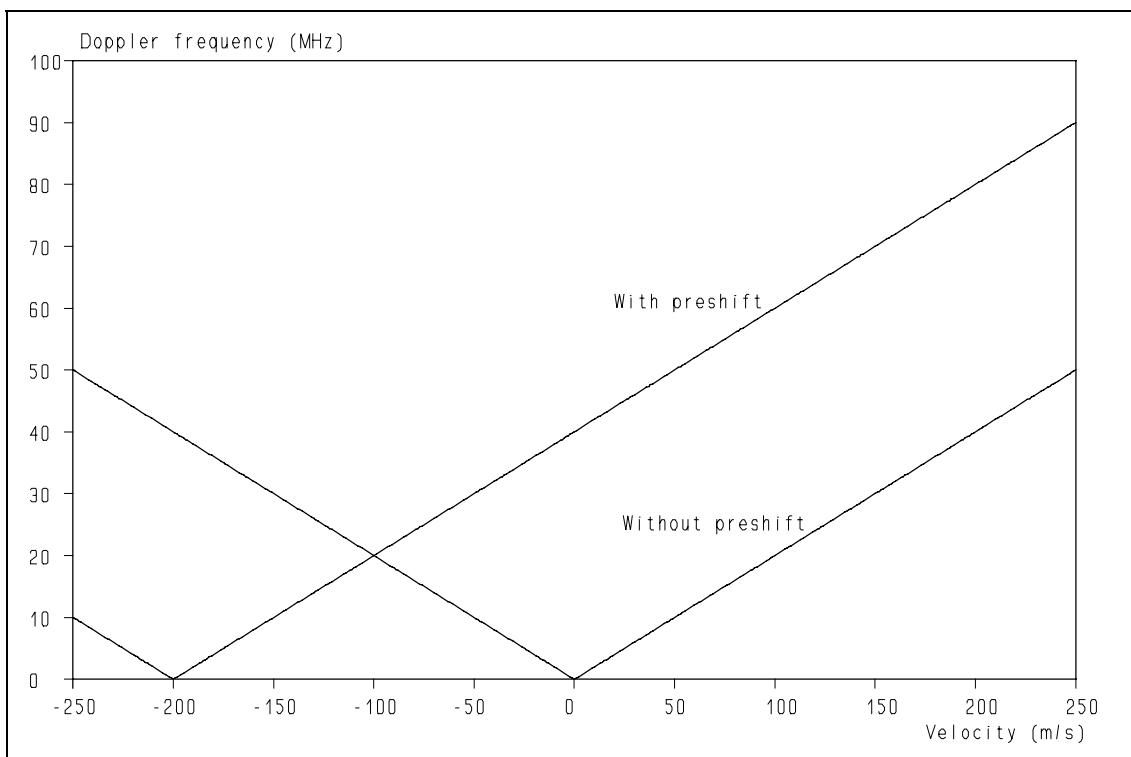


**Figure 1.2:** Frequency of the Doppler signal as function of velocity without (0 MHz at zero velocity) and with (40 MHz at zero velocity) preshift.

*Retrieval of turbulence and turbulence properties from LDA data with noise*

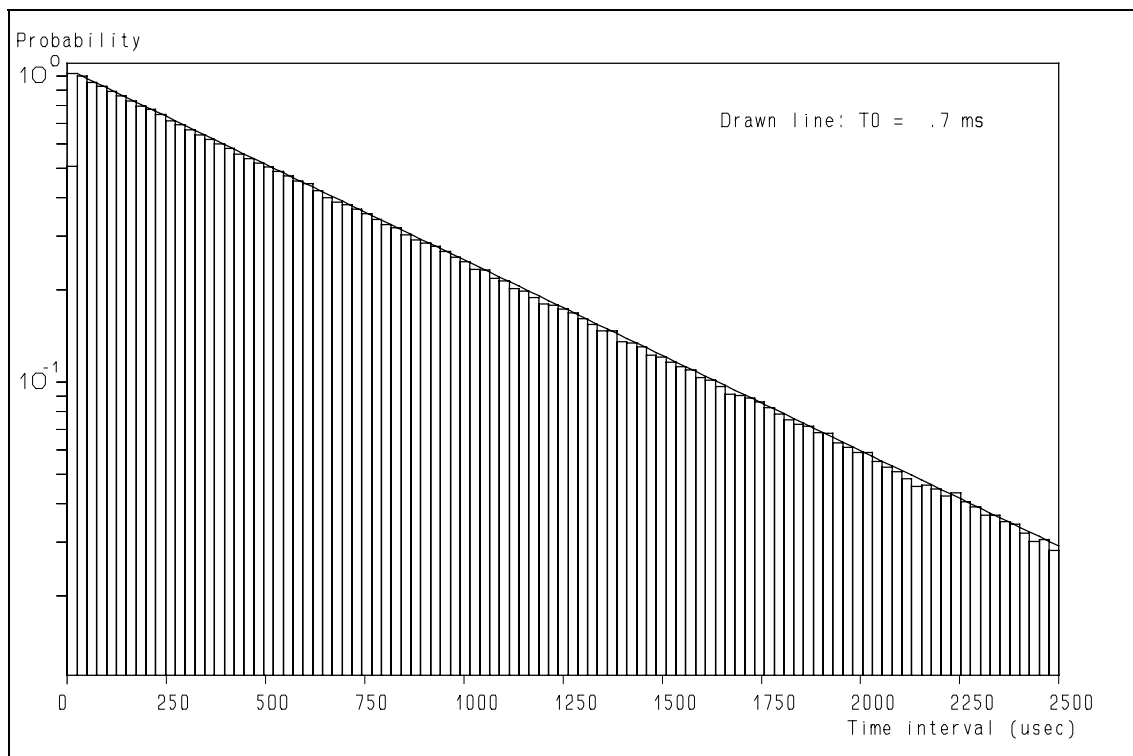


**Figure 1.3:** The exponential time interval distribution under ideal conditions, caused by the random (Poisson) distribution of the tracer particles in the fluid.

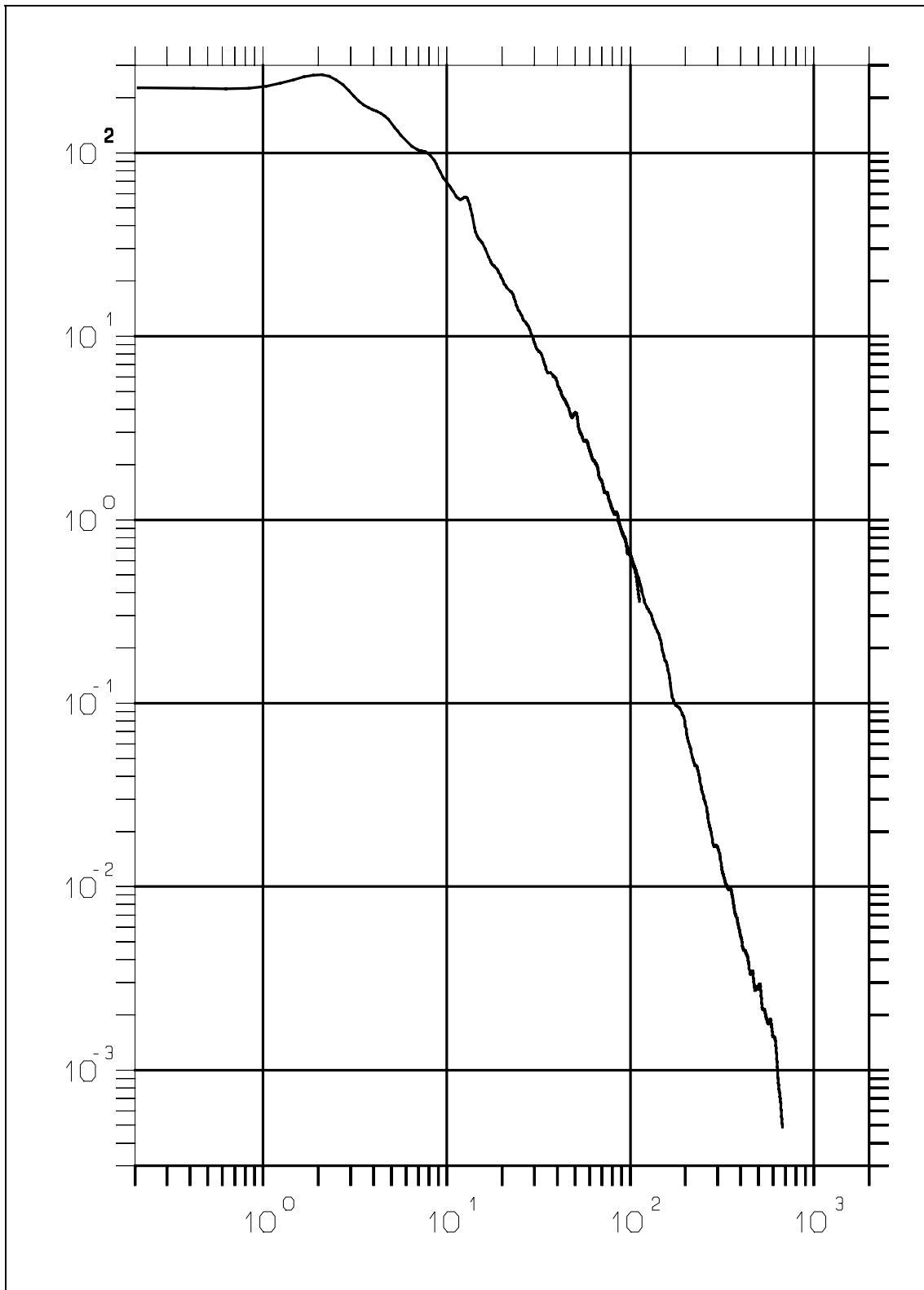


**Figure 1.4:** Turbulence power spectrum of the tangential component, measured in the jet of the Rushton turbine at 130 rpm.

*Retrieval of turbulence and turbulence properties from LDA data with noise*

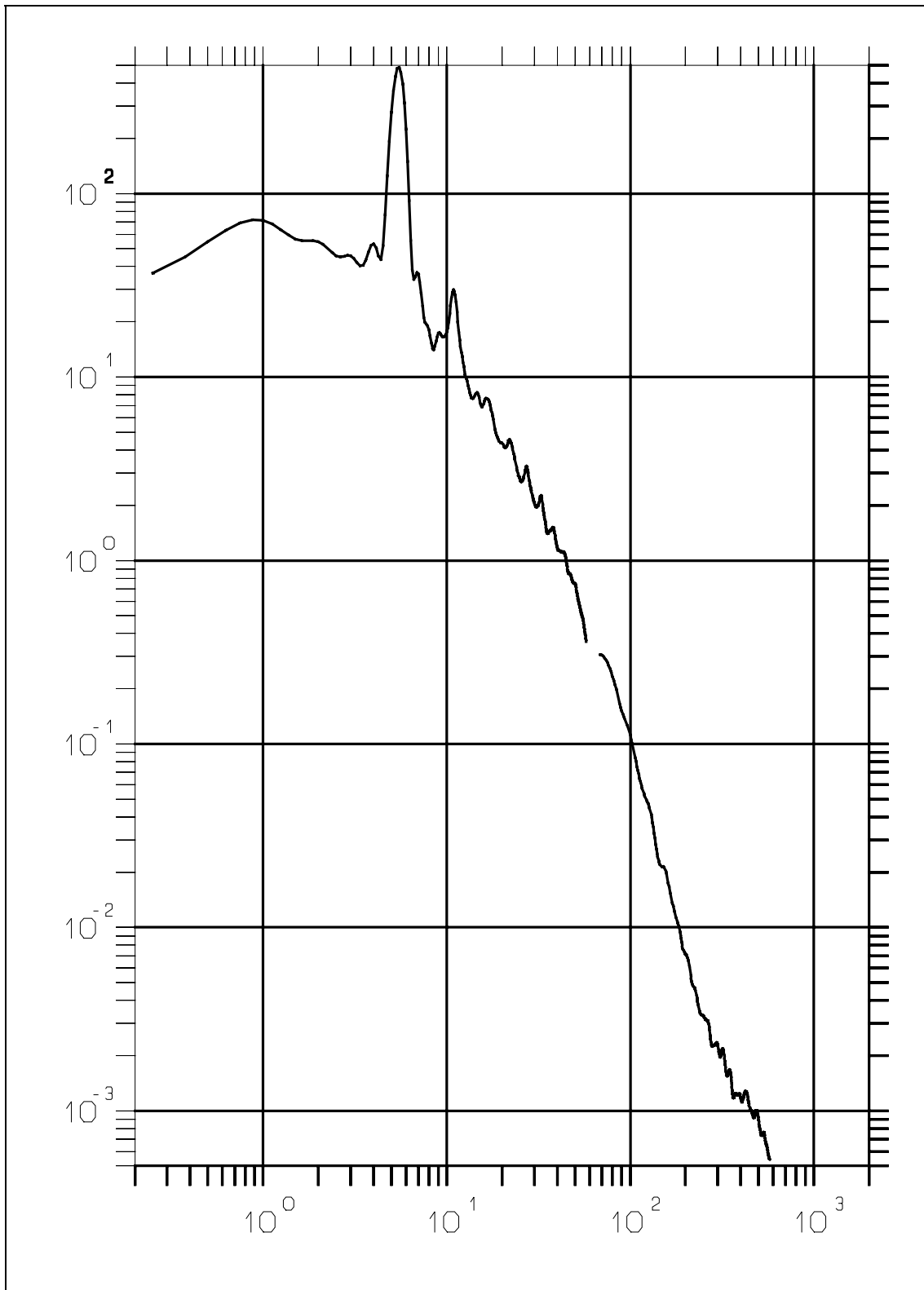


**Figure 1.5:** Turbulence power spectrum of the radial component, measured in the jet of the Rushton turbine at 55 rpm. Note the strong periodic component at 5.5 Hz, caused by the stirrer blades.

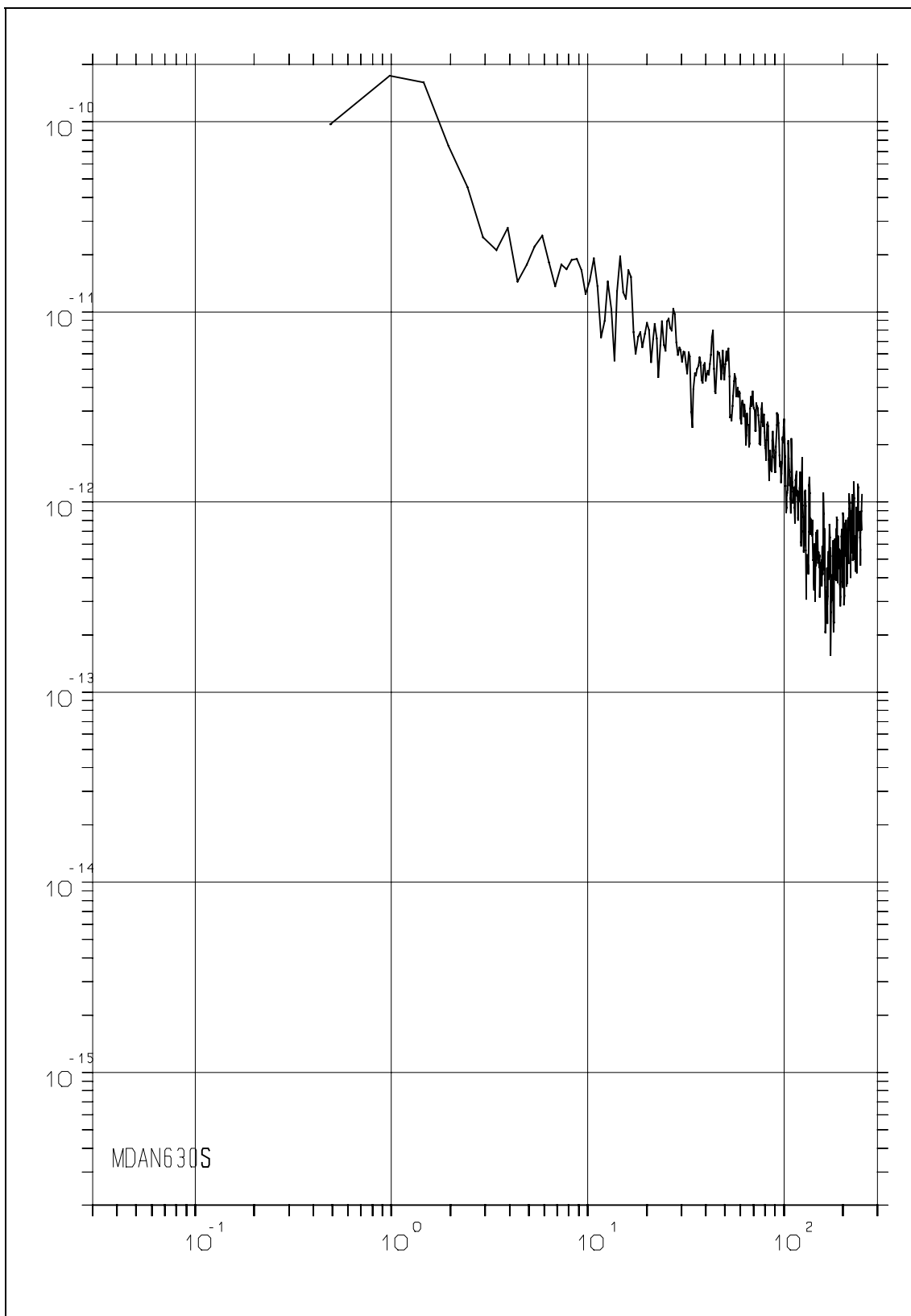


**Figure 1.6:** Turbulence power spectrum of the radial component (as fig. 1.5) as calculated by the software of a modern processor. Presentation of the results by the author.

# Chapter 2

## Monte Carlo Simulations

*There is one thing certain, namely,  
that we can have nothing certain;  
therefore it is not certain that  
we can have nothing certain.*  
Samuel Butler.

### 2.1 Introduction.

The analysis of the dynamic behaviour of turbulence measurement equipment is complicated by the fact that there are no simple ways to calibrate these. Turbulence itself is only reproducible in its statistical properties like average velocity, turbulence intensity, the auto correlation function (ACF) of the turbulent velocity fluctuations and the like, but the velocity fluctuations themselves are not repeatable. Some investigators have tried to put a Hot-Wire Anemometry (HWA) probe and a Laser Doppler Anemometry (LDA) measurement volume close together and to compare their behaviour (ref. 68), but such an experiment is hampered by the need of LDA for tracer particles, whereas HWA prefers clean air. Also, because tracer particle problems are less in liquids, many investigators want to apply LDA in liquids and the translation of such experiments from air to liquid is not simple as long as the mechanisms, that govern the behaviour of an LDA system are not well understood. The use of well-defined flows (e.g. vortex streets) could be helpful, but it still requires certain assumptions about the background turbulence and this makes the distinction between noise and background turbulence not an easy task. The use of solid bodies (e.g. rotating disks or vibrating surfaces) is not a very realistic simulation and it is not easy to interpret the results for the measurement of turbulent flows. On top of that the problem comes that an LDA is a complicated piece of equipment where noise contributions sneak in at many different (and sometimes unexpected) places (see Chapter 3). To separate the influence of all these different error sources is virtually impossible. Therefore, extensive use has been made of Monte-Carlo simulations in order to determine the influence of different noise sources and to develop novel data-processing algorithms. In this chapter we will describe the techniques that we have used to obtain the different simulated data-sets which are required.

### 2.2 Generation of random numbers with different probability distributions.

The analysis of systems using statistical techniques is common. To simplify this approach using a computer, all computers are nowadays equipped with a so-called "Random Number Generator", which generates a sequence of uncorrelated numbers in the range 0 - 1 with a homogeneous probability distribution. An example is shown in fig. 2.1. This sequence of numbers can be used to generate a sequence of random numbers with a different probability distribution, required for a certain application. The general procedure is to regard the homogeneous distribution as the cumulative distribution of the required distribution. Integration of the analytical probability distribution of the required distribution yields a function which -when inverted- can generate the desired probability distribution from the homogeneous distribution between 0 - 1. This can be illustrated by an example. If we e.g. want to obtain the exponential time interval distribution<sup>1</sup> as given by

---

<sup>1</sup> Note that this distribution is a straight line on a lin-log scale and that in the ideal case the data-rate (= number of independent Doppler signals per second) equals  $1/t_0$ .

## Retrieval of turbulence and turbulence properties from LDA data with noise

$$P(\Delta t) = \frac{1}{t_0} e^{-\frac{\Delta t}{t_0}} \quad [2.1]$$

in which:

$P$  = Probability density distribution.

$\Delta t$  = Time between two successive Doppler signals. S

$t_0$  = Characteristic time of the distribution S

the following procedure is applied:

Calculate the cumulative probability distribution:

$$C(\Delta t) = \int_0^{\Delta t} \frac{1}{t_0} e^{-\frac{\Delta z}{t_0}} d\Delta z = 1 - e^{-\frac{\Delta t}{t_0}} \quad [2.2]$$

in which:

$\Delta z$  = integration variable S

The result is illustrated in fig. 2.2. Now put the cumulative probability distribution equal to the homogeneous probability distribution as generated by the Random Number Generator of the computer:

$$RND = 1 - e^{-\frac{\Delta t}{t_0}} \quad [2.3^a]$$

$$e^{-\frac{\Delta t}{t_0}} = 1 - RND \quad [2.3^b]$$

By taking the inverse function and by noting that  $1 - RND$  is just as random as  $RND$ , the result is:

$$\Delta t = -t_0 \cdot \text{LOG}(1 - RND) = -t_0 \cdot \text{LOG}(RND) \quad [2.4]$$

So by using eq. [2.4] a set of numbers can be generated which have an exponential distribution<sup>2</sup>. That this technique works is shown in fig. 2.3, in which the probability distribution of such a set is shown (note the lin-log scale, for details see Chapter 4).

The technique, described in the previous paragraph is very powerful, but it requires that:

- the probability distribution has an analytical description.
- the analytical probability distribution can be integrated to yield an analytical cumulative probability distribution.
- the inverse function of the analytical cumulative probability distribution can be found.

Although this is possible for many distributions, not all fulfil the above mentioned requirements. The most notably of those is the Gaussian probability distribution. Fortunately, however, there is a way around this problem (ref. 69):

The probability distribution of the random numbers, generated by the computer, is homogeneous between 0 - 1. If 0.5 is subtracted from each number, the distribution becomes homogeneous between -0.5 and 0.5, as is illustrated in fig. 2.4. Call the set of these numbers  $R(1)$ . Adding two elements of  $R(1)$  results in a different set which we will call  $R(2)$ . The probability distribution of  $R(2)$  is a triangle with its top at 0 (zero) and intersections with the x-axis at -1 and +1 as is shown in fig. 2.5. Adding an element

---

<sup>2</sup> If no base is indicated in the logarithm, "log" will mean logarithm with base e (natural logarithm). Other bases will be indicated like e.g.  $^{10}\log$ .

## 2. Monte Carlo simulations

of  $R(1)$  and one of  $R(2)$  results in the set  $R(3)$  which has a sort of bell-shaped distribution as is shown in fig. 2.6. Elements of  $R(10)$  have a distribution which closely resembles a Gaussian distribution as is illustrated in fig. 2.7. In the simulations that we have used in this thesis we have applied elements of  $R(21)$ . For all practical purposes this is sufficiently close to Gaussian.

The first step of this procedure is mathematically described in the following way: The joint probability distribution of two sets  $R(1)$  yields  $R(2)$  and can be found by (ref. 69):

$$R(2) = P(z) = \int_{-\infty}^{\infty} P_1(x) \cdot P_1(z-x) dx \quad [2.5]$$

in which:

$P_1 = R(1)$  probability distribution, which is 1 (one) when  $-0.5 < x < +0.5$  and 0 (zero) elsewhere. The integral can be evaluated by realising that the distributions are either 0 (zero) or 1 (one), so these can be accounted for by the integration boundaries, as the product is 1 if and only if both distributions are 1. For the  $P_1(x)$  this is clear, the  $P_1(z-x)$  some reworking needs to be done:

$$\begin{aligned} -0.5 &< z-x < +0.5 \\ -z-0.5 &< -x < -z+0.5 \\ z-0.5 &< x < z+0.5 \end{aligned}$$

The integral can now be rewritten as:

$$R(2) = P(z) = \int_{\max(-0.5, z-0.5)}^{\min(0.5, z+0.5)} 1 dx \quad [2.6]$$

For  $z \leq 0$  the lower boundary is  $-0.5$ , the upper boundary  $z + 0.5$ , which leads to

$$P(z) = 1 + z \quad -1 \leq z \leq 0 \quad [2.7^a]$$

For  $z \geq 0$  the lower boundary is  $z-0.5$  and the upper boundary is  $0.5$ , which leads to

$$P(z) = 1 - z \quad 0 \leq z \leq 1 \quad [2.7^b]$$

Note that  $P(z)$  should be  $\geq 0 \forall z$ , so  $P(z) = 0$  elsewhere. This result is the triangular shape as shown in fig. 2.5.

The two distributions discussed above are the basis of the simulations. Using these simulations we have generated simulated signals of:

- Doppler signals with narrow band noise.
- Non-ideal time interval distributions<sup>3</sup>.
- Turbulence-like signals using two different power spectra.
- Simulated LDA data-sets on the basis of these turbulence-like signals.
- Simulated LDA data-sets on the basis of HWA signals.

### 2.3 Simulation of Doppler signals with narrow band noise.

In order to see what the lower limits of accuracy are that can be obtained with a certain noise level of the Doppler signal, it is necessary to have simulated Doppler signals with a noise contribution available. As in practice all LDA systems incorporate band-filters into their design, the noise should be narrow-band in this case also. Such signals can be obtained in the following way:

---

<sup>3</sup> These will be discussed in Chapter 4 on preliminary diagnostic testing of experimental data-sets.

## *Retrieval of turbulence and turbulence properties from LDA data with noise*

1. Select a frequency of the Doppler signal such that it is not an integer fraction of the sampling frequency and that approximately 40 - 50 periods of the cosine will fit into the time window chosen.
2. Multiply the cosine of the at step 1 chosen frequency with a Gaussian shaped envelope. Choose the  $\sigma$  of the Gaussian envelope such that the number of periods that have an amplitude larger than  $1/e^2$  of the maximum amplitude is approximately 30, corresponding to nominal values in many LDA systems.
3. Generate a block of 1024 or 2048 sampling points which contain the above defined signal (the required sampling frequency is roughly 20 - 30 times the frequency of the Doppler signal). An example is shown in fig. 2.8.
4. To each of the samples of the signal, obtained at step 3, a Gaussian distributed noise contribution is to be added. The variance of the noise has to be found by trial-and-error. An example can be seen in fig. 2.9, in which the Doppler signal is completely drowned in the noise.
5. The signal of fig. 2.9 is Fourier Transformed and the resulting amplitude spectrum is shown in fig. 2.10. The peak corresponds to the frequency of the Doppler signal and is easily recognised.
6. The spectrum, obtained at step 5 is subsequently filtered by application of a band-pass filter, as is common in LDA practice. The amplitude spectrum after filtering is shown in fig. 2.11.
7. Inverse Fourier Transformation brings the signal back into time domain and represents the Doppler signal, generated at step 2 and 3, accompanied by narrow band noise. The result is presented in fig. 2.12.

The use of different seed values for the Random Number Generator yields different readings for the noise contributions and in this way a large number of different Doppler signals with the same underlying Doppler frequency can be simulated and the different frequency estimation algorithms can be compared.

### **2.4 Turbulence-like signals according to predefined power spectra.**

Turbulent velocity fluctuations are -in general- not reproducible, only their statistical properties are. This means that it is virtually impossible to determine the amount of noise, left in the output data of a measured velocity signal. The only possibility to do this is by simulating LDA data on the basis of either simulated turbulence or e.g. HWA data. Before we come to this we will discuss how we can generate simulated turbulence. The procedure consists of the following steps:

1. Define a turbulence power spectrum in accordance with the current knowledge of turbulence. Bessem<sup>4</sup> et. al. (ref. 60 and 70) have given a useful description of such as spectrum, as well as Von Kármán-Pao (ref. 71). The equations of the Bessem and the Von Kármán-Pao spectra can be found in the Appendix to this chapter. The ACF, corresponding (for the parameters chosen) of the Bessem spectrum is shown in fig. 2.13 and the actual spectrum in fig. 2.14.
2. Regard the spectrum as a low-pass filter and calculate the impulse response of this filter using an Inverse Fourier Transformation<sup>5</sup>. Convolve a series of Gaussian distributed noise samples, generated in the way as described in the previous paragraphs, with the impulse response obtained at step 1. The procedure is illustrated in fig. 2.15. However, some practical aspects need to be addressed:
  - Because the temporal width of the impulse response of the filter is limited (in other words: the values of the impulse response are only different from zero in a limited part of the time window),

---

<sup>4</sup> This spectrum has been proposed by J.M. Bessem, based on literature. For ease of notation we will refer to this spectrum with cut-off frequencies of 1 and 50 Hz as "the Bessem spectrum".

<sup>5</sup> Keep in mind that these spectra are *power spectra* and therefore the square root needs to be taken to obtain the *amplitude spectra*. To complete the specification for the transfer function: for the phase any desired function can be chosen, but the simplest approach is to take zero phase shift for all frequencies. Now all requirements for the correct determination of the filter by Inverse Fourier Transformation are fulfilled.

## 2. Monte Carlo simulations

the convolution only needs to be calculated over this time window. This also means that the series of Gaussian distributed noise only needs to be available over this time window. That saves a lot of computer memory and the rest can be generated when needed.

- Theoretically, the impulse response can be different from zero for all time. This would mean that the above statement is no longer valid. However, in practice the impulse response rapidly decays and can be truncated outside a certain time window. This could lead to small "ringing" contributions because of the discontinuities at the time window boundaries. This can be eliminated by shifting the impulse response over the value at the boundaries, thus making sure that the impulse response is continuous over all time (see also Chapter 8).
- The time window boundaries can be chosen in such a way that the impulse response is -in absolute sense- smaller than e.g.  $10^{-7}$  of the maximum value for all time outside the window. This has proven to be sufficiently accurate for all cases studied.
- Choose the sampling frequency relatively high compared to the frequency where the dissipation begins (in the Bessem spectrum example 1000 Hz vs. 50 Hz). The reason for this is that the random sampling will generate instants in time in between two successive samples. The velocity at these instants needs to be estimated from the samples just before and just after this instant by linear interpolation. To avoid the introduction of additional error sources, one must be sure that the velocity has not changed so much that linear interpolation is not an accurate way of estimating the velocity.
- Using the procedure described above one obtains the fluctuating part of the velocity only. However, an average velocity can be added to one's desire or requirements.

Results of the technique described are shown in the fig. 2.16 - 2.21. Fig. 2.16 shows a small part of the thus generated "turbulence", fig. 2.17 a larger part. Fig. 2.18 presents the probability distribution (close to Gaussian), fig. 2.19 shows the ACF, fig. 2.20 the ACF simultaneously with the theoretical one and finally fig. 2.21 presents the power spectrum with the theoretical spectrum. Fig. 2.20 and 2.21 make evident that the procedure has given the proper results.

In this way we can obtain a simulated velocity signal that is known in any detail and that can be used as the basis of simulated LDA data. These data-sets can -on their turn- be used to evaluate different data-processing algorithms and their outcome can be compared to the original velocities.

### 2.5 Simulated LDA data-sets on the basis of simulated turbulence or HWA data.

Using the above described "ingredients" we can generate simulated LDA data-sets, based on either simulated or real turbulence, measured by HWA, by applying the following procedure:

- The sampling is done using the exponential time interval distribution. A desired data-rate is selected and the time intervals are generated by using the procedure described. The data-rate can be obtained from the tracer particle concentration, the effective size of the measurement volume and the magnitude of the fluid velocity through the measurement volume (which is not always the average value of the velocity component measured!).  
If desired, the  $t_0$  of the exponential time interval distribution can be varied according to the instantaneous velocity in order to simulate velocity bias. To simulate a dead time of the processor, the time intervals below a certain threshold value can be ignored.
- Every individual velocity estimate is accompanied by a Gaussian distributed noise contribution.

The instants, generated by the exponential time interval distribution, are used to determine the actual velocity by linear interpolation of the simulated velocity or HWA signal. A Gaussian distributed noise contribution is added and the "arrival time" and the "measured velocity" are written to file. Such a file would be similar to a file of measured data. The  $\sigma_n$  of the noise contribution can be derived from a desired ratio of the  $\sigma_t$  of the turbulence. Practical values are  $\sigma_n = 0.1 - 0.3$  of  $\sigma_t$ . An example of a thus obtained simulated data-set is shown in fig. 2.22.

## APPENDIX

### The turbulence power spectra used for the simulation of turbulence.

The Bessem Power Spectrum  $S_B(f)$  is given by (ref. 60 and 70):

$$S_B(f) = \frac{S_B(0)}{1 + \left(\frac{f}{f_1}\right)^{5/3} \cdot \left[1 + \left(\frac{f}{f_2}\right)^4\right]^{4/3}} \quad [2.8]$$

in which:

$S_B(0)$  = the static gain of the Power Spectrum m<sup>2</sup>/s or V<sup>2</sup>s  
 $f_1, f_2$  = the first and second cut-off frequency Hz  
 Below  $f_1$  the spectrum has a slope of 0 (zero) on a log-log scale, this is the production subrange. The subrange between the two cut-off frequencies is the inertial subrange with a slope of -5/3, consistent with the Kolmogoroff spectrum law (ref. 72). The dissipation subrange starts globally at  $f_2$  and has a slope of -7. The parameters used are:  $S_B(0) = 1 \text{ V}^2\text{s}$ ,  $f_1 = 1 \text{ Hz}$  and  $f_2 = 50 \text{ Hz}$ .

The Von Kármán - Pao Power Spectrum  $S_{KP}(f)$  is given by (ref. 71):

$$S_{KP}(k) = \alpha_k \frac{v^2}{\eta_k} \left(\frac{L}{\eta_k}\right)^{5/3} \frac{(kL)^4}{[1 + (kL)^2]^{17/6}} e^{-\frac{3}{2}\beta_k(k\eta_k)^{4/3}} \quad [2.9]$$

which, for a given value of the kinematic viscosity  $\nu$ , contains four parameters:

- $\alpha_k$  = dimensionless parameter
- $\beta_k$  = dimensionless parameter
- $L$  = the integral length scale m
- $\eta_k$  = Kolmogoroff length scale m

This spectrum is function of the wavenumber ( $k = 2\pi/\lambda$ ), and is the Fourier transform of a spatial ACF. According to Taylor's hypothesis the velocity  $u(t)$  may identified as  $u(x/U)$ , in which  $U$  is the transverse speed of the probe. This can be used up to high values of the turbulence intensity (ref. 73). Using this theory the wavenumber  $k$  may be replaced by the frequency multiplied by a constant, yielding the power spectrum. The four parameters were set to:  $\alpha_k = 1$ ,  $\beta_k = 1$ ,  $L = 1.5 \text{ m}$  and  $\eta_k = 0.006 \text{ m}$ . Literature confirms that this spectrum is a good representation of measured spectra, especially at higher Reynolds numbers (ref. 1, 2, 74 and 75).

## 2. Monte Carlo simulations

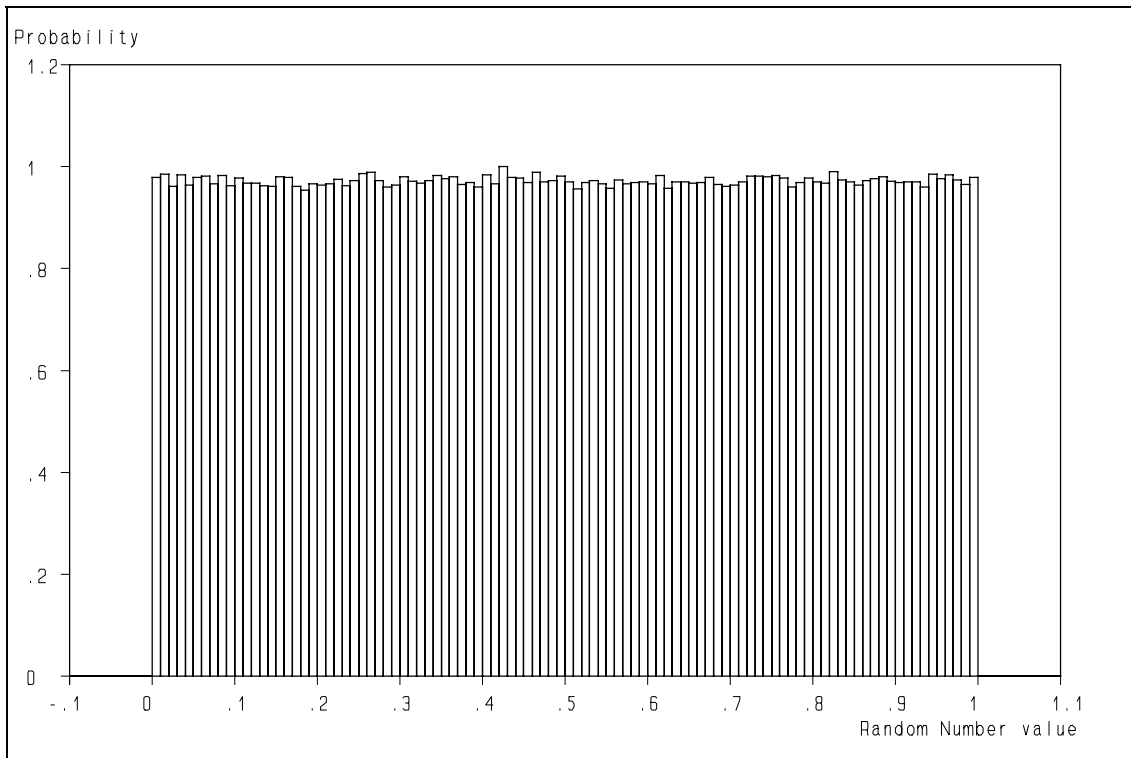


**Figure 2.1:** The distribution of the numbers from the Random Number generator.

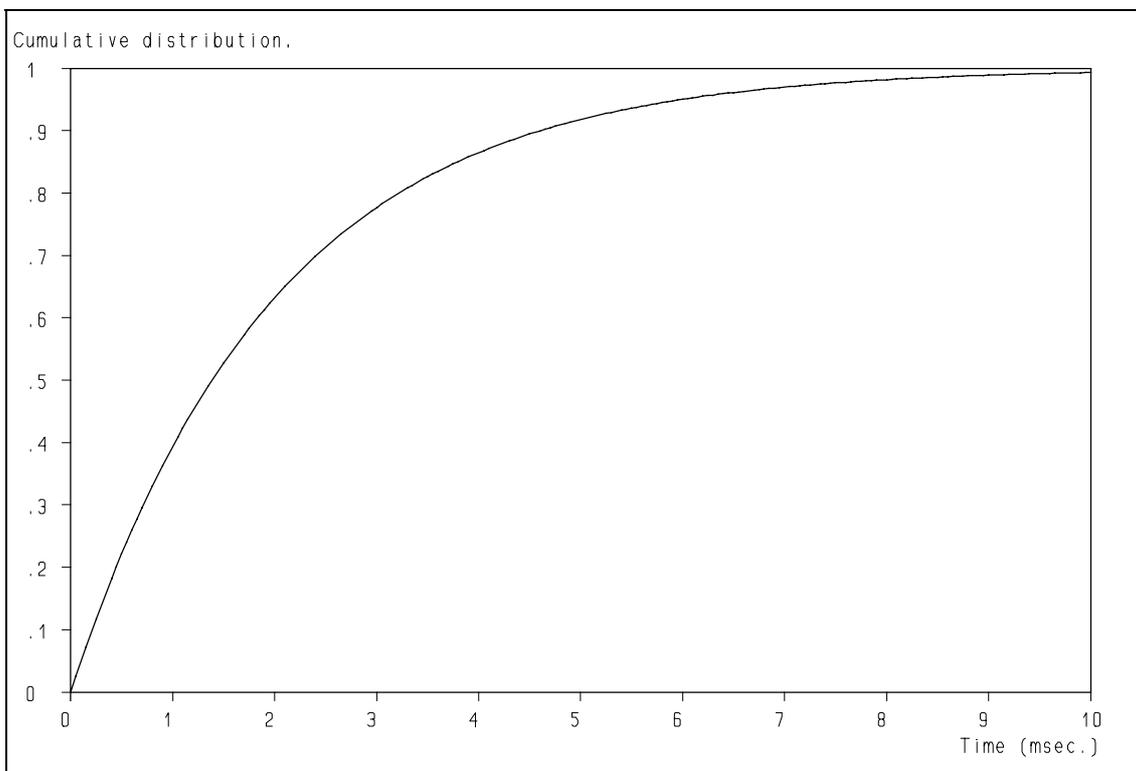


**Figure 2.2:** The cumulative distribution of the exponential time interval distribution ( $t_0 = 2.5$  msec.).

*Retrieval of turbulence and turbulence properties from LDA data with noise*

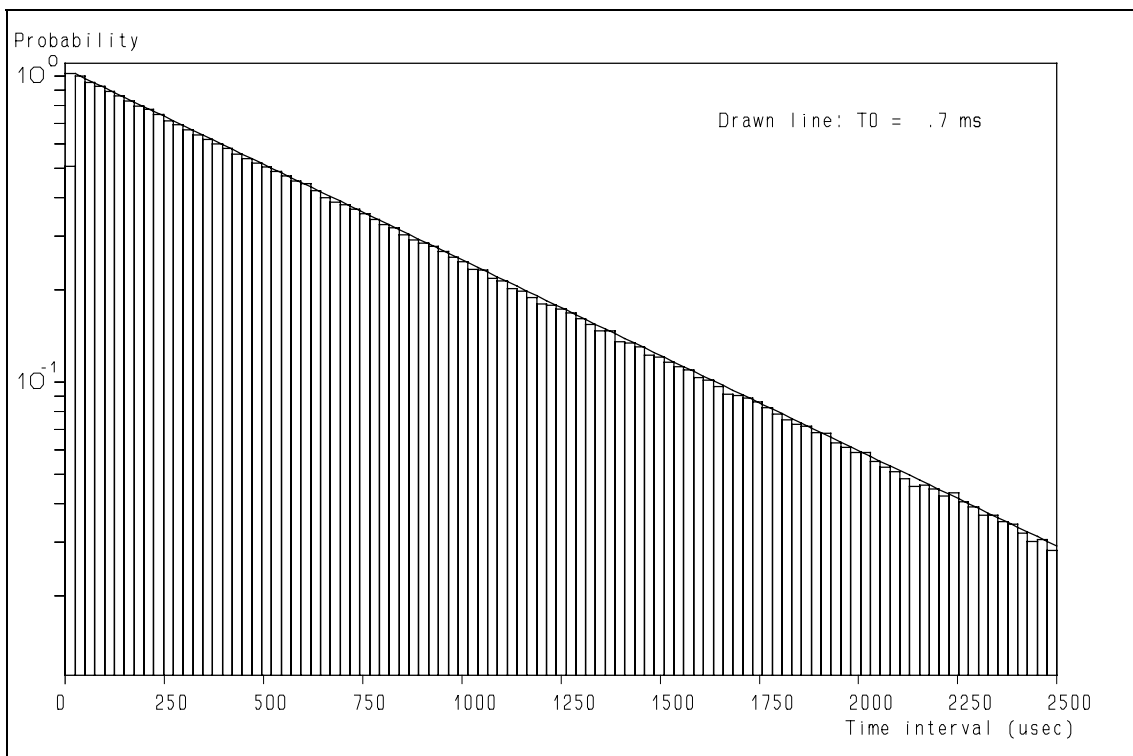


**Figure 2.3:** The exponential time interval distribution under ideal conditions.

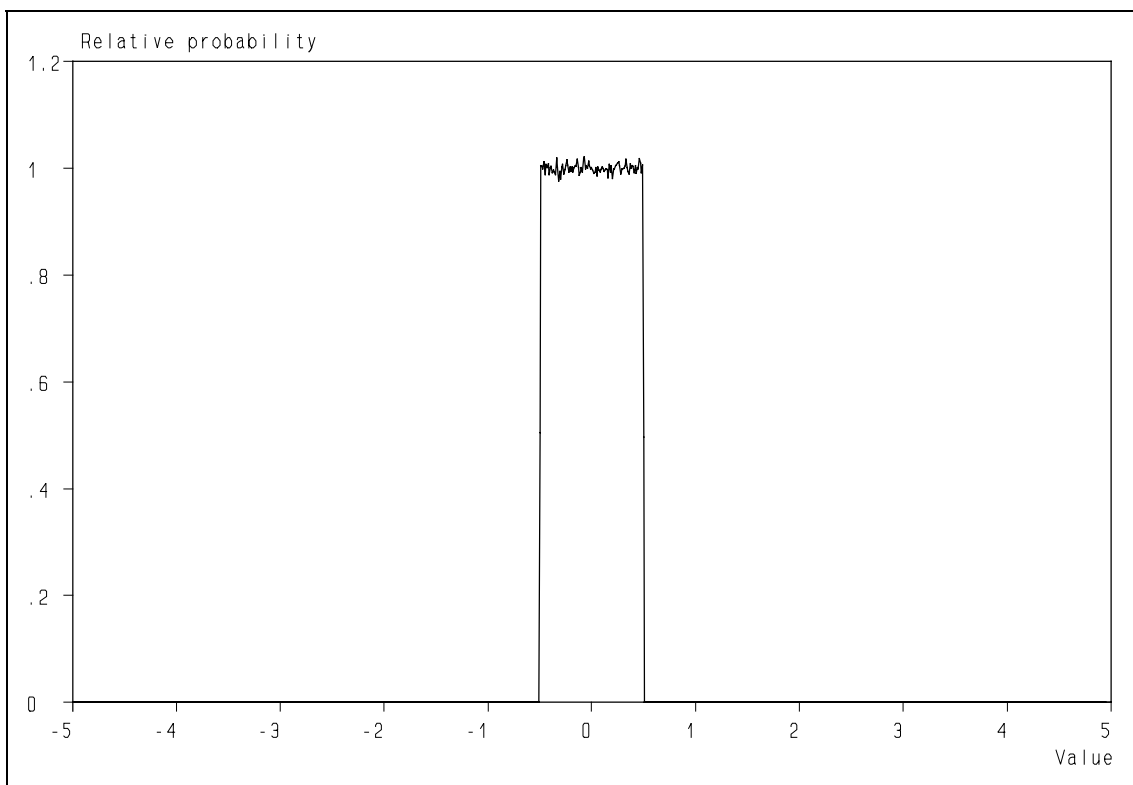


**Figure 2.4:** The RND generator produces values between 0 and 1, which can easily be shifted to -0.5 - +0.5.

## 2. Monte Carlo simulations

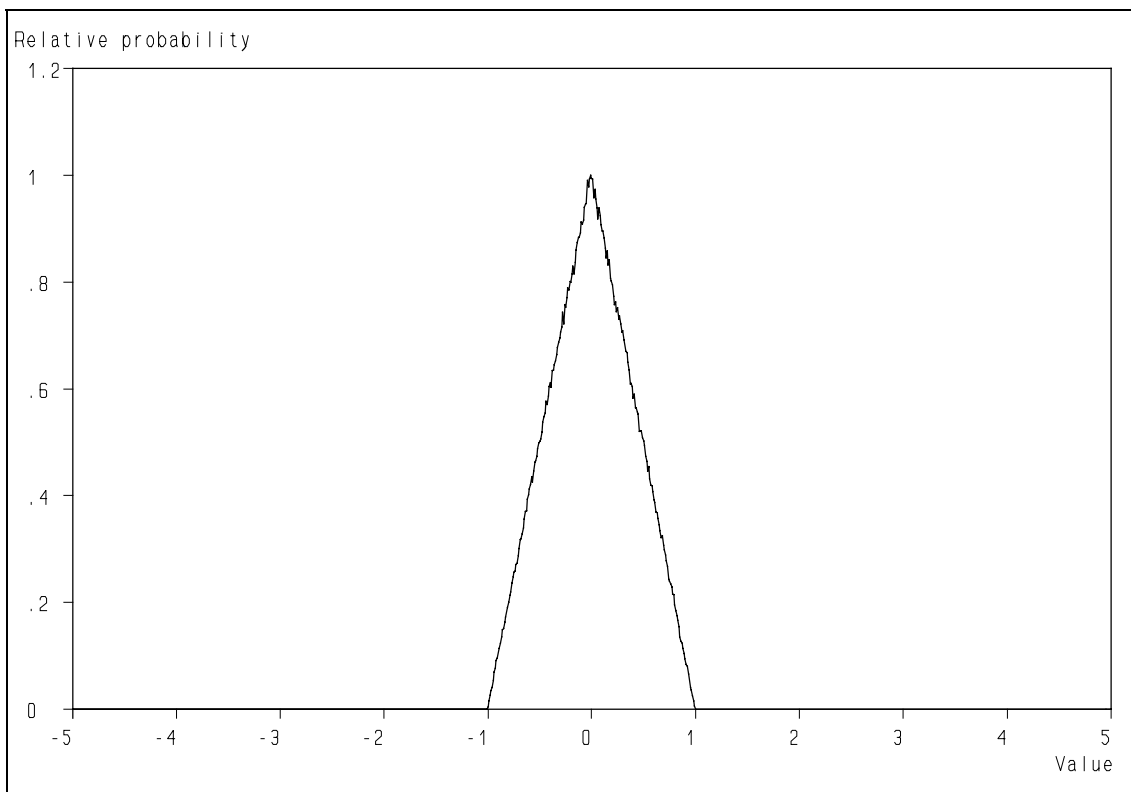


**Figure 2.5:** Adding two RND numbers from  $[-0.5, +0.5]$  yields a triangular distribution.

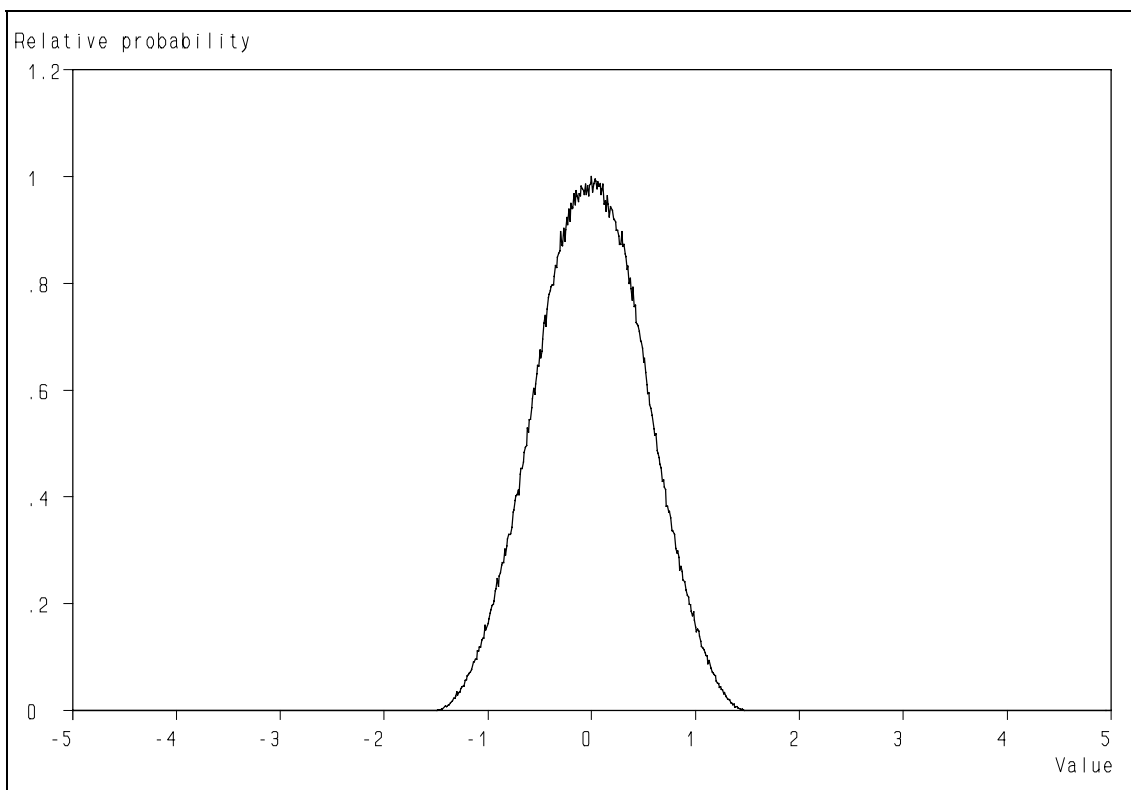


**Figure 2.6:** Adding three RND numbers from  $[-0.5, +0.5]$  yields a bell-shaped distribution.

*Retrieval of turbulence and turbulence properties from LDA data with noise*

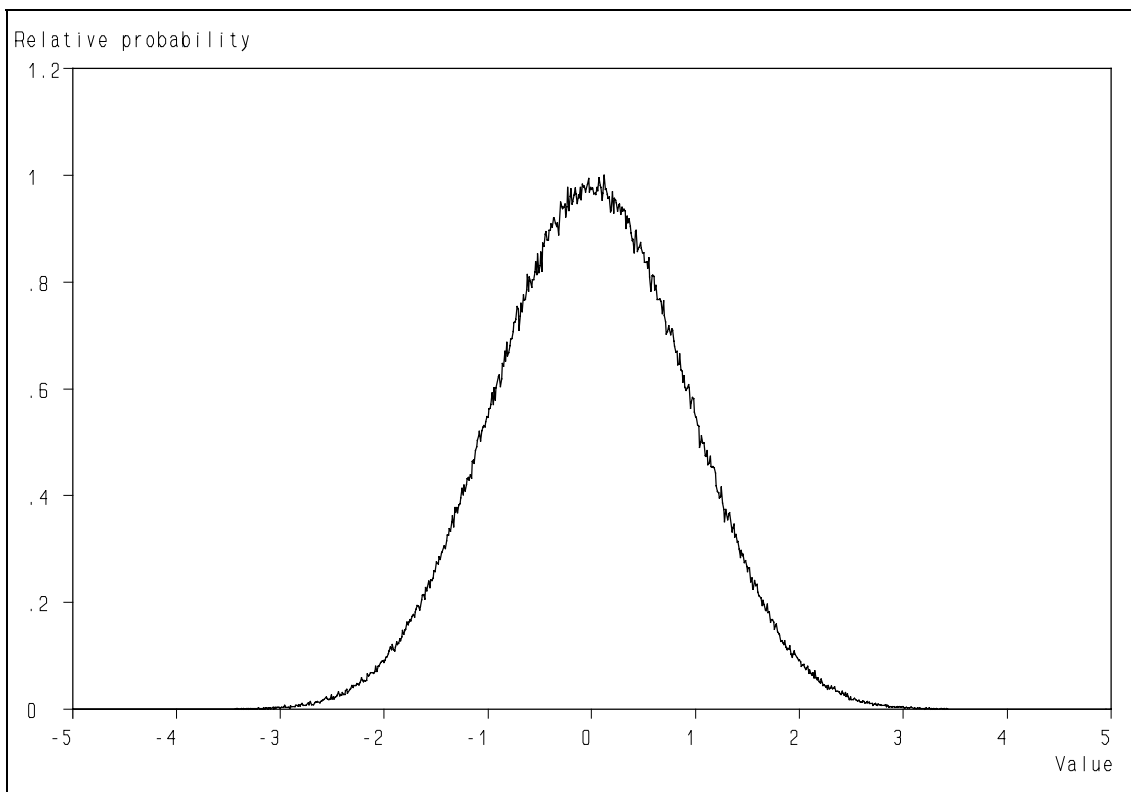


**Figure 2.7:** Adding 10 RND numbers from [-0.5 , +0.5] yields a distribution close to Gaussian.

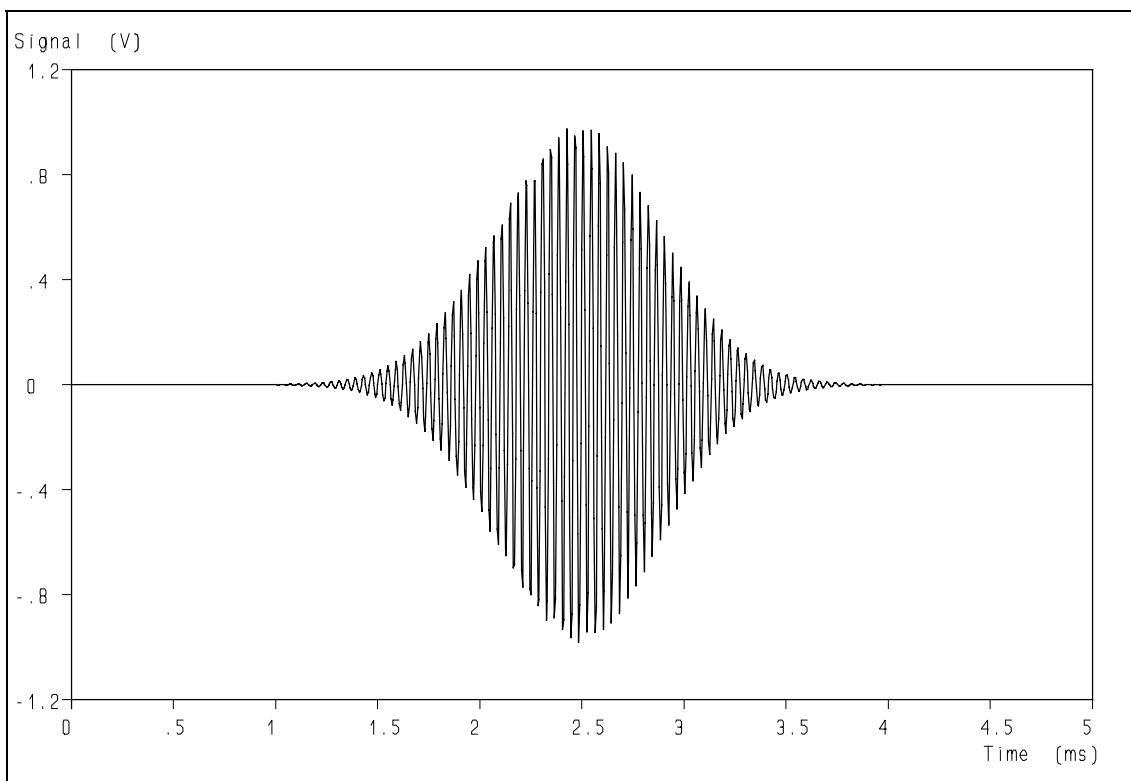


**Figure 2.8:** The ideal Doppler signal.

## 2. Monte Carlo simulations

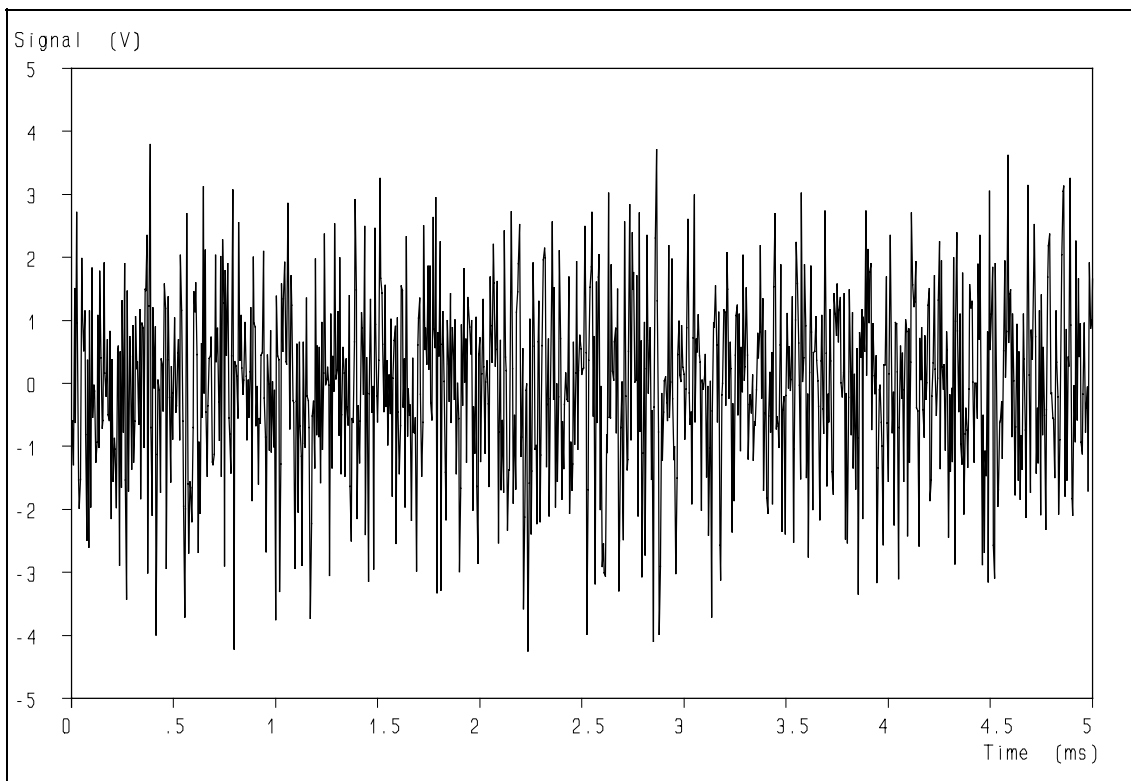


**Figure 2.9:** The Doppler signal of fig. 2.8 to which wide-band noise has been added.

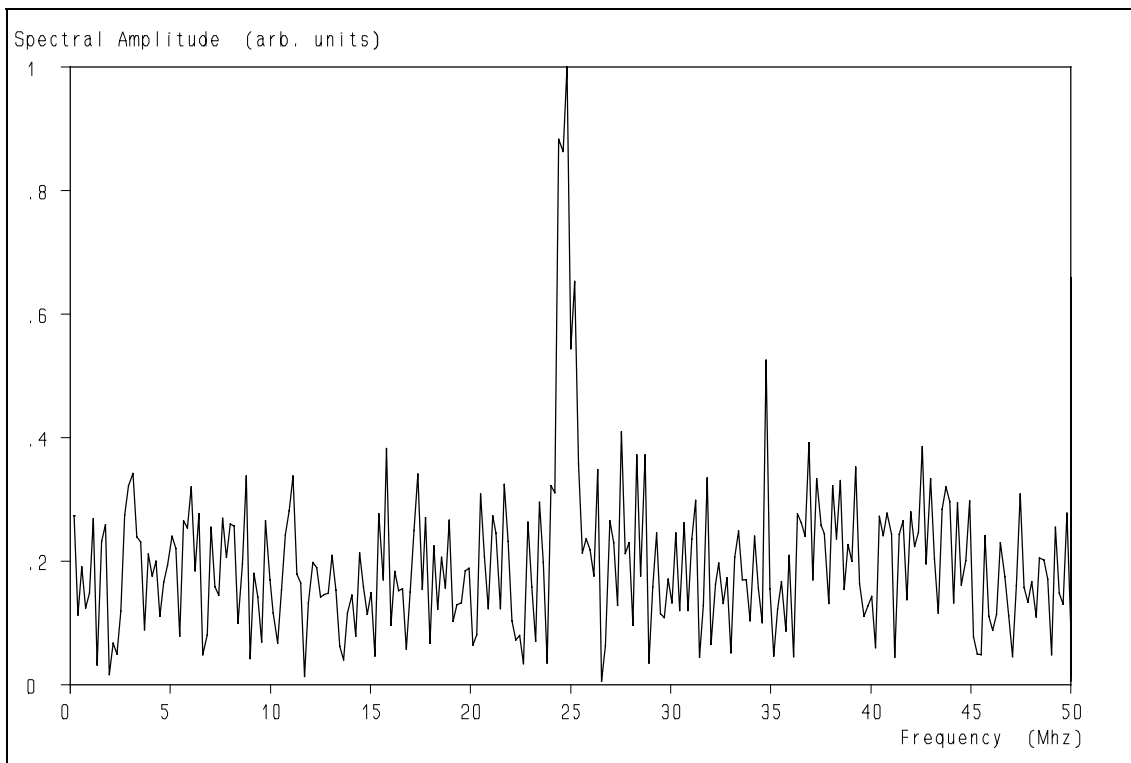


**Figure 2.10:** Modulus of the spectrum of the Doppler signal of fig. 2.9.

*Retrieval of turbulence and turbulence properties from LDA data with noise*

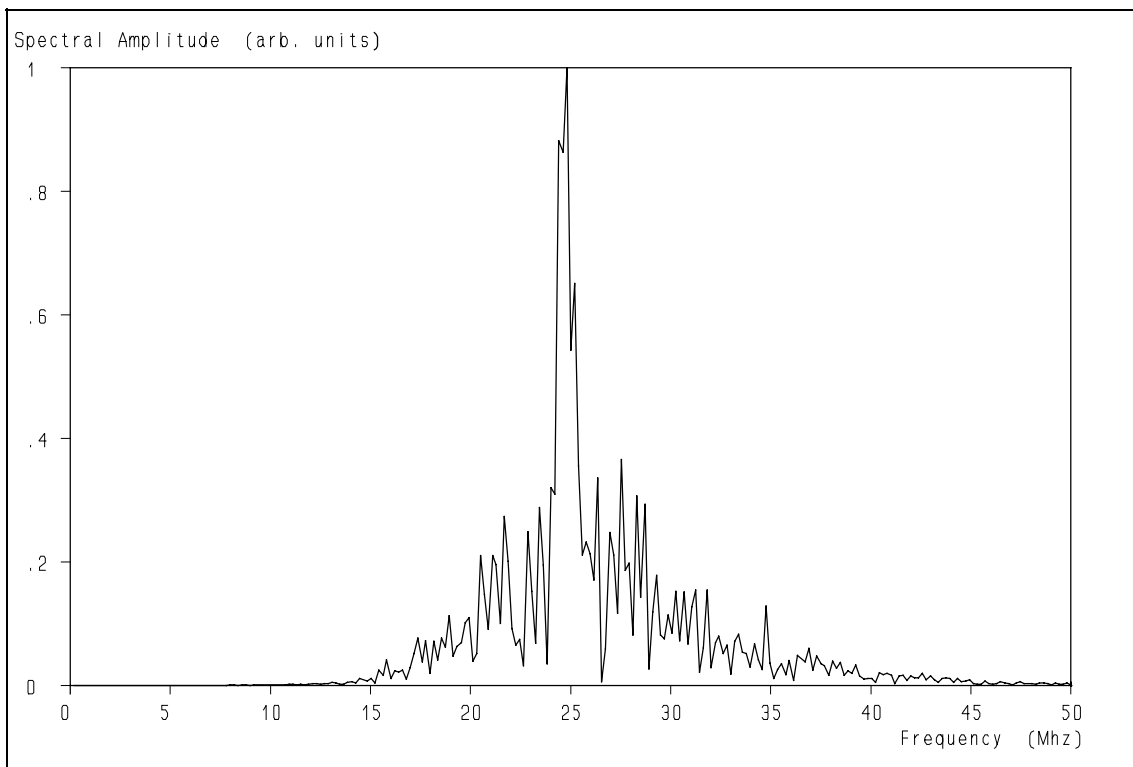


**Figure 2.11:** Spectrum of the Doppler signal of fig. 2.9 after the band-pass filter.

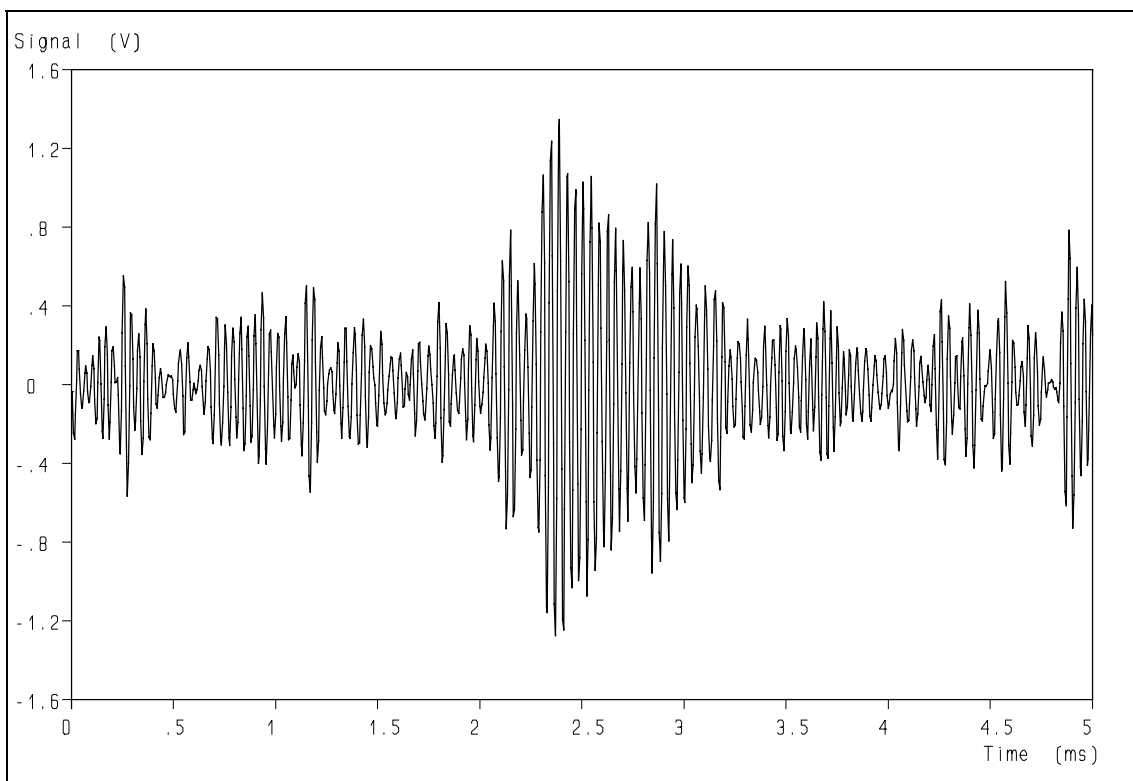


**Figure 2.12:** The Doppler signal of fig. 2.9 after the band-pass filter.

## 2. Monte Carlo simulations

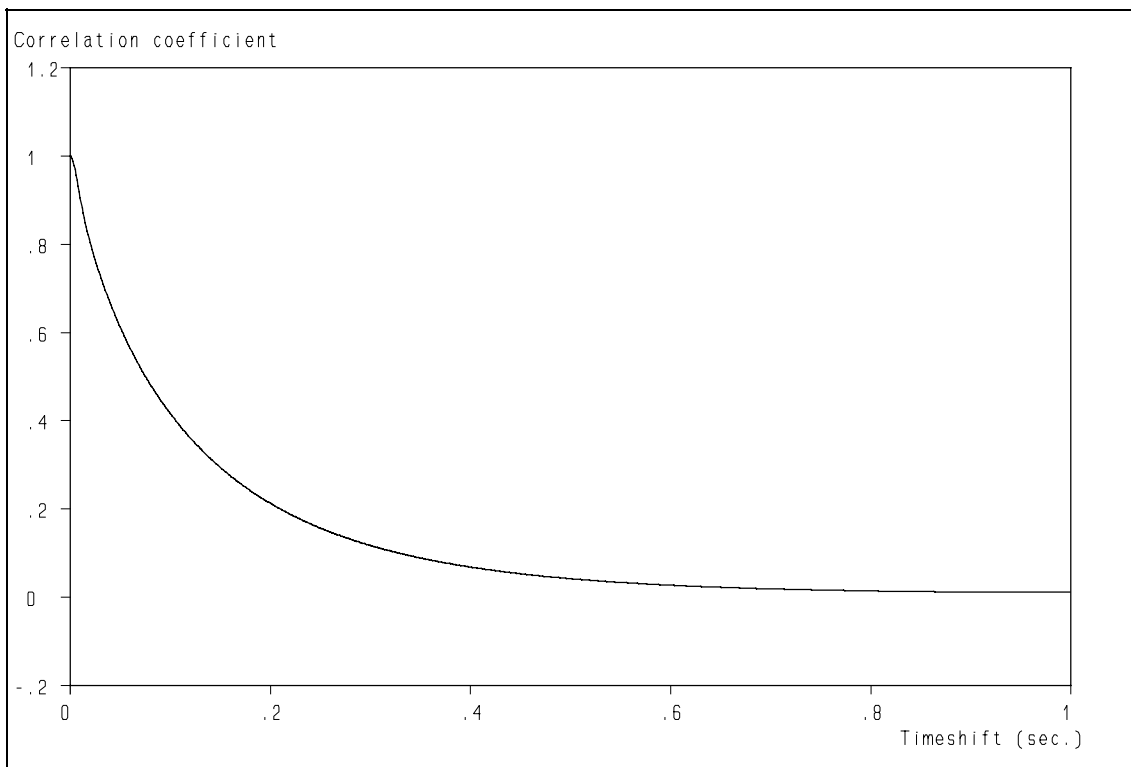


**Figure 2.13:** The theoretical auto correlation function, related to the Bessem turbulence power spectrum.

*Retrieval of turbulence and turbulence properties from LDA data with noise*

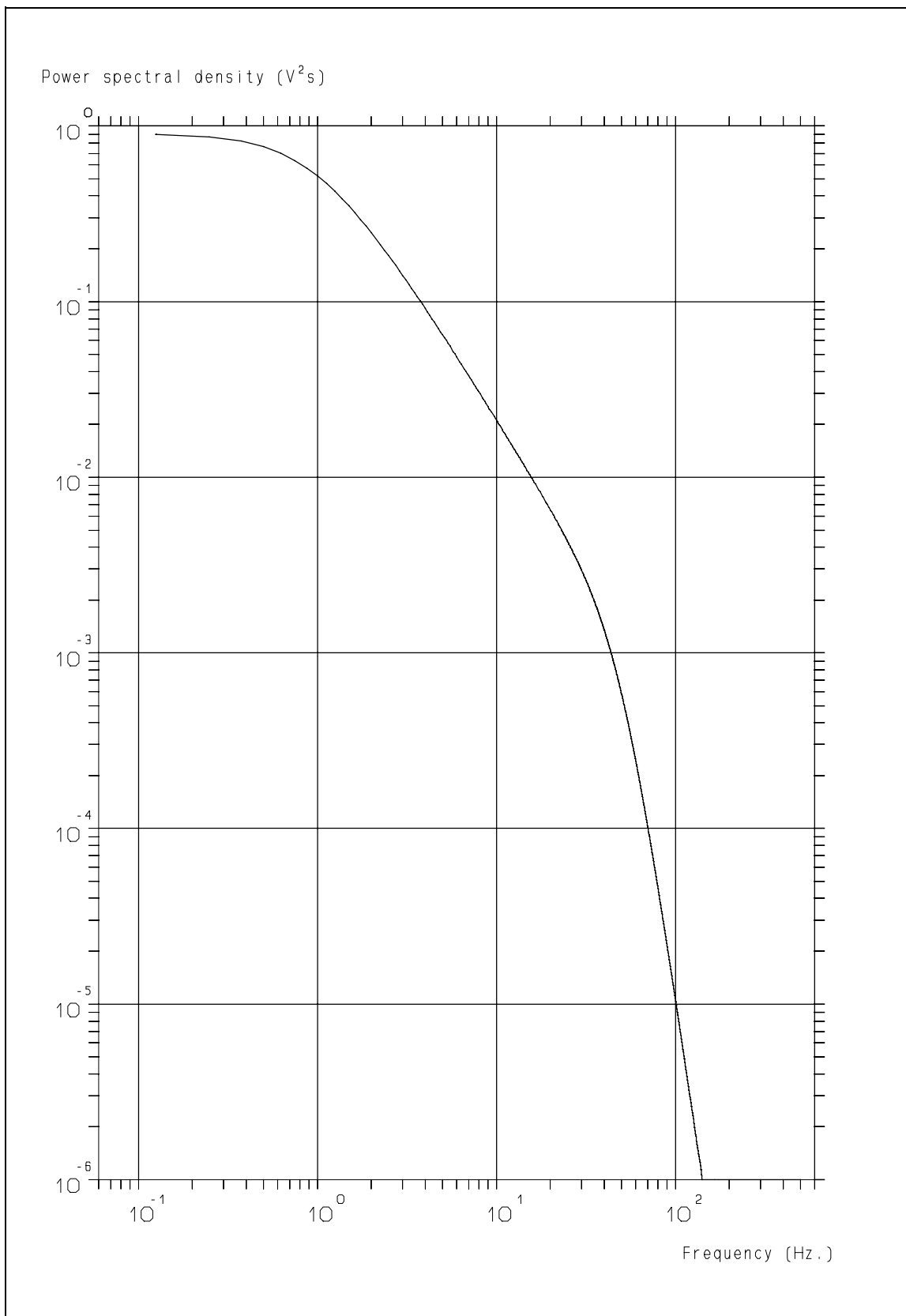


**Figure 2.14:** The Bessem turbulence power spectrum.

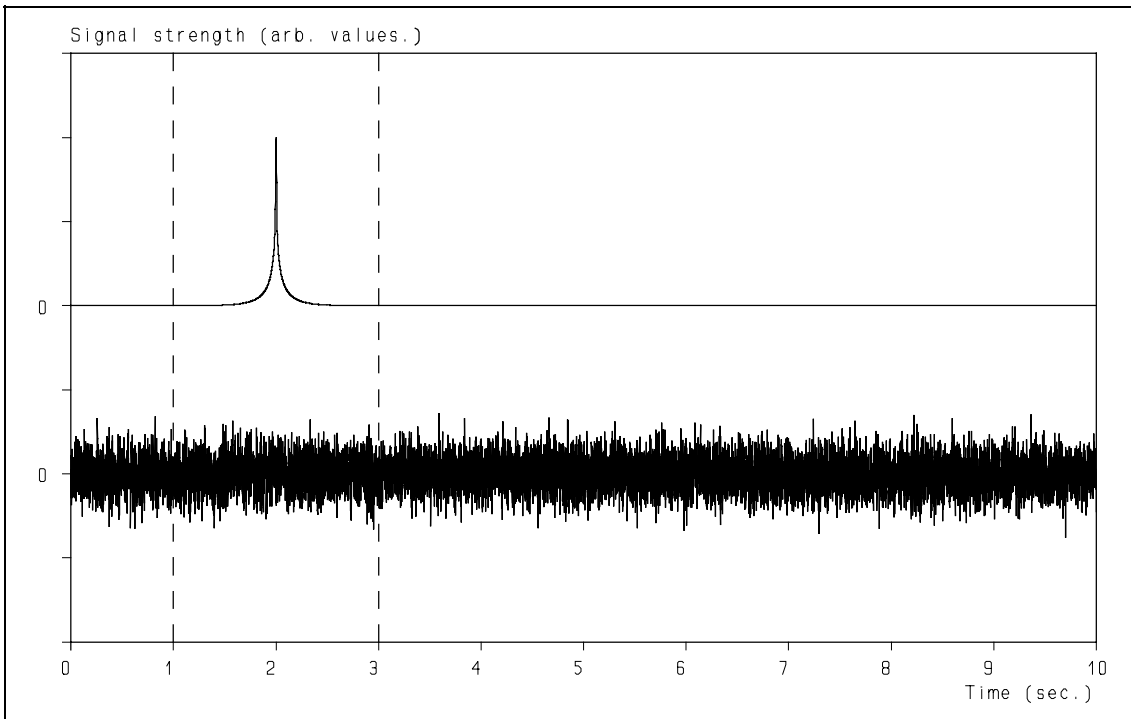


**Figure 2.15:** Illustration of the convolution algorithm. Between 1 and 3 sec. the IFT of the spectrum (upper trace) is different from zero and the integration with the noise (lower trace) can be limited to this interval.

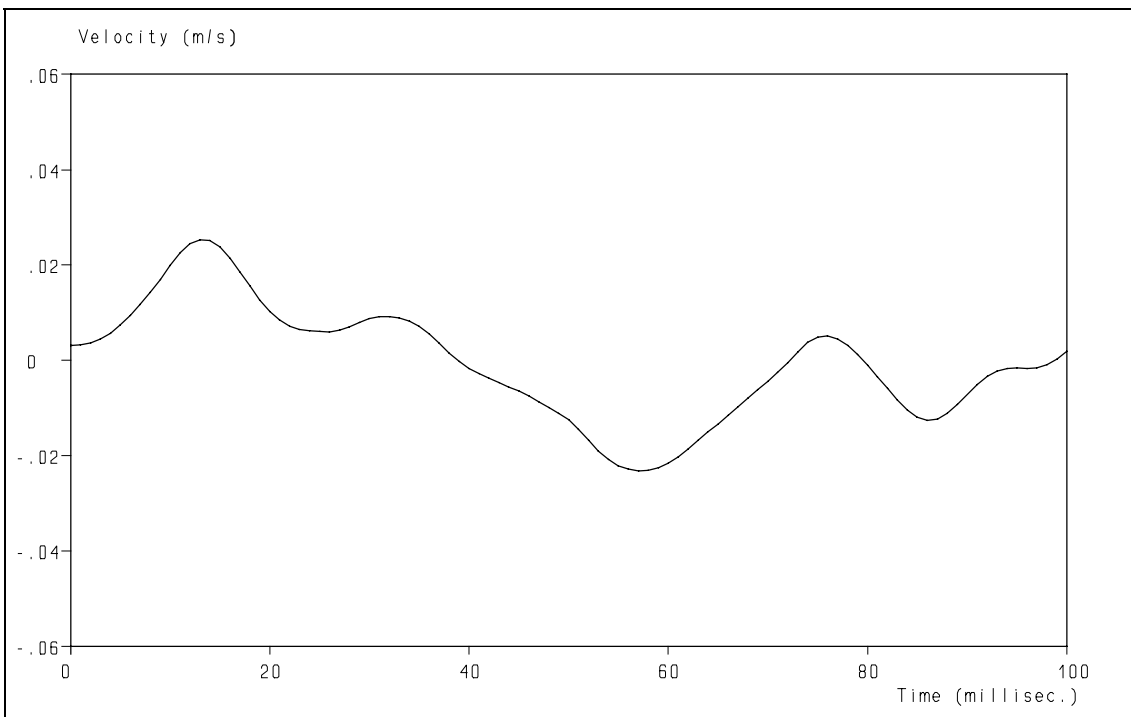


**Figure 2.16:** Example of a small part of the simulated turbulence according to the Bessem power spectrum.

*Retrieval of turbulence and turbulence properties from LDA data with noise*

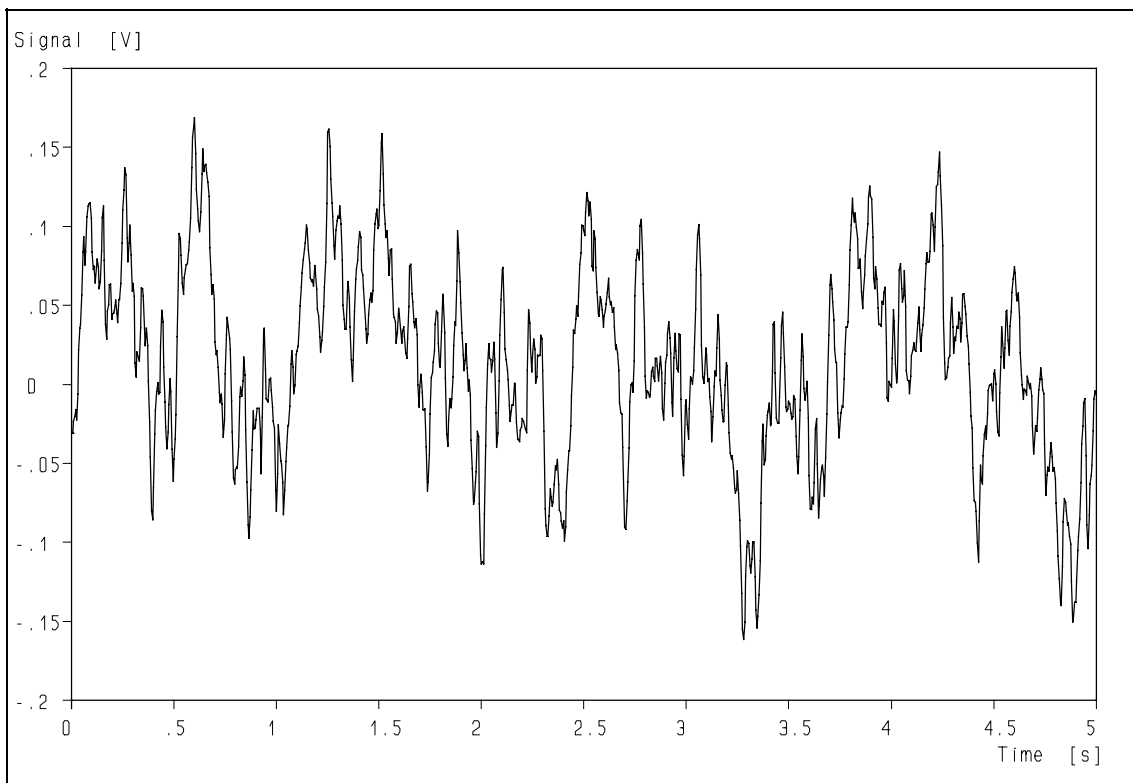


**Figure 2.17:** 5 seconds of simulated turbulence according to the Bessem power spectrum.

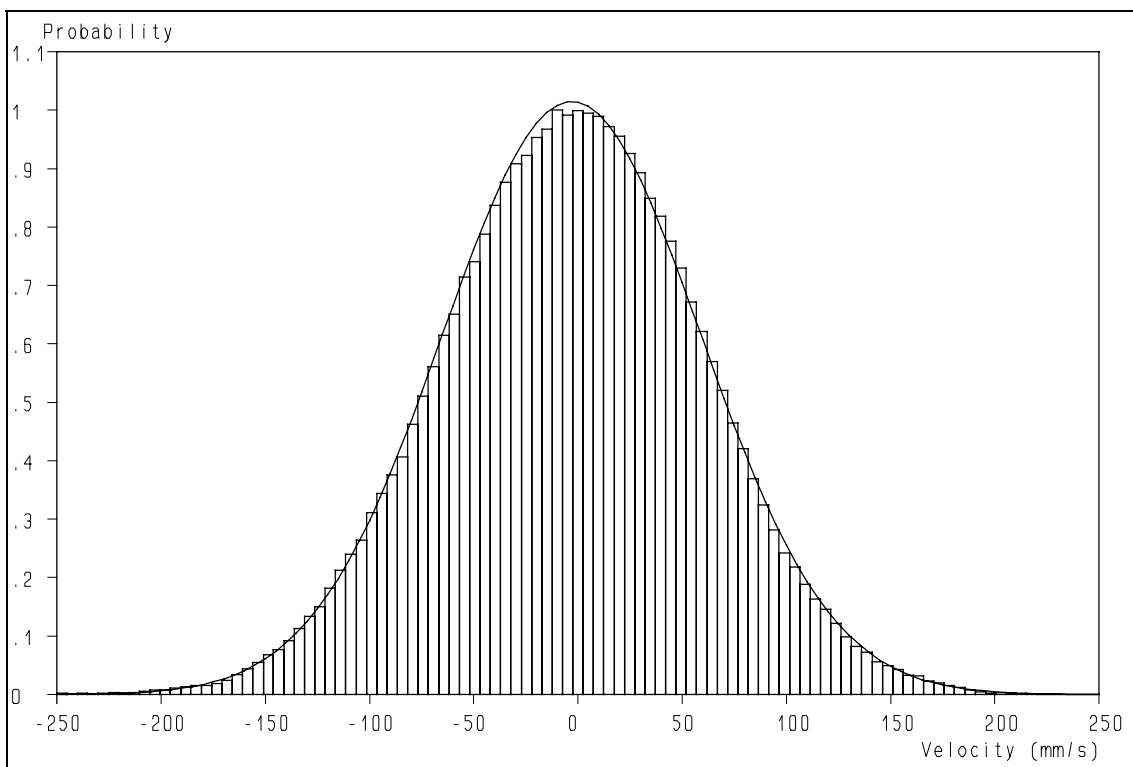


**Figure 2.18:** Histogram of the simulated turbulence. The drawn line is a Gaussian distribution.

## 2. Monte Carlo simulations

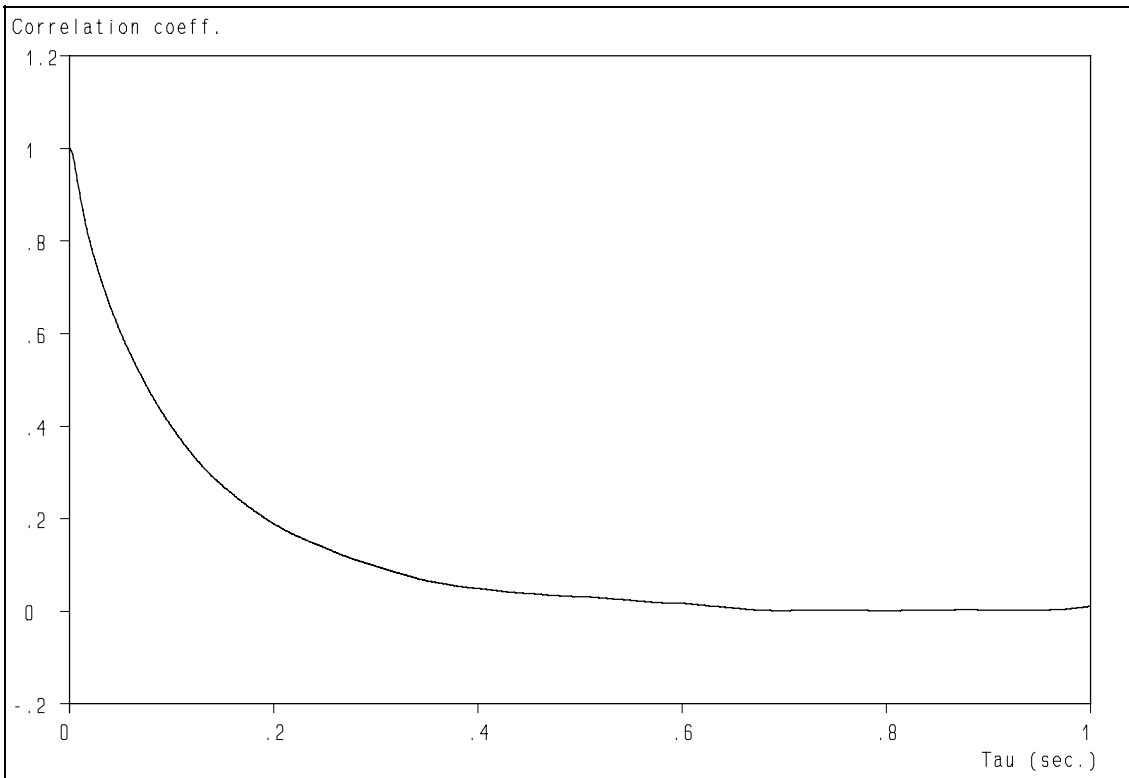


**Figure 2.19:** The auto correlation function of the simulated turbulence according to the Bessem power spectrum. Compare with fig. 2.13.

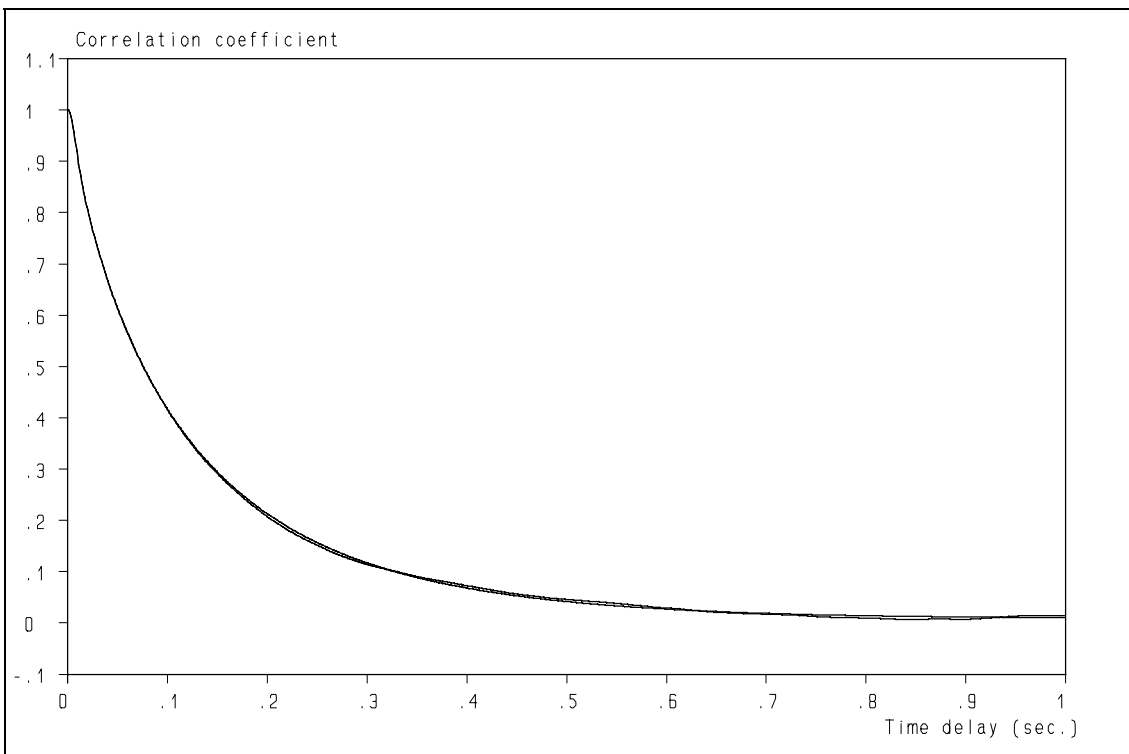


**Figure 2.20:** The auto correlation function of fig. 2.19 shown simultaneously with that of fig. 2.13.

*Retrieval of turbulence and turbulence properties from LDA data with noise*

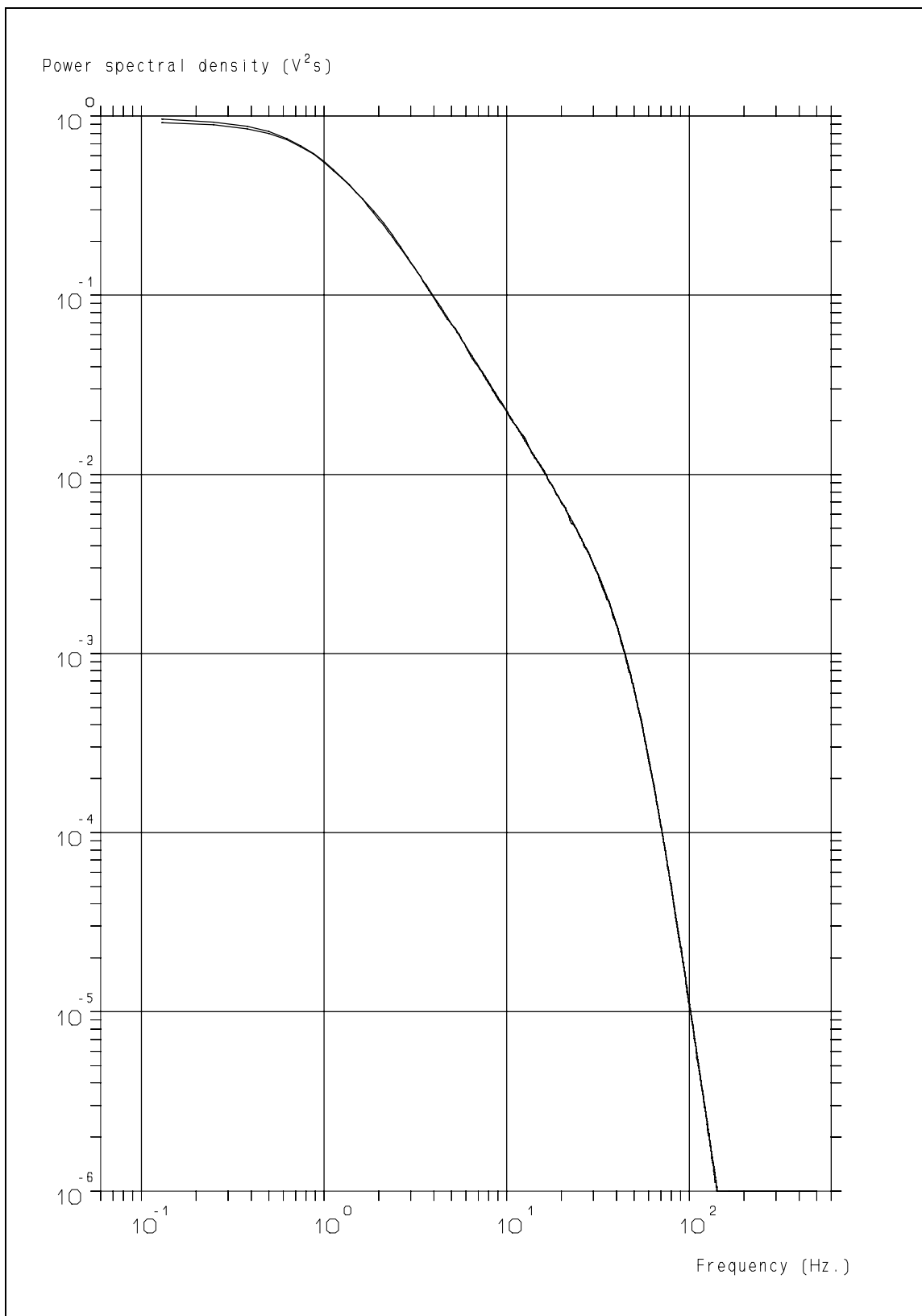


**Figure 2.21:** The power spectrum of the simulated turbulence shown simultaneously with that of fig. 2.14.

## 2. Monte Carlo simulations

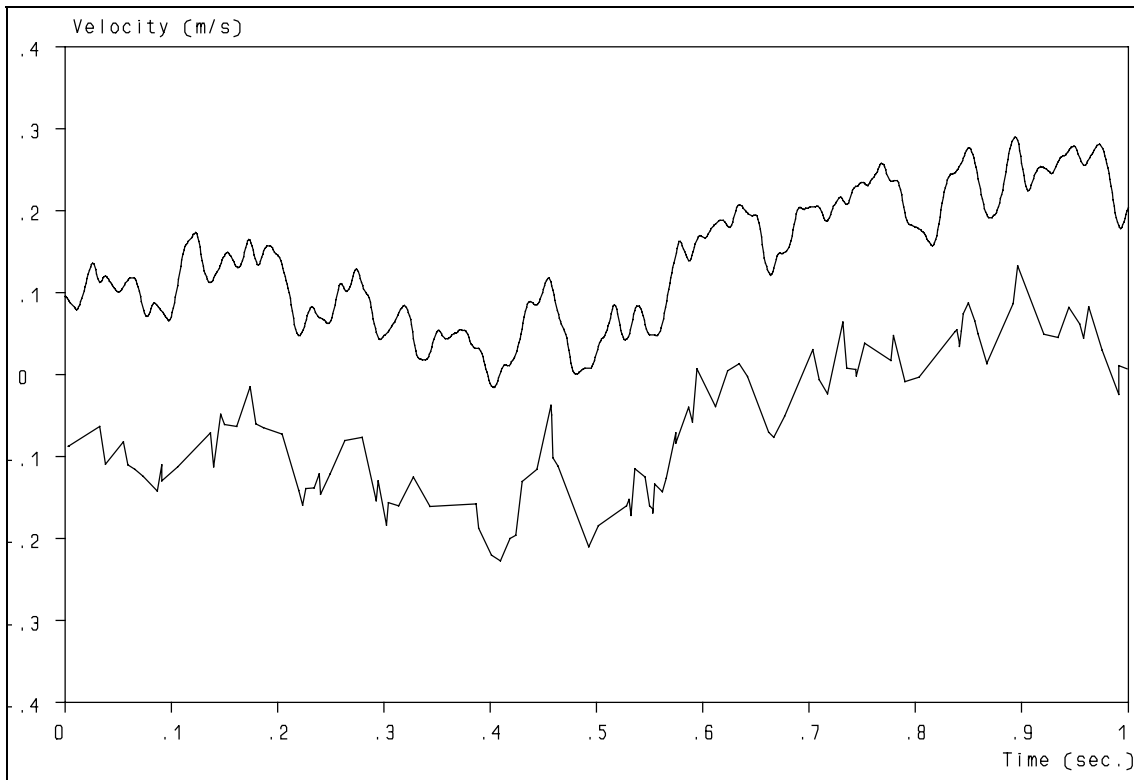


**Figure 2.22:** Graphical representation of a simulated processor file. The upper trace is the simulated turbulence, the lower trace is randomly sampled and Gaussian distributed noise is added.

# Chapter 3

## Noise in Laser-Doppler Anemometry

*The only certainty is  
that nothing is certain.*  
Pliny, the Elder

### 3.1 Introduction.

Noise occurs in every measurement process, but it plays a dominant, yet complex role in Laser Doppler Anemometry (LDA). As the following analysis will show, it will manifest itself at many different spots in the signal chain. Even with optimisation of the system, it is not possible with the current state-of-the-art to obtain a noise level in the resulting velocity estimates which is comparable to Hot-Wire Anemometry (HWA). Although the actual values are dependent on many different parameters and therefore an accurate number cannot be given, an indication is that with LDA a Signal-to-Noise ratio (SNR) of 5 - 8 is an excellent figure whereas with HWA an SNR of 300 is readily achieved. The reason why LDA is still an attractive technique lies in the advantages that LDA offers over HWA as has been described in Chapter 1.

In this thesis we will describe any deviation between the actual and the obtained velocity (as a function of time) as noise. However, the "translation" of the different noise sources into a noise contribution of the actual velocity estimate is not trivial. We will come back to this later.

### 3.2 Inventory of the noise and its sources.

In order to be able to optimise a Laser Doppler Anemometer, it is essential to know which noise sources contribute and to understand how they generate noise. It is important to make the distinction between noise and SNR. In general we want to optimize the SNR, which often *-but not always-* means to reduce the noise level. Therefore some aspects will be discussed separately, although they are intertwined. First we will make an inventory of the different noise sources and the following can be identified:

#### Noise in the Doppler signal:

1. Modulation noise of the laser.
2. Optical path difference of the incoming laser beams.
3. Phase front distortion by tracer particles in the incoming beams.
4. Distortion of the laser beams in the measurement volume due to the tracer particle.
5. Quantisation noise of the photocurrent.
6. Amplification noise of the photocurrent.
7. Electronic noise in the filters and amplifiers of the processor.

#### Aspects that are of influence on the SNR of the Doppler signal:

8. Laser power.
9. Dimensions of the measurement volume.
10. Quality and scattering properties of the tracer particles.
11. Collection angle and diaphragm diameter of the light collecting (receiving) optics.

## *Retrieval of turbulence and turbulence properties from LDA data with noise*

12. Projection of intersection volume of the laser beams onto the pinhole (spatial filter) in front of the photodetector.
13. Quantum efficiency of the photodetector.

### Noise in the velocity estimate:

14. Noise translation from Doppler signal → velocity estimate.
15. Non-optimised frequency estimation noise of the processor.
16. "Fringe" gradients.
17. Velocity gradients.
18. Arrival time estimation noise.
19. Random sampling.

### Additionally:

20. Quantisation noise of the A/D conversion.

### Aspects that are of influence on the data-rate:

21. Volume of the effective measurement volume.
22. Concentration of tracer particles.
23. Dead time of the processor.

### Ad 1.

The amount of light that the tracer particle can scatter depends on the amount of laser light that it receives. No light source is completely stable and the feedback mechanisms that can be applied to stabilize the output power of the laser require a certain time to react. As a consequence, the laser source is not stable on the time scales corresponding to the transit time of the tracer particle. This will - in general- result in a kind of modulation of the Doppler signal, which is similar to narrow-band noise, resulting in an error in the frequency estimation. We will discuss that in the following section. Using stable lasers is the only option to reduce this effect. Laser diodes are in this respect more critical than gas lasers because of the "mode hopping" that can occur in such lasers.

### Ad 2.

Current LDA systems often use fiber optics to bring the laser beams from the laser and beamsplitter to the probe, which includes a.o. the focusing lens. Although such an integrated concept is very practical, it could be possible that the optical path difference between the two laser beams is a significant part of the coherence length of the laser<sup>1</sup>. Non-coherent light does not contribute to the Doppler signal but does add to the noise in the detector signal. The only possibility to reduce this effect is to make the optical paths as equal as possible to each other, which can be verified by interference measurements. When possible, do not use optical fibers, as these can easily introduce path differences and reduce the coherence in the laser beams. Again, laser diodes are more critical because of their short coherence lengths.

### Ad 3.

Tracer particles are essential for the generation of Doppler signals. However, it is impossible to have these only in the measurement volume. They will also be present in the beams that are to build up the measurement volume. However, the tracer particles influence the wave front of the incoming laser beams, because the light has to pass around the tracer particles. As a result, the incoming wave front of the laser beams is not the idealised front that is mostly assumed for the calculations, but it is randomly distorted. Therefore the phase of the scattered light is not so well-defined either, but has a

---

<sup>1</sup> For an Argon-ion laser this length is approximately 20 mm.

### 3. Noise in Laser-Doppler Anemometry

random component as well, which is equivalent to a noise contribution (ref. 10). Using tracer particles with small diameters (because they distort the wave front the least) and at the lowest possible concentration (the less particles, the less distortion of the wave front) reduces this effect as much as possible, but it is contradictory to other noise sources as we will see shortly.

#### Ad 4.

Similar to the effect that the tracer particles in the beams, building up the measurement volume (see nr. 3) have, the tracer particle in the measurement volume itself influences the laser light. Theoretical calculations show that this can lead to deviations in the frequency from the expected Doppler signal. Naturally, the influence is larger when the tracer particle is bigger, but lowering the concentration has no effect, because it is caused by the particle that actually generates the Doppler signal. A detailed discussion can be found in ref. 76.

#### Ad 5.

The amount of light, scattered by the tracer particle, depends on the amount of laser irradiation, the size and the optical properties of the tracer particle and the scattering angle (ref. 15), but it will in general be small because the tracer particle is small (2 - 5  $\mu\text{m}$ ). The amount of light, collected by the detector is even smaller (see nr. 11) and as the detector itself has a quantum efficiency < 100%, the photocurrent is notably influenced by quantisation and therefore has a resulting noise contribution. The use of a high light intensity in the measurement volume (which is a combination of the laser intensity and the size of the measurement volume, see also nr. 8, 9 and 21) and detectors with a high quantum efficiency (see nr. 13) can reduce these effects.

#### Ad 6.

The photocurrent is too small to be processed directly. Therefore it has to be amplified first, which is usually done as close to the detector as possible, either by photo-multiplication or by avalanche photo detection (ref. 77). In both cases statistics determine the amplification process, thereby increasing the noise in the current. The paradoxical thing is that more amplification per stage gives less increase in the noise level! This means that the choice of the detector amplification can influence the noise level significantly. A Monte-Carlo simulation showed that increasing the amplification per stage from 1.5 to 2.5 for a total current amplification of 1500 reduced the noise level by 12 dB.

#### Ad 7.

The signal as it comes from the photodetector/amplifier combination is usually not yet strong enough for further processing. The main reason is that the signal is accompanied by wide-band noise which would saturate the amplification stages in the photodetector. Therefore the signal is filtered by a narrow band-filter first to remove the majority of the noise. Then the signal can be amplified by electronic amplifiers before it is processed for the determination of the frequency of the Doppler signal. It is unavoidable that these electronic filters and amplifiers will add noise to the signal. The noise contribution, however, can be small compared to the other noise sources, provided the parts of the LDA system, preceding the electronics, are optimised. This means that the signal, which is used for the input of the electronics, should be of sufficient strength.

#### Ad 8.

The *absolute* amount of laser power is one of the parameters that determine how much light is received by the photodetector (see also nr. 1). As has been pointed out above, this amount is of importance for the absolute noise level in the Doppler signal and is therefore of importance for the SNR of the Doppler signal. Studying the signals from the same tracer particle, the noise level *increases* with increasing light intensity, but the signal strength increases more and thus the SNR increases as well, albeit less than the laser power. The positive effect of the increasing SNR can be used by increasing the validation level of the burst detector with the same amount as the laser power. Then the signals coming from the good tracer particles will still be processed, but weak and still noisy signals coming from less ideal tracer particles will be eliminated without a reduction of the data-rate.

## *Retrieval of turbulence and turbulence properties from LDA data with noise*

### Ad 9.

The dimensions of the measurement volume are of importance for the SNR of the Doppler signal as the light from the laser is concentrated in the measurement volume. The smaller the beam diameter in the intersection volume, the higher the light intensity is and thus the amount of light that can be scattered by the tracer particles. This is attractive for a high SNR of the Doppler signal. However, the transit time of the tracer particles -and thus the duration of the Doppler signal- is reduced, thus making the determination of the frequency more susceptible to noise, as will be discussed in more detail in the following sections. Another potential problem is that a small measurement volume requires well-aligned optics, which is required to limit the "fringe gradients" (see nr. 16). Yet, a small measurement volume is attractive (see also nr. 17, 18, 19 and 22).

### Ad 10.

The quality and scattering properties of the tracer particles are of prime importance for the amount of light that will be scattered towards the photodetector. There is a vast volume of knowledge on the scattering by small particles and one should select those particles that fulfil the requirements for the specific optical configuration the best. Aspects that are of influence are e.g. the use of forward or backward scattering, the refractive index of the fluid and the like. More details can be found in ref. 15. Yet, one should never forget that these are *tracer particles*, which means that these are supposed to follow the flow and the turbulent velocity fluctuations. This puts upper limits to their dimensions on weight and diameter, which is -in general- more critical in gases than in liquids and depends also on the flow and turbulent properties. A well-known critical application is the study of the flow in cyclones, which primary use it is to remove solids from gases, which -as far as the cyclone is concerned- includes the tracer particles!

### Ad 11.

The collection angle of light collecting optics also have their influence on the SNR of the Doppler signal. Some tracer particles do not scatter significant amounts of light at certain angles, which should be taken into account when the light collecting (receiving) optics are configured. Also, the amount of light that can be collected depends on the diameter of the diaphragm of the collecting lens. One should keep in mind though that the *quality* of the light collecting lens is also of importance as the collected light needs to interfere with itself to generate the Doppler signal.

### Ad 12.

Many optical systems use an off-axis projection of the intersection volume of the laser beams onto the pinhole in front of the photodetector. This has several advantages:

- The length of the *effective* measurement volume is reduced. As the intersection volume is always long and thin, this increases the spatial resolution significantly.
- The part of the intersection which has the highest light intensity and the highest level of interference (ref. 9) is used only, thus increasing both the Doppler signal strength and the SNR of it.
- The increased spatial resolution allows a higher concentration of tracer particles, thus increasing the data-rate (see also nr. 21 and 22).

Such a configuration for the light collecting optics is attractive, provided the off-axis scattering angle is suitable for the tracer particles applied. However, the projection should use the central part of the intersection volume, else the advantages quickly turn into disadvantages. This requires accurate alignment, especially when the laser beams have a small diameter in the intersection volume (see nr. 9 and 21).

### Ad 13.

Just as the laser power is of importance for the SNR of the Doppler signal, so is the quantum efficiency of the photodetector. The reason for that is the quantum noise of the photocurrent (see also nr. 5). The higher the quantum efficiency, the higher the photocurrent and thus the higher the SNR of the Doppler signal. In general photodiodes & phototransistors have higher quantum efficiencies than photo multipliers.

### 3. Noise in Laser-Doppler Anemometry

#### Ad 14.

The noise in the Doppler signal translates into a noise contribution to the velocity estimate. This will be studied in more detail in the following section and in Chapter 5 when Monte-Carlo simulations of the Doppler signal are used to determine this translation more quantitatively.

#### Ad 15.

Noise in the Doppler signal is unavoidable, but the processors are not equally sensitive to it. Therefore, the noise contribution to the velocity estimate is different for different processors, even if the Doppler signals are identical. The additional noise contribution, related to the theoretical lower limit (the Cramer-Rao bound), depends on the properties of the processor and its settings. This will be discussed in more detail in Chapter 5.

#### Ad 16.

Optical aberrations lead to a non-ideal shape of the measurement volume. The scattering angle of the light is therefore not completely constant, but depends on the position of the tracer particle in the measurement volume. This effect is often referred to as "fringe gradient", based on the fringe model of LDA (ref. 9). The result is that the *same velocity* gives Doppler signals with *different frequencies*. Accurate optical alignment and correction for curved and non-perpendicular walls is essential to reduce this effect as much as possible.

#### Ad 17.

Because the measurement volume has a certain size, the velocity is not necessarily constant over the measurement volume, due to the gradient in the average velocity or the turbulent eddies with sizes similar or smaller than the measurement volume. So two successive Doppler signals can have a different frequency due to this effect because they have been generated in different parts of the measurement volume. These effects can be reduced by limiting especially the length of the measurement volume (see also nr. 9 and 12) and to position the measurement volume in such a way that the velocity gradients are in the shortest dimension of the measurement volume (ref. 13).

#### Ad 18.

The noise in the Doppler signal does not only introduce a noise contribution to the velocity estimate itself, but also in the estimation of the arrival time, as will be discussed in the following section. Usually, the arrival time of the Doppler signal is defined as the time at which the tracer particle is in the centre of the measurement volume. Or, to be more precise, when the distance that the tracer particle has travelled through the measurement volume is equal to the distance it still has to travel through it: usually the tracer particle does not move through the exact centre of the measurement volume. The noise in the Doppler signal, however, introduces an uncertainty in the estimation of this time and therefore an error in the localisation. However, in a turbulent flow the velocity is a function of time and therefore an error in the arrival time translates into an error in the velocity, which can be regarded as noise. This will be discussed in more detail in Chapter 4 and 5. Note that a short transit time reduces the possible error in the arrival time. This is another reason to use a small measurement volume (see also nr. 9 and 21).

Another aspect of importance for the arrival time uncertainty is the clock which is used. It is common to use digital clocks nowadays, which introduce a quantisation error in time. Depending on the resolution in the time domain, the accuracy used for storage of the arrival time in the data-file and the properties of the turbulence under study, this can lead to noticeable errors. It is to a certain extent comparable to the quantisation problems of the Analog-to-Digital (A/D) conversion of the velocity (see nr. 20). More details will be discussed in Chapter 4 on preliminary diagnostics of experimental data-sets.

#### Ad 19.

The Poisson distribution of the tracer particles in space results in the well-known exponential time interval distribution between two successive Doppler signals (ref. 11). As a result, there are longer periods of time over which no information about the development of the flow is available. No matter how sophisticated the velocity reconstruction algorithm used is, this will always result in a deviation between

## *Retrieval of turbulence and turbulence properties from LDA data with noise*

the actual velocity and the reconstructed velocity. By definition, this is noise. Note that the deviations increase with decreasing data-rate. Also, the phenomenon is more complicated as not all tracer particles pass through the centre of the measurement volume, scatter different amounts of light and the processor is not able to process all the data instantaneously, resulting in a dead-time (see also nr. 22 and 23). More details will be discussed in Chapter 4, 6 and 7.

### Ad 20.

The velocity value is in some processors or data-processing systems digitised using a Analog-to-Digital converter (ADC) with a limited number of bits. This adds noise to the velocity estimate, because there is a difference between the actual velocity estimate and the digitised value, as has been described and analyzed in more detail in ref. 60 and 70.

**N.B.** The importance of the data-rate on the resulting noise contribution to the velocity estimates is quite complex. It will be discussed extensively in the later chapters of this thesis. We will confine ourselves here to the remark that a high data-rate is attractive for several reasons. The data-rate can, however, be influenced by the configuration of the optical part of the LDA, both in the transmission and receiving optics.

### Ad 21.

The dimensions of the *effective* measurement volume determine the data-rate because of two important reasons:

- the light intensity (see nr. 9) and
- the concentration of tracer particles that can be realized.

A higher light intensity will usually mean that more Doppler signals have sufficient strength to be detected and validated, which will increase the data-rate. Most processors do not allow -or give erroneous results- when more than one tracer particle is present in the (effective) measurement volume. Reduction of the *volume* of the measurement volume increases the concentration of tracer particles that can be allowed before it will cause serious problems and thus increases the attainable data-rate.

### Ad 22.

The concentration of tracer particles is not only of importance for the noise level of the Doppler signals (see nr. 3), but also for the data-rate. As only Doppler signals can be generated when there is a tracer particle in the (effective) measurement volume, this is obvious. However, the higher the concentration, the more parasitic effects start playing a role (see nr. 3). Therefore it is of importance to determine the optimum tracer particle concentration experimentally by determination of the data-rate *and* the validation percentage as a function of the tracer particle concentration. A too high concentration will be detrimental to the end results.

### Ad 23.

The dead time of the processor determines the highest possible data-rate. The shorter the better and it can be influenced by the parameters of the Doppler signal detection and validation criteria. However, as will be discussed in Chapter 4, this can also lead to "multiple validation" of Doppler signals, which is detrimental to the results and has to be avoided. Note that the dead time is also dependent on the transit time and a small measurement volume reduces this, as well as the arrival time uncertainty. Both are attractive improvements.

### **3.3 Noise in the Doppler signal.**

In order to understand the way the different types of Doppler signal processors react to the Doppler signal and estimate its frequency (and thus the velocity of the tracer particle), it is essential to look in more detail to the noise contribution to the Doppler signal itself. This noise is the basis of many problems regarding the interpretation of LDA measurement data and there are numerous misunderstandings about it.

### 3. Noise in Laser-Doppler Anemometry

The essential task that every Doppler signal processor is confronted with is to estimate the frequency of the oscillating part of the Doppler signal. Reaching this goal is *always* hampered by the presence of the noise in the Doppler signal. We have made an inventory of the noise sources in the previous section and now we will see what the consequences are.

The ideal Doppler signal is shown in fig. 3.1. The "DC" contribution<sup>2</sup> is usually not of much interest and after high-pass filtering the Doppler signal looks as shown in fig. 3.2. Although the spectrum of the Doppler signal is broadened because of its limited duration (due to the Gaussian envelope), the frequency of the oscillating part can still be determined exactly: the position of the maximum of the amplitude spectrum corresponds precisely with the frequency we are looking for as is shown in fig. 3.3.

Unfortunately, there are a number of misunderstandings about the influence of noise in the Doppler signal. The most important are:

1. "The noise floor in the Doppler signal is white and therefore the spectrum of the Doppler signal is only lifted onto a pedestal with a constant level and that does not introduce any problem in the determination of its frequency".
2. "The noise only widens the spectrum of the Doppler signal, but its frequency remains the same".
3. "When band-pass filters with a narrow pass-band are applied, all the noise will be eliminated".
4. "The best estimate of the frequency is obtained by only using the central part of the Doppler signal, because that part has the highest SNR".
5. "Noise in the Doppler signal is unimportant, the processor has been designed to work with noisy signals".

Although some of these statements sound reasonable, they all are misunderstandings. This will be clear after a thorough analysis of the effects of noise on the frequency estimation. This can easiest be done by using a number of simulations. The advantage of simulations is that the Doppler signal and the noise can be separated completely and their effects studied. It also offers the possibility to apply statistical analysis to a large number of signals with identical properties. This would be very hard to do in practice as noise and Doppler signal are indistinguishable. How a Doppler signal, accompanied by narrow-band noise, can be simulated has been described in the previous chapter.

The first simulation shows that sometimes demonstrations of the noise with the Doppler signal are misleading. Fig. 3.4 shows an often used presentation of a Doppler signal with noise; an enlargement is shown in fig. 3.5. But looking at the spectrum of this signal, as shown in fig. 3.6, one sees that the spectral amplitude of the noise is only above zero at frequencies higher than the Doppler frequency and thus the noise could easily be filtered off. So this is not a realistic condition. Because of the narrow band-filter, the spectrum of the Doppler signal with noise looks as shown in fig. 3.7, and the Doppler signal itself looks as shown in fig. 3.8. *The bandfilter gives the noise properties similar to that of the Doppler signal itself.* It is important to analyze the consequences of this phenomenon. Note that the apparent position of the Doppler signal is shifted by approximately 250  $\mu\text{s}$  (its maximum can be found at 1250  $\mu\text{s}$ , whereas that of the input signal is located at 1000  $\mu\text{s}$  as can be seen from fig. 3.2), which, however, is nothing but an artefact from the noise contribution.

Sometimes it is stated that the noise contribution is white, which would only lift the spectrum of the Doppler signal as is shown in e.g. fig. 3.9. But the properties of "white" noise only show after a "sufficiently long" averaging time. However, the meaning of "sufficiently long" depends on what variance in the estimators is acceptable, but in general the transit time of the tracer particle will not be "sufficiently long" as is illustrated in fig. 3.10, which shows the spectrum of "white" noise with a duration, equal to the transit time of a tracer particle. This adds to the spectrum of the Doppler signal and the result is presented in fig. 3.11. This figure shows that the noise contribution shifts the peak of the Doppler signal

---

<sup>2</sup> This contribution is also called "the pedestal", especially in early publications on LDA.

## *Retrieval of turbulence and turbulence properties from LDA data with noise*

in the spectrum: the noise and the Doppler spectra are indistinguishable and the frequency estimator deviates from the ideal value and so will the velocity estimator. The latter means that the velocity estimator is accompanied by a noise contribution. A similar effect can be seen in time-domain: the noise causes a "phase-jitter", which leads to an uncertainty in the frequency, as is clear from fig. 3.12. This illustrates how noise in the Doppler signal is "translated" into noise in the velocity estimator and it illustrates too why the statement #1 is a misunderstanding. The only measurand which is not influenced by a white noise floor is the estimation of the *average* velocity, but still it can not be estimated accurately -not even in a laminar flow- from a single Doppler signal.

As can be seen from fig. 3.9 (compare with fig. 3.11), the width of the peak in the Doppler signal is *independent* of the presence of noise. The spectrum of fig. 3.11 (with noise) often leads to this misunderstanding. The width of the peak is determined by the transit time of the tracer particle and because this is equal to the averaging time of the noise spectrum, it seems attractive to have a long transit time. However, this is counteracted by other effects (see nr. 9, 18, 19 and 22).

As can be seen from fig. 3.11 and 3.12, the Doppler signal and the noise are neither in time-domain nor in frequency-domain distinguishable from each other. Filtering is therefore unable to improve the situation. So statement #3 is a misunderstanding as well.

Statement #4 seems logical and is therefore often mentioned. Yet, it is incorrect. Heuristically, this can be understood by realizing that the stronger parts of the Doppler signal are still influenced by noise and that -on the other hand- the weaker parts still carry information. A simulation shows this effect beyond any doubt. Fig. 3.13 shows the spectra of an ideal Doppler signal and of one with noise simultaneously. We see a similar effect as in fig. 3.11. This Doppler signal with noise was subsequently split into five separate parts and these have been used to determine the frequency. The results are presented in fig. 3.14 and the different parts of the Doppler signal can be recognised because low spectral amplitude corresponds directly to low signal amplitude (and vice versa). Note that the horizontal scale has been widened by a factor of 4 compared to fig. 3.13, because the "transit time" has been reduced significantly. The variance in the estimation of the frequency -and thus velocity- has markedly increased, as is obvious. Another way to determine this is by looking at the phase-jitter as shown in fig. 3.12: this phase-jitter determines the uncertainty in the frequency estimation. This phase-jitter will be of more influence if only one single cycle is used for this purpose than e.g. 10. But as the Doppler signal weakens, the phase-jitter increases. There must be some optimum and ways to determine which will be discussed in Chapter 5. However, these results show that the use of the largest possible part of the Doppler signal is to be recommended and the use of only the central part will lead to an unnecessarily high noise contribution to the velocity estimator.

We have seen why and how noise in the Doppler signal translated itself into noise in the individual velocity estimators. Although one type of processor is more sensitive to noise than the other, *none* of them is *insensitive* to it, simply because the Doppler signal and noise are indistinguishable. Some processors may be able to give a velocity estimate, based on weak, noisy Doppler signals, but such an estimate is *always* accompanied by a relatively large noise contribution. This noise contribution increases as the noise in the Doppler signal increases, as is illustrated in fig. 3.15. The SNR of the Doppler signal should thus be as high as possible.

That the noise in the Doppler signal represents a fundamental problem is again illustrated by the calculation of the auto correlation function of the Doppler signal. One might expect that the correlation of the narrow-band noise decays rapidly, leaving the tail of the correlation function to be dominated exclusively by the Doppler signal, opening the possibility to eliminate the effects of the noise contribution. However, this decay only occurs when the averaging time of the correlation function is "sufficiently long" and -in a similar way as with the spectral analysis of the Doppler signal with noise- the transit time of the tracer particle is *not* "sufficiently long". This is presented in fig. 3.16, which shows that the "tail" of the correlation function still shows phase-jitter. which -again- leads to an uncertainty in

### 3. Noise in Laser-Doppler Anemometry

the frequency estimator. The reason behind this all is that the Doppler signal and the noise are again indistinguishable.

#### 3.4 Experimental results.

In order to compare the simulation results with reality, two Doppler signals have been recorded using a fast digitizing oscilloscope. Fig. 3.17 shows a "strong" Doppler signal, one which could easily be detected and validated. This is obvious from the interpolated spectrum, which is presented in fig. 3.18. Yet, the velocity that is retrieved from the different parts of the Doppler signal varies notably, as is illustrated in fig. 3.19 (the positions correspond with those of fig. 3.17). Fig. 3.20 shows a "weak" Doppler signal, which was on the verge of detection and validation. Its interpolated spectrum is shown in fig. 3.21. This shows that the spectrum of the Doppler signal barely rises above the noise floor. Fig. 3.22 shows in a similar way as fig. 3.19 the estimated velocity as a function of the position within the Doppler signal (note the vertical scale!) and the effects are clear. The results, obtained from the simulations, are thus confirmed by the experiments.

If the noise floor is not white, but e.g. decreases with increasing frequency as shown in fig. 3.23, a bias is introduced. The reason for this is the extension of the Doppler spectrum around the central frequency in combination with the slope in the noise floor. In the case, shown in fig. 3.23, the low-frequency side is lifted more than the high-frequency side. As a result the position of the peak is shifted to lower frequencies on average and so is the estimated velocity. This is made clear by fig. 3.24. This kind of bias can cause problems when relatively low average velocities have to be measured with a high accuracy. Noise can thus lead to systematic errors and this has been the only explanation for such a systematic error in one of the experiments.

#### 3.5 On the definition of the Signal-to-Noise Ratio of the Doppler signal.

Up to now, no unique definition on the Signal-to-Noise Ratio of Doppler signals has been agreed upon (e.g. ref. 56 and 78 - 80), probably because there is -at this moment- no logical definition possible (maybe in the future, based on the Wavelet Transform, see Chapter 5). As a result there are numerous, yet different, ways to state these numbers which are usually incompatible. This can easily be demonstrated by the following examples: by widening the bandwidth of the filter, more noise is let through, thus reducing the "SNR" of the Doppler signal. But that is not important for the accuracy of the frequency estimation: this is determined by the *local*, and not the *global*<sup>3</sup>, SNR. Another example is increasing the time interval over which the spectrum of the Doppler signal is calculated: this increases the noise contribution and thus decreases the "SNR", but where are the limits of the Doppler signal? At  $1/e^2$  of the maximum amplitude? At 1 % of it? And how has the maximum amplitude been determined? It is all arbitrary, so it can easily be manipulated. This is a severe problem for users, because it is not possible to compare the numbers given by the different manufacturers in a sensible way. The obvious solution would be to establish a definition that -although arbitrary- everybody agrees upon. This would enable a useful comparison between processors and systems.

#### 3.6 Concluding remarks.

It is worth while to increase the Signal-to-Noise ratio of the Doppler signal as far as possible in order to reduce both the random and systematic errors in the velocity estimates. The random error in the individual velocity estimates will prove to be a major obstacle for the study of the details of the turbulence as will be shown later. But noise also hampers the estimation of average velocities because it increases the measurement (averaging) time required to reach a certain level of uncertainty: the variance decreases with the square root of the measurement time, so a factor of 2 lower SNR must be compensated by a factor of 4 longer averaging time. Optimisation of the entire measurement chain is

---

<sup>3</sup> Local and global in frequency domain.

### *Retrieval of turbulence and turbulence properties from LDA data with noise*

essential to get the best results and this requires insight into all the problems that can be encountered in the measurement process. As solutions of different problems are often conflicting, a high level of expertise is required and essential.

A definition of the SNR of Doppler signals should be created that everybody agrees upon, so different systems and processors can be compared. The current situation, in which many different definitions are used, is unacceptable from a users' point of view. But any definition will probably comprise some arbitrary aspects.

### 3. Noise in Laser-Doppler Anemometry

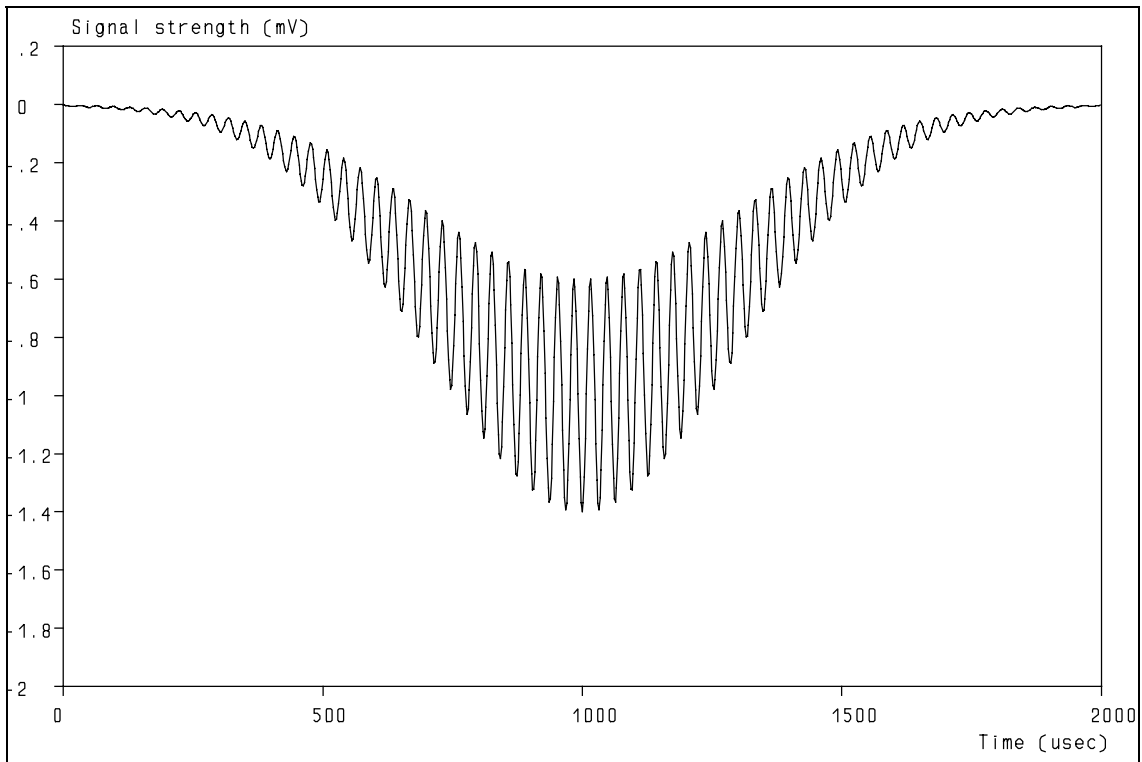


**Figure 3.1:** The ideal Doppler signal as it comes from the photo multiplier.

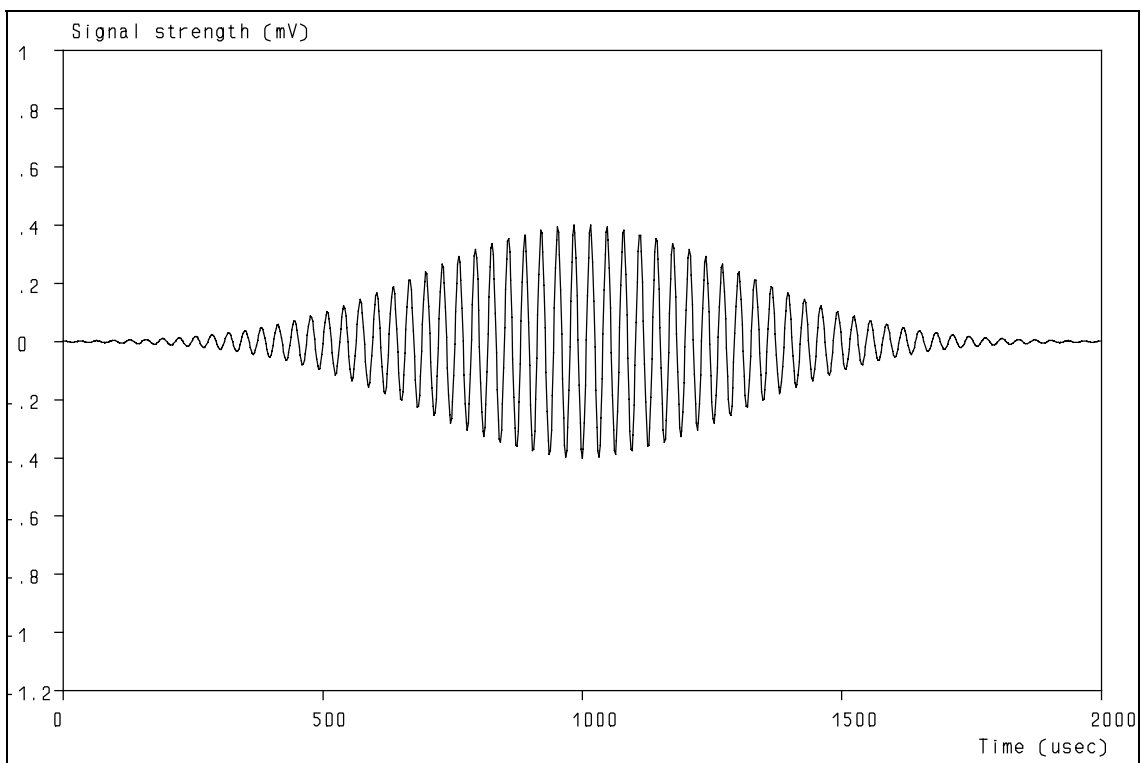


**Figure 3.2:** The ideal Doppler signal as it comes from the photo multiplier after removal of the "DC" component or "pedestal".

*Retrieval of turbulence and turbulence properties from LDA data with noise*

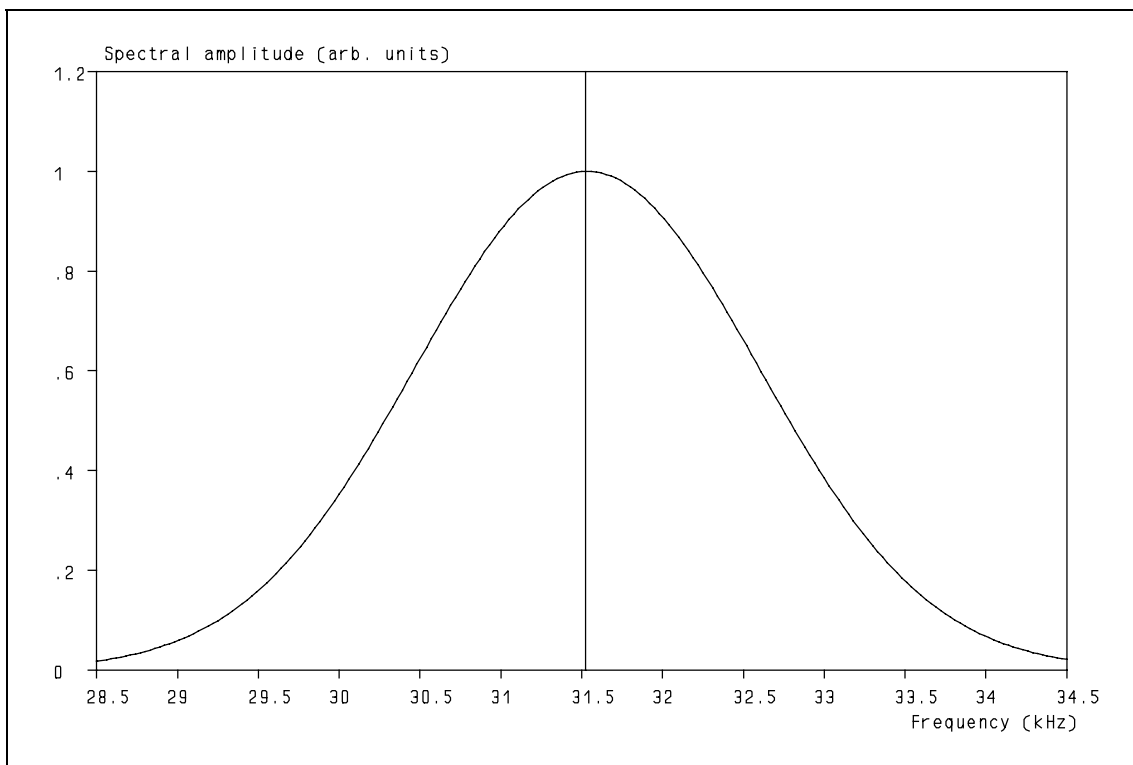


**Figure 3.3:** Although the spectrum of the Doppler signal is broadened, the maximum still corresponds to the frequency which is to be established.

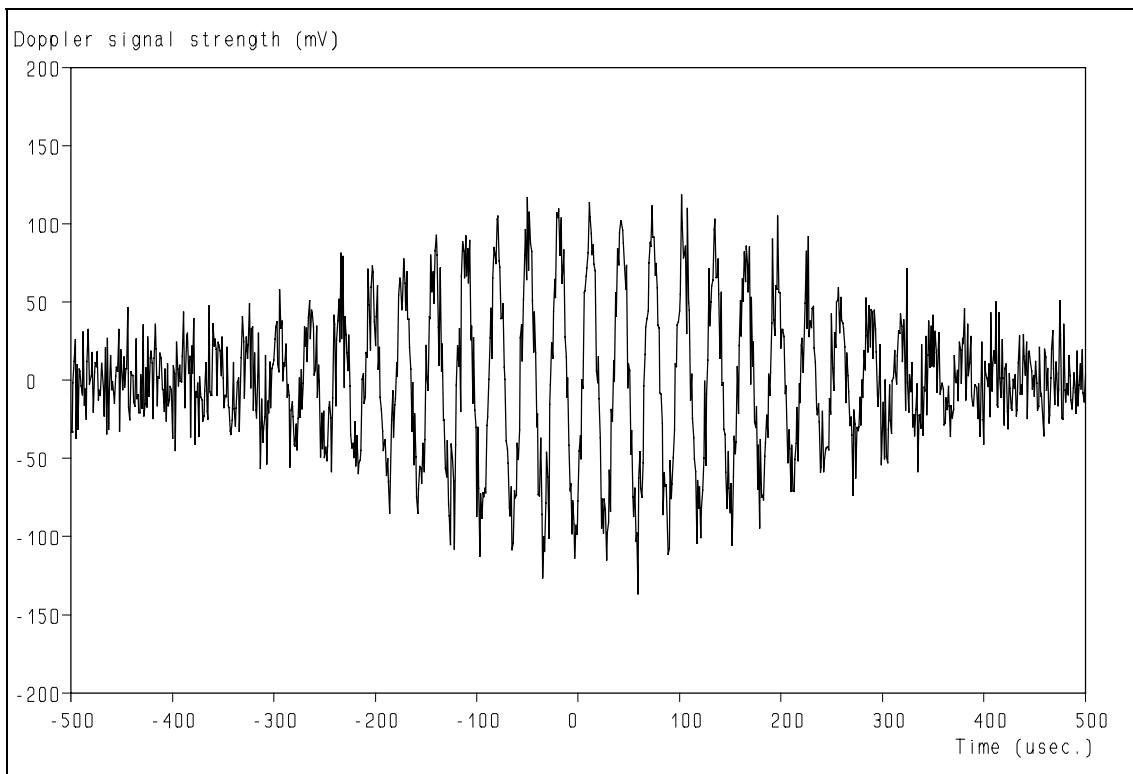


**Figure 3.4:** Often noise in the Doppler signal is represented like this.

### 3. Noise in Laser-Doppler Anemometry

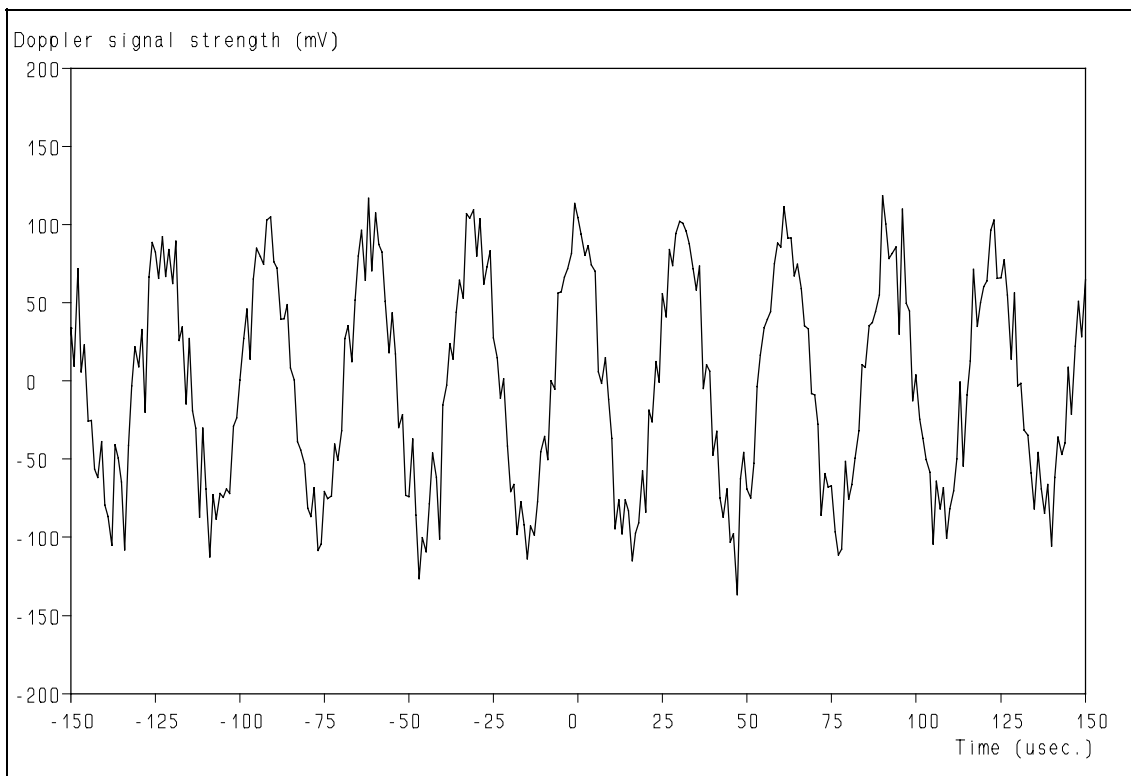


**Figure 3.5:** Often noise in the Doppler signal is represented like this (enlargement).

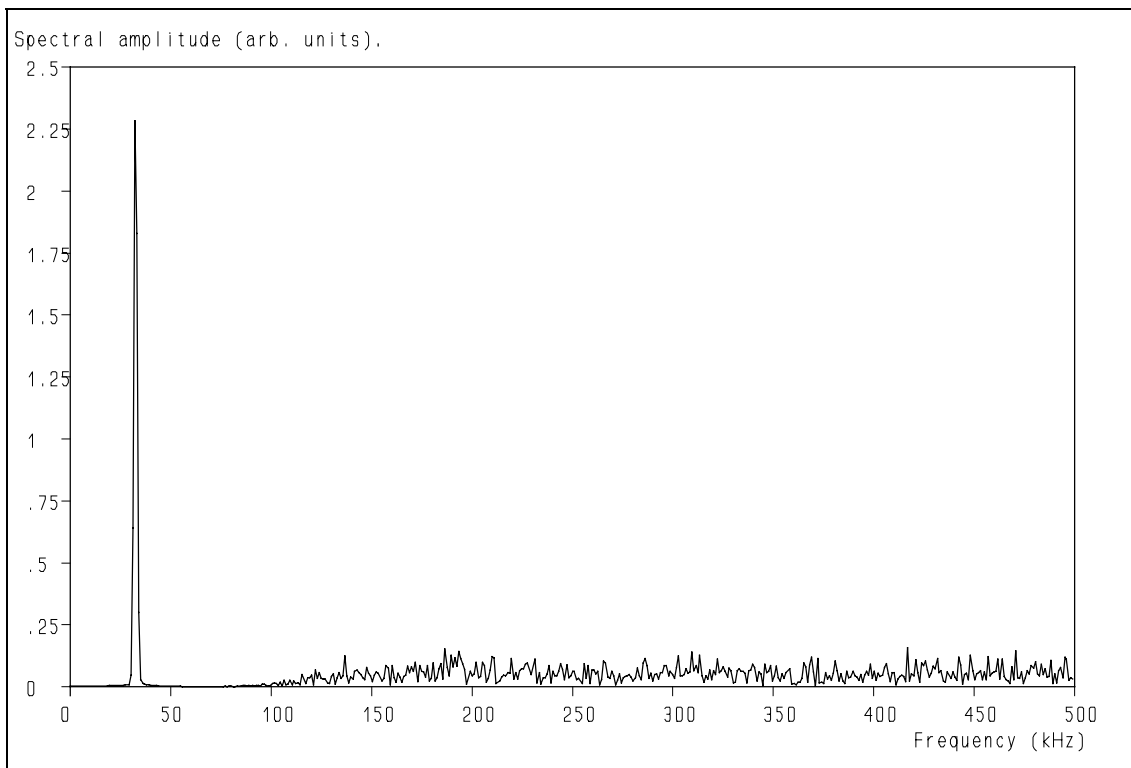


**Figure 3.6:** In such a case the noise could simply be filtered off: the spectrum shows that the Doppler signal and the noise are located in different frequency ranges.

*Retrieval of turbulence and turbulence properties from LDA data with noise*

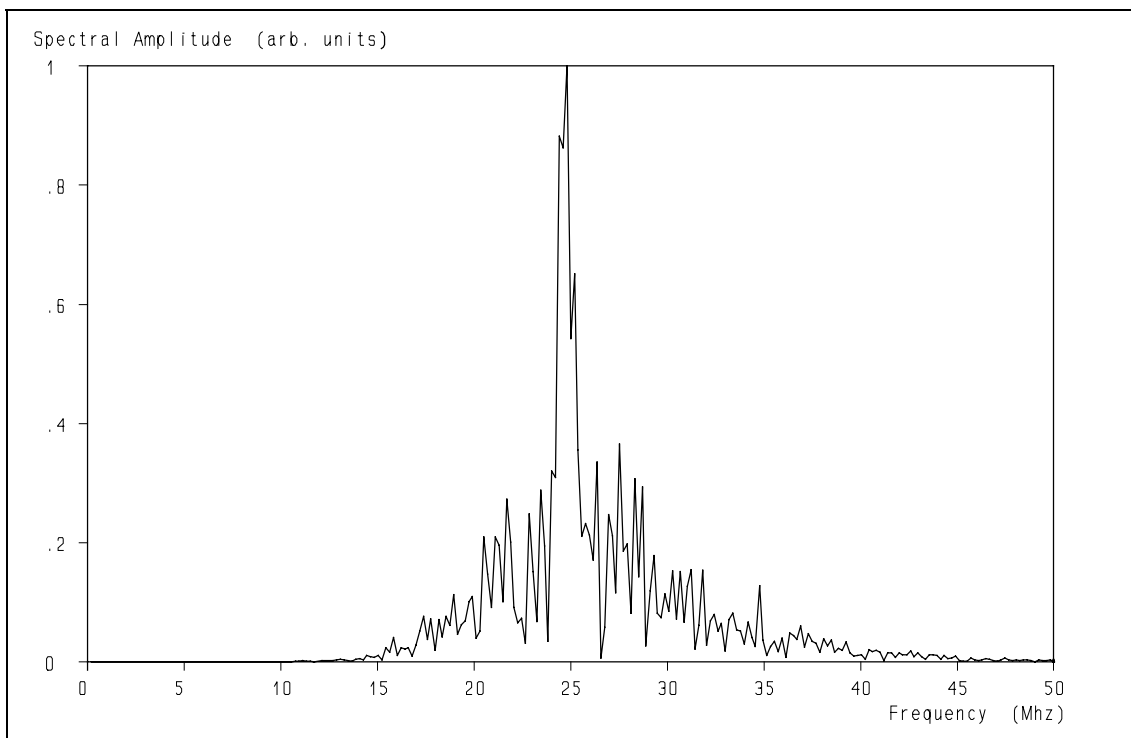


**Figure 3.7:** The spectrum of a Doppler signal consists of a peak accompanied by narrow-band noise.

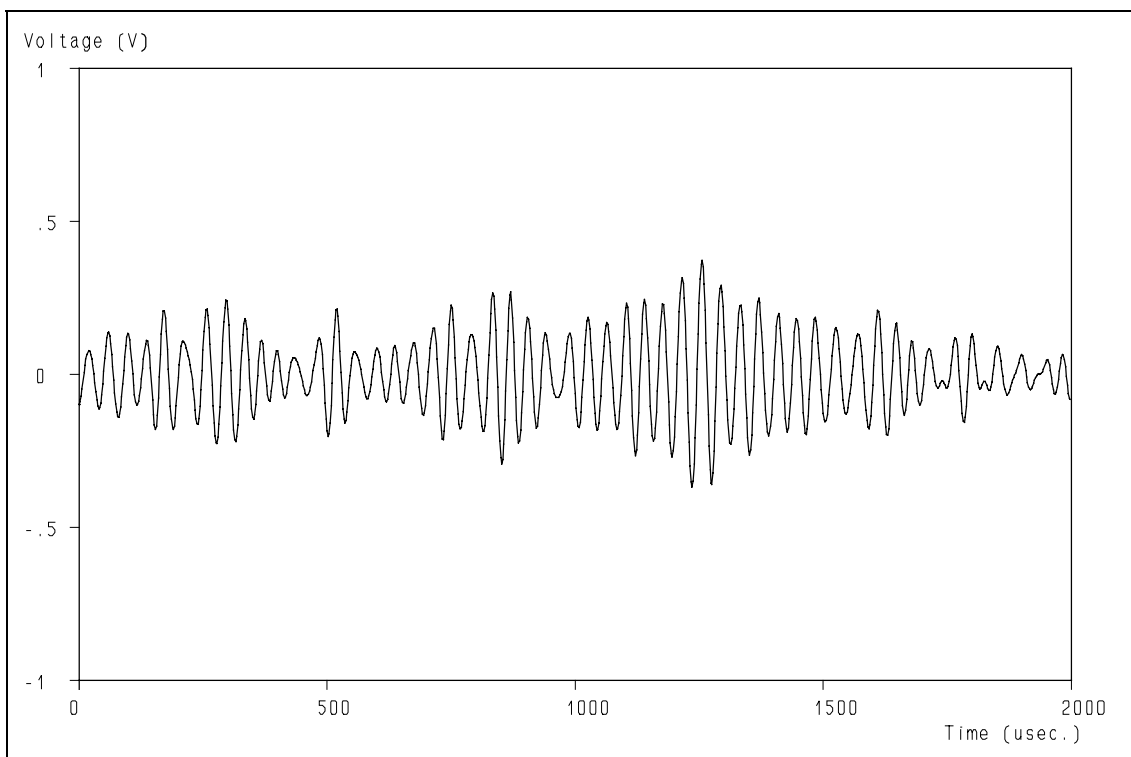


**Figure 3.8:** As a result, the structures of the narrow-band noise and the Doppler signal intertwine.

### 3. Noise in Laser-Doppler Anemometry

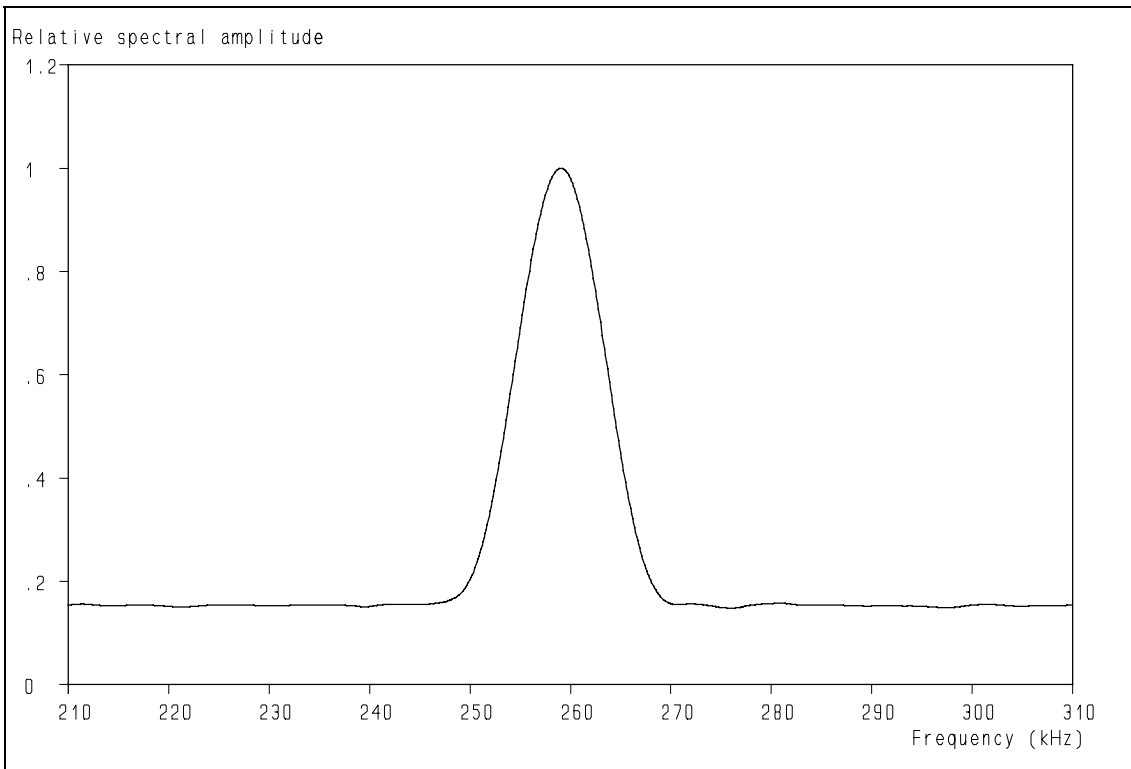


**Figure 3.9:** The white character of the noise only shows after a large number (1000) of averages.

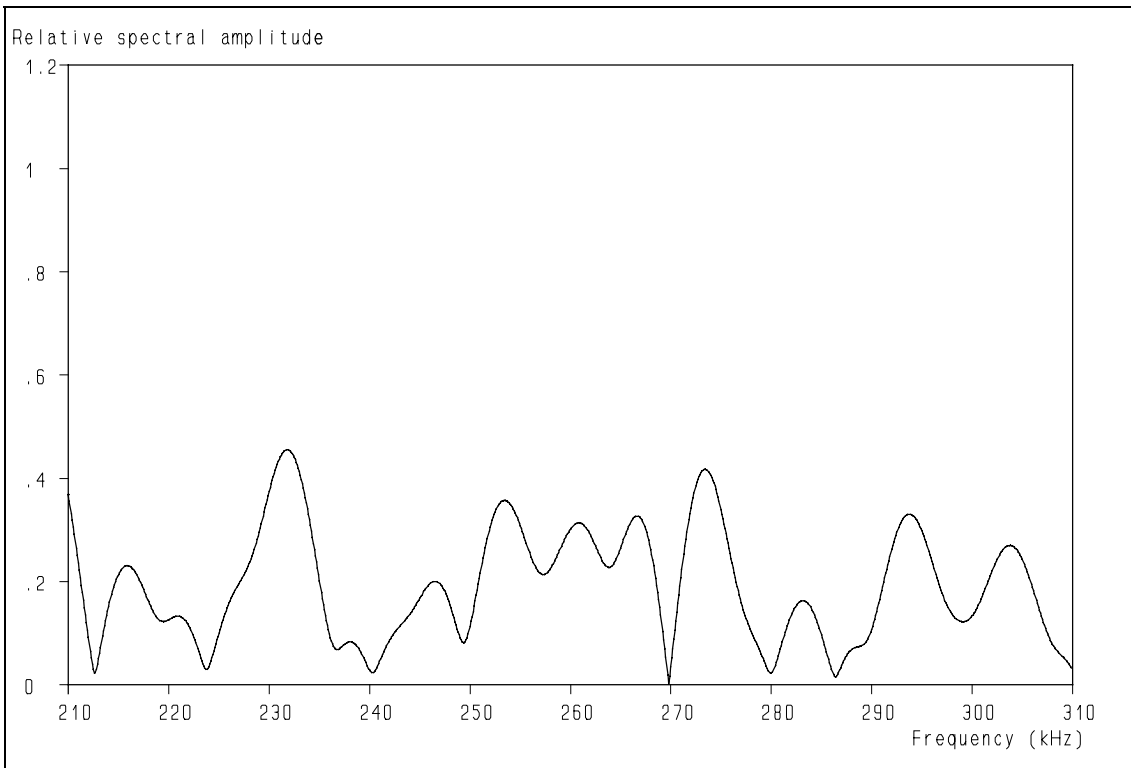


**Figure 3.10:** The noise contribution to a single Doppler signal presented separately.

*Retrieval of turbulence and turbulence properties from LDA data with noise*

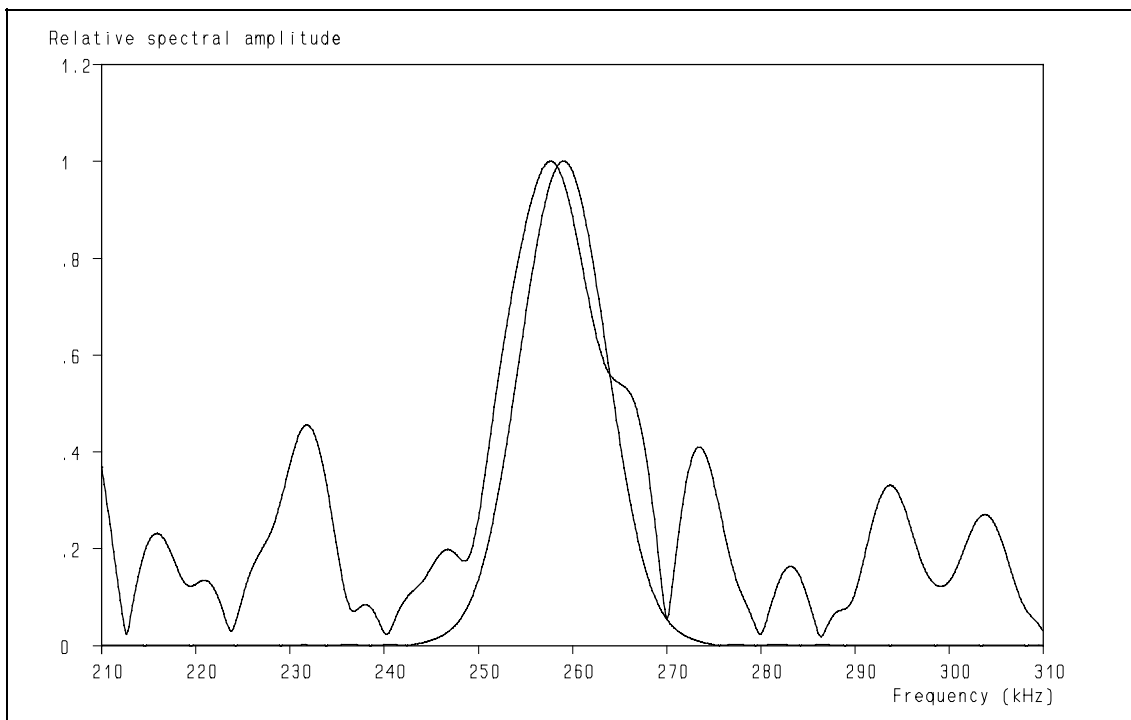


**Figure 3.11:** The spectrum of a Doppler signal with (which is  $> 0$  for all frequencies) and without a noise contribution (which is zero outside the Doppler peak) shown simultaneously.

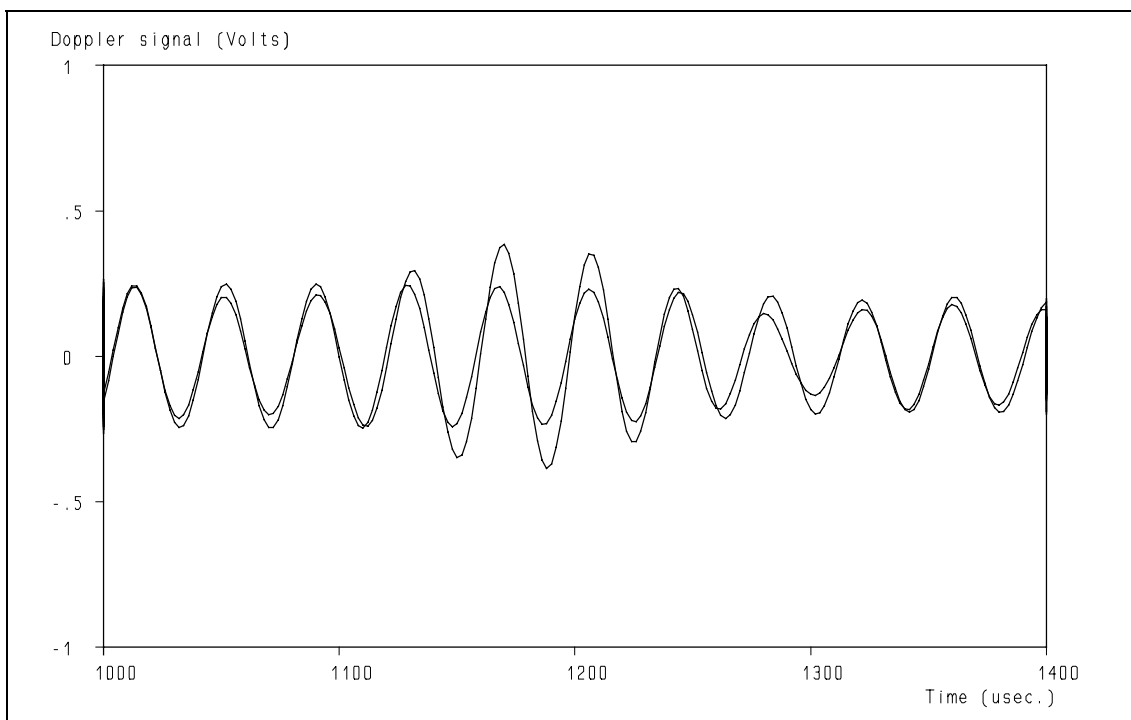


**Figure 3.12:** Narrow-band noise leads to phase-jitter in the Doppler signal, which translates into frequency fluctuations. The ideal Doppler signal has an almost constant amplitude, the actual a modulation, compare fig. 3.2 & 3.8).

### 3. Noise in Laser-Doppler Anemometry

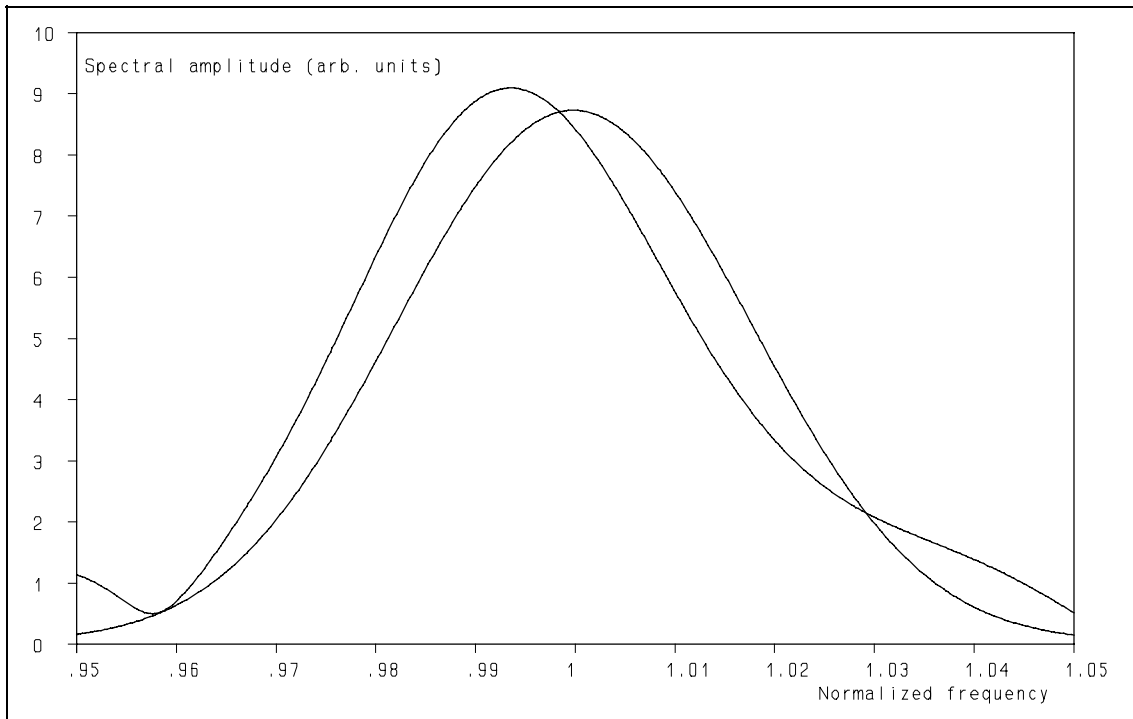


**Figure 3.13:** The high-resolution spectra of an ideal (lower at left) and a realistic Doppler signal show that noise leads to a deviation of the frequency estimator and thus to a noise contribution in the velocity estimate.

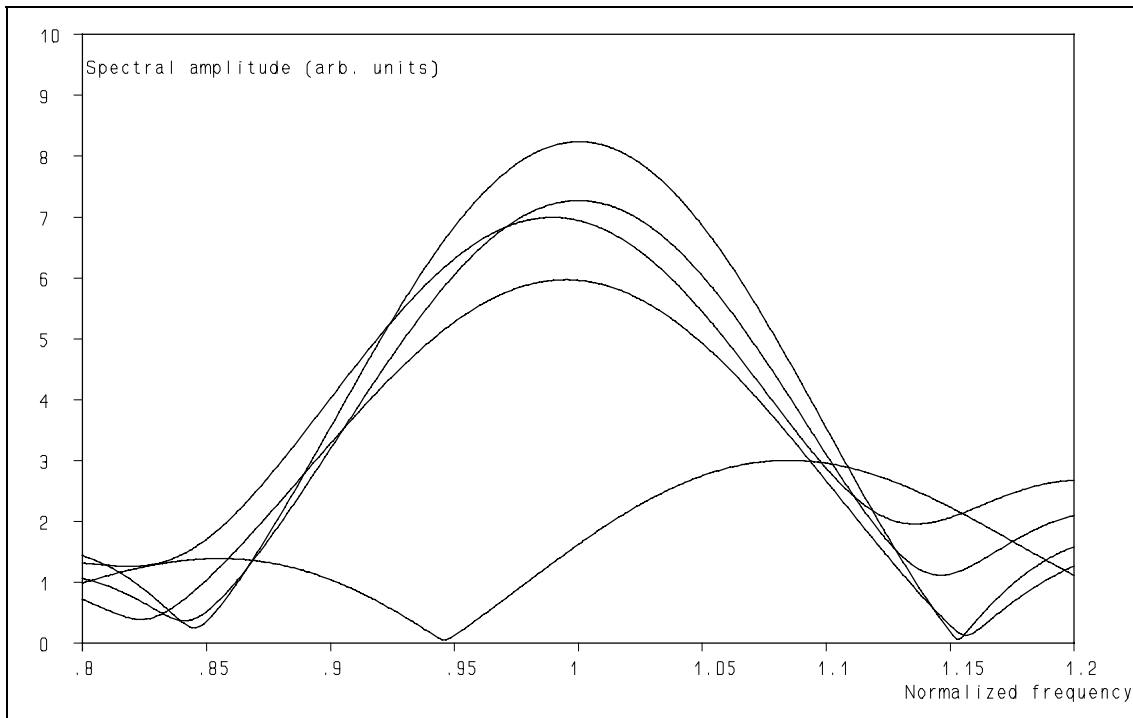


**Figure 3.14:** Spectral analysis of *parts* of the Doppler signal shows that the estimated frequency depends on the part chosen. Note the scale which runs from  $0.8 F_{gem}$  to  $1.2 F_{gem}$ .

Retrieval of turbulence and turbulence properties from LDA data with noise

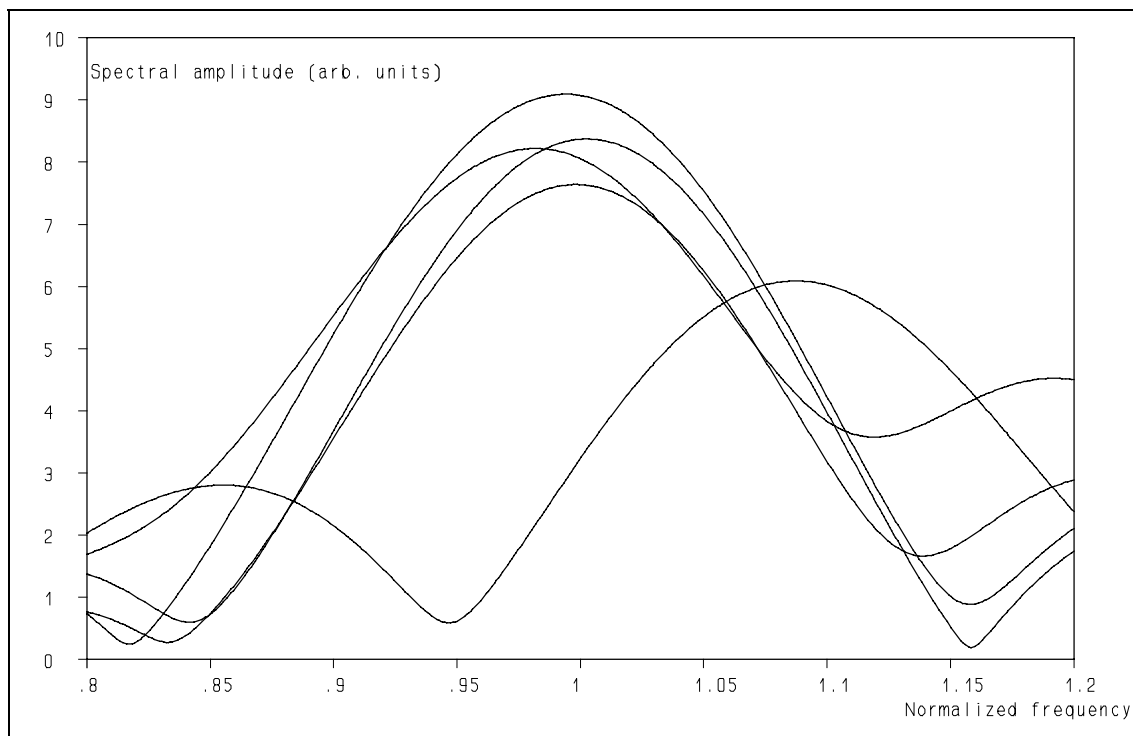


**Figure 3.15:** As the previous figure, but with a two times higher noise level. As is to be expected the accuracy of the estimator decreases. The scale is from  $0.8 F_{gem}$  to  $1.2 F_{gem}$ .

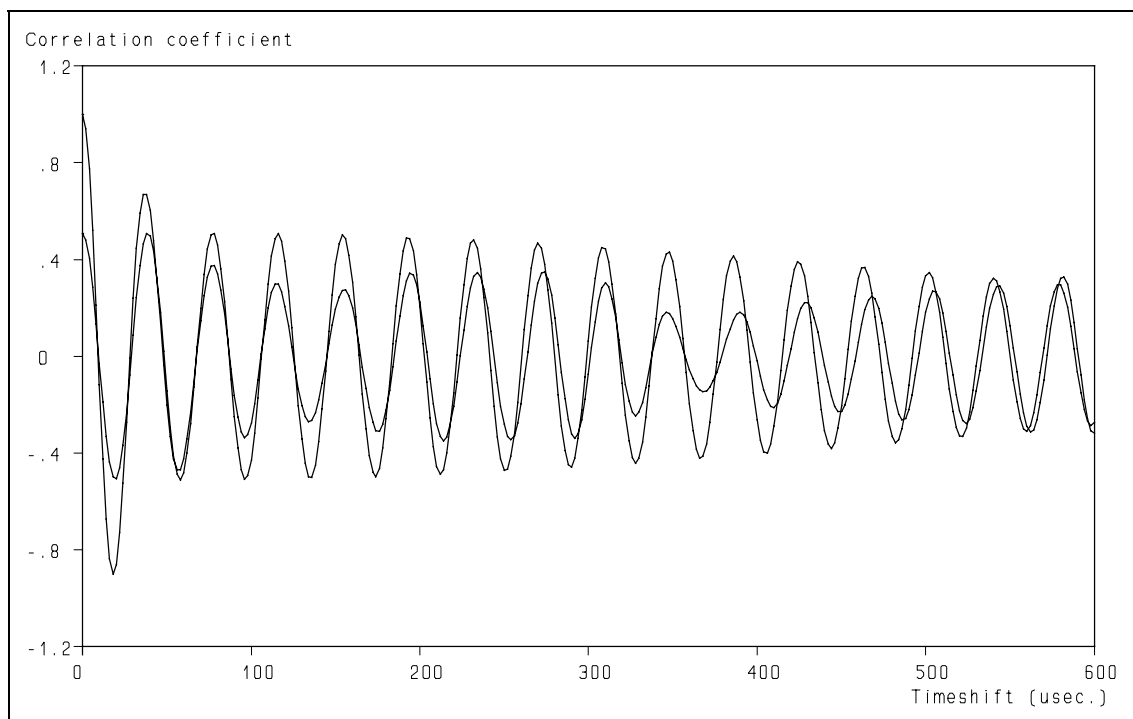


**Figure 3.16:** The auto correlation functions of an ideal and a realistic Doppler signal. The phase-jitter, caused by the narrow-band noise, gives rise to an uncertainty in the estimation of the frequency too.

### 3. Noise in Laser-Doppler Anemometry

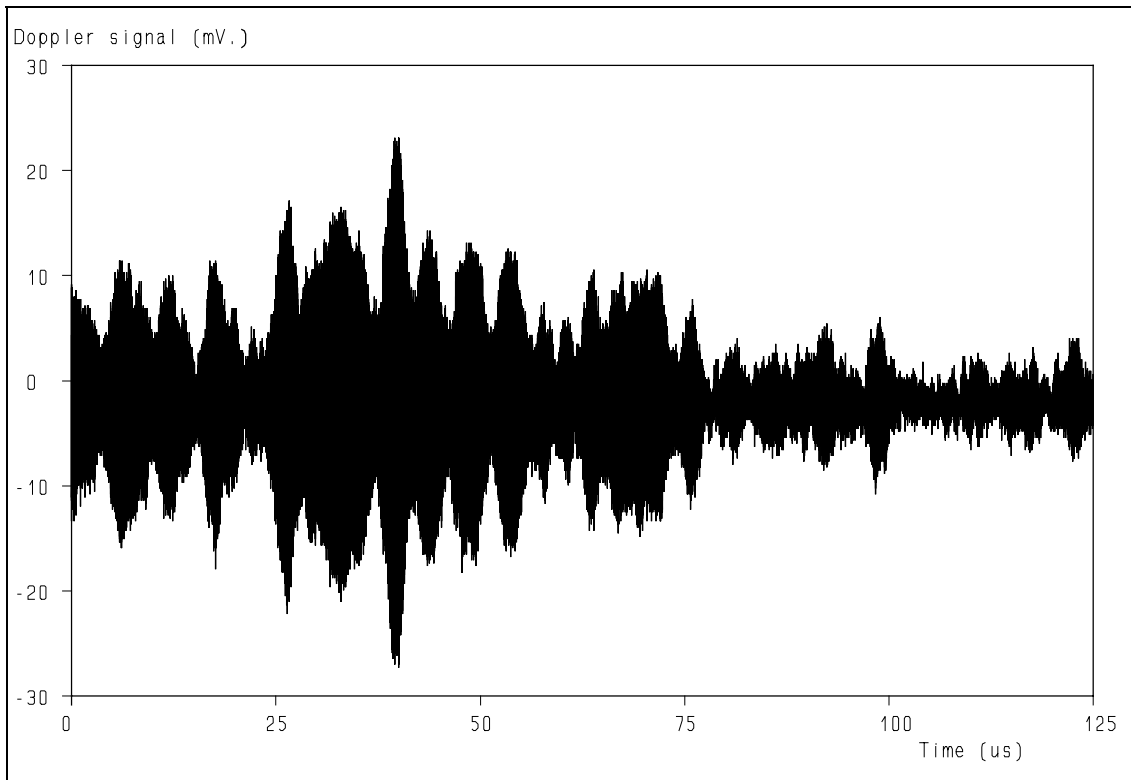


**Figure 3.17:** "Strong" Doppler signal, recorded by a digitizing oscilloscope.

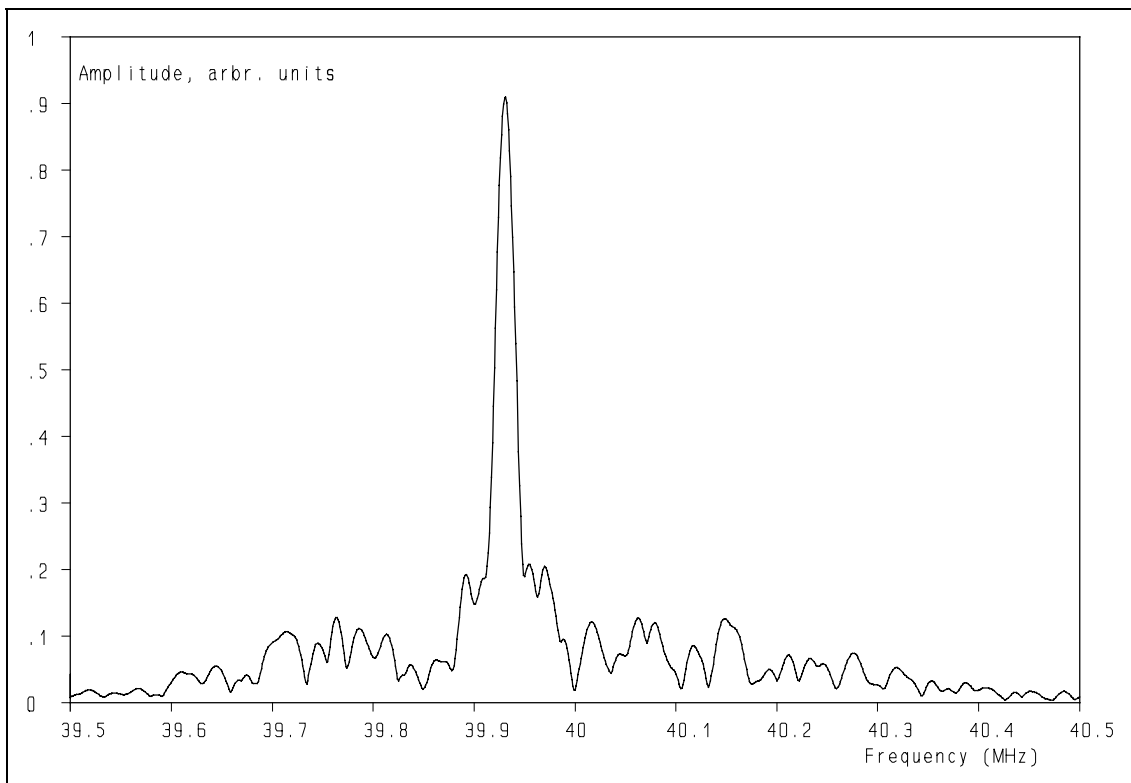


**Figure 3.18:** The spectrum of the "strong" Doppler signal.

*Retrieval of turbulence and turbulence properties from LDA data with noise*

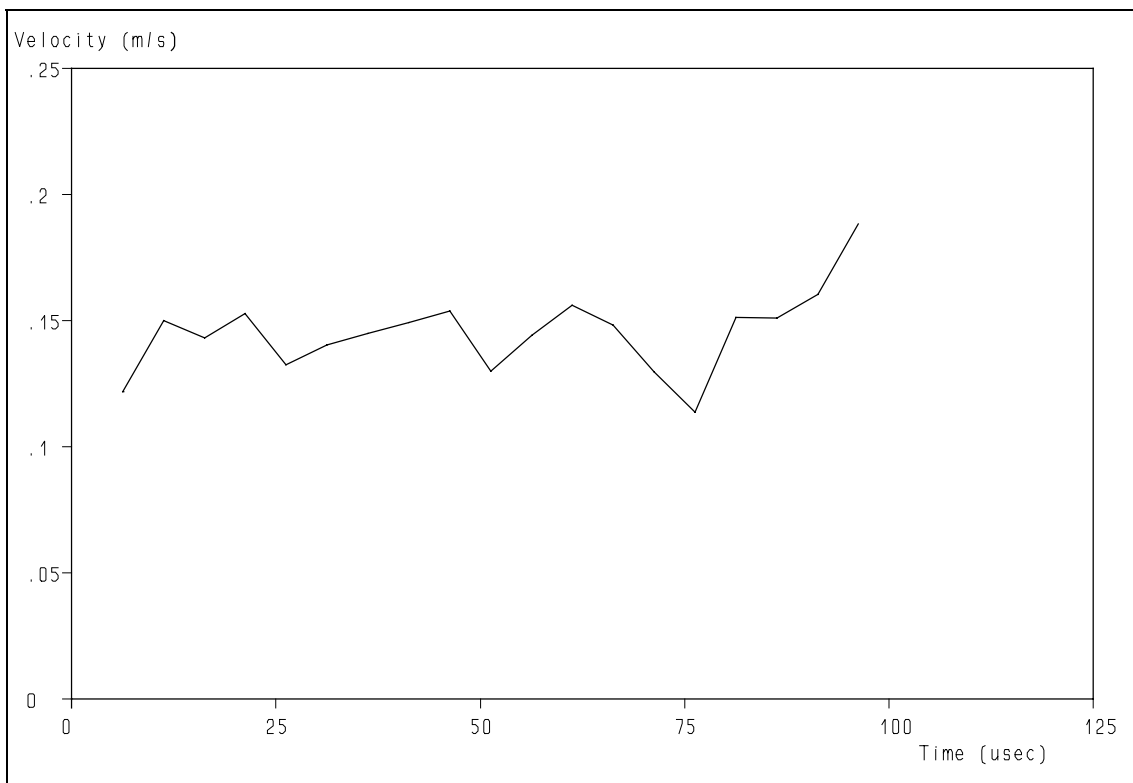


**Figure 3.19:** The velocity as estimated from parts of the "strong" Doppler signal.

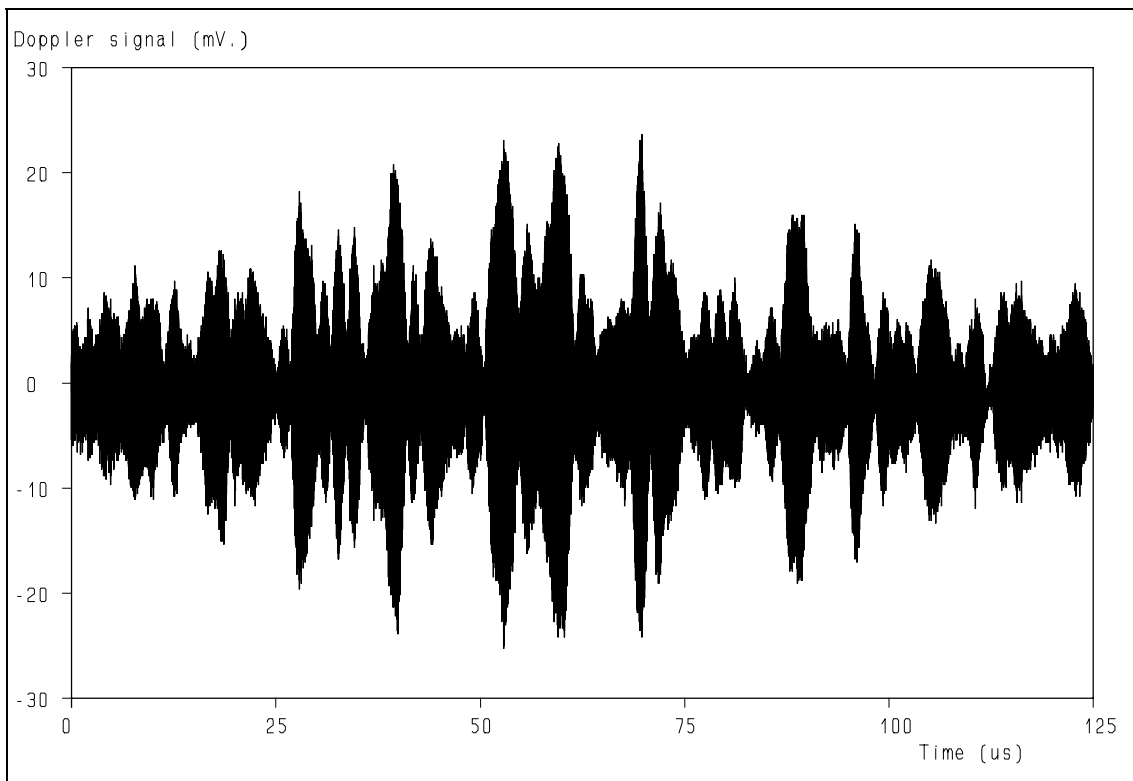


**Figure 3.20:** "Weak" Doppler signal, recorded by a digitizing oscilloscope.

### 3. Noise in Laser-Doppler Anemometry

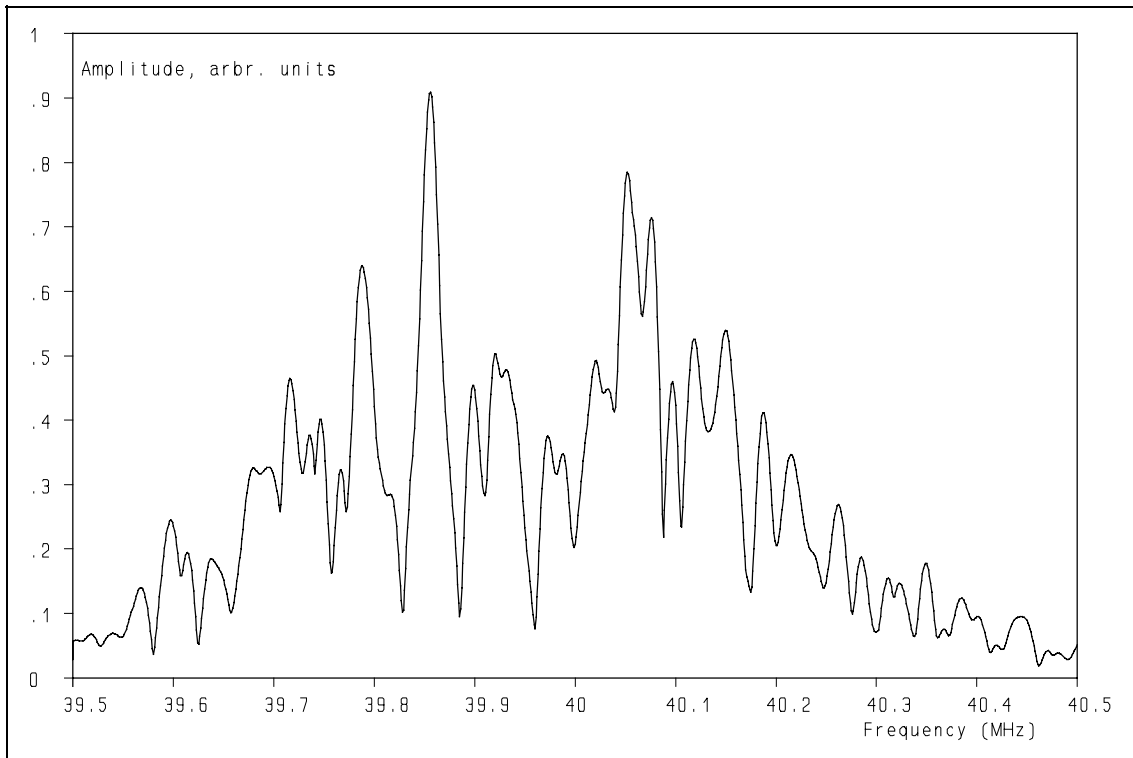


**Figure 3.21:** Spectrum of the "weak" Doppler signal.

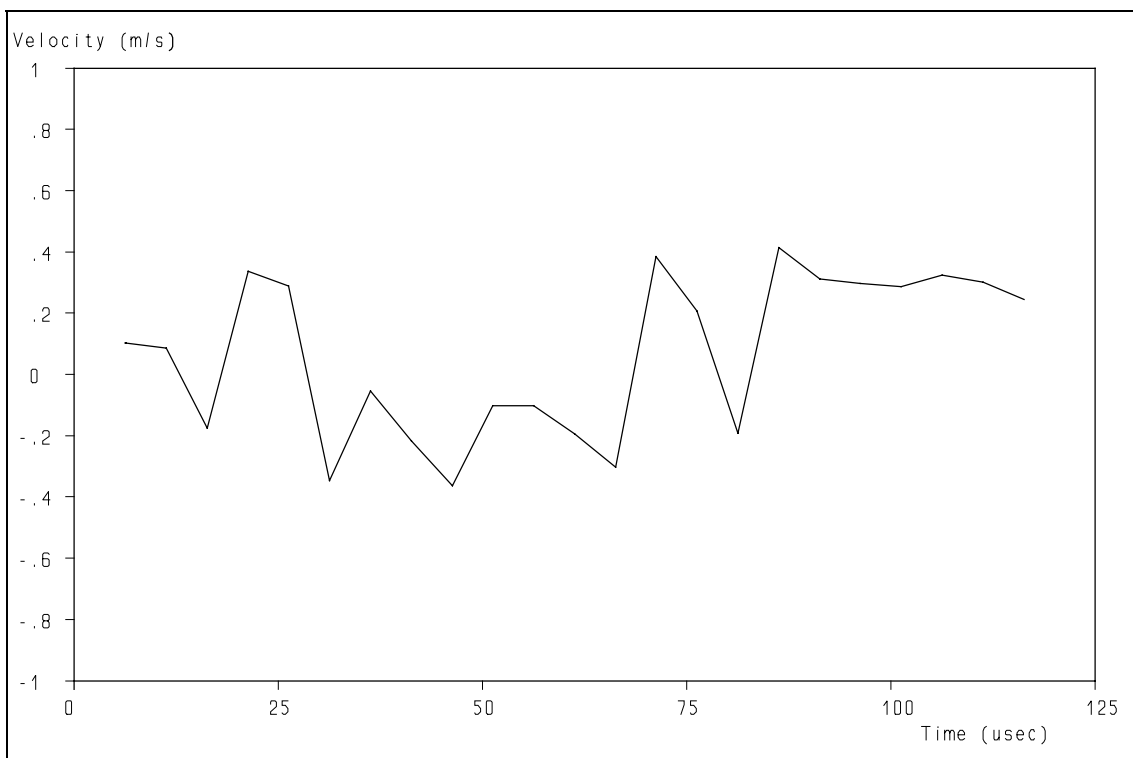


**Figure 3.22:** Velocity as derived from parts of the "weak" Doppler signal. Note the vertical scale compared to fig. 3.19!

*Retrieval of turbulence and turbulence properties from LDA data with noise*

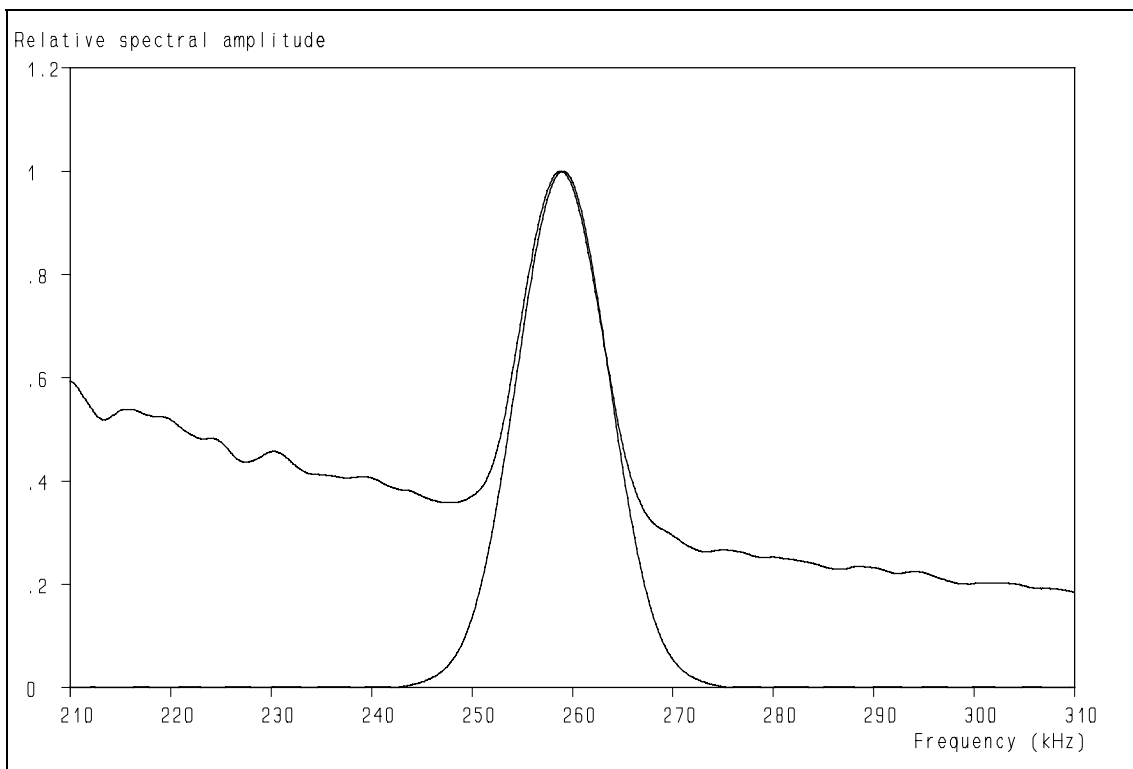


**Figure 3.23:** Because of the non-white noise floor, the peak of the Doppler signal shifts, causing a systematic error.

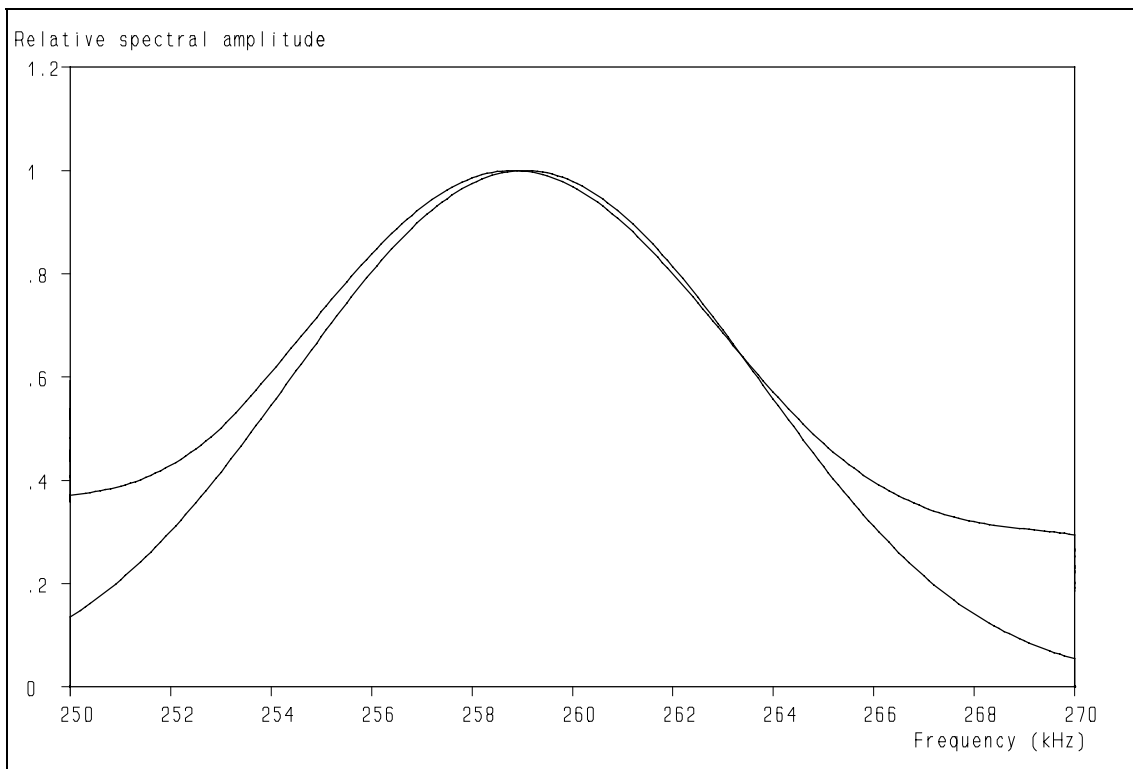


**Figure 3.24:** The shift becomes more clear in this enlargement of the previous figure.

# Chapter 4

## Preliminary Diagnostic Testing of Experimental Data-Sets

*If a man will begin with certainties,  
he shall end in doubts,  
but if he will content to begin with doubts,  
he shall end in certainties.*  
Francis Bacon

### 4.1 Introduction.

Making measurements using Laser-Doppler Anemometry (LDA) is a time intensive effort. It is therefore essential to obtain an indication on the quality of the experimental data, preferably during or shortly after the data have been collected, in order to be able to re-run the experiment if the data are of insufficient quality. To that end several tools have been developed, which will be discussed in the following sections.

### 4.2 The Time Interval Distribution.

Before the time interval distributions will be discussed, some comments should be made about the way these are constructed and presented here as choices have to be made. The first is the length of the maximum time interval, the range of the distribution. The second is the division of this range into bins, which have a certain width. In this thesis the range is roughly  $4 \cdot t_0 - 5 \cdot t_0^1$ , whereas the number of bins is chosen to be 100, resulting in a resolution of  $\approx 0.05 \cdot t_0$ . Note that the probability at  $4.6 \cdot t_0$  is roughly 0.01 of the maximum value. Any observation of a time interval that falls within the boundaries of a bin is assigned to that bin. This is a kind of quantisation in itself, which is inevitable in order to obtain a certain number of observations within each bin. The variance of this number is determined by statistics and increases with increasing time interval lengths, as can be seen from fig. 4.1, which shows the theoretical distribution (in this case in spatial separation). This is caused by the lower number of observations in these bins, which explains the choice of the range. This variance also puts a lower limit to the width of the bins that can be used in practice<sup>2</sup>. An upper limit to the bin-width is obtained from the maximum bias that is allowed: any non-linear distribution will have a certain amount of bias due to the non-linear averaging over the finite width of the bins. As the time interval distribution is non-linear, the bins should not be too wide to avoid noticeable bias. It should be emphasized that the choices made are arbitrary, yet determine the characteristics of the distribution obtained and are therefore open for discussion. Yet, I think that the choices made yield, within the practical boundaries, distributions which are suited for their purpose: diagnostics. However, it can very well be that different choices are better for different measurement conditions.

The presentation of the distributions is a bit different from the common way. The distributions are shown on a lin-log scale to begin with. The reason for this is that the distributions should be linear on such a scale and any deviation from a straight line can easily be distinguished. As the range has been chosen to be  $4 \cdot t_0 - 5 \cdot t_0$ , a vertical range of two decades will suffice. In order to keep the total probability

---

<sup>1</sup> Note that the average data-rate is  $1/t_0$ .

<sup>2</sup> Using these choices, the bins at the upper end of the distribution contain roughly 0.045% of the observations. The variance can subsequently be estimated using the total number of observations.

## *Retrieval of turbulence and turbulence properties from LDA data with noise*

1 (one), the values should be divided by the total number of observations and the bin-width. This, however, complicates the interpretation and comparison of distributions from measurements with a different data-rate. Therefore the distributions are "normalised" by dividing the numbers in each bin by the highest number in the distribution. Also, a straight line (remember this is a lin-log scale!) is fitted through the distribution in order to obtain the best estimator for the  $t_0$ , which in non-ideal cases may differ from the inverse of the data-rate. This fitted line should go through (0,1) in the ideal case (see fig. 4.1) when the distributions are presented in this way. Deviations can therefore be used to quantify the differences of the distribution and the ideal one. This straight line also helps to detect deviations from the linear behaviour of the distribution.

### 4.2.1 The theoretical Time Interval Distribution.

The homogeneous, but random, distribution of the tracer particles in space leads to an exponential distribution of the distances between two particles along the same line. In case of a laminar flow, this leads to the well-known exponential time interval distribution between two successive Doppler signals (e.g. ref. 11). This is known from statistics, but it can easily be confirmed by a Monte-Carlo simulation as is illustrated in fig. 4.1. The parameters that have been used for this simulation are:

- 1 million tracer particles dispersed in a volume of  $1 \times 1 \times 1 \text{ mm}^3$ .
- Cross-sectional area of measurement volume:  $100 \mu\text{m}^2$ , resulting in an average distance of  $10 \mu\text{m}$  between tracer particles that hit the measurement volume.

When the flow would convey these tracer particles with a constant velocity  $U$  through the measurement volume, the distance of  $10 \mu\text{m}$  would translate in a time, equal to  $10 \mu\text{m} / U$  sec. So the theory is correct, yet it shows in practice that these distributions show deviations from the ideal shape. These deviations can be used to determine the quality of the experimental data.

### 4.2.2 Practical Time Interval Distributions.

In the fig. 4.2 - 4.8 a number of time interval distributions are shown, which are obtained from different experiments. Although all have a certain resemblance to the ideal exponential time interval distribution, most show to a certain extent deviations from it. The causes of these deviations could provide us with information about the differences between the idealised picture, painted above, and the practical reality. As the time interval distribution can be available shortly after the termination of the data-collection, it fulfils the requirement for a diagnostic tool.

The most important deviations, which can be distinguished in the fig. 4.2 - 4.8 are:

- The absence of measurements for the shortest time intervals.
- The shape of the time interval distribution for short intervals is convex.
- The time interval distribution is concave in the vicinity of the average value of the interval time.
- The time interval distribution shows a crenellate structure over a large part of the range.
- A limited numbers of bins of the time interval distribution do not contain observations.
- A large number of bins of the time interval distribution do not contain observations.
- The time interval distribution shows a doublet structure with two, clearly distinct, characteristic times.

In many cases the observed distributions show a combination of several of these deviations simultaneously.

In order to find explanations for the above listed deviations, Monte-Carlo simulations have been run. The ideal distribution (see fig. 4.1) has been the starting point and assumptions have been made for different causes of the deviations. The simulation then tells us whether the assumption is correct or not. The major causes for the deviations that have been identified will be discussed below.

## 4. Preliminary Diagnostic Testing of Experimental Data-Sets

### 4.3 Causes of the deviations of the Time Interval Distribution.

#### 4.3.1 The dead time of the processor.

Every processor has a "dead time" in which it is determining the frequency and arrival time of a Doppler signal that just has been detected and validated. Including such a time into the distribution, in which the processor is not able to accept newly arriving Doppler signals, removes the observations for the shortest time intervals, as is shown in fig. 4.9. But the boundary is sharp, which differs from what is observed in practice, where a more gradual boundary is the rule. The dead time of the processor is therefore only a partial explanation for the deviations, observed at short time intervals. Yet, it is an important parameter for the optimisation of the LDA system that can be estimated from the time interval distribution, because it determines the high-frequency limits of the data-set: the dead time introduces a quasi-periodical sampling of the velocity next to the random sampling, which limits the frequency due to the Shannon-Nyquist sampling theorem. But also for the slotting technique (see Chapter 10) it is a disadvantage, as any slot below the dead time will remain empty. This enforces a minimum slot width, which limits the range and resolution of the turbulence power spectrum. Reduction of the dead time is therefore attractive, but as will be shown later, this is often in conflict with other requirements. Note that the total dead time of the LDA system is also related to the transit time of the tracer particles.

#### 4.3.2 Round-off errors in the data-file.

Usually computers do their calculations with a certain, limited accuracy, dependent on the kind of operating system, the programming language and possibly some limitations, introduced by the programmer. This could, also in combination with the limited accuracy used in the data-file itself, lead to problems: the total duration of an experiment will -in general- be long in comparison to the average time in between two successive Doppler signals. When the processor stores the (cumulative!) *arrival time* in the data-file, and not the time in between the Doppler signals, the resolution in the arrival time can become of the same order of magnitude as the shorter time intervals. The round-off errors will then play a role, as can be seen from the following example: assume that the average data-rate is 1 kHz and that the duration of the measurement is 1000 seconds. The resolution of the numbers in the computer is 1 to  $10^7$  (which is quite normal for single-precision values), which limits the resolution near the end of the experiment to 100  $\mu$ sec, which is 10% of the  $t_p$ . The time interval distribution, however, (see e.g. fig. 4.2) has a much higher resolution than 100  $\mu$ sec. The round-off errors start to interfere with the inherent quantisation in the time interval distribution and are therefore noticeable in it. Because this phenomenon only occurs after the arrival time has reached a certain value, the first part of the file will behave normally, but from a certain moment on a number of bins will no longer collect observations, which causes the crenellate structure of the distribution.

This phenomenon is confirmed by simulation. The results are shown in fig. 4.10. This means that with the use of longer measurement times (at least with several processors, not all of them) the arrival time is no longer recorded with sufficient accuracy, leading to an additional, but unnecessary, noise contribution to the velocity estimators. More details will be discussed later.

#### 4.3.3 Round-off errors in the internal clock of the processor.

The internal clock of a processor has its limitations too. This can lead to round-off errors in the interval times, which is -of course- unacceptable. The resolution of the clock should be chosen sufficiently high in order to avoid unnecessary errors.

This phenomenon could be modelled very well, as is shown in fig. 4.11. Less extreme cases may go unnoticed, as may be the case in fig. 4.12, but it is still not correct. Therefore it is important to study these distributions in minute detail. Note that the choices made for the construction of the time interval distribution enable the detection of round-off errors of roughly  $0.01 \cdot t_p$  and larger. This holds for the

## *Retrieval of turbulence and turbulence properties from LDA data with noise*

round-off errors in the data-file as well as those of the internal clock of the processor. This should be sufficient for most cases, but if a lower detection limit is required, the bin-width should be reduced.

### 4.3.4 Arrival time estimation noise.

The simulated distribution of fig. 4.12 already has a close resemblance to the distribution of fig. 4.6, but there are still some distinctions. Especially the difference between the completely empty bins of the simulation and the partially filled bins of the experimental distribution are remarkable. The cause of this difference is the uncertainty in the individual arrival time estimators. This could be christened "arrival time estimation noise", because when the individual velocity estimators are plotted, one should define an "error value" for the velocity estimator, but also an error value for the *arrival time estimator*. This will show up again with the Wavelet Transform (see Chapter 5) and it causes an additional noise contribution to the estimators of the properties of the turbulence.

Assuming a certain size for the arrival time estimator uncertainty results in the distribution, presented in fig. 4.13, which shows indeed the structure of the distribution of fig. 4.6. Another effect worth noting is the convex shape of the distribution at short time intervals, as is shown in fig. 4.14, so this phenomenon is explained as well. Note that this phenomenon causes the fitted line to intersect the vertical axis above 1 (one). This can be used as a measure of this error source. As will be discussed in more detail at the Wavelet Transform, this arrival time uncertainty is an unattractive phenomenon, but at this moment it can only be suppressed as much as possible by using strong Doppler signals which have a high Signal-to-Noise ratio (SNR) in combination with a small measurement volume. See Chapter 3 for more details.

### 4.3.5 Velocity bias.

Velocity bias is a much debated phenomenon in LDA, which is still not resolved. An extensive discussion can be found in ref. 67. This phenomenon is caused by a correlation between the (measured) velocity component and the data-rate. In order to study the influence of this correlation on the time interval distribution, a simulation has been run in which a 1-D flow system<sup>3</sup> has been analyzed by adding an average velocity to the simulated turbulence and to take the data-rate proportional to the instantaneous velocity. The results for a turbulence intensity of 30% are presented in fig. 4.15 and those for a turbulence intensity of 100% in fig. 4.16. These results show that correlation between velocity and data-rate causes a concave shape of the time interval distribution, which increases with increasing turbulence intensity. This deviation corresponds to deviations which have been noticed in several experimental time interval distributions (see also Chapter 11).

The time interval distribution can thus be used to note the occurrence of velocity bias. This can warn the experimenter to take counteracting measures, but it can also be used to give a rough indication of the seriousness of the problem.

### 4.3.6 Bias caused by tracer particle concentration fluctuations.

Another cause of bias in LDA is the mixing or confluence of fluids with different tracer particle concentrations or changes in the tracer particle concentration by e.g. centrifugal effects. An example of the latter is the cyclone, which is designed for the separation of solids from the fluid. To study the influence of this kind of bias on the time interval distribution another simulation has been run in which the fluids had a concentration difference of a factor 4 and a factor of 2. Each fluid spent 50 % of the time in the measurement volume under the assumption that these times are far longer than the  $t_0$  of the time interval distribution. The results are presented in fig. 4.17 (factor 4) and in fig. 4.18 (factor 2). These figures show that this kind of bias introduces similar deviations from the ideal time interval

---

<sup>3</sup> This is the most extreme case. More details will be discussed in Chapter 10.

#### 4. Preliminary Diagnostic Testing of Experimental Data-Sets

distribution as the correlation between velocity and data-rate does, but that the concentration difference of a factor of 2 gives deviations which are hardly noticeable. This is a bit disappointing from a diagnostic point of view, but still it could be indicative in extreme cases when e.g. one of the seeding generators has ceased functioning.

##### 4.3.7 Multiple validation.

As has been demonstrated when the narrow-band noise contribution to the Doppler signal was discussed, this noise leads to an amplitude modulation of the Doppler signal. This -on its turn- can give rise to so-called "multiple validation" of the Doppler signal. In popular terms: the Doppler signal detection and validation system has been fooled by the amplitude modulation and was made to think that the signal consisted of the Doppler signals of two (or even more) tracer particles. It is not surprising that this multiple validation influences the time interval distribution as a large number of observations with short interval times (with a maximum of the transit time of the tracer particles!) are added. The time interval distributions which are measured when multiple validation occurs will show a kind of double structure in the decay, one characteristic time corresponding to the transit time and the other to the actual interval time. This phenomenon is clearly illustrated in fig. 4.19, which shows the results of a simulation in which two different characteristic times have been used. Compare it with fig. 4.8. Note that multiple validation leads to an intersection of the fitted line with the vertical axis below 1 (one). This can be used as a measure of this phenomenon. Only few experimental distributions will give a fit with an intersection close to 1 (one), e.g. the distribution of fig. 4.2, but most will give a value above 1. This is caused by e.g. the dead time which is an unavoidable phenomenon in LDA (see e.g. fig. 4.9). Therefore intersections below 1 should warn the user of serious error(s) in the measured data.

One might think that it not such a bad idea to use multiple validation to increase the data-rate artificially and to obtain information on the small scales. However, the noise contribution to the Doppler signals sees to it that the best estimate for its frequency will be obtained when the *complete* Doppler signal is used and not only a part of it (see the discussion in Chapter 3). The dramatic effect on the velocity estimators becomes obvious by comparing fig. 4.20 and 4.21: fig. 4.20 shows the velocity as a function of time without multiple validation and in fig. 4.21 with it. No further comments are necessary in my view. One can therefore conclude that multiple validation is something to avoid at -virtually- all costs. And this holds for all processors: fig. 4.22 and 4.23 show a similar behaviour for another type of processor. This is to be expected as it is a property of the Doppler signal itself.

Multiple validation can be avoided by correct settings of the Doppler signal detection and validation system. This often means that the dead time of the processor is increased, but that is a price one has to pay. However, the dead time of the processor never needs to be longer than the transit time of the tracer particles, thus by choosing a small measurement volume, this can be reduced as much as possible. A small measurement volume also increases the spatial resolution, it increases the light intensity and it allows higher concentrations of tracer particles before the chances become too big that more than one tracer particle will be present in the measurement volume. Reduction of the dimensions of the measurement volume is therefore an attractive approach for optimisation (see also the discussion in Chapter 3). Apart from this, the settings of the Doppler signal detection and validation system are quite critical in highly turbulent flows, as the transit time may vary considerably due to the differences in the local, instantaneous velocity. If fast signals are allowed to be processed, there is a chance for multiple validation at low velocities, whereas suppressing the fast signals may result in the loss of Doppler signals from the high velocities, which is unacceptable too. The best thing to do would be to apply dynamic validation criteria, which could adapt to the "instantaneous" flow conditions. But a processor with such a dynamic system is -as far as my knowledge goes- not (yet) on the market. Fortunately the time interval distribution offers a tool to see the influence of the settings on the results and can thus be helpful in finding the optimum settings.

## *Retrieval of turbulence and turbulence properties from LDA data with noise*

### **4.4 The actual velocity trace.**

The velocity trace itself can give indications about the way the experiment goes. Although measurements are made because it is unknown how the flow develops, one can still use common sense and this will tell that such strange excursions, as are shown in fig. 4.21 and 4.24, are not correct. The velocity trace can also indicate the amount of noise, present in the signal (velocity estimates). However, it is only a qualitative judgement that can be made and also, a nice looking signal is no guarantee at all that the experiment is running nice and smooth. Observation of the velocity trace falls into the category "required, but insufficient".

### **4.5 The linear Velocity Probability Distribution.**

The velocity probability distribution of most turbulent flows usually has a more or less Gaussian shape, shifted over the average velocity of the component being measured (ref. 1, 2 and 74). An example is shown in fig. 4.25. Skewed probability distributions are rather the rule than the exception and in oscillating flows bimodal probability distributions can occur. One should therefore keep the flow conditions in mind when judging the velocity probability distribution. But when the probability distribution deviates strongly from what one could expect under the given conditions, there is a severe chance that something or some part is not functioning correctly. It is also important to keep in mind that the probability distribution is necessarily a continuous function and when this is not the case it is also a clear indication that something is not working properly. An example is shown in fig. 4.26, where the probability distribution shows a "comb-like" structure, which points at round-off errors due to quantisation by the processor. The most probable cause is a far from optimum choice of the velocity range of the processor for the experimental conditions. Fig. 4.27 shows another probability distribution which contains a small number of observations at elevated velocities. However, such small contributions can still have a significant influence on the values of the higher moments of the probability distribution. But as these small contributions are hard to distinguish in probability distributions on a *linear* scale it is attractive to use a *logarithmic* scale vertically.

### **4.6 The logarithmic Velocity Probability Distribution.**

There is no real difference between the logarithmic and linear velocity probability distributions, only the vertical scale is different to enhance small contributions. This is shown clearly in fig. 4.28. The small contributions at the higher velocities can easily be distinguished and those above 0.2 m/s are obviously suspect. Calculation of the higher moments of the probability distribution can reveal whether this suspicion is correct or not.

### **4.7 The Auto Correlation Function estimated using the Local Normalisation.**

In Chapter 10, the estimator for the auto correlation function, using the slotting technique with Local Normalisation, will be described and extensively discussed. This has shown to be a good approach, *provided the raw data are reliable*. Although this algorithm was never intended to be a quality tester, it showed that it is very sensitive to multiple validation: the estimated auto correlation becomes uninterpretable. Fig. 4.29 shows an estimator for the auto correlation function like one might expect. The variance in the vicinity of  $\tau = 0$  is limited and it has a clear noise peak at the origin. In contrast, fig. 4.30 shows one which has been effected by multiple validation. The large variance for all values of  $\tau$  indicates that something is seriously wrong. This is an attractive property which can be used for diagnostic purposes. Note that the noise peak at  $\tau = 0$  is an objective measure of the noise contribution to the individual velocity estimates. This will be discussed in more detail in Chapter 10.

## 4. Preliminary Diagnostic Testing of Experimental Data-Sets

### 4.8 The number of products in the slotted Auto Correlation Function.

When calculating the auto correlation function using the slotting technique, in each slot a number of products is collected. This number of products is -on average- equal to:

$$N_p = N_t \cdot \left( \frac{\Delta t}{t_0} \right) = T_m \cdot \left( \frac{\Delta t}{t_0^2} \right) \quad [4.1]$$

in which:

$N_p$  = number of products in each slot (on average)

$N_t$  = total number of velocity observations in the data

$\Delta t$  = slot width

S

$t_0$  = characteristic time of distribution (= 1/data-rate)

S

$T_m$  = Total measurement time

S

This can be understood by realising that the chance to find an observation within a (slot) width  $\Delta t$  is equal to  $\Delta t/t_0$  and because the total measurement time is  $N_t \cdot t_0$ . As the variance of the individual correlation coefficient also depends on the number of products in a slot, this number should at least be several thousand. Verification of this number indicates the quality of the individual correlation coefficients that will be obtained. This is generally in agreement with experimental observations, but deviations from the number of products in a slot from the average value can be used as a diagnostic tool. This is illustrated in fig. 4.31, in which the low number of products in the first slots are indicative for a low number of observations with short time intervals (see fig. 4.32) and the comb-or crenellate-like structure for round-off errors in the data-file. Note that the latter is not so obvious from the time interval distribution, shown in fig. 4.32. Although the calculation of the auto correlation function is usually done as off-line data-processing, it can be used for diagnostic analysis.

### 4.9 Concluding remarks.

Unfortunately, diagnostics has not received the attention with the development of the LDA measurement technique that it should have had. It is -in my view- very important that it during -or at least shortly after the termination of- the experiment becomes clear whether the data, that have been collected, are useful or not. The analyses that have been described above can help in that respect, without pretending that these will give the final answer. But if the data pass these tests, there is a fair chance that these are useful. In the future additional diagnostic tools may be developed, which can increase the probability of detecting data which are not OK. Such tools should be used to eliminate data-sets which cannot stand the test in order to avoid that incorrect conclusions might be drawn from the data. These tools are also valuable for the training of novel users, because they give feedback to the experimenter. This training task is often neglected as well.

*Retrieval of turbulence and turbulence properties from LDA data with noise*

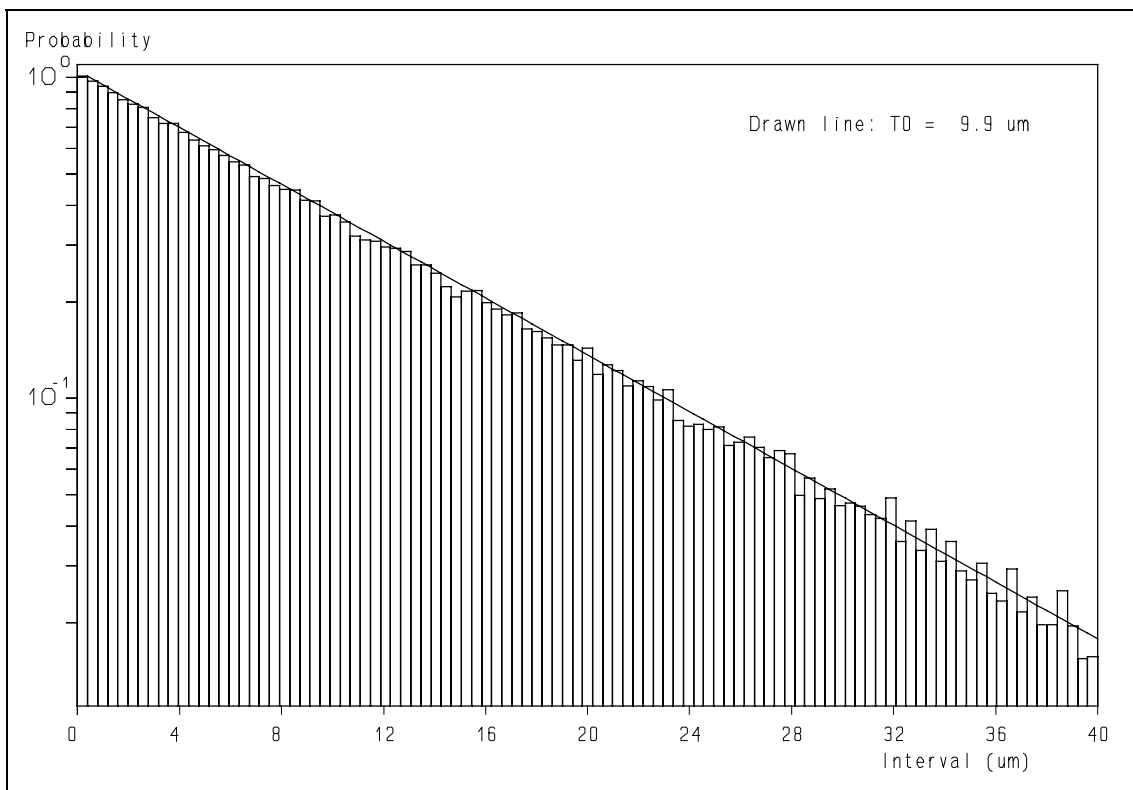


**Figure 4.1:** Histogram of the positional distribution of homogeneously, but randomly, distributed point-like particles.

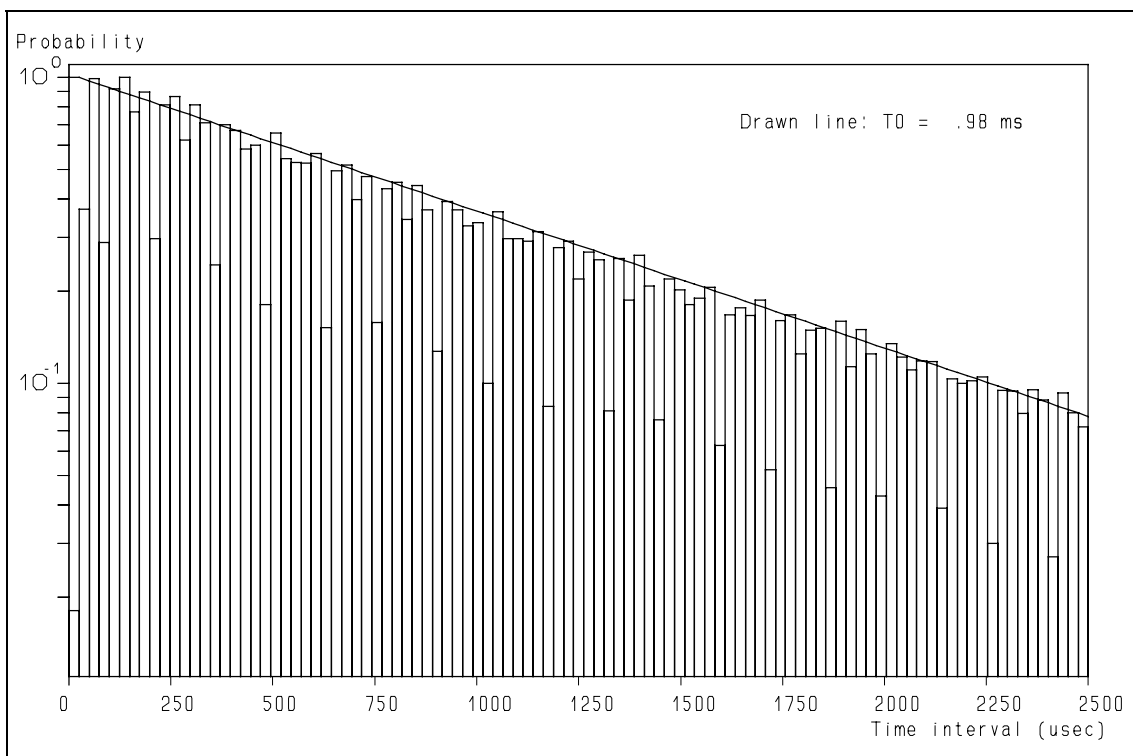


**Figure 4.2:** Time interval distribution with an average data-rate of approximately 1 kHz.

#### 4. Preliminary Diagnostic Testing of Experimental Data-Sets

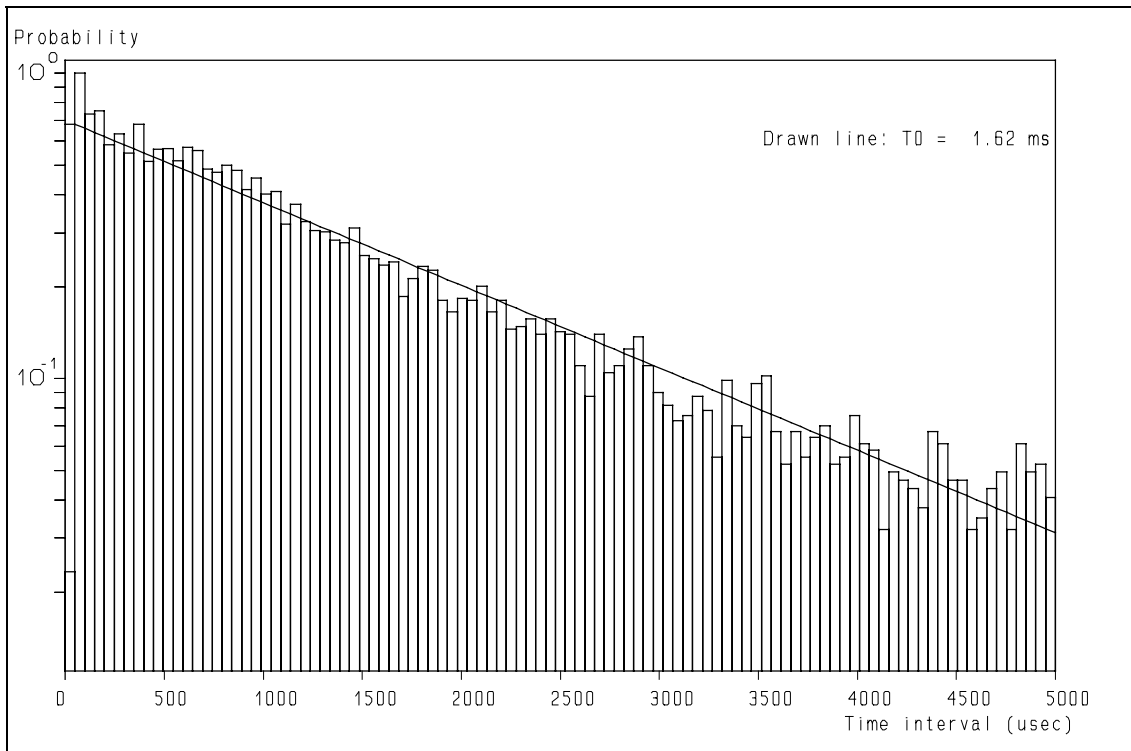


**Figure 4.3:** Deviations: elevated below 150  $\mu\text{sec}$ , reduced between 150 and 500  $\mu\text{sec}$ , reduced around 2500  $\mu\text{sec}$  and elevated at 5000  $\mu\text{sec}$ .

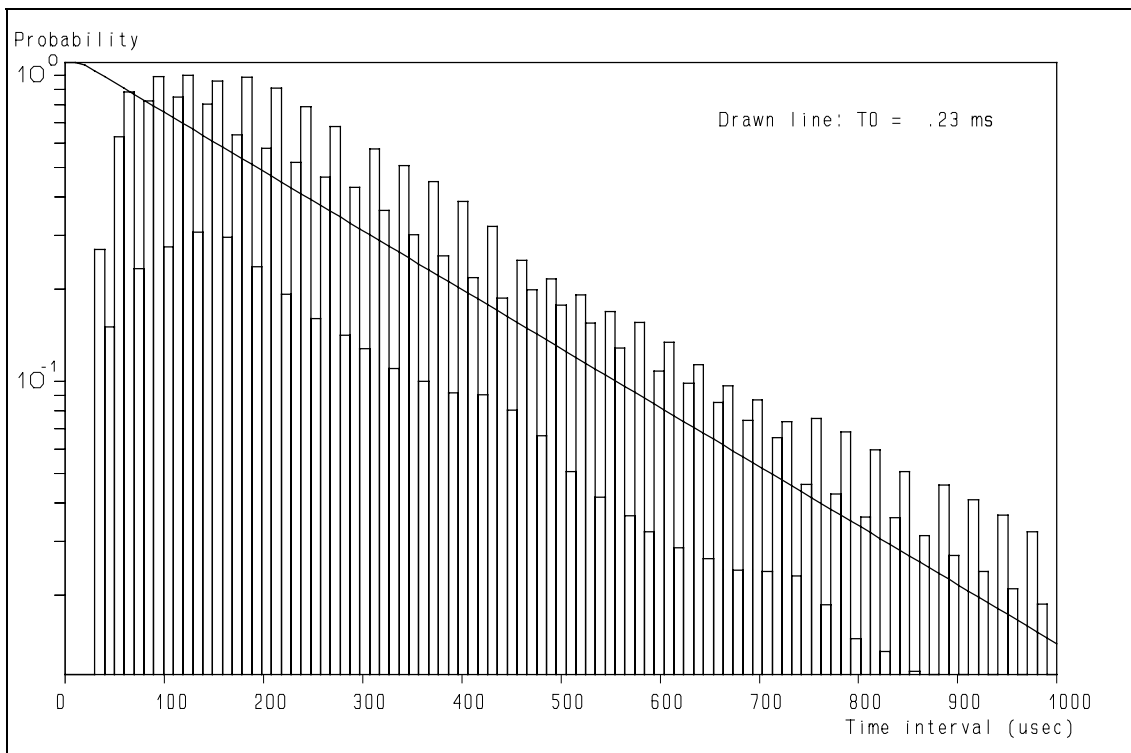


**Figure 4.4:** Deviations: no observations below 30  $\mu\text{sec}$ , convex up to 200  $\mu\text{sec}$ , concave shape and crenellate structure.

Retrieval of turbulence and turbulence properties from LDA data with noise

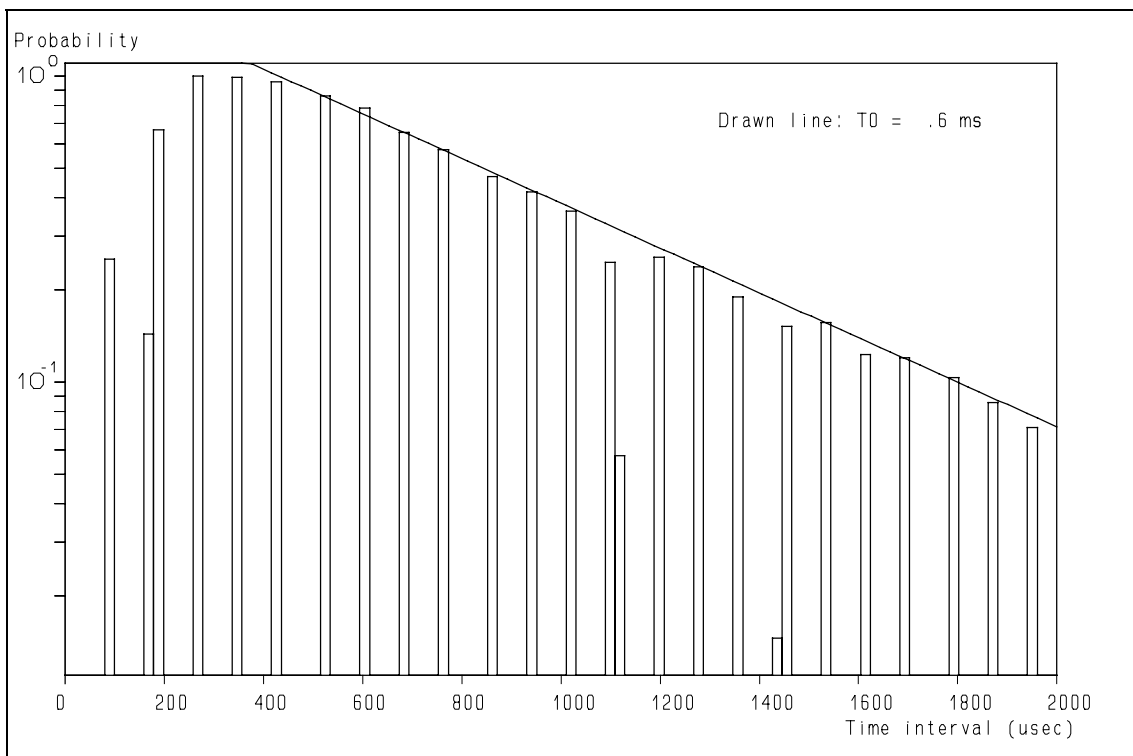


**Figure 4.5:** Deviations: convex up to 400  $\mu\text{sec.}$ , a large number of bins do not contain observations.

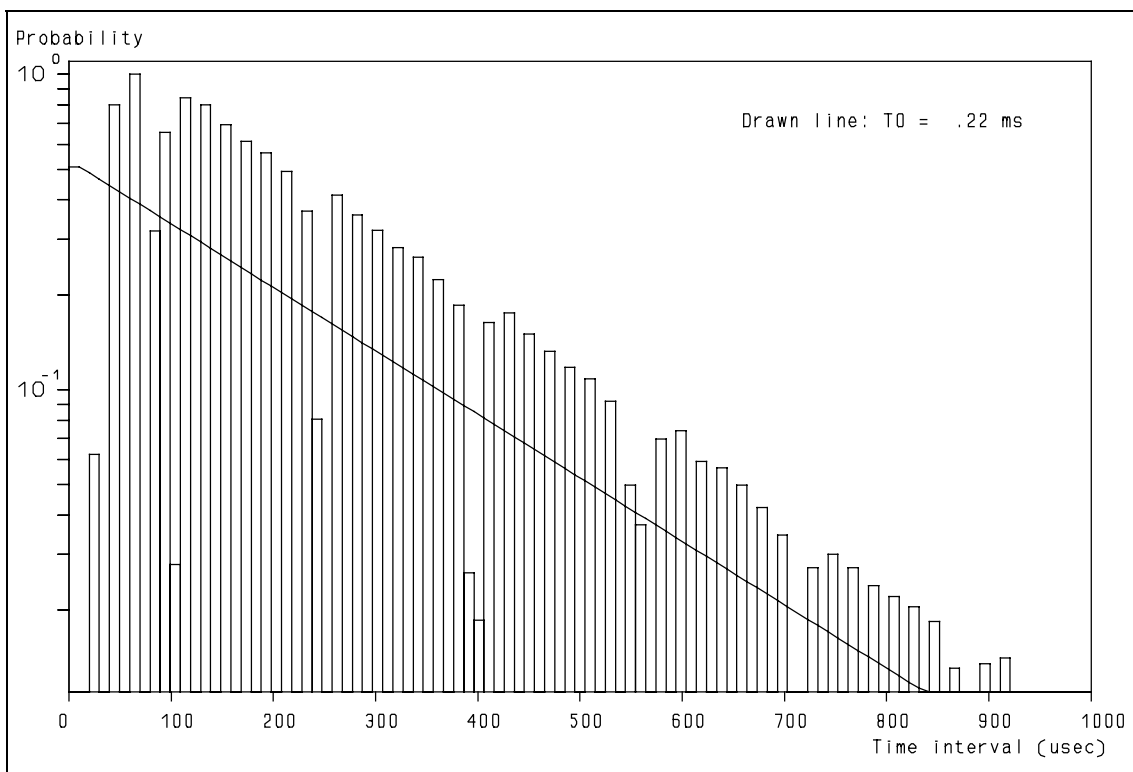


**Figure 4.6:** Deviations: no observations below 30  $\mu\text{sec.}$ , convex up to 70  $\mu\text{sec.}$  and a number of bins does not contain observations.

#### 4. Preliminary Diagnostic Testing of Experimental Data-Sets

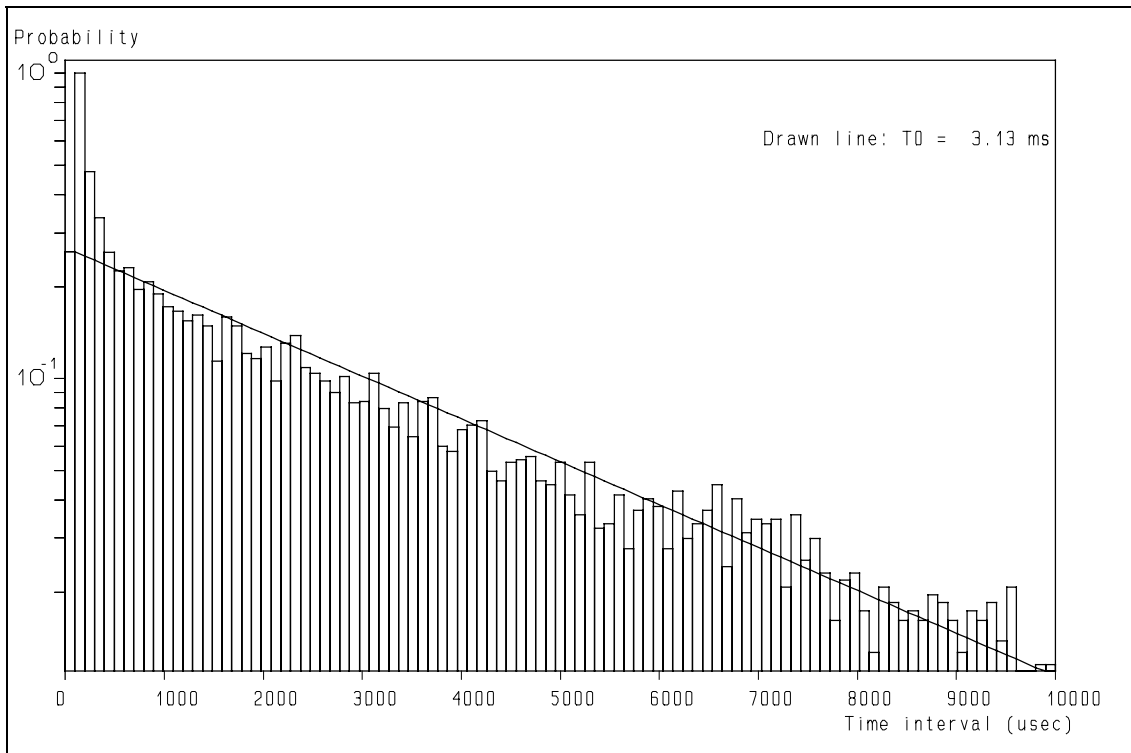


Figure 4.7: Deviation: double  $t_0$  structure.

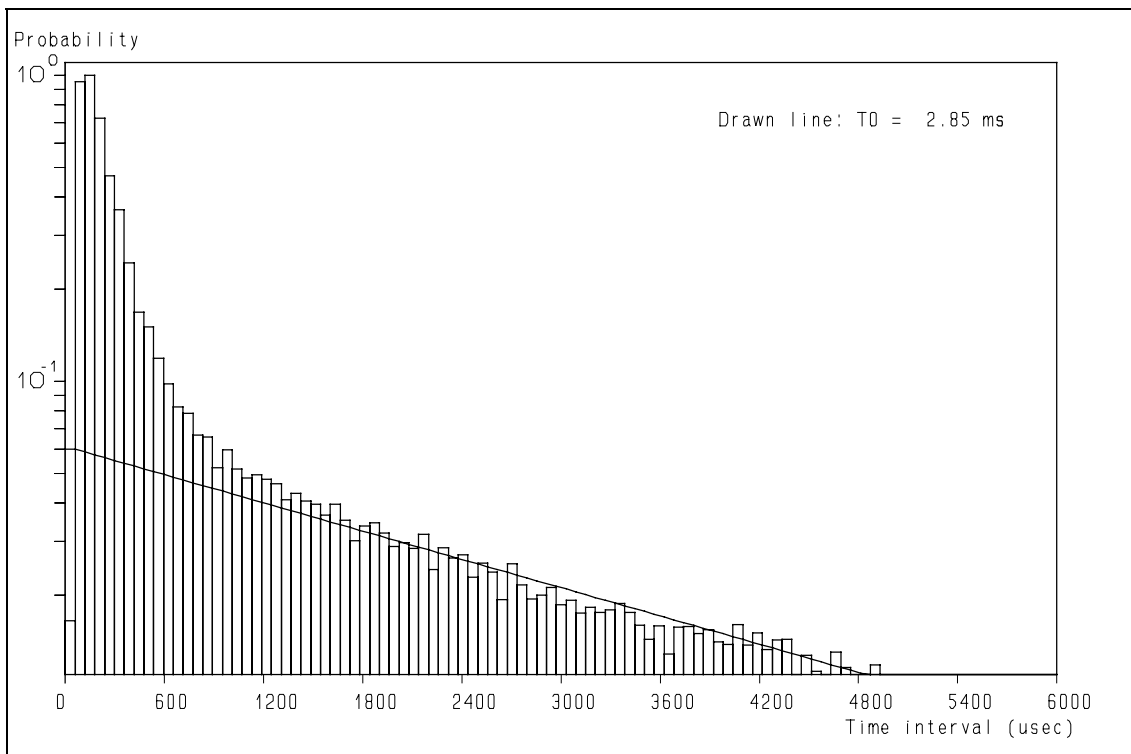
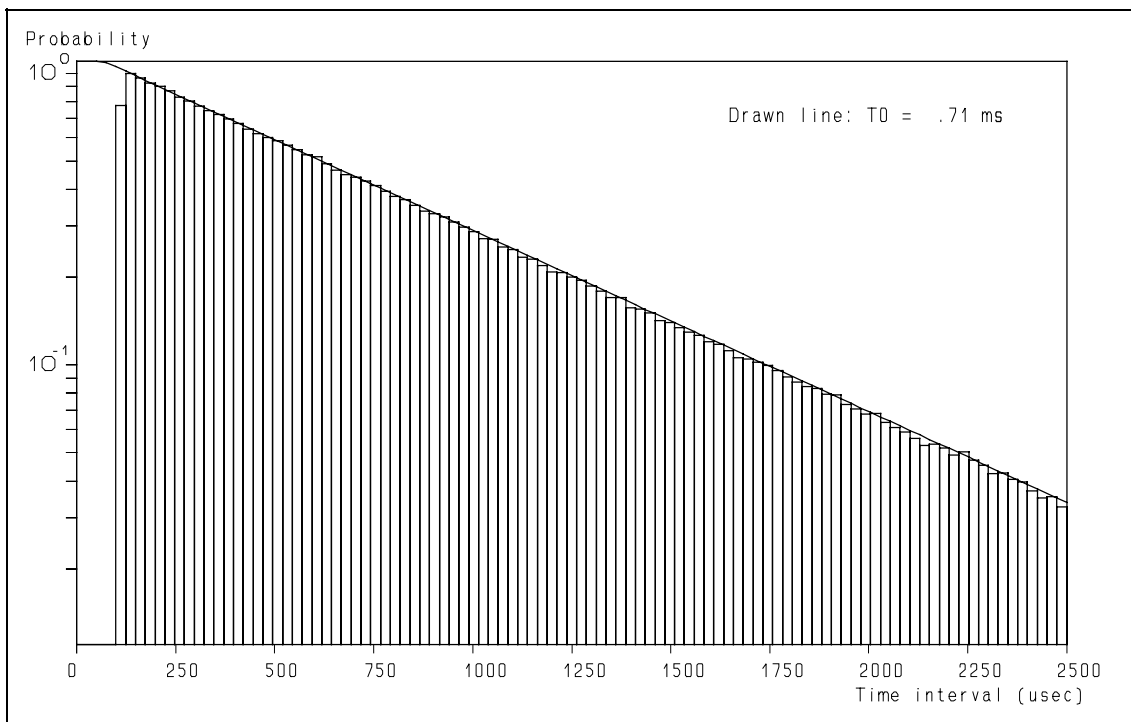
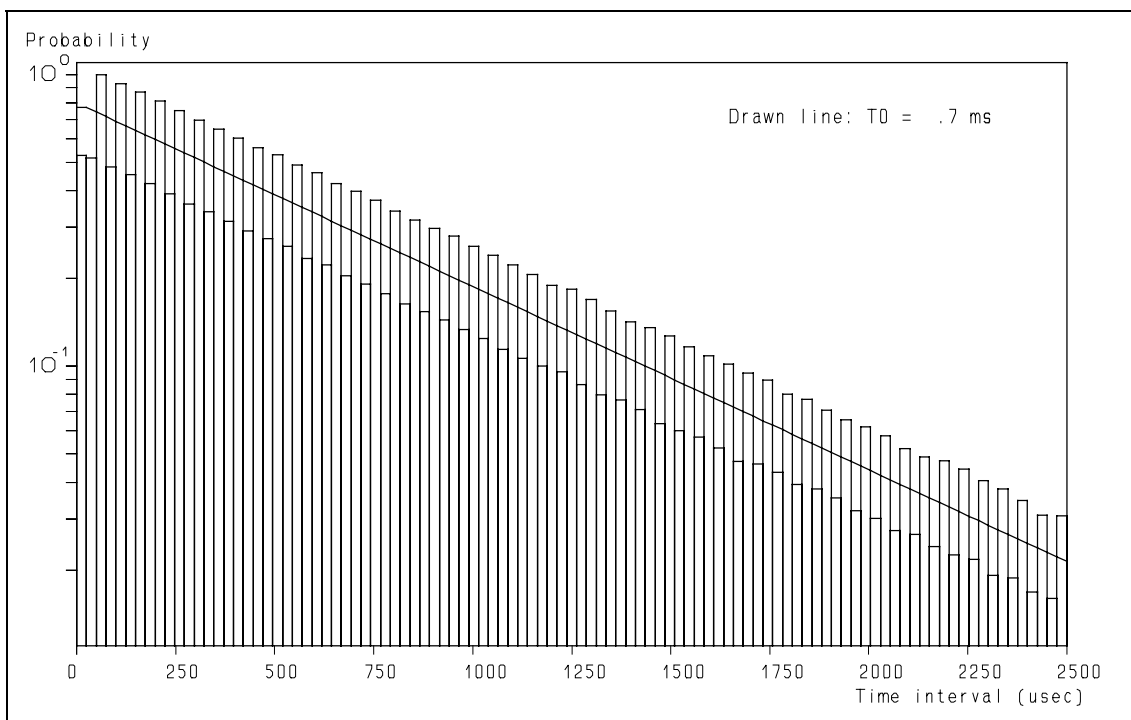


Figure 4.8: Deviation: double  $t_0$  structure.

*Retrieval of turbulence and turbulence properties from LDA data with noise*



**Figure 4.9:** A dead time of the processor explains the lack of observations for short time intervals. Note, however, the sharp boundary.



**Figure 4.10:** When the accuracy, which is used to record the arrival time in the data-file, is insufficient, round-off errors cause a crenellate structure. This happens especially with long durations of the measurement.

#### 4. Preliminary Diagnostic Testing of Experimental Data-Sets

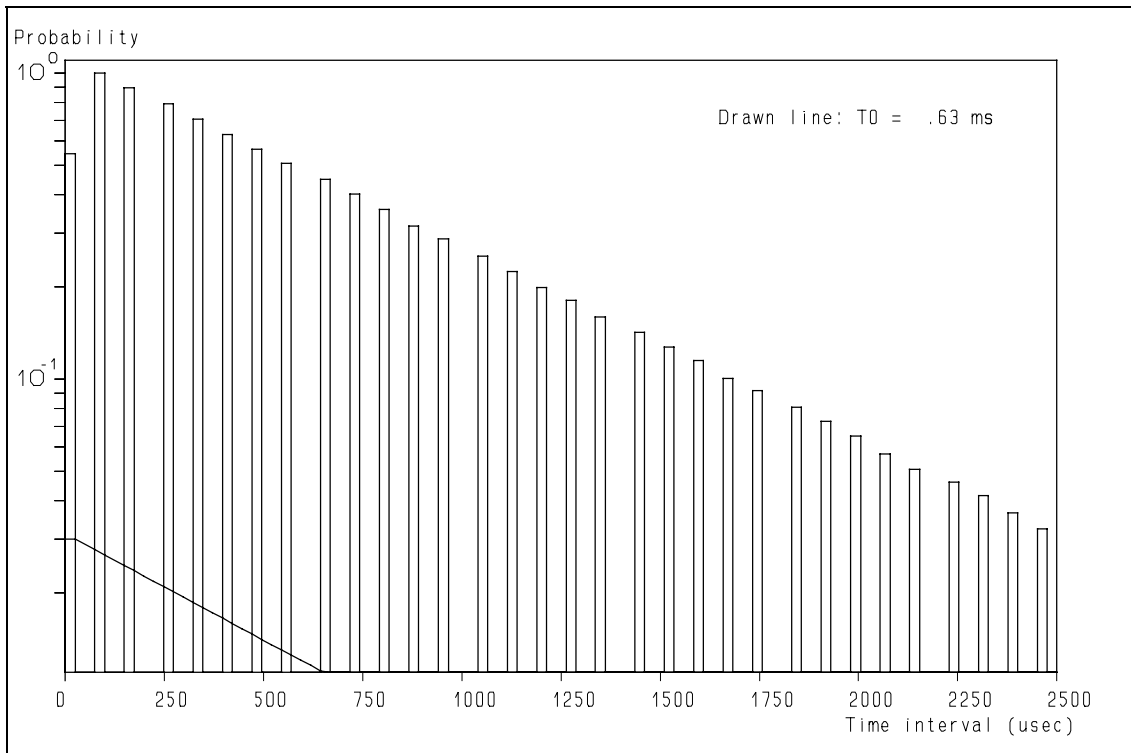


**Figure 4.11:** Round-off errors of the internal clock of the processor lead to a distribution with many bins without observations.

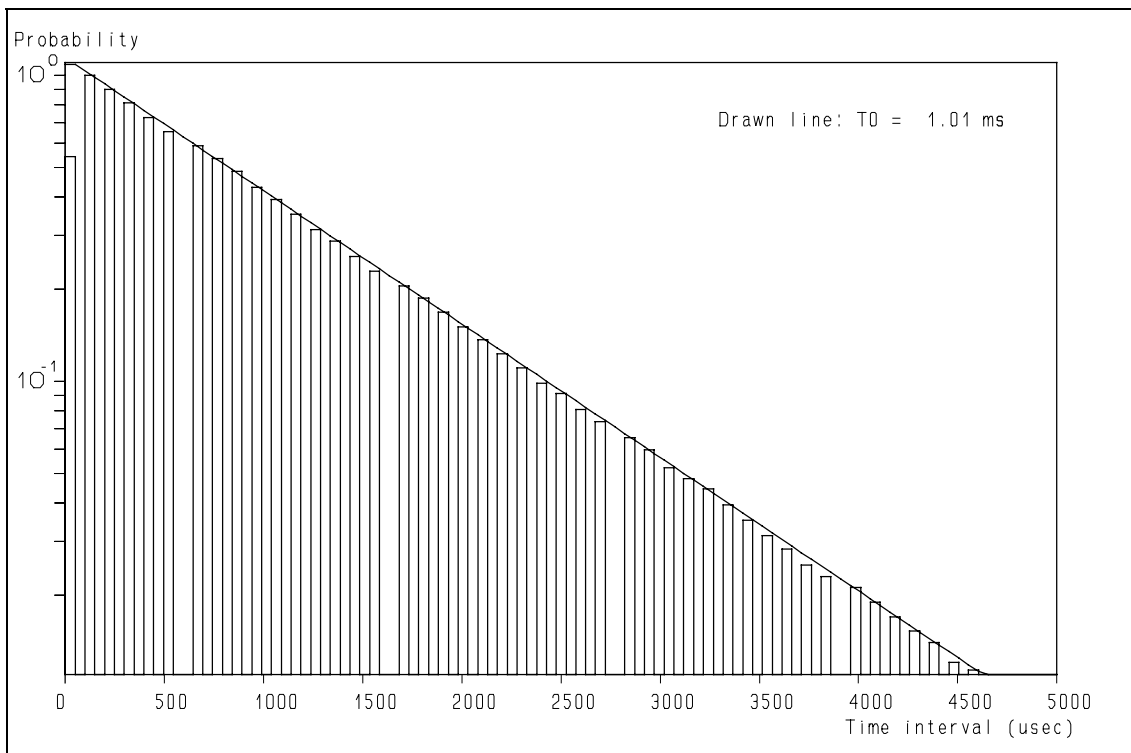


**Figure 4.12:** The round-off errors of the clock do not explain the measured deviations completely.

*Retrieval of turbulence and turbulence properties from LDA data with noise*

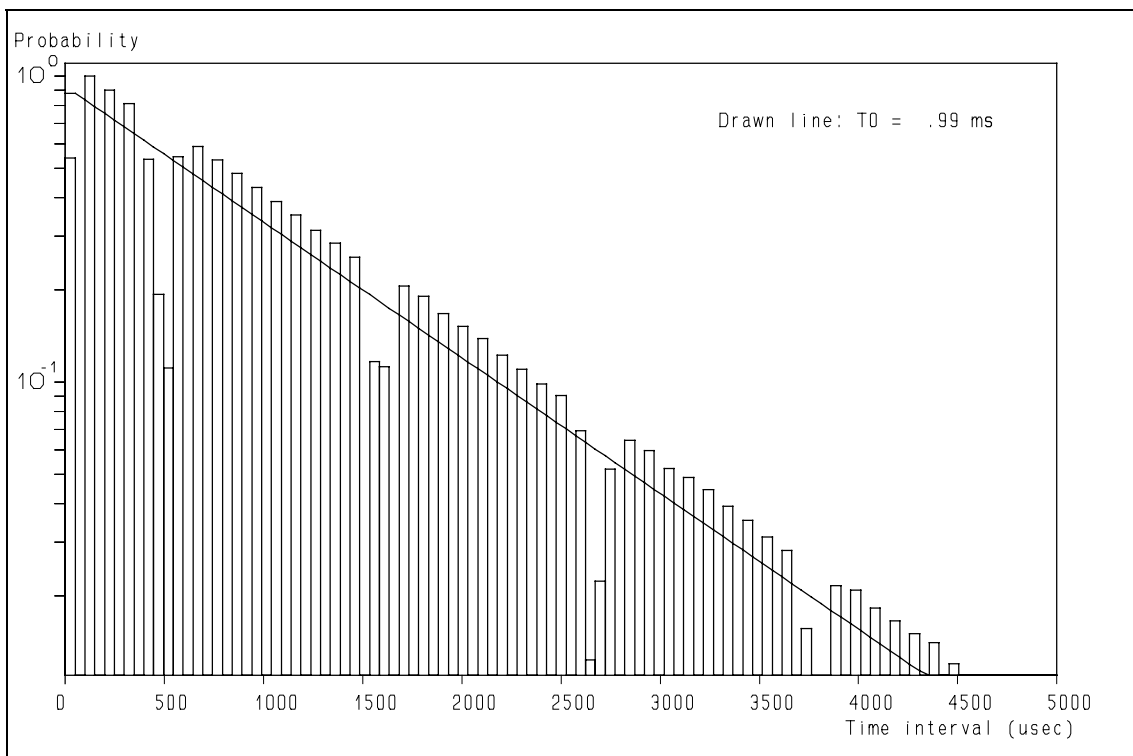


**Figure 4.13:** A combination of the uncertainty in the arrival time and the round-off errors of the clock creates the observed deviations.

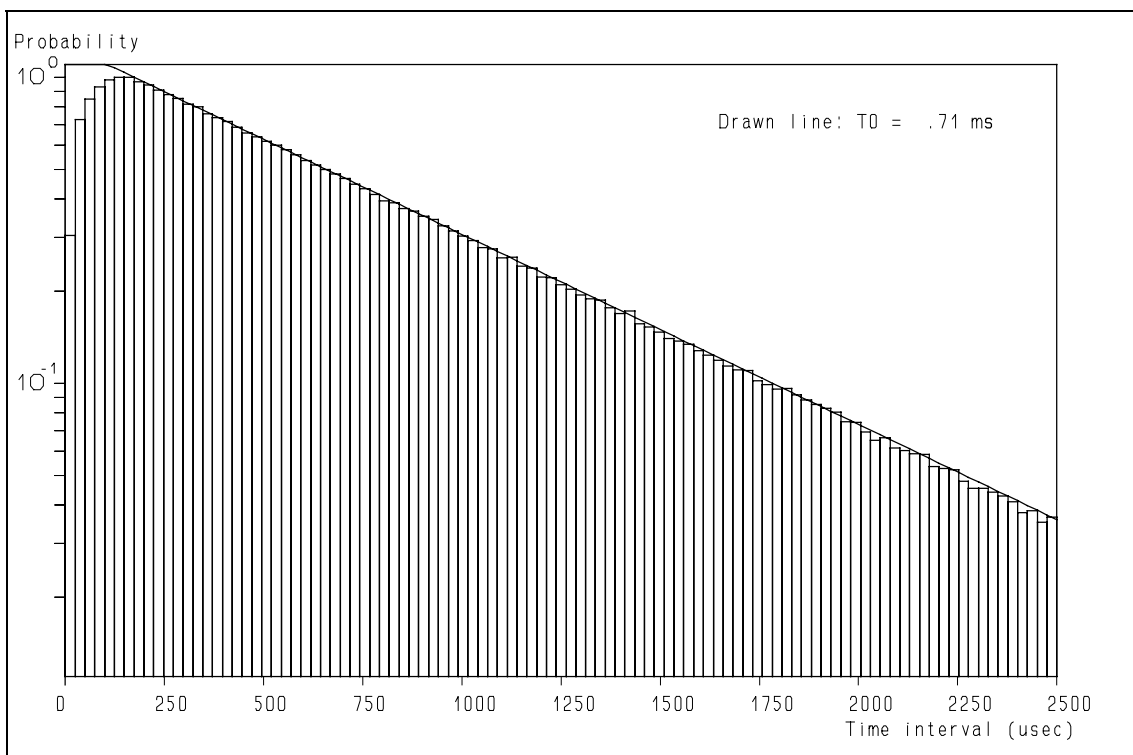


**Figure 4.14:** Uncertainties in the arrival time estimators give rise to a convex shape at short time intervals.

#### 4. Preliminary Diagnostic Testing of Experimental Data-Sets

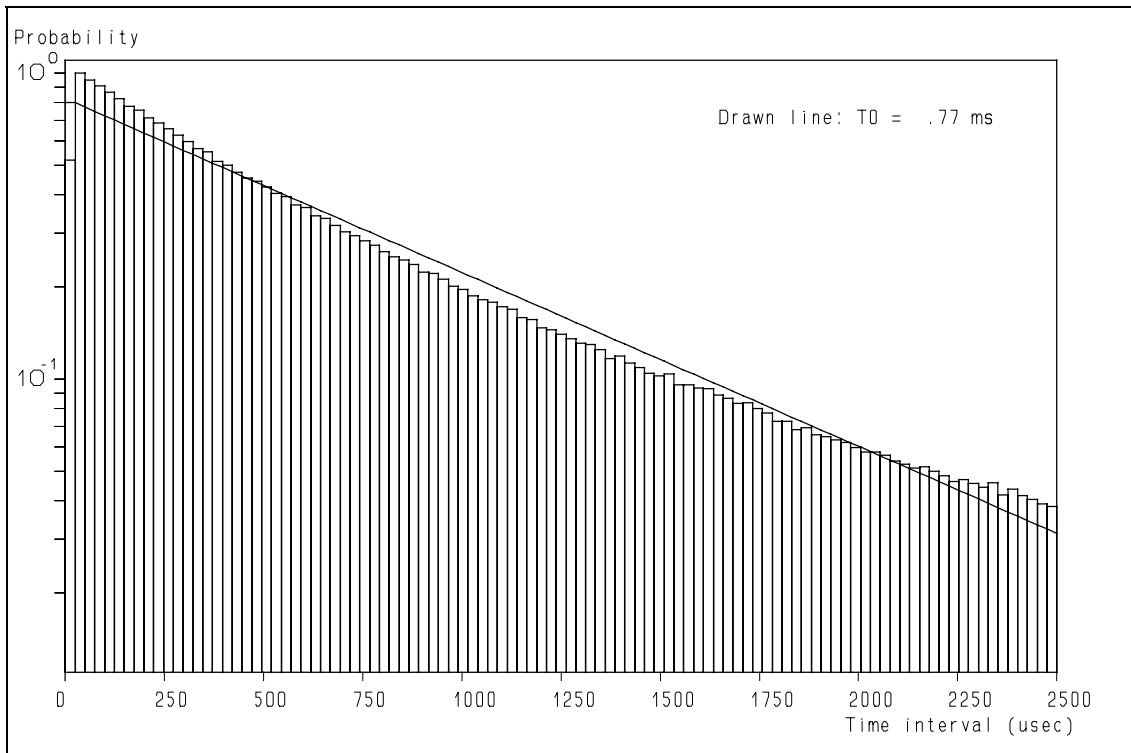


**Figure 4.15:** A turbulence intensity of 30 % in combination with 1-D velocity bias creates a slightly concave shape of the time interval distribution.

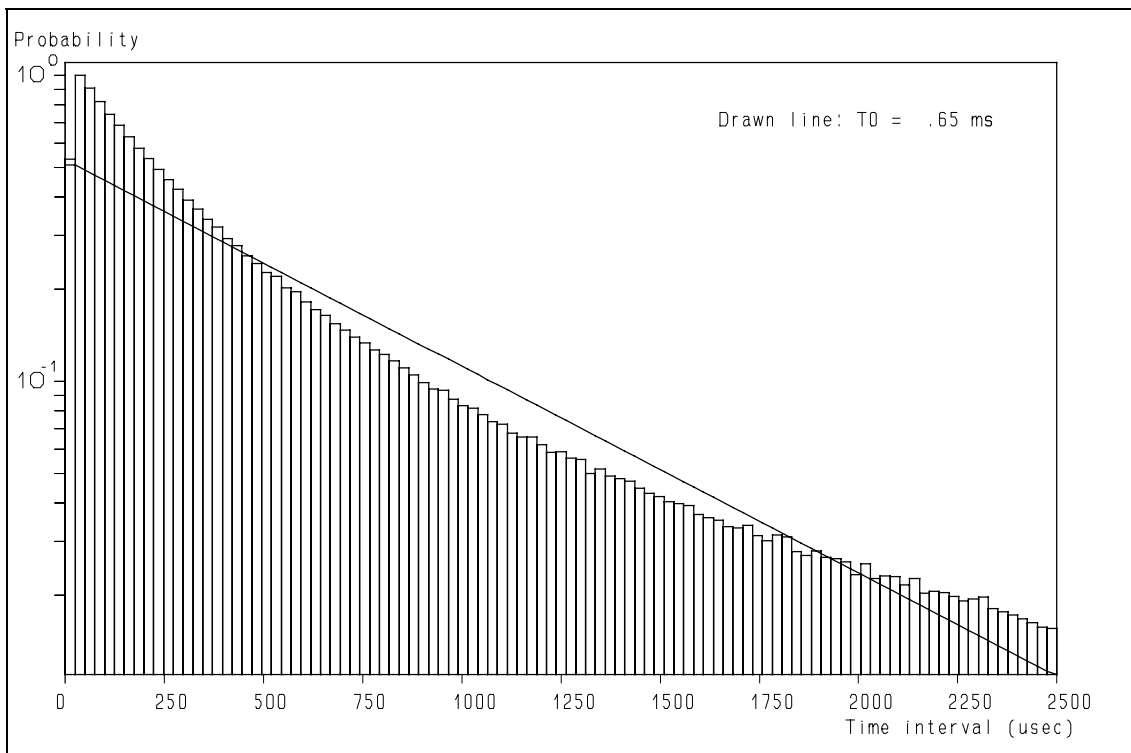


**Figure 4.16:** A turbulence intensity of 100% and up creates a strong concave shape of the time interval distribution.

*Retrieval of turbulence and turbulence properties from LDA data with noise*

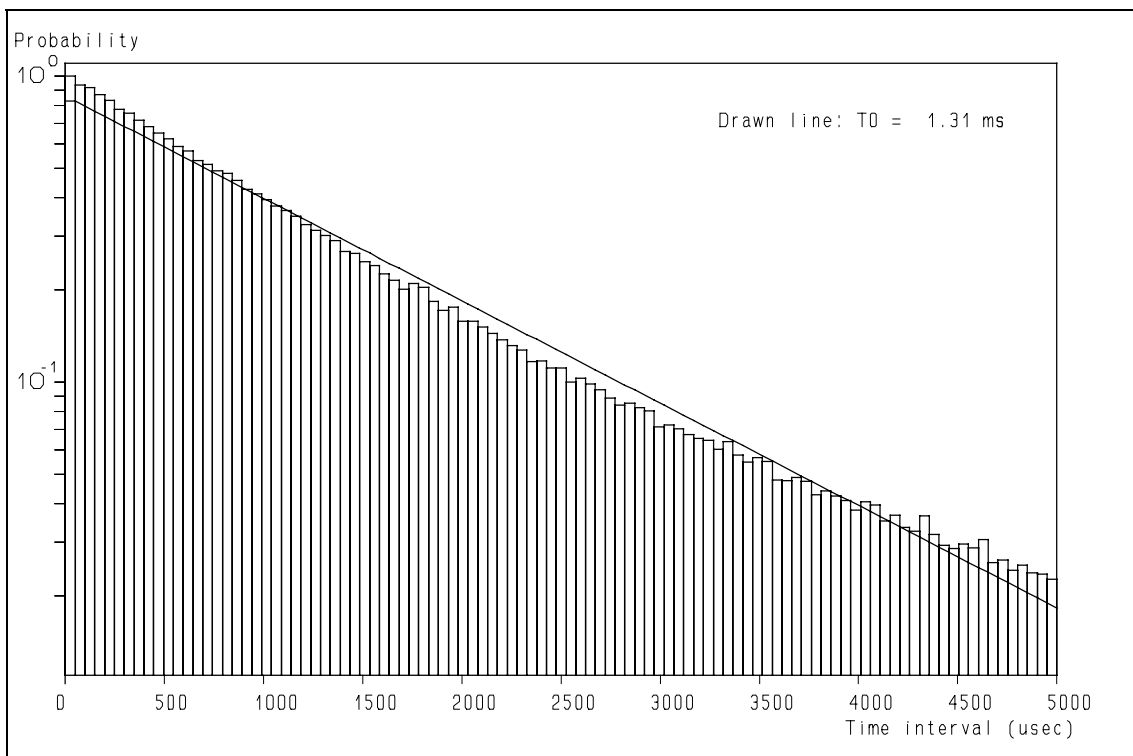


**Figure 4.17:** The time interval distribution of mixing fluids. The concentrations of the tracer particles differs by a factor of 4, 50 - 50 ratio of the fluids.

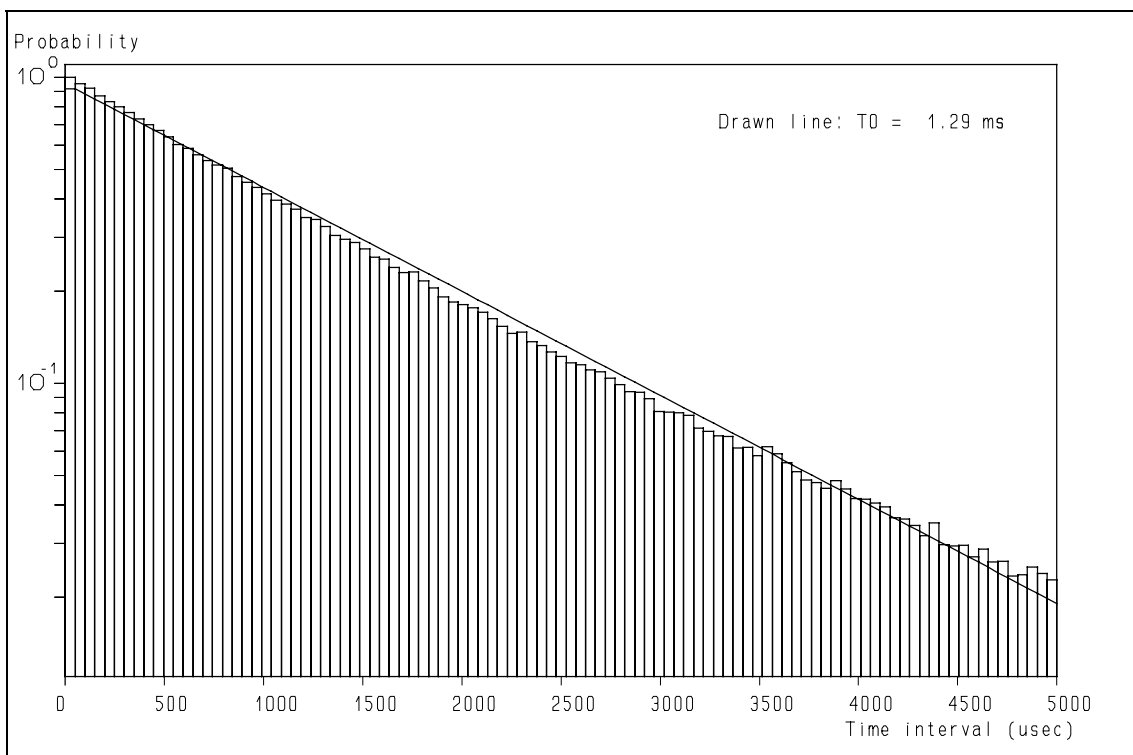


**Figure 4.18:** The time interval distribution of mixing fluids. The concentration of the tracer particles differs by a factor 2, 50 - 50 ratio of the two fluids.

#### 4. Preliminary Diagnostic Testing of Experimental Data-Sets

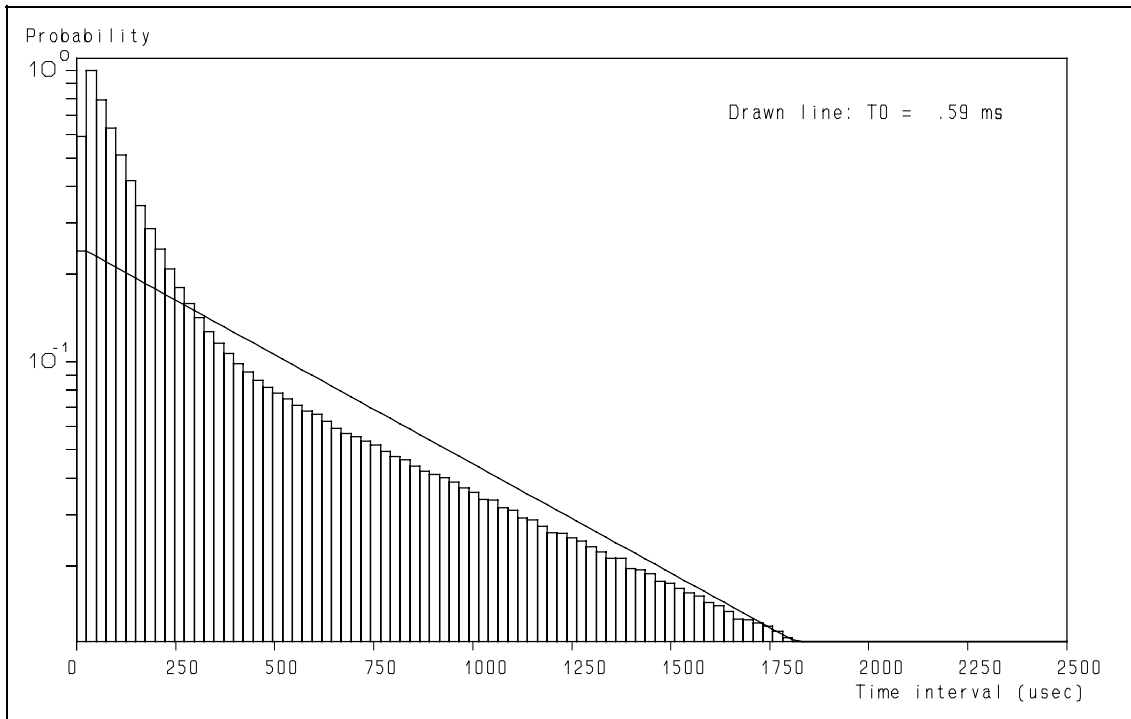


**Figure 4.19:** Multiple validation of the same Doppler signal leads to a time interval distribution with a double  $t_0$  structure: the transit time and the interval time.

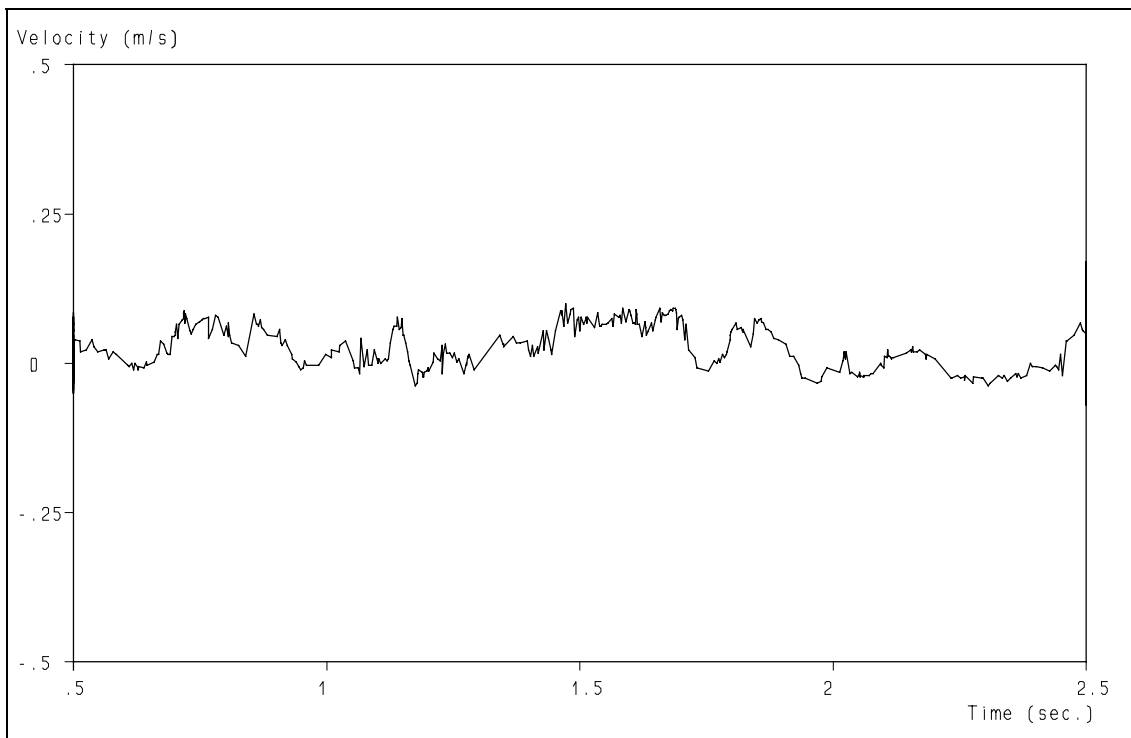


**Figure 4.20:** Velocity fluctuations as function of time, with the settings of the Doppler signal detection and validation scheme such that multiple validation of the same Doppler signal is avoided.

*Retrieval of turbulence and turbulence properties from LDA data with noise*

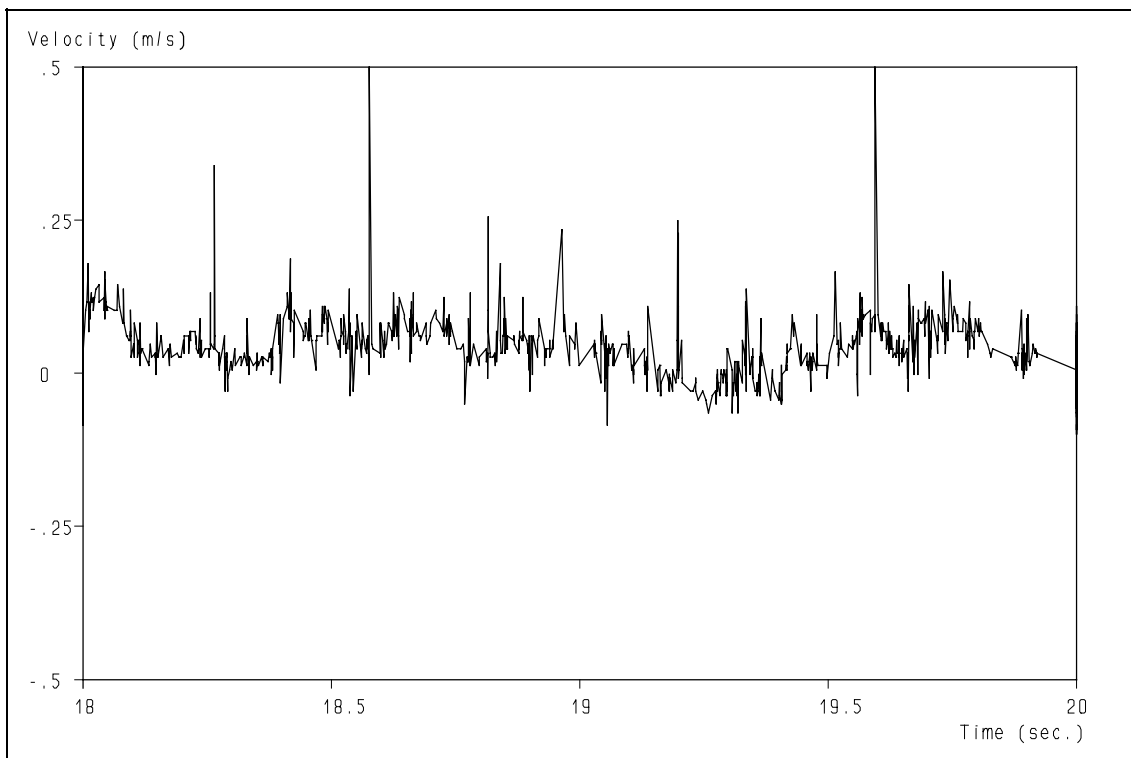


**Figure 4.21:** Velocity fluctuations as a function of time, with the settings of the Doppler signal detection and validation scheme such that multiple validation can occur.

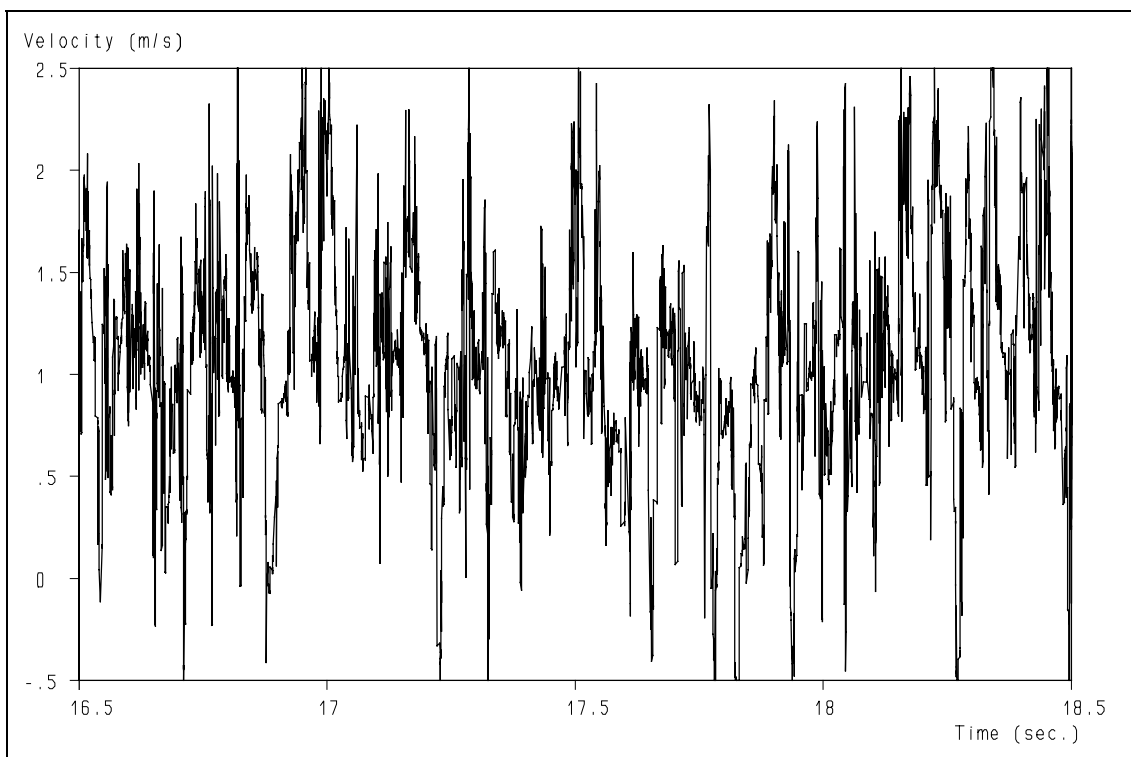


**Figure 4.22:** Other processors show excursions too when multiple validations occurs.

#### 4. Preliminary Diagnostic Testing of Experimental Data-Sets

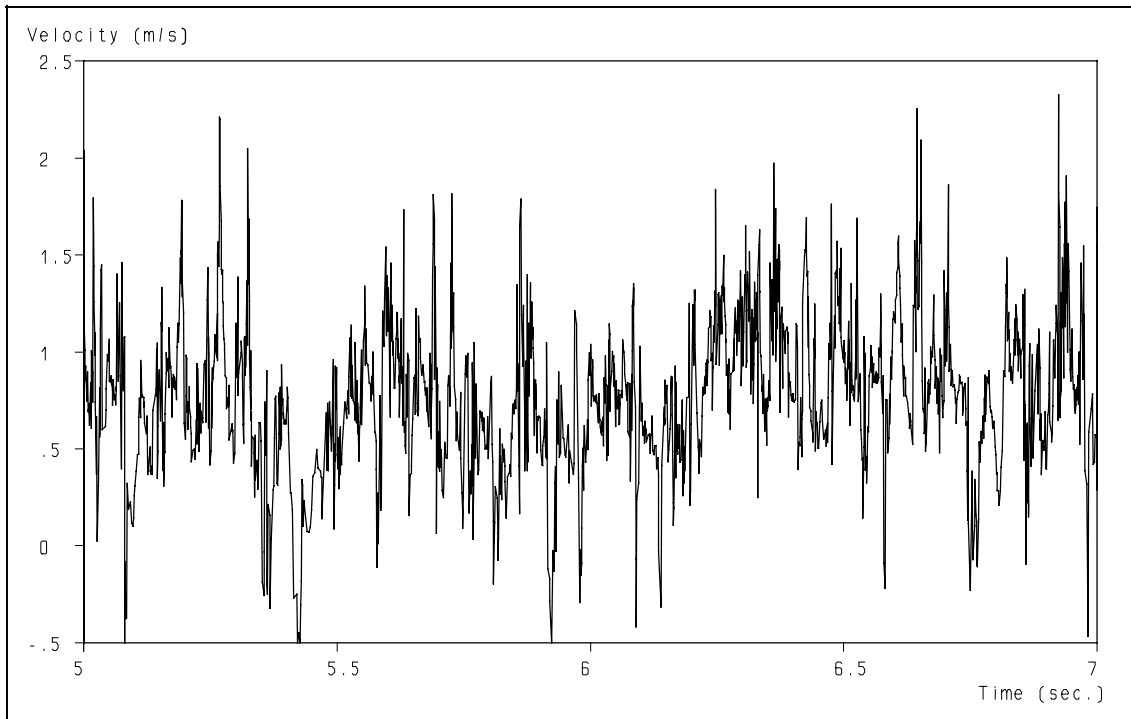


**Figure 4.23:** The behaviour improves clearly when the settings for the Doppler signal detection and validation scheme are adjusted in such a way that multiple validation cannot occur. Compare with fig. 4.22.

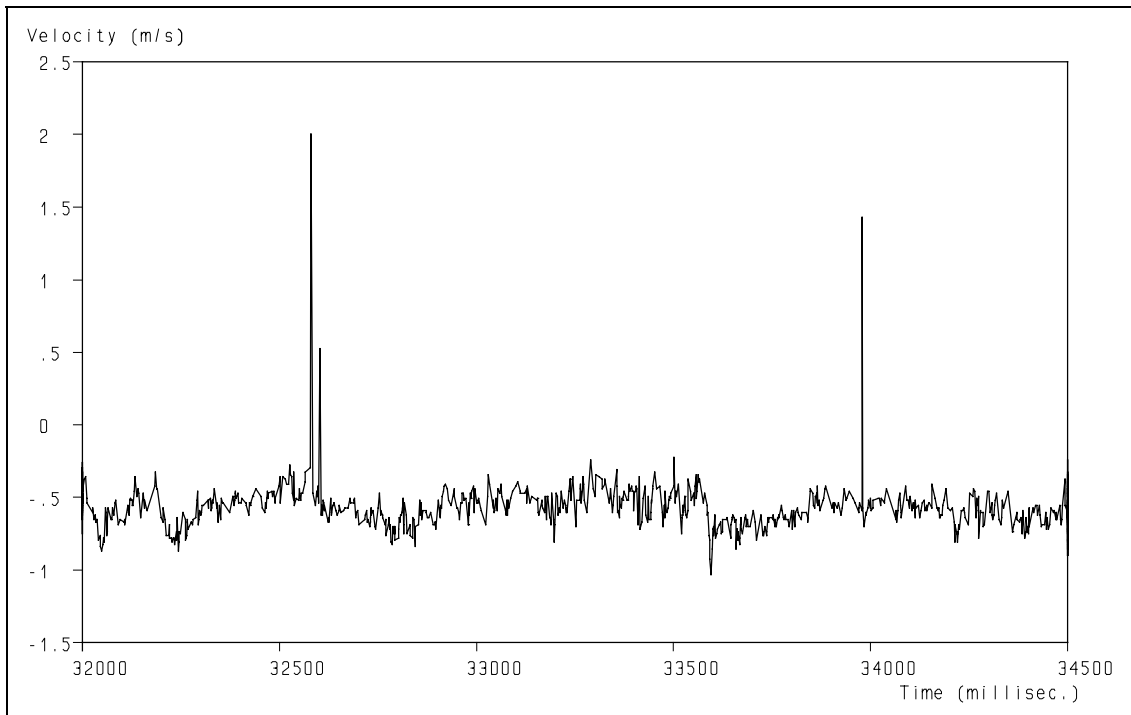


**Figure 4.24:** Example of the raw velocity trace, which contains a few excursions, which indicate erroneous behaviour.

*Retrieval of turbulence and turbulence properties from LDA data with noise*

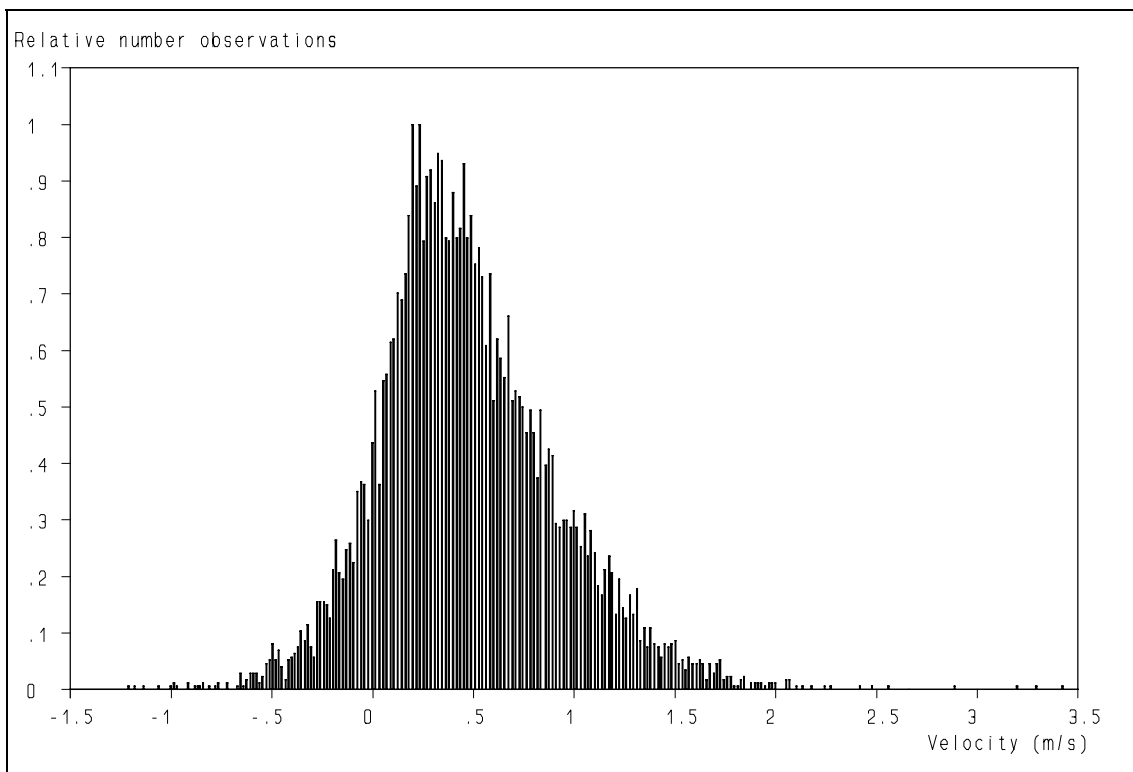


**Figure 4.25:** An example of a velocity probability distribution.

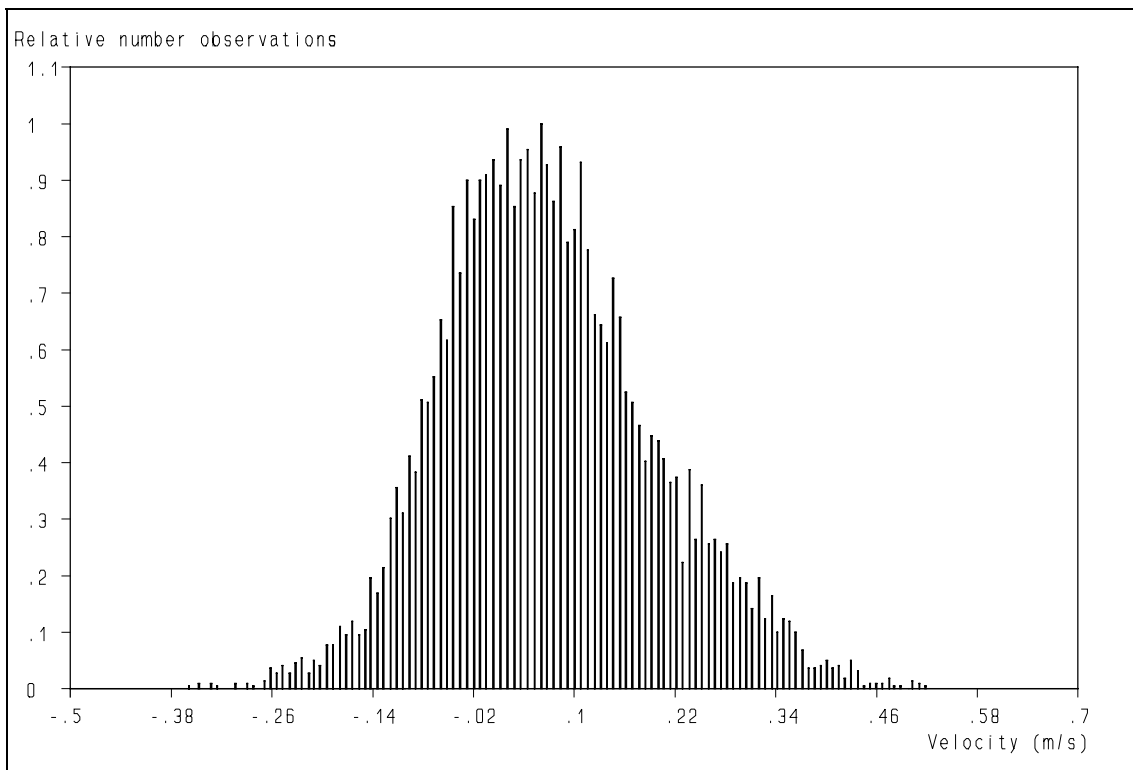


**Figure 4.26:** An example of a velocity probability distribution with a "comb-like" structure.

#### 4. Preliminary Diagnostic Testing of Experimental Data-Sets

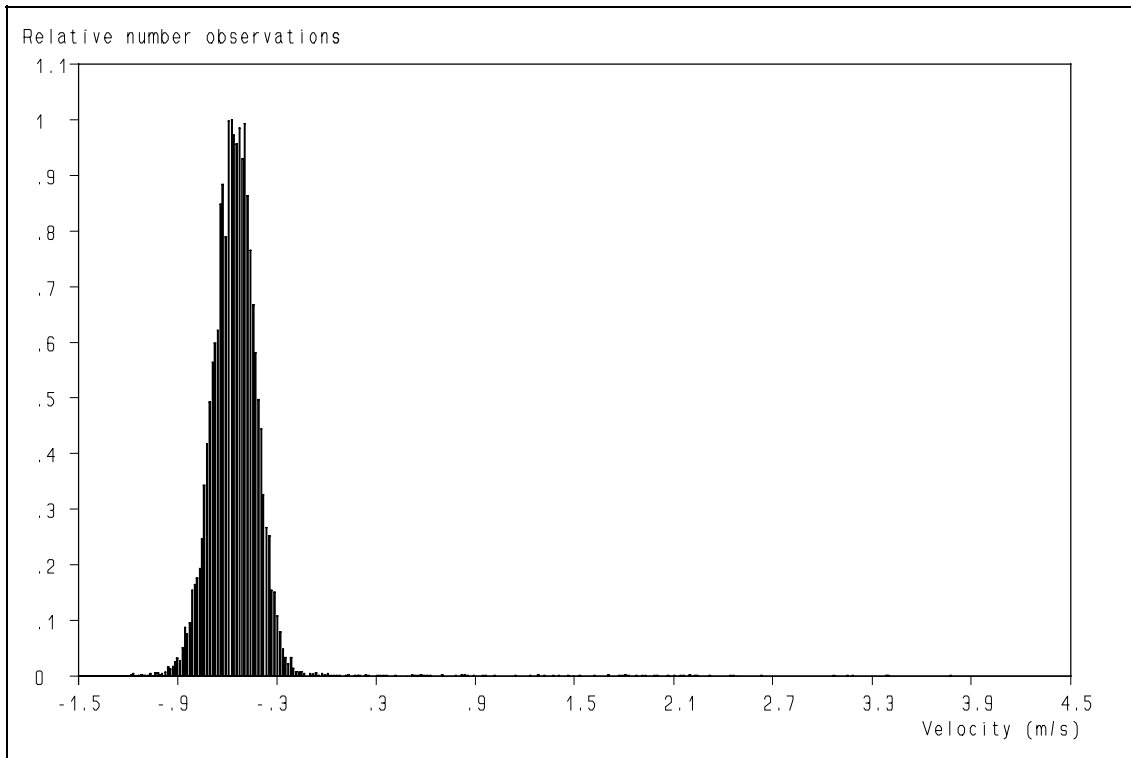


**Figure 4.27:** An example of a velocity probability distribution with a small number of observations at elevated velocities.

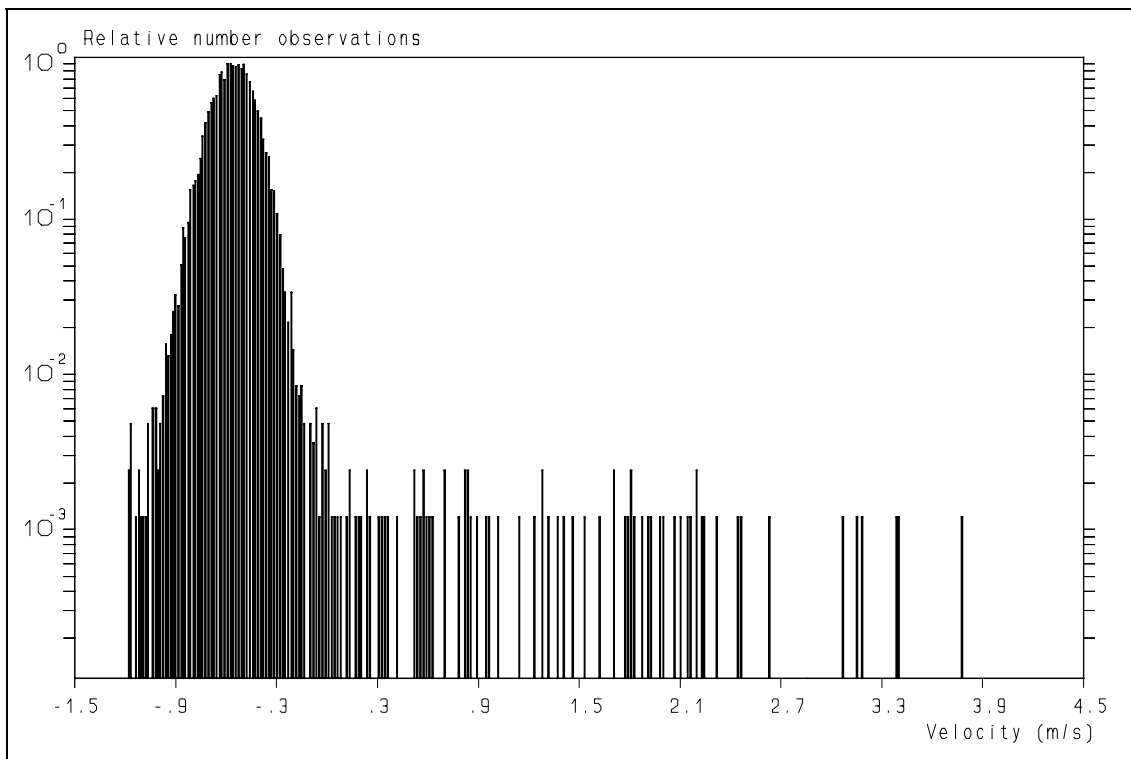


**Figure 4.28:** The same velocity probability distribution as shown in fig. 4.27, but the vertical axis has a logarithmic scale now.

*Retrieval of turbulence and turbulence properties from LDA data with noise*

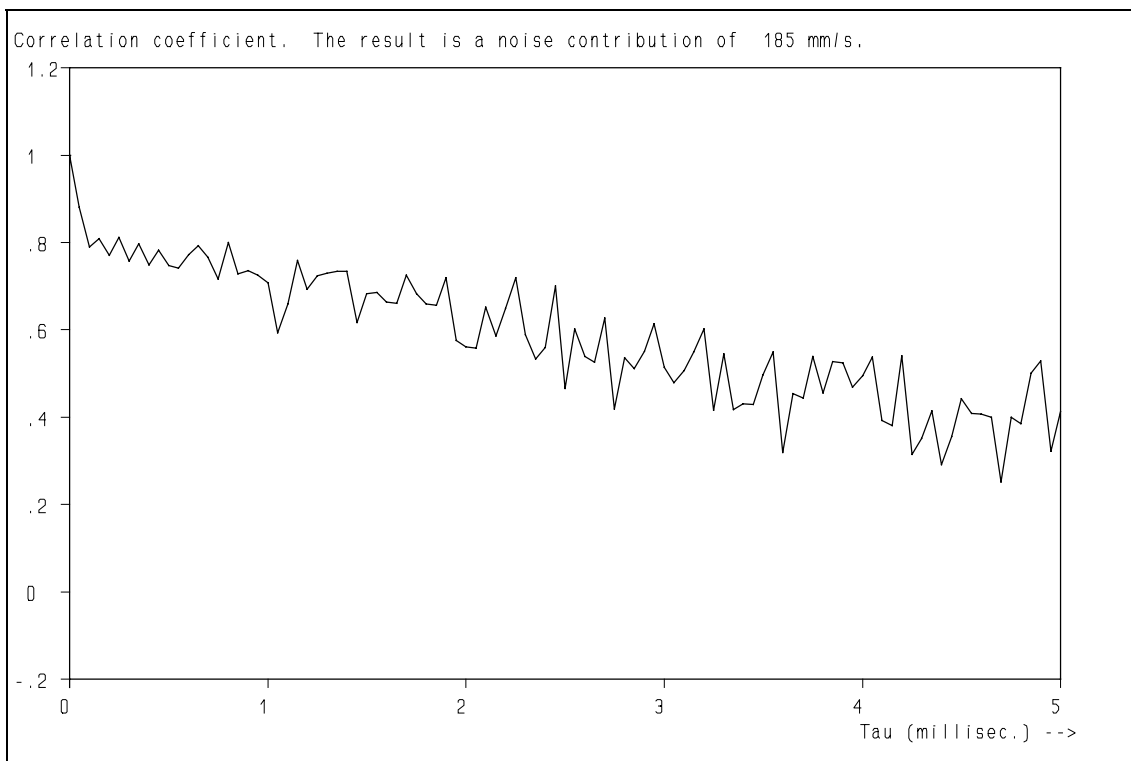


**Figure 4.29:** The auto correlation function with Local Normalisation when the data are OK.

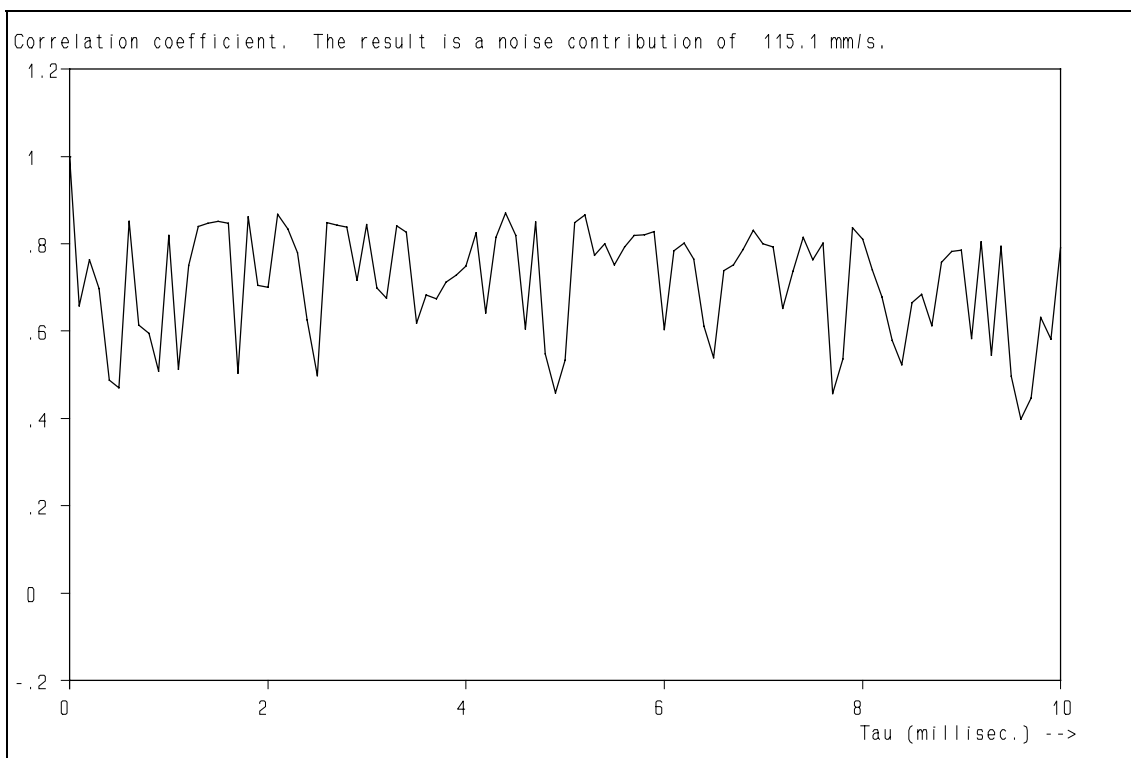


**Figure 4.30:** The auto correlation function when multiple validation occurs. Note the high variance for all values of  $\tau$ . Compare with fig. 4.29.

#### 4. Preliminary Diagnostic Testing of Experimental Data-Sets

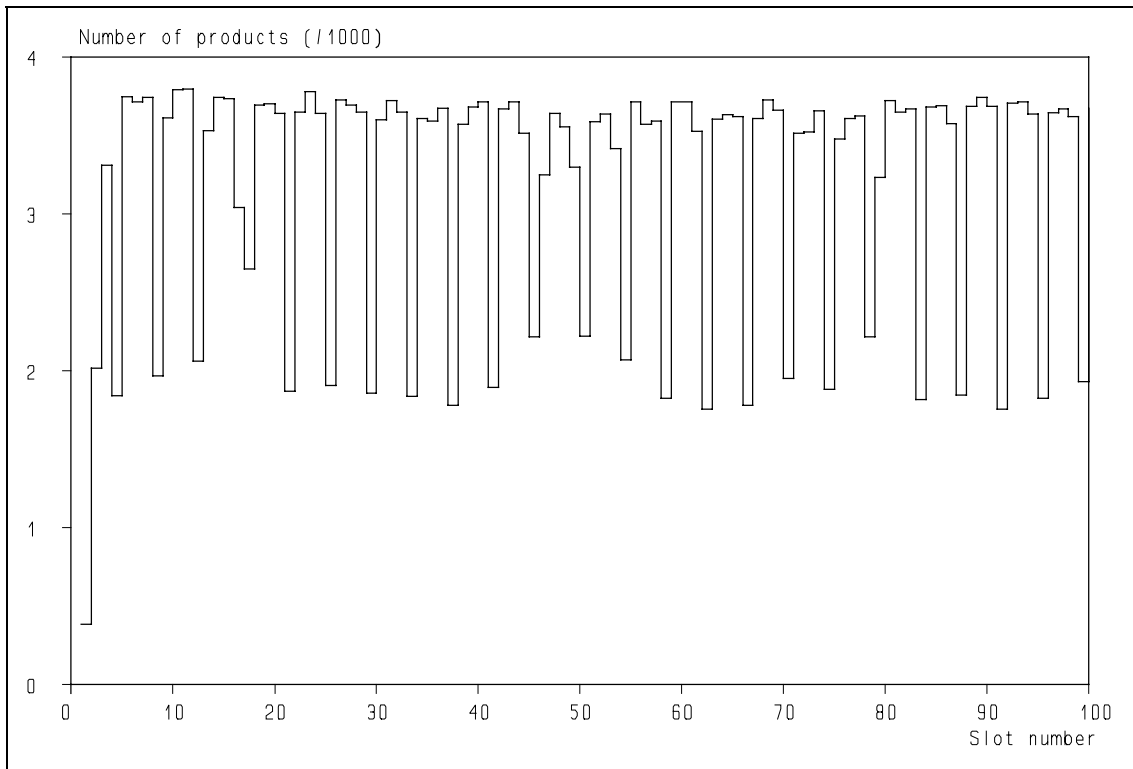


**Figure 4.31:** Deviations of the number of products from the average can be used for diagnostics.

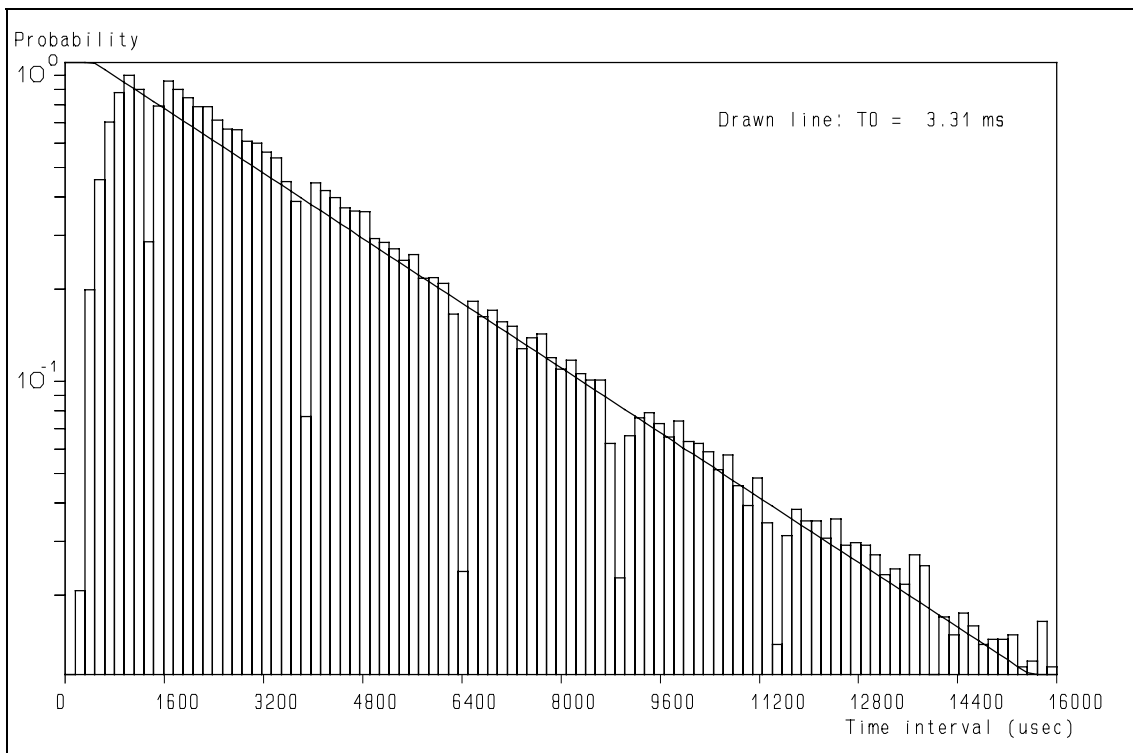


**Figure 4.32:** Time interval distribution which shows a lower number of observations for the short time intervals and round-off errors in the data-file. Compare with fig. 4.31.

# Chapter 5

## Application of the Wavelet Transform to Laser-Doppler Signal Processors

*If we wait until we've satisfied  
all the uncertainties,  
it may be too late.*  
Lee Iacocca

### 5.1 Introduction.

An essential step in the data-processing of signals from a Laser-Doppler Anemometer (LDA) is the estimation of the frequency of the Doppler signal, which is a direct estimate for the velocity of the tracer particle in the measurement volume. Many different techniques for the estimation of the frequency of the Doppler signal have been realised, such as frequency to voltage converters, counters, Fourier Transformation (FT) processors, correlation based processors, etc. (ref. 25, 53, 57, 81 - 86). Every technique has its advantages and disadvantages, which we will not summarize here. An essential problem that every processor has to deal with is the noise, accompanying the Doppler signal as has been discussed in Chapter 3. This causes an error in the estimation of the frequency, which translates into an error in the velocity estimation (ref. 63). Further processing of the data to e.g. a turbulence power spectrum leads to a "noise floor" which obscures the study of the small eddies, which e.g. are responsible for the dissipation of the turbulent kinetic energy and the mixing in chemical engineering applications. Reconstruction of the turbulent velocity fluctuations is also hampered by this unavoidable problem (ref. 87). Of course, an LDA system could be optimized in order to reduce the noise contribution, but to the best of our knowledge, this optimisation has not yet been completed and further extension is possible.

An additional aspect that is easily overlooked, is that for the retrieval of turbulence properties not only the estimation of the *frequency* needs to be optimised, but also the *moment in time* at which the tracer particle passes the centre of the measurement volume, the arrival time. An error in arrival time leads to an additional error in the velocity estimation:

- the actual velocity at the designated time will differ from the estimated velocity because of the change in velocity due to turbulence and
- a part of the Doppler signal is either ignored or replaced by noise<sup>1</sup>.

The optimum processing of LDA signals should therefore include an optimal estimation of both the frequency of the Doppler signal *and* its arrival time. Optimisation of the transmission & receiving optics and the electronics for detection & amplification of the Doppler signal is essential in order to reduce the noise to the Doppler signals as much as possible, but it is impossible to eliminate it completely. The question which remains is what kind of *processing* of the Doppler signal will enable the (close to)

---

<sup>1</sup> This effect can be understood by looking at fig. 5.4 and 5.5. The duration of the Doppler signal is approximately 1500  $\mu\text{sec}$  as is clear from fig. 5.4. The arrival time of the actual Doppler signal is estimated at approximately 1250  $\mu\text{sec}$ , as can be seen in fig. 5.5. When the signal of fig. 5.5 is used from 500 to 2000  $\mu\text{sec}$ , thus over the entire duration of the Doppler signal, the part from 250 to 500  $\mu\text{sec}$  is ignored and effectively replaced by the noise from 1750 to 2000  $\mu\text{sec}$ . To avoid the latter, the signal could be used from 750 to 1750  $\mu\text{sec}$ , ignoring the information from 250 to 750  $\mu\text{sec}$ . In both cases (and anything in between) the error in the frequency estimator is higher than necessary as has been discussed in Chapter 3.

## Retrieval of turbulence and turbulence properties from LDA data with noise

optimum estimation of both the frequency and the arrival time. The Wavelet Transform might be optimum way to do it, at least it is better than the current techniques, as will be shown later.

### 5.2 The Signal-to-Noise Ratio of the Doppler signal revisited.

Up to now, no unique definition on the Signal-to-Noise Ratio (SNR) of Doppler signals has been agreed upon (e.g. ref. 56 and 78 - 80) and those that are proposed are often not consistent. The definition used in ref. 88 for example, defines the SNR as the ratio of the Mean Square (MS) of the Doppler signal over the variance of the noise, the noise taken to be white up to the Nyquist frequency. As a result, the SNR is indeterminate:

- the length of the sampling period is indeterminate and thus the mean square of the signal is indeterminate too and
- the noise bandwidth is equal to the Nyquist frequency, which would mean that by e.g. doubling the sampling frequency (assuming a white noise floor of the same level in both cases), the SNR would go *down* by 3 dB<sup>2</sup> but the choice of the sampling frequency -and thus of the Nyquist frequency- is purely arbitrary.

Mathematically, the problem can be described by the following equations:

$$\int_{-\infty}^{\infty} f_d(t)^2 dt < \infty \quad [5.1]$$

$$\int_{-\infty}^{\infty} n(t)^2 dt = \infty \quad [5.2]$$

in which:

$f_d(t)$	=	Doppler signal	V
$n(t)$	=	noise signal	V
$t$	=	time	s

In order to avoid the SNR to be zero, the integration of the noise signal has to be limited in time, however, assuming "white" noise up to the bandwidth limitation of the noise:

$$\int_{-T/2}^{T/2} n(t)^2 dt = N_f(\omega) \cdot B_w \quad [5.3]$$

in which:

$T$	=	integration time	s
$N_f(\omega)$	=	noise floor in spectrum, proportional to the integration time $T$	V <sup>2</sup> s <sup>2</sup>
$B_w$	=	bandwidth of the noise signal	Hz

The noise *value* can therefore be chosen arbitrarily, whereas the only important parameter is the *noise floor level* in the spectrum, as has been elucidated in Chapter 3.

The confusion is further extended by the fact that *in practice* the noise does not extend up to the Nyquist frequency, because that would result in aliasing. To avoid this, the signal is band-pass filtered,

---

<sup>2</sup> Assuming white noise, the variance of the noise is proportional to the bandwidth. This follows directly from Parseval's theorem, but can also be understood by realising that the integral of the power spectrum is equal to the Mean Square of the signal. This integral is in the case of white noise equal to the product of the noise level and the bandwidth.

## 5. Application of the Wavelet Transform to LDA Signal Processors

which reduces the noise variance by reducing its bandwidth. How should these practical conditions be translated into this (or any other) definition of the SNR?

In several papers the results of a processor or processing technique are compared with the Cramer-Rao bound. Regarding the problems mentioned above, this seems already questionable, but the problem is further enhanced by the fact that the Cramer-Rao bound assumes that the noise contributions to the individual samples (in time) are *uncorrelated*. However, the application of band-pass filters introduces severe correlation into the noise signal because such filters have a wide impulse response in time domain (ref. 60, 70, 89 - 92). The correlation, introduced by a band-pass filter is presented in fig. 5.1. It shows the auto correlation function of band-pass filtered, initially uncorrelated, white noise, obtained with a Monte-Carlo simulation. As is clear, the assumption of an uncorrelated noise contribution is no longer valid. Therefore, it would be better to compare different processing techniques by using simulated Doppler signals with *realistic* properties. Such signals should thus be accompanied by narrow-band (filtered) noise, using the procedure described in Chapter 2. Although the parameters chosen would still be arbitrary, direct comparison under more realistic conditions would reveal the behaviour of different processing techniques better. For example, the use of counters is virtually impossible when wide band noise is present, but after band-pass filtering good results can be obtained. Therefore we have used such a simulation in this thesis to determine whether the Wavelet Transform (WT) would improve the processing of Doppler signals compared to e.g. Fourier Transform processing.

As we have seen in Chapter 3 on the noise contributions, the relative noise level is a function of the position in the Doppler signal: at the centre it is higher than at the boundaries, yet it showed that the use of only the central part of the Doppler signal gave rise to frequency estimators with a higher variance than those based on the entire Doppler signal. However, there must be a limit to this, because the use of longer time windows will eventually increase the amount of noise more than the amount of information, as is illustrated by eq. [5.3], so the variance must reach a minimum for the optimum time interval length. However, the weaker parts of the Doppler signal should contribute less to the frequency estimator, as the information is more corrupted by the noise. Therefore a *weighted* estimator, which takes the local strength of the Doppler signal into account, would be attractive. This is precisely what the Wavelet Transform does. A short description of the technique, focused on this specific application, will be outlined in the next section.

### 5.3 Wavelet Transformation.

Fourier Transformation is a well-known mathematical technique (e.g. ref. 89 - 91) which is a one-to-one projection from time into frequency domain. The frequency space is spanned up from sine- and cosine functions which act as independent vectors in the frequency space. Although it is possible to truncate the transformation window (in time domain), all points within the transformation window are equally important. This has two major consequences for the application of the FT for the estimation of the frequency of the Doppler signal: the noisier<sup>3</sup> parts of the Doppler signal contribute equally to the frequency estimator as the better parts (in the centre) and the technique is not very well suited for the positioning of signals in time as the amplitude spectrum does not depend at all on the position of the ideal Doppler signal in time. This is different with Wavelet Transforms.

There is a certain similarity between the FT and the WT. In the WT the basic vectors (functions) are time-limited functions with a self similarity. This means that all the functions can be obtained from a single function by scaling (expansion/compression in time) and shifting (in time). Many different functions can be chosen and a more detailed description can be found in ref. 93 and 94. It is important

---

<sup>3</sup> This means the part where the relative noise level is higher than in the centre of the Doppler signal.

## Retrieval of turbulence and turbulence properties from LDA data with noise

to realise that the WT is a transformation to *two independent variables*, in this case time and frequency. We will use as basic vector functions the Gaussian enveloped cosine and sine functions:

$$x_1(t) = \sqrt{a} e^{-\frac{1}{2}\left(\frac{at'}{\sigma_t}\right)^2} \cos[\omega_0(at')] \quad [5.4]$$

$$x_2(t) = \sqrt{a} e^{-\frac{1}{2}\left(\frac{at'}{\sigma_t}\right)^2} \sin[\omega_0(at')] \quad [5.5]$$

in which:

$a$  = scaling factor

$t'$  =  $t - t_s$  s

$t$  = time s

$t_s$  = shift in time s

$\sigma_t$  = sigma of Gaussian envelope s

$\omega_0$  = radial frequency rad/s

The factor  $\sqrt{a}$  is added for normalisation reasons. The WT can now be performed with the scaling factor (which is the equivalent of frequency) and the time shift as variables. The values of these variables which fit the signal best yield the estimate for the frequency and the arrival time of the Doppler signal. Intuitively one could expect that this is the optimum value because the functions used in the WT resemble the ideal Doppler signal better than those in the FT. As a result, these automatically reduce (but not neglect) the influence of the noisier parts of the Doppler signal and the choice of the time window is not critical, as it is with the FT, because the functions are time-limited themselves and the (arrival) time is an *independent* variable. Because of the latter, it is likely that the WT will give an estimate for the arrival time which is less susceptible to noise. This WT output is illustrated in fig. 5.2, which shows the 3-dimensional result, obtained from the noisy Doppler signal of fig. 5.3.

The question which remains is how the WT compares to e.g. FT based processors. To answer that question a numerical simulation has been used, which will be discussed in the next section.

### 5.4 Numerical simulation.

In order to study the influence of the processing technique on the accuracy of the frequency -and thus velocity- estimate, a numerical simulation has been performed. For each simulation 10000 ideal Doppler signals of known frequency, as shown in fig. 5.4, have been generated and a white, Gaussian distributed noise contribution has been added. The thus obtained signal is fed through a band-pass filter (Butterworth 8<sup>th</sup> order high and low-pass), resulting in "actual" Doppler signals as shown in fig. 5.5. Note that the apparent position of the Doppler signal is shifted by approximately 250  $\mu$ s, which is nothing but an artefact from the noise contribution. Using these signals, the frequency is estimated using the FT (using the central part of the actual Doppler signal) and the WT. The distribution of frequencies is calculated from these sets of 10000 Doppler signals. The estimation of the frequency using the FT is obtained by curve-fitting a parabola through the highest three points of the amplitude spectrum.

To estimate the arrival time, the maximum of the envelope of the Doppler signal is estimated using a fit to a parabola. In order to get three points for the fit, the absolute value of the Doppler signal is calculated, the maximum value of the signal is selected and this is used with the closest maxima to the left and right as input for the fit to a parabola (see fig. 5.6). The maximum value of the parabola is taken as the arrival time. Note that the fit does not always improve the estimation of the arrival time compared to just taking the maximum value of the same signal as can be seen in fig. 5.6 (the arrival time is 2.5 ms).

## 5. Application of the Wavelet Transform to LDA Signal Processors

The optimum (maximum) value of the Wavelet Transform will be reached when the best estimates for the frequency and the arrival time are used. The whole area of interest could be scanned for the optimum value but that would take far too much time (see fig. 5.2) for the calculations. To find the maximum value of the "wavelet-mountain", the fit to a parabola is used once more, but this time for a function of two independent variables. As a starting point, the estimated arrival time using a fit to a parabola and the maximum value of the filtered spectrum (with a fit to a parabola to interpolate between subsequent points) is used with two additional points for both the frequency- and the time-axis (1.1 times and 0.9 times the initial estimate). The fit is applied alternating for the frequency- and the time-axis. The next fit gives a new and better value closer to the top. The distance between the new fit and the previous fit is taken as the error. When both the errors of frequency and arrival time drop below a certain value, it is assumed that the maximum value has been found with sufficient accuracy.

### 5.5 Results and discussion.

In fig. 5.7 the probability distributions of the frequency estimates of the two different techniques are shown. One is obtained by the use of the FT on the central part of the Doppler signal (with known position in time) and the other by using the WT. The variance of the WT is clearly lower than that of the FT, in this case the error of the FT is approximately 100 % higher than that of the WT. The use of the known position in time of the Doppler signal reduced the variance of the FT technique. However, the use of only the central part increased it. Thus there are different influences which partly cancel each other effects: the use of the central part, and thus a shorter duration, virtually eliminates the chance of just looking at noisy parts, but, on the other hand, neglects the information contained in the weaker parts of the signal. But in all the cases that we have explored, the WT gave the lowest variance, although the reduction was relatively small ( $\approx 30\%$ ) when the Doppler signals had a high SNR and the FT was used over the full Doppler signal. The major advantage of the WT thus occurs when the SNR is lower. This is an attractive property in practice, as this means that the "weaker" Doppler signals do not as easily lead to extreme values for the estimated velocity as sometimes happens with common processors (see Chapter 4). Note that in the subsequent data-processing the velocity estimators are regarded as equally important. It would be better to record the SNR of the Doppler signal too in order to take the noise contribution to each velocity estimator into account! The advantages of the WT are also illustrated by the arrival time estimation.

The estimation of the arrival time using the maximum of the envelope as described above resulted in the probability distribution, shown in fig. 5.8. The WT resulted in the histogram, shown in fig. 5.9 and the improvement is clear. For ease of comparison both distributions are shown in fig. 5.10. This indicates that with most processors the estimation of the arrival time is not very accurate. This corresponds with measured time interval distributions. These often show a rounding in the vicinity of  $\Delta t = 0$ , as can be seen -amongst other deviations from the ideal distribution- in fig. 5.11 (see Chapter 4). A Monte Carlo simulation of errors in the arrival time has shown a similar deviation in this distribution as can be seen from fig. 5.12. Improvement of the arrival time estimation will therefore improve the quality of the results of the LDA measurements. The WT shows to be very promising in this respect.

### 5.6 Proposal for a design of a Wavelet Transform Processor.

Fourier Transform based processors for Doppler signals have been around for almost 20 years (e.g. ref. 52, 56 and 57). These processors are based on the Fast Fourier Transform (FFT) algorithm, which is available in hardware. Up to this moment there is no equivalent "Fast Wavelet Transform" algorithm, let alone a hardware implementation of it, which would be required for on-line, real time processing of Doppler signals. Off-line processing would require (far) too large storage of the sampled Doppler signals, so this is -at this moment- no real alternative. However, it should be possible - in theory at least- to build a "Quasi-Wavelet Transform processor", using the properties of the Doppler signal.

## Retrieval of turbulence and turbulence properties from LDA data with noise

The Doppler signal  $f_d(t)$  can be described (idealised case without noise) by:

$$f_d(t) = A_0 e^{-\frac{1}{2}\left(\frac{t'}{\sigma_t}\right)^2} \cos(\omega_0 t') \quad [5.6]$$

in which:

$A_0$	= maximum amplitude	V
$t'$	= $t - t_a$	s
$t$	= time	s
$t_a$	= arrival time	s
$\sigma_t$	= sigma of Gaussian envelope	s
$\omega_0$	= radial frequency	rad/s

This is basically the product of a cosine wave with a Gaussian envelope, but it has a close resemblance to the wavelet as described by eq. [5.4]. The only difference is that the Gaussian envelope has a fixed  $\sigma_t$ , whereas in the Wavelet Transform it is coupled to the transformation function. The Fourier Transform of such a Doppler signal has a Gaussian shape as well, the  $\sigma$  of the spectral function is inversely related to the  $\sigma_t$  (ref. 89). The (real part of the) Fourier Transform of this signal is

$$f_d(\omega) = A_0 \int_{-\infty}^{\infty} e^{-\frac{1}{2}\left(\frac{t'}{\sigma_t}\right)^2} \cos(\omega_0 t') \cdot \cos(\omega t') dt' \quad [5.7]$$

However, as the spectral width of the spectrum of a Doppler signal is relatively narrow<sup>4</sup>, the differences between a fixed and coupled  $\sigma_t$  are minor because the frequency range of a Doppler signal is quite limited. Thus the Wavelet Transform of a Doppler signal could, for a certain time shift, be closely approximated by a *windowed Fourier Transform*. This could be achieved by multiplying the integrand of eq. [5.7] with a moving Gaussian window with a fixed  $\sigma_t$ . By varying the time shift of the windowing function, a transformation could be created, which comes close to the Wavelet Transform, as is illustrated in fig. 5.13. The incoming signal from the photodetector, shown in row 1, is used to estimate the  $\sigma_t$  of the Doppler signal. Subsequently, envelope signals with this  $\sigma_t$  are generated with different time shifts as is shown in row 2. The incoming signal of row 1 is multiplied with these envelope functions, resulting in the signals shown in row 3. These signals are Fourier Transformed, resulting in the spectra of row 4, which can be joined to create the Quasi-Wavelet Transform of row 5. Although it is only an approximation, it is a close approximation due to the properties of the Doppler signal. It could be realised by parallel processing of a number of FFT hardware processors. In fig. 5.13 we have shown only 5 parallel channels for the sake of clarity, however, in practice a larger number would probably be required, the exact number will depend on the precise implementation. It should be possible to reduce the amount of superfluous calculations by a clever pre-selection of the time-frequency range which is analyzed (see section 5.4). Although such a processor would not be cheap, the improvement of the estimators for turbulence research would be significant, thus extending the experimental possibilities and increasing the accuracy of the measurements.

---

<sup>4</sup> Loosely speaking is the spectral width  $\Delta\omega/\omega = 1/N$ , in which  $N$  is the number of cycles in the Doppler signal.  $N$  is usually 20 - 40 so the spectral width is relatively narrow.

## *5. Application of the Wavelet Transform to LDA Signal Processors*

### **5.7 Concluding remarks.**

The estimation of frequency and arrival time of the Doppler signals is an essential step in the processing of Laser-Doppler Anemometry. Any further processing of these raw data will take the inaccuracies in the estimates along. Therefore these inaccuracies should be as small as possible.

A numerical simulation has shown that the Wavelet Transform, in which the basic vector functions are Gaussian enveloped sine and cosine functions with a structure similar to the Doppler signal itself, yields an improvement of the estimates of both frequency and arrival time compared to current techniques. It also showed to produce more accurate results with Doppler signals with a low SNR, which reduces the chances of erroneous velocity estimates in the data-set. Application of a processor, based on a Wavelet Transformation would result in a data-set with less variance and would thus increase the amount of detail of the turbulence that can be retrieved from it. Part of this work has been reported at a conference in Lisbon, Portugal (1996, ref. 95), but the concepts for realisation of a processor, based on the Wavelet Transform have only been mentioned there and are not included in the proceedings.

*Retrieval of turbulence and turbulence properties from LDA data with noise*

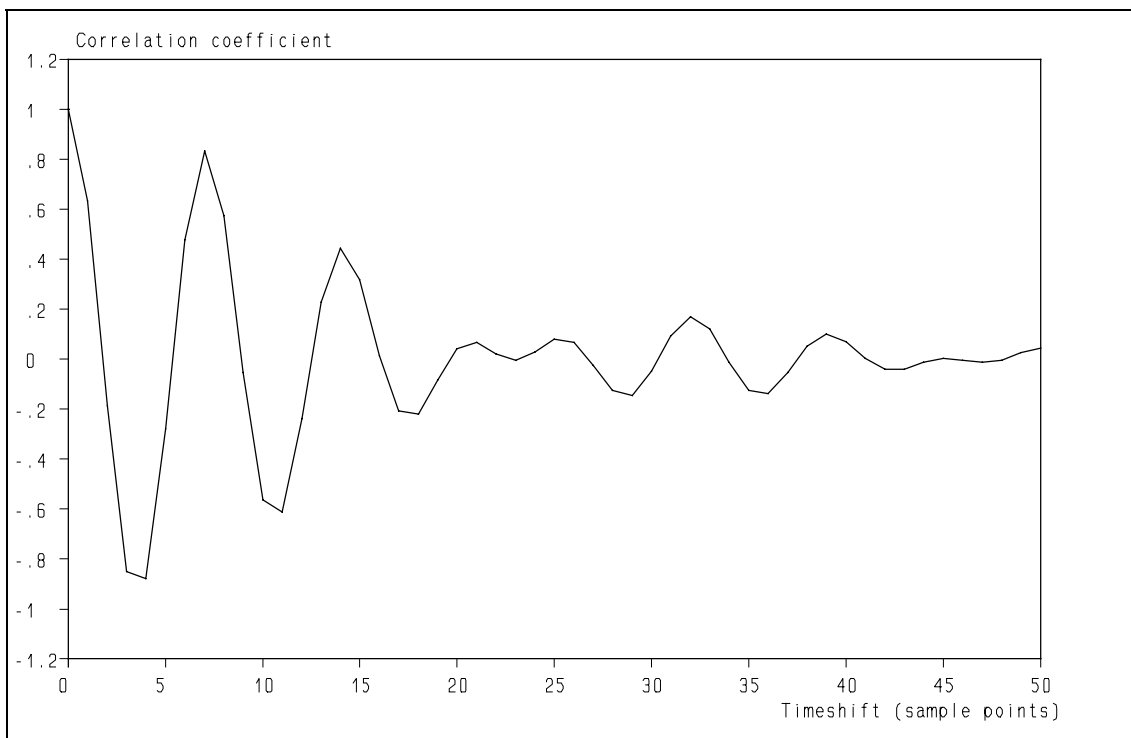


**Figure 5.1:** Auto correlation function of narrow band noise. Bandwidth 0.22 of centre frequency, the Nyquist frequency is 3.6 times the centre frequency.

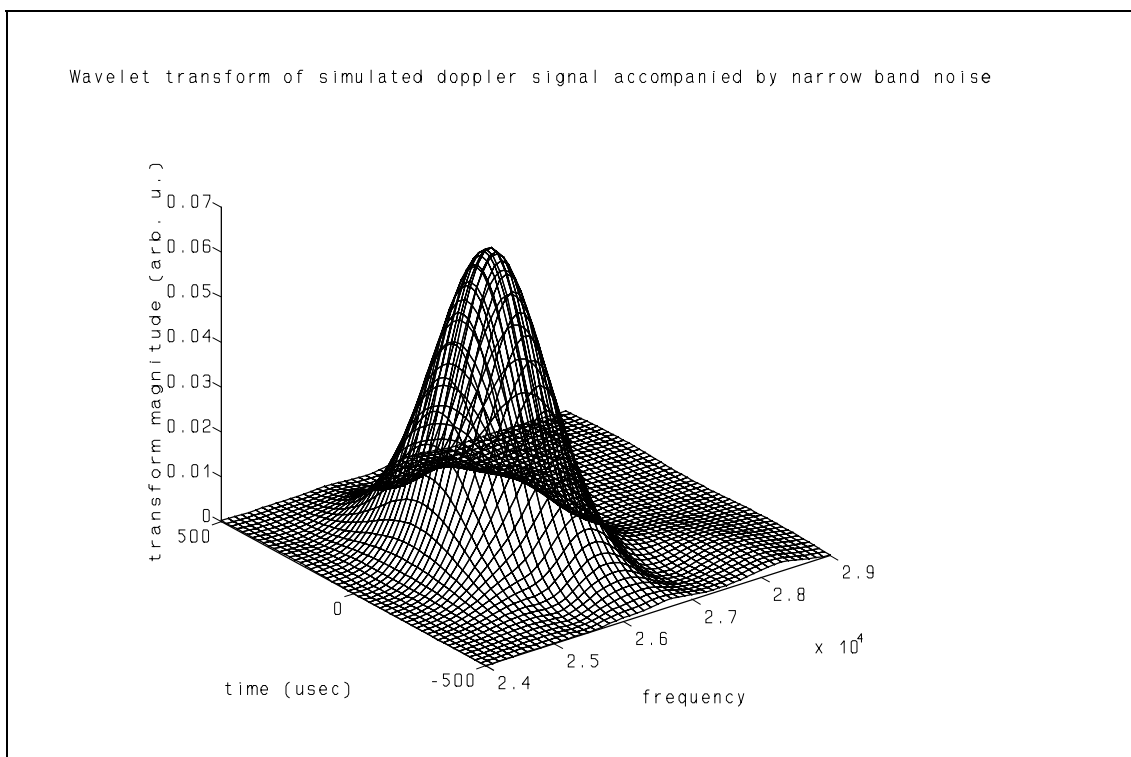


**Figure 5.2:** The 3-D plot of the Wavelet Transform of the noisy Doppler signal of fig. 5.3.

## 5. Application of the Wavelet Transform to LDA Signal Processors

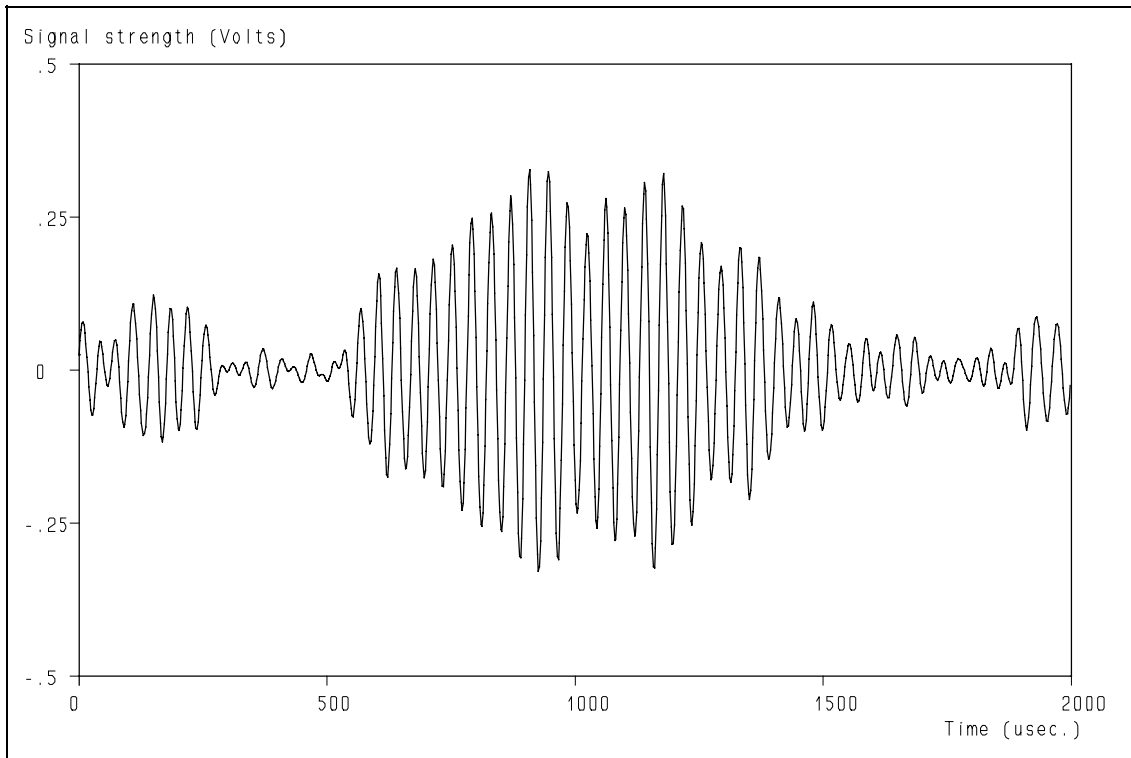


**Figure 5.3:** The Doppler signal which was used for the wavelet transformation of fig. 5.2.

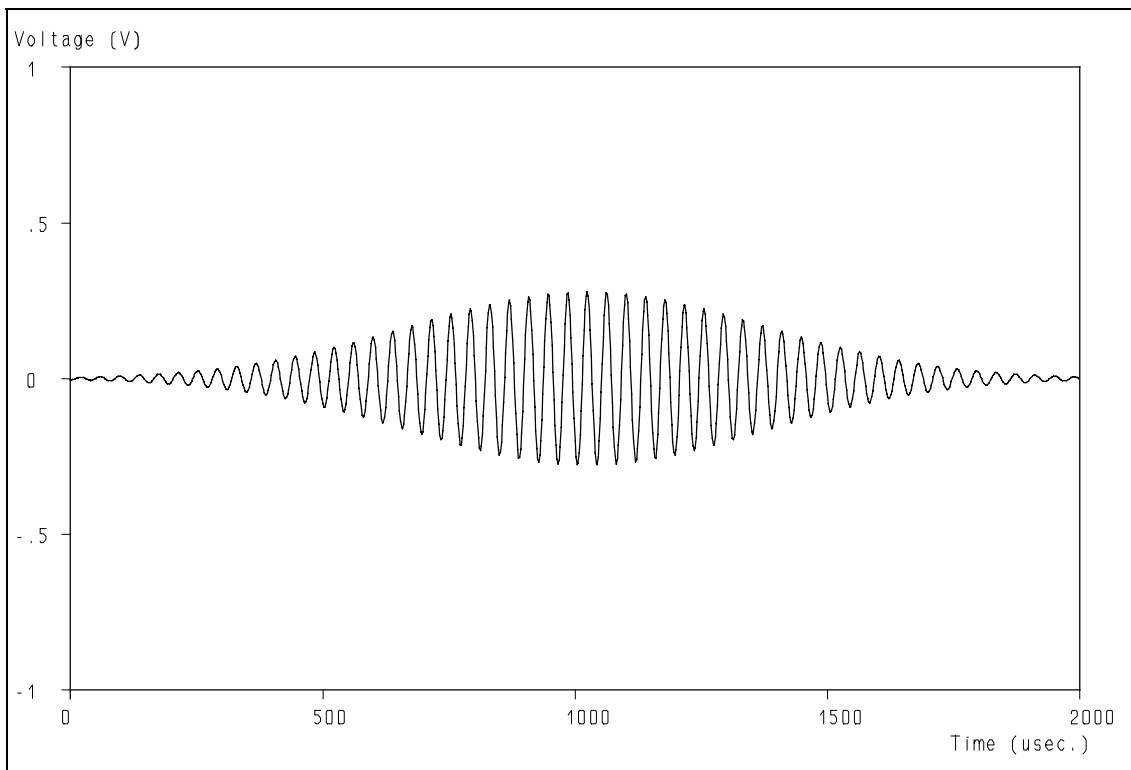


**Figure 5.4:** Doppler signal when no noise is present.

*Retrieval of turbulence and turbulence properties from LDA data with noise*

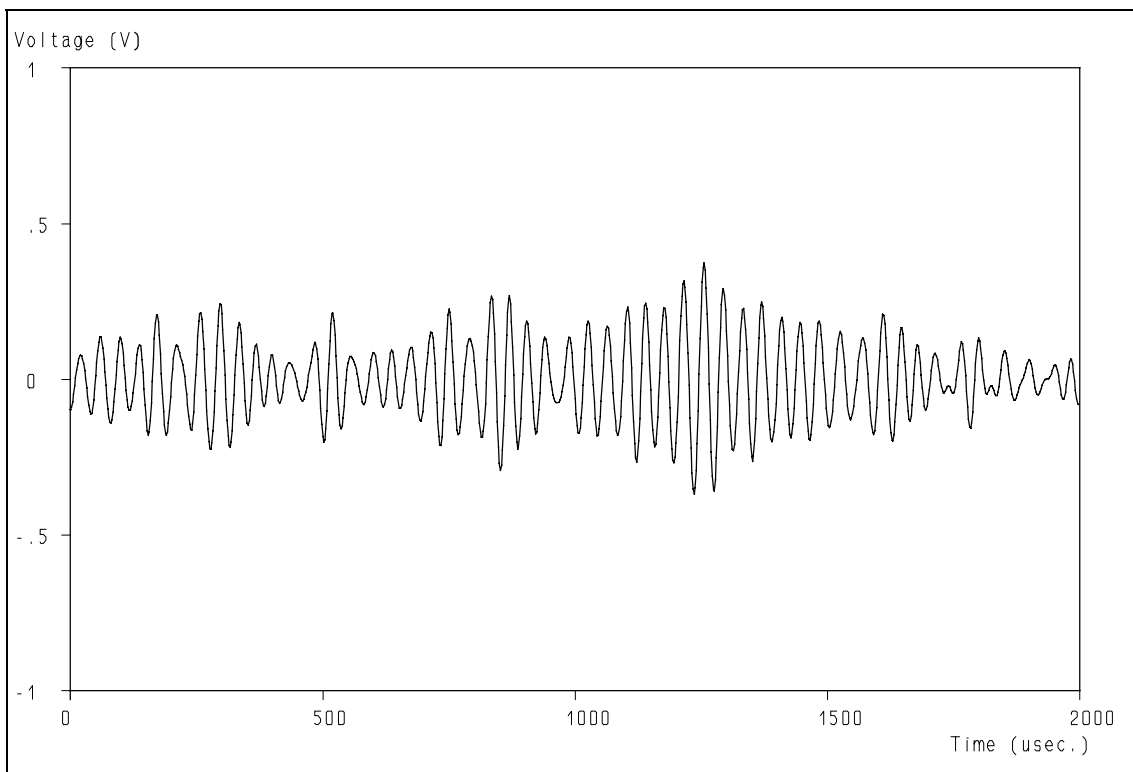


**Figure 5.5:** As figure 5.4, but with narrow band noise added. Note the apparent shift in time.

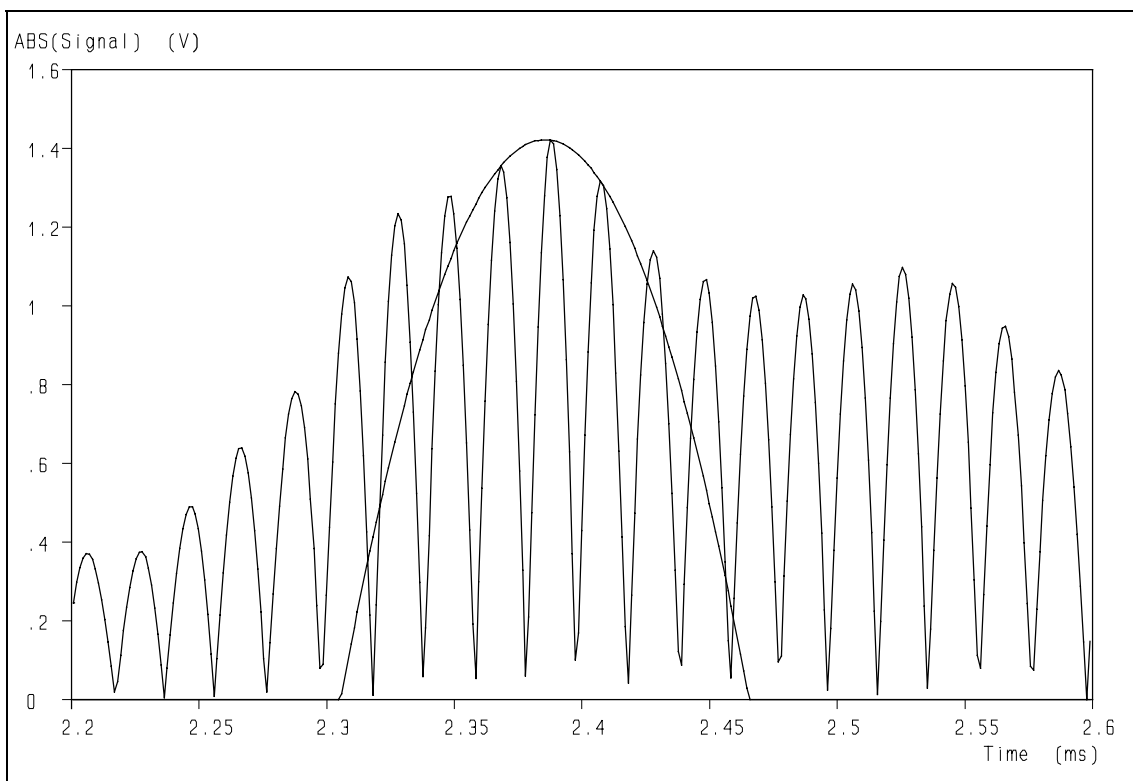


**Figure 5.6:** Enlargement of a part of the rectified Doppler signal with a fit to a parabola.

## 5. Application of the Wavelet Transform to LDA Signal Processors

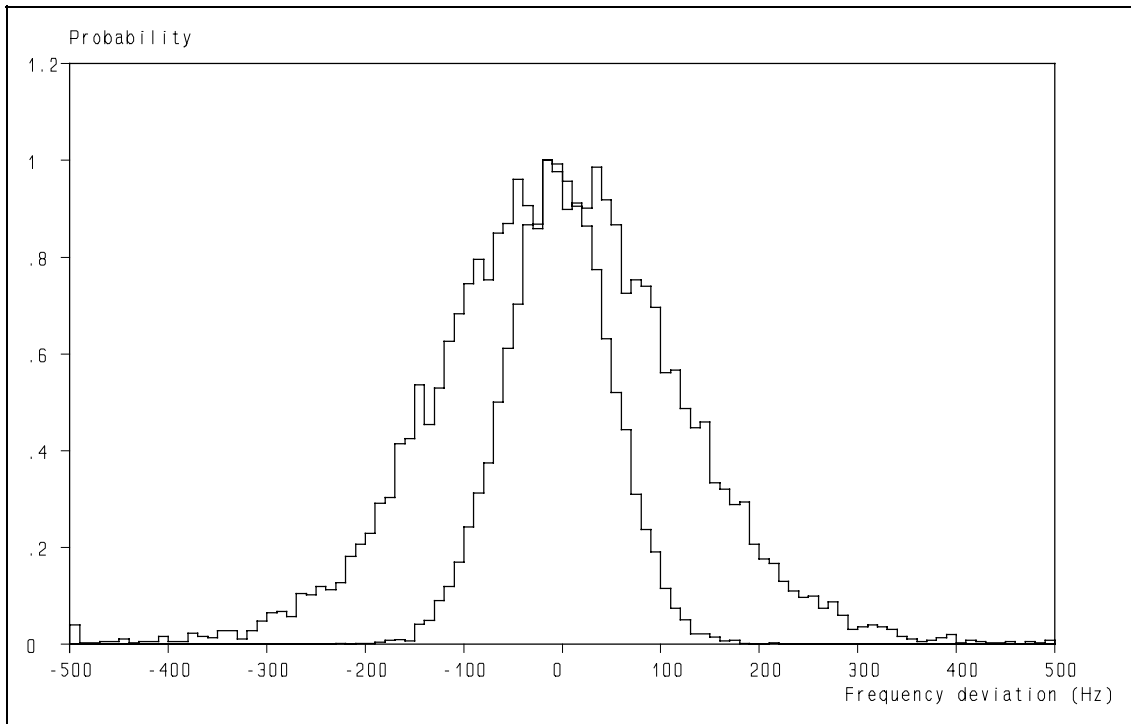


**Figure 5.7:** Histograms of the non-normalised frequency estimation distributions for FFT processing using 1/4 of the Doppler signal (outer curve) and wavelet transform (inner curve).

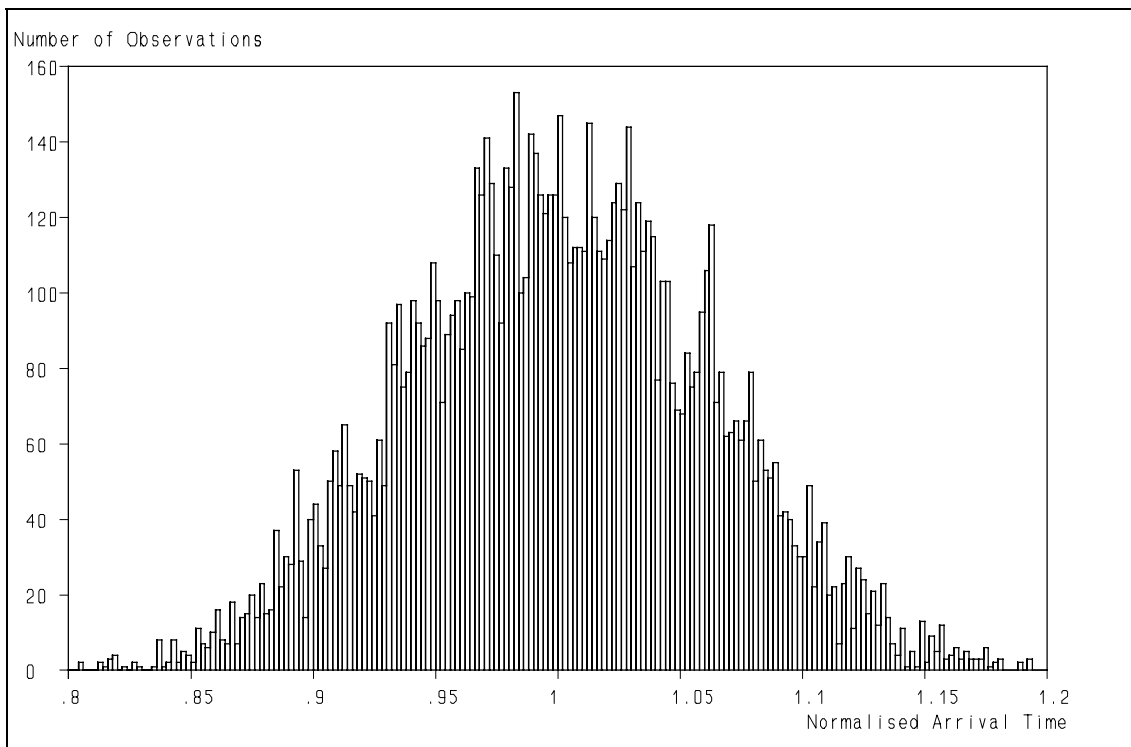


**Figure 5.8:** Probability distribution of the estimated arrival time using a fit to a parabola.

*Retrieval of turbulence and turbulence properties from LDA data with noise*

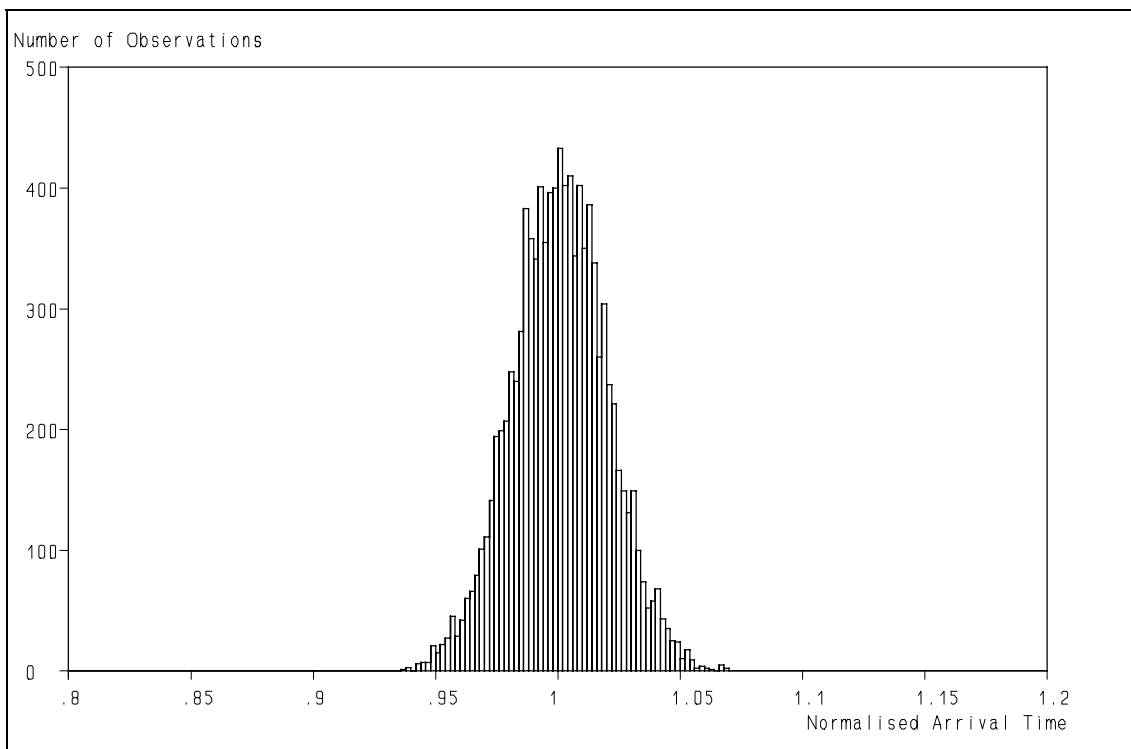


**Figure 5.9:** Probability distribution of the estimated arrival time using the wavelet transform.

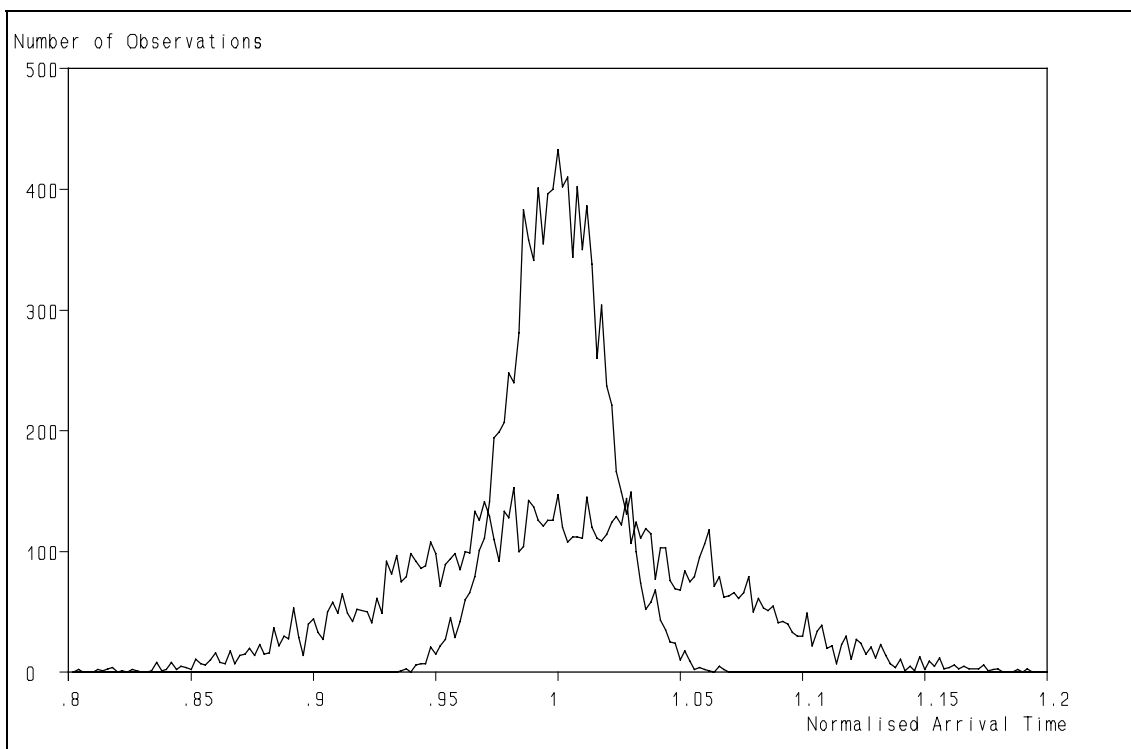


**Figure 5.10:** Comparison of the probability distributions of the arrival time estimators using the parabola fit and the wavelet transform.

## 5. Application of the Wavelet Transform to LDA Signal Processors

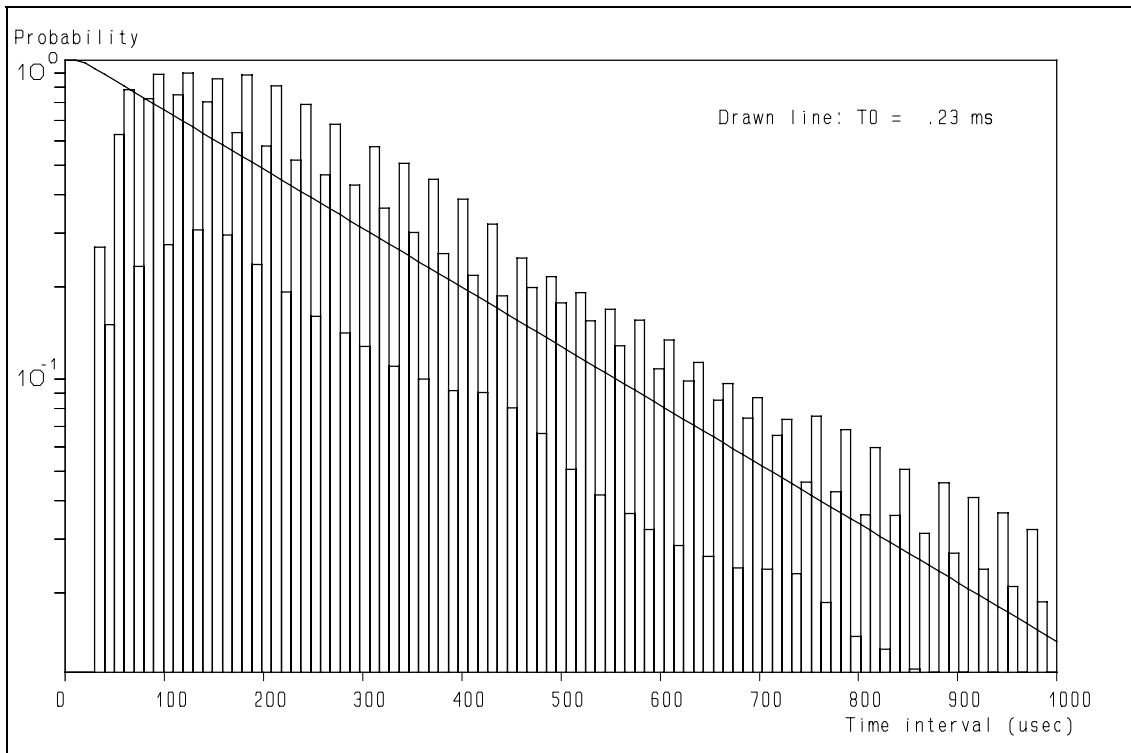


**Figure 5.11:** The time interval distribution as retrieved from a measurement of the radial component of the velocity in the jet of a stirrer.

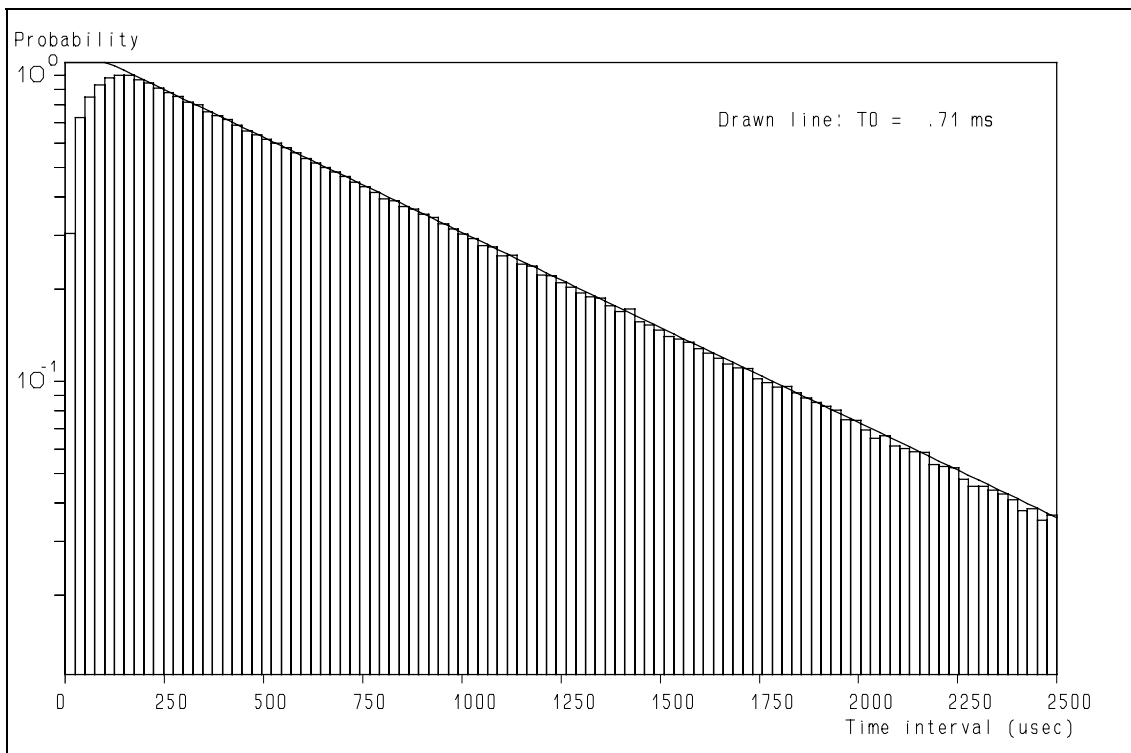


**Figure 5.12:** The time interval distribution when inaccuracies in the arrival time estimation of the Doppler signals occur.

*Retrieval of turbulence and turbulence properties from LDA data with noise*

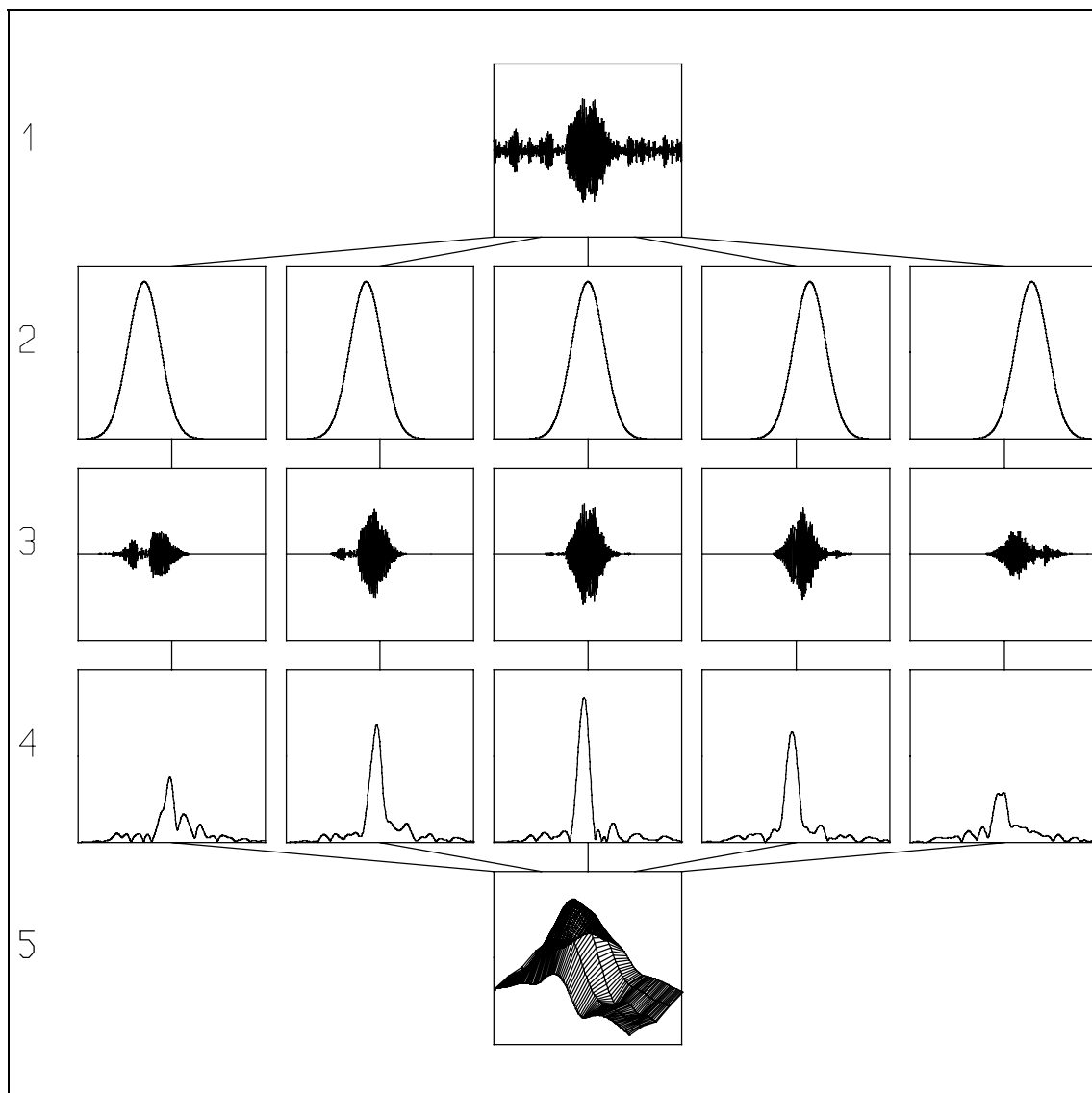


**Figure 5.13:** Concept for a processor, based on the Wavelet Transform. By parallel processing of the windowed signal from the photodetector and subsequent parallel Fourier Transformation, a Quasi-Wavelet Transform can be realized.

# Chapter 6

## Data-rate requirement for velocity signal reconstruction

*Great men have not been concerned with fame.  
The joy of achievement that comes from  
finding something new in the universe  
is by far their greatest joy.*  
William P. King

### 6.1 Introduction.

Velocity signal reconstruction is an attractive approach for the further processing of Laser-Doppler Anemometry (LDA) data, as will be shown in the next chapter. However, before we are able to discuss the specific problems of velocity signal reconstruction it is necessary to study the question about the minimum data rate required to make it feasible. This will be the subject of this chapter.

### 6.2 Statement of the problem.

The velocity information arrives randomly when a tracer particle traverses the measurement volume. Even in the case that the corresponding velocity estimates would be exact, this leaves the development of the velocity between two successive estimates unknown. Therefore it is required to choose one or other interpolation scheme to "bridge" the gap between two successive velocity estimates. Several different schemes can be selected, but they all have one thing in common: they introduce *correlation* into the reconstructed velocity signal. The reason for that is simple: the interpolation will -in one or other way- be based on the information in the vicinity of the point that needs to be interpolated. This information is therefore "smeared out" in time, creating a correlation that previously was not there. This can be illustrated by using the simplest interpolation: zero-order reconstruction (Sample-and-Hold cq. S&H) or "track-and-hold" as has been used by the trackers too (ref. 50 and 96). The output of such a reconstruction algorithm is shown in fig. 6.1 which is a simulation of a tracker signal, which used a hardware implementation of the S&H reconstruction. Let us assume that the fluctuations to be reconstructed are white noise. The random sampling gives a limited number of samples and the S&H creates a signal like is shown in fig. 6.2, which is obtained from a Monte-Carlo simulation. The auto correlation function of this signal is an exponentially decaying curve with a time constant  $t_0 = 2$  ms.:

$$\rho_{ff}(\tau) = e^{-\frac{\tau}{t_0}} \quad [6.1]$$

in which:

$\rho_{ff}$  = auto correlation function

$\tau$  = time delay

$t_0$  = characteristic time of the time interval distribution

and which is shown in fig. 6.3. This result can be understood by the following reasoning: the samples are uncorrelated, thus the correlation is only different from zero for the hold time of the system. The probability distribution of the time intervals (and thus of the hold times) is the exponential of eq. [6.1] and the auto correlation function is therefore identical to it. To verify this result, the auto correlation function of a simulated signal, as shown in fig. 6.2 is calculated and the result is also shown in fig. 6.3. The line, obtained by the Monte-Carlo simulation virtually coincides with the curve, obtained from eq. [6.1]. This shows that S&H does indeed introduce correlation into the signal, but this phenomenon also

## Retrieval of turbulence and turbulence properties from LDA data with noise

acts as a low-pass filter with a cut-off frequency of  $1/(2\pi t_0)$ , because the Fourier transform of eq. [6.1] is

$$S(f) = \frac{S(0)}{1 + (2\pi f t_0)^2} \quad [6.2]$$

in which:

$S$  = power spectral density m<sup>2</sup>/s  
 $f$  = frequency Hz  
 $t_0$  = characteristic time of exponential time interval distribution s

This spectrum decays for frequencies above the cut-off frequency, as is shown in fig. 6.4, upper trace<sup>1</sup>. But remember that the input signal was white noise, which has a constant power spectrum for all frequencies. We have to conclude that the combination of the random sampling and the reconstruction limits the frequency response of the system. For S&H this has been reported in the literature before (ref. 39), but it holds for any kind of reconstruction. An example is the first-order reconstruction: as can be seen in fig. 6.4, lower trace, a similar decay occurs. The level of the noise floor is lower and the slope above the cut-off frequency may be different, steeper in this case, but the cut-off frequency itself is not. As both S&H and first-order reconstruction only interpolate in between two successive velocity estimators, the time span of the correlation which is introduced is limited to the exponential time interval distribution. It is therefore to be expected that the cut-off frequencies of S&H and first-order reconstruction will be similar. However, other approaches might use information from other samples as well, thus increasing the time span over which correlation is introduced and as a consequence lowering the cut-off frequency of the reconstructed signal. A high data-rate (at least  $2\pi$  times the highest frequency) is required in order to reconstruct the velocity fluctuations, but for certain reconstruction schemes a higher rate may be required. As we will use first-order reconstruction as the basis of our reconstruction scheme, we will use the factor of  $2\pi$  as the ratio between the data-rate and the highest frequency to be reconstructed.

The velocity fluctuations develop in between two successive samplings, whereas *any* reconstruction scheme can only make approximations for the development of the velocity in time. Therefore a difference will exist between the actual velocity and the reconstructed velocity. Because of the step-shaped result of the S&H reconstruction, this has been referred to as "step noise" (e.g. ref. 39). However, it also occurs with e.g. first-order reconstruction in which case the term "step noise" is less appropriate. As it will occur in *any* reconstruction scheme, it would be better to name it "reconstruction noise" and we will use this terminology in this thesis.

It is possible -in theory at least- to correct the power spectrum for the low-pass filtering of the random sampling<sup>2</sup> and two examples are shown in fig. 6.5 and 6.6. The noise floors in these spectra can easily be distinguished, but the levels are significantly higher than those obtained in earlier work using low-power lasers and trackers (ref. 50 and 64 - 66), an example of which is shown in fig. 6.7. This unexpected result can be explained by the determination of the noise floor as a function of the data-rate.

---

<sup>1</sup> Note that the obtained spectrum is identical to that of first-order low-pass filtered white noise. The random sampling in combination with S&H reconstruction thus acts as a first-order low-pass filter.

<sup>2</sup> From here on we will refer to the low-pass filtering due to the random sampling in combination with the velocity signal reconstruction as "the particle rate filtering", in line with literature. Keep in mind that the low-pass filtering only occurs in combination with the reconstruction.

## 6. Data-rate requirement for velocity signal reconstruction

### 6.3 Noise level as a function of the data-rate.

As has been shown in the previous section, the highest frequency that can be reconstructed is  $1/2\pi$  times the data-rate. At first one might think that it does not make any sense to increase the data-rate any further, but that is not the case: the *distribution* of the noise power over the frequencies also depends on the data-rate as can be shown by the following analysis:

Remember that the integral of the power spectrum is equal to the Mean Square (MS) value of the signal. Integration of the power spectrum of S&H reconstructed noise (eq. [6.2])

$$S(f) = \frac{S(0)}{1 + (2 \Pi f t_0)^2} \quad [6.2]$$

yields the MS value of the noise contribution:

$$MS = \int_0^{\infty} \frac{S(0)}{1 + (2 \Pi f t_0)^2} df = \quad [6.3^a]$$

$$= \frac{S(0)}{2 \Pi t_0} \int_0^{\infty} \frac{1}{1 + z^2} dz = \quad [6.3^b]$$

$$= \frac{S(0)}{2 \Pi t_0} [\arctan z]_0^{\infty} = \frac{S(0)}{2 \Pi t_0} \frac{\Pi}{2} = \frac{S(0)}{4 t_0} \quad [6.3^c]$$

from which follows that

$$S(0) = 4 MS t_0 \quad [6.4]$$

In other words: the level of the noise<sup>3</sup> in the turbulence power spectrum is proportional to  $t_0$  and thus inversely proportional to the data-rate for a fixed MS of the noise. A Monte-Carlo simulation confirmed this result as is shown in fig. 6.8. It is similar to the result presented at the conference in Lisbon, Portugal (ref. 97). This also (partly) explains the big differences between fig. 6.5 & 6.6 on the one hand and fig. 6.7 on the other: trackers operate best with a high data-rate, obtained in forward scatter mode, whereas the other records have been obtained with backscatter, leading to a significantly lower data-rate (ref. 63). Similar results have been reported in the literature for turbulence power spectra (ref. 39).

For other reconstruction schemes a similar effect can be derived. Let us assume again that it is white noise which is to be reconstructed. As the correlation window of white noise is zero, the samples we obtain from the random sampling are uncorrelated. The reconstructed signal is therefore in its statistical properties linearly scaled to the  $t_0$  of the random sampling. As a consequence, the auto correlation function (ACF) of the reconstructed signal is, expressed in  $\tau/t_0$ , independent of  $t_0$ . Also, the distribution, and thus the MS and Root Mean Square (RMS) values, of the reconstructed signal are independent of the  $t_0$ . Thus the properties of any reconstruction scheme can be captured in a single curve, a dimensionless auto covariance function. The properties of S&H are described by eq. [6.1] and

---

<sup>3</sup> Note that this is about the noise contribution to the individual velocity estimates and not the reconstruction noise.

## Retrieval of turbulence and turbulence properties from LDA data with noise

those of first-order reconstruction are illustrated in fig. 6.9, which is the result of a Monte-Carlo simulation. In general, it can mathematically be expressed by:

$$R_{nn}(\tau/t_0) = MS \cdot \rho_{nn}(\tau/t_0) \quad [6.5]$$

in which

$R_{nn}$  = auto covariance function m<sup>2</sup>/s<sup>2</sup>

$\tau$  = time delay s

$t_0$  = characteristic time of the time interval distribution s

$\rho_{nn}$  = auto correlation function

The Fourier transform of  $R_{nn}$ , yielding the power spectrum, is

$$PSD_{nn} = \frac{1}{2\pi} \int_{-\infty}^{\infty} MS \cdot R_{nn}(\tau/t_0) \cdot \text{COS}(\omega\tau) \, d\tau \quad [6.6^a]$$

$$= \frac{MS \, t_0}{2\pi} \int_{-\infty}^{\infty} R_{nn}(\tau/t_0) \cdot \text{COS}(\omega t_0 \tau/t_0) \, d\tau/t_0 \quad [6.6^b]$$

$$= \frac{MS \, t_0}{2\pi} \int_{-\infty}^{\infty} R_{nn}(\tau') \cdot \text{COS}(\omega' \tau'/t_0) \, d\tau' \quad [6.6^c]$$

in which:

$\tau' = \tau/t_0$

$\omega' = \omega t_0$

Eq. [6.6] shows that the *shape* of the power spectrum of the noise is independent of  $t_0$ , which is not surprising as the ACF has a shape which is independent of  $t_0$  (see fig. 6.9), but that the position shifts with  $t_0$ : the cut-off frequency is inversely proportional to  $t_0$  and the low frequency level (the noise floor) is proportional to  $t_0$ . The latter follows when the integrand is evaluated for  $\omega$  goes to zero. These properties are evaluated for first-order reconstruction and the results are presented in fig. 6.10 for the auto covariance functions which correspond to cut-off frequencies of 2, 6 and 20 Hz<sup>4</sup>, shown in fig. 6.9. It is important to note that these properties only hold for the noise that accompanies the individual velocity estimates and not for the reconstruction noise. In general, the reconstruction techniques do not conserve the MS value of the turbulent velocity fluctuations, with S&H as the only exception. However, if the data-rate is sufficiently high, this is not a problem, as will be illustrated in the next section where the S&H and first-order reconstruction will be applied to periodic fluctuations.

### 6.4 Filtering of periodic signals.

One might wonder whether the analysis for the particle rate filtering of white noise is valid for signals with other spectral compositions as well. Although the theory of linear systems tells us this is the case in general (ref. 89 and 90), it is not straightforward to translate it to systems like these, regarding e.g. the assumption that there is no correlation in the signal. To verify whether this translation is valid, we have examined the opposite of white noise and used noise-free pure sinusoidal waves as input signals for a randomly sampling system in combination with S&H. Using a  $t_0$  of 6 msec, the filtering is shown in fig. 6.11 in combination with the theoretical curve of eq. [6.2]. This shows that eq. [6.2] holds

---

<sup>4</sup> Note that the noise floor with first order reconstruction is always lower than with S&H at the same data-rate.

## 6. Data-rate requirement for velocity signal reconstruction

for the extreme cases of pure sinusoidal waves and white noise. Therefore it is clear that the normal theory of linear systems may be applied. We can thus correct all the spectra obtained by LDA by using the inverse of eq. [6.2]. However, the analysis with sinusoidal waves has also revealed that there is a third reason to obtain a high data-rate, which is the *energy conversion*. The particle rate filtering is not completely similar to the filtering of electronic filters, which *reduces* the energy of the incoming signal at certain frequencies. The random sampling in combination with the S&H rather *re-distributes* the energy: the *reduction* of the energy at a certain frequency is compensated by an *increase* in the filtered white noise accompanying the signal. This can be illustrated by the following examples. Two of the signals that have been used in the above analysis are shown in fig. 6.12 (a 12 Hz sinusoid, a little below half the cut-off frequency) and in fig. 6.13 (a 55 Hz sinusoid, twice the cut-off frequency). The 12 Hz signal is still recognisable, but the 55 Hz signal has more resemblance to noise. Yet, in the auto covariance functions, shown in fig. 6.14 and 6.15, both frequencies can clearly be distinguished. But although the power of the 55 Hz signal is significantly lower than that of the 12 Hz signal (in agreement with the filtering properties), the MS value of both signals is the same (and equal to the MS of the actual signals), because the values at  $\tau = 0$  are identical (see also ref. 39), showing that S&H conserves the MS of the signals. This, however, means that the original power of the sine wave has been partly re-distributed as filtered white noise. This can be seen from the Auto Covariance Function which shows the typical decaying characteristics for short time intervals as is shown in more detail in fig. 6.16. This is confirmed by the spectra of these signals which are shown in fig. 6.17. In other words: the power of the signal is re-distributed by the random sampling into filtered white noise, which low-frequency level is again determined by the data-rate.

As we have seen in sec. 6.2 (fig. 6.4) the particle rate filtering also acts on first-order reconstructed signals. However, there are differences with periodic signals when compared to S&H reconstruction, as now there is correlation in the signal: the MS of the signals is no longer conserved and the re-distribution of the energy is modified. The first phenomenon is illustrated in fig. 6.18, which shows the auto covariance functions of the first-order reconstructed periodic signals. Comparing the values at  $\tau = 0$  with those of fig. 6.14 and 6.15 shows that the MS is lower for both signals, but that the value of the 55 Hz is lower than that of the 12 Hz signal. This means that the reconstruction noise is lower with first-order reconstruction than with S&H, which reflects itself also in the low-frequency noise floor in the power spectrum, as is illustrated in fig. 6.19. But as the re-distribution of the power over the frequencies follows a different scheme with first-order reconstruction than with S&H, the *ratio* between the low-frequency noise floors of the 12 and 55 Hz signals is different compared to the S&H case. Note that the noise floor in the 12 Hz spectrum is roughly a factor of 3 lower compared with the S&H, but that the noise floor in the 55 Hz spectrum is barely below that of the S&H case. Although first-order reconstruction is -from a noise point of view- more attractive than S&H, the behaviour of the reconstruction noise is more complicated than that of S&H. However, as long as the data-rate requirement is fulfilled, first-order reconstruction is to be preferred, because in that case we only have to deal with the noise contributions. We will discuss the differences in the presence of measurement noise between S&H and first-order reconstruction in the next chapter.

Note that the redistribution of the reconstruction noise power holds for *any* reconstruction scheme, not only for S&H. As turbulence power spectra tend to decay for higher frequencies, the amount of power to be re-distributed increases rapidly as the data-rate is reduced. This effect contributes therefore significantly to the noise "floor" in the spectra for low data-rates (in comparison with the frequencies in the turbulent velocity fluctuations) and is probably also partly responsible for the high noise floors in fig. 6.5 and 6.6. If, however, a significant part of the turbulent velocity fluctuations is effected by a low data-rate, systematic errors will occur with all reconstruction schemes, except S&H.

### **6.5 Concluding remarks.**

The highest frequency that can be reconstructed is at best equal to the data-rate/ $2\pi$ , but may be lower, dependent on the reconstruction scheme chosen. However, a higher data-rate is always attractive as this reduces the noise floor and reveals more of the small eddies (corresponding to high frequencies). Although in the next chapter techniques will be revealed to reduce the noise, one should always keep in mind that no technique is able to remove the noise completely and to resolve the turbulence. Therefore the better the input-data are for the velocity signal reconstruction, the better the output signal will be. High data-rate can be achieved by the use of forward scatter (ref. 15 and 63) and the use of beam expanders. These create a smaller diameter of the laser beams at the focus, thus reducing the volume of the measurement volume. Although this shortens the lengths of the Doppler signals, the Signal-to-Noise Ratio (SNR) of the Doppler signals remains roughly the same, because the light intensity is increased. The additional advantages, however, are that a smaller measurement volume allows higher concentrations of tracer particles and thus an increased data-rate and increased spatial resolution. More details can be found in Chapter 3.

## 6. Data-rate requirement for velocity signal reconstruction

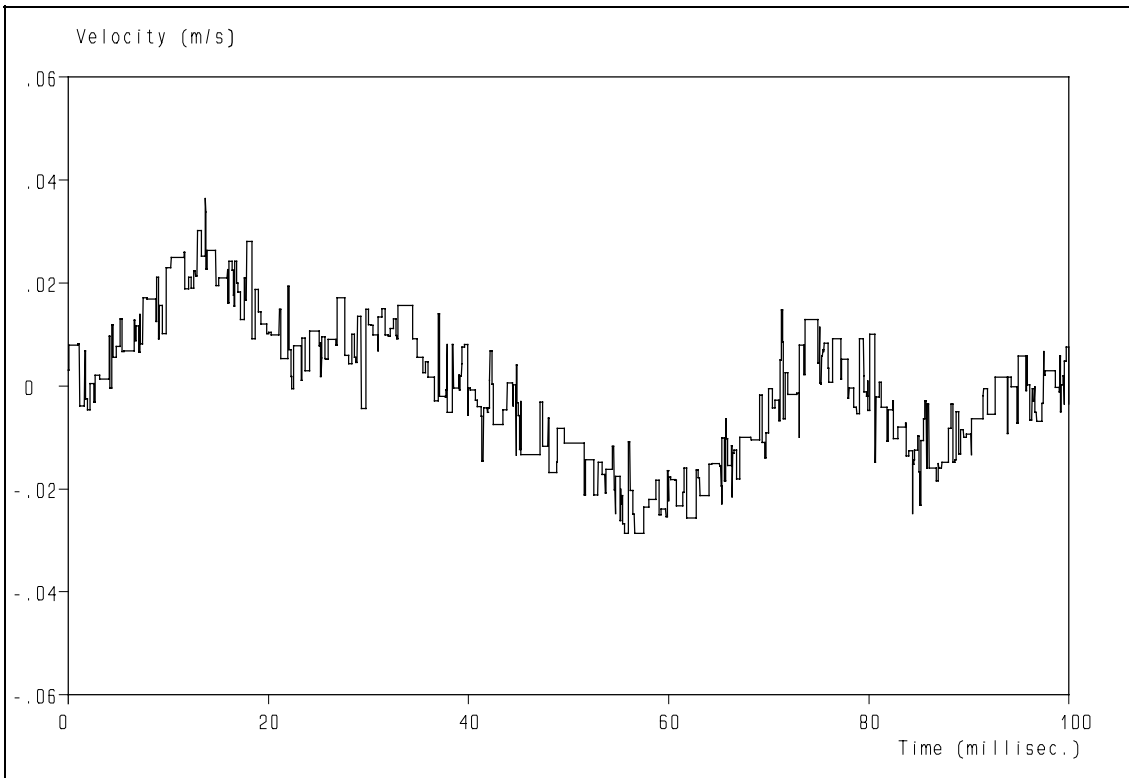


**Figure 6.1:** A tracker uses analog electronics for zero-order signal reconstruction. The high data-rate is responsible for the typical noise band around the turbulent velocity fluctuations.

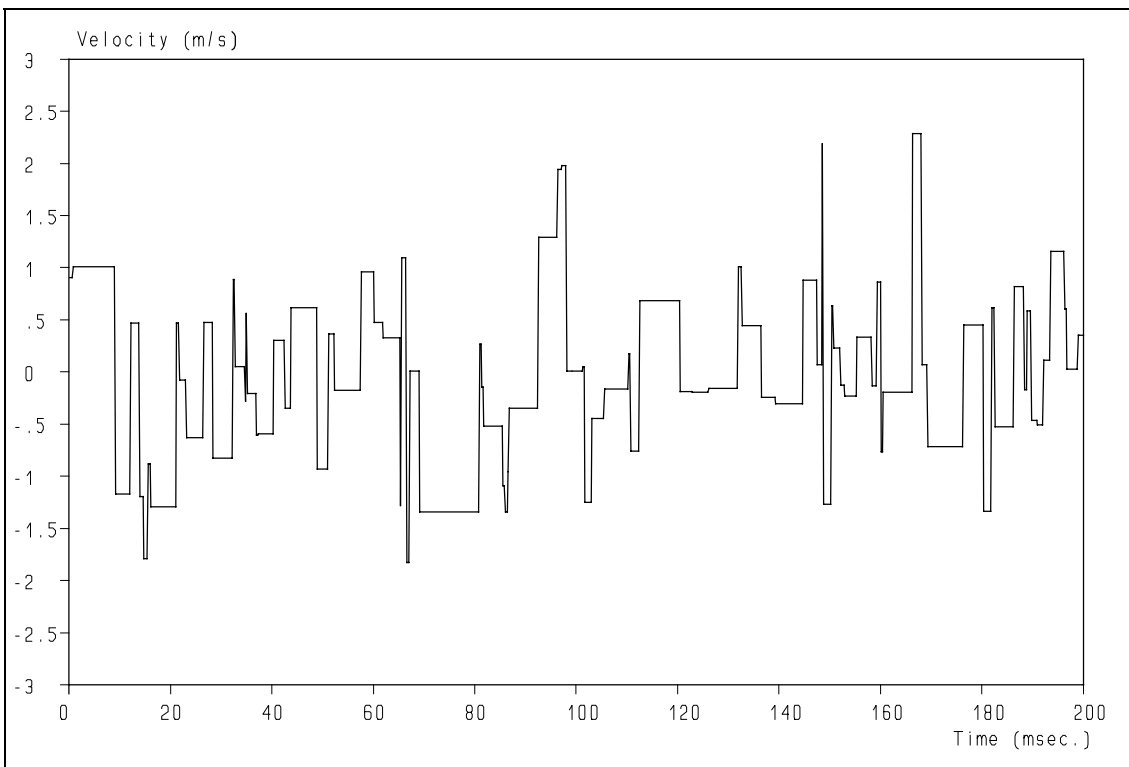


**Figure 6.2:** Zero-order (S&H) reconstruction of a randomly sampled white noise signal.

*Retrieval of turbulence and turbulence properties from LDA data with noise*

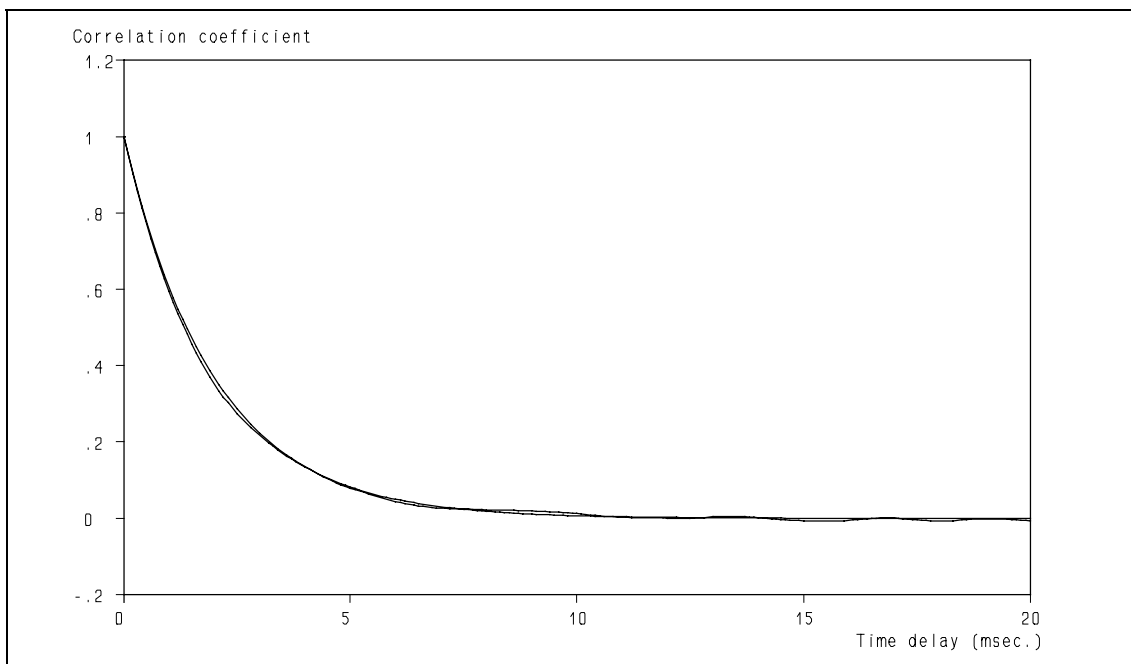


**Figure 6.3:** Auto Correlation Function of a zero-order reconstructed white noise signal, randomly sampled with an average data-rate of 500 Hz. For comparison an exponentially decaying function with a time constant of 2 ms. is shown.

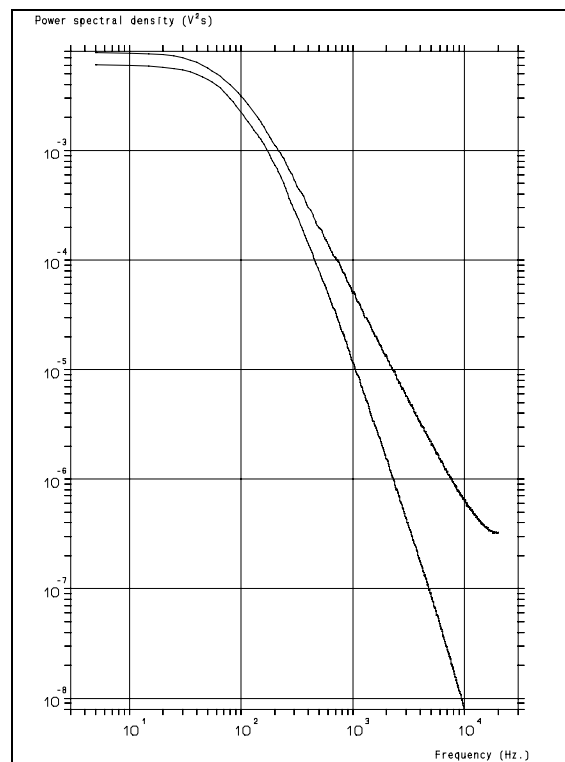


**Figure 6.4:** Power spectrum of a S&H (upper trace) and first-order reconstructed white noise signal. Note that the decay of both spectra starts at  $500/2\pi$  Hz.

## 6. Data-rate requirement for velocity signal reconstruction

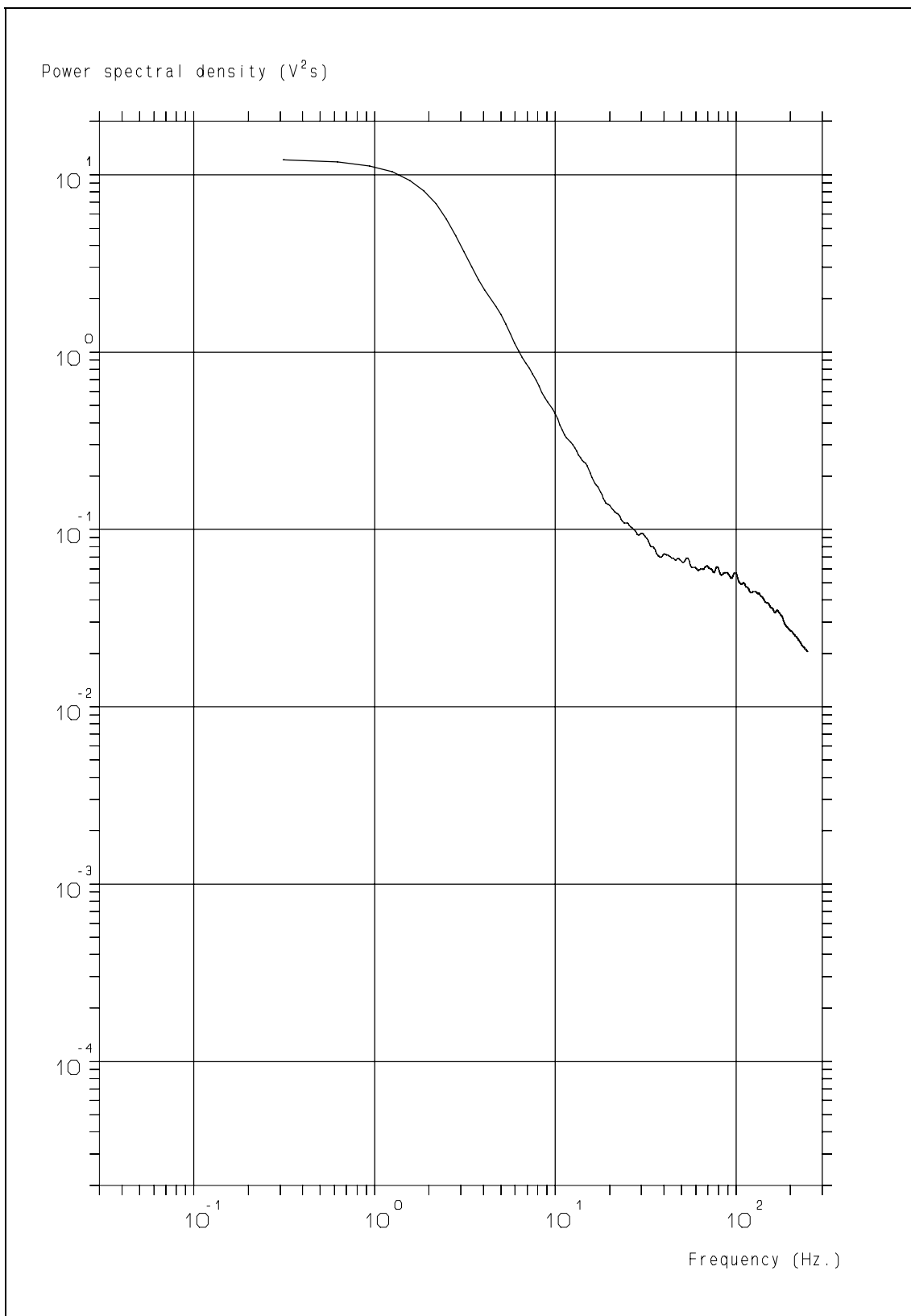


**Figure 6.5:** Power Spectrum obtained by first-order signal reconstruction and correction for the filtering, caused by the random sampling.

*Retrieval of turbulence and turbulence properties from LDA data with noise*

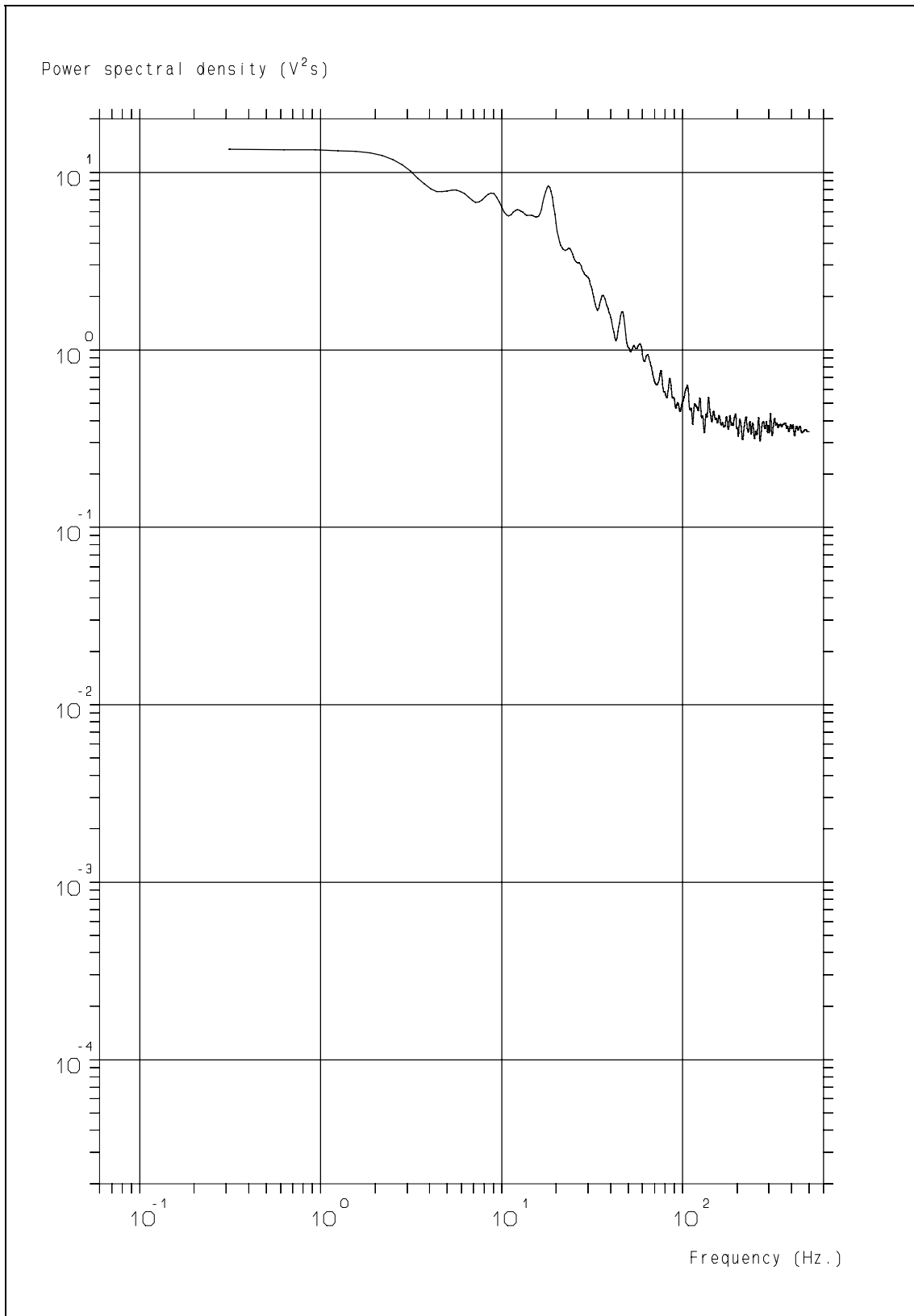


**Figure 6.6:** Power Spectrum obtained using first-order signal reconstruction and correction for the filtering, caused by the random sampling.

6. Data-rate requirement for velocity signal reconstruction

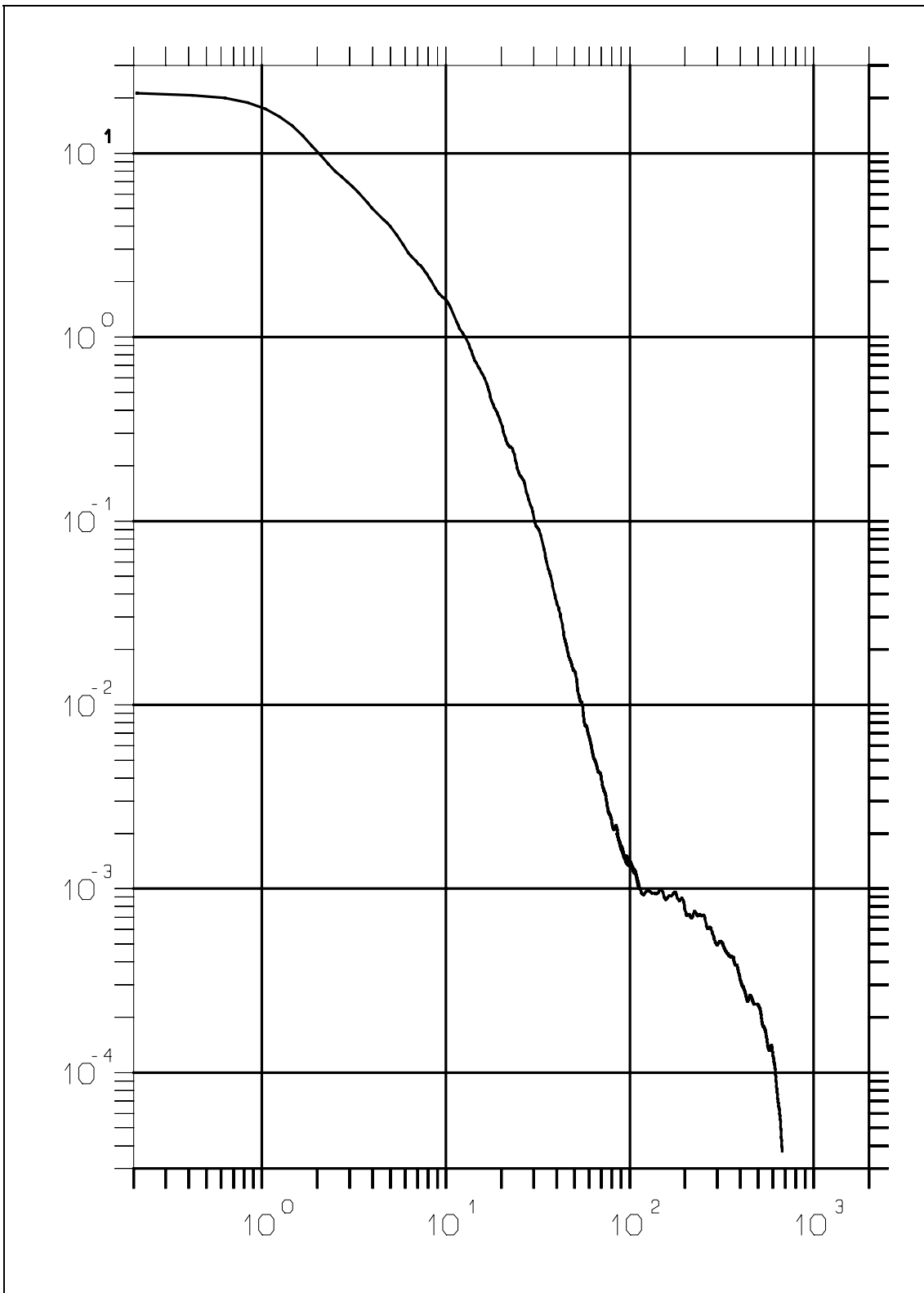


**Figure 6.7:** Turbulence Power Spectrum, measured in a vessel with a magnetic stirrer, using a tracker as processor. Compare the noise floor with those of fig. 6.5 & 6.6.

*Retrieval of turbulence and turbulence properties from LDA data with noise*

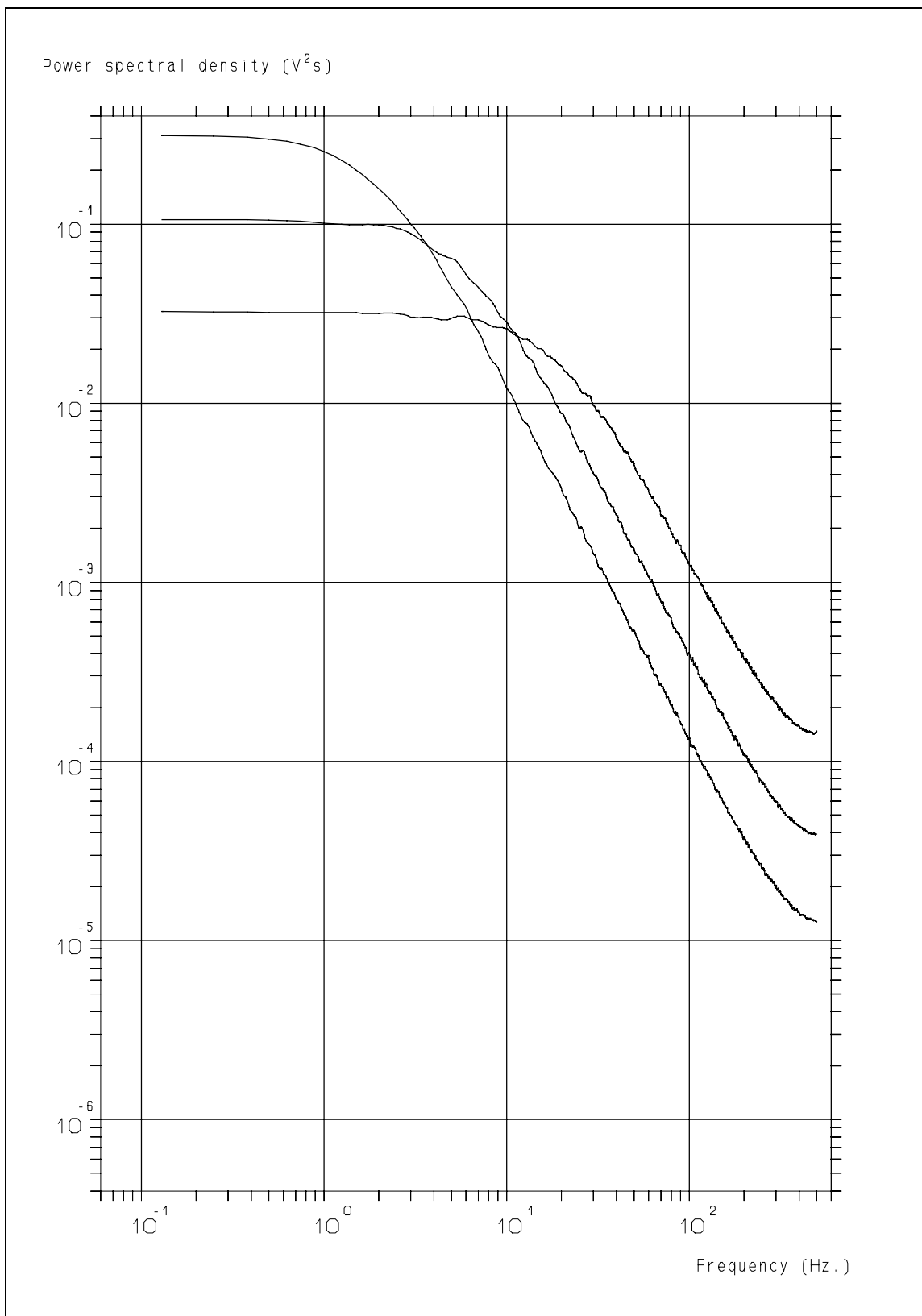


**Figure 6.8:** Monte Carlo simulation showing that the noise floor level depends on the  $t_0$ . The cut-off frequencies used are 2 Hz (highest level at 1 Hz), 6 Hz en 20 Hz (lowest level at 1 Hz).

## 6. Data-rate requirement for velocity signal reconstruction

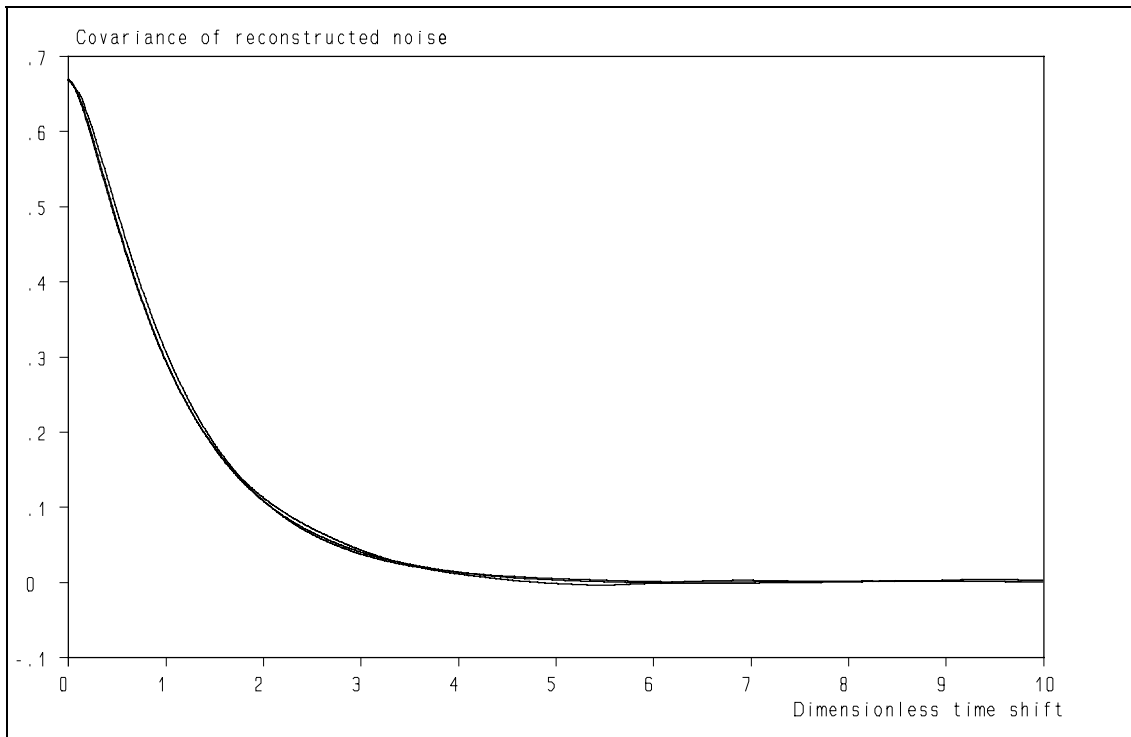


**Figure 6.9:** When the AVF's of first order reconstructed noise are plotted as a function of  $\tau/t_0$ , the curves coincide; the  $t_0$  values correspond to cut-off frequencies of 2, 6 and 20 Hz.

*Retrieval of turbulence and turbulence properties from LDA data with noise*

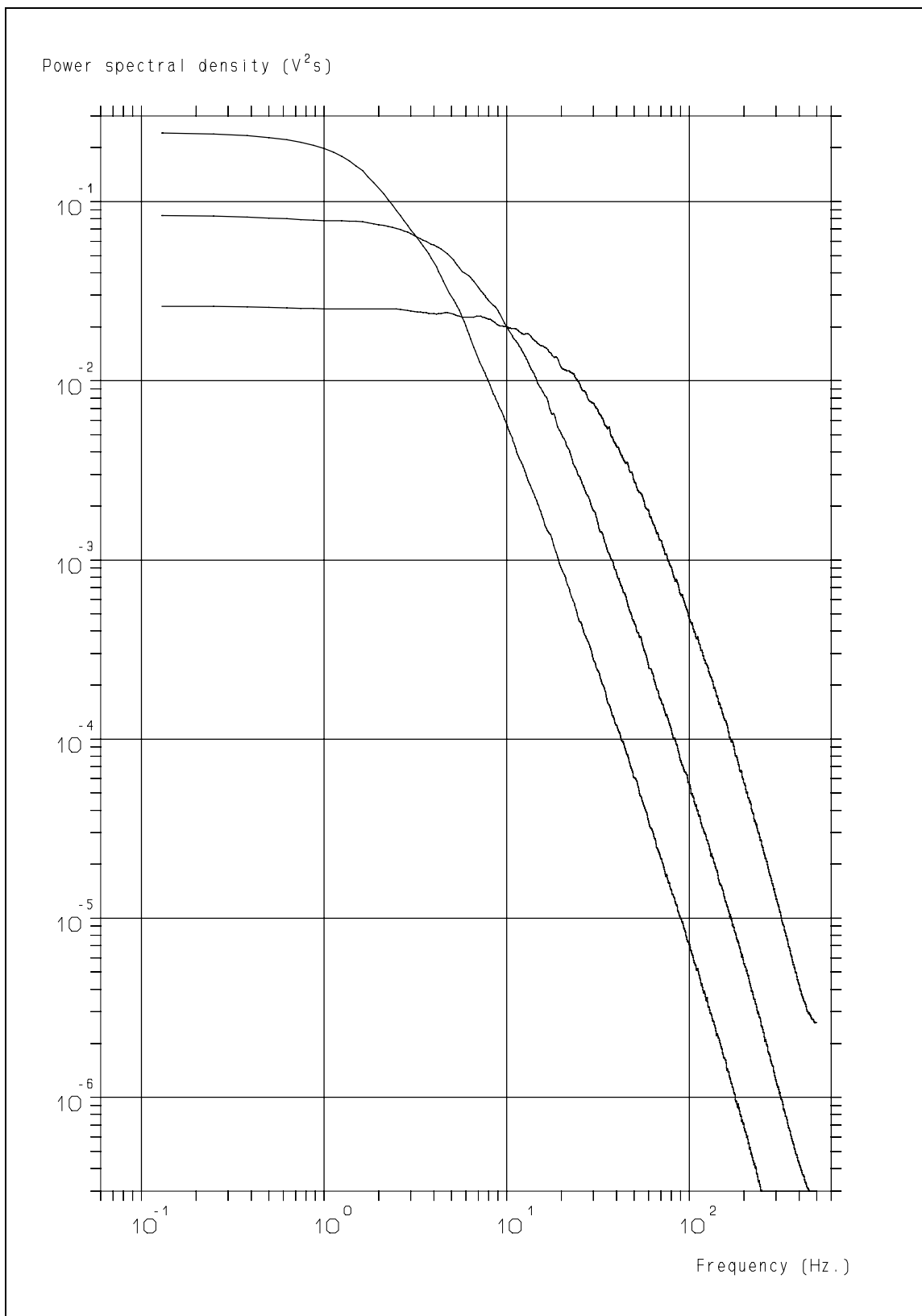


**Figure 6.10:** A simulation shows that the noise floor level with first order reconstruction depends on the  $t_0$  in the same way as with S&H. Conditions are identical to those of fig. 6.8.

## 6. Data-rate requirement for velocity signal reconstruction

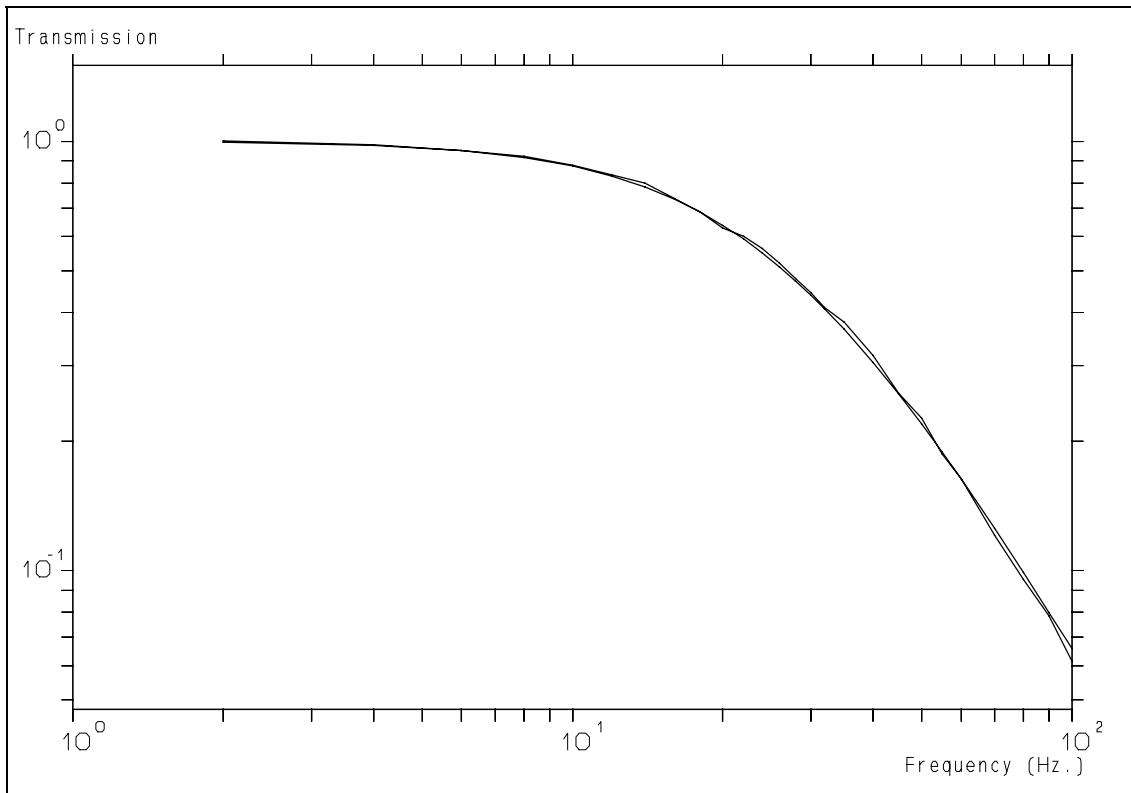


**Figure 6.11:** Filtering due to random sampling and S&H reconstruction of sinusoidal signals and the theoretical curve of eq. [6.2].

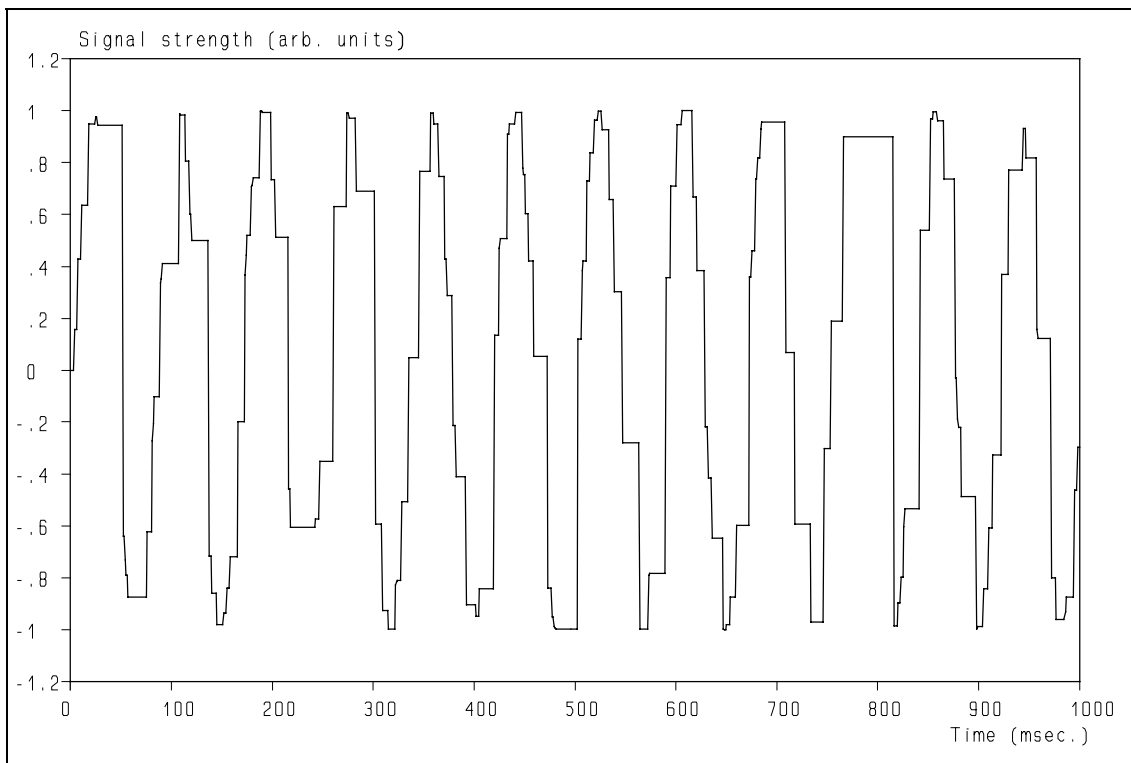


**Figure 6.12:** A sine wave of 12 Hz randomly sampled with a characteristic time ( $t_b$ ) of 6 ms.

Retrieval of turbulence and turbulence properties from LDA data with noise

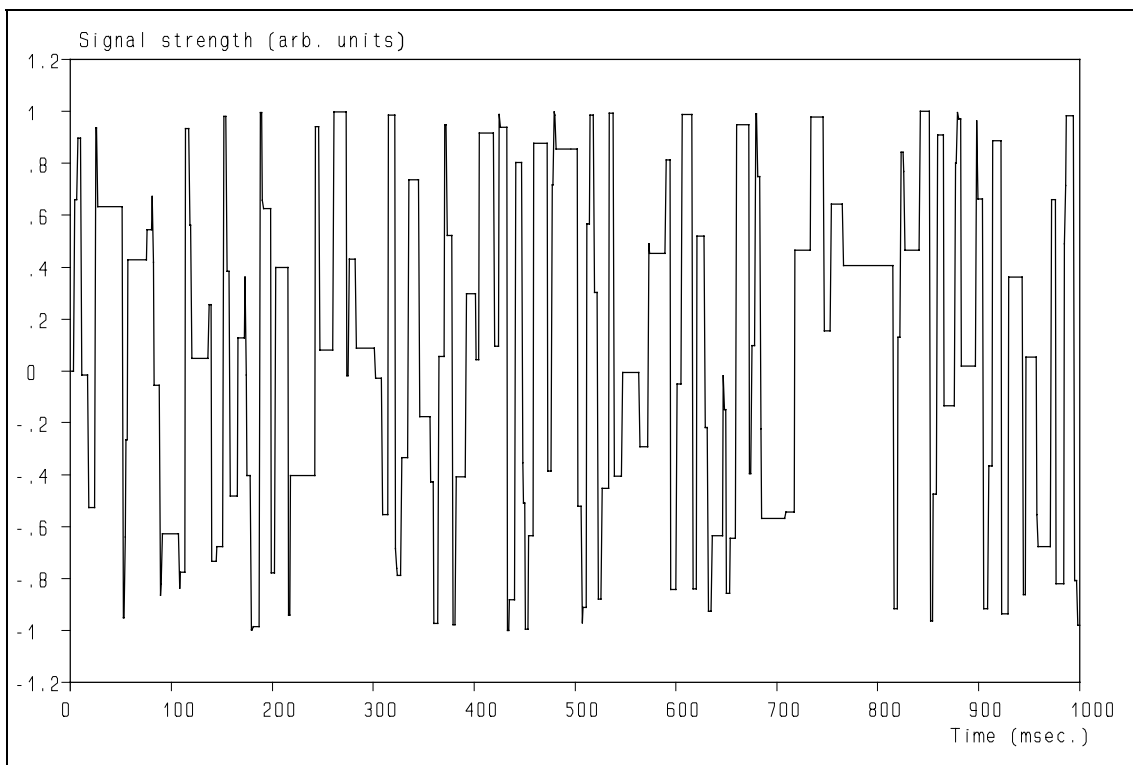


Figure 6.13: A sine wave of 55 Hz randomly sampled with a characteristic time ( $t_c$ ) of 6 ms.

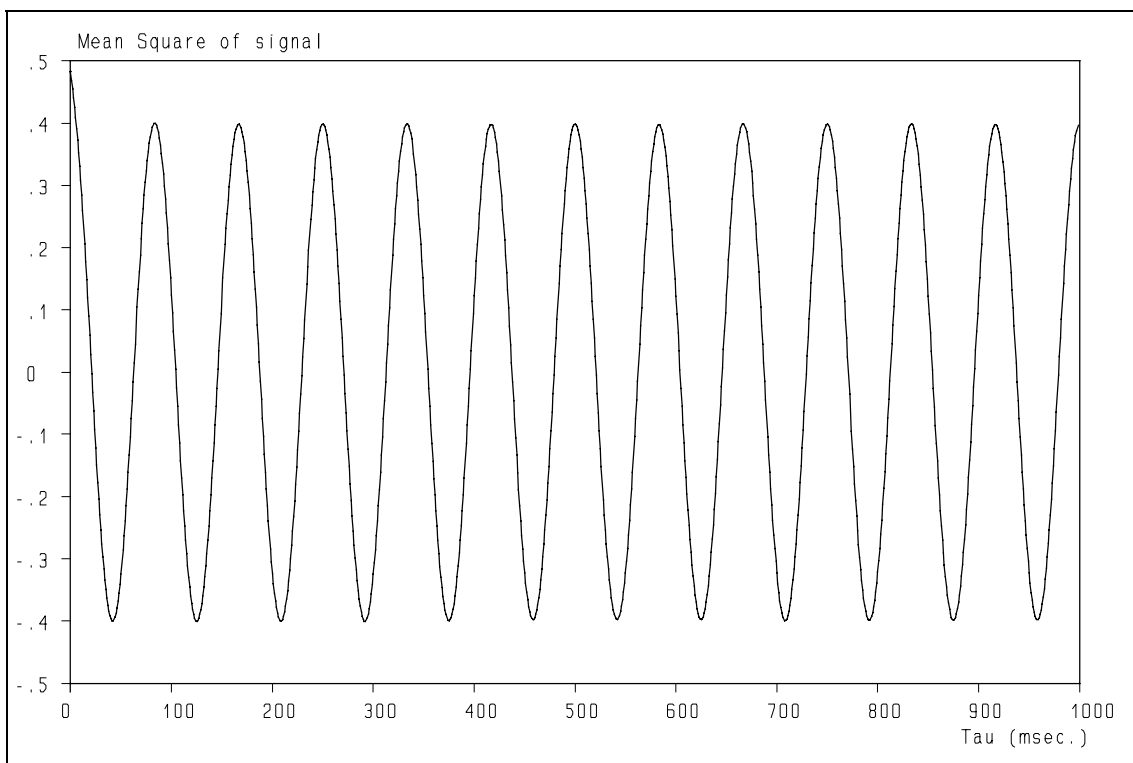


Figure 6.14: Auto covariance function of the 12 Hz signal of fig. 6.12.

6. Data-rate requirement for velocity signal reconstruction

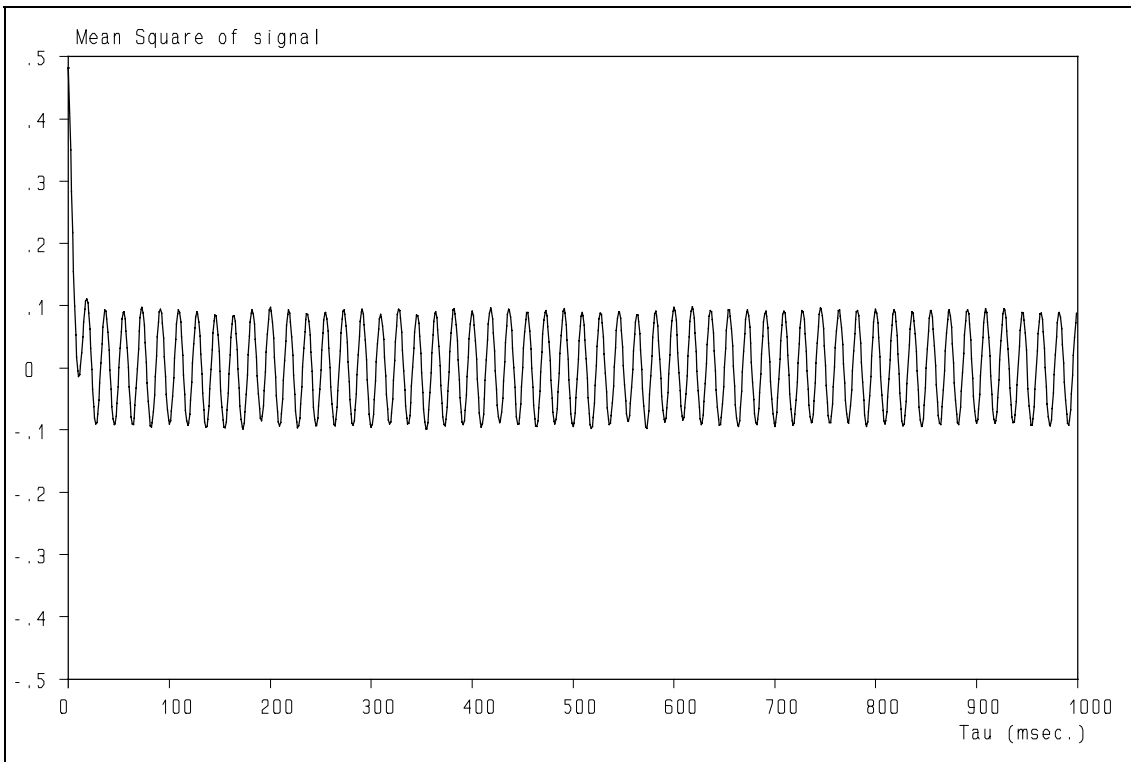


Figure 6.15: Auto covariance function of the 55 Hz signal of fig. 6.13.

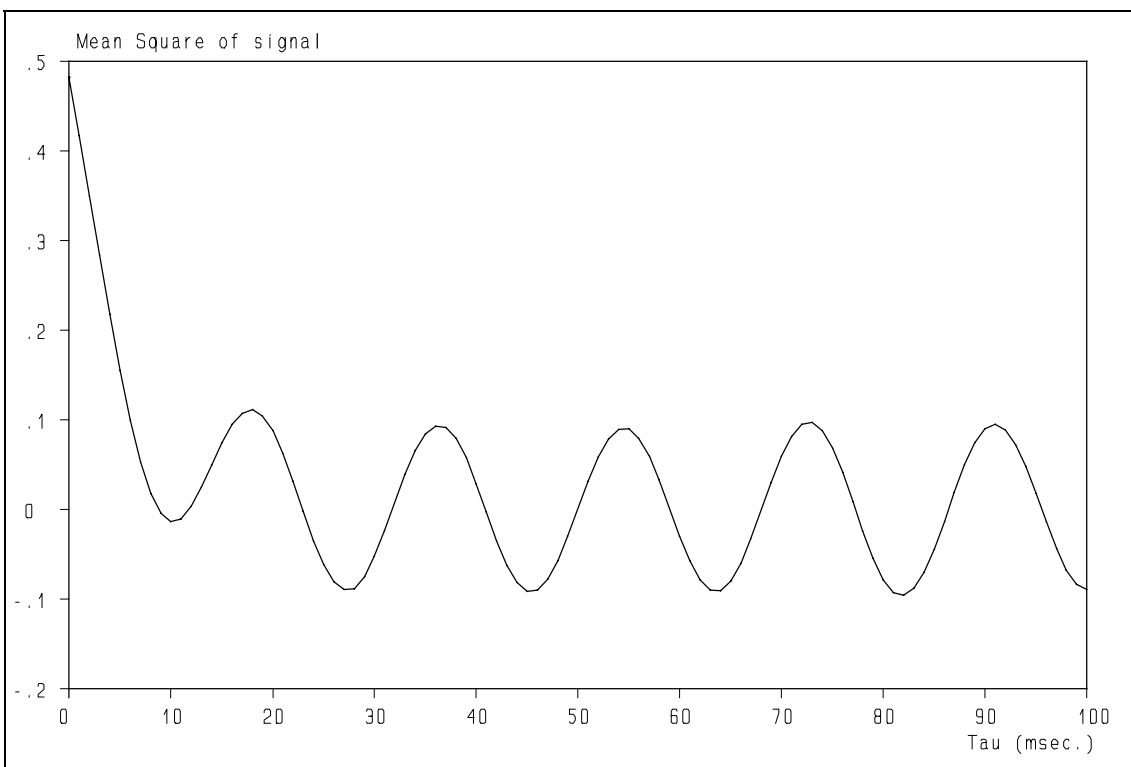
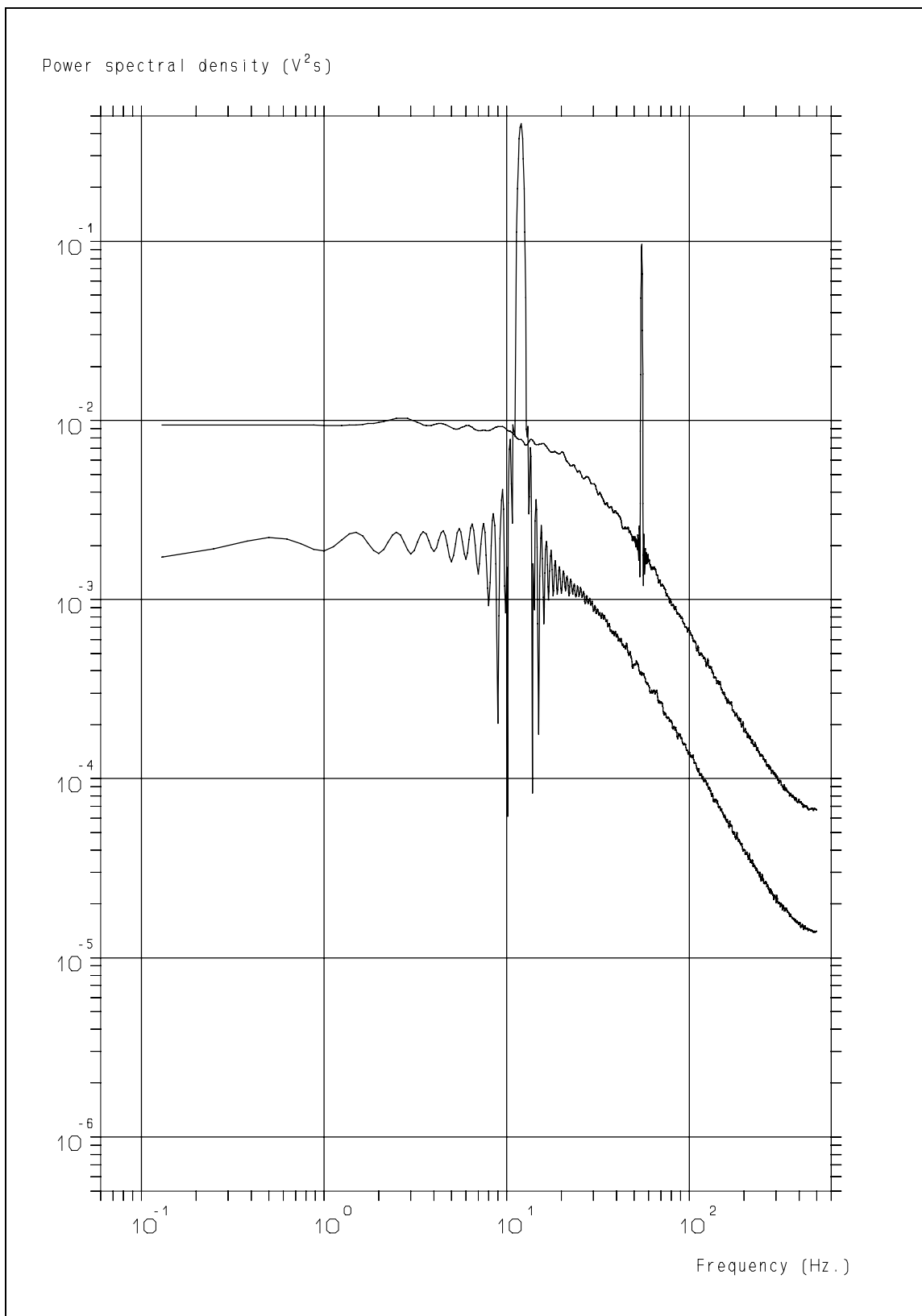


Figure 6.16: Auto covariance function of the 55 Hz signal of fig. 6.13 (enlargement of fig. 6.15).

*Retrieval of turbulence and turbulence properties from LDA data with noise*



**Figure 6.17:** Power spectra of the signals of fig. 6.12 (lower trace) and 6.13 (upper trace) showing the re-distribution of the energy.

6. Data-rate requirement for velocity signal reconstruction

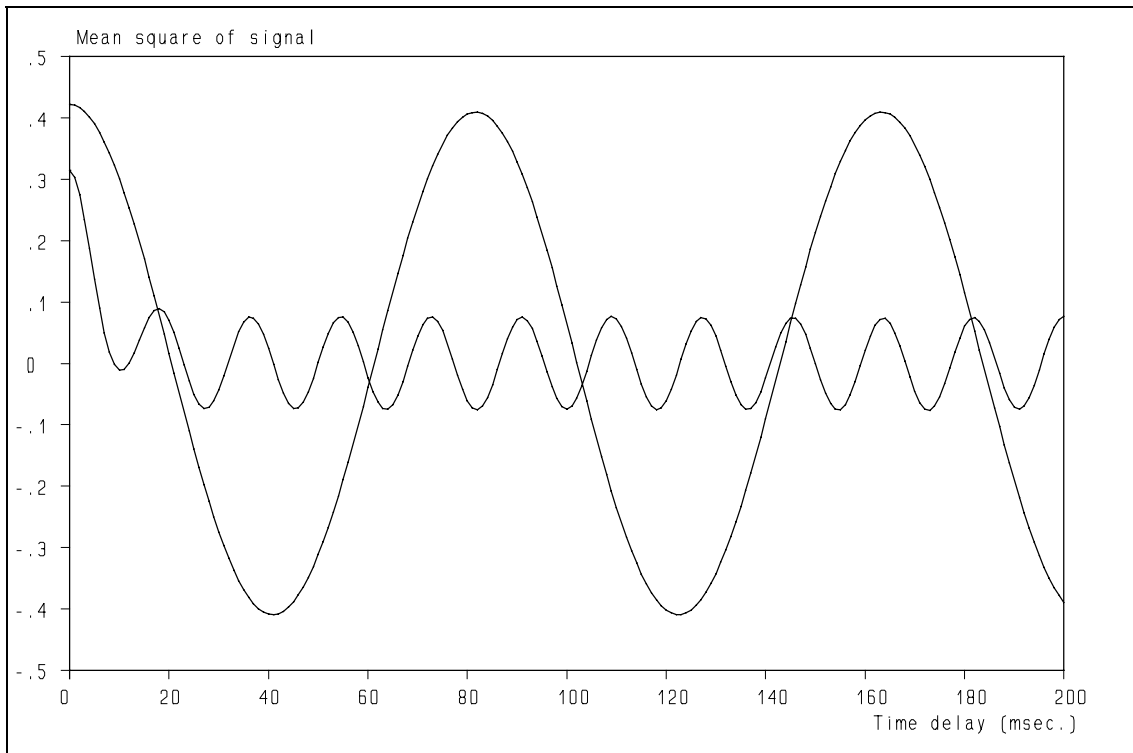


**Figure 6.18:** Auto covariance functions of first order reconstructed periodic signals, showing the dependence of the MS on the frequency.

*Retrieval of turbulence and turbulence properties from LDA data with noise*

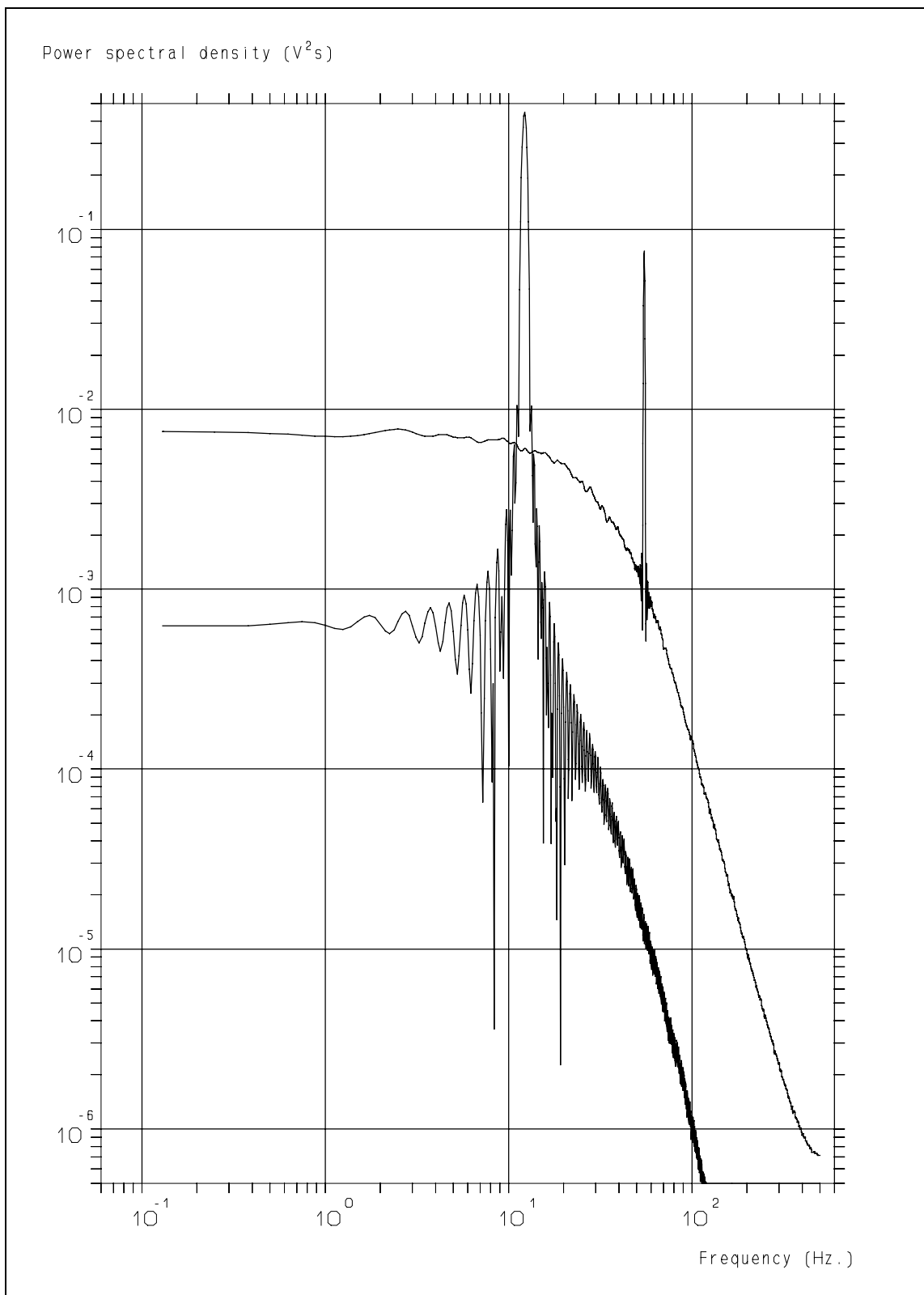


**Figure 6.19:** Power spectra of the first order reconstructed periodic signals showing the redistribution of the energy. Compare with fig. 6.17 and also note the difference in decay above the cut-off frequency.

# Chapter 7

## Velocity signal reconstruction I

*When we accept tough jobs  
as a challenge to our ability  
and wade into them  
with joy and enthusiasm,  
miracles can happen.*  
Arland Gilbert

### 7.1 Introduction.

Velocity signal reconstruction is an attractive approach for the further processing of Laser-Doppler Anemometry (LDA) data. Provided such a scheme would be feasible, it would solve a number of problems:

- Velocity and tracer particle concentration biases would be eliminated.
- The signals could be used to study instantaneous phenomena like bursting in boundary layers (ref. 13 and 98).
- Measurements of e.g. the instantaneous Reynolds shear stress would be possible (ref. 13).
- All the data-processing algorithms which have been developed for continuous and periodically sampled signals can be applied, which are further developed and more readily available than those for randomly sampled signals.

However, in order to apply velocity signal reconstruction two essential problems need to be solved:

1. How are the gaps in the information "bridged"?
2. How is the noise in the individual velocity estimates attacked?

#### Ad 1.

The velocity information arrives randomly when a tracer particle traverses the measurement volume. Even in the case that the corresponding velocity estimates would be exact, this leaves the development of the velocity, in between two successive estimates, unknown. Therefore it is required to choose one or other interpolation scheme to "bridge" the gap between two successive velocity estimates. However, as it is impossible to predict exactly the development in between two successive velocity estimators, there will be, no matter which reconstruction scheme is chosen, a difference between the actual and the reconstructed velocity, which we will refer to as "reconstruction noise" (see also Chapter 6). A useful criterion for the selection of a reconstruction scheme is therefore the amount of reconstruction noise generated: the lower the better.

#### Ad 2.

As we have seen in Chapter 3 on the noise contributions in LDA, each individual velocity estimate is accompanied by a noise contribution. This is an unavoidable fact of life and we will have to deal with it throughout the reconstruction scheme. This will become more clear in the next section.

Because of the above mentioned attractive properties of velocity signal reconstruction, several approaches to achieve this have been reported in the literature and a comprehensive overview can be found in ref. 99. Some of these techniques are focused on spectral estimation, whereas our efforts are primarily aimed at reconstruction of the velocity signal in time domain to obtain signals, similar to those

## *Retrieval of turbulence and turbulence properties from LDA data with noise*

of Hot-Wire Anemometry (HWA)<sup>1</sup>. The following discussion should be viewed with this background. The simplest polynomial reconstruction techniques, Sample and Hold (S&H) and first-order reconstruction, will be discussed in the next section. The other approaches mentioned in ref. 99 (Shannon Reconstruction, Fractal Reconstruction and Projection onto Convex Sets) did neither seem very promising for temporal reconstruction nor did cope with noise in the individual velocity estimates well. Therefore these approaches have not been evaluated further for reasons that will become clear in the next section.

After a discussion of the simplest polynomial reconstruction techniques and the influence of the measurement noise on the reconstruction noise, we will develop the first-order Kalman reconstruction scheme in this chapter. In Chapter 12 we will discuss the extended reconstruction filter, which will lead to the best estimators for the instantaneous velocity available at this moment.

### **7.2 Zero-order (S&H) and first-order reconstruction.**

The simplest approach for velocity signal reconstruction is the S&H technique, in which the latest measured value is used as the estimator of the velocity until the next measurement value is available<sup>2</sup>. We have encountered this in the previous chapter where the minimum required data-rate has been derived. The second option is -of course- first-order<sup>3</sup> reconstruction and the question is how well these approaches reconstruct the velocity fluctuations. To study this question let us use an ideal situation first: every velocity estimator is perfect, so no noise is added to it. Zero-order reconstruction will lead to an increasing difference between the actual velocity and the estimated velocity due to turbulence. The difference is the reconstruction noise, as is illustrated in fig. 7.1. This difference between the estimated and actual velocities is significantly lower when first-order reconstruction is used as is shown in fig. 7.2, in agreement with the results on periodic signals as discussed in Chapter 6. In the limiting case of the data-rate going to infinity, the error goes notably faster to zero than with S&H reconstruction. This would make first-order reconstruction an ideal approach as a high data-rate is required for reconstruction anyway, as has been shown in Chapter 6.

However, every estimator of the instantaneous velocity has a noise contribution and introducing this in the above calculation shows that the difference between the S&H and first-order reconstruction is far less, as can be seen from fig. 7.3 and 7.4. Yet, first-order reconstruction has an advantage over zero-order reconstruction as is illustrated in fig. 7.5 (in agreement with the results presented in Chapter 6) and therefore we will use it as the first step in our reconstruction approach. However, we can draw an essential conclusion at this stage: *any reconstruction technique that should give a realistic representation of the instantaneous velocity should take the noise contribution into account in order to compensate for it as much as possible*. This is the main reason why the alternative reconstruction schemes, studied in ref. 99 are not evaluated any further. It also means that more sophisticated reconstruction techniques than S&H and first-order are required. The first-order Kalman reconstruction, followed by an extended reconstruction filter, showed to be a fruitful approach.

Before we will describe this technique, it should be mentioned that any velocity signal reconstruction technique is -and always will be- the use of fragmentary information to re-create the whole. The dangerous pitfall of this is that one creates "self-fulfilling prophecies": what comes out are the assumptions one has put in. Therefore some people oppose this approach. To avoid this pitfall it is

---

<sup>1</sup> Note that perfect temporal reconstruction would automatically lead to a perfect estimator for the power spectrum. However, imperfect reconstruction might be optimised for either temporal or spectral estimation.

<sup>2</sup> Note that trackers did the same on a hardware basis.

<sup>3</sup> This is equivalent to piecewise linear interpolation.

## 7. Velocity signal reconstruction I

necessary to base the velocity signal reconstruction scheme on as little assumptions as possible and to support the ones we use with knowledge of turbulence already available or to use experimental evidence. Any other information that is required should be derived from the (raw) data itself. Although this is not trivial, it is feasible as we will show in the next sections and chapters.

### 7.3 Kalman velocity signal reconstruction.

#### 7.3.1 Background.

The noise in measurements can often be reduced by averaging. If more than one observation of the same measurand is available, the error in the estimation can be reduced by using the averaged value of the observations and the standard deviation of the error in the observation is reduced by the square root of the number of observations. Something similar can be done with LDA velocity estimates: we know that each of the velocity estimates has a noise contribution and we know that the velocity cannot change too fast, as the forces are finite and the fluid has mass and is viscous as well. Therefore it should be possible to obtain a better estimate for the instantaneous velocity by looking at the measurements in the "vicinity" of the current observation too. The word "estimator" should be emphasized as it should be noted -again- that the higher the quality of the input data, the better the output of the reconstruction algorithm will be. The Kalman reconstruction is no miracle cure either. The concept of the first-order Kalman reconstruction algorithm will be described in the next sections.

#### 7.3.2 Derivation of the First-Order Kalman Reconstruction Algorithm.

Kalman filtering was originally developed for dynamic system estimation and control purposes. Based on the current knowledge, it constructs optimal estimates of internal ("state") variables, taken into account that the information is accompanied by noise. The noise level(s) need to be known and a dynamic model is required to describe the behaviour of the system under study. In this case, turbulence is the system of investigation. Unfortunately, assumptions are unavoidable, but we will try to restrict these as much as possible and to validate these.

##### 7.3.2.1 Assumptions.

For the first-order Kalman reconstruction scheme, four assumptions have been made. These are for steady flows:

1. The time-interval distribution of the times between two successive Doppler signals is exponential and the corresponding cut-off frequency of the filtering ( $1/2\pi t_0$ ) lies at or above the highest frequency of interest for the turbulence. This assumption is generally correct, but deviations of the ideal time interval distribution occur, as has been described in Chapter 4 on preliminary diagnostic testing of experimental data-sets. However, experiments have shown that the time interval distribution is close to exponential with well-done measurements. On top of that this assumption is not very critical, its main purpose is to validate the highest frequencies in the turbulence that can be reconstructed.
2. The power spectrum can be approximated by that of first-order (low-pass) filtered noise (see fig. 7.6). This assumption means that the turbulence power has a "constant" level below and is proportional to  $f^{-2}$  above a certain frequency. It comes close to a slope of -1.67 (on a log/log plot) which is often reported in literature for the inertial subrange (ref. 1, 2, 72 and 75) and the slope of -2.5 for developing flows (ref. 65 and 66). This is related to the situations where the accelerations of the fluid are limited by inertial and frictional forces. The turbulence cut-off frequency can be estimated from the power spectrum (e.g. from a Fourier transformation of the slotted auto covariance function, which will be discussed in Chapter 10). In case of bias, the auto covariance function could be obtained from the signal reconstruction scheme as will be described in Chapter 8. In either way the information of the data itself is used for the determination of the important

## Retrieval of turbulence and turbulence properties from LDA data with noise

parameters. The auto covariance function can also be used for the determination of the Signal-to-Noise Ratio (SNR) of the velocity estimates.

3. The turbulence generating accelerations and the (measurement) noise contributions in the velocity estimates are not correlated with each other. This is illustrated in fig. 7.7 and 7.8, which show the slotted auto correlation functions of LDA data. The noise peak at  $\tau = 0$  clearly stands out<sup>4</sup> and has disappeared as soon as the time delay  $\tau$  becomes  $> 0$ . Although these figures show that the noise is not correlated with the velocity either, the *variance* of the noise is in some cases correlated with the velocity, as becomes clear by comparing fig. 7.9 and 7.10. Usually this is caused by the processor or the measurement set-up<sup>5</sup>. It should either be verified or taken into account in the scheme. As the latter will complicate the reconstruction algorithm, it is better to use a processor that has a velocity independent noise level.
4. The dynamic model that characterizes the turbulence dynamics is linear(izable) with respect to the state variables.

### 7.3.2.2. The Turbulence Model.

The following simple dynamic model for the evolution of the velocity  $v(t)$  over time  $t \geq t_{begin}$ , of a particle with mass  $m$  in a turbulent flow, is used (Newton's law):

$$\frac{d}{dt}v(t) = -\frac{\lambda^*}{m}v(t) + \frac{\zeta(t)}{m} = -\lambda v(t) + \xi(t) \quad [7.1]$$

in which:

$v(t)$	= velocity	m/s
$t$	= time	s
$\lambda^*$	= $\lambda \cdot m$	kg/s
$m$	= mass	kg
$\zeta(t)$	= $\xi(t) \cdot m$	kgm/s
$\lambda$	= characteristic radial frequency of first-order Kalman reconstruction filter	rad/s
$\xi(t)$	= turbulence generating white noise signal	m/s <sup>2</sup>

The driving acceleration term  $\xi(t)$  is assumed to be equivalent to a Gaussian distributed *continuous-time, white* noise signal with an intensity  $\sigma^2$ . The mean value of  $v(t)$  has to be zero. If this is not the case, the average of  $v(t)$  has to be subtracted from  $v(t)$  because we are only interested in the turbulent fluctuations of the velocity. The term  $-\lambda v(t)$  models the frictional de-acceleration, with parameter  $\lambda \geq 0$ . The velocity  $v(t)$  can be measured at stochastic, Poisson distributed times  $t_k$  (the innovations  $t_k - t_{k-1}$  being identically, independently exponentially distributed), yielding

$$v_k^{obs} = v(t_k) + \eta_k \quad ; \quad k = 0,1,2,\dots \quad [7.2]$$

in which:

$v_k^{obs}$	= velocity observation #k	m/s
$\eta_k$	= Gaussian distributed <i>white</i> noise sequence with variance $\rho^2$	m/s

<sup>4</sup> Note that the ACF at  $\tau = 0$  is equal to 1!

<sup>5</sup> There are several possibilities for a correlation between the velocity and the noise in the corresponding velocity estimate. An obvious one is a non-white noise floor in the Doppler signal (see also Chapter 3), but it can also be caused by the processor. If e.g. the number of cycles used by a counter processor depends on the frequency of the Doppler signal, the noise will depend on the frequency, as has been elucidated in Chapter 3.

## 7. Velocity signal reconstruction I

i.e.

$$\eta_k \sim \mathbf{N}(\mathbf{0}, \rho^2) \quad [7.2^a]$$

and

$$E[\eta_k \eta_l] = \mathbf{0} \text{ for all } k \neq l. \quad [7.2^b]$$

in which:

$E$  = expectation value of

Experimental data show the validity of this assumption, as can be seen from fig. 7.7 and 7.8.

### 7.3.2.3 Design of the Kalman Filter.

It is well known (see e.g. ref. 100 for the system-theoretic setting, or for a concise statistical treatment in discrete time ref. 101) that the optimal state-estimation problem leads to a Kalman filter design. Let  $\underline{x}$  be the dynamic state (vector) of the system which consists of all the variables needed to describe the system, then its evolution in time is (approximately) given by a set of first-order linear differential equations

$$\frac{d}{dt} \underline{x}(t) = \mathbf{A} \underline{x}(t) + \underline{\xi} \quad [7.3]$$

in which:

$\mathbf{A}$  = the system matrix

$\underline{\xi}$  = the stochastic driving term of the system.

$\underline{\xi}$  is a vector with white Gaussian noises with a mean of 0 (zero). The observation equation of this system is given by

$$\underline{y} = \mathbf{C} \underline{x} + \underline{\eta}. \quad [7.4]$$

in which:

$\mathbf{C}$  = observation matrix of the system

$\underline{y}$  = the measured quantities on the state of the system  $\underline{x}$  at a given time  $t$ .

$\underline{\eta}$  = the measurement noise.

This equation reflects the dependence of the measured quantities on the state of the system, showing that the measurement noise makes it impossible to carry out measurements which are exact. Both the measurement noise  $\underline{\eta}$  with variance  $\rho^2$  and the stochastic turbulence generating noise  $\underline{\xi}$  with variance  $\sigma^2$  are white and Gaussian distributed.

The optimal prediction of  $\underline{x}(t)$  is a (deterministic) vector which equals the conditional expectation

$$\hat{\underline{x}}(t) = E[\underline{x}(t) | \underline{y}(s); s \leq t] \quad [7.5]$$

in which:

$\hat{\underline{x}}$  = optimal prediction of  $\underline{x}(t)$

This is therefore the expected value for the unmeasured  $\underline{x}(t)$ , based on all past measurement information. This prediction can be shown to minimize the squared prediction error

## Retrieval of turbulence and turbulence properties from LDA data with noise

$$\int_0^t E \|\hat{x}(z) - x(z)\|^2 dz \quad [7.6]$$

in the class of all linear filters.

The optimum prediction can be calculated from

$$\frac{d}{dt} \hat{x}(t) = \mathbf{A} \hat{x}(t) + \mathbf{L} \mathbf{e}(t) ; \quad \mathbf{e}(t) = y(t) - \mathbf{C} \hat{x}(t) \quad [7.7]$$

in which:

$\mathbf{L}$  = the filter gain

$\mathbf{e}(t)$  = the difference between the actual measured value and the value which should have been measured based on the values of the predictions (internal state variables) of the system.

The dynamics of the predictions (estimations) partly follow the dynamics of the system model and are partly corrected for the deviations of the measurements from the internal state. When  $\mathbf{L}$  is small, the filter mainly trusts its own internal system model and the feedback based on actual measured values is small. When  $\mathbf{L}$  is large, the measurements are regarded as more trustworthy. In real-time applications, the filter gain is also a function of time which converges towards a constant value. In this case, the LDA measurements have already been done and simplifications can be made by calculating the filter gain in advance (off-line) using the static equations for the filter gain.

The (static) Kalman *filter gain (matrix)* equals

$$\mathbf{L} = \mathbf{A} \mathbf{C}' \mathbf{\Pi}^{-1} \quad [7.8]$$

in which:

$\mathbf{\Lambda}$  = the (positive definite) matrix, which is the solution to a Ricatti equation:

$$\mathbf{\Lambda} \mathbf{A} + \mathbf{A}' \mathbf{\Lambda} - \mathbf{\Lambda} \mathbf{C}' \mathbf{\Pi}^{-1} \mathbf{C} \mathbf{\Lambda} + \mathbf{\Sigma} = \mathbf{0} \quad [7.9]$$

$\mathbf{C}'$  = transpose of  $\mathbf{C}$ ;  $C'_{ij} = C_{ji}$

$\mathbf{\Sigma}$  = the covariance matrix of  $\xi$ .

$\mathbf{\Pi}$  = the covariance matrix of  $\eta$ .

If one applies the equations of the Kalman filter to the equations of the first-order turbulence model (with  $A = -\lambda$ ,  $C = 1$ ,  $\Pi = \rho^2$  and  $\Sigma = \sigma^2$ ), the optimal filter gain is seen to be

$$L = -\lambda + \sqrt{\lambda^2 + \frac{\sigma^2}{\rho^2}} \quad [7.10]$$

Note that in this application  $L$  is scalar.

Using the equation to compute the optimum prediction, it follows that the filter dynamics behave according to

## 7. Velocity signal reconstruction I

$$\frac{d}{dt} \hat{v}(t) = -\sqrt{\lambda^2 + \frac{\sigma^2}{\rho^2}} \hat{v}(t) + \left(-\lambda + \sqrt{\lambda^2 + \frac{\sigma^2}{\rho^2}}\right) v^{obs}(t) = -\gamma \hat{v}(t) + \delta v^{obs}(t) \quad [7.11]$$

$$\hat{v}(t_0) = v_0^{obs} \quad [7.11^a]$$

in which:

$$\gamma = \sqrt{\lambda^2 + \frac{\sigma^2}{\rho^2}} = L + \lambda \quad [7.12]$$

$$\delta = -\lambda + \sqrt{\lambda^2 + \frac{\sigma^2}{\rho^2}} = L \quad [7.13]$$

The variables  $\gamma$  and  $\delta$  have been introduced for later convenience. Since  $\lambda \geq 0$  and  $\sigma/\rho \geq 0$ , the filter is stable in the bounded input, bounded output sense.

There is, however, one structural difficulty, namely that the specific continuous-time Kalman filter requires continuous measurements of the velocities  $v^{obs}(t)$ ,  $t \geq t_{begin}$ . If the Kalman reconstruction filter is applied directly to the time series, only discrete-time measurements are available and some assumption on the intermediate behaviour has to be formulated. When the time intervals of the time series are constant because some signal reconstruction has already been applied to the signal, the same procedure can be followed.

As has been discussed in Chapter 6, we have chosen to use first-order reconstruction as the first step. This is straightforward and is offered by using linear components, i.e. for  $k = 0, 1, 2, 3, \dots$

$$v^{obs}(t) = \alpha_k t + \beta_k \quad (t_k \leq t \leq t_{k+1}) \quad [7.14]$$

in which:

$$\alpha_k = \frac{v_{k+1}^{obs} - v_k^{obs}}{t_{k+1} - t_k} \quad [7.14^a]$$

$$\beta_k = \frac{t_k v_{k+1}^{obs} - t_{k+1} v_k^{obs}}{t_k - t_{k+1}}. \quad [7.14^b]$$

With this "measurement" signal, the scalar, linear differential equation can be solved analytically in a sequential fashion.

## Retrieval of turbulence and turbulence properties from LDA data with noise

For  $k = 0, 1, 2, 3, \dots$ , and  $t_k \leq t \leq t_{k+1}$ , the (forward) solution can be recursively obtained from

$$\hat{v}^f(t) = (\hat{v}^f(t_k) - \frac{\delta}{\gamma}(\alpha_k(t_k - \frac{1}{\gamma}) + \beta_k))e^{-\gamma(t-t_k)} + \frac{\delta}{\gamma}(\alpha_k(t - \frac{1}{\gamma}) + \beta_k) \quad [7.15]$$

for given

$$\hat{v}^f(t_{begin}) = v_0^{obs} \quad [7.15^a]$$

This shows that the filter update terms are subject to an (unavoidable) time delay  $1/\gamma$ . In order to correct for the effects of this phase shift, one can apply "bi-directional" Kalman filtering if the measured data are available in batch and (thus) limited in size. Let  $t_N$  be the final measurement time and the corresponding velocity measurement  $v_N^{obs}$ . One then additionally constructs the *backward* filtered prediction, by processing the data using the same procedure in reverse order using the "initial" velocity

$$\hat{v}^b(t_N) = v_N^{obs}. \quad [7.16]$$

This gives for  $k = N-1, N-2, \dots, 1, 0$  and  $t_k \leq t \leq t_{k+1}$

$$\hat{v}^b(t) = (\hat{v}^b(t_{k+1}) - \frac{\delta}{\gamma}(\alpha_k(t_{k+1} + \frac{1}{\gamma}) + \beta_k))e^{-\gamma(t_{k+1}-t)} + \frac{\delta}{\gamma}(\alpha_k(t + \frac{1}{\gamma}) + \beta_k). \quad [7.17]$$

The overall bi-directional prediction can be taken as the average of forward and backward predictions

$$\hat{v}(t) = \frac{\hat{v}^f(t) + \hat{v}^b(t)}{2} = \mathbf{A} + \mathbf{B} + \mathbf{C} \quad [7.18]$$

in which:

$$\mathbf{A} = \frac{\delta}{\gamma}(\alpha_k t + \beta_k) \quad [7.18^a]$$

$$\mathbf{B} = \frac{1}{2}(\hat{v}^f(t_k) - \frac{\delta}{\gamma}(\alpha_k(t_k - \frac{1}{\gamma}) + \beta_k))e^{-\gamma(t-t_k)} \quad [7.18^b]$$

$$\mathbf{C} = \frac{1}{2}(\hat{v}^b(t_{k+1}) - \frac{\delta}{\gamma}(\alpha_k(t_{k+1} + \frac{1}{\gamma}) + \beta_k))e^{-\gamma(t_{k+1}-t)}. \quad [7.18^c]$$

Consequently the bi-directional prediction or estimator is phaselag-free as can be seen from the formulas given above. Note that in the middle of each of the successive time intervals the above expression reduces to

$$\hat{v}(\frac{t_{k+1} + t_k}{2}) = \mathbf{D} + \mathbf{E} \cdot \mathbf{F} \quad [7.19]$$

in which:

$$\mathbf{D} = \frac{\delta}{\gamma}(\alpha_k(\frac{t_{k+1} + t_k}{2}) + \beta_k) \quad [7.19^a]$$

## 7. Velocity signal reconstruction I

$$E = \frac{v^f(t_k) + v^b(t_{k+1})}{2} - \frac{\delta}{\gamma} (\alpha_k \frac{t_{k+1} + t_k}{2} + \beta_k) \quad [7.19^b]$$

$$F = \theta^{-\gamma \left( \frac{t_{k+1} - t_k}{2} \right)} \quad [7.19^c]$$

The first-order Kalman reconstruction scheme is shown schematically in fig. 7.11.

### 7.3.2.4 Determination of the Turbulence Model Parameters.

In order to use the above described filter algorithm, the parameters associated with the turbulence model and the measurement process have to be specified or estimated from the experimental data. These parameters are:

$\lambda$	: first cut-off frequency of the power spectrum of the turbulence	rad/s
$\sigma^2$	: the variance of the driving acceleration term of the turbulence model	m <sup>2</sup> /s <sup>4</sup>
$\rho^2$	: the variance of the measurement noise	m <sup>2</sup> /s <sup>2</sup>

The friction (dissipation) parameter  $\lambda$  can be found to equal the frequency point (in rad/s) where the velocity power spectrum falls off on a log-log plot.

The next quantity to be found is  $(\sigma/\rho)^2$  which is related to the SNR in the measurements because  $\sigma^2$  is the intensity of the driving acceleration of the turbulence and  $\rho^2$  is the variance of the noise in the measurements which can be obtained from the slotted auto covariance function (see Chapter 10). The value in the first slot equals the variance of the velocity fluctuations plus the variance of the noise:  $\sigma_v^2 + \rho^2$ . The value in the second slot is close to the variance of the velocity  $\sigma_v^2$ , so subtracting the value in the second slot from the value in the first slot gives us the parameter  $\rho^2$  (see also Chapter 10).

The last parameter we need to know is the variance of the driving acceleration of the turbulence  $\sigma^2$  which can be derived from the variance of the velocity  $\sigma_v^2$ . The turbulence model reads:

$$\frac{d}{dt} v(t) = -\lambda v(t) + \xi(t) \quad [7.1]$$

The transfer function  $G(j\omega)$  of the model is:

$$G(j\omega) = \frac{1}{\lambda} \frac{1}{1 + j \left( \frac{\omega}{\lambda} \right)} \quad [7.20]$$

The spectrum  $S(\omega)$  can be calculated from eq. [7.1], eq. [7.20] and eq. [6.4], with replacing  $t_0$  by  $1/\lambda$ :

$$S(\omega) = S(0) G(j\omega) G(j\omega)^* \sigma^2 = \frac{4}{\lambda^3} \frac{\sigma^2}{1 + \left( \frac{\omega}{\lambda} \right)^2} \quad [7.21]$$

According to Parseval, the total (mean square) power  $P_s$  contained in this spectrum is equal to:

## Retrieval of turbulence and turbulence properties from LDA data with noise

$$P_S = \frac{1}{2\pi} \int_{-\infty}^{\infty} S(\omega) d\omega = \frac{1}{2\pi} \frac{4}{\lambda^3} \int_{-\infty}^{\infty} \frac{\sigma^2}{1 + \left(\frac{\omega}{\lambda}\right)^2} d\omega = \frac{2}{\lambda^2} \sigma^2 = \sigma_v^2 \quad [7.22]$$

Now, the mean square of the acceleration can be calculated:

$$\frac{2}{\lambda^2} \sigma^2 = \sigma_v^2 \Rightarrow \sigma^2 = \frac{\lambda^2 \sigma_v^2}{2} \quad [7.23]$$

The Kalman reconstruction algorithm does not critically depend on the specific value of the filter gain so its value does not have to be known exactly (ref. 87). Monte Carlo simulations have been performed to search for a filter gain for which the Mean Square Error (MSE) is minimized.

### 7.4 Results.

As stated above, Monte Carlo simulations have been used to determine the "mean squared prediction error", (eq. [7.6]). This is a measure of the difference between the original turbulent velocity fluctuations and the reconstructed turbulence, based on samples obtained as described in Chapter 2. This MSE does not depend strongly on the filter gain, as shown in fig. 7.12. As this filter gain is mainly determined by the SNR of the individual velocity estimates, the determination of the SNR is not critical. This is fortunate as the SNR estimation is influenced by e.g. velocity bias (ref. 102 and Chapter 10). Note that fig. 7.12 also shows that for no value of the filter gain the error becomes zero. It will remain an estimation of the velocity with its limitations.

As a second test, the reconstructed turbulence was compared with the input turbulence of the simulated signal. Two examples are shown in fig. 7.13 and 7.14, showing that the extreme excursions, due to the noise, have disappeared. As a result the reconstructed velocity resembles the input signal a lot better. Similar improvements, albeit only qualitatively<sup>6</sup>, are obtained when we apply the first-order Kalman reconstruction to experimental data, as is shown in fig. 7.15 and 7.16.

Because the first-order Kalman reconstruction limits the accelerations, this should be clear by comparison of the accelerations in the raw and the Kalman reconstructed signals. Fig. 7.17 confirms this and it shows that the extreme values of more than 10 km/s<sup>2</sup> are effectively suppressed. The distributions of the accelerations, shown in fig. 7.18 and 7.19, illustrate this even more clearly because the distribution after first-order Kalman reconstruction is in better agreement with the current knowledge of turbulence than the distribution before the first-order Kalman reconstruction.

The distributions of the raw velocity data and after first-order Kalman reconstruction show that the bias has been eliminated by the Kalman reconstruction (as it would have been by any other reconstruction scheme). This can be seen from fig. 7.20. Note that the distribution is not purely Gaussian, but that has not caused any problems with the first-order Kalman reconstruction. The deviations due to bias are corrected, but the skewness itself remains intact.

Fig. 7.21 shows the power spectrum as it is obtained using first-order reconstruction (linear interpolation) when noise is present in the individual velocity estimates. Also drawn is the Bessem power spectrum from which the signal has been derived. Note that the deviations are already noticeable above the noise floor itself. Using first-order Kalman reconstruction, the deviations are significantly smaller as

---

<sup>6</sup> Unfortunately, the original velocity fluctuations are unknown, so the signals have to be examined with general knowledge of turbulence only.

## *7. Velocity signal reconstruction I*

can be seen from fig. 7.22. Especially the retrieval of the frequency where the dissipation begins is more accurate. Application of the first-order Kalman reconstruction to measured data results in the spectrum of fig. 7.23, which can be compared to the spectrum of fig. 7.24, which has been obtained by the cross-covariance technique applied to tracker signals (ref. 50).

Others have made comparisons between several data-processing techniques and the first-order Kalman reconstruction. These have shown to be favourable for the first-order Kalman reconstruction for the estimation of the auto correlation function and the turbulence power spectrum (ref. 103) as well as for the estimation of structure functions (ref. 104). These experiences are in agreement with those reported in this chapter, but some limitations were reported as well. These are caused by the limitations of the turbulence model used in the first-order Kalman reconstruction.

### **7.5 Concluding remarks.**

The fig. 7.13 - 7.23 show that the first-order Kalman reconstruction leads to better results than different approaches, which is confirmed by the work of others (ref. 103 and 104). However, it is obvious that still residual noise is present in the reconstructed signals. Further improvement can be obtained by optimal use of the information, contained in the raw LDA data and when the power spectrum of the turbulence is available. These developments will be the subject of the following chapters.

## Retrieval of turbulence and turbulence properties from LDA data with noise

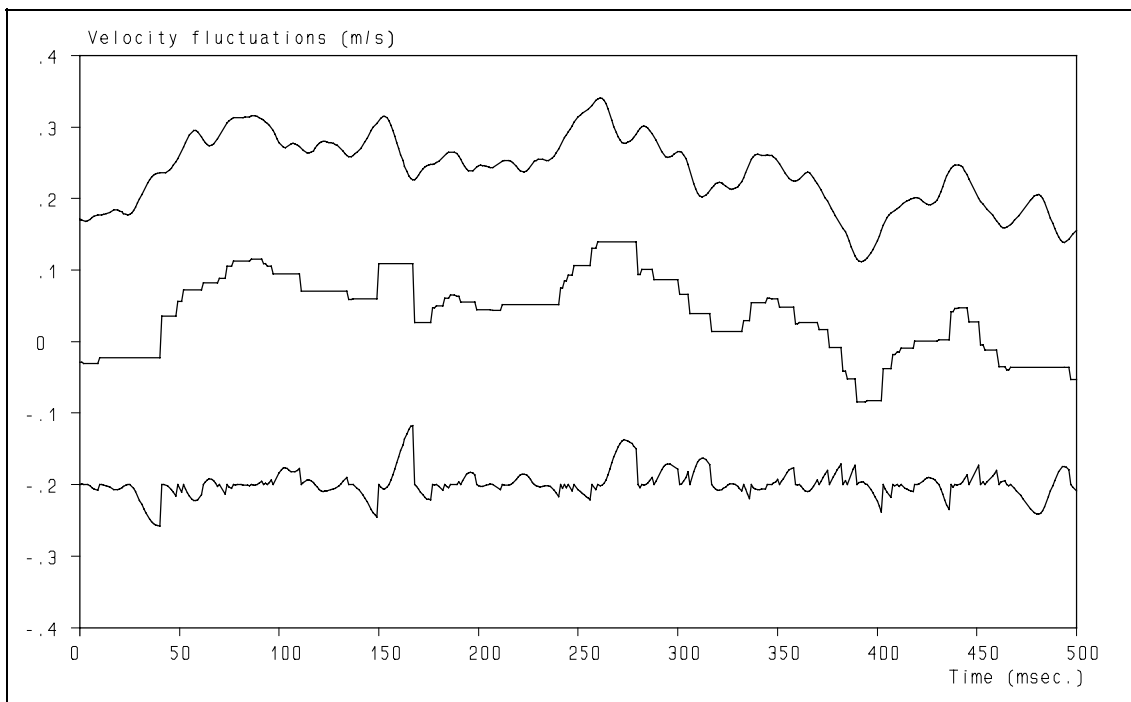


**Figure 7.1:** The difference between the actual and the S&H reconstructed signal is the reconstruction noise, even with perfect velocity estimators.

For fig. 7.1 - 7.4 holds: Upper trace: actual velocity (shifted 0.2 m/s up). Middle trace: reconstructed velocity. Lower trace: reconstruction noise (shifted 0.2 m/s down).

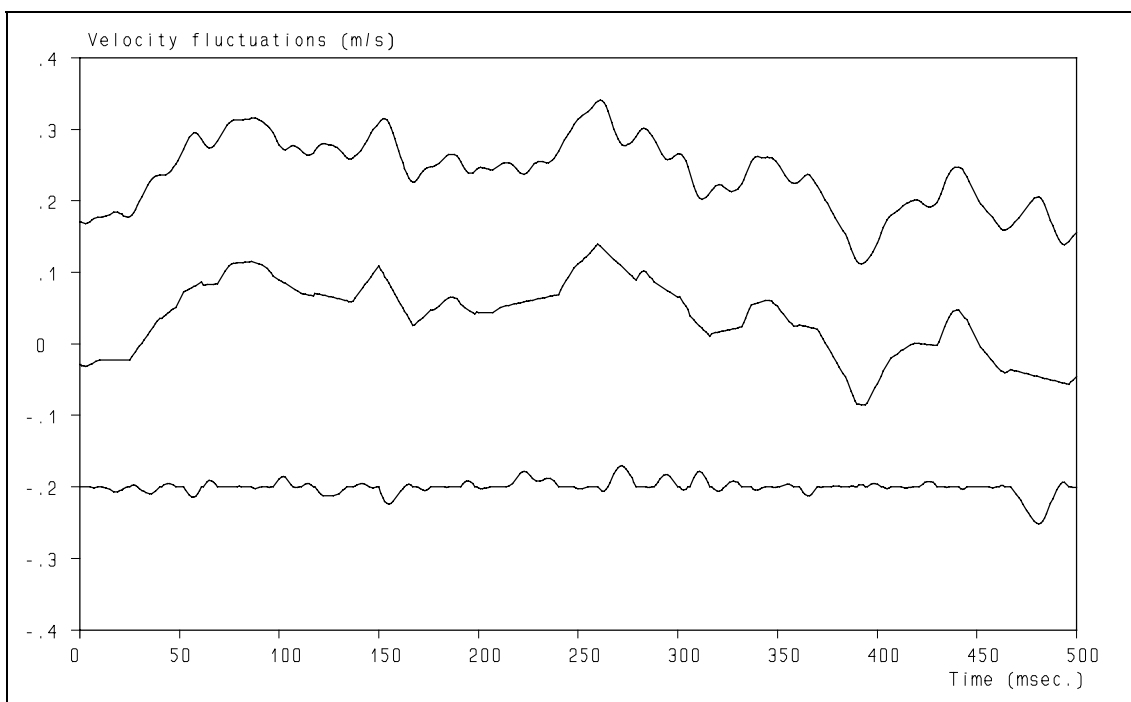


**Figure 7.2:** When the velocity estimators are noise-free, the reconstruction noise is significantly less with first-order reconstruction. Compare with fig. 7.1.

## 7. Velocity signal reconstruction I

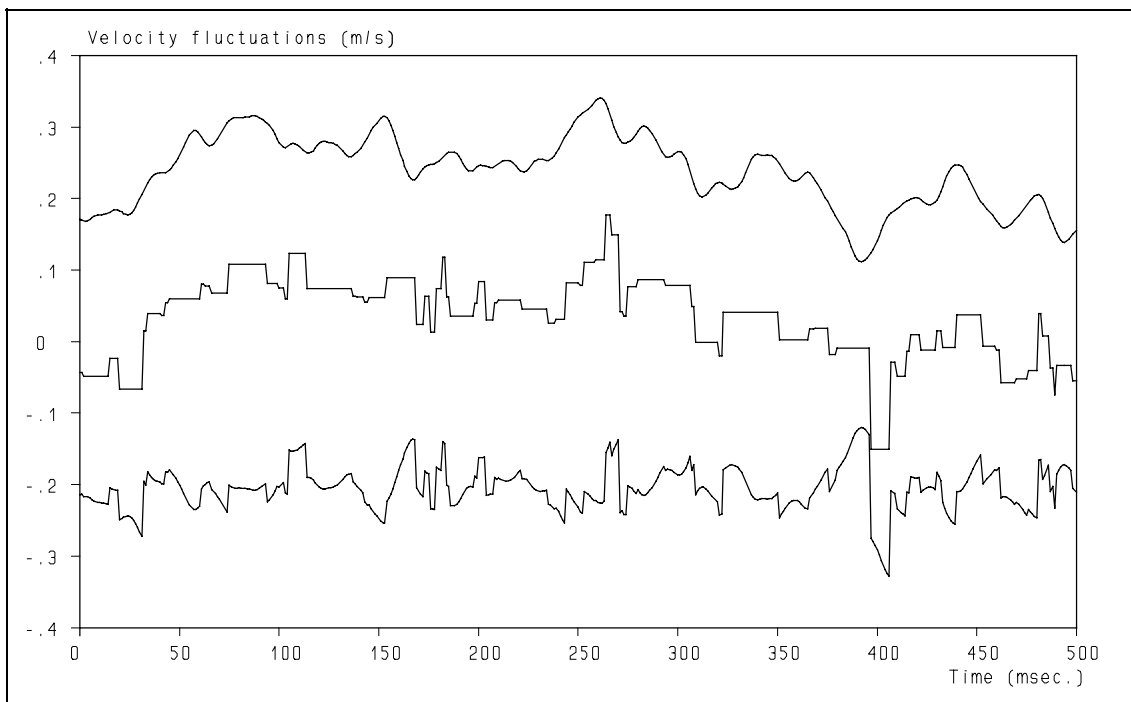


**Figure 7.3:** However, when the individual velocity estimates have a noise contribution, the differences between S&H and first order reconstruction are significantly less. Compare with fig. 7.1, 7.2 and 7.4.

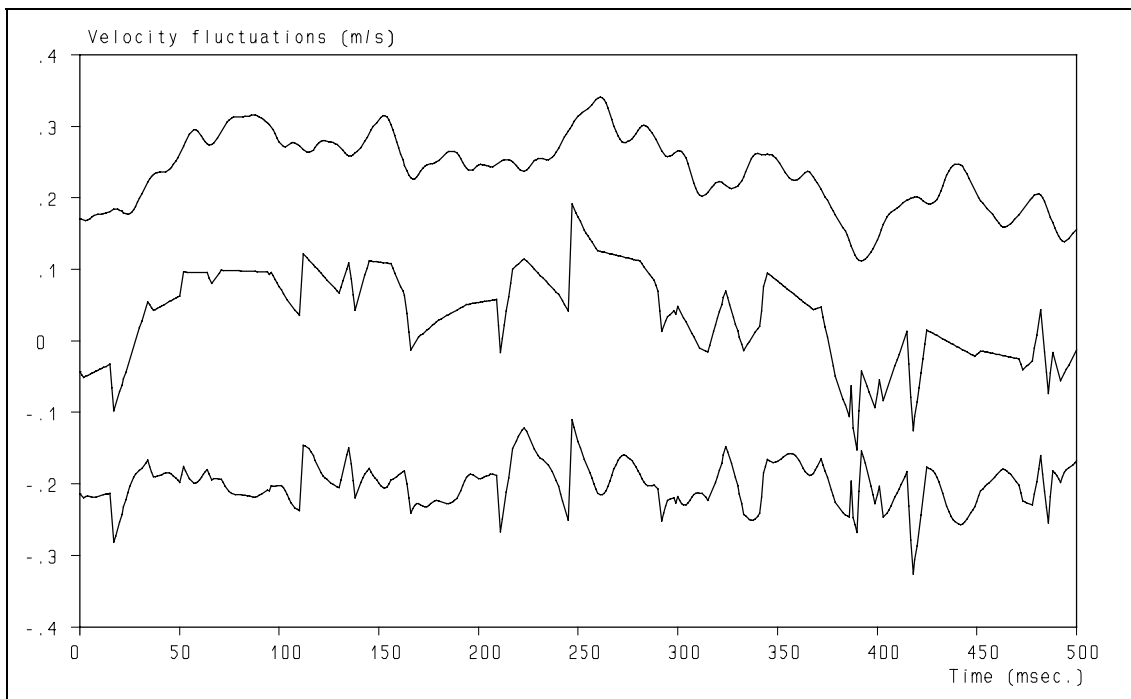


**Figure 7.4:** The reconstruction noise with first order reconstruction and a noise contribution to the individual velocity estimates. Compare with fig. 7.1 - 7.3.

*Retrieval of turbulence and turbulence properties from LDA data with noise*

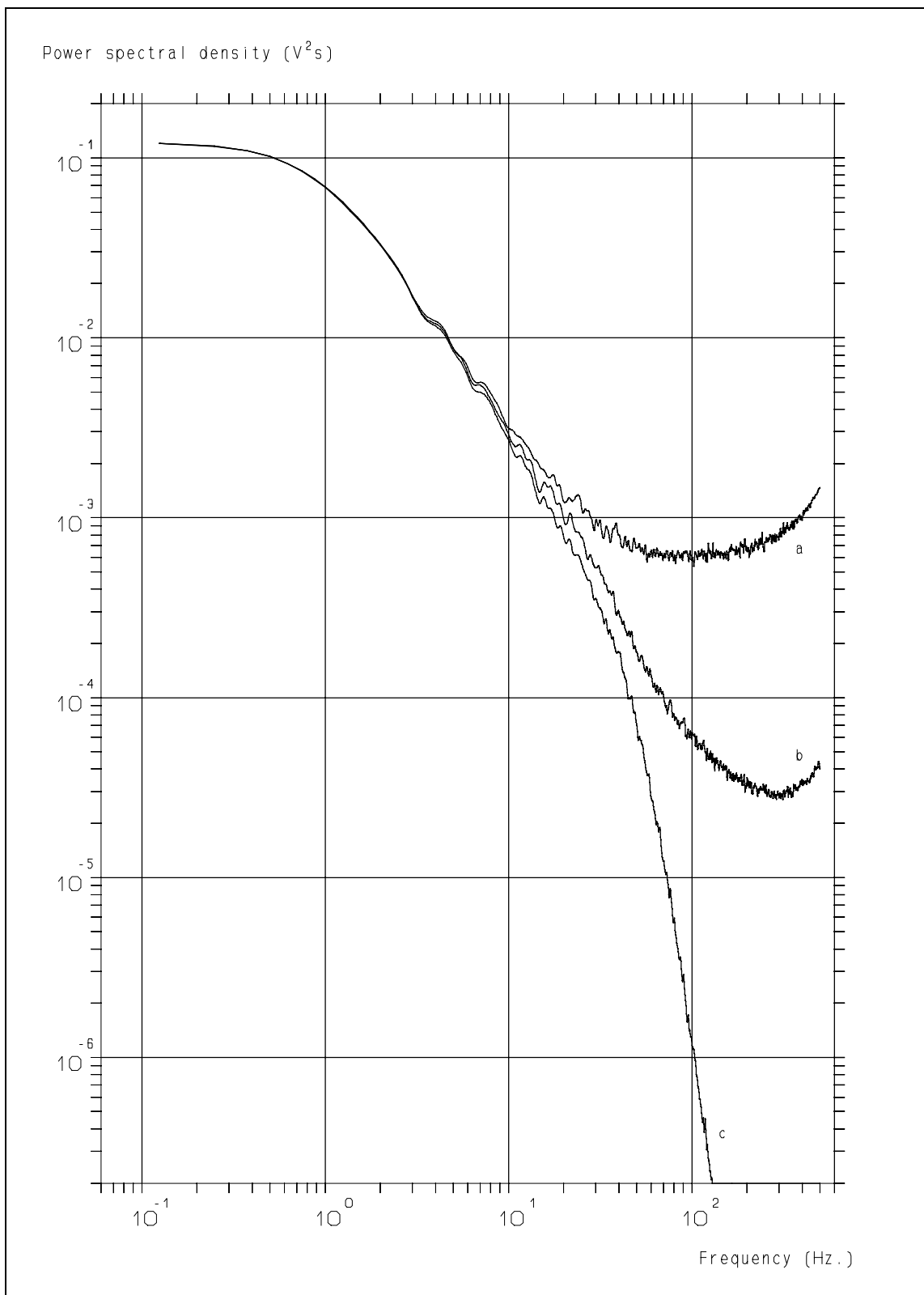


**Figure 7.5:** Even when the velocity estimates have a noise contribution, there is a difference between the zero-order (curve a) and first-order (curve b) reconstructions. Curve c is the actual spectrum of the turbulence.

## 7. Velocity signal reconstruction I

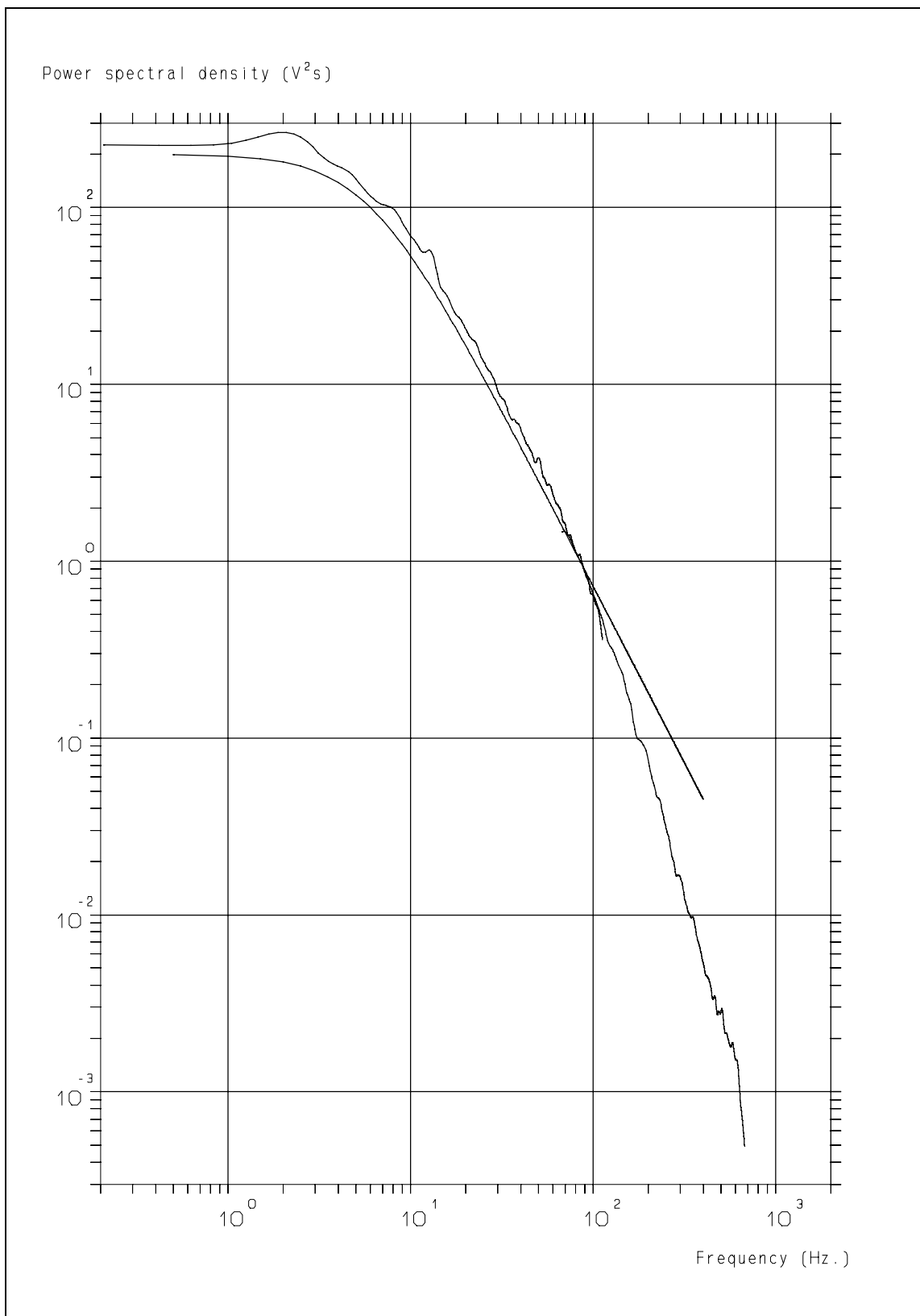


**Figure 7.6:** As can be seen from this turbulence power spectrum, a slope of -2 on a log-log scale gives a reasonable description of its structure.

*Retrieval of turbulence and turbulence properties from LDA data with noise*

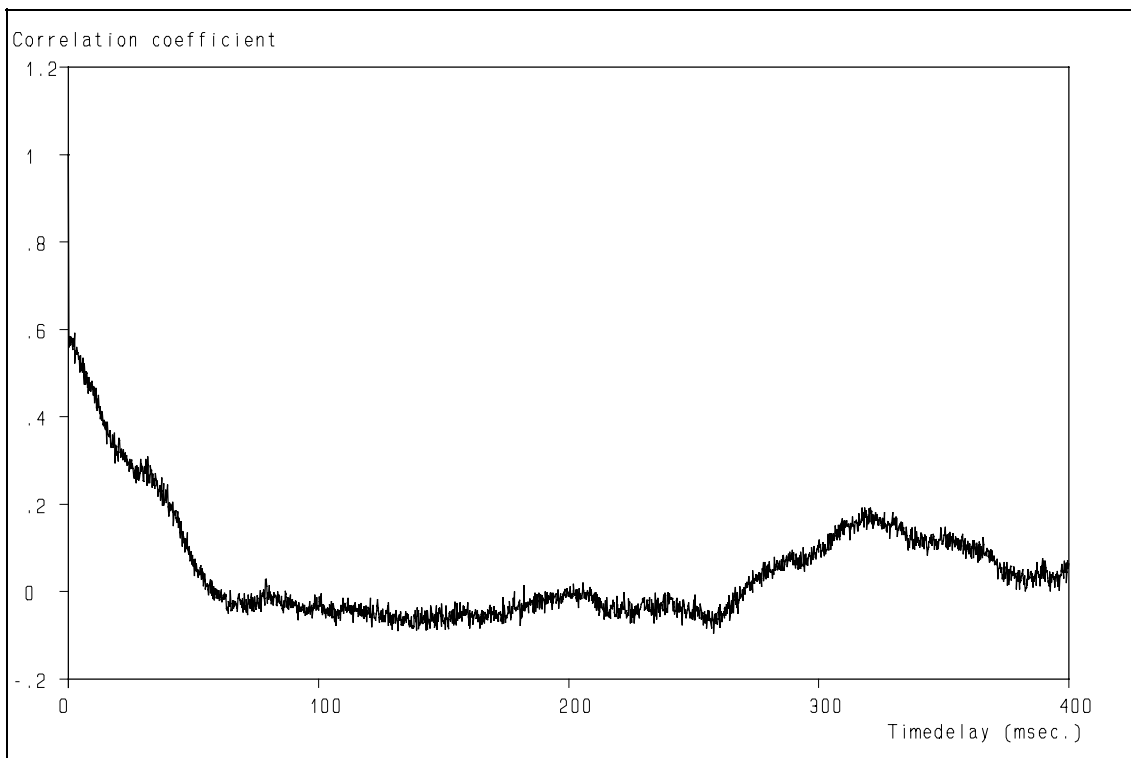


**Figure 7.7:** The auto correlation function shows a clear  $\delta$ -peak at  $\tau = 0$ , where the correlation coefficient is 1. This shows that the noise is not correlated with itself.

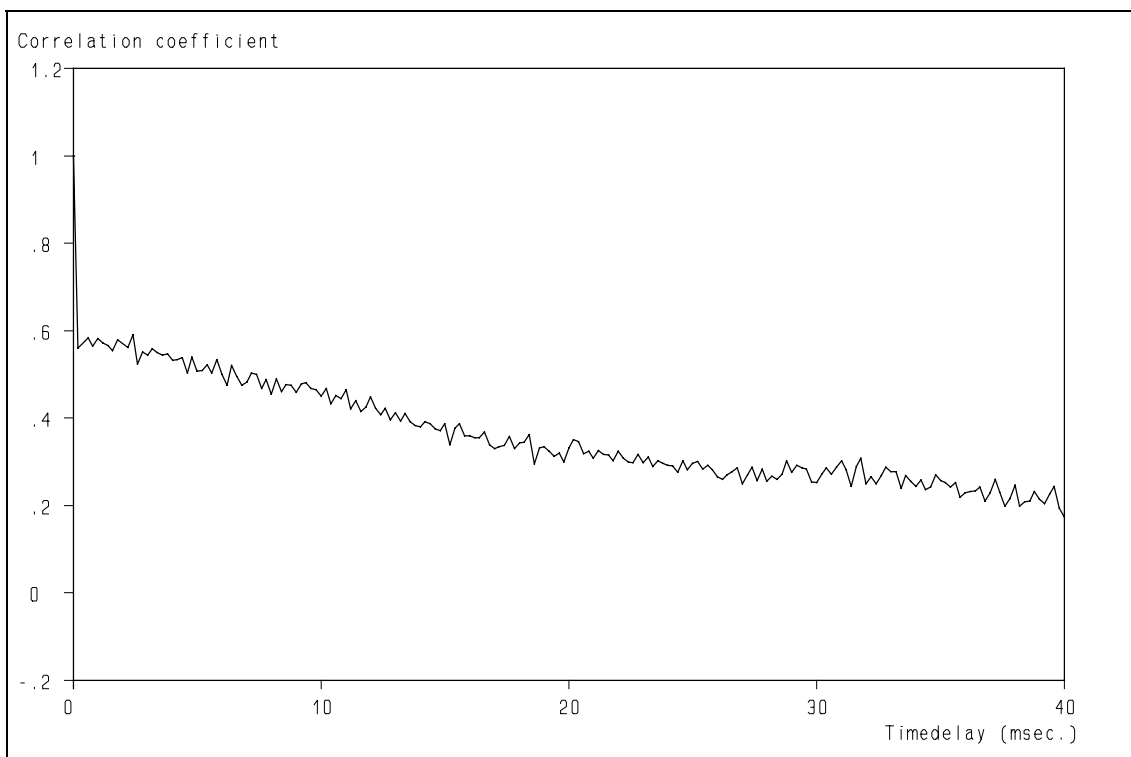


**Figure 7.8:** Even an enlargement of the beginning of the auto correlation function of fig. 7.7 does not show any correlation of the noise with itself.

## 7. Velocity signal reconstruction I

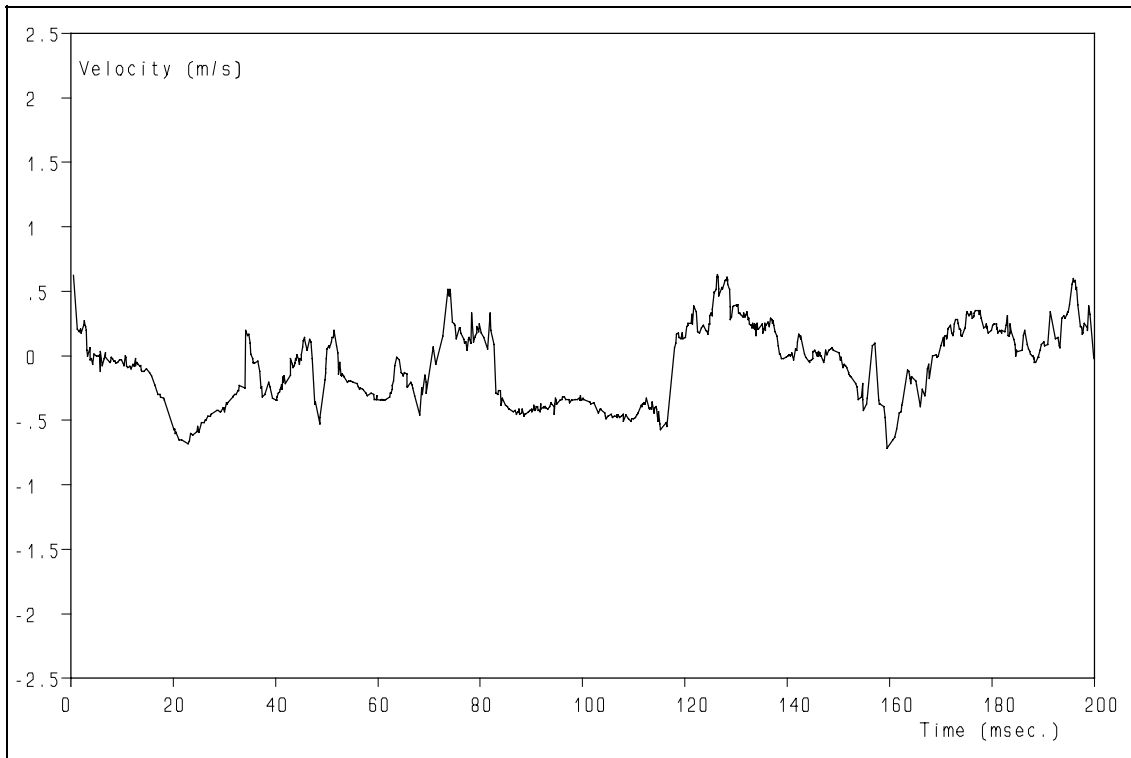


**Figure 7.9:** The raw velocity signal of a processor which shows little or no correlation between the velocity and the noise or noise variance.

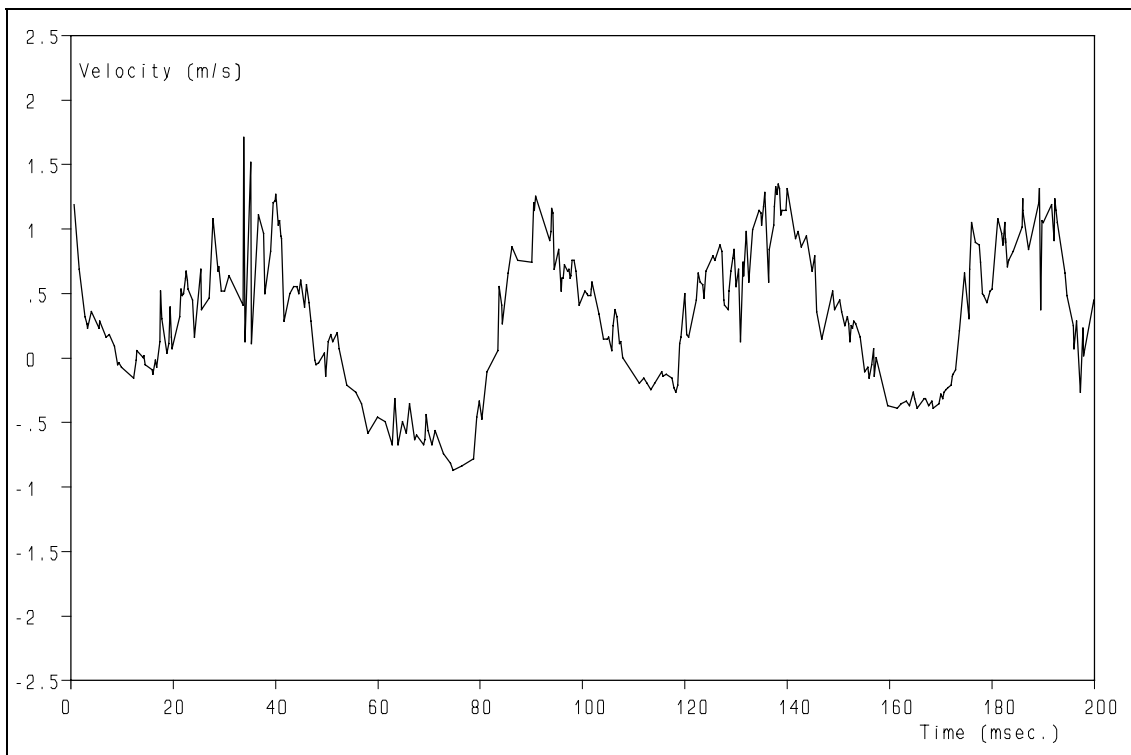


**Figure 7.10:** The raw velocity signal of a processor which seems to show a correlation between the velocity and the noise or noise variance.

Retrieval of turbulence and turbulence properties from LDA data with noise

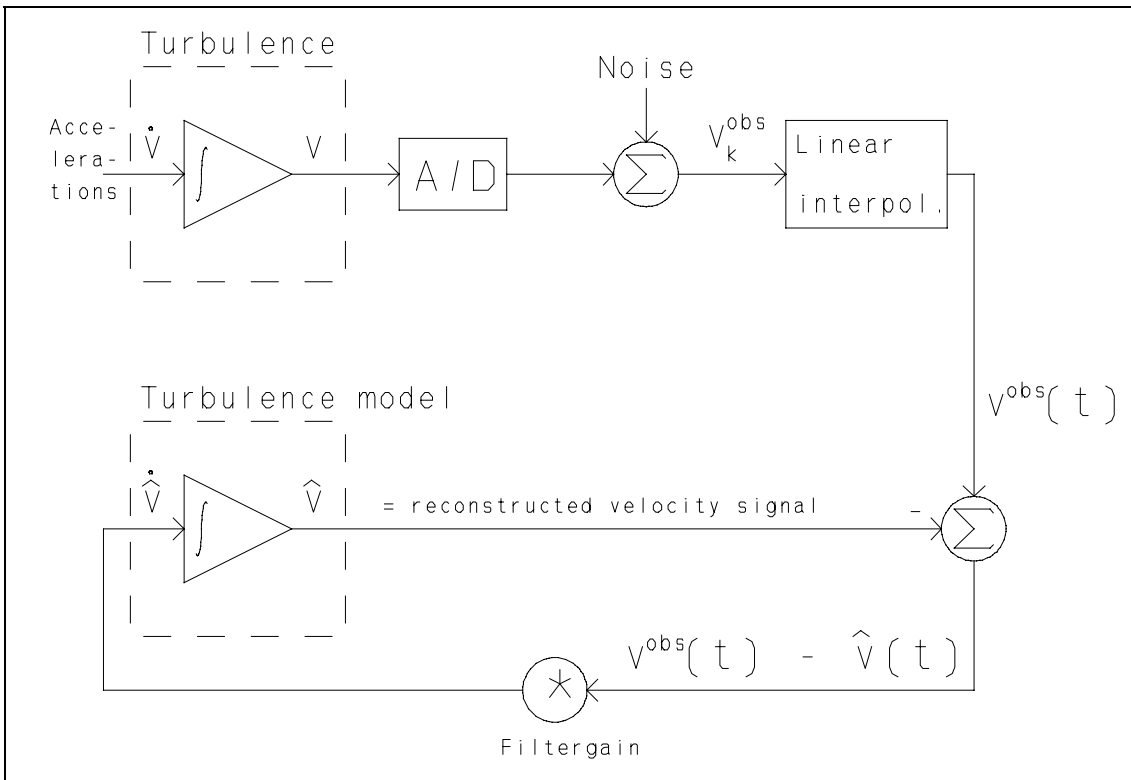


Figure 7.11: Schematic diagram of the first-order Kalman reconstruction filter.

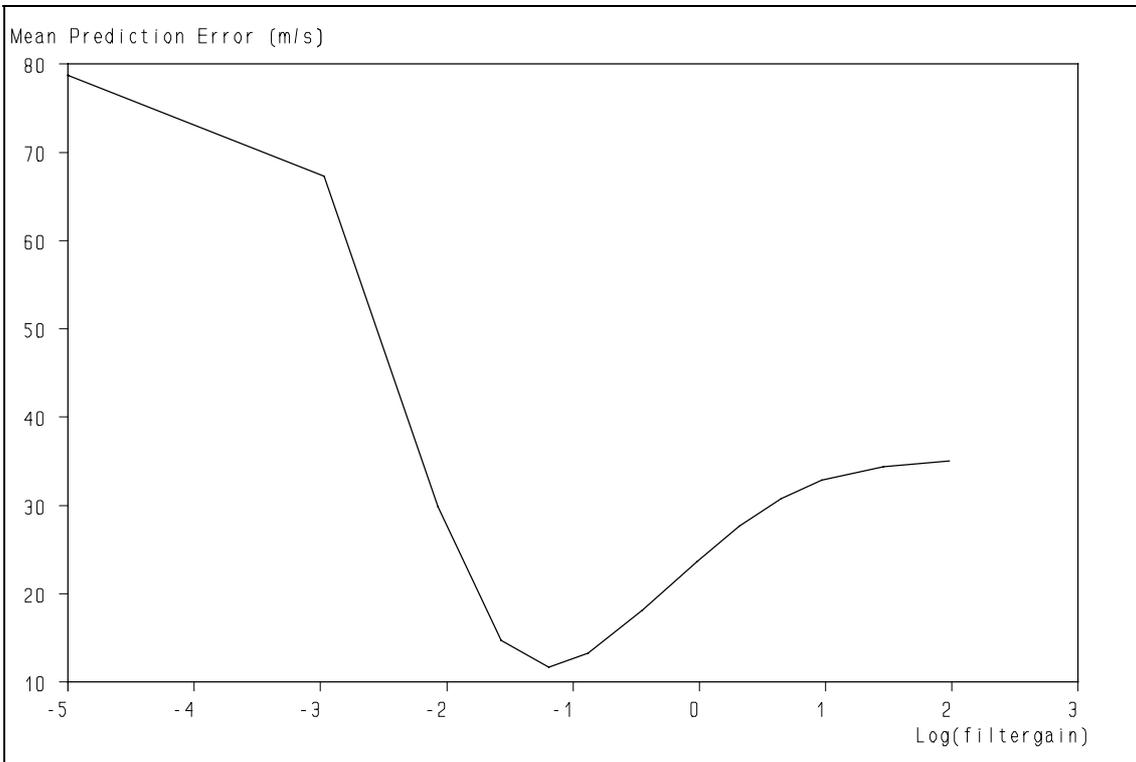
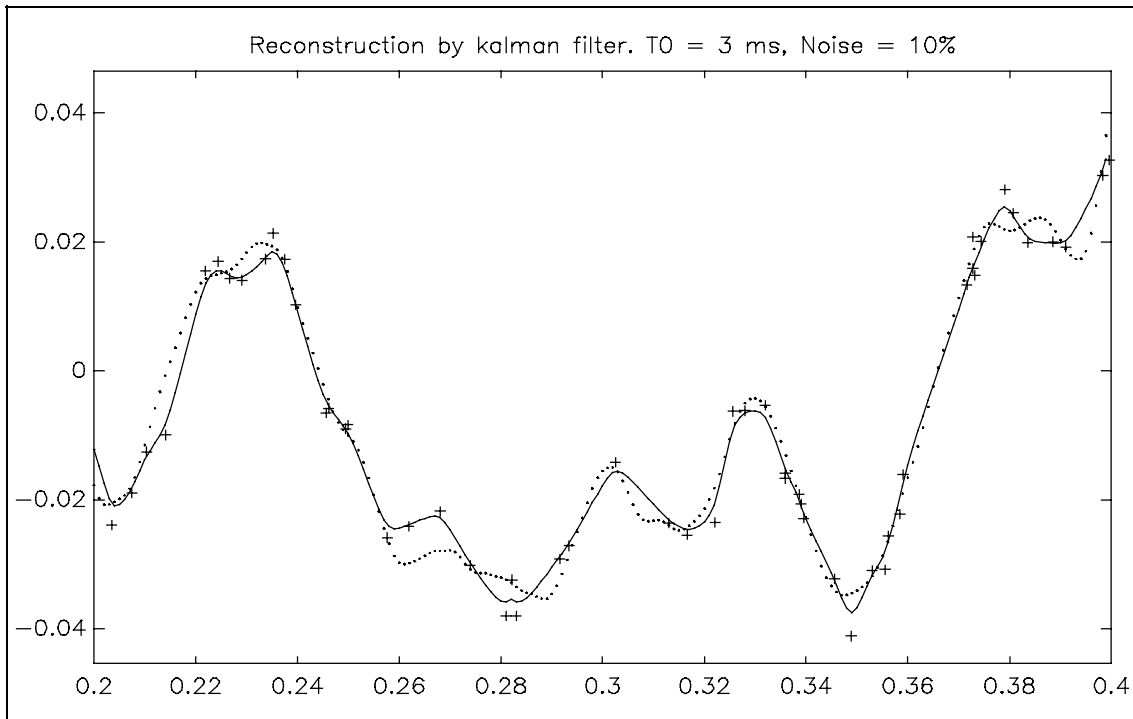
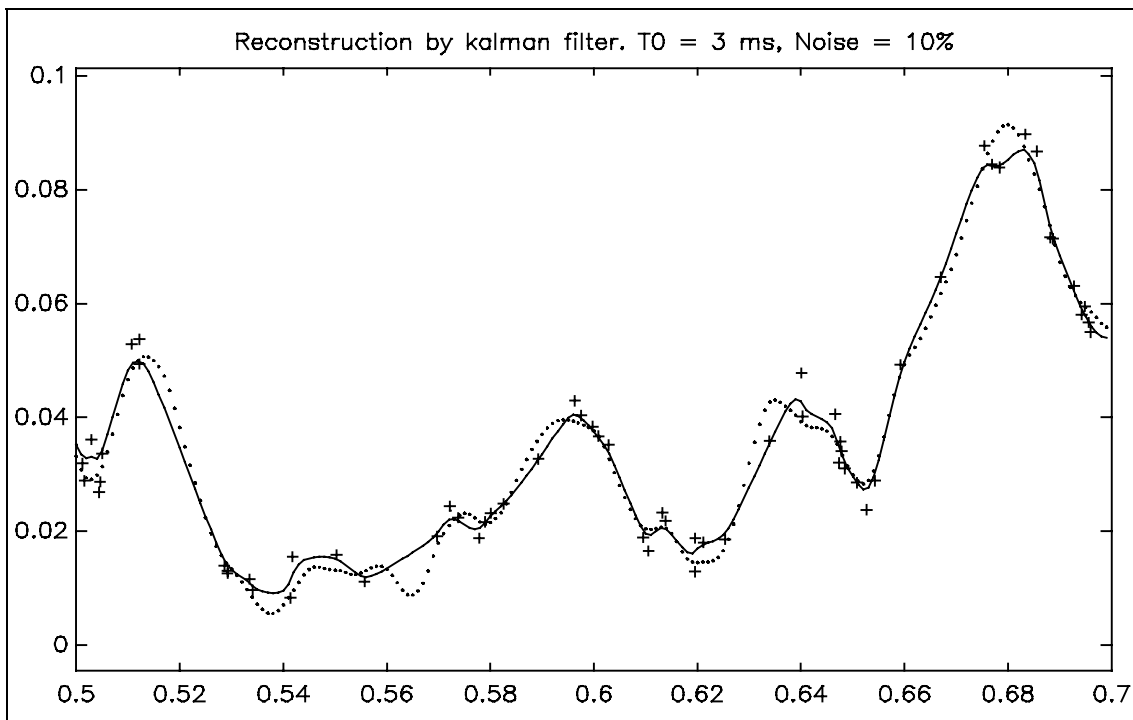


Figure 7.12: The mean prediction error of the bidirectional Kalman reconstruction algorithm as a function of the filter gain.

## 7. Velocity signal reconstruction I



**Figure 7.13:** First-order Kalman reconstruction of simulated turbulence. The dotted line is the input signal, the drawn line the reconstructed signal. "+"s are "measured" values.



**Figure 7.14:** First-order Kalman reconstruction of simulated turbulence. The dotted line is the input signal, the drawn line the reconstructed signal. "+"s are "measured" values.

*Retrieval of turbulence and turbulence properties from LDA data with noise*

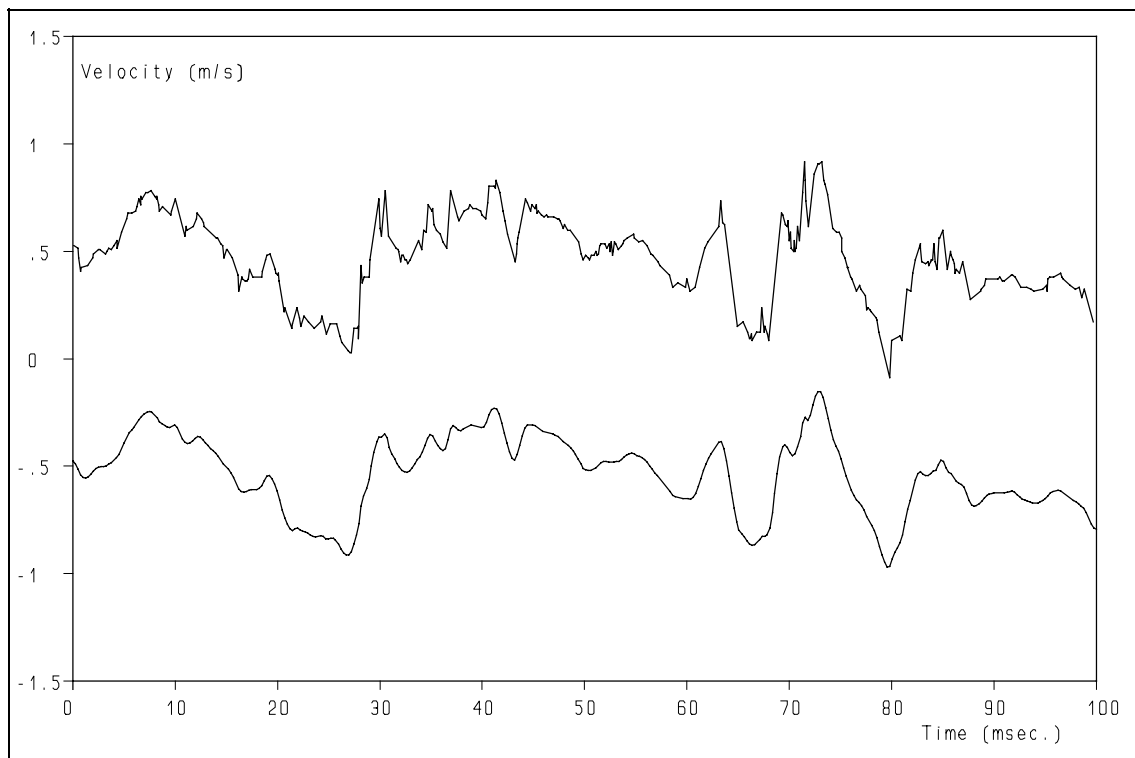


**Figure 7.15:** Raw (upper trace) and first-order Kalman reconstructed signal (lower trace) of experimental data.

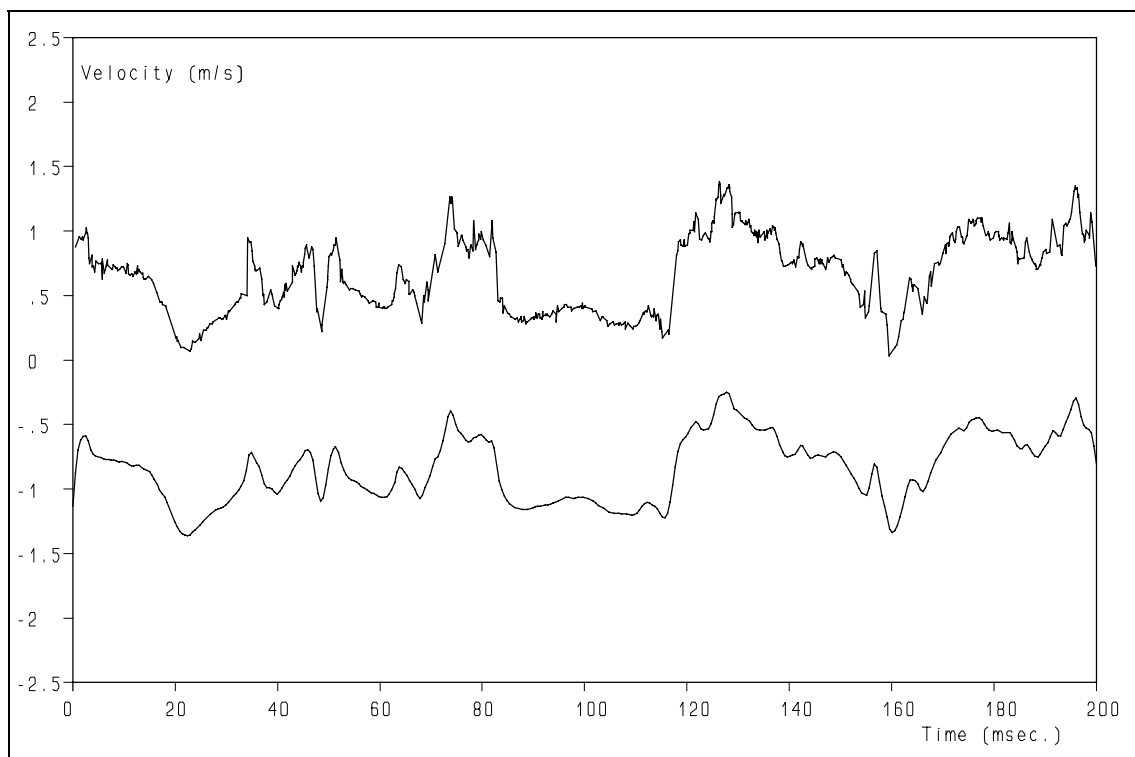


**Figure 7.16:** Raw (upper trace) and first-order Kalman reconstructed velocity (lower trace) from experimental data.

## 7. Velocity signal reconstruction I

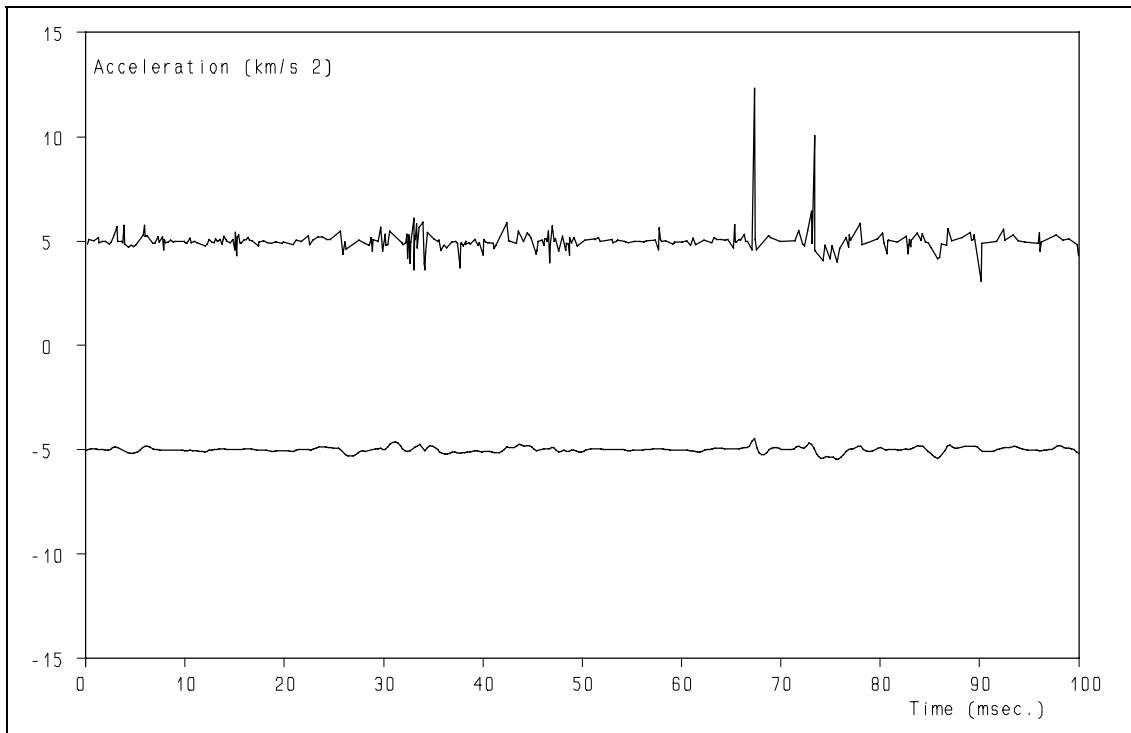


**Figure 7.17:** Accelerations as obtained from the raw (upper trace) and the first-order Kalman reconstructed velocity (lower trace) from the experimental data of fig. 7.15. Note the peaks in the raw data.

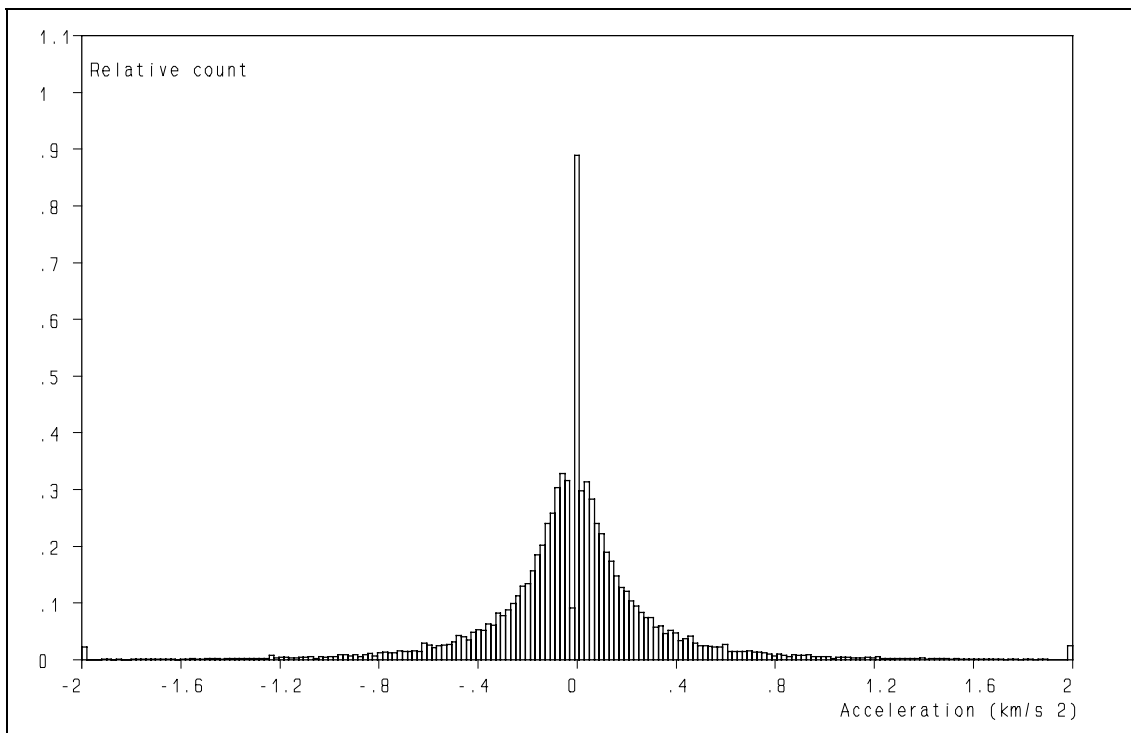


**Figure 7.18:** Distribution of the accelerations obtained from the raw experimental data. Note the accelerations outside the range of  $\pm 2$  km/s<sup>2</sup>.

*Retrieval of turbulence and turbulence properties from LDA data with noise*

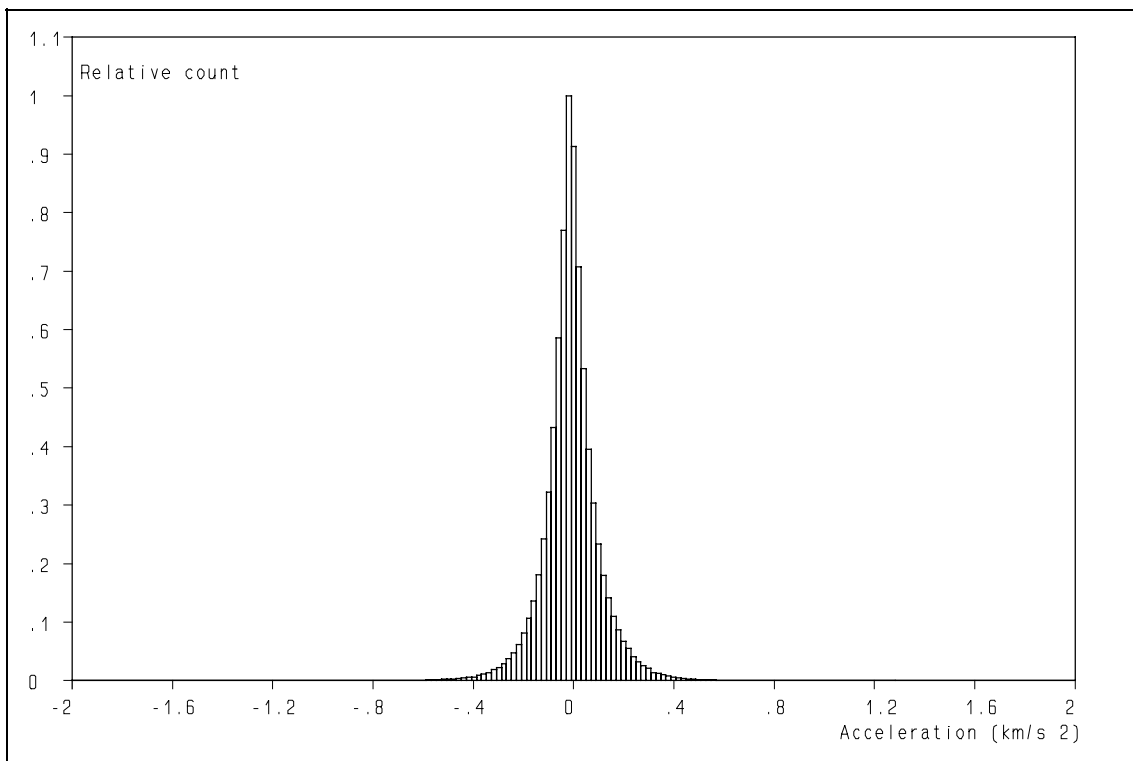


**Figure 7.19:** Distribution of the accelerations obtained from the first-order Kalman reconstructed velocity from experimental data.

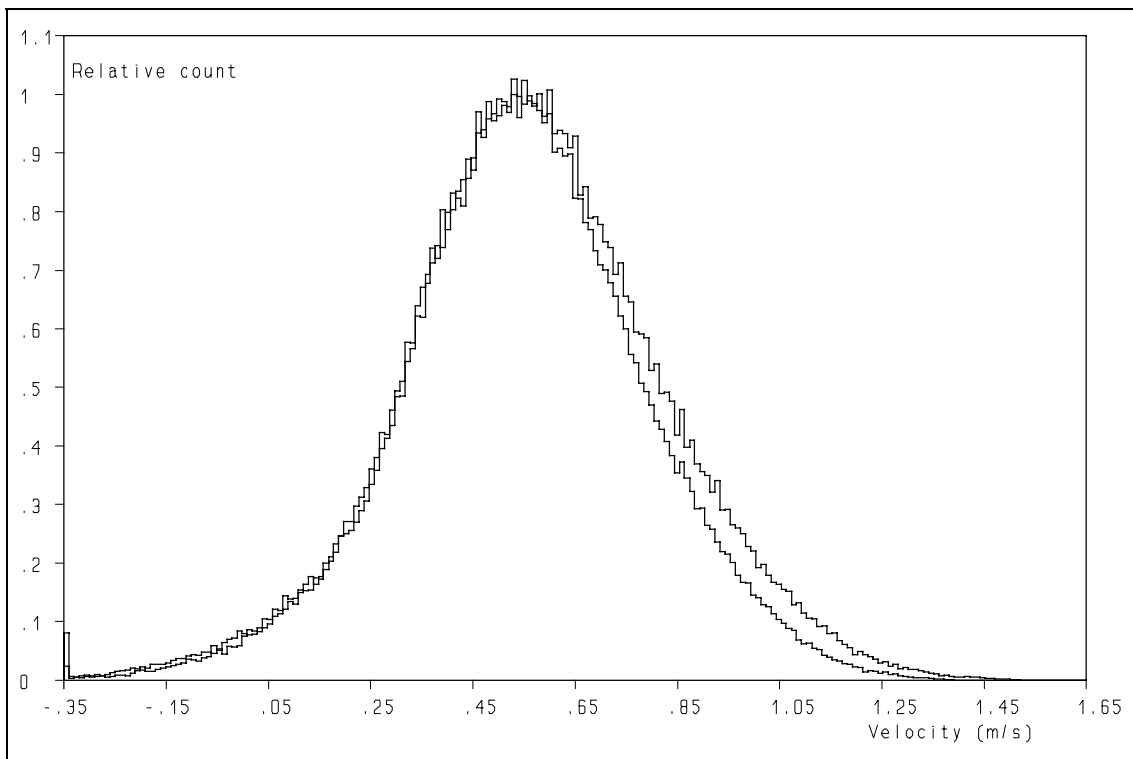


**Figure 7.20:** Distributions of the raw data (upper trace) and of the first-order Kalman reconstructed signal.

## 7. Velocity signal reconstruction I

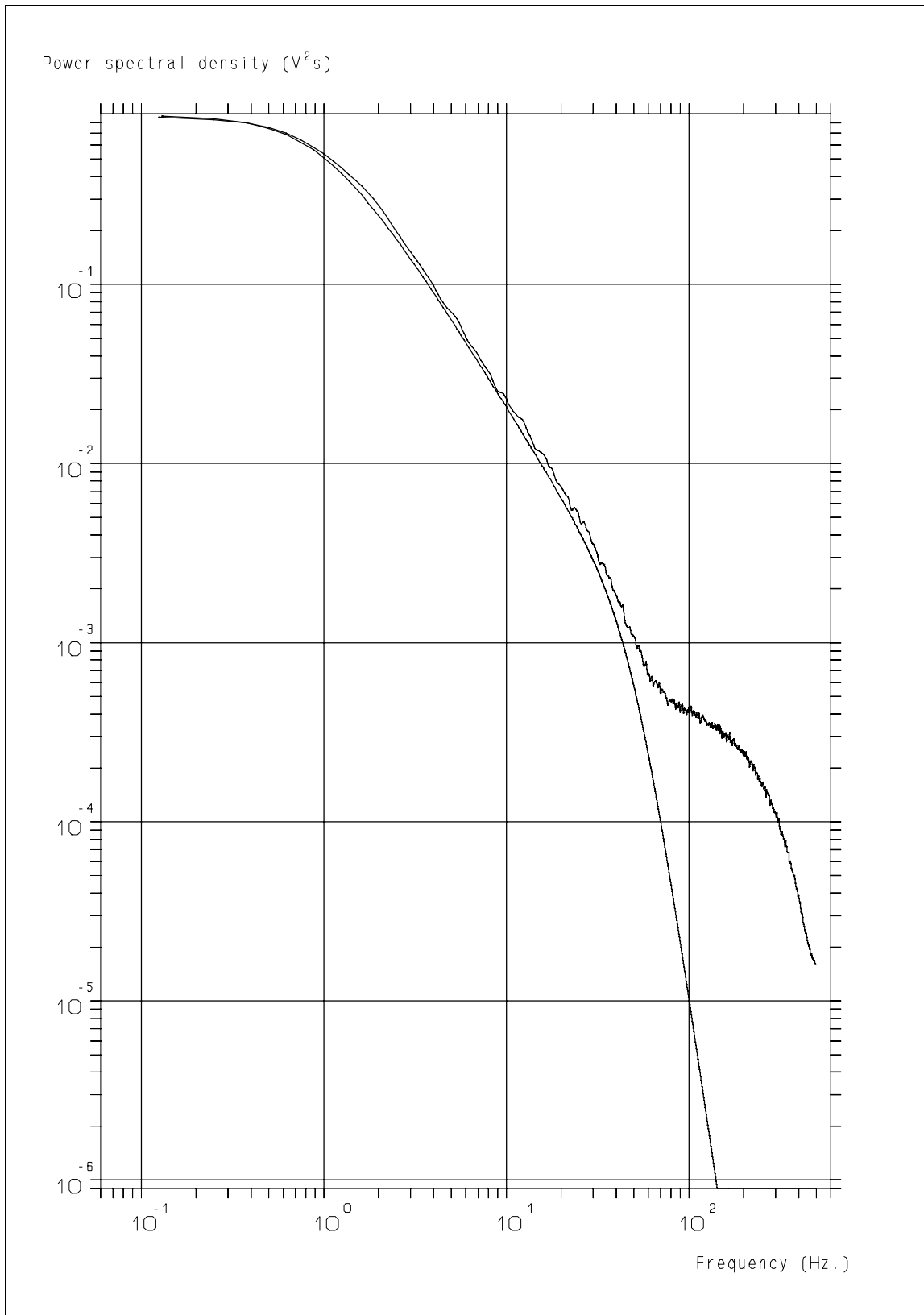


**Figure 7.21:** The Bessem power spectrum (lower trace) and the spectrum, obtained from first-order reconstruction.

*Retrieval of turbulence and turbulence properties from LDA data with noise*

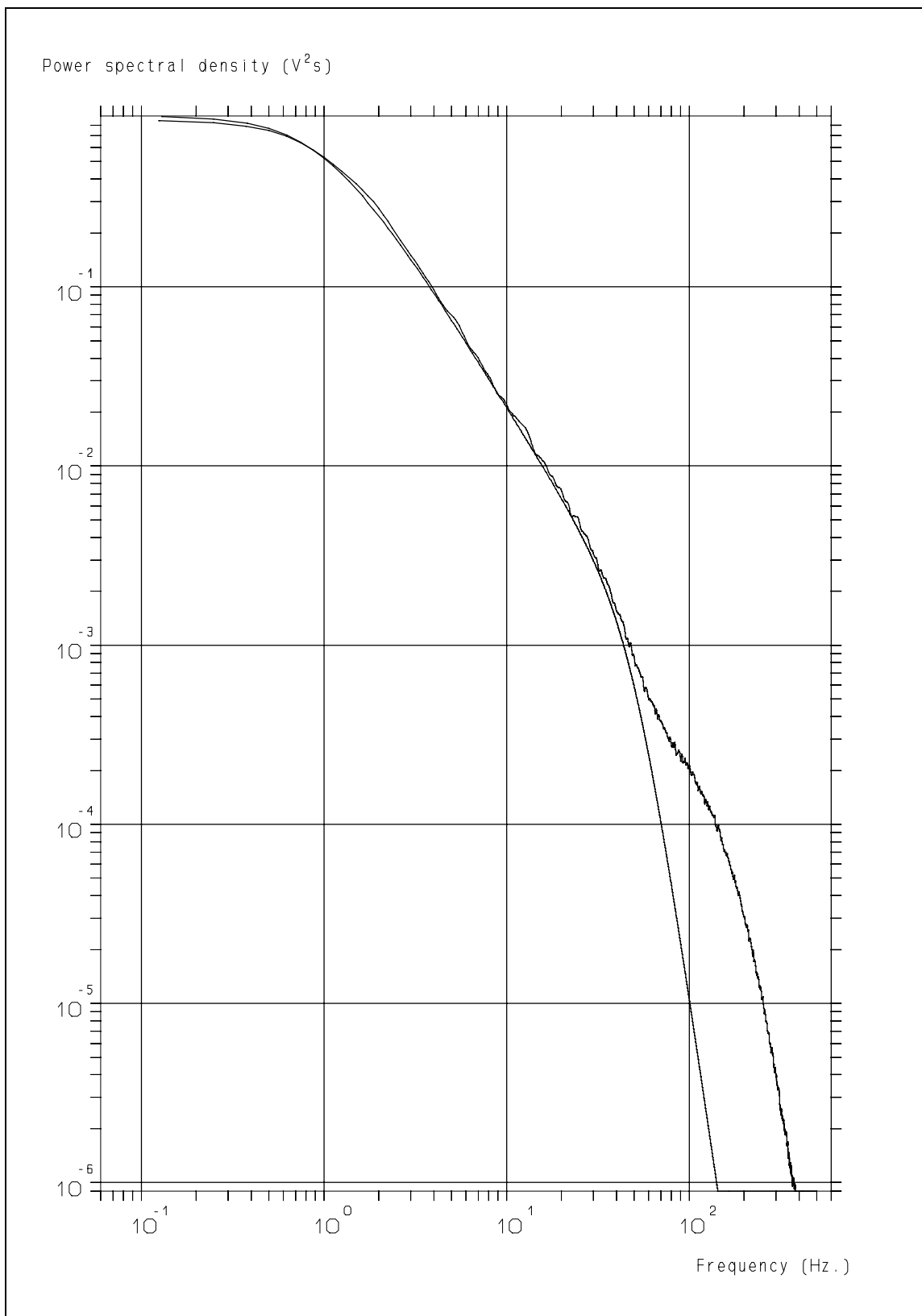


**Figure 7.22:** The Bessem power spectrum (lower trace) and the spectrum obtained from first-order Kalman reconstruction. Compare with fig. 7.21.

## 7. Velocity signal reconstruction I

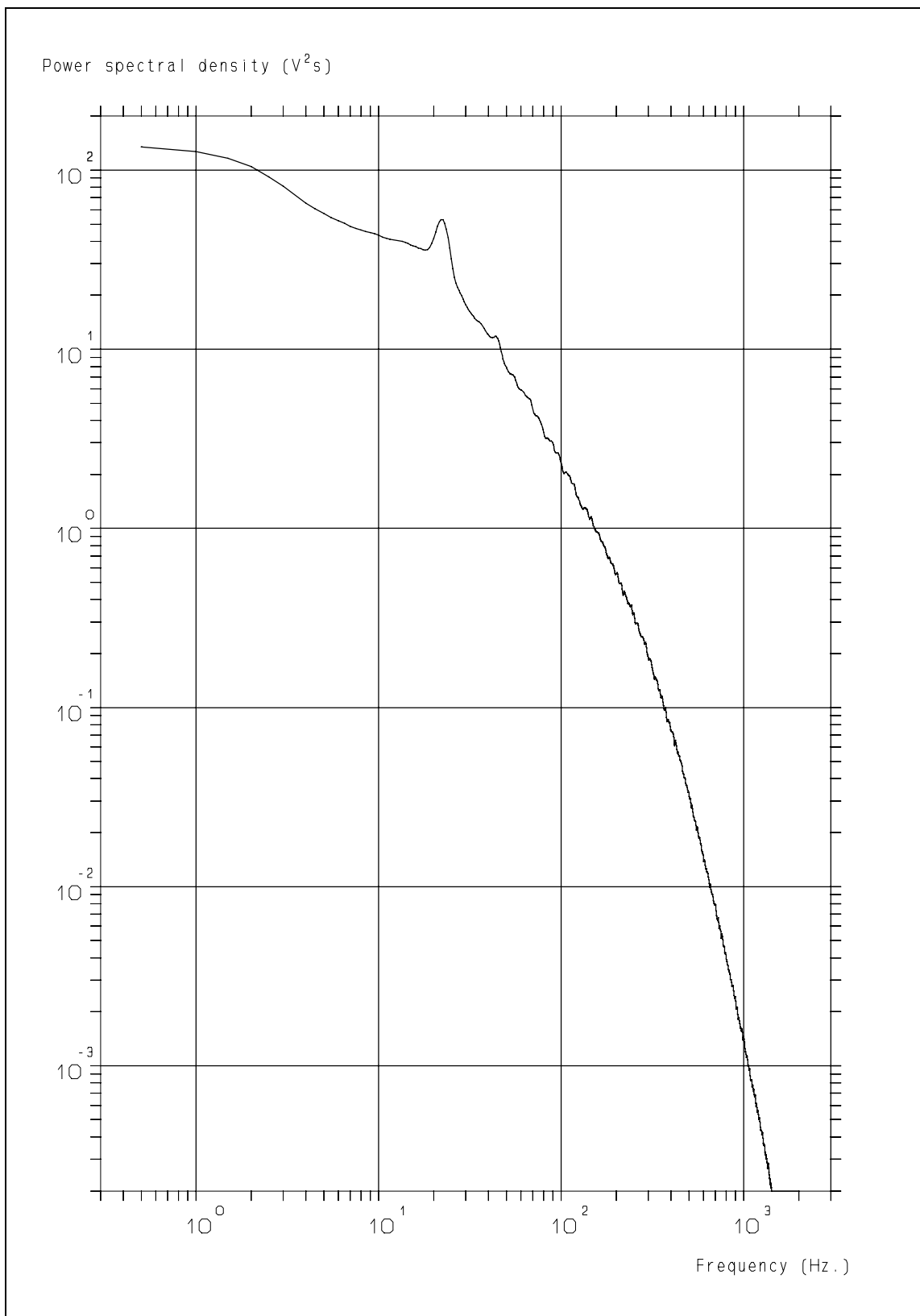


**Figure 7.23:** Power spectrum obtained from experimental data using first-order Kalman reconstruction.

*Retrieval of turbulence and turbulence properties from LDA data with noise*

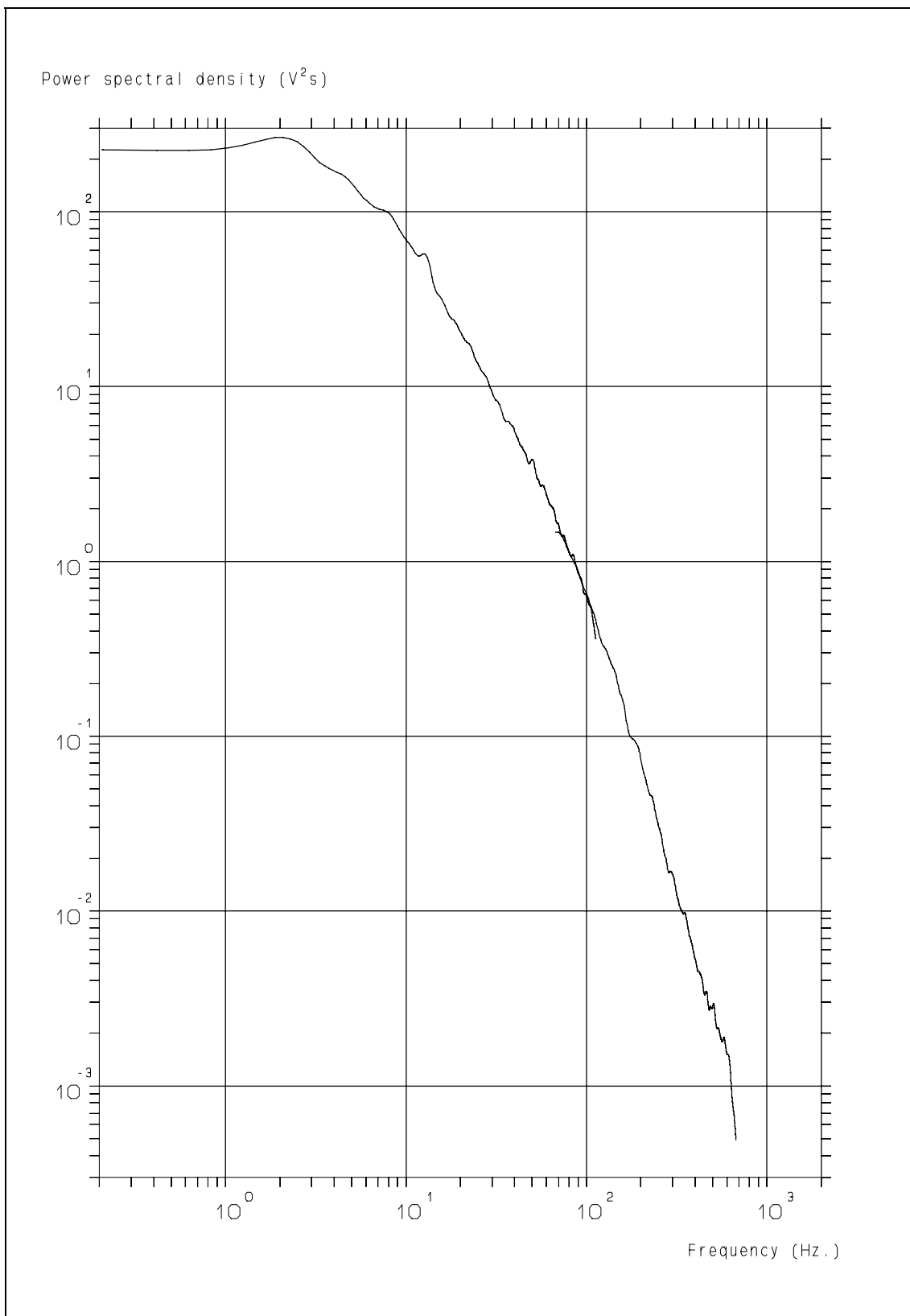


**Figure 7.24:** Power spectrum obtained using the cross covariance technique (see Chapter 9) from tracker signals. Compare with fig. 7.23.

# Chapter 8

## High interpolation rate pre-processing of LDA data

*Sharing what you have  
is more important  
than what you have.*  
Albert M. Wells, Jr.

### 8.1 Introduction.

Turbulence is a phenomenon with statistical properties which spans scales of several orders of magnitude. This causes a fundamental problem for the study of turbulence: to estimate its properties with low variance from the measured velocity fluctuations, a long measuring time is required (at least several times the largest time-scales occurring in the flow). On the other hand, the study of the small scale phenomena requires a high data-rate, as we have seen in Chapter 6. As a result, a large number of samples (typical  $10^5 - 10^6$ ) is necessary. To complicate things further, the Doppler signals arrive with an exponential time interval distribution, but almost all efficient data-processing techniques require an equidistant (periodic) sampling of the data. A simple, straightforward approach is to re-sample at predefined times and to estimate the velocity at those instants by linear interpolation of the closest available measured values before and after the selected instant. Such an approach was chosen for the first-order Kalman reconstruction of the previous chapter. In order to maintain the size of the data-set at roughly the size it has, the re-sampling frequency is usually chosen at a value similar or lower than the original data-rate. The reason for this is that periodically sampled signals can carry information from zero to half the sampling frequency (Nyquist/Shannon sampling theorem, see ref. 89 - 91), whereas reconstruction of randomly sampled signals results in a low-pass filtering at  $1/2\pi$  of the data-rate (the particle rate filter, see Chapter 6). Assuming now that a sufficiently high-data rate has been obtained<sup>1</sup>, a similar or lower re-sampling frequency can be used. This, however, leads to an undesirable effect: due to the exponential time interval distribution<sup>2</sup> of the original samples: the majority ( $\approx 63\%$ ) of the samples arrives within the same sample interval of the re-sampled data-set, as can be seen in fig. 8.1. This means that only 37% of the data is -effectively- used. This increases the inaccuracy in the reconstructed velocity estimates, because a large portion of the information is ignored. This is illustrated in fig. 8.2, in which the vertical lines indicate the sampling interval of the re-sampled data-set. Of course, this could be avoided by the use of a periodic re-sampling frequency that is far higher (say by a factor of 10) than the average data-rate of the Laser-Doppler Anemometry (LDA) data, as is illustrated in fig. 8.3, but that would lead to a data set which is also a factor of 10 larger than the original data-set. This set is already  $10^5 - 10^6$  samples large, leading to excessive processing times and causing problems with the mass storage devices, as each measurement file would be 20 - 40 Mbyte large. To avoid this, the average sampling rates of the reconstructed, equidistant, data-set is preferably chosen about equal to the data-rate of the original, randomly distributed, data-set. To achieve this without discarding the largest part of the available information, a different approach has been developed.

---

<sup>1</sup> By this we mean that the data-rate  $> 2\pi$  times the highest frequency of interest.

<sup>2</sup> Note that the exponential time interval distribution tells that the highest probability of another Doppler signal is immediately after the previous one!

## *Retrieval of turbulence and turbulence properties from LDA data with noise*

### **8.2 The novel approach.**

The new approach uses an intermediate step, which consists of the following parts:

1. The velocity is reconstructed at equidistant samples with a data-rate which is approximately 10 times the data-rate of the original data-set, using piecewise linear interpolation<sup>3</sup>.
2. The thus obtained reconstructed velocity is digitally low-pass filtered using convolution with a minimised time-smear response.
3. The filtered signal is (re-)sampled using equidistant intervals at the desired data-rate, which is about equal to the original data-rate or lower.

#### Ad 1.

The use of a data-rate which is 10 times higher than the original enables the use of virtually all (> 90% <sup>4</sup>) of the measurement data because the chance that two independent measurements fall in the same re-sampling interval is less than 10 %.

#### Ad 2 and 3.

The details of the filtering technique are described in the next section, but the effect is a reduction of the noise contribution to the filtered estimates, compared to that of the original estimates. This can be understood from this filtering: the filtered samples are obtained by "averaging" of the original samples by the filter<sup>5</sup>, thus reducing the noise. The result of the filtering is illustrated in fig. 8.4, which shows that the variance due to the noise contribution of the original estimates (indicated by the "+" symbols) is reduced in the filtered estimates (drawn line), because indeed an averaging over the re-sampling interval has occurred due to the filtering.

### **8.3 The minimised time-smear anti-aliasing filter.**

#### 8.3.1 Aliasing in periodically sampled data.

The periodic sampling of analog signals requires that the analog signal does not contain any spectral components above the Nyquist frequency<sup>6</sup> (ref. 89 - 91). If this requirement is not fulfilled, aliasing occurs when such signals are sampled periodically, leading to improper results. The spectral components which were originally above the Nyquist frequency show up below the Nyquist frequency and have become indistinguishable from the correct components at those frequencies. This is, of course, not acceptable. As it is, in general, impossible to guarantee that no components above the Nyquist frequency are present (ref. 60 and 70), the common solution is to use an anti-aliasing filter. An additional advantage is that the noise is reduced and thus the Signal-to-Noise Ratio (SNR) of the measurement data is improved.

One should realise that re-sampling of periodically sampled signals at a lower frequency is prone to the same aliasing errors: if an analog signal is correctly sampled at the original, high frequency, periodic re-sampling at a lower rate will give rise to aliasing of the components between the Nyquist

---

<sup>3</sup> Piecewise linear interpolation means that the velocity at the instant  $t_i$  is estimated as the value, obtained by linear interpolation between the latest measured value before  $t_i$  and the first measured value after  $t_i$ . See also Chapter 7.

<sup>4</sup> If the time interval distribution would be truly exponential, the fraction of the samples used would be 90.5%. However, the distribution is influenced for short time intervals by the unavoidable dead time of the processor (see Chapter 4) and as a consequence an even larger fraction will be used.

<sup>5</sup> This can be visualised by convolving the original estimates with the impulse response of the filter.

<sup>6</sup> The Nyquist frequency is equal to the sampling-frequency/2.

## 8. High interpolation rate preprocessing of LDA data

frequencies of the re-sampling and the original sampling. The only way to do this correctly is to filter the signal, sampled at the high frequency, digitally (e.g. in the computer) and to re-sample the *filtered signal* at the lower sampling frequency. This procedure has the additional advantage that the noise, due to the quantisation of the Analog-to-Digital Converter (ADC) is also reduced (ref. 60 and 70). However, in this particular case, the filter chosen may have a relatively high transmission up to the Nyquist frequency of the re-sampling frequency, because the turbulence signal has a low-pass characteristic of itself and therefore a more efficient choice of the filter cut-off frequency is possible and allowed (ref. 60 and 70) without increasing the level of aliasing.

### 8.3.2 Possibilities for the digital filtering.

There are two different approaches that can be used for the creation of the digital filter. It could either be realised in time or in frequency domain (ref. 89 - 91). Mathematically speaking these approaches are identical, but for the practical realisation there are differences. Before a choice will be made, both techniques will be described briefly.

#### 8.3.2.1 Filtering in frequency domain.

Filtering in frequency domain can be accomplished by the following calculation steps:

- Calculate the Fourier Transform (FT) of the signal with the high sampling frequency.
- Multiply the spectrum with the (complex) transfer function of the desired filter.
- Reduce the spectral width of the filtered spectrum to the Nyquist frequency of the low sampling frequency.
- Calculate the Inverse Fourier Transform (IFT) of the reduced spectrum. The result is the re-sampled version of the signal.

The route to filter and re-sample the data in frequency domain has some advantages:

- The choice of the filter is clear.
- The filter can be chosen such that the transfer function is zero above the Nyquist frequency of the low sampling frequency.
- If use is made of Fast Fourier Transformation (FFT) algorithms, it can be reasonably fast.

The major disadvantages are:

- FFT algorithms usually require a number of samples which is a power<sup>7</sup> of 2. Data-sets that do not fulfil this requirement could be extended by addition of zero's to complete the set. This does, however, lead to a lot of manipulation with zero's.
- The influence of the filter in time domain at boundaries of the interval is neither determined nor simple to estimate. Unfortunately, filter characteristics which seem very well suited in *frequency domain* have severe influence in *time domain* (ref. 60, 70 and 92). This will be discussed in more detail when the filter will be selected.
- The FT for large data-sets can become very time consuming<sup>8</sup> and/or lead to problems with computer memory. With e.g. systems which have a 16-bit pagination, the limit is usually 8192 data-points.

---

<sup>7</sup> This is not fundamental, basically only the requirement is set that the number of samples can be decomposed in a product of (as small as possible) primes. For each of the decomposed basis is then a kind of FT calculated. For practical simplicity all commercial FFT algorithms are based on decomposition of the prime 2 (which is the smallest that can be used).

<sup>8</sup> The calculation time increases with  $N^2 \log N$  and thus more than proportional to the number of samples in the signal.

## *Retrieval of turbulence and turbulence properties from LDA data with noise*

- Because the FT assumes periodic repetition of the signal, it is not possible to split the signal into smaller blocks which could be processed separately without the penalty of incorrect coupling of the different blocks at their boundaries of the re-sampled signal (ref. 89 - 91). This is in many cases not acceptable.

### *8.3.2.2 Filtering in time domain.*

The filtering can also be achieved in time domain by calculation of the convolution of the signal with the impulse response (which is the IFT of the complex transfer function) of the filter (ref. 89 - 91). The procedure for this approach is:

- Select a (normalised) impulse response of the filter<sup>9</sup>.
- Truncate the impulse response to a practical limit.
- Calculate the convolution integral (in this case sum) of the signal at the high sampling rate with the impulse response for those points in time which correspond to the re-sampled signal.

The advantages of the time domain filtering are:

- The effect of the filtering at the boundaries is well-known.
- The filtering can take place over any length of signal, because only a limited part of the signal needs to be in active memory.
- The calculation time is linearly proportional to the number of data points.

The disadvantages of the time domain filtering are:

- The filter characteristic is only known after Fourier Transformation of the chosen impulse response.
- Because of practical limitations, the impulse response needs to be finite, leading to truncation errors, which usually show up as bounces in the filter characteristic.

Regarding the above, a time domain filtering approach has been selected.

### 8.3.3 Filter selection.

The calculation time for filtering in time domain is determined by the product of the length of the signal and the length of the impulse response. A short impulse response is therefore attractive. However, filters which seem to have a (close to) ideal behaviour in frequency domain have a large (wide) impulse response in time domain. Filters which show a narrow impulse response give only a minor reduction in frequency domain and are therefore unsuitable as anti-aliasing filter (ref. 60, 70, 89 - 92). The optimum (filter efficiency vs. length of the impulse response) is given by a Gaussian filter characteristic with linear phase behaviour, leading to a Gaussian impulse response (ref. 60, 70, 89 - 92). Such a filter is therefore the most appropriate choice.

The major disadvantage of a Gaussian filter characteristic is that a Gauss curve is  $> 0$  for all values of time. The impulse response must therefore be truncated. Arbitrarily, the truncation limit has been set at those times at which the value of the non-normalised Gauss distribution (which is 1 for  $t = 0$ ) is equal to 0.001, corresponding to  $\pm 3.72\sigma$ . The truncation is smoothed by shifting all the values of the Gauss curve 0.001 downward to avoid a step at the boundaries. This is illustrated in fig. 8.5 for a more severe case. The resulting impulse response, used for this filter, is shown in fig. 8.6. The Fourier Transform of this impulse response is shown in fig. 8.7, which reveals some bouncing, which is nowhere above  $10^{-4}$  (equal to -80 dB or equivalent to 13 - 14 bits). For most applications the currently selected response will be sufficient, because most signals tend to decay with increasing frequency (ref. 60 and 70), which would bring the filter efficiency to approximately 16 bits. This is higher than the SNR of almost all measurement signals and further improvement in the filter algorithm would not yield any improvement

---

<sup>9</sup> This can either be chosen directly or by IFT of the complex transfer function of a desired filter characteristic.

## 8. High interpolation rate preprocessing of LDA data

in the end result. Yet, if further improvement is required, the impulse response should be truncated at a lower value than 0.001, leading to a wider impulse response and increased calculation times.

The -3 dB frequency was chosen at 0.55 of the Nyquist frequency, which is a reasonable compromise between the influence on the turbulence power spectrum and the remaining aliasing. As far as aliasing is concerned one should also take into account that the highest frequency that can be reconstructed from such a data-set is  $1/(2\pi \cdot t_0)$  which corresponds to 0.3 of the Nyquist frequency (ref. 39, 63 and 87). Also, the contribution of turbulence to the signal is small at these frequencies as the signal is dominated by noise contributions, so a bit of aliasing is not really a problem, provided that the folded noise is sufficiently low at 0.3 of the Nyquist frequency. This is obtained with this choice of the filter. The relation between the  $\sigma_t$  of the impulse response and the re-sampling frequency can be found from the (numerically determined) simple relation:

$$\text{Re-sampling frequency} \cdot \sigma_t = 0.4845 \quad [8.1]$$

### 8.4 Results.

A step signal has been applied to the filter and the response of the algorithm is shown in fig. 8.8. This response shows clearly the non-causality of the filter. The non-causality of the filter is only a problem if the re-sampled data do not describe the original data correctly, which only occurs if the re-sampling rate is chosen too low. As is well-known, a step signal cannot be described with any sampling frequency (ref. 89 - 91) because its spectral composition is  $> 0$  for any frequency and the decay with frequency is moderate, thus clearly showing the effect of non-causality.

Application of the complete re-sampling algorithm to LDA data has been presented already in fig. 8.4, showing the reduction of the variability of the reconstructed signal in comparison with the raw velocity data.

The effectiveness of the algorithm for the processing of LDA data can be illustrated by looking at the Mean Square Error (MSE) of the resulting re-sampled signal (which equals the Mean Square value of the difference between the actual and estimated velocity). We have calculated this for the simulated turbulence which corresponds to the "Bessem" power spectrum (ref. 60, 70 and 87, see also Chapter 2) with a Signal-to-Noise Ratio of 10 in the individual velocity estimates, a data-rate of 500 Hz and a re-sampling frequency of 1000 Hz. The obtained MSE's are:

1 kHz direct linear interpolation:	MSE = 9.47 E-5
Novel algorithm:	MSE = 3.02 E-5

The MSE of the novel algorithm is only 32 % of the MSE of the straightforward linear interpolation. The algorithm thus not only gives a periodically re-sampled velocity signal as output, but reduces the noise contribution to the velocity estimates as well.

The re-sampling algorithm is flexible as it allows any desired re-sampling frequency. One can choose a frequency which is lower, equal to or higher than the original data-rate, depending on the requirements. It will always give an output signal that has conserved the information of the original data close to the maximum possible and allow the application of all the data-processing techniques available. The improvement in the SNR is also illustrated by the need to be use a higher SNR value for the determination of the parameters for the first-order Kalman reconstruction than is originally estimated, based on the raw data.

We want to emphasize that this re-sampling algorithm gives close to optimum results for the changeover from random to periodic sampling. It does not improve the information contained in the LDA data, although one might be tempted to think so when the SNR is increased. It sounds trivial, but *the higher the quality of the input data, the higher the quality of the output data*. This re-sampling algorithm

## *Retrieval of turbulence and turbulence properties from LDA data with noise*

is no miracle cure either as none of the algorithms is. The conclusions that can be drawn from the measurements depend on the quality of the data and a high quality of the data requires optimisation of the complete measurement- and the data-processing chain. This algorithm has been developed with this philosophy in the back of our minds.

### **8.5 Concluding remarks.**

A novel algorithm has been developed which converts a randomly sampled LDA data-set into a periodically sampled velocity signal without significant loss of information. The obtained periodically sampled velocity signal has a lower noise contribution compared to the original velocity estimates. Yet it does not take up more storage space than the original information. Actually, it can be less, because it is no longer necessary to store the time with each sample: this can easily be retrieved from the time at the beginning, the re-sampling frequency and the number of the sample. The described algorithm will be used as a "pre-processor" for the first-order Kalman reconstruction which gives less residual noise when the input signal has less noise. These results have been presented at the international conference in Karlsruhe (Germany), September 1997 (ref. 105).

## 8. High interpolation rate preprocessing of LDA data

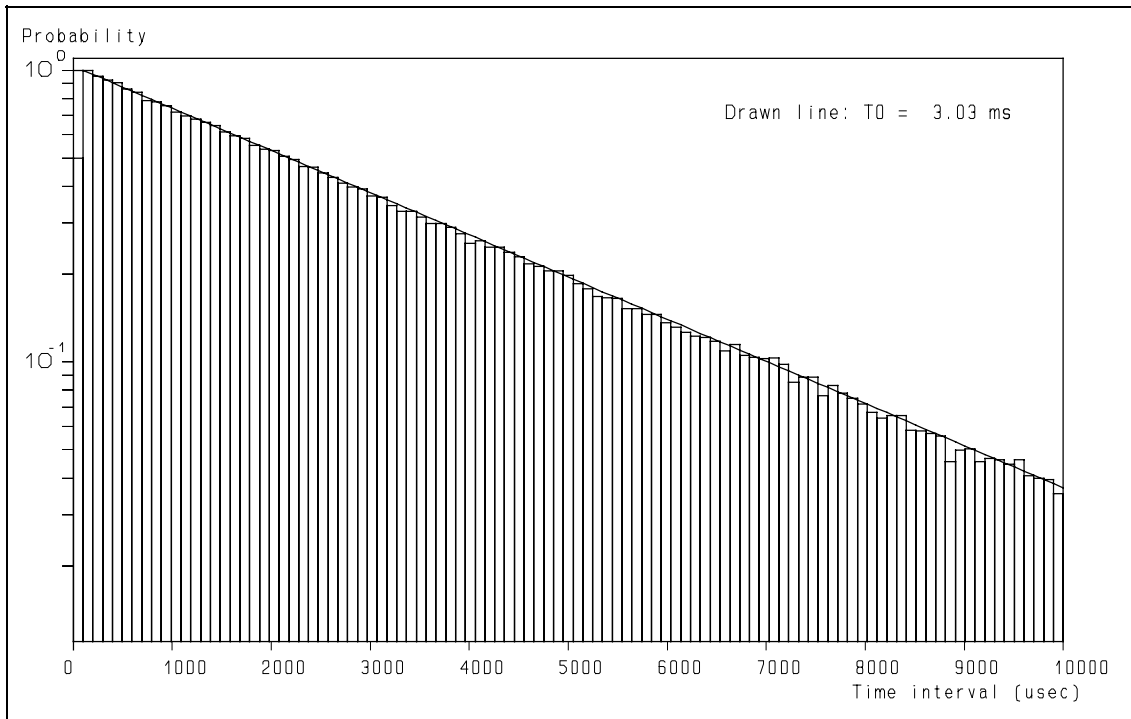


**Figure 8.1:** An example of the time interval distributions used in the simulation. The chosen value of the  $t_0$  was 3 ms. in this case.

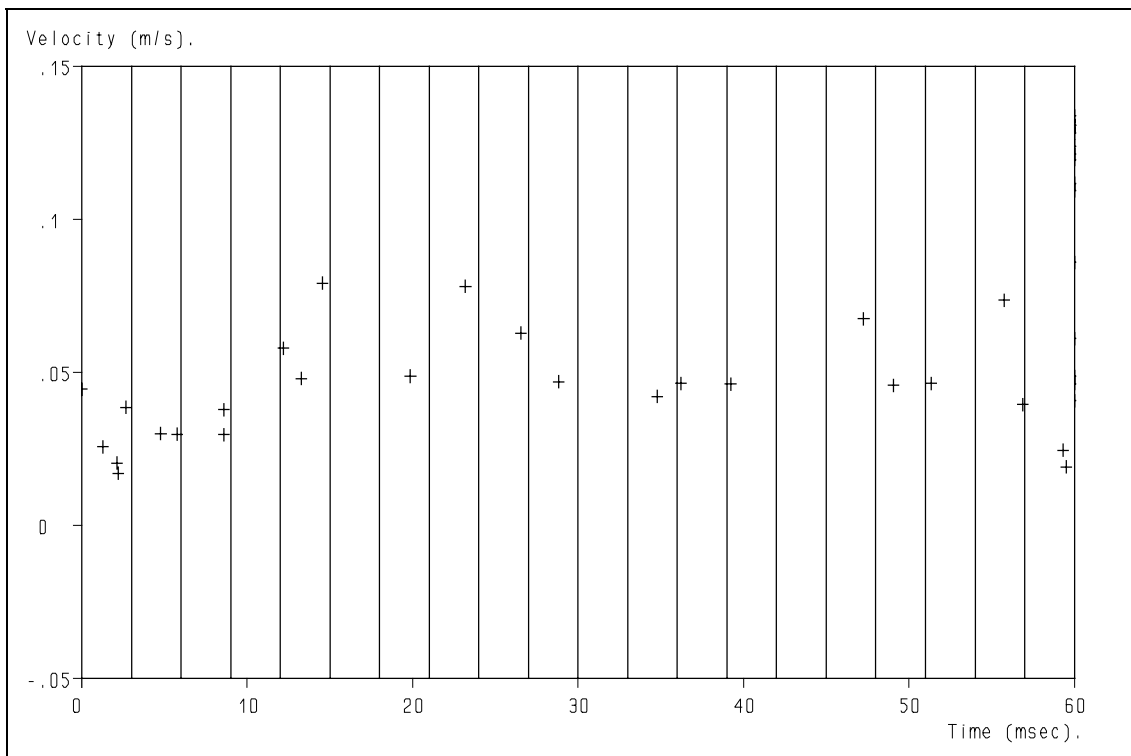


**Figure 8.2:** Due to the exponential time interval distribution often several samples lie within a single re-sampling interval, 3 ms. wide, indicated by the vertical bars.

*Retrieval of turbulence and turbulence properties from LDA data with noise*

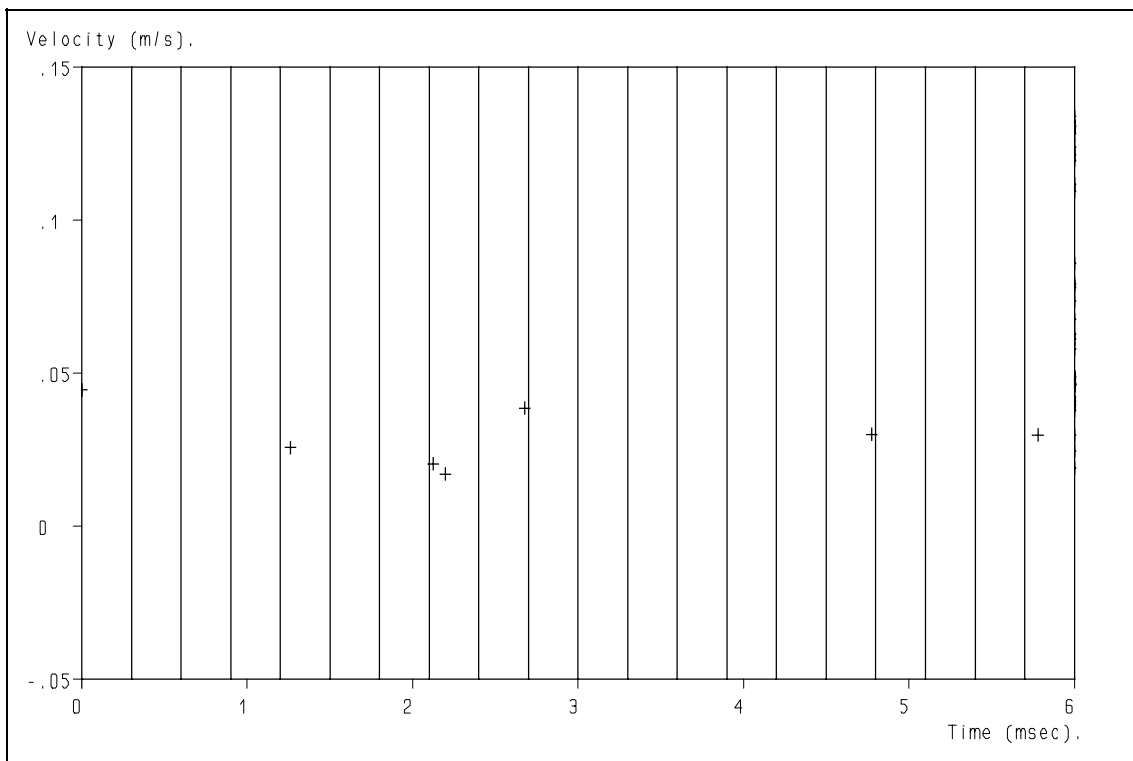


**Figure 8.3:** Sampling at a rate, which is 10 times the average data-rate virtually solves the problem.

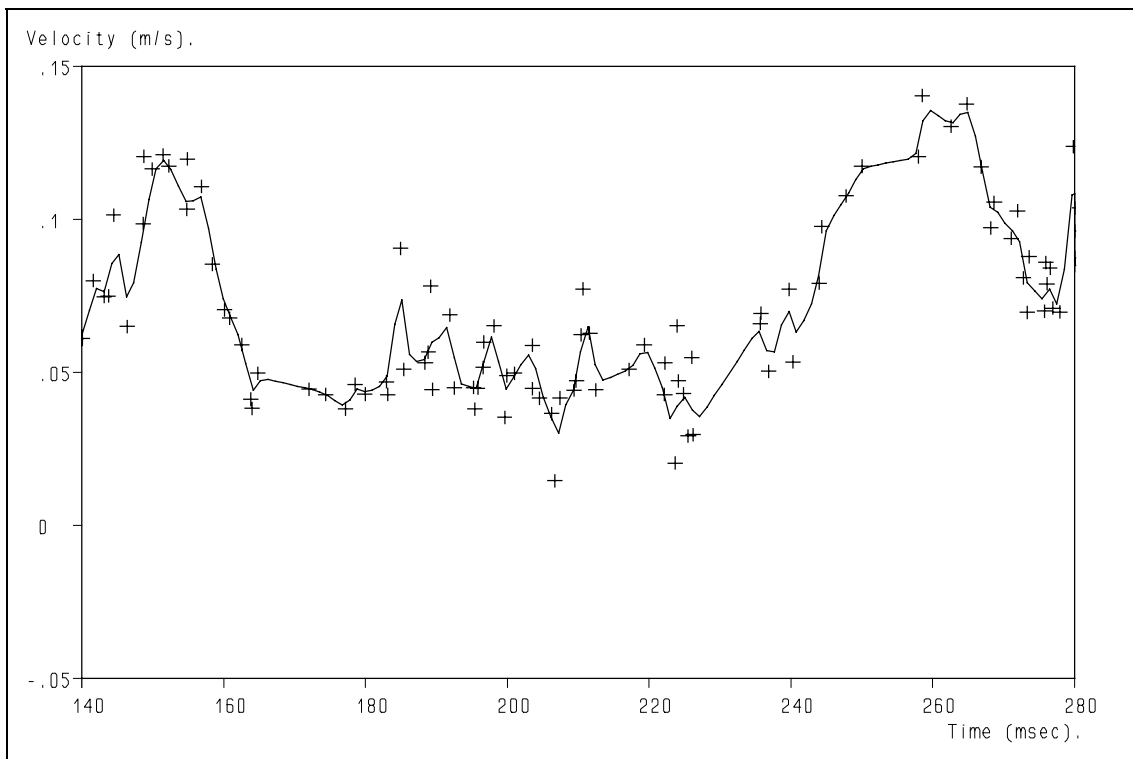


**Figure 8.4:** The result of the high sampling and filtering algorithm on the velocity estimation. + indicates measured data, the drawn line the resulting velocity estimates.

## 8. High interpolation rate preprocessing of LDA data

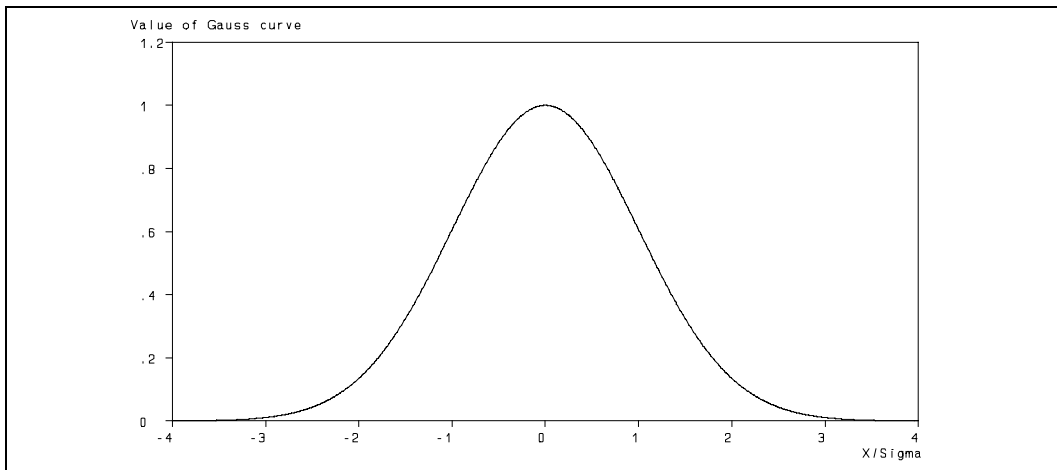


**Figure 8.5<sup>a</sup>:** Non-normalized Gauss curve.

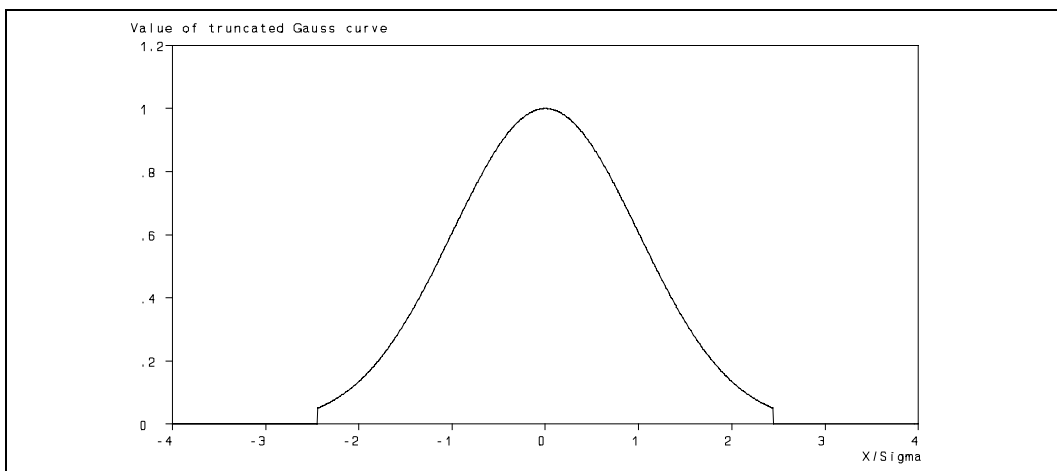


**Figure 8.5<sup>b</sup>:** Gauss curve truncated when its value drops below 0.05 of the maximum value. Note the step at the boundaries, leading to undesired effects in the filtering.

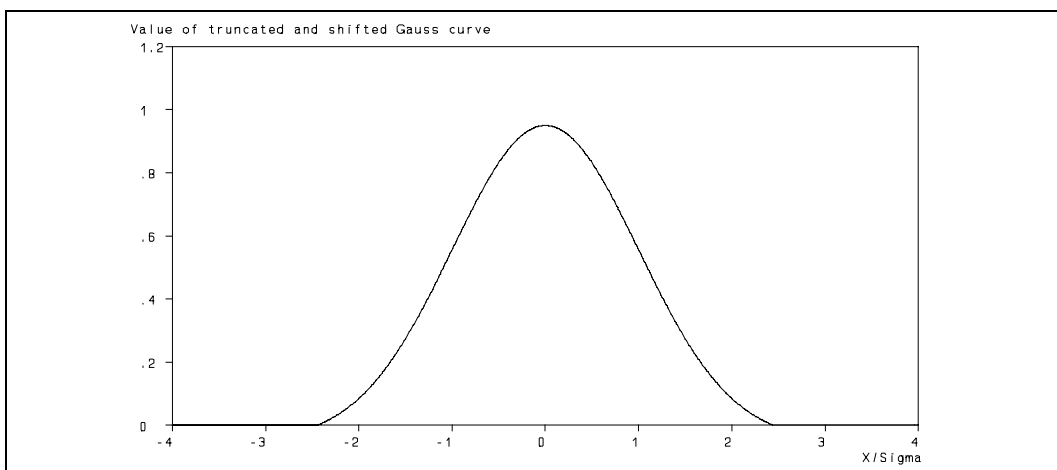


**Figure 8.5<sup>c</sup>:** Shifting of the complete curve over 0.05 in this case reduces the undesired truncation effects (discontinuity reduces to discontinuity in the derivative).

*Retrieval of turbulence and turbulence properties from LDA data with noise*

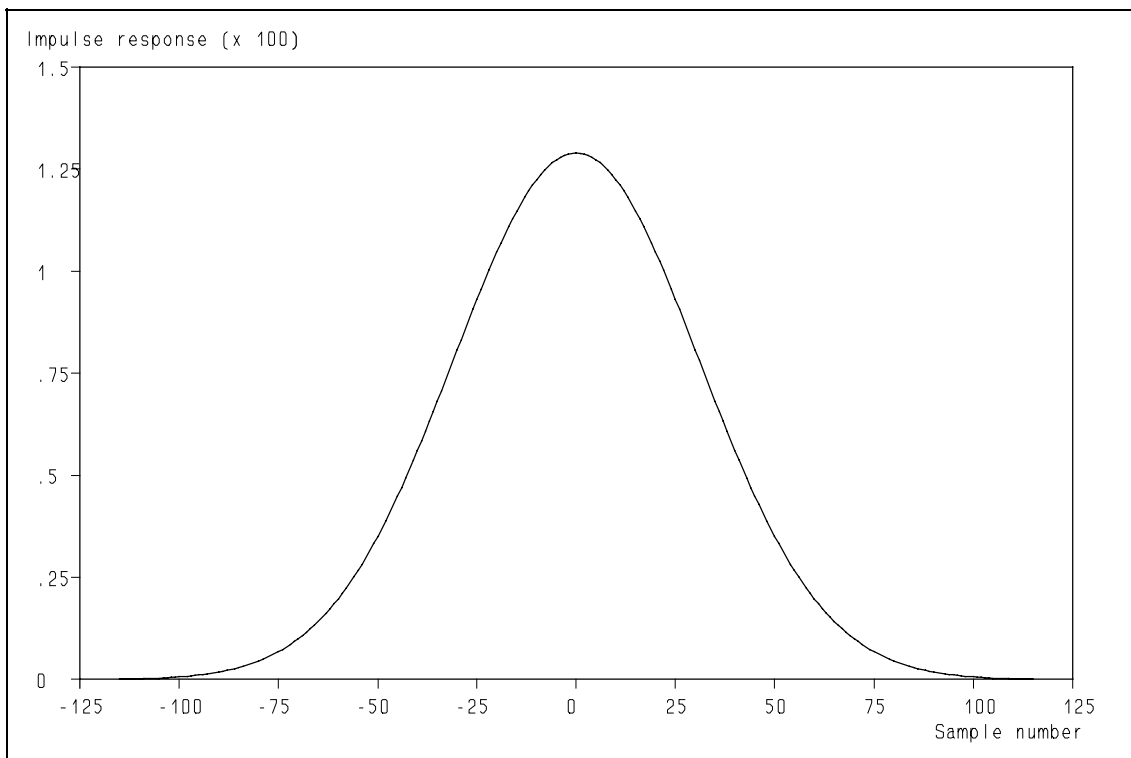


**Figure 8.6:** Impulse response of the filter for a sample rate reduction of 20. Amplitude of the impulse response is multiplied by 100 for clarity.

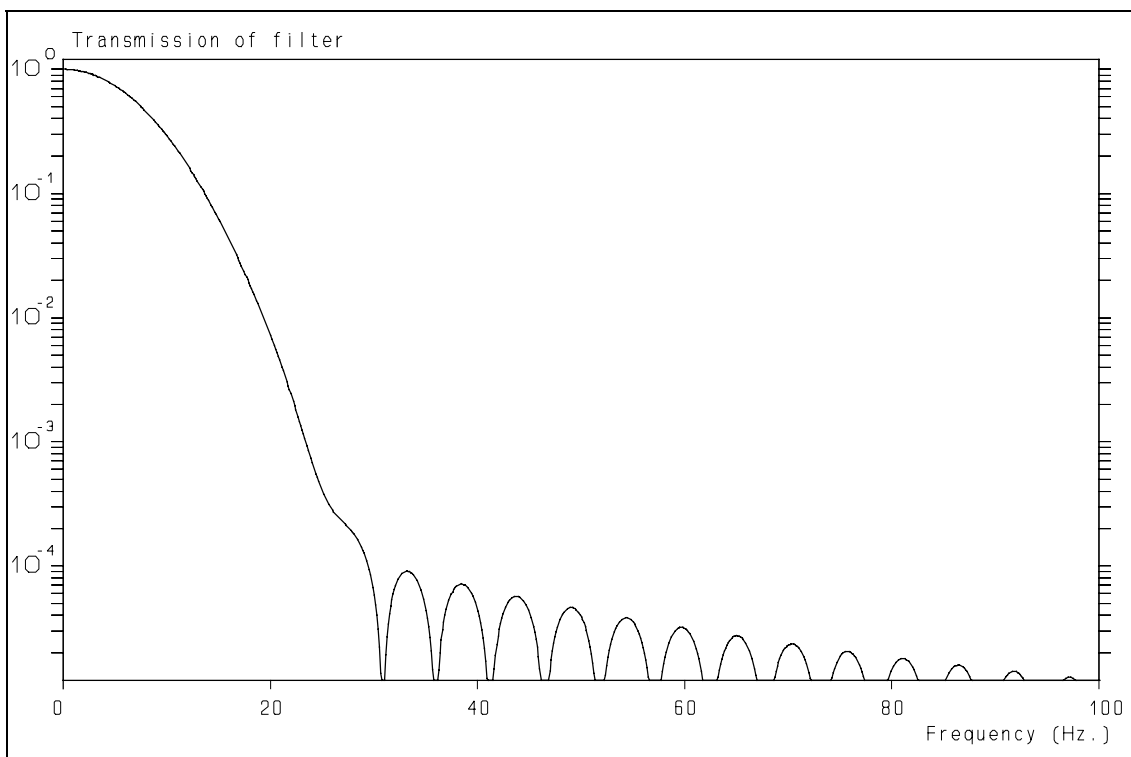


**Figure 8.7:** Filter characteristic of the chosen impulse response when the  $\sigma$  of the impulse response is 25 milliseconds.

## 8. High interpolation rate preprocessing of LDA data

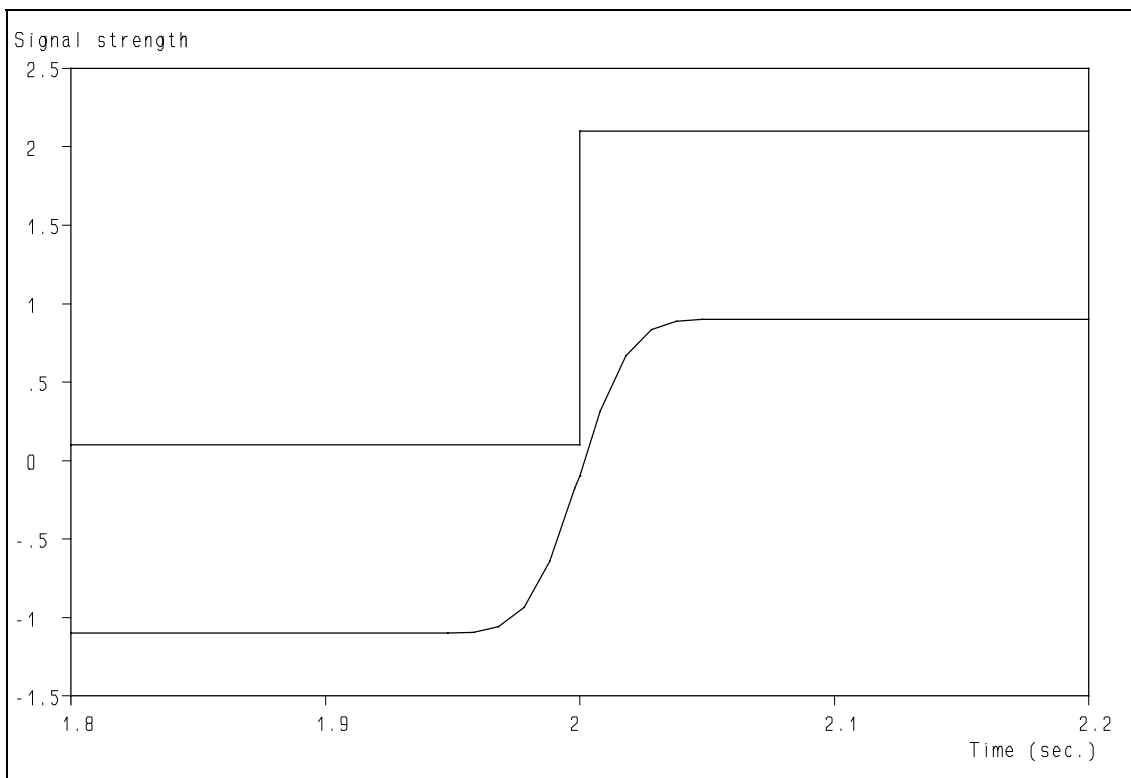


**Figure 8.8:** Step response of the chosen filtering. Upper trace input signal, lower trace output signal. Both are shifted for clarity. Note the non-causality of the filter.

# Chapter 9

## The Cross-Covariance Technique

*It takes time to succeed  
because success is merely the natural reward  
for taking the time to do anything well.*  
Joseph Ross

### 9.1 Introduction.

The turbulence power spectrum is an important measurand for the retrieval of the properties of the turbulence (e.g. ref. 72 and 74). However, as we have seen in previous chapters, estimation of the turbulence power spectrum using Laser-Doppler Anemometry (LDA) is seriously hampered by the random sampling and the noise contribution to the individual velocity estimates. In this chapter we will discuss a technique in which the power spectrum can be estimated roughly 1.5 - 2 decades below the noise floor, based on an old idea (ref. 50), which will be extended. It will also be shown that the obtained spectrum is indeed to correct estimator, something which could only be made plausible in 1975. After a description of the technique we will apply it to simulated data to determine the level of improvement and to proof that the correct spectrum is obtained.

### 9.2 Spectral estimates using the cross covariance technique.

Assuming that a velocity signal reconstruction technique has been applied to the LDA data (see Chapters 6, 7 and 8), a continuous estimation trace of the turbulent velocity fluctuations has been obtained. However, this signal consists of the actual velocity fluctuations with a noise contribution and therefore the auto covariance function has a noise "spike" in the vicinity of  $\tau = 0$ , which obscures the contribution of the small eddies to the power spectrum. In case of velocity reconstruction, the width of this noise "spike" is not zero due to the correlation that has been introduced (see ref. 39, 63, 87 and Chapter 6) and it can therefore not easily be separated from the turbulence contributions. Yet, the Power Spectral Density (PSD) of the velocity fluctuations can still be estimated with a reduced noise contribution if two *independent* measurement signals of the velocity fluctuations are available (ref. 50). This so-called cross covariance technique is based on the idea that the *cross covariance function* of the two independent measurement signals is equal to the *auto covariance function* of the velocity fluctuations alone, provided that the noises are not correlated. The determination of the turbulence power spectrum can subsequently be realised by Fourier transformation of the thus obtained "auto" covariance function of the velocity fluctuations (ref. 89 - 91). We will show that shortly, but to simplify the notation we will first introduce some "shorthand".

Consider a function  $f(t)$ , then the bar-notation can be introduced to denote the time average of  $f(t)$ :

$$\bar{f} \equiv \frac{1}{T} \int_0^T f(t) dt. \quad [9.1]$$

in which:

$T$  = integration time s

Using this notation, the auto covariance function  $R_{ff}(\tau)$  can be defined as the time averaged product of  $f(t)$  and  $f(t+\tau)$ :

Retrieval of turbulence and turbulence properties from LDA data with noise

$$R_{ff}(\tau) \equiv \overline{f(t) f(t+\tau)} = \frac{1}{T-\tau} \int_0^{T-\tau} f(t) f(t+\tau) dt ; \quad \tau < T \quad [9.2]$$

in which:

$\tau$  = the time over which the signal is shifted before it is multiplied with itself s

If two signals  $f(t)$  en  $g(t)$  are available, the cross covariance function  $R_{fg}(\tau)$  is, in analogy with eq. [9.2], defined as:

$$R_{fg}(\tau) \equiv \overline{f(t) g(t+\tau)} = \frac{1}{T-\tau} \int_0^{T-\tau} f(t) g(t+\tau) dt ; \quad \tau < T. \quad [9.3]$$

Assume that two independent measurements of the velocity at a certain measurement position are available. Both measurements are accompanied by a certain amount of noise. We will describe both measurements signals as:

$$f_1(t) = u'(t) + n_1(t) ; \quad f_2(t) = u'(t) + n_2(t) \quad [9.4]$$

in which:

$f_1(t)$	= first measurement signal (including noise)	m/s
$f_2(t)$	= second measurement signal (including noise)	m/s
$u'(t)$	= fluctuating part of velocity signal (without noise)	m/s
$n_1(t)$	= noise contribution to the first measurement signal	m/s
$n_2(t)$	= noise contribution to the second measurement signal	m/s

The cross covariance function of these two signals  $f_1(t)$  en  $f_2(t)$  is:

$$R_{f_1 f_2}(\tau) = \overline{(u'(t) + n_1(t)) \cdot (u'(t+\tau) + n_2(t+\tau))} = \quad [9.5^a]$$

$$\overline{u'(t) u'(t+\tau) + u'(t) n_2(t+\tau) + n_1(t) u'(t+\tau) + n_1(t) n_2(t+\tau)} = \quad [9.5^b]$$

$$\overline{u'(t) u'(t+\tau) + u'(t) n_2(t+\tau) + n_1(t) u'(t+\tau) + n_1(t) n_2(t+\tau)} = \quad [9.5^c]$$

$$R_{u'u'}(\tau) + R_{u'n_2}(\tau) + R_{n_1 u'}(\tau) + R_{n_1 n_2}(\tau) \quad [9.5^d]$$

If the velocity is not correlated with the noise and the noises are not correlated with each other, then in the limiting case (i.e. infinite duration) all but the first term, which is the auto covariance function of the velocity fluctuations, disappear. In other words: the cross covariance function of the two signals *with* noise converges to the auto covariance function of the turbulent velocity fluctuations *without noise*. This eliminates the contribution of the noise and thus enables correct estimation of the turbulence power spectrum. The effectiveness of the technique is illustrated in fig. 9.1.

### 9.3 Discussion.

Although this technique opens the possibility for more accurate estimation of the PSD of the turbulent velocity fluctuations, three complications play a role:

1. The limited averaging time.
2. Correlated noise sources.
3. Practical limitations.

#### Ad 1.

If the contribution of the velocity fluctuations to the cross covariance function becomes very small, very long averaging times are required as the noise level is reduced only with the square root of the number of samples and thus to the duration of the measurement. This poses a practical upper limit to this technique. The effect is illustrated in fig. 9.2, which shows the higher noise level in the spectrum when less samples are used (compare with fig. 9.1). However, the reduction of the noise that has been obtained in fig. 9.1 required more than three times the amount of samples. The number of samples is related to the duration of the experiment and the data-rate. A high data-rate is attractive because it reduces the noise contribution to the individual measurement signals (see Chapter 6, 7 and 8). It also reduces the time, required to collect sufficient samples for a significant noise reduction and thus reduces the time that the flow system should be steady. A high data-rate has thus two attractive properties.

#### Ad 2.

Not all the noise contributions to the velocity estimates in the two independent measurement signals are uncorrelated. This limits the reduction of the noise contribution to the "auto" covariance function by this technique, as only uncorrelated noise sources will be reduced. Referring to the discussion in Chapter 3, a separation of correlated and uncorrelated noise sources can be made. Correlated noise sources, which contribution to the cross covariance function can only be reduced by reducing the noise from these sources themselves, are<sup>1</sup>:

- Modulation noise of the laser.
- Optical path difference of the incoming laser beams.
- Phase front distortion by tracer particles in the incoming beams.
- Distortion of the laser beams in the measurement volume due to the tracer particle.
- "Fringe" gradients.
- Velocity gradients.
- Dead time of the processor.

Uncorrelated direct noise sources, which contribution to the cross covariance technique can be reduced, are:

- Quantisation noise of the photocurrent.
- Amplification noise of the photocurrent.
- Electronic noise in the filters and amplifiers of the processor.
- Arrival time estimation noise.
- Quantisation noise of the A/D conversion.

The indirect noise contributions, as discussed in Chapter 3, partly determine the noise contribution to the reconstructed velocity signal. The lower the noise contribution to the reconstructed velocity signals, the lower the remaining noise contribution to the cross covariance function under identical conditions.

---

<sup>1</sup> Note that a large fraction of these noise sources are related to the properties of the measurement volume, which is logical as both detectors obtain the Doppler signals from the same measurement volume.

## Retrieval of turbulence and turbulence properties from LDA data with noise

### Ad 3.

A practical implementation of the cross covariance technique consists of doubling the detection and processing electronics. The use of two different detectors, which detect signals from the same (part of the) measurement volume has been reported (ref. 50), but in general it will be difficult to get a perfect overlap of the two fields of view of the two detectors. This, however, does not necessarily pose a problem. The question is: does a slightly different measurement volume result in different (or partly uncorrelated) reconstructed velocity signals? As the measurement volume averages the velocity fluctuations across it, the spatial resolution determines the eddy size that can be resolved. As long as the non-overlapping part of the two measurement volumes is small, compared to the actual size of these, the influence on the signals is not significant, as the eddies, which could be effected, are already averaged out by the measurement volume(s) themselves. This phenomenon has even been used to reduce the noise further by deliberately shifting the measurement volumes a small distance apart (ref. 50). With current LDA processors, the effective size of the measurement volume can be reduced by using the coincidence detection, because then only the Doppler signals are processed when a tracer particle is present in the overlapping part of the measurement volume. It can therefore be concluded that as long as the non-overlapping part of the measurement volumes is either small, compared to their actual size, or coincidence processing is used, the non-perfect overlap of the measurement volume does not pose a problem for the cross covariance technique and sometimes even can be used for further noise reduction or reduction of the effective size of the measurement volume.

In practical situations, the PSD can be extended by 1.5 - 2 decades because of the above mentioned problems. It is therefore important that the whole LDA system is optimised as -again- the cross-covariance technique is no "miracle cure" either.

To answer the question whether the cross covariance technique yields the *correct* estimates for the PSD's of turbulent velocity fluctuations, a simulation has been run. In this simulation "turbulence" of known properties has been used, generated using the technique described in ref. 60, 70 and 87 and Chapter 2. The PSD of the simulated, so-called "Bessem", turbulence, which can be motivated on theoretical grounds, is defined as:

$$S_B(f) = \frac{S_B(0)}{1 + \left(\frac{f}{f_1}\right)^{\frac{5}{3}} \cdot \left[1 + \left(\frac{f}{f_2}\right)^4\right]^{\frac{4}{3}}} \quad [9.6]$$

in which:

$S_0$	= low frequency level of spectrum	$V^2s$
$f$	= frequency	Hz
$f_{1,2}$	= characteristic frequencies	Hz

More details of this simulated turbulence can be found in Chapter 2 on Monte Carlo simulations. From this simulated turbulence, data-sets as obtained from LDA using two different detectors have been derived using random sampling and addition of a white, Gaussian distributed, "measurement" noise contribution, as described in ref. 87, 102 & 105 and in Chapter 2. These data-sets have been used for first-order Kalman reconstruction of the velocity fluctuations with the low-frequency re-sampling pre-processing as described in Chapter 8. Using the scheme "Data Processing I" on page 157, the PSD has been estimated and the result is shown in fig. 9.1, together with the theoretical PSD. This shows that the cross covariance technique does indeed give the correct estimate for the PSD, provided that the filter gain of the first-order Kalman reconstruction filter is set at the correct value (rather a bit too

## 9. The Cross-Covariance Technique

high than too low)<sup>2</sup>. The thus obtained PSD can therefore be used for determination of the properties, required for the extended reconstruction filter, which will be discussed in Chapter 12.

Some discussion on the Kalman filter gain should be made here. It is important to realise that the first-order Kalman reconstruction acts to a certain extent as a low-pass filter, albeit its parameters are determined from the signal properties themselves. However, the gain setting is determined by optimisation of the Mean Square Error (MSE), as has been discussed in Chapter 7 and 8. But as the contributions to the turbulent velocity fluctuations decrease with increasing frequency, a relatively strong reduction of the higher frequencies does not influence the MSE much. In other words: the MSE tends to give a larger relative weight to the larger eddies than to the smaller ones. So the situation may occur that the optimum filter gain will result in the best estimator for the instantaneous velocity, but has suppressed the higher frequencies too much. Such a condition can occur when the Signal-to-Noise ratio (SNR) is low, because the Kalman reconstruction scheme will tend to suppress the noise. Yet, as we try to reduce the noise by the cross covariance technique too, the filtering should not be so severe that the information on the small eddies has been suppressed as well. The possibility exists that the optimum filter gain for the signal itself may be too low for the application of the cross covariance technique. The detrimental effects of erroneous filter gain settings are depicted in fig. 9.3, in which the obtained spectra are shown with increasing filter gain (from left to right). When the gain is set at a too high value (curve a), the noise contribution is still clearly visible. When the gain is set too low (curve c), the turbulence itself is suppressed. The best approach is to start off with a high value of the gain and to decrease the filter gain gradually. When the gain is at its optimum setting, the turbulence is not yet effected, as can be seen in curve b. As a large part of the turbulence power spectrum is distinguishable from the noise when using the cross covariance technique, this distinction is possible, as is clear by comparing curve a and b. However, in case of doubt it is possible to obtain an *independent* estimate of the PSD by using the auto correlation function, derived using the slotting technique with local normalisation, in combination with the curve-fit technique, which will be discussed in the Chapters 10 and 11. The influence of a too low Kalman gain, applied to a simulated data-set is illustrated in fig. 9.4, which shows that the contribution of the small eddies is estimated too low. The use of a higher filter gain resulted in the PSD of fig. 9.1.

The above mentioned effect is enhanced by the noise reduction obtained by the pre-processor, described in ref. 105 and Chapter 8, as it tends to reduce the noise level and thus to increase the SNR, as is illustrated in fig. 9.5 and the corresponding increase in filter gain in fig. 9.6. However, the noise reduction obtained is attractive: the lower the noise levels in the input signals, the higher the final dynamic range in the PSD is. The reason for that is simple: the *noise reduction factor* depends on the averaging time and this is independent of the noise level. The final noise level is determined by the noise level in the input signals for the cross covariance technique and this noise reduction factor. This is confirmed by Monte Carlo simulations, which will be described in Chapter 12. Some results are presented in fig. 9.7 and 9.8 which show the difference between the power spectra obtained by application of the cross covariance technique to first-order and first-order Kalman reconstructed signals. The lower noise level of fig. 9.8 is easily understood as the noise levels in the first-order Kalman reconstructed signals are significantly lower than those in the first-order reconstructed signals.

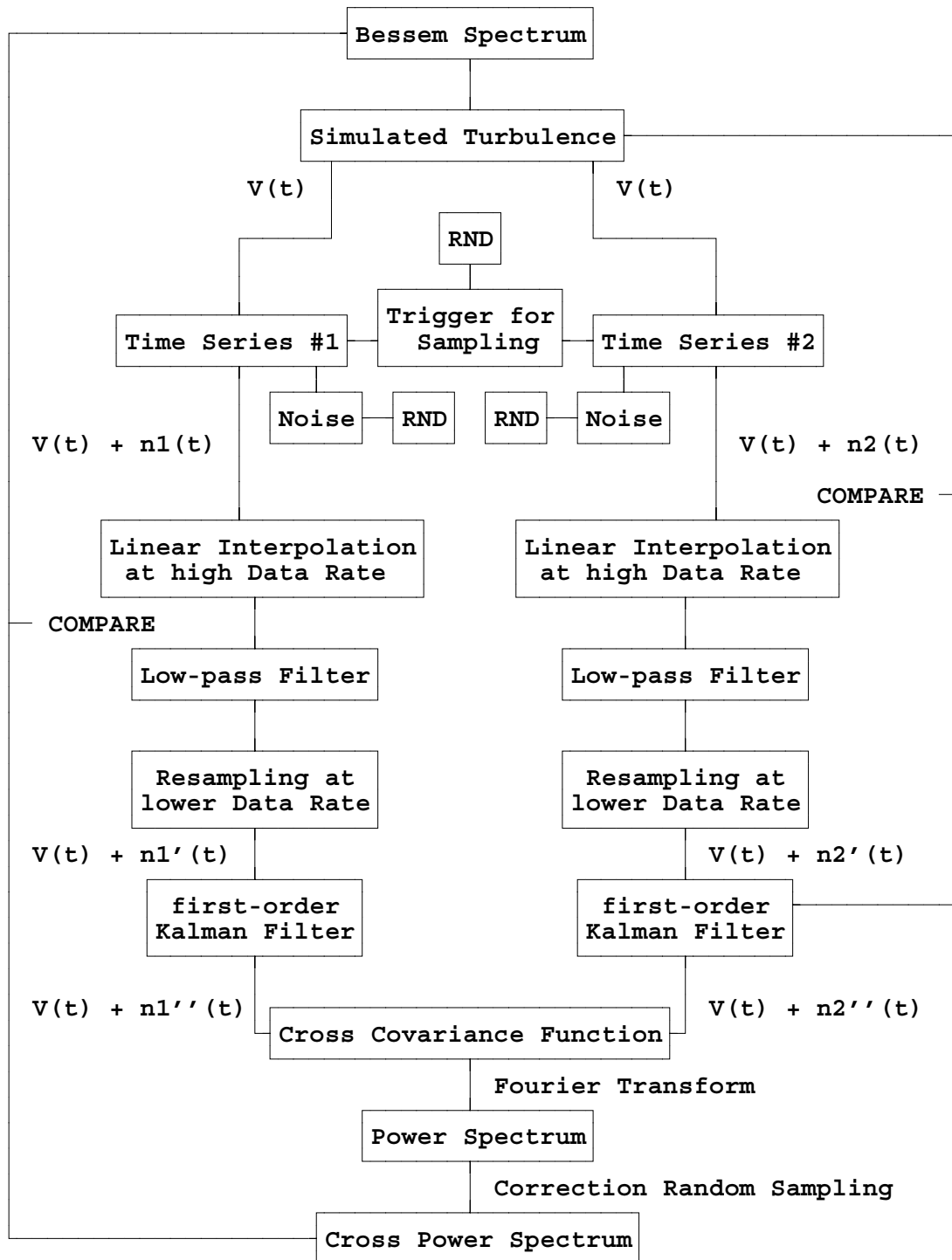
---

<sup>2</sup> For the determination of the filter gain (which is a function of the Signal-to-Noise ratio), one should take into account that the first steps of the reconstruction algorithm (see fig. 8.4 and ref. 105) reduce the noise contribution and thus increase the SNR of the input signal for the Kalman reconstruction filter.

**9.4 Concluding remarks.**

We have shown now that the velocity signal reconstruction using the pre-processor and the first-order Kalman reconstruction results in signals which still have a residual noise contribution, albeit at a low level. It is reasonable to assume that this noise level is close to the theoretical minimum that is achievable given the properties of the individual velocity estimates and the data-rate. With a proper setting of the filter gain of the first-order Kalman reconstruction filter, the residual noise contribution can be reduced with the application of the cross covariance technique for the determination of the turbulence power spectrum. Monte Carlo simulations have shown that this turbulence power spectrum is the correct estimator. The turbulence properties that have been retrieved from the data will be used in a later stage for the extension of the velocity reconstruction filter (this will be discussed in Chapter 12) but before that we will describe another approach to obtain information about the turbulence properties without the use of velocity signal reconstruction.

Data Processing I



*Retrieval of turbulence and turbulence properties from LDA data with noise*

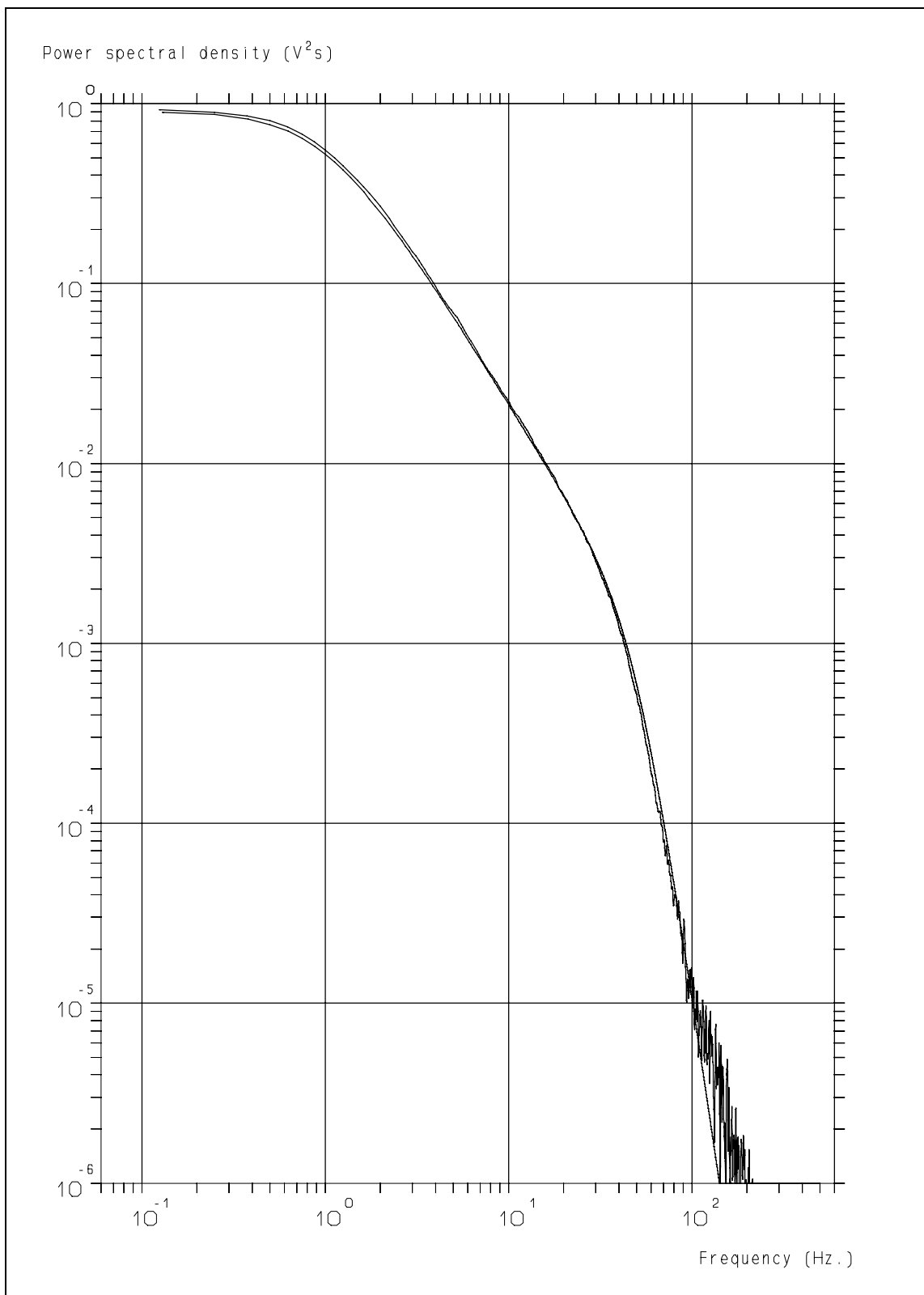


**Figure 9.1:** PSD derived from the cross covariance function of first-order Kalman reconstructed turbulence, including the pre-processor of Chapter 8 ( $10^6$  samples, wiggly at bottom) and the Bessem spectrum.

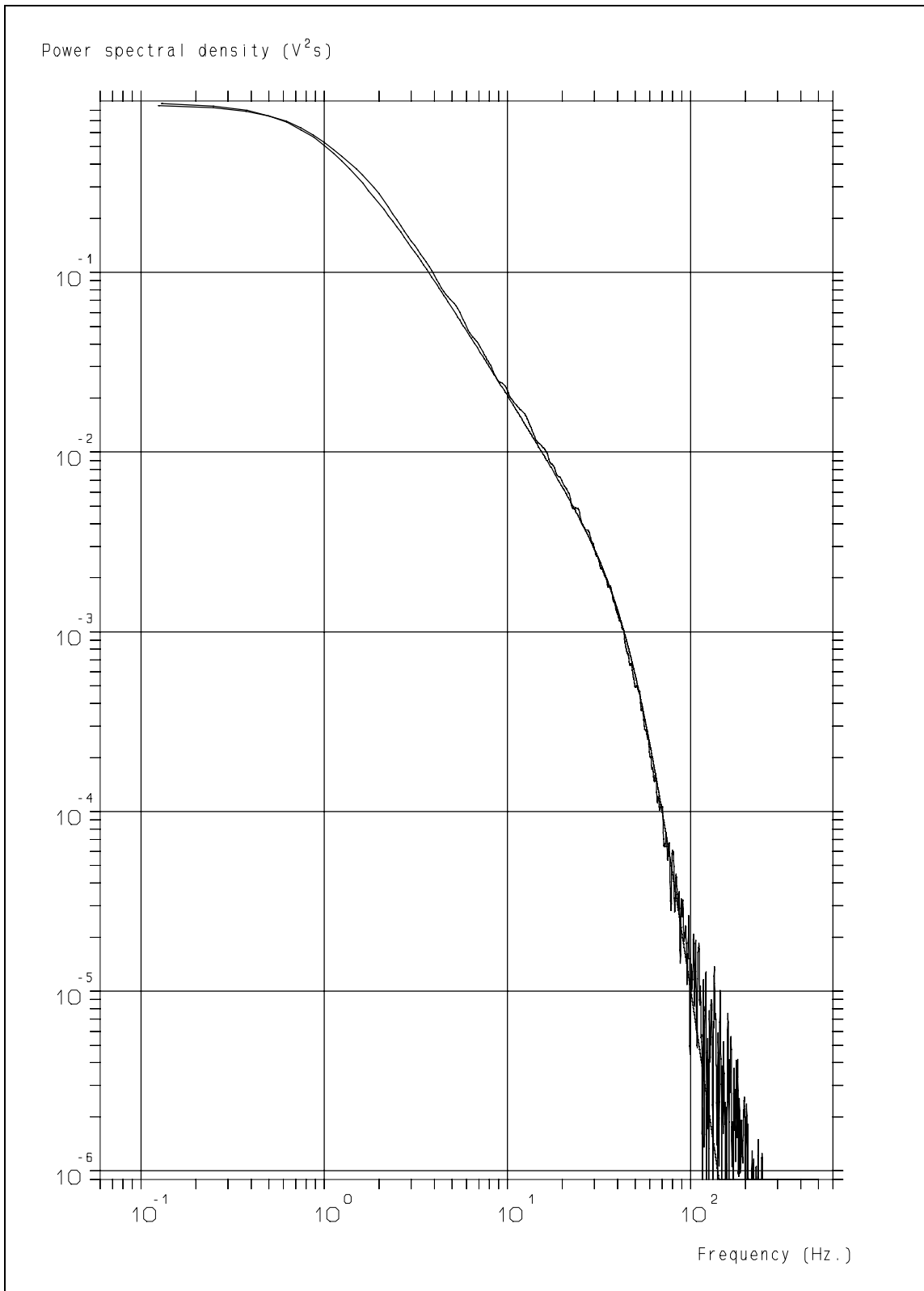


**Figure 9.2:** PSD derived from the cross covariance function of first-order Kalman reconstructed turbulence, including the pre-processor of Chapter 8 ( $3 \cdot 10^5$  samples, wiggly at bottom) and the Bessem spectrum.

*Retrieval of turbulence and turbulence properties from LDA data with noise*

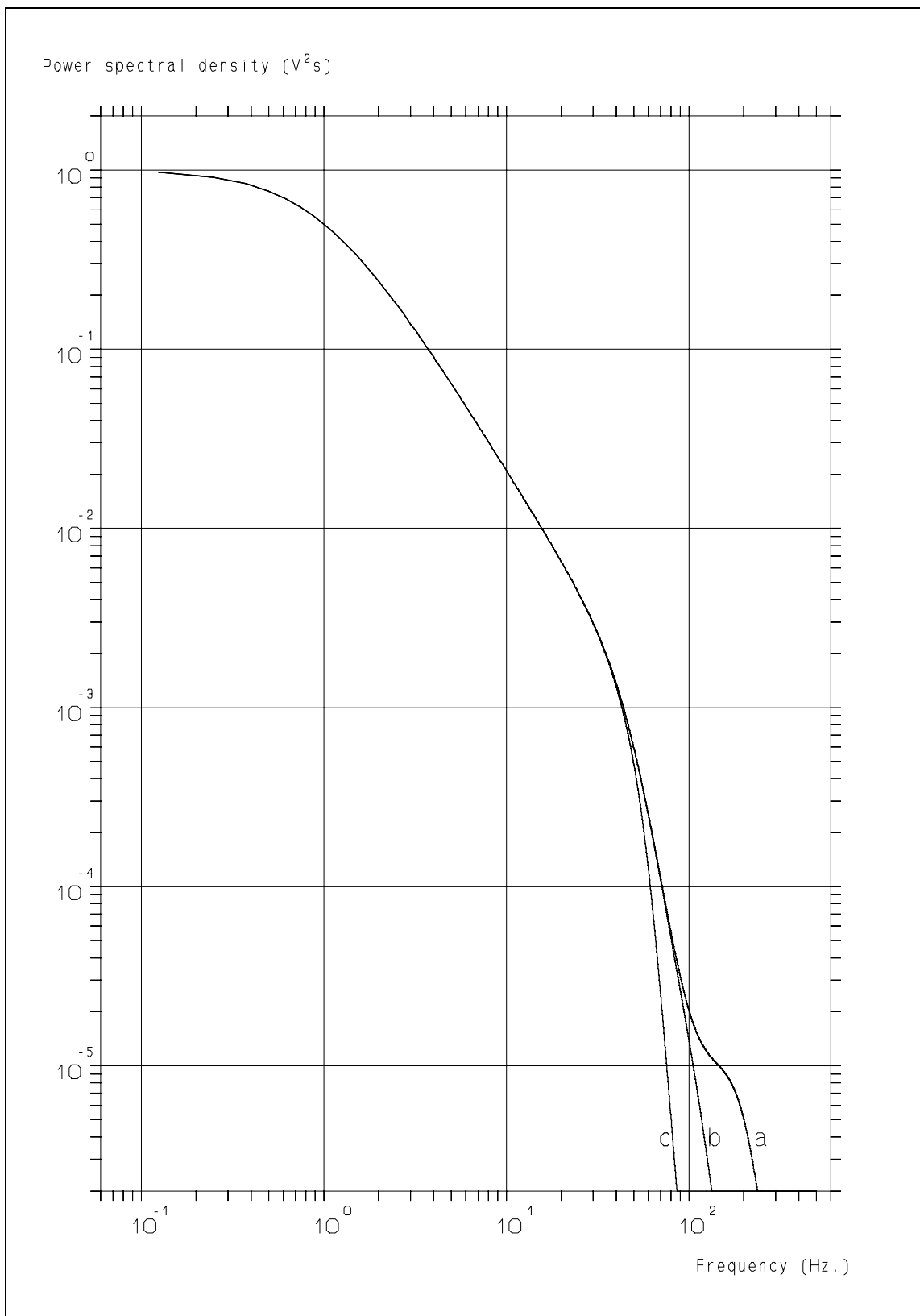


**Figure 9.3:** Influence of the Kalman gain setting on the PSD: curve a: gain too high, noise clearly present; curve c: gain too low, turbulence contributions suppressed; curve b: gain optimal.

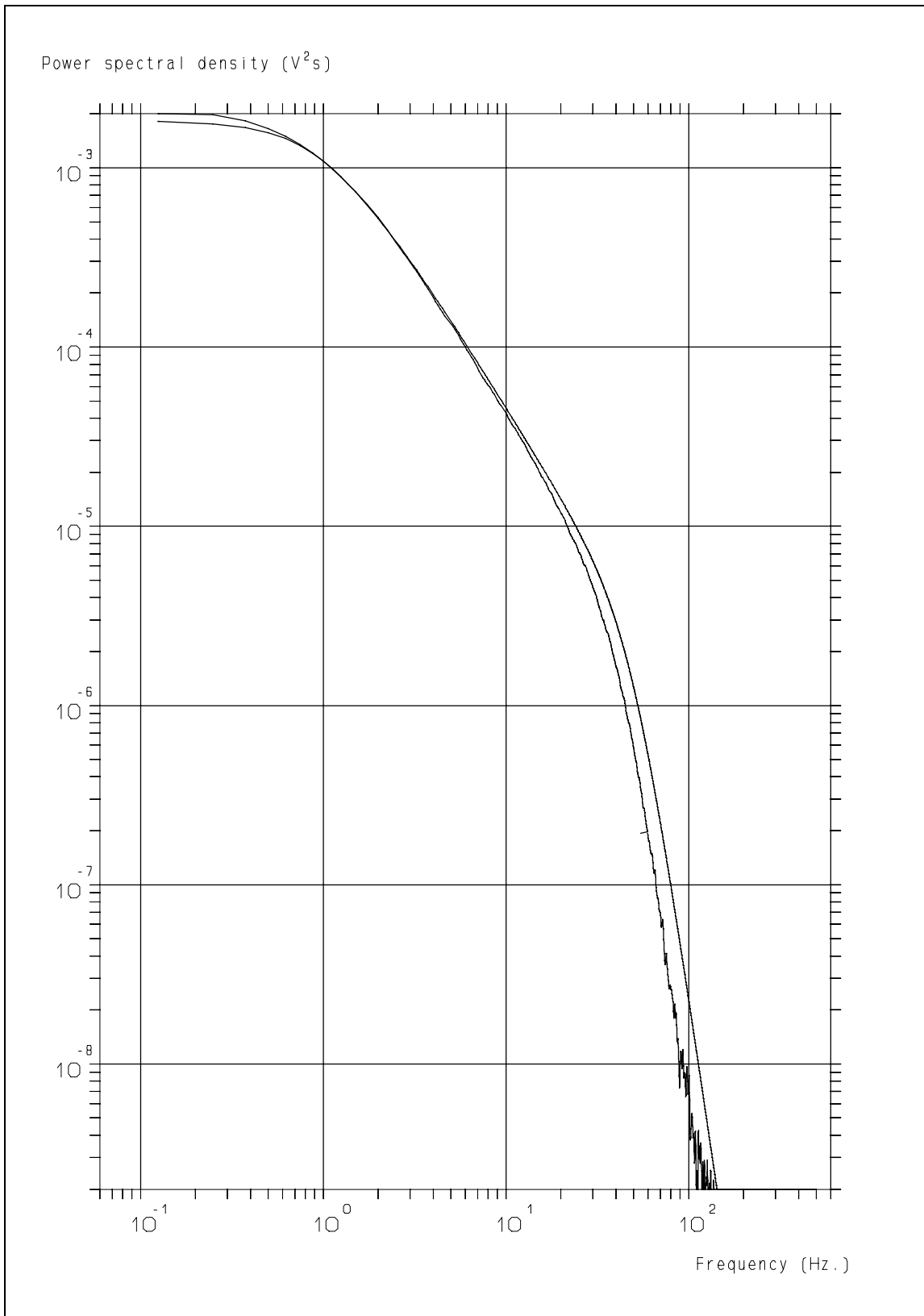


**Figure 9.4:** Power spectrum obtained using the optimum filter gain of the first-order Kalman filter and the cross-covariance technique (lower trace) and the Bessel spectrum.

*Retrieval of turbulence and turbulence properties from LDA data with noise*

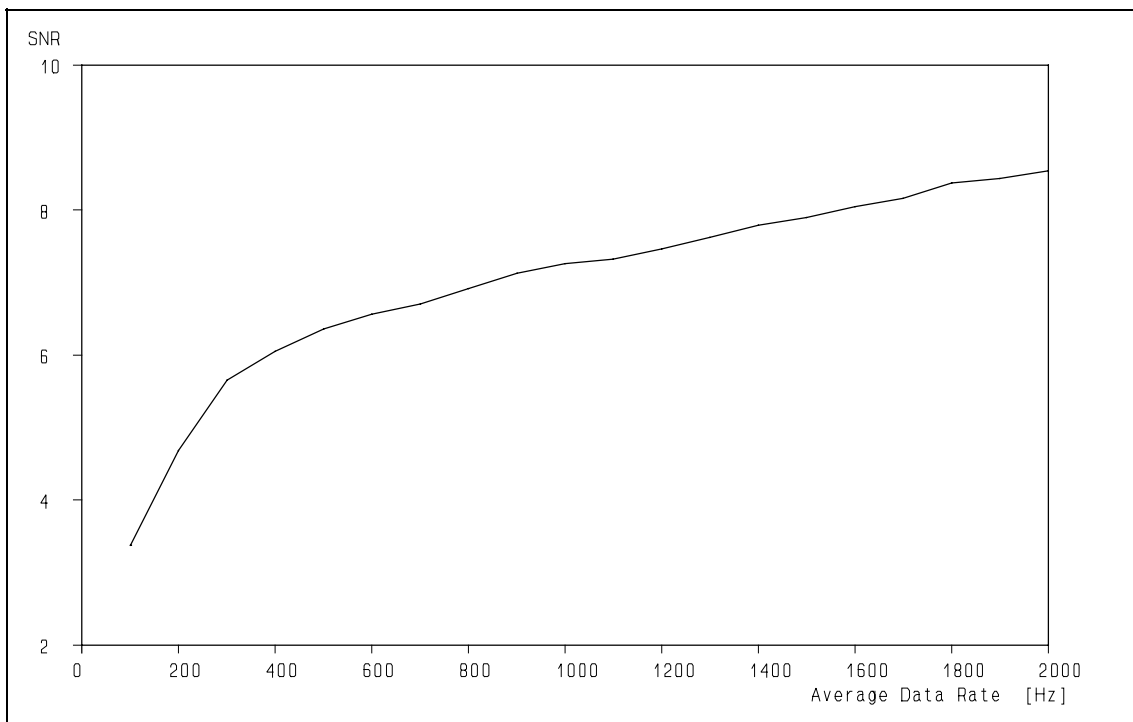


**Figure 9.5:** The signal fed to the Kalman filter has a Signal-to-Noise ratio which depends on the average data rate of the velocity measurements when the pre-processor is used (see Chapter 8).

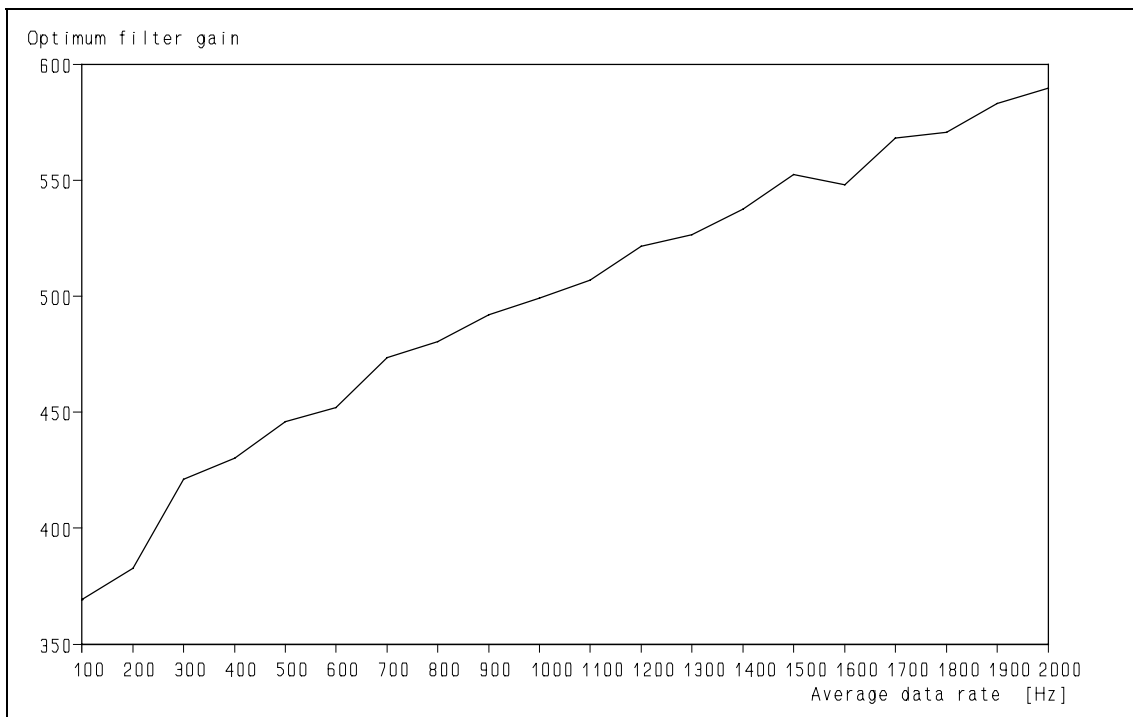


**Figure 9.6:** The optimum filter gain varies with the average sampling rate when the pre-processor of Chapter 8 is used.

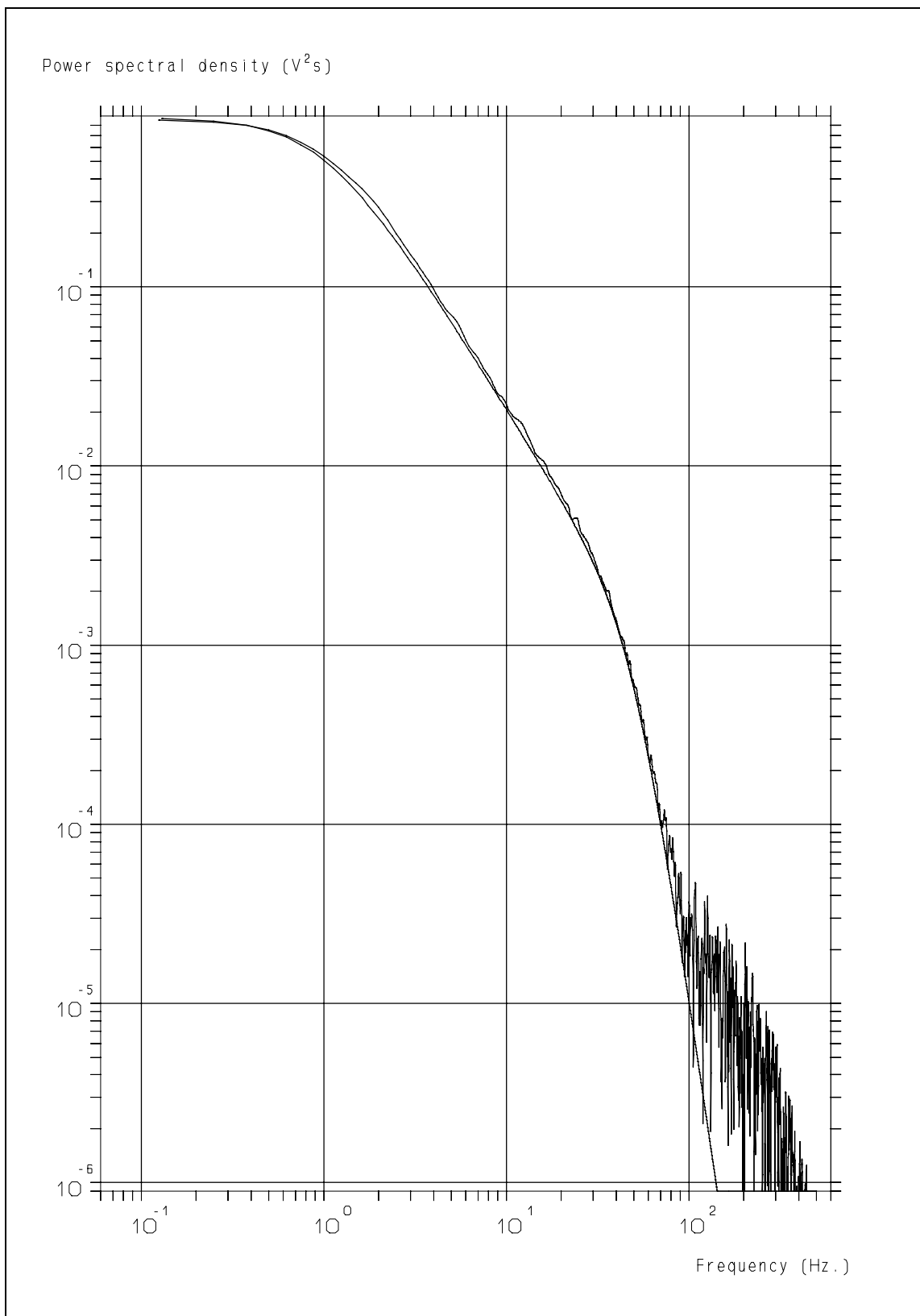


**Figure 9.7:** Power spectrum, obtained using the cross covariance technique and first-order reconstruction (wiggly at bottom) and the Bessem spectrum.

*Retrieval of turbulence and turbulence properties from LDA data with noise*

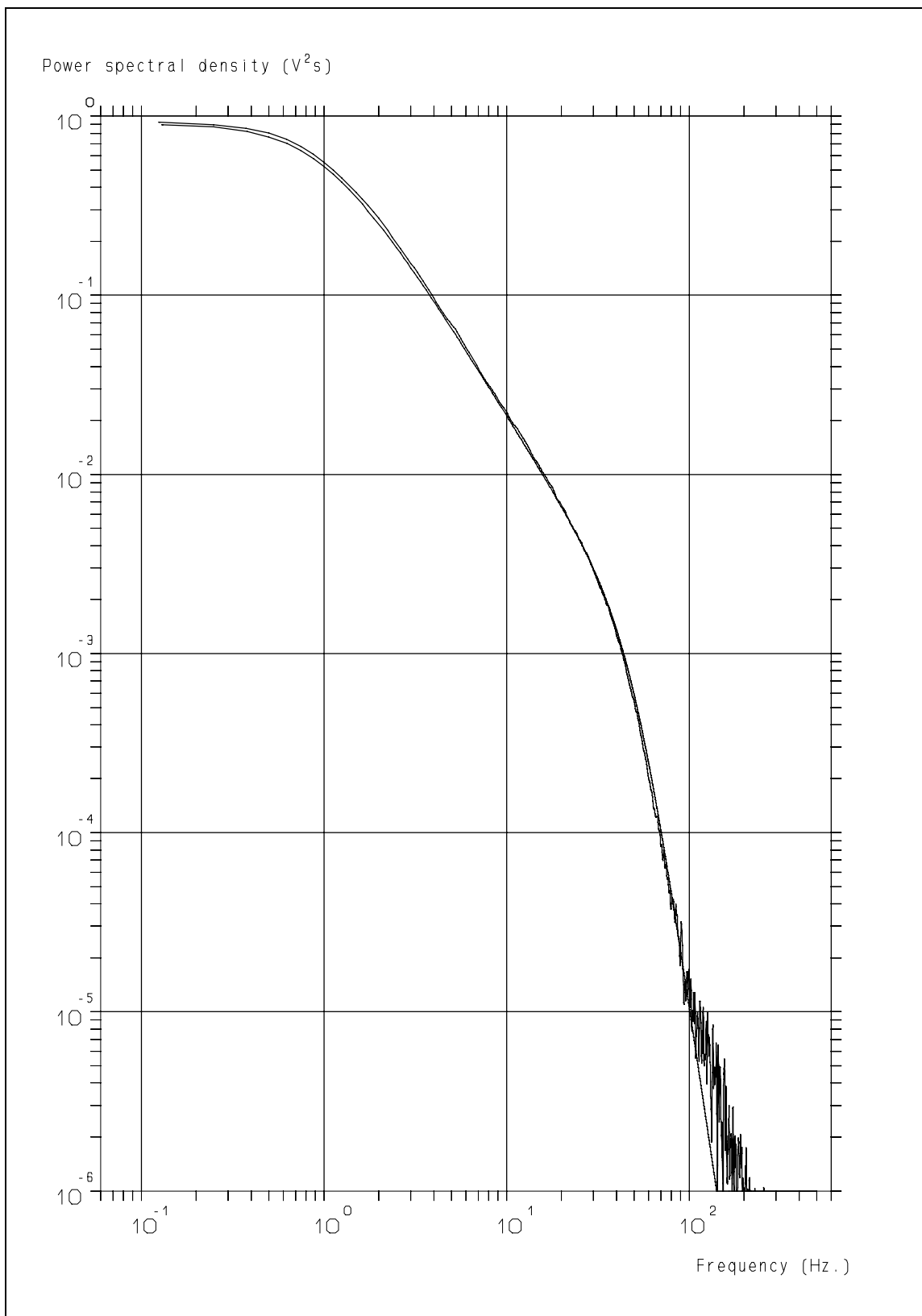


**Figure 9.8:** Power spectrum, obtained using the cross covariance technique and first-order Kalman reconstruction (wiggly at bottom) and the Bessem spectrum.

# Chapter 10

## The auto correlation estimation using the slotting technique with Local Normalisation

*Each day comes bearing its own gifts.  
Untie the ribbons!*  
Ruth Ann Schabacker

### 10.1 Introduction.

In previous chapters we have seen that the distribution of the time intervals in between two successive Doppler signals is exponential because of the random distribution of the tracer particles (ref. 11). This is often a disadvantage as it complicates the processing of Laser-Doppler Anemometry (LDA) data significantly. In the Chapters 6, 7 and 8 we have seen how this random sampling leads to a low-pass (particle rate) filter characteristic when reconstruction (with periodic re-sampling) is applied and how the unavailability of information during the longer time intervals leads to a noise contribution. However, the exponential time interval distribution, which is a consequence of the random tracer particle distribution, has also one advantage: because the highest probability to obtain a Doppler signal is immediately after the previous one, there is information available on the short time scales, *no matter how low the data-rate is* and this information is relatively plentiful. This phenomenon has been pointed out already in the early years of LDA (ref. 18 and 28). Mayo (ref. 22 and 23) was the first to develop an algorithm, using this phenomenon, to estimate the auto correlation function (ACF) of the turbulent velocity fluctuations. Unfortunately, this algorithm showed to give estimators of the individual correlation coefficients with a high variance and on top of that the individual estimators could become  $> 1$  in the case of velocity bias or due to the large variance. In the next section we will describe this algorithm in more detail with its drawbacks, followed by a novel estimator, based on Local Normalisation, proposed by Tummers et. al. (ref. 73). Subsequently, the ACF's obtained with this novel estimator will be analyzed in more detail and its limitations outlined.

### 10.2 The slotting technique.

As the algorithms are aimed at estimating the ACF, we will define it here as:

$$\rho_{u'u'}(\tau) = \frac{\overline{u'(t) \cdot u'(t+\tau)}}{u'^2} \quad [10.1]$$

in which:

$\rho_{u'u'}$  = auto correlation function of  $u'$

$u'$  = fluctuating part of the velocity (average value of  $u'$  is zero)

$\tau$  = time lag

m/s  
s

The overbar denotes time averaging, see eq. [9.1].

The ACF is a measure for the similarity of a signal with itself, shifted over the time lag  $\tau$ . This can be used to determine a number of timescales of the turbulent fluctuations, such as the Taylor timescale  $T_\lambda$  which follows from the curvature of the ACF at zero lag time:

## Retrieval of turbulence and turbulence properties from LDA data with noise

$$T_\lambda^2 = \frac{-2}{\left( \frac{d^2 \rho_{u'u'}(\tau)}{d\tau^2} \right)_{\tau=0}} \quad [10.2]$$

This equation shows that very accurate estimates of  $R_{u'u'}$  at small time scales are required when the  $T_\lambda$  is to be determined from experimental data.

The algorithm, proposed by Mayo (ref. 22 and 23), for the estimation of the ACF from randomly sampled data has become known as the slotting technique, because it assigns products of two individual velocity estimates to "slots" of a finite width, depending on the time difference of the two velocity estimates. In mathematical description:

$$\rho_{u'u'}(k\Delta\tau) = \frac{\sum (u'_i u'_j)_{(k\Delta\tau)}}{N_{k\Delta\tau} [\overline{u'(t)}]^2} \quad [10.3]$$

in which:

$\Sigma (u'_i u'_j)_{k\Delta\tau}$  = sum of all cross products  $u'(t_i)u'(t_j)$  that are separated by a lag time in the interval  $(k - 1/2) \Delta\tau \leq (t_j - t_i) \leq (k + 1/2) \Delta\tau$

$N_{k\Delta\tau}$  = number of products within the above defined slot (note that  $\Delta\tau$  is the width of a slot)

The Mean Square (MS) value of the velocity fluctuations is estimated using:

$$[\overline{u'(t)}]^2 = \frac{1}{N} \sum_{i=1}^N [u'(t)]^2 \quad [10.4]$$

However, this technique suffers from several serious drawbacks:

- The variance of the estimator of the ACF in each slot (the individual correlation coefficients) is large compared to other techniques.
- the estimator of the individual correlation coefficients can rise above 1 for  $\tau > 0$  because of velocity bias (ref. 63, 67 and 102). The effect is shown in fig. 10.1. The occurrence of velocity bias in this data-set is shown by the decrease of the number of products, as shown in fig. 10.2 (see also Chapter 4).
- Separation of noise and turbulence contributions is difficult, in most cases even impossible, because of the above mentioned problems. As can be seen from fig. 10.1, estimation of the Taylor time scale is impossible when velocity bias occurs. As velocity bias is rather the rule than the exception<sup>1</sup>, this is a serious drawback.

As a result, the Mayo algorithm has not found many applications and the potential of the random sampling to obtain information on the small scales has not materialized. Improvement can, however, be obtained with a different approach, called Local Normalisation, which has been proposed and applied by Tummers et al. (ref. 73).

---

<sup>1</sup> We will prove the existence of velocity bias in Appendix A.

## 10. The ACF estimation using the slotting technique with Local Normalisation

### 10.3 Description of the ACF estimation with Local Normalisation.

Local Normalisation uses the following property of a stationary flow:

$$\overline{[u'(t)]^2} = \sqrt{\overline{[u'(t)]^2}} \cdot \sqrt{\overline{[u'(t+\tau)]^2}} \quad [10.5]$$

Substituting this into the equation for the slotting technique, the ACF can be estimated as:

$$\rho_{u'u'}(k\Delta\tau) = \frac{\sum (u'_i u'_j)_{(k\Delta\tau)}}{\sqrt{\sum (u'_i u'_i)_{(k\Delta\tau)}} \cdot \sqrt{\sum (u'_j u'_j)_{(k\Delta\tau)}}} \quad [10.6]$$

This yields the modified ACF estimator which showed to be very promising, as reported by Tummers (ref. 73) and in more detail in ref. 102. The properties of the Local Normalisation estimator will be evaluated here using numerical simulations and subsequently it will be applied to measured data. A numerical simulation is required as that is the only way to know the properties of the turbulence the algorithm is to reproduce, as has been discussed in Chapter 2.

### 10.4 Analysis of the properties of the ACF estimated with Local Normalisation.

For the analysis of the properties of the ACF, estimated using Local Normalisation, simulated turbulence according to the "Bessem" power spectrum has been used. From this simulated turbulence, simulated LDA data have been derived by random sampling and the addition of Gaussian distributed noise to each individual velocity estimate. The properties of the simulated turbulence and the generation of the simulated LDA data-set have been described in Chapter 2, the Signal-to-Noise Ratio (SNR) used was 5. Also, one-dimensional velocity bias has been introduced when required. This can easily be achieved by adding an average velocity to the simulated turbulence and subsequently taking the actual data-rate proportional to the instantaneous velocity<sup>2</sup>. In the rare case that the actual data-rate would become lower than 0.01 of the average data-rate, the data-rate was set to 0.01 of the average data-rate to avoid excessive and thus unrealistic time intervals. The ratio of the Root-Mean-Square value of the simulated turbulence and the average velocity determines the amount of bias (expressed in the turbulence intensity).

For reference: the auto correlation function corresponding to the "Bessem" spectrum is shown in fig. 10.3 and the Taylor time scale of this simulated turbulence is 27 msec. The first analysis was to determine the differences between the actual ACF and the ACF's, estimated by the two algorithms when no velocity bias was introduced, only a noise contribution. The result is presented in fig. 10.4 and from this figure<sup>3</sup> some properties can be derived:

1. The noise peak stands out clearly for both algorithms.
2. The variance of the individual correlation coefficients obtained with the Mayo algorithm is high compared to the variance of those, obtained with Local Normalisation.
3. The variance of the individual correlation coefficients using Local Normalisation increases with decreasing values of the correlation coefficients.

---

<sup>2</sup> Note that the "effective  $t_0$ " is thus inversely proportional to the actual velocity.

<sup>3</sup> The different curves are very hard to label, but they can be identified using their properties: the noise peaks of the ACF's obtained using Mayo's algorithm and the Local Normalisation coincide at  $\tau = 0$ , but for  $\tau > 0$  the theoretical ACF and the ACF using Local Normalisation virtually coincide. Note the large variance of the ACF obtained using Mayo's algorithm.

## Retrieval of turbulence and turbulence properties from LDA data with noise

The properties 2 and 3 have been investigated further using a sinusoidal signal which was randomly sampled and had a noise contribution with an SNR of 10. The ACF, obtained using Local Normalisation, is shown in fig. 10.5 and this shows that the variance in the estimators of the individual correlation coefficients is dependent on the *absolute value* of the correlation coefficient. Compare fig. 10.5 with fig. 10.6 which shows the result when the Mayo algorithm is applied to the same data-set. The differences are obvious and fig. 10.6 also shows that the variance of the individual correlation coefficients is virtually *independent* of the value of the correlation coefficient. The differences between the two algorithms are even more clear from fig. 10.7 which shows an enlargement of the two ACF's in the vicinity of  $\tau = 0$ . Note that the Mayo algorithm leads to estimators  $> 1$  due to variance, because no velocity bias has been introduced. However, when the value of the individual correlation coefficients approaches zero, both algorithms lead to the same estimator, as is illustrated in fig. 10.8, where virtually no difference between the two estimators can be distinguished. The Local Normalisation thus gives optimum estimators for the ACF, especially in the vicinity of  $\tau = 0$  and when the SNR is as high as possible<sup>4</sup>. This is another important reason to optimise the LDA measurement system.

Both above mentioned analyses showed very promising properties of the Local Normalisation, but as the Mayo algorithm proved very sensitive to velocity bias, the next set of analyses concentrated on the influence of velocity bias on the estimated ACF's, obtained by Local Normalisation. Therefore the simulated turbulence has been randomly sampled with a  $t_0$  of 6 ms. and the turbulence intensities ranged between 33 and 200 % with the introduction of one-dimensional velocity bias. The effect of velocity bias on the time interval distribution is shown in fig. 10.9, which shows the characteristic shape as has been discussed in Chapter 4 on preliminary diagnostic testing of experimental data-sets. The simulated LDA data have been processed with slots of 0.2 and 1 msec. wide.

### 10.5 Results.

The estimation of the ACF's, using Local Normalisation, from data-sets with one-dimensional velocity bias does not lead to values of the individual correlation coefficients  $> 1$  even if the turbulence intensity is increased to 200 %. This is illustrated in the fig. 10.10 - 10.14. Fig. 10.10 illustrates the difference between the Mayo algorithm and the Local Normalisation on simulated data and it is similar to fig. 10.1 where the same difference is illustrated when both algorithms are applied to real (measured) data. In fig. 10.11 - 10.14 the influence of velocity bias on the estimated ACF's is illustrated and the differences with the actual ACF<sup>5</sup> can be distinguished.

Because the values of the individual correlation coefficients do not rise above 1, it is now possible to determine the Taylor time scale from these ACF's by fitting a parabola to the ACF at  $\tau = 0$  using the least-squares approach. When no velocity bias is present, the estimated Taylor time scale is correct. The Taylor time scale has been determined using a large number of turbulence intensities with one-dimensional velocity bias and the results are presented in fig. 10.15. The noise peak at  $\tau = 0$  is clearly distinguishable in all cases, albeit its size depends on the turbulence intensity, as can be seen from the fig. 10.11 - 10.14. Therefore, the SNR is also estimated, assuming that the noise and turbulence are not correlated (which is a correct assumption in the simulations, but also in most practical cases, see Chapter 7). The correlation coefficient at  $\tau = 0$  is thus the normalised sum of the MS of the turbulence and the MS of the noise. The turbulence contribution can be estimated from the extrapolation of the parabola, obtained from the Taylor time scale. From these two values the SNR can easily be estimated:

---

<sup>4</sup> Note that the correlation coefficient for  $\tau > 0$  is below 1 (one) because the noise contribution disappears. The smaller the noise contribution, the closer the correlation coefficients stay to 1 (one) and thus the lower the *variance* in the correlation coefficients will be.

<sup>5</sup> The estimated ACF's can be recognised by their wiggly appearance for the smaller values of the correlation coefficients.

## 10. The ACF estimation using the slotting technique with Local Normalisation

$$SNR = \sqrt{\left( \frac{\sigma_t^2}{1 - \sigma_t^2} \right)} \quad [10.7]$$

in which:

$\sigma_t$  = contribution of turbulent velocity fluctuations to the ACF at  $\tau = 0$ .

The obtained estimates for the SNR are presented in fig. 10.16. From both figures it can be seen that:

- The Taylor time scale rises above the actual value (27 ms.) for turbulence intensities above 100%.
- The Taylor time scale is below the actual value for turbulence intensities below 100%.
- The Taylor time scale is close to the actual value for turbulence intensities of 100% and for the limiting case of the turbulence intensity going to 0%.
- The noise peak at  $\tau = 0$ , indicative for the SNR of the velocity fluctuations, is too small for high turbulence intensities.

### 10.6 Discussion.

The retrieval of the turbulence properties of a steady flow up to the smallest scales has proven to be difficult at low mean data-rates. The reasons are:

- The noise contributions to each individual velocity estimate obscure the contribution of the small eddies.
- The original (Mayo's) slotting algorithm is sensitive to velocity bias and has a large variance in the individual ACF estimates.

Although the Local Normalisation is still sensitive to velocity bias, it solves some of the above mentioned problems. Important is its low variance in the vicinity of  $\tau = 0$  where the correlation coefficient is high. This enables not only an accurate determination of the Taylor time scale, but as the power spectral distribution for small scales is determined by the auto correlation function at the short time scales (ref. 89 and 90), it may open the opportunity to determine the turbulence power spectrum with a higher accuracy than previously. This will be the subject of the next chapter.

One might be tempted to think that small slot widths are attractive because the slot width determines the highest frequency in the spectrum (Nyquist/Shannon theorem) and it would give a detailed estimator for the ACF for the short time intervals. However, there are lower limits to what is possible. In the first place the transit time of the tracer particles: as only one signal can be processed at a time, slot widths smaller than the transit time will not contribute to the ACF. Also, the dead time of the processor will set a lower limit, as slots, corresponding to delay times below the dead time will remain empty, which is unacceptable. Thirdly, the arrival time error (see Chapter 5) introduces uncertainties in the measured time difference between two velocity estimators. Increasing the resolution in the time delays of the ACF will not contribute to more accurate results. And last-but-not-least: the variance in the estimators of the individual correlation coefficients will increase as the number of products in each slot decreases. The average number of products in each slot is equal to:

$$N_p = N_t \cdot \left( \frac{\Delta\tau}{t_0} \right) = T_m \cdot \left( \frac{\Delta\tau}{t_0^2} \right) \quad [10.8]$$

in which:

$N_p$  = number of products in each slot (on average)

$N_t$  = total number of velocity observations in the data

$\Delta\tau$  = slot width

$t_0$  = characteristic time of distribution (= 1/data-rate)

$T_m$  = total measurement time

s

s

s

## *Retrieval of turbulence and turbulence properties from LDA data with noise*

This can be understood by noting that the chance to find an observation within a (slot) width  $\Delta t$  is equal to  $\Delta t/t_0$  and that the total measurement time is  $N_r t_0$ . As the variance of the individual correlation coefficient also depends on the number of products in a slot, this number should at least be several thousand, and the lower the SNR, the higher this number should be. Note that this number is proportional to the measurement time and proportional to the data-rate *squared*. This shows again the importance of the data-rate, even when no velocity signal reconstruction is applied.

### **10.7 Concluding remarks.**

Using Local Normalisation with the slotting technique, an improved estimation of the auto correlation function of turbulent velocity fluctuations, measured with a Laser-Doppler Anemometer, has been obtained. The use of simulated LDA data-sets has revealed that:

- The variance of the estimator is significantly lower than the estimator of the original algorithm for high absolute values of the correlation coefficient: the higher the absolute value of the correlation coefficient, the lower the variance.
- The estimator, obtained with Local Normalisation, is identical to the estimator of the original algorithm when the absolute value of the correlation coefficient is close to zero.
- The erroneous result of the original algorithm when velocity bias occurs (correlation coefficients  $> 1$ ) does not happen with Local Normalisation.
- This new algorithm is also sensitive to velocity bias, albeit in a different way. The velocity bias effects the results for the values of the Taylor time scale and the Signal-to-Noise Ratio, derived from the estimated ACF.

The ACF estimator has a low variance for higher absolute values of the correlation coefficients. High values of the correlation coefficient often occur for shorter time delays and these correspond to the higher frequencies in the spectrum, which are usually obscured by noise (ref. 63). This fortunate coincidence can be used to estimate the turbulence power spectrum *below* the noise floor by noting that the fluctuations in the correlation function, which occur at longer time delays, cannot be caused by turbulence. This will be the subject of the next chapter.

10. The ACF estimation using the slotting technique with Local Normalisation

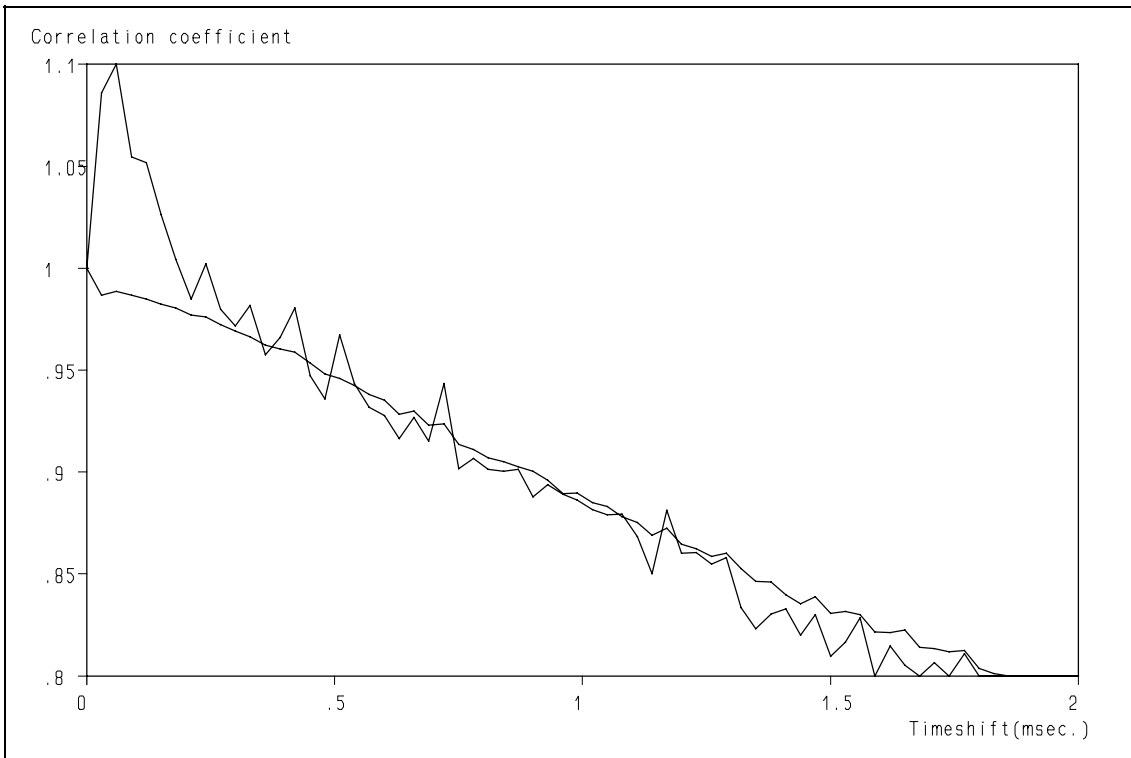


**Figure 10.1:** Velocity bias leads to estimators of the correlation coefficients  $> 1$  when the Mayo algorithm (upper curve) is used. The lower curve is a better estimator.

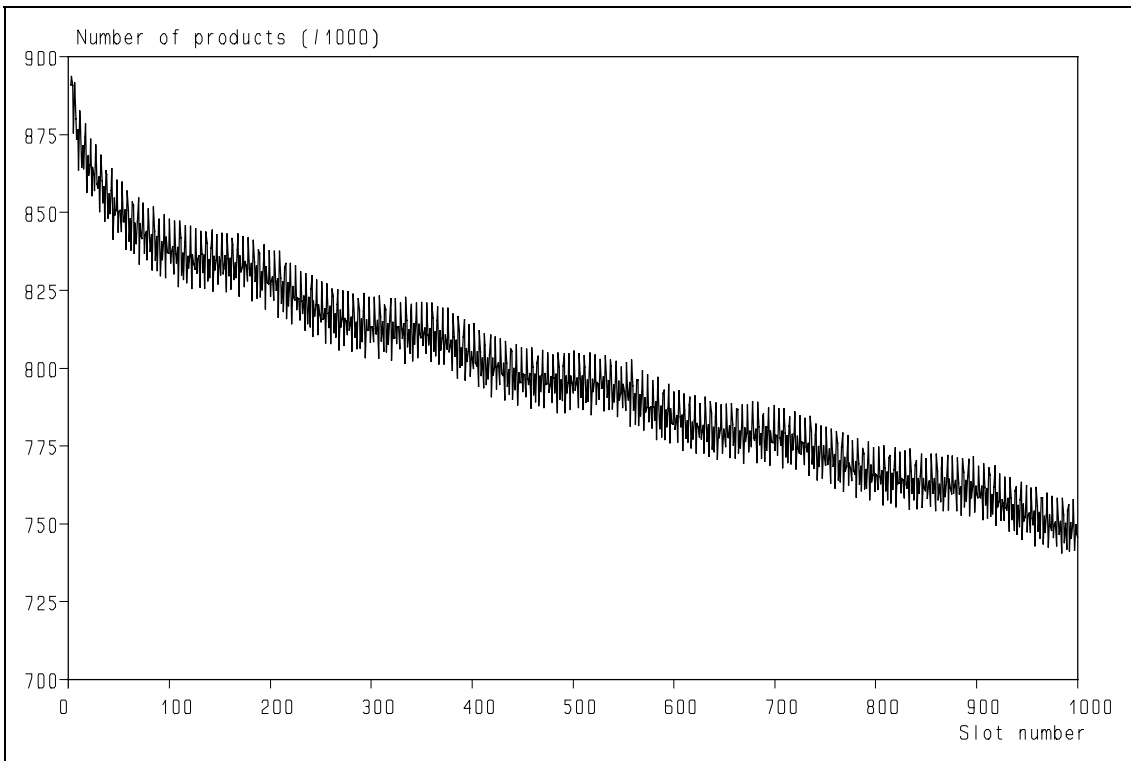


**Figure 10.2:** The decrease of the number of products as a function of slot number shows that the data-set used in fig. 10.1 shows velocity bias.

*Retrieval of turbulence and turbulence properties from LDA data with noise*

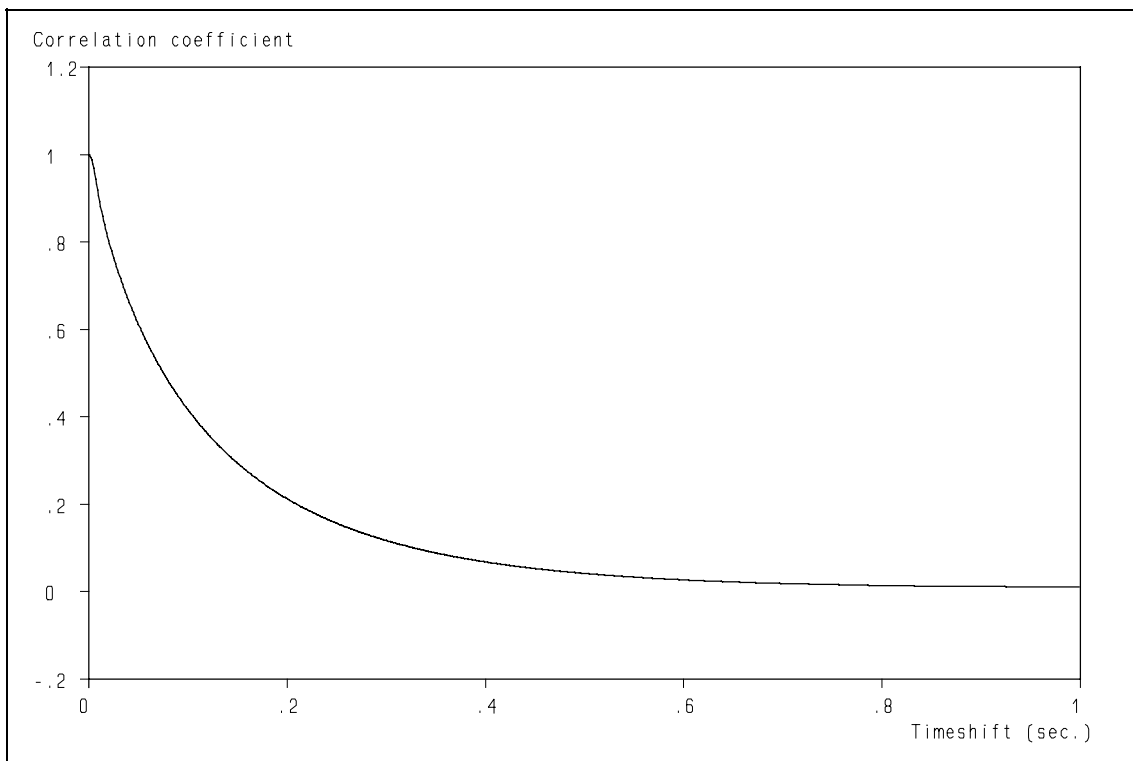


**Figure 10.3:** The theoretical auto correlation function, corresponding to the Bessem power spectrum.

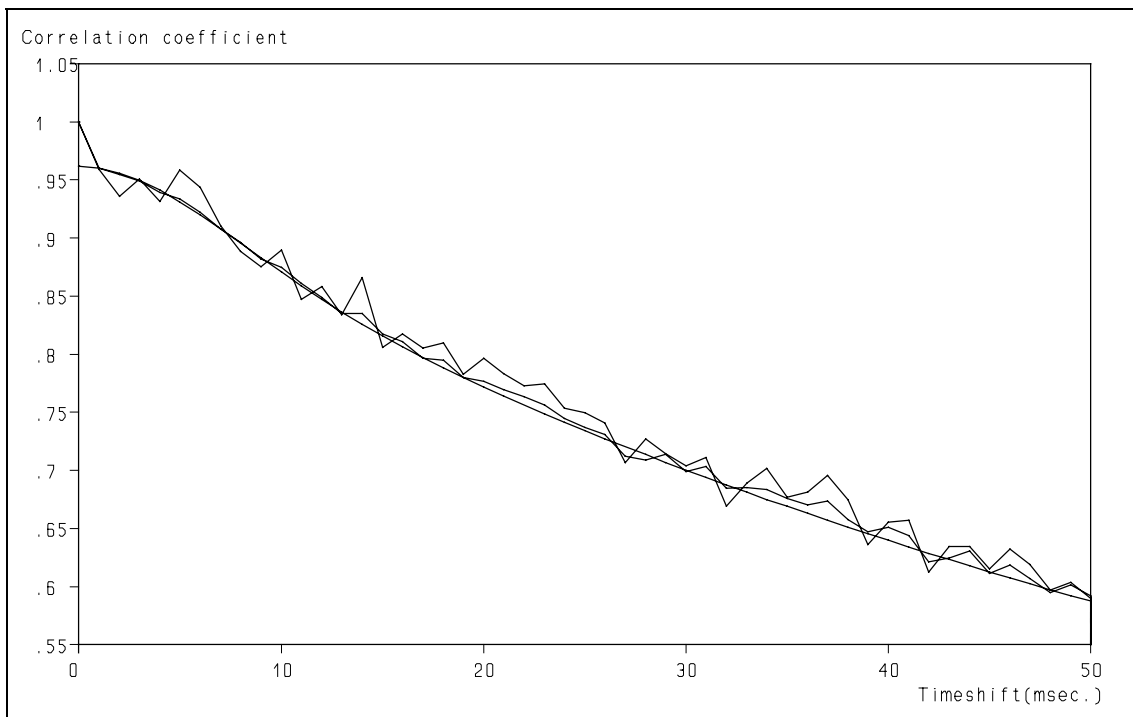


**Figure 10.4:** Comparison of the ACF estimates according to the ideal, the Mayo and the Local Normalisation algorithms. Note that the LN and ideal ACF's almost coincide for small values of  $\tau$ .

## 10. The ACF estimation using the slotting technique with Local Normalisation

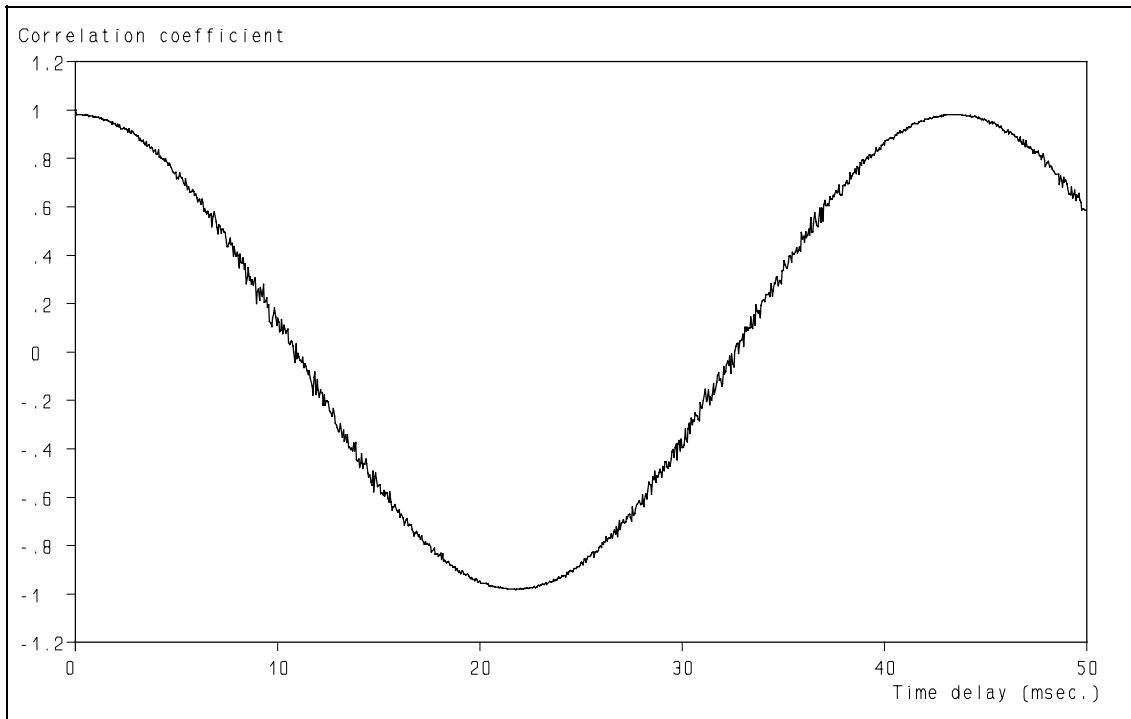


**Figure 10.5:** Slotted ACF, using the Local Normalisation, of a periodic signal with 10 % Gaussian white noise added. Note that the variance depends on the *absolute value* of the correlation coefficient.

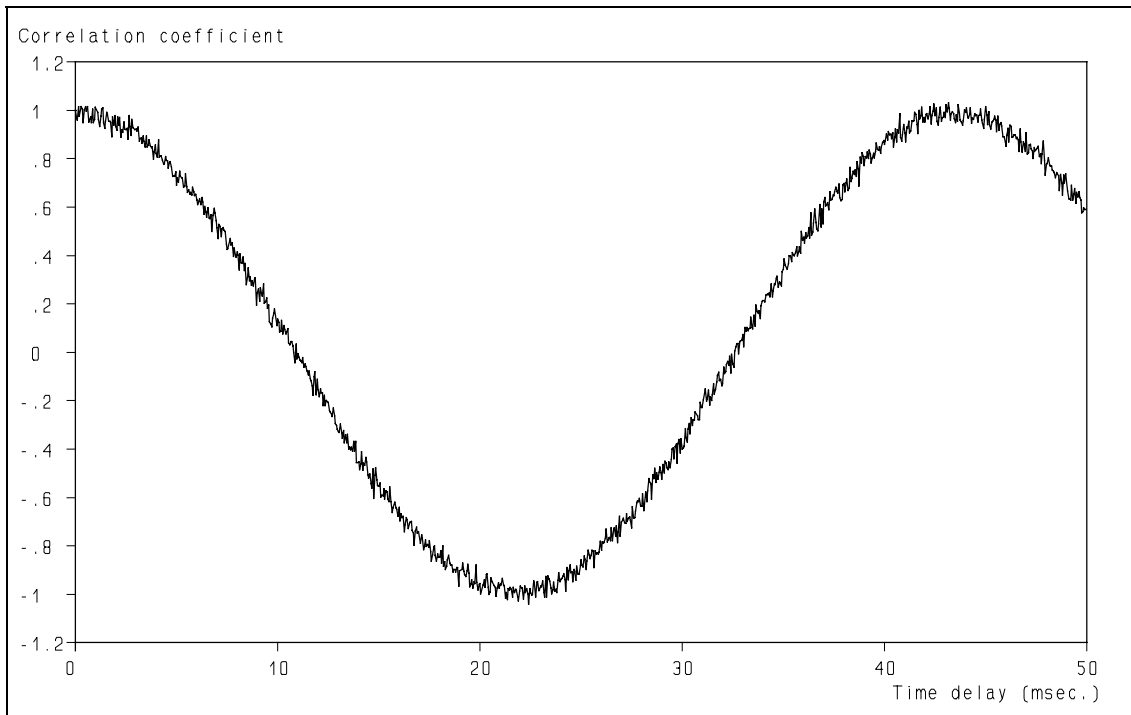


**Figure 10.6:** Slotted ACF, using Mayo's algorithm, of a periodic signal with 10 % Gaussian white noise added. Note that the variance is independent of the value of the correlation coefficient.

*Retrieval of turbulence and turbulence properties from LDA data with noise*

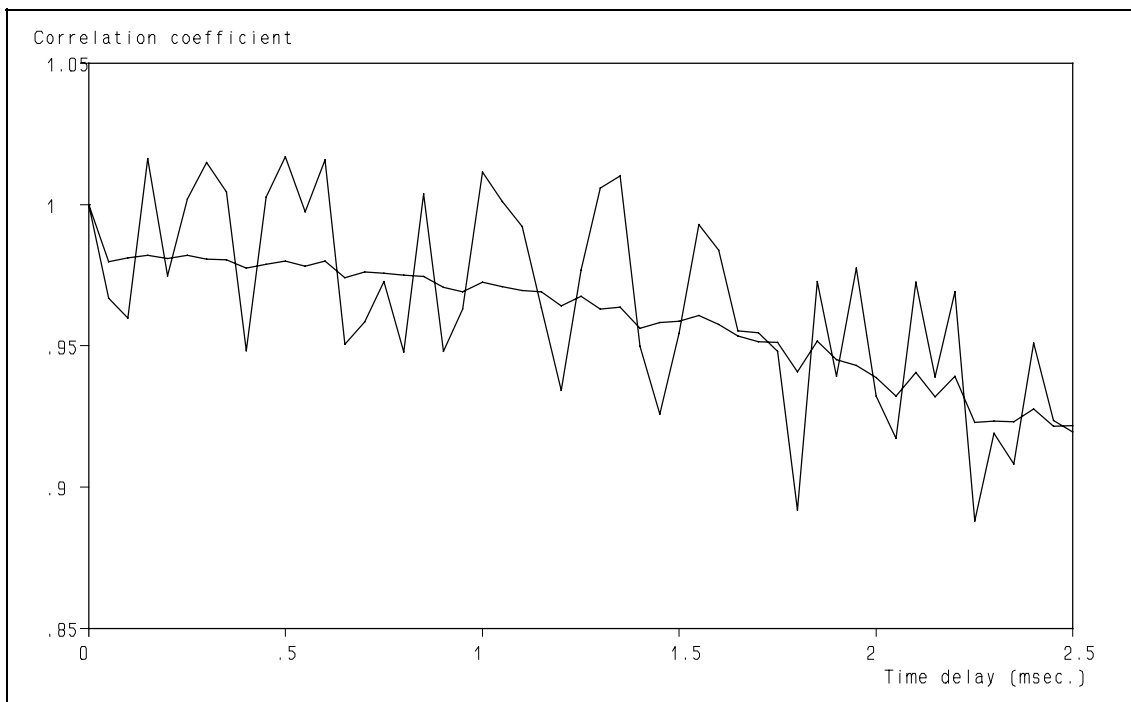


**Figure 10.7:** Enlargements of slotted ACF's of fig. 10.5 and 10.6. Note the difference in variance for large values of the correlation coefficient. The rise above 1 is caused by variance, not by velocity bias.

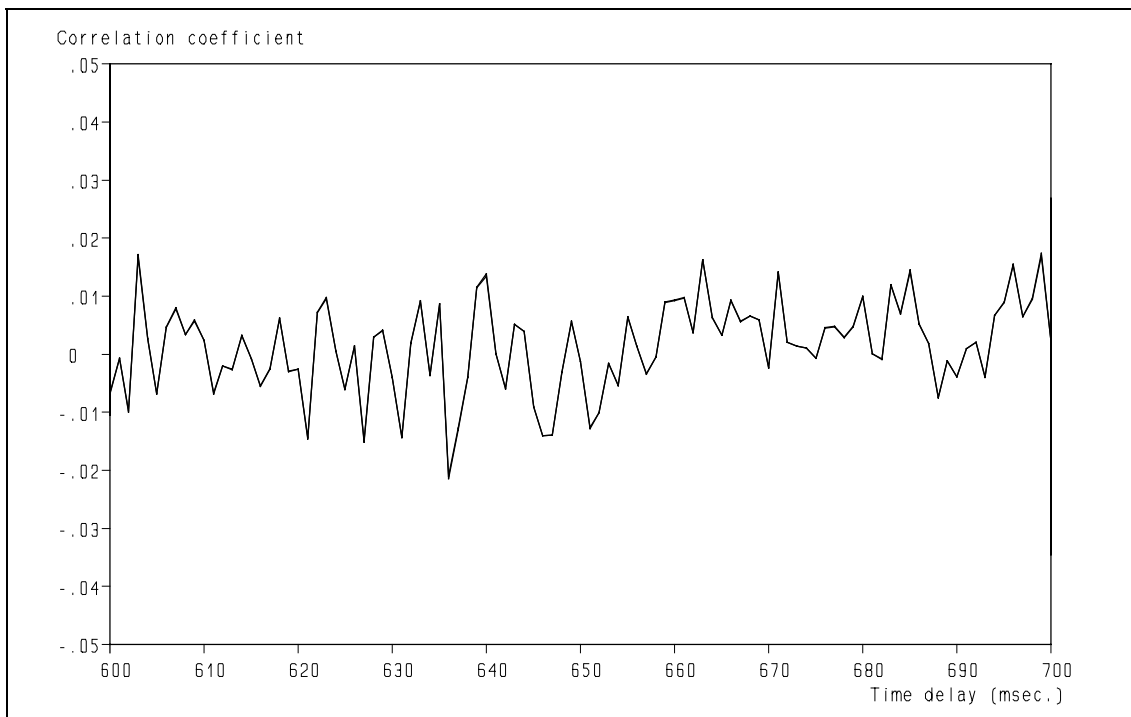


**Figure 10.8:** Comparison of the ACF estimates using Mayo's algorithm and the Local Normalisation. Note that the variances are identical for low values of the correlation coefficient: the traces are virtually indistinguishable.

10. The ACF estimation using the slotting technique with Local Normalisation

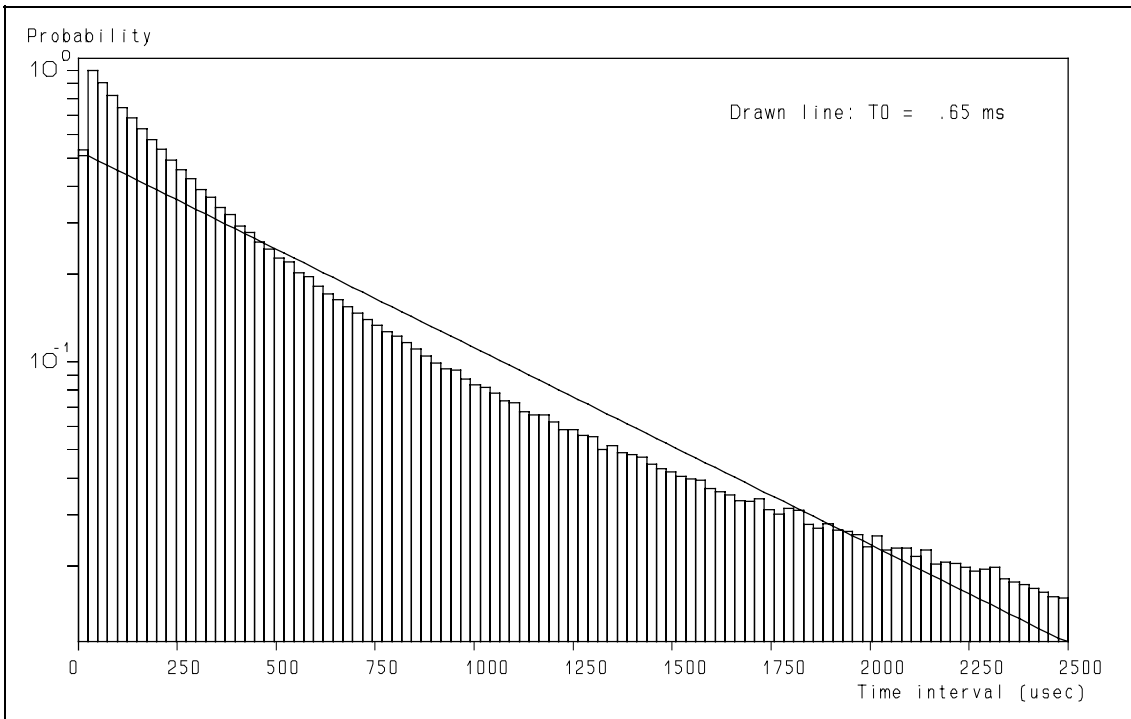


**Figure 10.9:** The time interval distribution when strong velocity bias occurs (turbulence intensity 100% and up). See also Chapter 4.

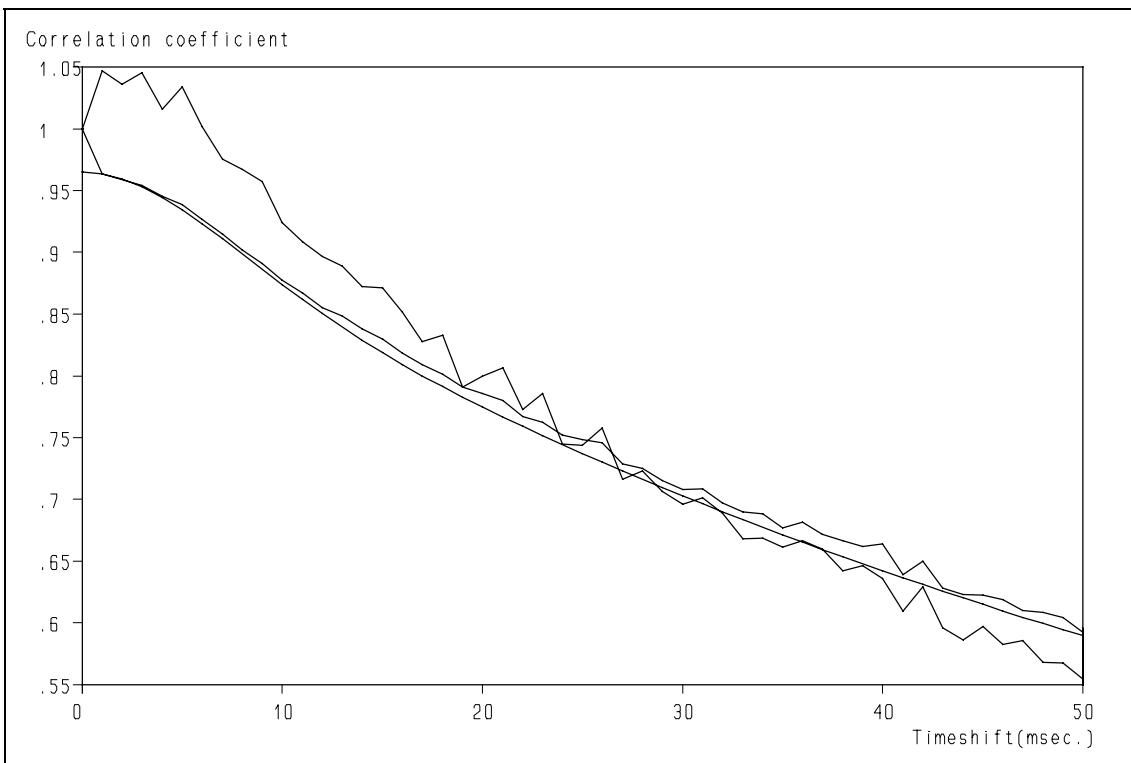


**Figure 10.10:** As figure 10.4, but with velocity bias introduced.

*Retrieval of turbulence and turbulence properties from LDA data with noise*

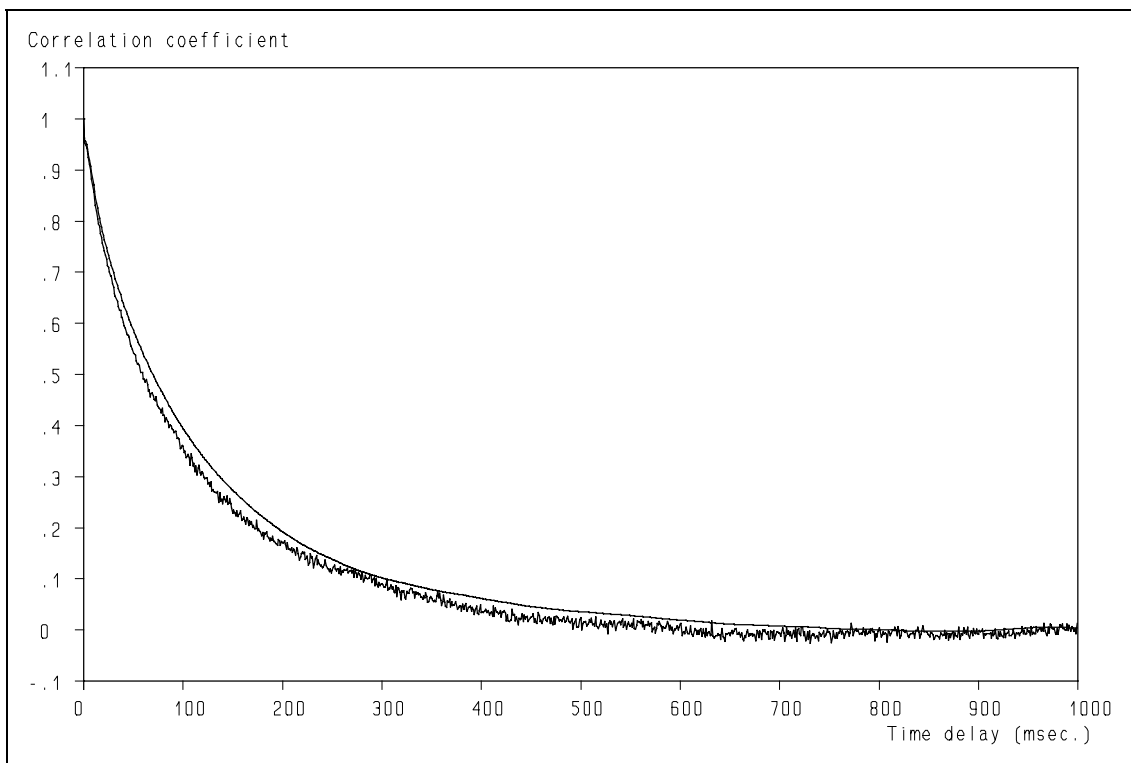


**Figure 10.11:** Estimate of the ACF using the Local Normalisation and the theoretical ACF, slot width 1 ms. Turbulence intensity 33 %, 1-dimensional velocity bias introduced.

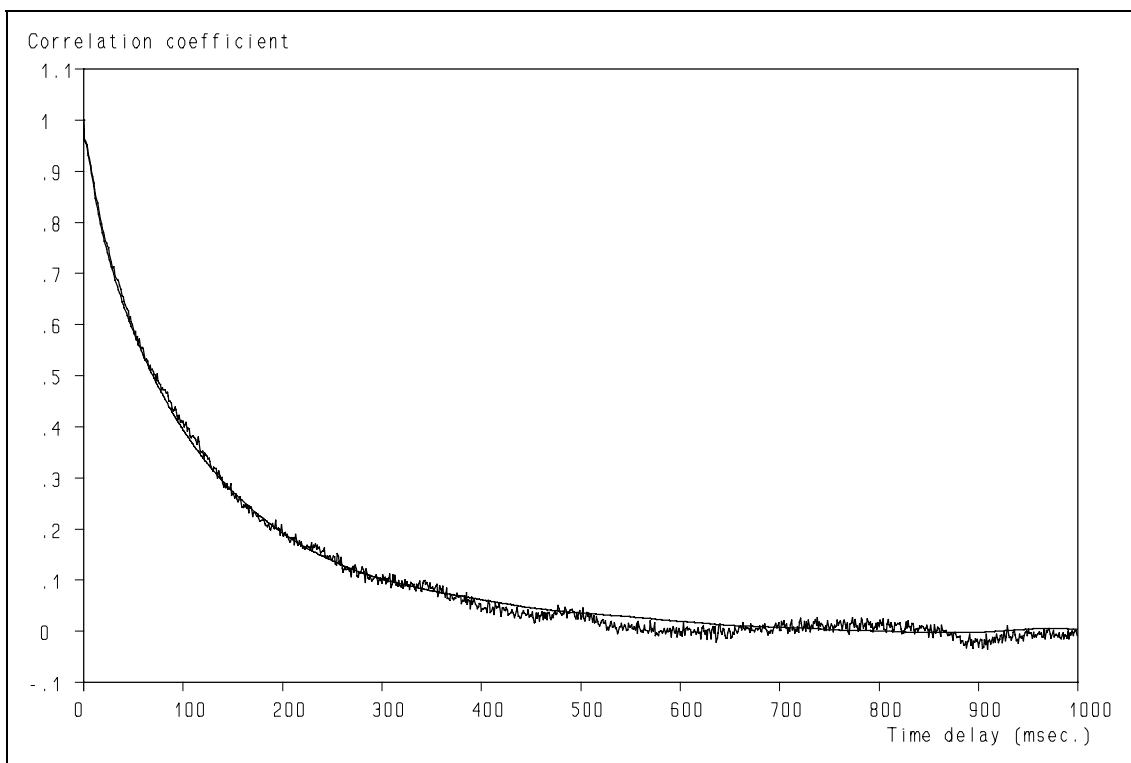


**Figure 10.12:** Estimate of the ACF using the Local Normalisation and the theoretical ACF, slot width 1 ms. Turbulence intensity 100 %, 1-dimensional velocity bias introduced.

10. The ACF estimation using the slotting technique with Local Normalisation

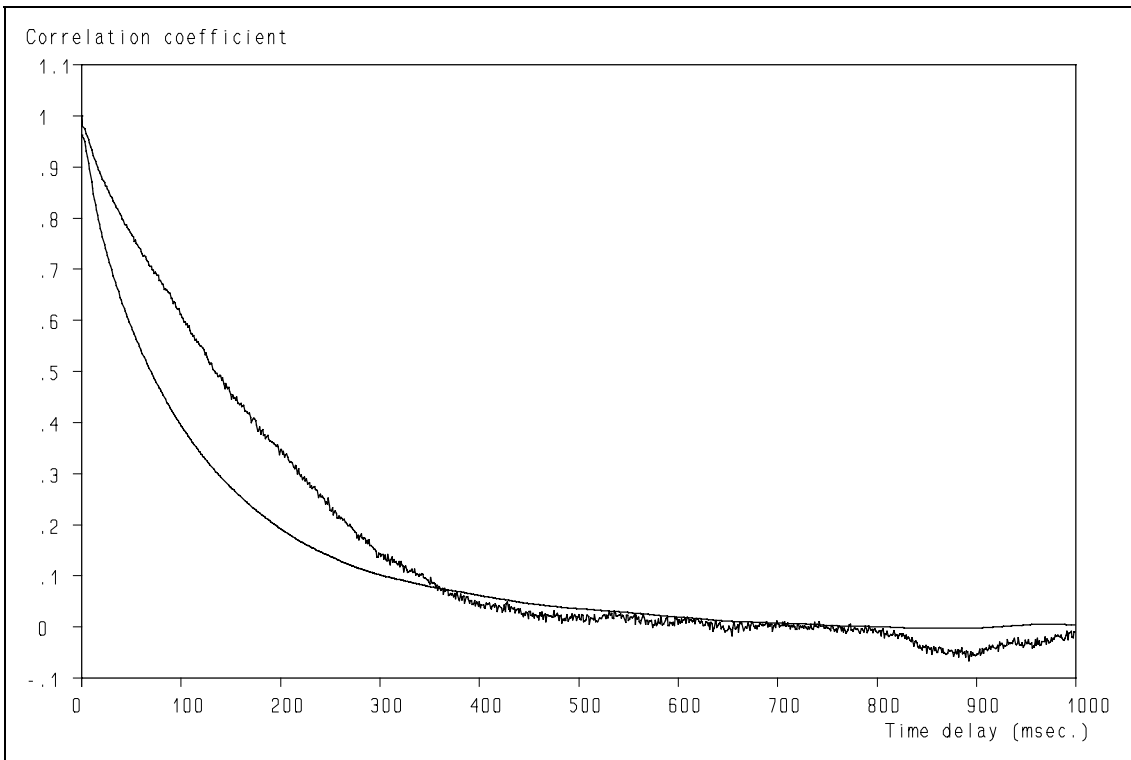


**Figure 10.13:** Estimate of the ACF using the Local Normalisation and the theoretical ACF, slot width 1 ms. Turbulence intensity 200 %, 1-dimensional velocity bias introduced.

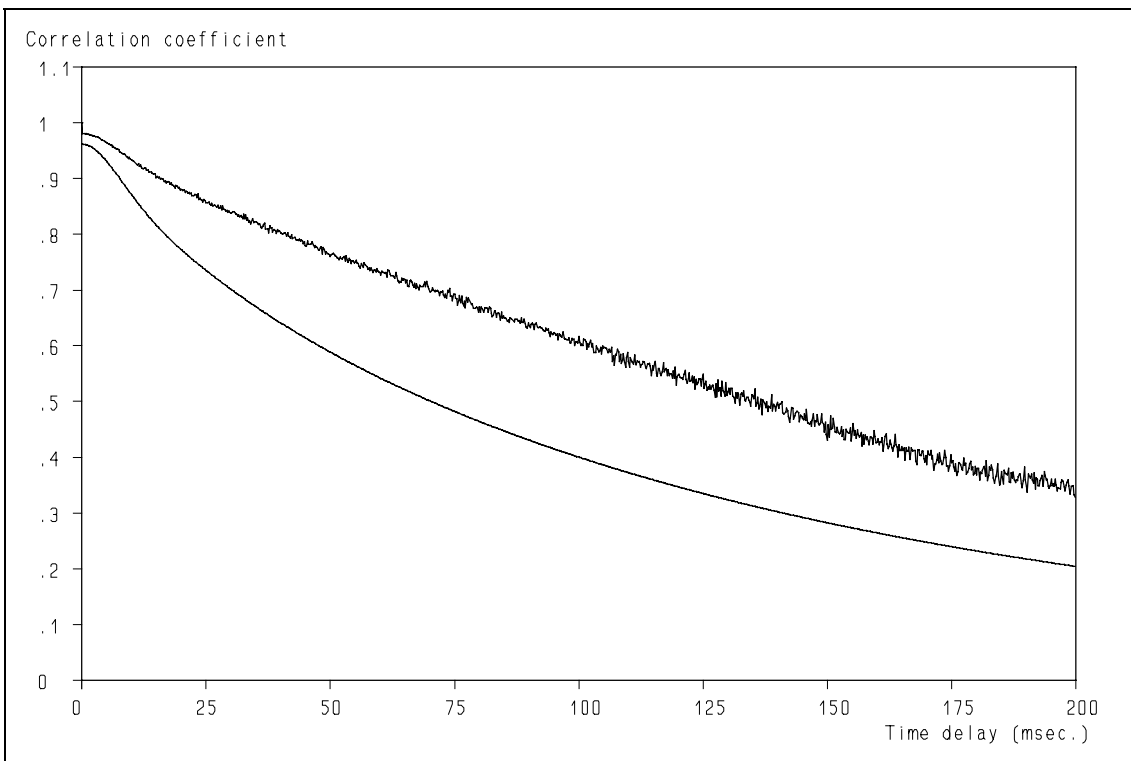


**Figure 10.14:** Estimate of the ACF using the Local Normalisation and the theoretical ACF, slot width 0.2 ms. Turbulence intensity 200 %, 1-dimensional velocity bias introduced.

*Retrieval of turbulence and turbulence properties from LDA data with noise*

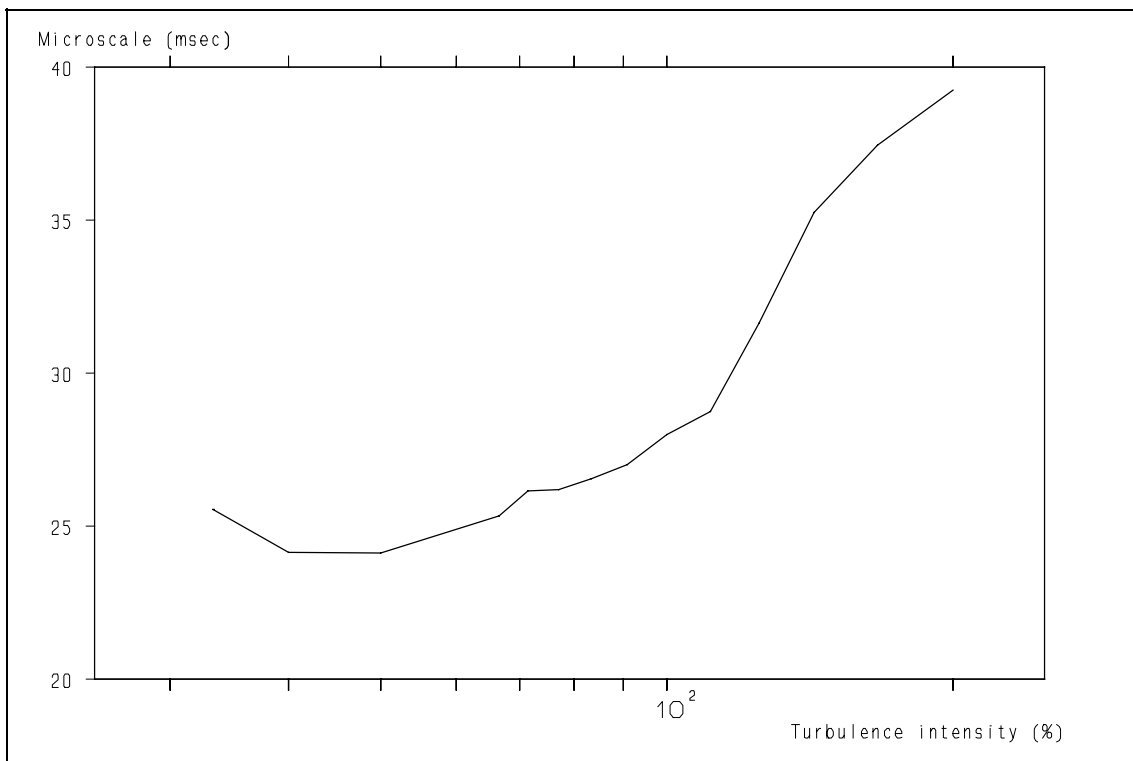


**Figure 10.15:** Taylor time scale as a function of the turbulence intensity when one-dimensional velocity bias is introduced.

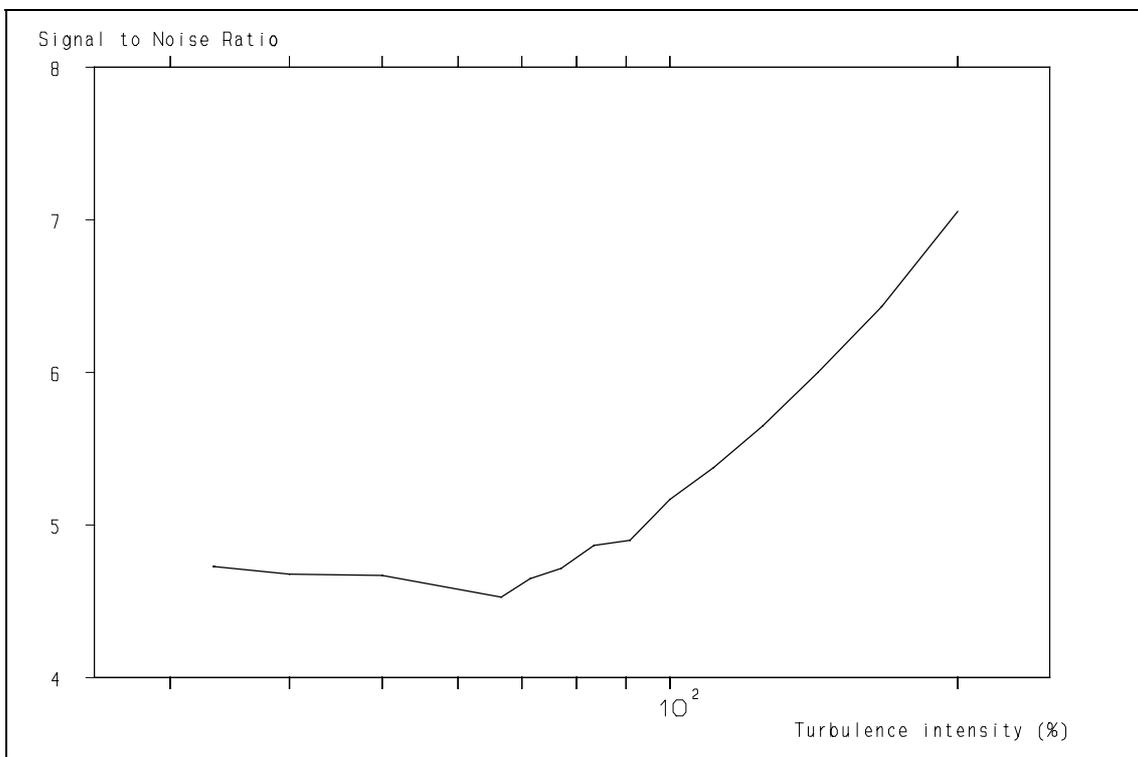


**Figure 10.16:** Signal to noise ratio as a function of the turbulence intensity (input value = 5) when one-dimensional velocity bias is introduced.

# Chapter 11

## Estimation of Turbulence Power Spectra by Curve-Fit to the Auto Correlation Function

*Soon after a heart-wrung decision,  
something inevitably occurs to cast doubt on your choice.  
Holding steady against that doubt usually proves your decision.*  
R.I. Fitzhenry

### 11.1 Introduction.

In the previous chapter a technique has been presented which can be used for the estimation of the auto correlation function (ACF) in case the data-rate is not sufficiently high for velocity signal reconstruction as described in Chapter 6 - 8. As the ACF is estimated with a low variance in the vicinity of  $\tau = 0$ , this might open the possibility to estimate the turbulence power spectrum for small scales as these are determined by the short time lags of the ACF (ref. 89 and 90). However, direct Fourier Transformation of a slotted ACF still leads to a noise floor which is similar to that when the Mayo slotting algorithm is applied, as can be seen from fig. 11.1 and 11.2. The reason for this lack of improvement is that there is still a noise peak at  $\tau = 0$  and the increase of the variance of the correlation coefficients when the correlation declines. The first problem could easily be solved by substituting the extrapolated value of the parabola for the Taylor time scale estimate at  $\tau = 0$ , thus eliminating the noise spike. The second problem is, however, harder to tackle. In the literature subtraction of the noise has been demonstrated (ref. 106) and it showed to give significant improvement, but the limitation there was still the variance in the spectral estimators. As this variance reduces only slowly with increasing size of the data-set, there is a practical limit to it, determined by the measurement duration, stability of the equipment and the like. The approach that will be described in this chapter circumvents this variance problem by the application of a curve-fit to the ACF, based on knowledge of turbulence. In literature an attempt to estimate parameters, based on *signal properties*, has been reported (ref. 107), but in this approach we use the *turbulence properties* as the starting point. This has also recently been reported in the literature (ref. 108 and 109), but care should be taken that the description of the turbulence is sufficiently flexible to avoid "self fulfilling prophecies". Especially the prescription of the well-defined slope of the inertial subrange (ref. 108) looks attractive, but it only occurs in fully developed flows. In less well developed flows different slopes have been reported (ref. 64 - 66) and have also been encountered in practical flow conditions as will be presented later in this chapter. These different slopes should -of course- be retrieved correctly.

As a first step an analytical expression for the turbulence power spectrum will be given, from which an analytical expression for the ACF can be derived. This ACF is fully determined by a small number (6) of parameters and these parameters can be optimised in order to obtain the closest fit to the ACF, derived from the experimental data. The technique will be tested using simulated Laser-Doppler Anemometry (LDA) data, based on both simulated turbulence and Hot-Wire Anemometry (HWA) data. Subsequently, the technique will be used to estimate power spectra from real (measured) LDA data-sets in order to determine the spectra below the noise floor.

## Retrieval of turbulence and turbulence properties from LDA data with noise

### 11.2 The curve-fit approach.

#### 11.2.1 Requirements for the curve-fit approach.

As is known from theory (ref. 89 and 90) the auto covariance function<sup>1</sup> and the power spectrum are each others' Fourier Transforms. So in order to result in a useful approximation of the turbulence power spectrum, the ACF should fulfil a number of requirements as the requirements set for one are reflected in requirements for the other. It is therefore convenient to specify the requirements in properties of the power spectrum where possible as more is known about the properties of the turbulence power spectrum than those of the ACF. The following properties for spectra of random turbulence (so without periodic components) have -at least- to be fulfilled (ref. 1, 2, 71, 72 and 74):

1. The spectrum should decay monotonically with increasing frequency above a first start frequency.
2. The decay of the spectrum should increase monotonically with increasing frequency above a second start frequency.
3. The slope of the power spectrum should be -4 dec./dec. above a third start frequency. This is required in order to fulfil the requirement that the derivative of the ACF is zero at  $\tau = 0$ . This is explained in detail in Appendix B.
4. The spectrum should be able to include slopes with non-integer values (expressed in dec./dec.) in order to describe e.g. the inertial subrange (which has a slope of -5/3 dec./dec., see ref. 72).
5. The shape of the spectrum must be very flexible in order to accommodate many different flow conditions. This includes different slopes, variable slopes, parts with constant slopes and continuously changing slopes of the spectrum on a log-log scale.
6. The analytical description of the spectrum should preferably be analytically Inverse Fourier Transformable in order to obtain an analytical expression for the ACF in order to reduce the time, required for the iteration<sup>2</sup>.
7. The number of parameters that can be chosen should be as small as possible in order to limit the time required to optimize the parameters and to guarantee stability and independence of starting values of the iteration.
8. The spectrum should describe the actual power spectrum correctly within an accuracy of  $\pm 25\%$  of the *actual* value over a dynamic range of 6 decades. The choice of 25% is purely arbitrary, but based on previous experience with turbulence power spectra, it is an ambitious goal.

These requirements are partly conflicting and an extensive analysis has shown that it is not possible to combine requirement 4 and 6. Therefore a "compromise" has been adopted in which the parts with a non-integer slope are approximated by a combination of increasing and decreasing terms. As will be shown later on, this compromise still fulfilled requirement 8, but it is to a certain extent conflicting with requirement 2.

#### 11.2.2 Choices made for the spectrum description.

The analytical description of the spectrum chosen consists of one phase-advance network in combination with four low-pass networks. The equation which describes the spectrum is:

---

<sup>1</sup> The auto covariance function is equal to the auto correlation function multiplied by the mean square value of the signal.

<sup>2</sup> In principle it is possible to use numerical Fourier and Inverse Fourier transformations. However, this increases the computational load significantly compared to the analytical transformations: the parameters describe both the spectrum and the ACF, it is just a matter of substitution. The use of analytical transforms also increases the flexibility of the curve-fit algorithm, as any desired number of points in the ACF can be handled.

## 11. Estimation of Turbulence PSD by Curve-Fit to the Auto Correlation Function

$$S_a(f) = S_a(0) \left[ 1 + (f/f_0)^2 \right] \prod_{k=1}^n \frac{1}{1 + (f/f_k)^2}, \quad k \in \mathbb{N} \quad [11.1]$$

in which:

$S_a(f)$	= analytical power spectrum	m <sup>2</sup> /s
$f$	= frequency	Hz
$S_a(0)$	= static gain of the power spectrum	m <sup>2</sup> /s
$f_0, f_k$	= parameters	Hz
	totally $n+1$ ; $n=5$ in our selection.	

In total the description requires six parameters, which leads to a high degree of flexibility of the power spectrum as is shown in fig. 11.3. The static gain of the spectrum is determined by integration of the power spectrum. This integral should equal the Mean Square (MS) value of the turbulent velocity fluctuations (ref. 1, 89 and 90).

The above described spectrum can be analytically Inverse Fourier Transformed (IFT) to obtain an auto covariance function and thus an ACF, described by these six parameters. The IFT is not easily done and details can be found in Appendix C. The ACF  $\rho_a(\tau)$  obtained is:

$$\rho_a(\tau) = \frac{S_a(0)}{R_a(0)} \pi \sum_{k=1}^n \left[ e^{-\frac{2\pi|\tau|}{\tau_k}} \left( 1 - \frac{\tau_0^2}{\tau_k^2} \right) \frac{1}{\tau_k} \prod_{l=1, l \neq k}^n \left( \frac{\tau_k^2}{\tau_k^2 - \tau_l^2} \right) \right] \quad [11.2]$$

in which:

$\tau$	= time shift	s
$R_a(0)$	= autocovariance at $\tau = 0$ (= MS of turbulent velocity fluctuations)	m <sup>2</sup> /s <sup>2</sup>
$\tau_0, \tau_k$	= parameters, $\tau_{0,k} = 1/f_{0,k}$	s

The ACF's show a similar flexibility as the spectra, as is shown in fig. 11.4. However, only the application to actual data from different sources can reveal whether the flexibility is enough or not. But first a curve-fit procedure will have to be developed followed by a test using simulated data of which all the properties are known in detail.

### 11.3 The curve-fit procedure.

The original slotted ACF is approximated by the function, given by eq. [11.2]. The six parameters have to be adjusted and this will be done by minimizing the Weighted Mean Square Error (WMSE): assume one is approximating a function, given by N data points  $(x_i, y_i)$   $i = 1, \dots, N$ , by a function which has M adjustable parameters  $a_j$ ,  $j = 1, \dots, M$ , i.e. M degrees of freedom. This is mathematically described by:

$$y(x) = y(x; \mathbf{a}_1 \dots \mathbf{a}_M) \quad [11.3]$$

The Weighted Mean Square Error is in this case:

$$WMSE = \sum_{i=1}^N w_i [y_i - y(x_i; \mathbf{a}_1 \dots \mathbf{a}_M)]^2 \quad [11.4]$$

in which:

$w_i$	= weightfactor
-------	----------------

## *Retrieval of turbulence and turbulence properties from LDA data with noise*

The WMSE can thus be regarded as an M-dimensional function with the parameters  $a_i$  as the independent variables. The global minimum of this function should be found as this corresponds to the best approximation to the input (the slotted auto correlation) function. This has to be done numerically using an iterative approach. The concepts of the algorithm that has been applied in this work can be found in ref. 110, but any technique that finds the global minimum of eq. [11.4] can be used for this purpose.

The six parameters (which we will denote as  $P_1 - P_6$ ) describe in principle the ACF, but for practical purposes two extra parameters are added. One is needed for the correction of the noise contribution to the slotted ACF, the second is used to take residual DC or periodic component contributions into account. We will discuss these separately.

As has been discussed in the previous chapter, the slotted ACF has a peak at  $\tau = 0$ . This is caused by the noise contribution to the individual velocity estimates. Because different noise contributions are uncorrelated, they only show up at the origin, where they correlate with themselves (see also Chapter 10). As a result, however, the contribution of the turbulent velocity fluctuations to the ACF is lower than unity, which has to be corrected for. This is done by the first additional parameter (which we will denote as  $P_7$ ), which is used to scale the amplitude of the approximate ACF to unity at  $\tau = 0$ .

As we use the curve-fit approach especially to retrieve details of the small eddies, which correspond to high frequencies, we tend to use small slot widths for the estimation of the ACF as the frequency range is proportional to  $1/\tau$  (ref. 89 and 90). However, the integral time scale does -of course- not depend on the choice of the slot width and consequently it can happen that the ACF at the end of the correlation window (which is usually 1000 times the slot width  $\Delta\tau$ ) is not yet zero. However, the ACF estimator corrects for "DC" contributions at the window boundary<sup>3</sup> and thus subtracts the end value from the estimated correlation coefficients before scaling. The value of the slotted ACF can therefore be too low near the window boundary. But the approximated ACF will tend to be above zero because it tries to fit to the *decay* of the correlation function. To overcome this problem an offset (which we will denote as  $P_8$ ), equal to the curve-fit function value at the window boundary ( $= 1000 \Delta\tau$ ), has been introduced into the slotted ACF. It also showed to be useful to compensate for small (remnants of) periodic components. We will discuss this when the results are presented.

The spectrum at high frequencies is determined by the correlation coefficients of the shorter time intervals (small values of  $\tau$ ) where the Local Normalisation reduces the variance of the individual correlation coefficients, as has been discussed in Chapter 10. However, the remaining variance in the other parts of the ACF obscures the spectrum with a noise floor at high frequencies as can be seen in fig. 11.2. Because the variance of the estimates of the slotted ACF depends on the absolute value of the correlation coefficient, the weight factors for the determination of the WMSE also depend on the absolute value of the correlation coefficient. These values have been estimated by "trial and error" and are given in Table 11.1.

---

<sup>3</sup> Note that a DC contribution to the input data leads to a constant, positive, value of the ACF at the correlation window boundary, no matter how wide this window is.

## 11. Estimation of Turbulence PSD by Curve-Fit to the Auto Correlation Function

Correlation coefficient absolute value	Weightfactor
>0.9	200.000
>0.85	1.000
>0.8	200
>0.7	10
>0.5	5
>0.3	2
>0.1	1

**Table 11.1:** The weightfactors

It seems at first sight that the weightfactors are quite unbalanced, but extensive experimentation on these values has revealed that these give the best results. The reasons for this phenomenon are:

- The variance of the individual correlation coefficients increases with decreasing values, thus the high values give more reliable estimates and can therefore be attributed higher weightfactors.
- The number of slots with a correlation coefficient  $> 0.9$  is usually small, which reduces their contribution to the total WMSE, even with high weightfactors.
- The high frequency part of the power spectrum usually has low values and subsequently only a small contribution to the ACF. It is also the most difficult part of the spectrum to estimate because of the obscuration by the noise. This high frequency part is, however, determined by the short time intervals (ref. 89 and 90), so this is the most important part to be fitted by the curve-fit algorithm (see also section 11.5). Fortunately, the short time intervals have the highest correlation coefficients and should thus be given the highest weightfactors, which is possible because they have the lowest variance.
- The other parts of the ACF still contribute to the WMSE and its *total* value is minimized. Thus only the *importance* of the value of the correlation coefficients for longer time delays is reduced, but they are not ignored.

However, it might be possible that for different conditions these weightfactors are not the optimum choice. It is -of course- simple to adjust these, but this will require a Monte-Carlo simulation which is representative for the conditions under study.

### 11.4 Verification of the curve-fit algorithm.

In the preceding section it has been demonstrated that the six parameters enable a large flexibility in the shape of the turbulence power spectrum. The next step is to apply the algorithm to different types of data in order to verify the capability of estimating the power spectrum within the required accuracy. Often the dynamic range of turbulence power spectra from LDA data is only 2 to 3 decades and the higher frequency part is obscured by a noise floor (see e.g. fig. 11.2). This prohibits the estimation of the frequency of the onset of the dissipation range and the slope of the spectrum in that range. We have applied the algorithm to different types of data in order to verify the accuracy of the results in comparison with our requirements:  $\pm 25\%$  over six decades. The data-sets that have been used are:

- simulated turbulence without random sampling and noise contributions.
- simulated turbulence with random sampling and noise contributions.
- HWA measured data with random sampling and noise contributions.
- LDA data from four different measurement set-ups.

## Retrieval of turbulence and turbulence properties from LDA data with noise

First the algorithm will be applied to simulated turbulence. The advantage of such data is that the power spectrum is known over the entire spectral range, thereby making it possible to evaluate the power spectrum obtained by the algorithm. As a second test these data-sets are randomly sampled with an exponential time interval distribution and Gaussian distributed noise is added to the individual velocity estimates. These estimates then have similar characteristics as LDA measured velocity estimates, as has been described in Chapter 2. Using these LDA-like data, the ACF is determined using the slotting technique, which is subsequently used as input for the algorithm, which should still be able to retrieve the underlying spectral properties. These analytical power spectra and the simulated turbulence derived from those spectra are, however, only an approximation of real turbulence. Therefore, HWA data of grid turbulence are used to generate a record of LDA-like velocity estimates to verify the behaviour of the algorithm on realistic turbulence data. Finally the algorithm is applied to a wide variety of LDA data from different experimental configurations. In the following sections the characteristics of the data and the experimental conditions in which they have been measured are presented, together with the results.

### 11.4.1 Simulated velocity estimations.

Two different spectra have been used as input for the simulations. The first data-set to which the algorithm has been applied is "turbulence" generated according to the "Bessem" power spectrum (ref. 60 and 70, see also Chapter 2) with cut-off frequencies  $f_1 = 1$  Hz and  $f_2 = 50$  Hz. The record consists of  $2 \cdot 10^6$  samples with a sampling frequency of 1000 Hz; the total duration of the signal is 2000 s. The ACF of this equidistant data set is estimated using

$$\rho_{u'u'}(k\Delta t) = \frac{\frac{1}{N-k} \cdot \sum_{n=1}^{N-k} u'(n\Delta t) \cdot u'((n+k)\Delta t)}{\frac{1}{N} \cdot \sum_{n=1}^N (u'(n\Delta t))^2} \quad [11.5]$$

in which:

- $\rho_{u'u'}$  = auto correlation function
- $k$  = integer number
- $\Delta t$  = sampling interval (= 1 / sampling-frequency) s
- $N$  = total number of observations
- $u'(t)$  = turbulent velocity fluctuations m/s

The integral time scale is estimated by integration of the ACF and the Taylor micro scales are estimated by fitting a parabola through the 1<sup>st</sup>, 2<sup>nd</sup> and 3<sup>rd</sup> point and a parabola through the 1<sup>st</sup>, 3<sup>rd</sup> and 5<sup>th</sup> point of the ACF. The average value of the interceptions of the two parabolas at the time-shift axis is taken as the micro time scale. Fig. 11.5 shows the ACF of the Bessem power spectrum together with the resulting approximation. Fig. 11.6 shows the Bessem power spectrum and the result of the curve-fit. To enhance the errors left by the curve-fit algorithm, the ratio of these spectra is shown in fig. 11.7, showing that the error is limited to  $\pm 25\%$ .

The second data-set consists of a record of  $2 \cdot 10^6$  samples which has been generated using the Von Kármán - Pao power spectrum, as specified in Chapter 2, with a duration of 500 s. ( $f_s = 4000$  Hz). The ACF, the integral and the Taylor time scale are estimated in the same way as described above.

The ACF, calculated using eq. [11.5] and the fit are presented simultaneously in fig. 11.8. Both spectra are shown in fig. 11.9 and the ratio of these two spectra is presented in fig. 11.10. The approximate spectrum is thus able to describe the actual spectra within the required accuracy of  $\pm 25\%$  and the curve-fit algorithm is able to find the parameters that correspond with these spectra if the ACF's are not distorted by noise and variance. The next step is thus to verify the behaviour of the algorithm when the ACF's resemble the ACF's of actual LDA measurements more closely.

## 11. Estimation of Turbulence PSD by Curve-Fit to the Auto Correlation Function

### 11.4.2 Simulated velocity estimations with a noise contribution.

To obtain more realistic ACF's, the simulated turbulence signals have been randomly sampled and to each individual velocity estimate a Gaussian distributed noise contribution has been added. The ACF obtained using this procedure with the simulated turbulence according to the Bessem power spectrum is shown in fig. 11.11. The  $t_0$  of the random sampling is 6.6 ms., resulting in an average data-rate of 150 Hz, which would set an upper limit of 24 Hz for the velocity signal reconstruction. Note that the ACF tends to 0.96 when approaching  $\tau = 0$ , which points at the noise peak at  $\tau = 0$  and also note the increasing variance when the correlation coefficient decreases. Fig. 11.11 also shows the fit to the ACF. Fig. 11.12 shows the spectra, derived from the ACF by Fourier Transformation and from the curve-fit. The curve-fit results in a close approximation in the part that lies above the noise floor, the part above approximately 40 Hz. To compare the fitted spectrum with the -underlying- Bessem power spectrum, both are shown in fig. 11.13. The curve-fit shows a close approximation to the actual spectrum up to the highest frequency presented, approx. 140 Hz, which is *close to the average data-rate* and six times above the frequency limit for velocity signal reconstruction. The close resemblance of the fitted and original spectra is even more clearly illustrated in fig. 11.14, which presents the ratio of these spectra, which shows that the error is limited to  $\pm 25\%$ . In fig. 11.15 - 11.18 similar results are presented for the LDA data, simulated according to the Von Kármán-Pao power spectrum and sampled with a data-rate of 1 kHz. Also in this case the error is limited to  $\pm 25\%$ , again to frequencies above the frequency limit for velocity signal reconstruction. The curve-fit algorithm is able to retrieve the underlying power spectrum over a range of 6 decades with an error of  $\pm 25\%$  from the "noisy" ACF's of simulated turbulence. The next step is to verify the results of the curve-fit algorithm to real turbulence signals.

### 11.4.3 Hot-Wire Anemometry velocity estimations.

The data have been measured in a wind-tunnel using three hot-wires with a pyramid shape from which the  $u$ ,  $v$  and  $w$  component of the velocity vector have been resolved. Turbulence has been generated by means of a grid with a mesh of 40 mm and the HWA-probe was located approximately 1 meter downstream of the grid. The duration of the measurement was 90 s. with a sampling frequency of 20 kHz (approximately 1 800 000 samples). The three power spectra have been estimated by calculation of the ACF using eq. [11.5] and subsequent Fourier Transformation of these ACF's. These spectra are used as reference for comparison with the curve-fit results. It was found that the  $u$  component contained a periodic component, as shown in fig. 11.19, which hampered the curve-fit algorithm and therefore has been removed. We will discuss compensation of periodic components in section 11.4.4.3 when the measurements in a mixing vessel will be presented.

The HWA-data have been "transformed" to LDA-like velocity estimates by random sampling using a  $t_0$  of 0.3 ms. and by adding Gaussian distributed noise, similar to the procedure used with the simulated turbulence, as described in more detail in Chapter 2. The presentation is also similar to those of the simulated turbulence. The results for the  $u$ -component are shown in the fig. 11.20 - 11.24, for the  $v$ -component in the fig. 11.25 - 11.27 and for the  $w$ -component in the fig. 11.28 - 11.30, except for the spectra which are similar to fig. 11.22. These results show again that the spectrum, derived from the curve-fit to the "noisy" ACF's, has an error of less than  $\pm 25\%$  from the actual spectrum up to frequencies of 9 kHz. Yet, the average data-rate of the random sampling was only 3.3 kHz, resulting in an upper limit for velocity signal reconstruction of only 530 Hz! The curve-fit algorithm thus performs satisfactorily on the real turbulence data. The only remaining question therefore is if the flexibility of the chosen spectrum (and corresponding ACF) is sufficient for different flow conditions. This will be presented in the next section.

## Retrieval of turbulence and turbulence properties from LDA data with noise

### 11.4.4 Measured LDA velocity estimates.

From different sources LDA data have been collected. This to ensure that different flow conditions would be represented and to avoid "experimenter bias" (influence of experience of the experimenter). Four different data-sets have been analyzed and these will be described below.

#### 11.4.4.1 Pipe flow.

The LDA measurements have been performed in a re-circulating pipe flow. The length of the pipe is 34 metres with an internal diameter of 40 mm. A trip-ring with a height of 5 mm is inserted in the pipe to force transition to turbulence. Two different kinds of fluids have been used, i.e. water seeded with pigment, acting as a Newtonian fluid, and a polymer-water solution. The polymer used is Superfloc A110, which is relatively resistant to mechanical degradation, with a the concentration of 20 wppm. Measurements have been performed at 11.9 mm (Newtonian fluid) and 11.7 mm (polymer solution) distance from the wall. The LDA was located 30 m downstream of the ring, measuring the streamwise (axial) component using the forward scatter mode. The results are presented in a similar way as the previous results and can be found in the fig. 11.31 - 11.33 for the experiment using water and in the fig. 11.34 - 11.36 for the experiment using the polymer solution. In both cases the fitted spectrum has a close resemblance to the spectrum derived from the slotted ACF, indicating that the flexibility of the curve-fit is sufficient to describe these spectra.

#### 11.4.4.2 Mixing-layer flow.

The data have been measured in a mixing-layer between two horizontal parallel water flows which serves as a model for the confluence of two rivers. The width of the mixing layer is approximately 600 mm and the water depth is 60 mm. The measuring volume of the LDA was located at the end of the channel in the middle of the mixing layer at 0.4 times the water depth above the bottom of the channel. The horizontal velocity components have been measured in the backward scattering mode, because the fluctuating water surface makes it impossible to use the forward scattered light. This results in a relatively low data-rate (147 Hz for the  $u$  component and 95 Hz for the  $v$  component) which would limit the velocity signal reconstruction to roughly 23 and 15 Hz, which is too low to retrieve information about the smaller eddies. The approach described in this chapter, however, enables the estimation of the spectra to frequencies above the average data-rate. The results are presented in the fig. 11.37 - 11.39 for the  $u$ -component and in the fig. 11.40 - 11.42 for the  $v$ -component. The curve-fit algorithm yields spectra which again have a close resemblance to the spectra derived from the slotted ACF's, so the flexibility is also sufficient for this type of flow.

#### 11.4.4.3 Mixing vessel flow.

A one-dimensional LDA, operating in the forward scatter mode, has been used to measure the turbulent velocity fluctuations in a mixing vessel containing water seeded with tracer particles of approximately 2.5  $\mu\text{m}$ . Measurements have been performed in the jet of the stirrer, an eight bladed Rushton turbine. These blades give rise to a periodic component in the flow, consisting of the blade passing frequency and several harmonics. These periodic component(s) show up in the ACF as damped cosine contributions of the same frequency, as is illustrated in fig. 11.43. They can be described by:

$$g_{per}(\tau) = A \cos(2\pi f_b \tau) \cdot e^{-\frac{\tau}{\tau_a}} + B \cos(4\pi f_b \tau) \cdot e^{-\frac{\tau}{\tau_b}} + C \cos(6\pi f_b \tau) \cdot e^{-\frac{\tau}{\tau_c}} + \dots \quad [11.6]$$

in which:

$g_{per}$  = contribution to the ACF by the periodic components

$A$  = relative "amplitude" of first harmonic

$B$  = relative "amplitude" of second harmonic, etc.

## 11. Estimation of Turbulence PSD by Curve-Fit to the Auto Correlation Function

$f_b$	= blade passing frequency	Hz
$\tau_a$	= damping of first harmonic	s
$\tau_b$	= damping of second harmonic, etc.	s

As the function chosen to describe the turbulence power spectrum does not include such periodic components, compensation is required to obtain a monotonously decreasing power spectrum and ACF. The most convenient method is to subtract the function of eq. [11.6] from the ACF. This has been done manually, by trial and error, and in this particular case it has been found that two harmonics with the same damping suffice. The parameters used are:

$f_b$	= 22.4 Hz,
$A$	= 0.11
$B$	= 0.004
$\tau_a$	= 0.35 s
$\tau_b$	= 0.35 s

After subtraction of these periodic components, the ACF of fig. 11.44 remains. Application of the curve-fit algorithm to this ACF yields the results presented in fig. 11.44 - 11.46. Although quite different from the spectra in the previous cases, the curve-fit does again yield a spectrum with a close resemblance to the spectrum, derived from the slotted ACF.

### 11.4.4.4 Airfoil flow.

In a wind tunnel the  $v$ -component of the turbulent velocity fluctuations in the lag of a wing profile have been measured. The measuring volume of the LDA was located 130 mm behind the profile with an  $y$ -shift of 9 mm. Oil droplets with a diameter of approximately 1  $\mu\text{m}$  have been used as tracer particles. The combined average velocity of all the three components is 0.295 m/s whereas the Root Mean Square value (RMS) of the fluctuations of the  $v$ -component is 1.216 m/s. This yields an extremely high turbulence intensity of 412%. At these high intensities velocity bias can be a real problem. This is demonstrated by the time interval distribution, which is shown in fig. 11.47. This distribution has a concave shape, quite different from the ideal distribution which is linear on a lin-log scale as has been discussed in Chapter 4 on preliminary diagnostic testing of experimental data-sets. The deviation is caused by bias (see Chapter 4 and ref. 102). Also, the ACF, shown in fig. 11.48 shows deviations similar to those predicted by simulations as reported in Chapter 10 and ref. 102. As a consequence, the curve-fit is not as good as with the previous data-sets, as can be seen from fig. 11.48. Also, the power spectra derived from the slotted and fitted ACF's show questionable deviations from what is to be expected in general. In fig. 11.49 the power spectrum derived from the curve-fit is shown, in fig. 11.50 also the Fourier Transform of the slotted ACF is shown. The *decrease* of the slope at approximately 60 Hz is a strange phenomenon, which is not easily explained by turbulence theory. However, the spectrum, derived from the curve-fit does reproduce this behaviour to a limited extent, indicating that the curve-fit has a high degree of flexibility. As has been shown previously (see Chapter 10 and ref. 102), the slotting algorithm is sensitive to bias and it is likely that these deviations are caused by bias. We will come back to this aspect in the next section.

The experimental conditions of the LDA measurements are summarized in table 11.2 and the parameters are tabulated in table 11.3.

*Retrieval of turbulence and turbulence properties from LDA data with noise*

	number sampl.	tot. time [sec]	int. time scale [msec]	Taylor time scale [msec]	RMS [m/sec]	SNR	average velocity [m/sec]	Turbu- lence intensity [%]
Bessem	2·10 <sup>6</sup>	2 000	133.23	29.20	0.0624	*	0	**
von Kármán-Pao	2·10 <sup>6</sup>	509.2	54.45	11.45	0.0426	*	0	**
Bessem with noise	296 716	1 950.1	119.45	30.01	0.0649	5.00	0	**
Von Kármán-Pao with noise	508 879	509.2	69.20	11.61	0.0443	5.00	0	**
HWA <i>u</i> comp.	296 719	90.15	4.61	0.51	0.480	6.86	9.11	5.27
HWA <i>v</i> comp.	296 716	90.15	1.09	0.40	0.3821	6.83	0	4.29
HWA <i>w</i> comp.	296 716	90.15	1.31	0.41	0.3409	6.77	0	3.74
Water pipe-flow	196 115	82.3673	27.81	10.36	0.0845	4.99	0.257	32.83
Polymer pipe-flow	196 348	84.2022	37.21	14.90	0.0783	7.17	0.295	26.54
Mixlayer- <i>u</i>	88 266	600	171.71	35.88	0.0182	9.01	0.193	9.48
Mixlayer- <i>v</i>	56 833	600	58.27	20.01	0.0152	10.31	0	7.83
Stirrer-jet	10 <sup>6</sup>	298	7.27	3.27	0.291	8.51	0.590	49.33
Airfoil	434 376	1 367	19.09	2.25	1.216	16.53	-0.105	412.20

**Table 11.2:** The experimental conditions.

\* No noise has been added to these simulated signals.

\*\* The turbulence intensity given in this table is the RMS of a separate velocity component divided by the average velocity of all components.

## 11. Estimation of Turbulence PSD by Curve-Fit to the Auto Correlation Function

Data set	param. 1	param. 2	param. 3	param. 4	param. 5	param. 6
Bessem	7.304	2.044	22.820	52.012	70.645	70.891
von Kármán-Pao	17.268	2.049	22.874	199.029	324.752	337.936
Bessem, noise	8.582	1.198	18.799	62.975	66.135	67.832
von Kármán-Pao, noise	19.642	2.034	26.271	144.294	373.439	400.395
HWA <i>u</i> comp.	433.311	50.979	819.406	3176.619	4851.979	7288.763
HWA <i>v</i> comp.	369.150	96.493	1095.214	1767.547	3462.713	12373.381
HWA <i>w</i> comp.	361.620	97.908	858.611	2552.334	5729.576	6317.507
Water pipe-flow	11.481	4.153	28.232	69.229	94.568	109.252
Polymer pipe-flow	9.201	3.380	17.511	42.862	71.048	174.981
Mixlayer- <i>u</i>	1.899	0.577	3.954	18.788	12500.657	12510.325
Mixlayer- <i>v</i>	4.173	2.011	9.174	418.095	8309941	15508770
Stirrer-jet	138.129	21.108	169.517	688.103	18518895	6581744
Airfoil	64.362	6.173	108.423	3864.209	3864.589	3871.630

**Table 11.3:** The six fit-parameters.

### 11.5. Discussion

In the previous section the curve-fit algorithm has been applied to a number of different simulated LDA signals, derived from simulated turbulence and Hot-Wire Anemometry data. In all cases the algorithm was able to retrieve the underlying turbulence power spectrum over a dynamic range of 6 decades with an accuracy of  $\pm 25\%$ , even though the Signal-to-Noise ratio (SNR) of the individual velocity estimates was 5 - 7. The data-rate requirement for velocity signal reconstruction,  $2\pi$  times the highest frequency present in the turbulence, is not required for power spectrum estimation using this curve-fit approach and it is even possible to estimate the power spectrum at frequencies *above the average data-rate* as is e.g shown in fig. 11.13, 11.23 and 11.41. This attractive property has been evaluated further by a more extreme simulation. A simulated data-set as described in section 11.4.2, using the Bessem power spectrum as the underlying turbulence, has been generated with an average data-rate of 50 Hz, leading to a particle rate filter frequency of approximately 8 Hz. The same data-processing procedure has been applied and the power spectrum was estimated up to 250 Hz. This is more than thirty times the particle rate filter frequency and the value of the power spectrum is almost eight decades below the maximum value at that frequency and more than four decades below the noise floor. Still the power was estimated within 25% of the actual value, as is illustrated in fig. 11.51, illustrating the power of the curve-fit algorithm. Although this is the result of a simulation, it is reasonable to expect that with real measured LDA data this property will hold up to at least two times the data-rate as long as the ACF is not hampered by the dead time of the processor (ref. 111). The property to estimate the power spectrum above the data-rate is very attractive for flows where backscatter has to be used for various reasons, like the mixing layer flow (see section 11.4.4.2), or where even forward scatter does not yield enough samples as in e.g. most gas flows. Also turbid flows like these occur in two-phase flows can profit from this property. The only requirement left is that the flow should be steady. This approach thus offers a practical solution for a problem that has been around ever since LDA has been used. But it can also be applied for the extended velocity signal reconstruction, as will be demonstrated in Chapter 12.

## Retrieval of turbulence and turbulence properties from LDA data with noise

The accuracy of the curve-fit algorithm can further be illustrated by looking at the slopes of the spectra, derived from the curve-fitted ACF's. In fig. 11.52 the fitted spectrum of fig. 11.6 is re-drawn with the estimated slopes added. The resulting slopes are -1.61 for the inertial subrange (theoretically -1.667) and -7 in the dissipation range (equal to the theoretical value). The cut-off frequencies are  $\approx 0.9$  and 50 Hz, which is close to the original 1 and 50 Hz. Identical values are obtained from fig. 11.53, in which the fitted spectrum from fig. 11.13 is re-drawn. This illustrates again -just as fig. 11.7, 11.14 and 11.51- that the random sampling and noise contribution do not influence the results of the curve-fit algorithm worth mentioning! Because the Kármán-Pao power spectrum does not have as well defined slopes as the Bessem power spectrum these slopes cannot be estimated, but the close resemblance of the spectra of fig. 11.9 and 11.17, as well as the ratios, shown in fig. 11.10 and 11.18, is convincing.

The analysis of different data-sets has revealed that basically two problems are still remaining:

- the compensation of periodic components which e.g. occur in stirred vessels.
- the influence of velocity bias.

The first problem can basically be solved by using a contribution to the ACF as described by eq. [11.6]. In most practical cases correction up to the third harmonic will suffice, which leads to an additional 7 parameters, the frequency of the blade passage and the amplitude and damping of the three harmonics. However, the frequency of the blade passage can be estimated from the drive shaft revolution frequency and the amplitude of the first harmonic from the ACF. Although the additional parameters do increase the time required for the iteration, the summation of the random turbulence ACF and the damped periodic components (eq. [11.6]) enables such an iteration, thus the problem is -at least in principle- solvable.

The second problem is harder to tackle, but fortunately it is not required to eliminate velocity bias completely. As is shown in literature (ref. 112), the scaling from frequency to wavenumber can still be done within narrow bounds when the turbulence intensity is as high as 40%. As has been shown previously (see Chapter 10 and ref. 102), the estimation of the ACF is hampered by the velocity bias. It would therefore be a better approach to scale the *time intervals* in the raw data file directly to *distance intervals* using the local "instantaneous" velocity and subsequently calculate the ACF. This ACF would thus become a function of *distance difference* instead of *time difference*, converting it to a sort of *spatial* correlation function instead of a temporal correlation function. Although this translation from  $\Delta t$  to  $\Delta x$  could probably not be done perfectly, it might reduce the effective velocity bias to an acceptable amount (below 40 %), especially when the velocity in the main flow direction is known. This would, however, require further study to see what kind of smoothing is required to reduce the influence of noise to the velocity estimates and what the contribution of the other velocity components to the transport velocity is. Simultaneous measurement of two or three components would, of course, alleviate this conversion.

The large weightfactors for small lag times ensure an appropriate fit round  $\tau = 0$ . This is essential to get a good prediction of the power spectrum for higher frequencies below the noise floor. This choice of the power spectrum is further confirmed by the estimated Taylor micro timescales of the fitted function, 30.01 msec (Bes.) and 11.61 msec (K-P), i.e. the micro timescales of the slotted "original" ACF are respectively 29.20 msec and 11.45 ms. This also indicates the importance of an optimized LDA: the higher the SNR of the individual velocity estimates, the smaller the "noise peak" at  $\tau = 0$  and the higher the correlation coefficients in the vicinity of  $\tau = 0$  and the larger the part of the ACF is where the correlation coefficient  $> 0.9$ . In other words: this curve-fit approach is no "miracle cure", it tries to squeeze as much information as possible from the data, but -as always- *the quality of the results will reflect the quality of the input data*. Another important aspect in this respect is that the variance does not depend on the correlation coefficient only. Also the number of products in each slot is of importance (see also Chapter 10). Therefore a sizeable data-set is required to obtain ACF estimates in the vicinity of  $\tau = 0$  with a low variance, required to get an accurate estimation of the power spectrum. In most cases we have used data-sets of 300 000 - 1 000 000 data points.

## 11. Estimation of Turbulence PSD by Curve-Fit to the Auto Correlation Function

Most attention is given to the prediction of the power spectra for higher frequencies, where the noise floor usually obscures the power spectrum itself. Therefore the prediction is less well for lower frequencies as can be seen from e.g. fig. 11.17, 11.39 and 11.50. We do not regard this as a serious problem because other techniques give good results for the estimation of the power spectra at lower frequencies (ref. 60, 68, 70, 89 and 90). Still, the higher frequency part is predicted accurately by the curve-fit approach. One should keep in mind that although narrower  $\tau$ -slots are attractive because they give spectra with a higher upper frequency, the slots cannot be made arbitrarily narrow: lower limits are set by the transit time of the tracer particles and the dead time of the Doppler signal processor (see also ref. 111). Too narrow slots will result in empty slots, which is unacceptable. Optimization is also here the keyword. See for more details Chapter 10.

Another problem may occur if the flow has a high ratio between the integral and Taylor time scales. The use of sufficiently narrow slots in order to resolve the high-frequency part of the power spectrum may result in an insufficient decay of the ACF at the window boundaries. Although the curve-fit algorithm can take a small offset ( $< 0.2$ ) at these boundaries into account, it does not work well if the remaining offset is too high. The solution in such cases is to extend the *number* of slots in the ACF. The algorithm can easily be adapted, but the calculation time of the iteration increases roughly proportional to the number of slots in the ACF. In the cases that we have tested, the 1000 slots sufficed, but in larger flow systems this may not be the case.

Although the flow conditions that have been tested cover a wide variety of flow velocities, turbulence intensities and geometries, this does not *guarantee* that *any* turbulence power spectrum can be estimated accurately using this approach. Yet, we do not expect many exceptions apart from the extensions that we have described above. If, however, a class of turbulence power spectra is uncovered that is not described by eq. [11.1], this does not mean that the approach described in this chapter cannot be used any longer. The problem that needs to be solved is to find an analytical description which covers the power spectra with sufficient accuracy and which -preferably, but not necessarily- can be Inversely Fourier Transformed in order to obtain an ACF which is determined by a limited number of parameters. Adding terms as are already present in the nominator and denominator of eq. [11.1] can increase the types of shapes that the power spectra can adopt. However, the larger the amount of parameters, the more important the initial "guess" of the parameter values becomes. But further extension of this curve-fit approach is possible, if need be.

This technique has been compared with other approaches to estimate the power spectrum from LDA data by means of a "benchmark" test, organised by the University of Erlangen (Germany) and the results have been presented in Lisbon (ref. 113, 1998). The technique showed to perform very well for the short time scales (e.g. estimation of Taylor time scale) and the estimation of the power spectrum at higher frequencies. The integral time scale was less well estimated, which is not surprising because of the focus on the shorter time scales and the higher frequencies in the power spectrum. Both findings are therefore in agreement with the results, presented in this chapter. A general conclusion from this benchmark test was that the parametric estimators performed superior compared to the direct estimators. Because of their tendency to reduce variance, this is not surprising and it was this concept that was the basis of the work, reported in this chapter. Another conclusion was that both the Local Normalisation and the "fuzzy" slotting technique improved the estimators of the ACF and it was therefore proposed to combine both techniques. This showed to be possible and this has already been published (ref. 114). The combination of the ACF estimation using the Local Normalisation and the curve-fit approach, described in this chapter, have been used successfully by others (ref. 115).

## *Retrieval of turbulence and turbulence properties from LDA data with noise*

### **11.6 Concluding remarks.**

The use of six parameters for the description of turbulence power spectra yields sufficient flexibility for the description of turbulence of many different flow conditions. Application to a wide variety of simulated and experimental data has confirmed this.

The deviation over the first six decades (in power) of the spectra, yielded by the curve-fit algorithm, from the actual value was in the range of  $\pm 25\%$ , which fulfils the requirement, set at the onset of this investigation. This requirement has been met for both the "noise-free" and "noisy" data-sets, obtained from both simulated and Hot-Wire Anemometry data.

The curve-fit algorithm can estimate the power spectrum at frequencies which are above the data-rate. Simulations have shown that it was able to do this even at five times the data-rate with an accuracy of  $\pm 25\%$ , at values more than four decades below the noise floor. Although it might be less in practical situations, it is reasonable to expect that it will perform up to twice the data-rate at least.

Because the algorithm has successfully predicted the turbulence power spectrum of LDA-like data-sets, obtained from both simulated and real (measured) turbulence, we expect it to give accurate results on real LDA data as well. This expectation is also based on the accurate prediction of the part of the power spectrum that is revealed by Fourier Transformation of the slotted ACF of these data-sets.

Simulations have shown that the slopes in the turbulence power spectrum which describe the inertial subrange and the dissipation range obtained by the algorithm are sufficiently accurate.

The curve-fit algorithm yields an accurate estimation of the frequency where the dissipation range begins.

Up to 50% turbulence intensity the estimated ACF coincides with a high degree of accuracy with the experimental ACF, a further increase of the intensity leads to noticeable differences. However, in such cases the estimation of the ACF itself is hampered by velocity bias and alternative estimators should be considered.

The ACF of velocity estimates with a periodic component can be described by an ACF of random (non-periodic) turbulence and a damped cosine function with several harmonics. If the frequency of the first harmonic of the periodic component is below the spectral resolution of the turbulence power spectrum, it tends to a DC contribution and it can therefore be compensated by the offset, build into the algorithm.

Comparison in a benchmark test with other techniques to retrieve the power spectrum has shown that the combination of the ACF, based on Local Normalisation, and the curve-fit approach leads to good results. Further improvement is obtained when the "fuzzy" slotting technique is merged with the Local Normalisation in order to reduce the variance of the individual correlation coefficient estimators in the ACF further.

## 11. Estimation of Turbulence PSD by Curve-Fit to the Auto Correlation Function

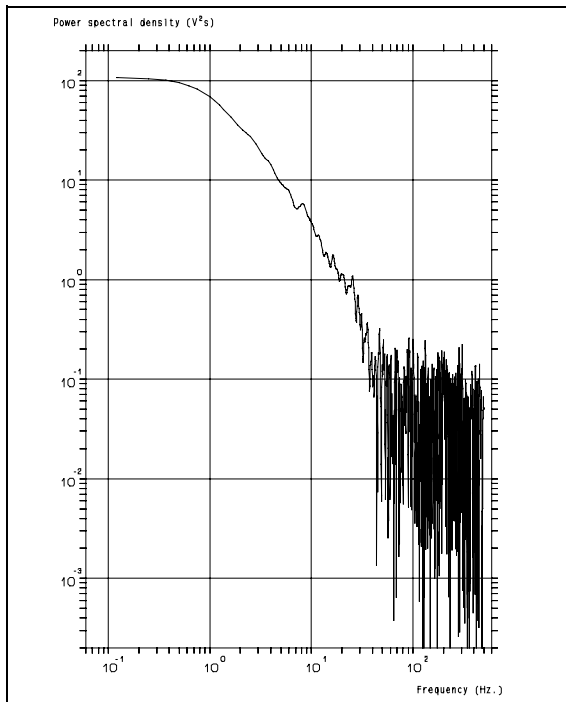


**Figure 11.1:** Power Spectral Density, obtained by Fourier Transformation of ACF estimated using the Mayo algorithm, eq. [10.3].

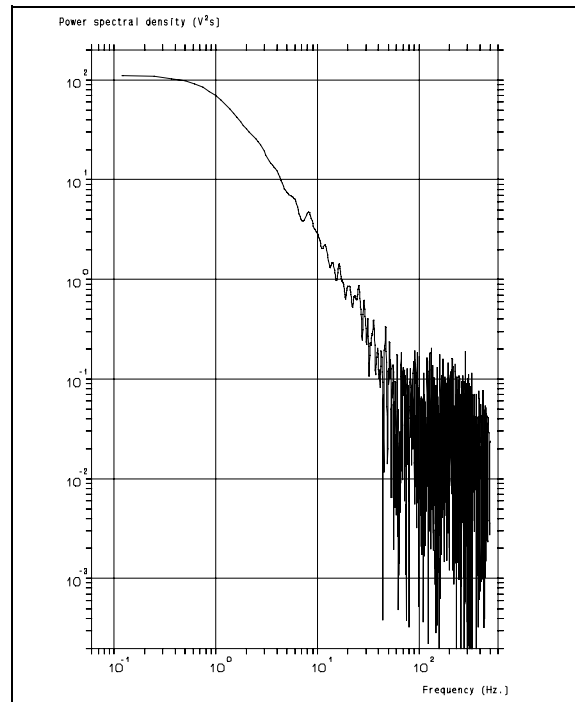


**Figure 11.2:** Power Spectrum, obtained by Fourier Transformation of an ACF, estimated using the slotting technique of eq. [10.6]. Note the noise floor at higher frequencies (> 40 Hz) and the variance > 7 Hz.

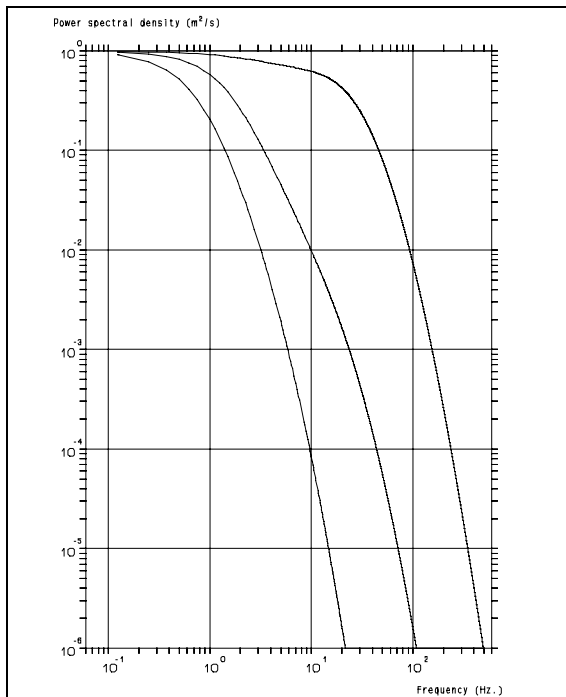


**Figure 11.3:** Flexibility of the Power Spectrum as described by eq. [11.1] as the three spectra are obtained by a different choice of the parameter values.

Frequency parameter	Left curve	Centre curve	Right curve
$f_0$	75 Hz	7.5 Hz	10 Hz
$f_1$	0.75 Hz	1.5 Hz	20 Hz
$f_2$	7.5 Hz	30 Hz	40 Hz
$f_3$	10 Hz	40 Hz	110 Hz
$f_4$	25 Hz	42 Hz	115 Hz
$f_5$	30 Hz	48 Hz	120 Hz

**Table 11.4:** The parameters used for fig. 11.3

*Retrieval of turbulence and turbulence properties from LDA data with noise*

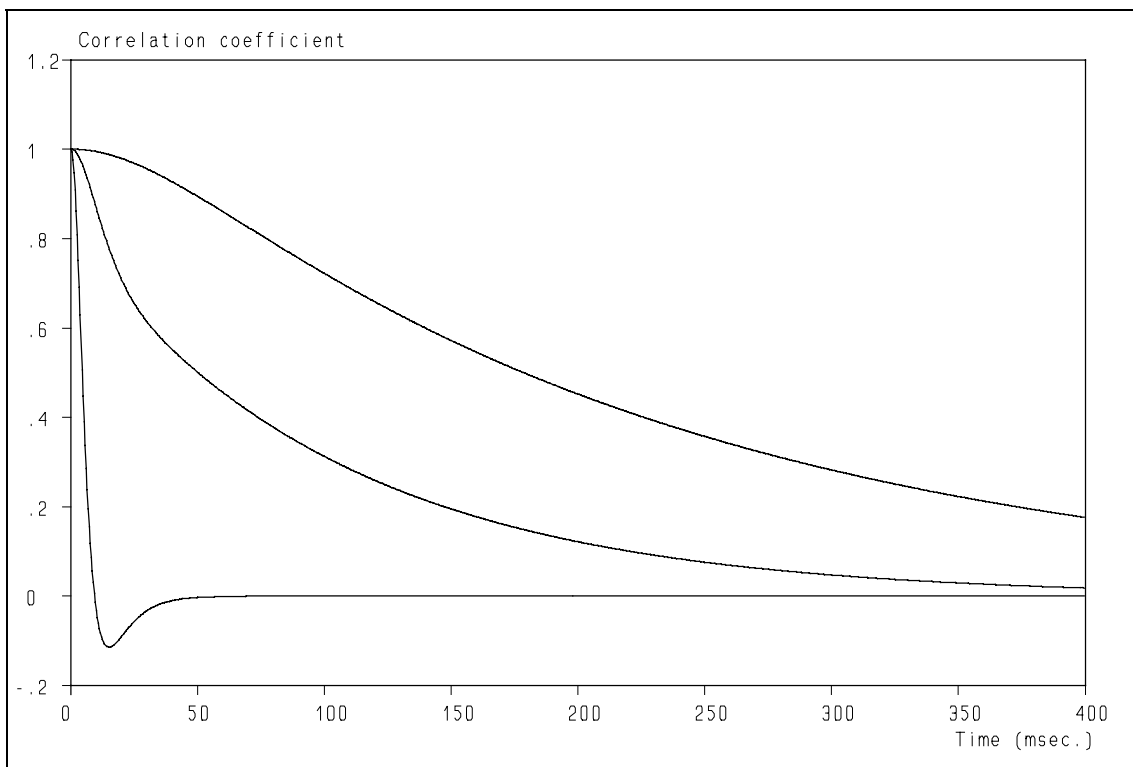


**Figure 11.4:** Flexibility of the ACF, described by the six parameters. Upper curve corresponds to the left curve of fig. 11.3, the lower curve to the right curve of fig. 11.3.

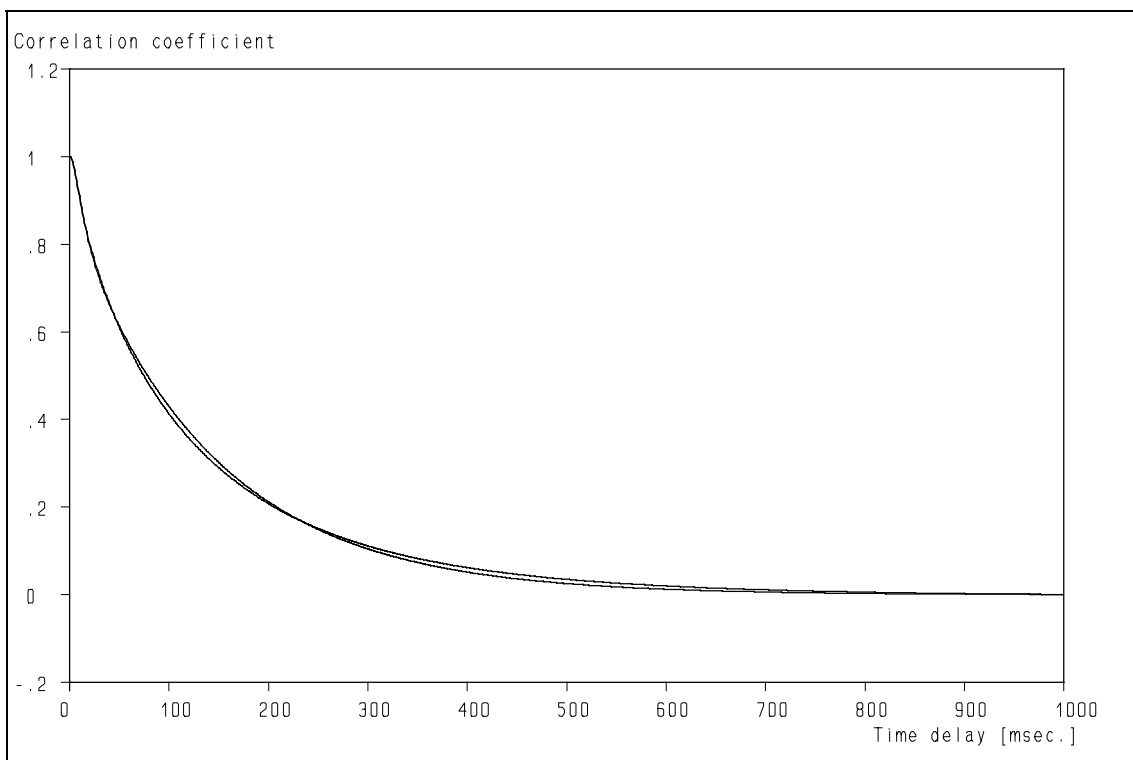


**Figure 11.5:** The ACF corresponding to the Bessem Power Spectrum and the fitted ACF.

### 11. Estimation of Turbulence PSD by Curve-Fit to the Auto Correlation Function

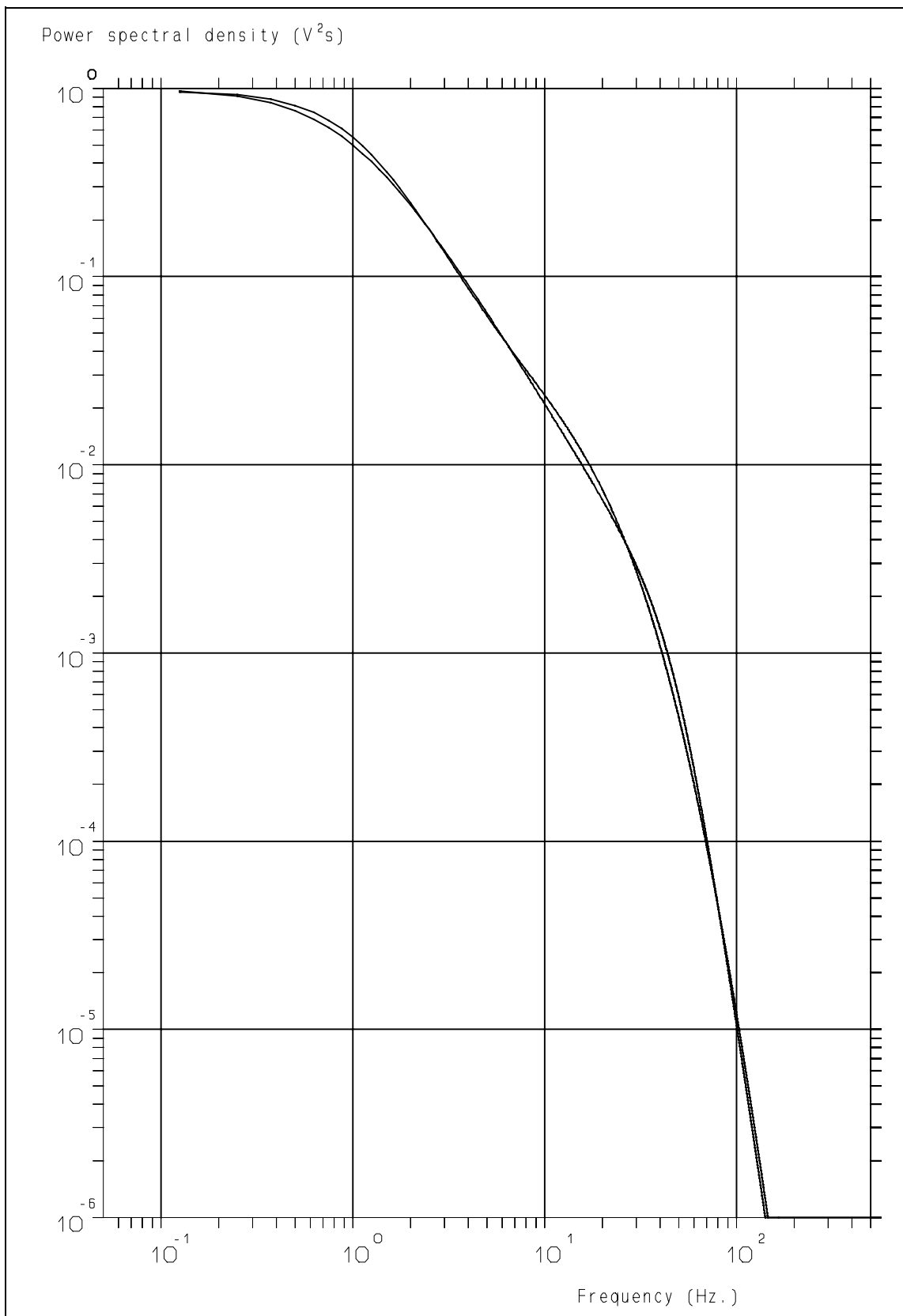


**Figure 11.6:** The Bessem Power Spectrum and the fit, derived from the ACF of fig. 11.5.

*Retrieval of turbulence and turbulence properties from LDA data with noise*

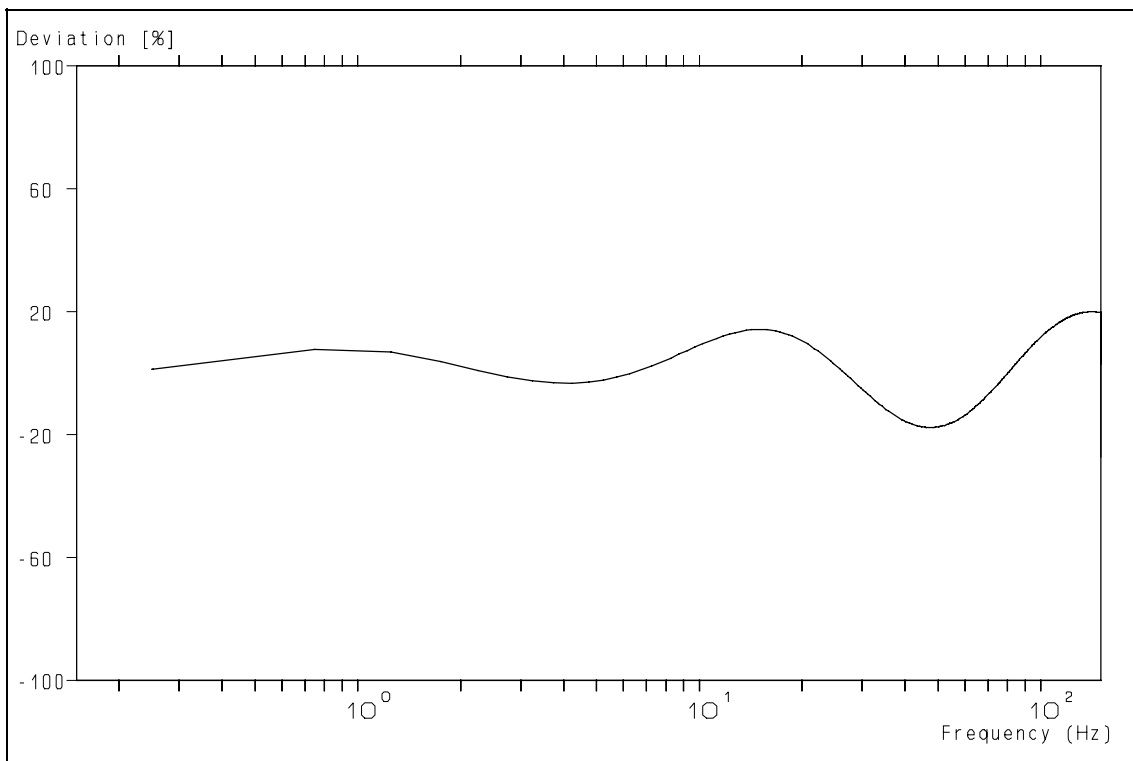


**Figure 11.7:** Deviation between the Bessem Power Spectrum and the Power Spectrum, derived from the fitted ACF of fig. 11.5.

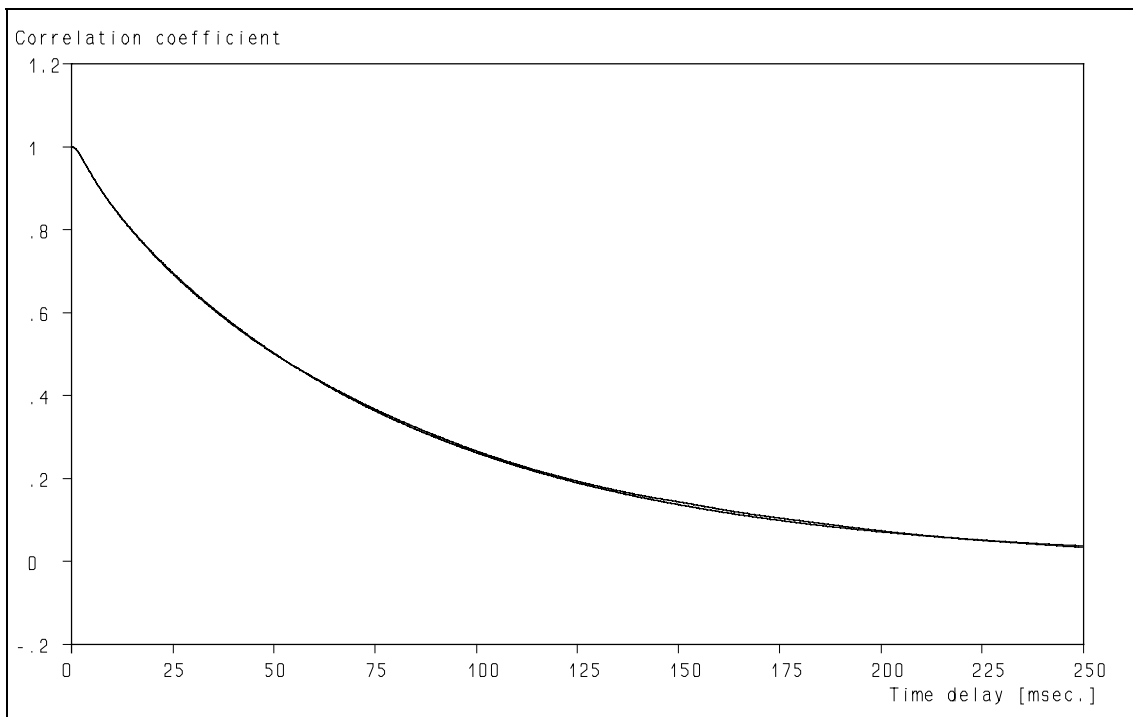


**Figure 11.8:** The ACF corresponding to the Von Kármán - Pao Power Spectrum and the fitted ACF.

### 11. Estimation of Turbulence PSD by Curve-Fit to the Auto Correlation Function

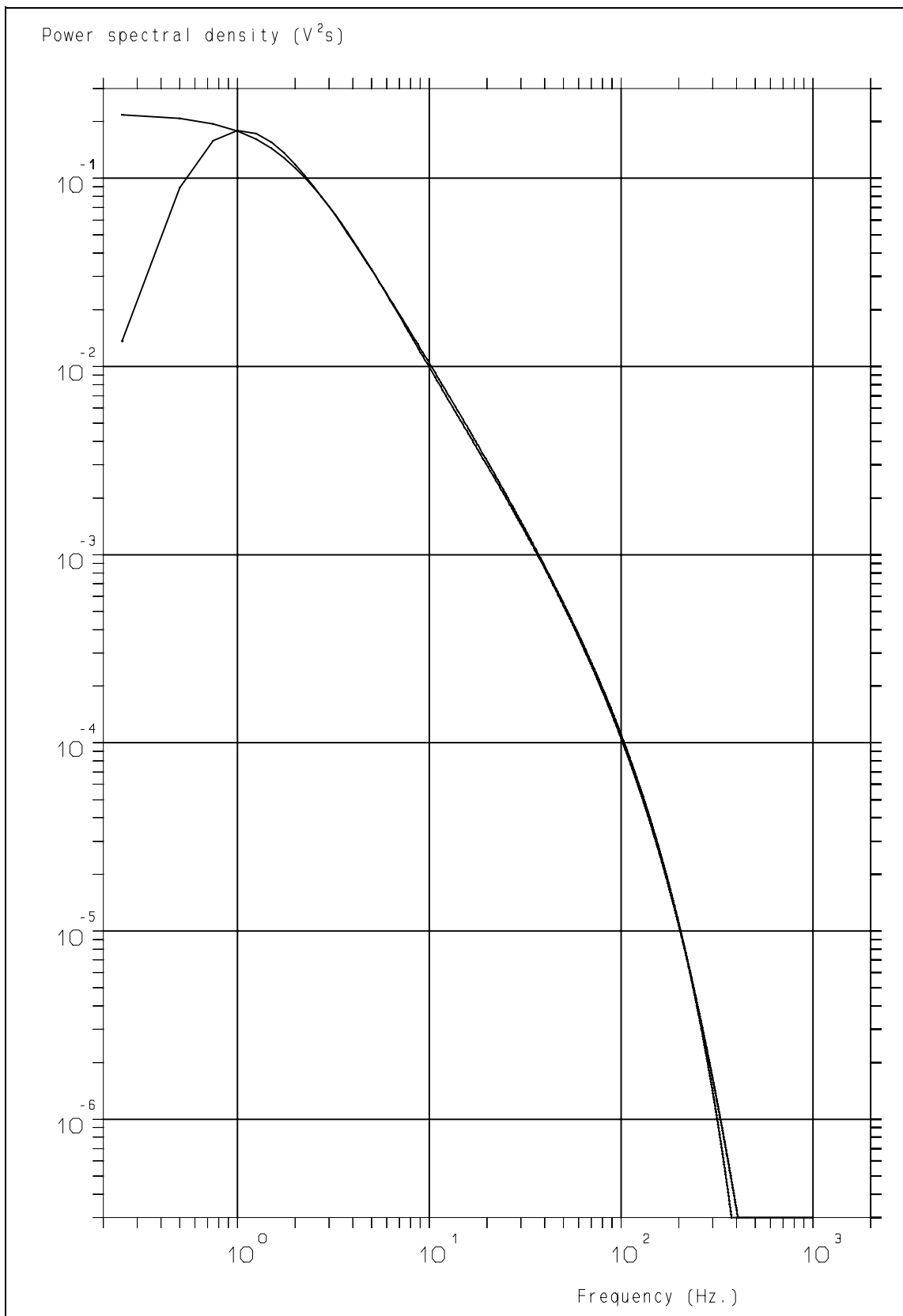


**Figure 11.9:** The Von Kármán-Pao Power Spectrum and the fit obtained from the ACF of fig. 11.8.

*Retrieval of turbulence and turbulence properties from LDA data with noise*

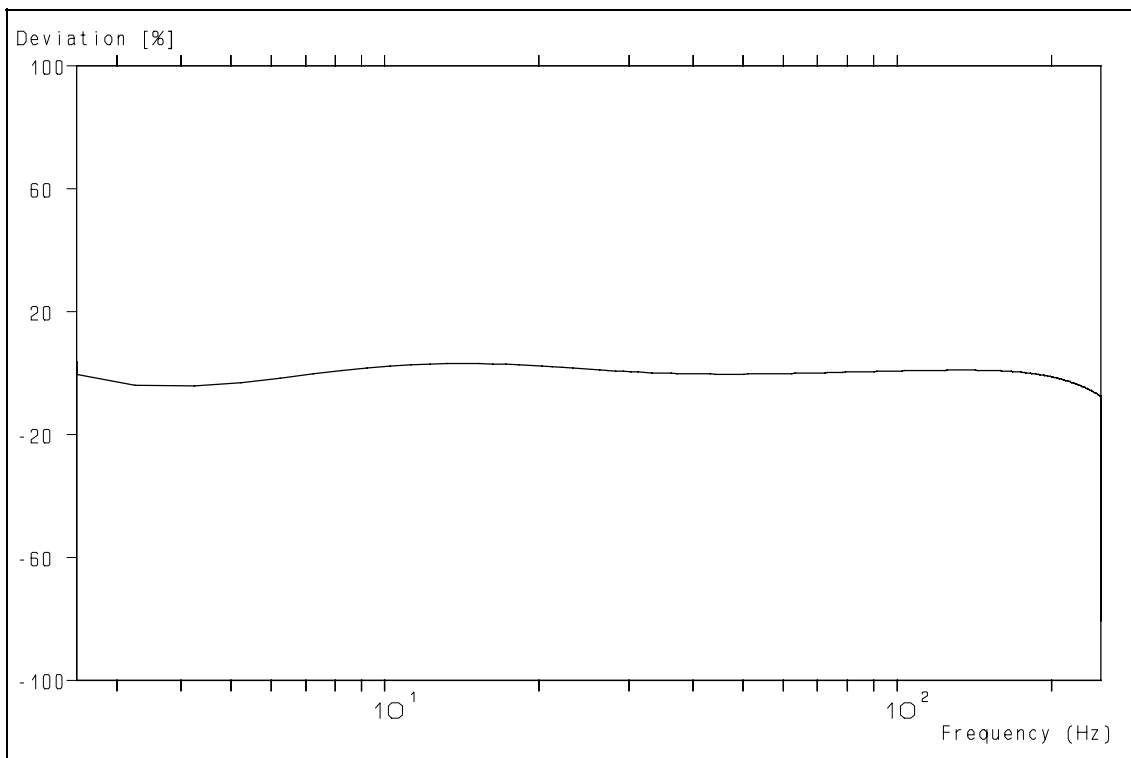


**Figure 11.10:** Deviation between the Von Kármán - Pao Power Spectrum and Power Spectrum derived from the fitted ACF of fig. 11.8

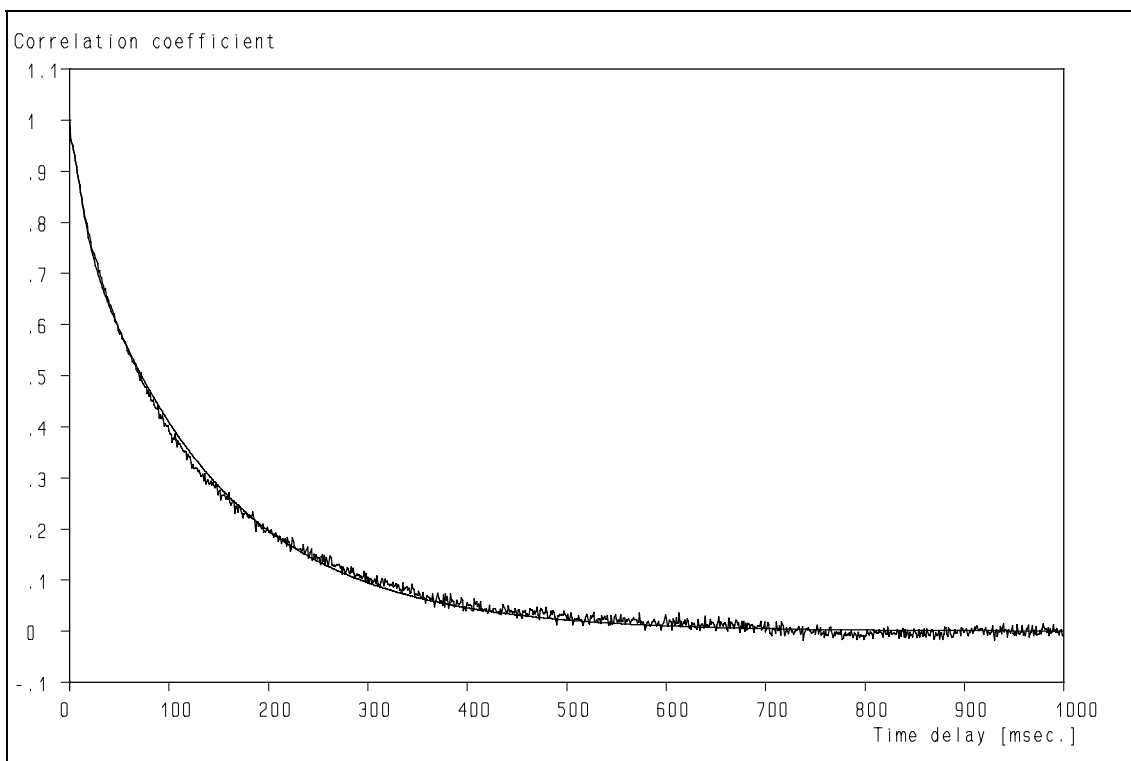


**Figure 11.11:** The Slotted ACF of simulated turbulence according to the Bessem power spectrum with noise added to the individual velocity estimates and the fitted ACF.

### 11. Estimation of Turbulence PSD by Curve-Fit to the Auto Correlation Function

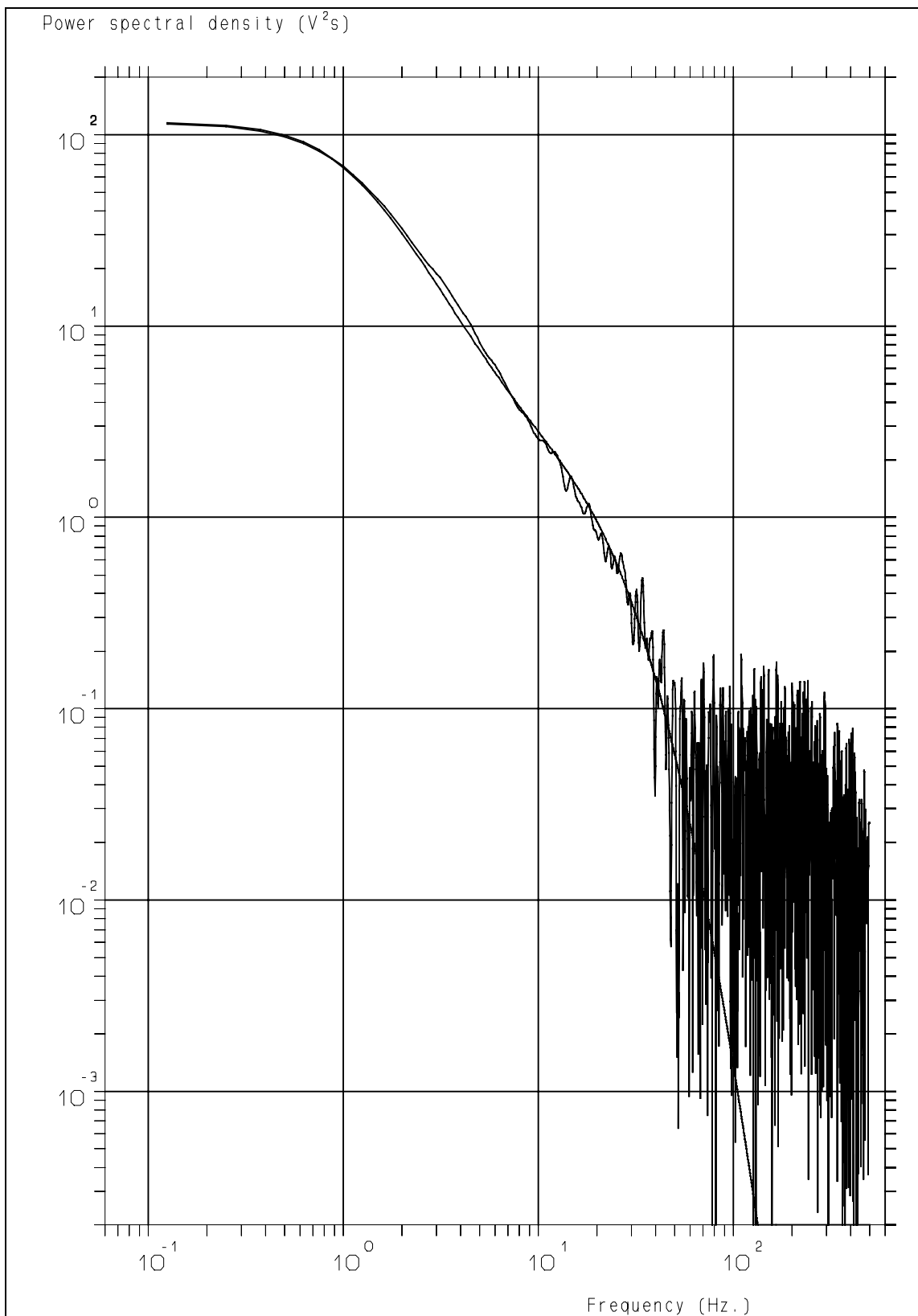


**Figure 11.12:** The Power Spectrum obtained from the slotted ACF of fig. 11.11 and the Power Spectrum, obtained from the fitted ACF.

*Retrieval of turbulence and turbulence properties from LDA data with noise*

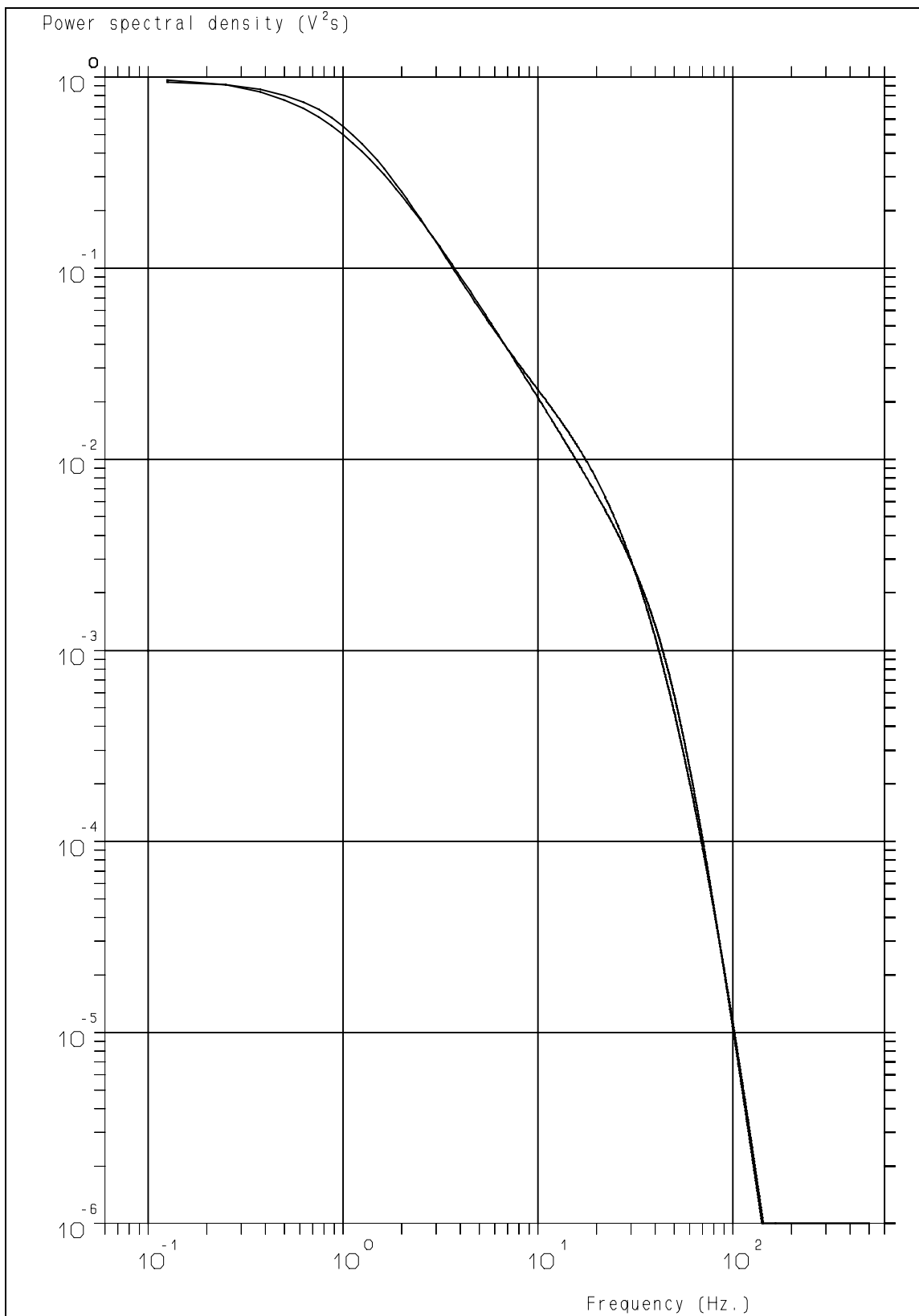


**Figure 11.13:** The Bessem Power Spectrum and the Power Spectrum obtained from the fitted ACF of fig. 11.11.

## 11. Estimation of Turbulence PSD by Curve-Fit to the Auto Correlation Function

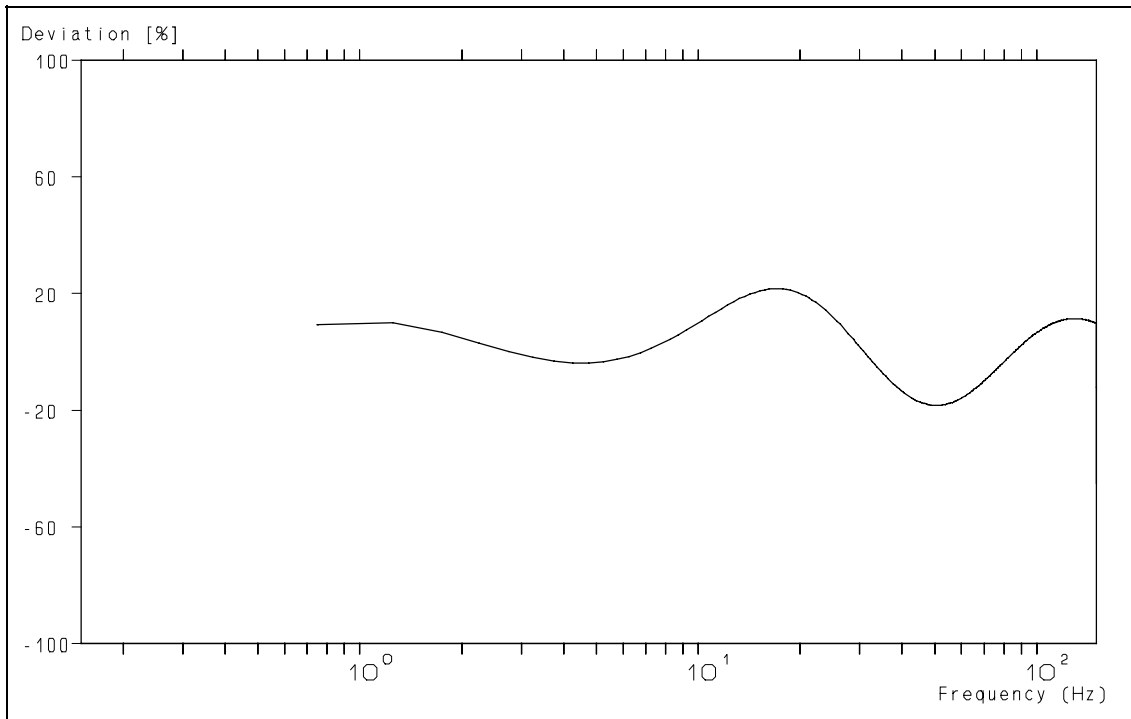


**Figure 11.14:** Deviation between the Bessem Power Spectrum and the Power Spectrum derived from the ACF, fitted to the "noisy" ACF, both shown in fig. 11.11.

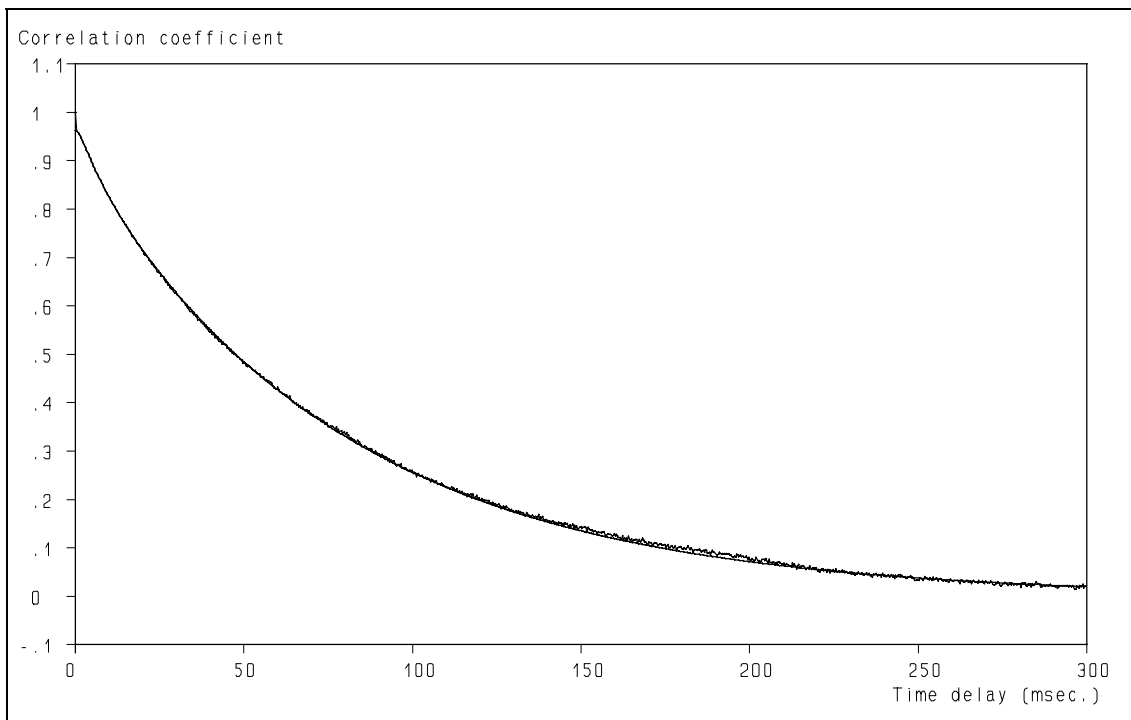


**Figure 11.15:** The ACF of simulated turbulence according to the Von Kármán - Pao Power Spectrum with noise added to the individual velocity estimates and the fitted ACF.

*Retrieval of turbulence and turbulence properties from LDA data with noise*

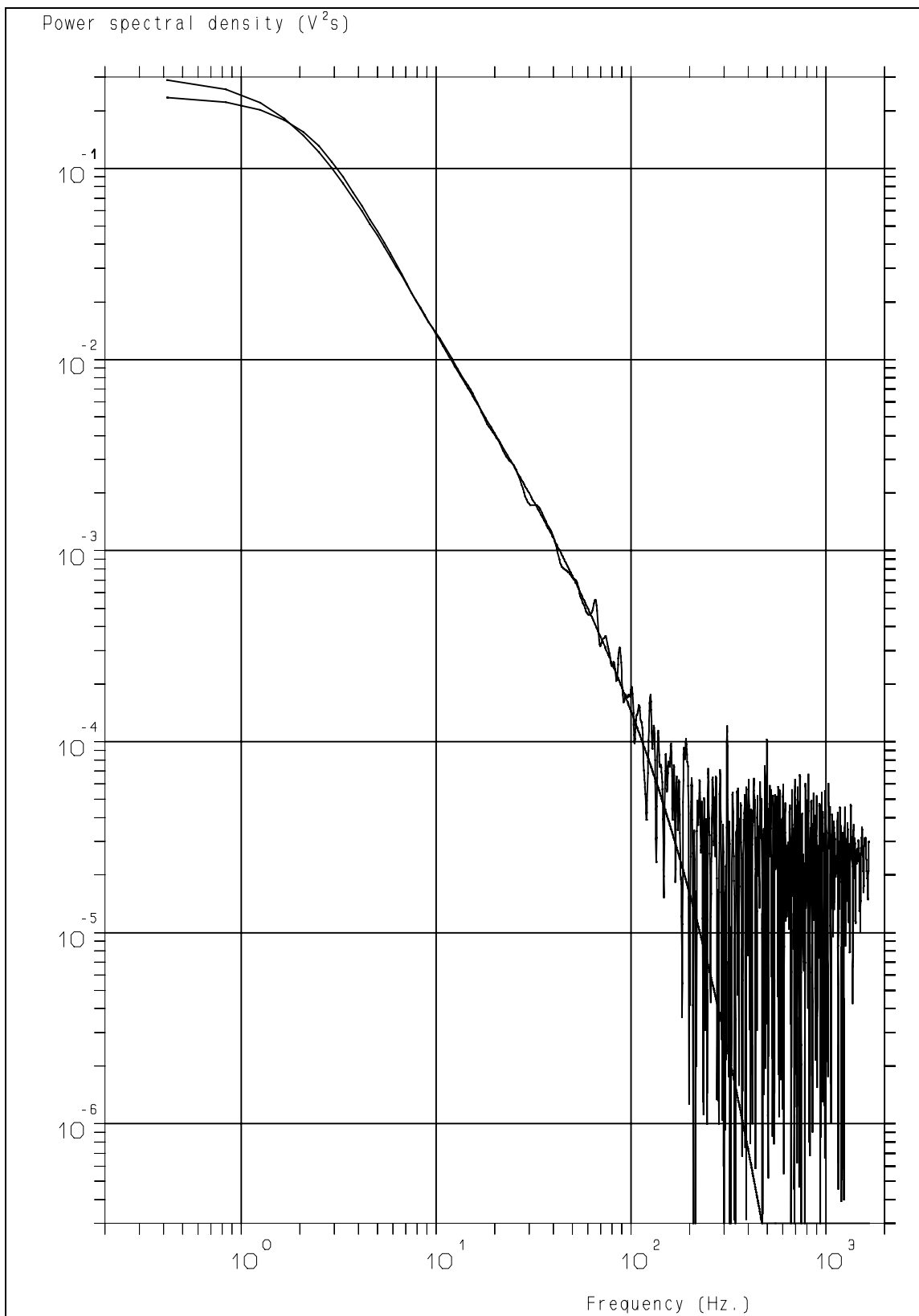


**Figure 11.16:** The Power Spectrum obtained from the slotted ACF of fig. 11.15 and the Power Spectrum, derived from the fitted ACF.

### 11. Estimation of Turbulence PSD by Curve-Fit to the Auto Correlation Function

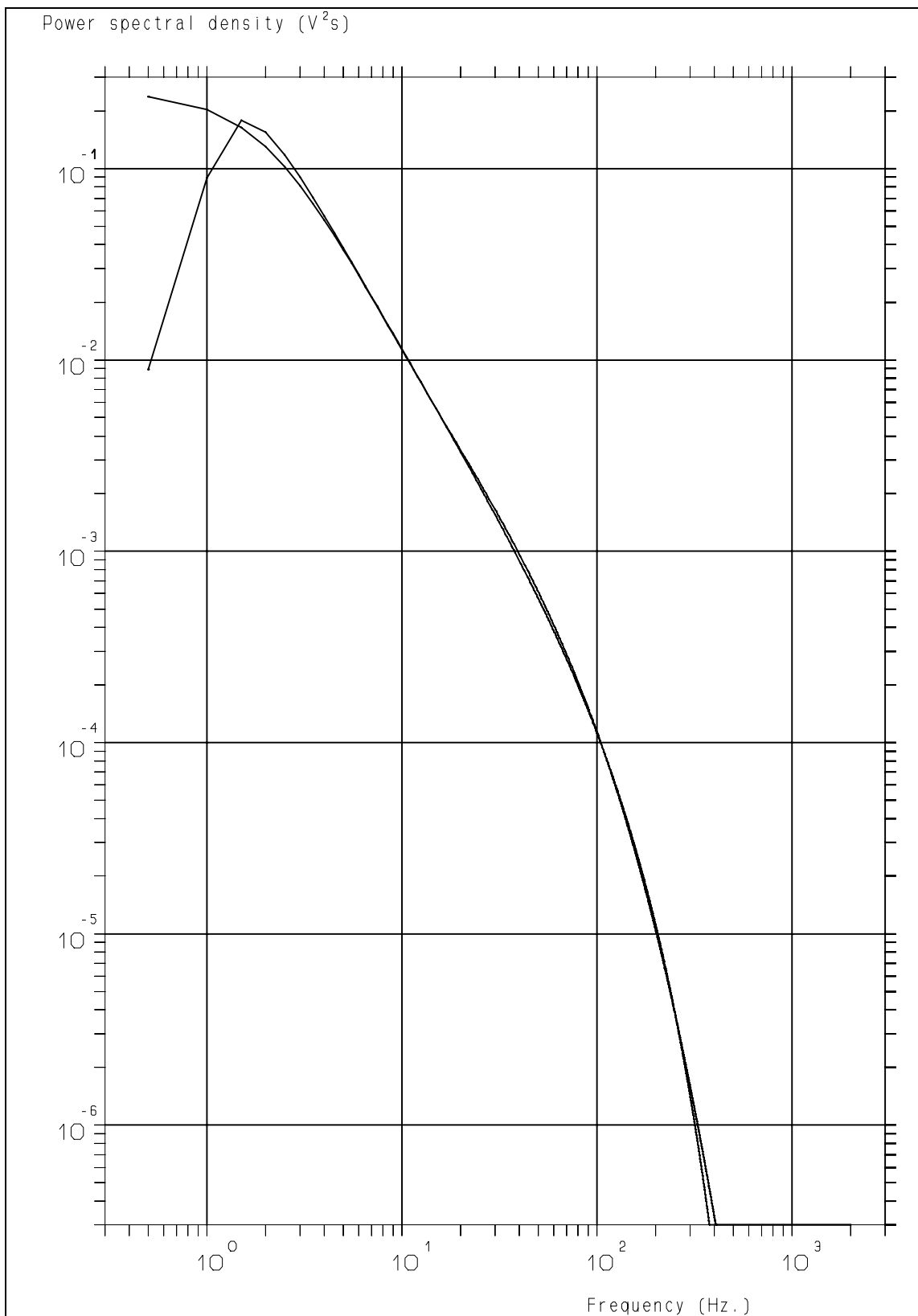


**Figure 11.17:** The Von Kármán-Pao Power Spectrum and the Power Spectrum obtained from the fitted ACF of fig. 11.15.

*Retrieval of turbulence and turbulence properties from LDA data with noise*

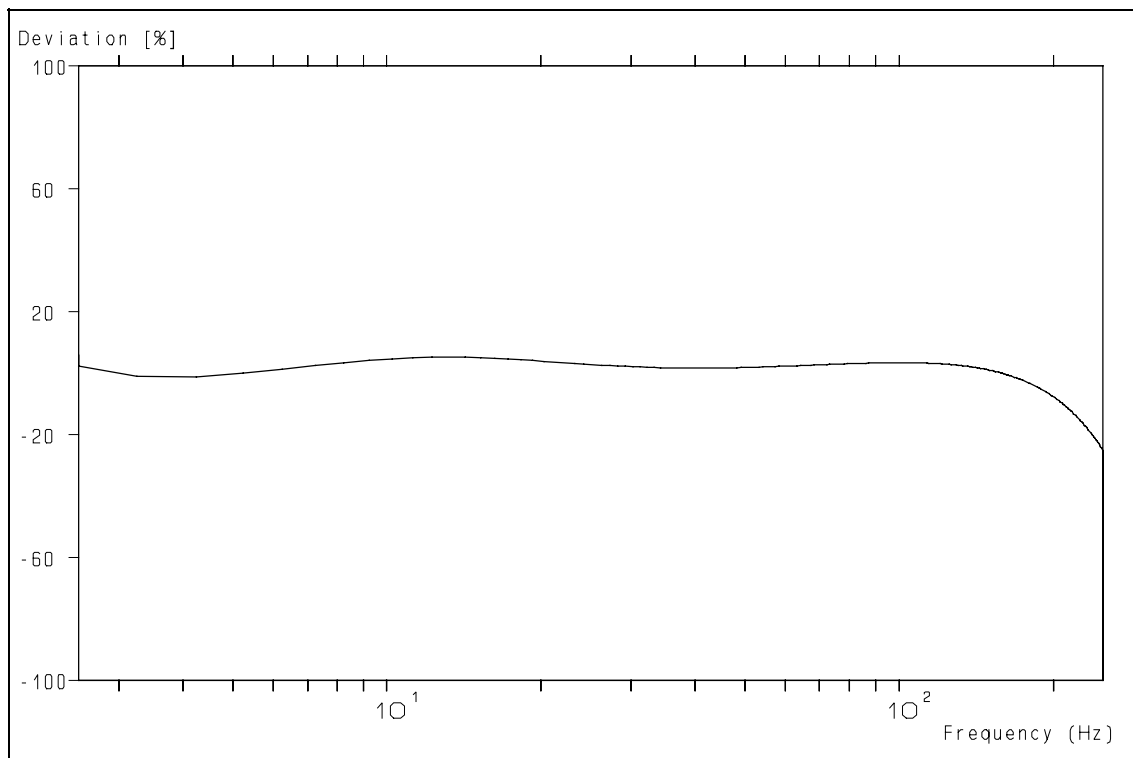


**Figure 11.18:** Deviation between the Von Kármán-Pao Power Spectrum and the Power Spectrum, obtained from the fitted ACF of fig. 11.15.

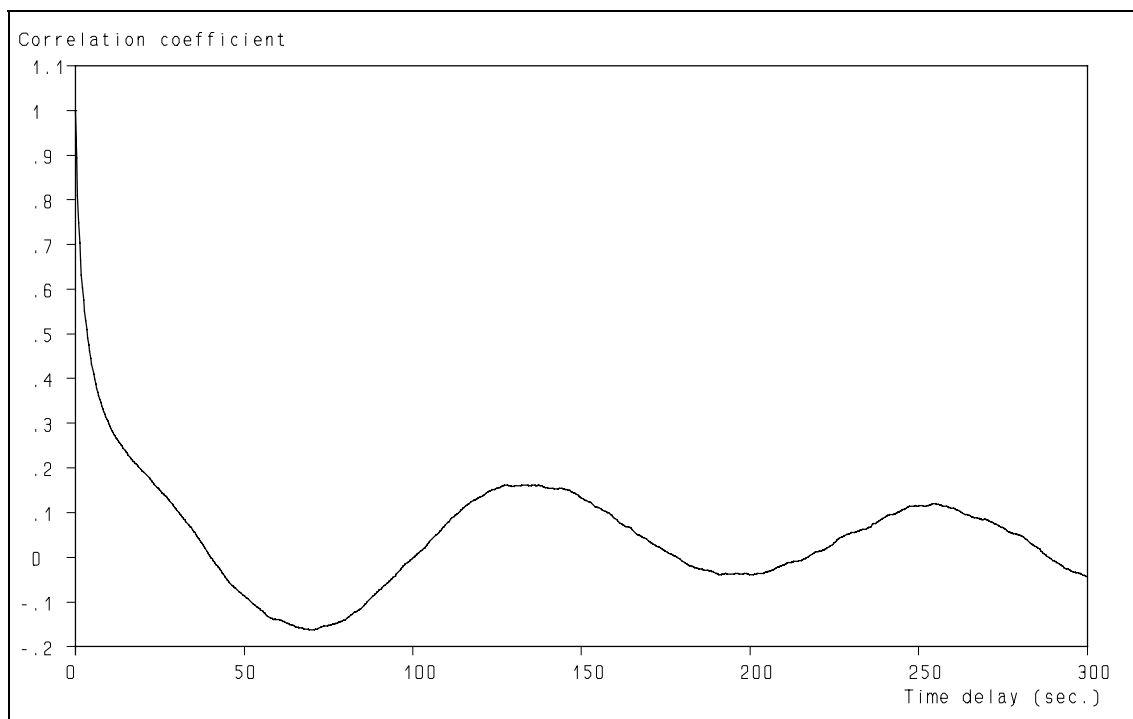


**Figure 11.19:** The ACF of the  $u$ -component of the Hot-Wire Anemometry data shows a periodic component.

## 11. Estimation of Turbulence PSD by Curve-Fit to the Auto Correlation Function

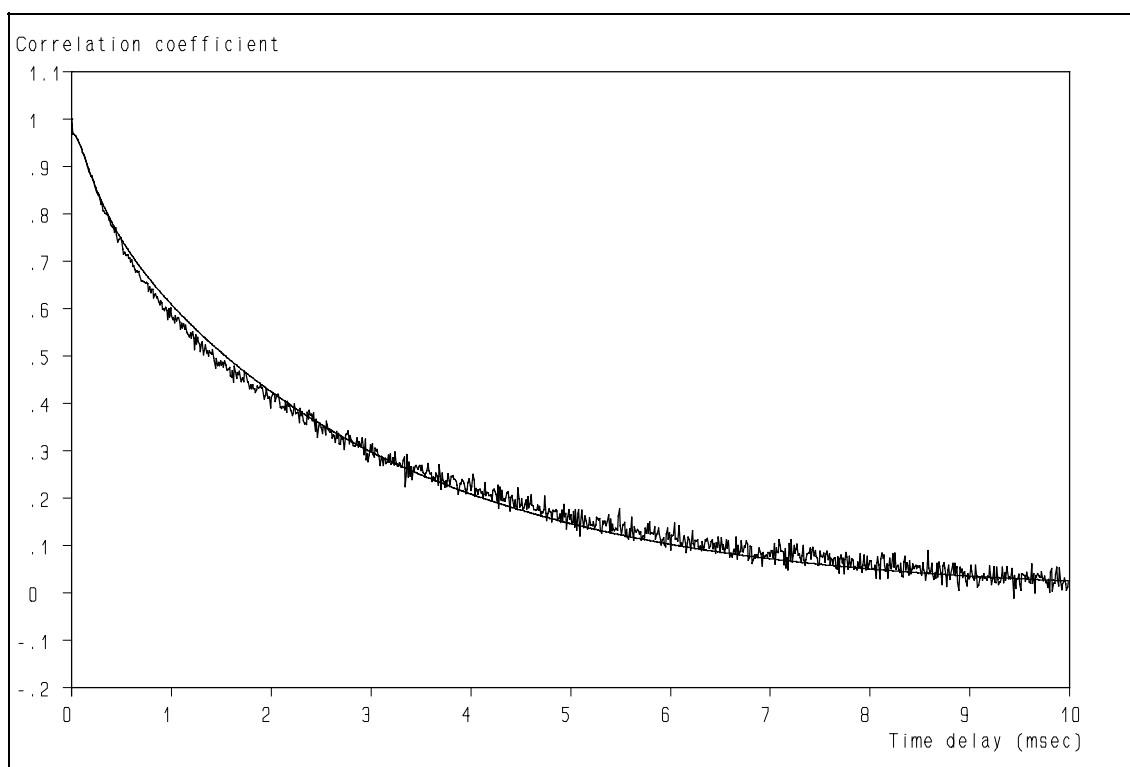


**Figure 11.20:** The ACF of the "LDA-like" HWA data ( $u$ -component) and the fitted ACF.

*Retrieval of turbulence and turbulence properties from LDA data with noise*

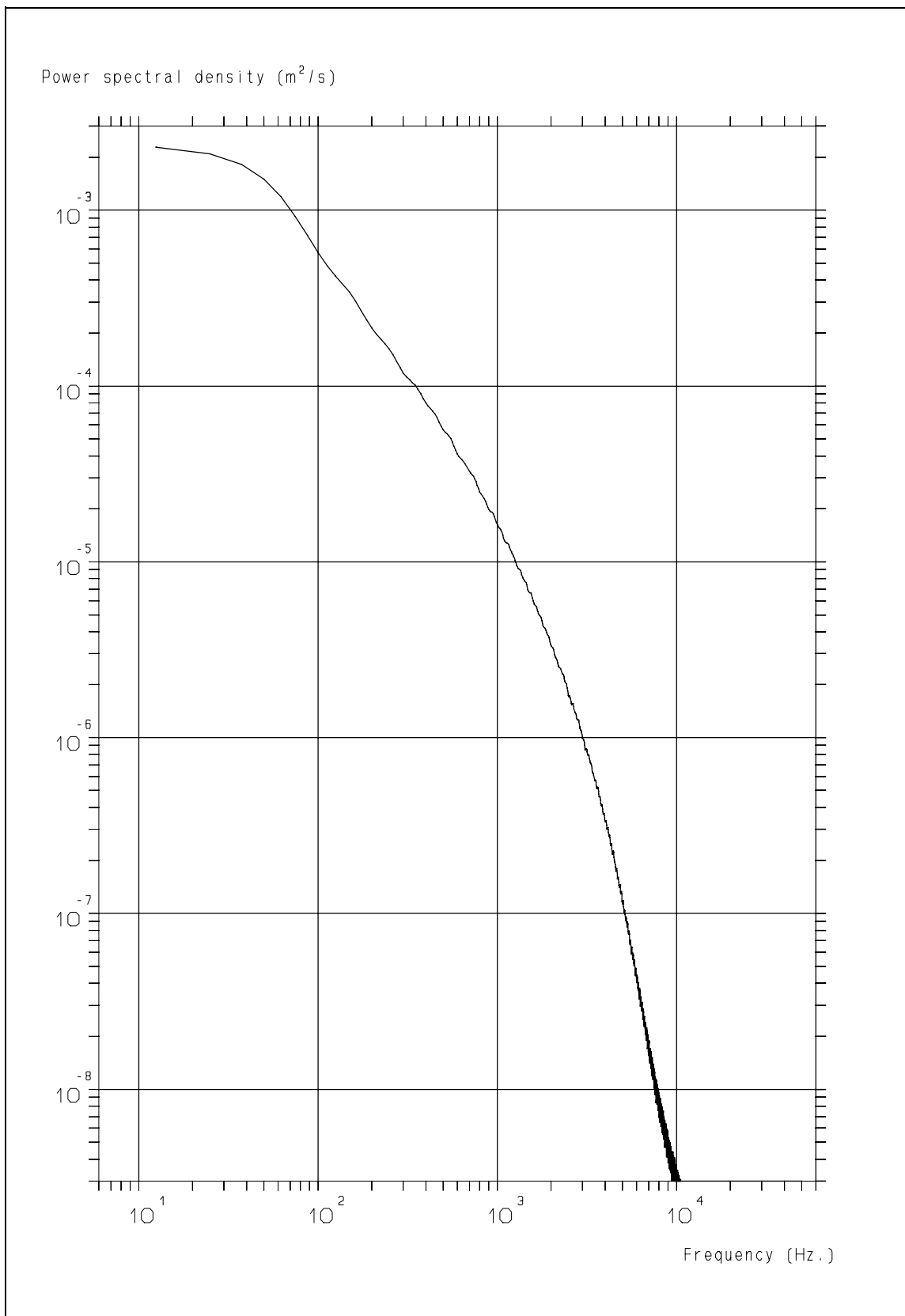


**Figure 11.21:** The Power Spectrum of the  $u$ -component of the HWA data.

## 11. Estimation of Turbulence PSD by Curve-Fit to the Auto Correlation Function

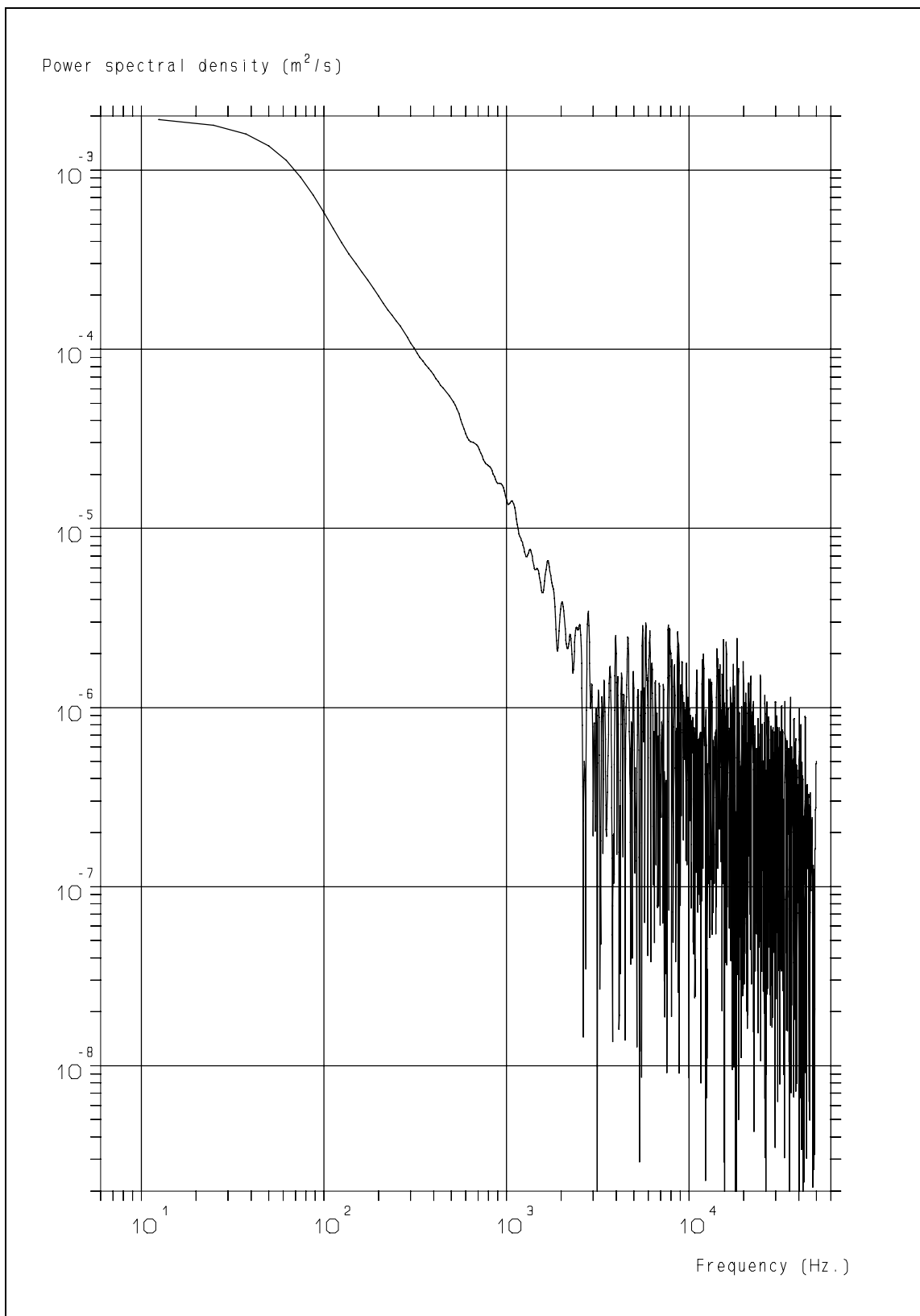


**Figure 11.22:** The Power Spectrum of the HWA data after random sampling and noise contribution to make them "LDA-like" ( $u$ -component).

*Retrieval of turbulence and turbulence properties from LDA data with noise*

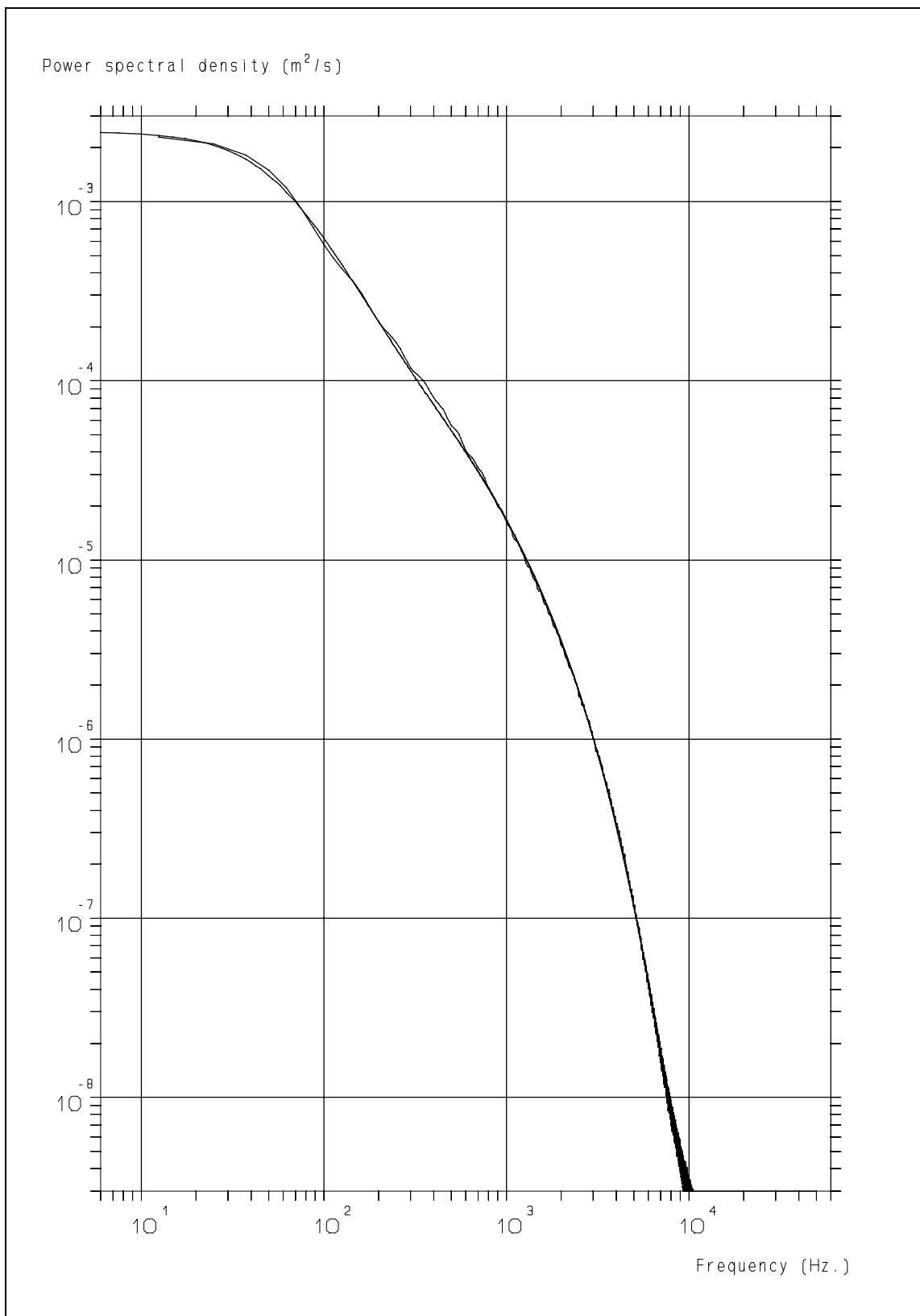


**Figure 11.23:** The Power Spectrum of the  $u$ -component of the HWA data and the Power Spectrum derived from the fitted ACF of fig. 11.20. The data-rate of the simulated LDA data is only 3.3 kHz!

### 11. Estimation of Turbulence PSD by Curve-Fit to the Auto Correlation Function

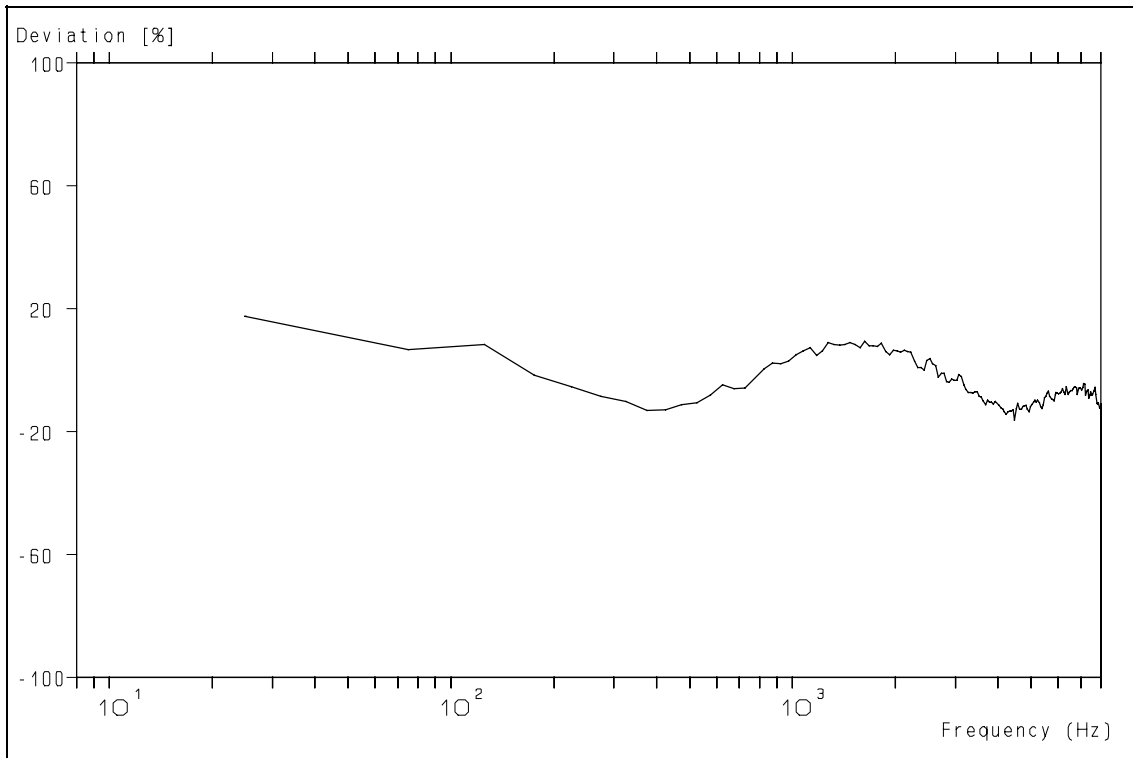


**Figure 11.24:** The deviation between the Power Spectrum of the  $u$ -component of the HWA data and the Power Spectrum, derived from the fitted ACF of fig. 11.20.

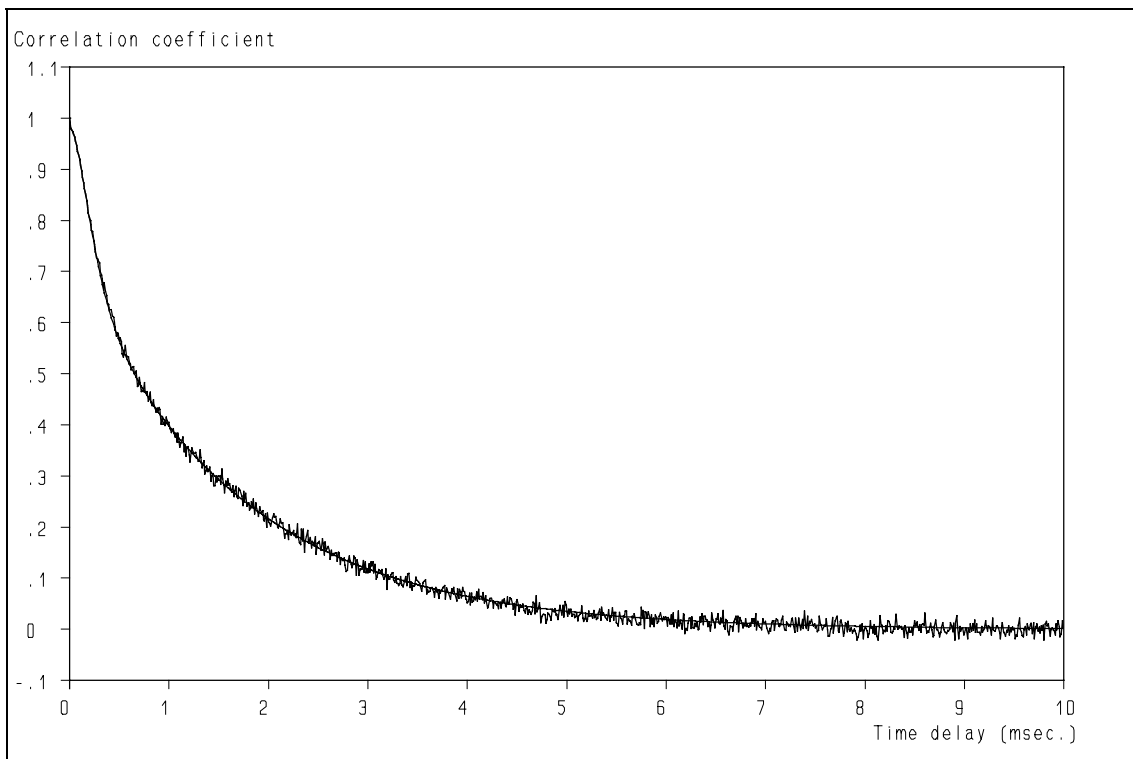


**Figure 11.25:** The ACF of the "LDA-like" HWA data ( $v$ -component) and the fitted ACF.

*Retrieval of turbulence and turbulence properties from LDA data with noise*

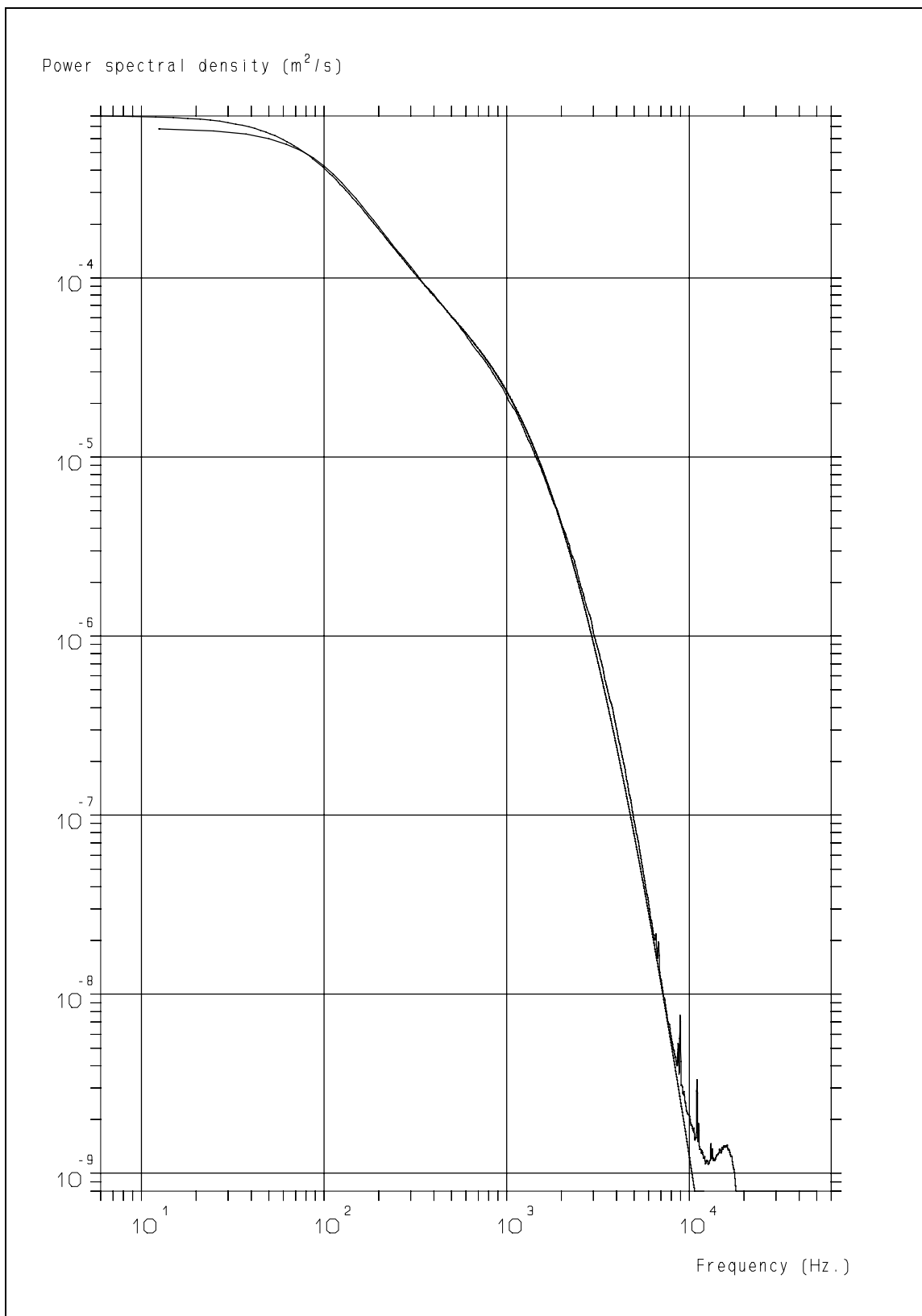


**Figure 11.26:** The Power Spectrum of the  $v$ -component of the HWA data and the Power Spectrum derived from the fitted ACF of fig. 11.25. The data-rate of the simulated LDA data is only 3.3 kHz!

## 11. Estimation of Turbulence PSD by Curve-Fit to the Auto Correlation Function

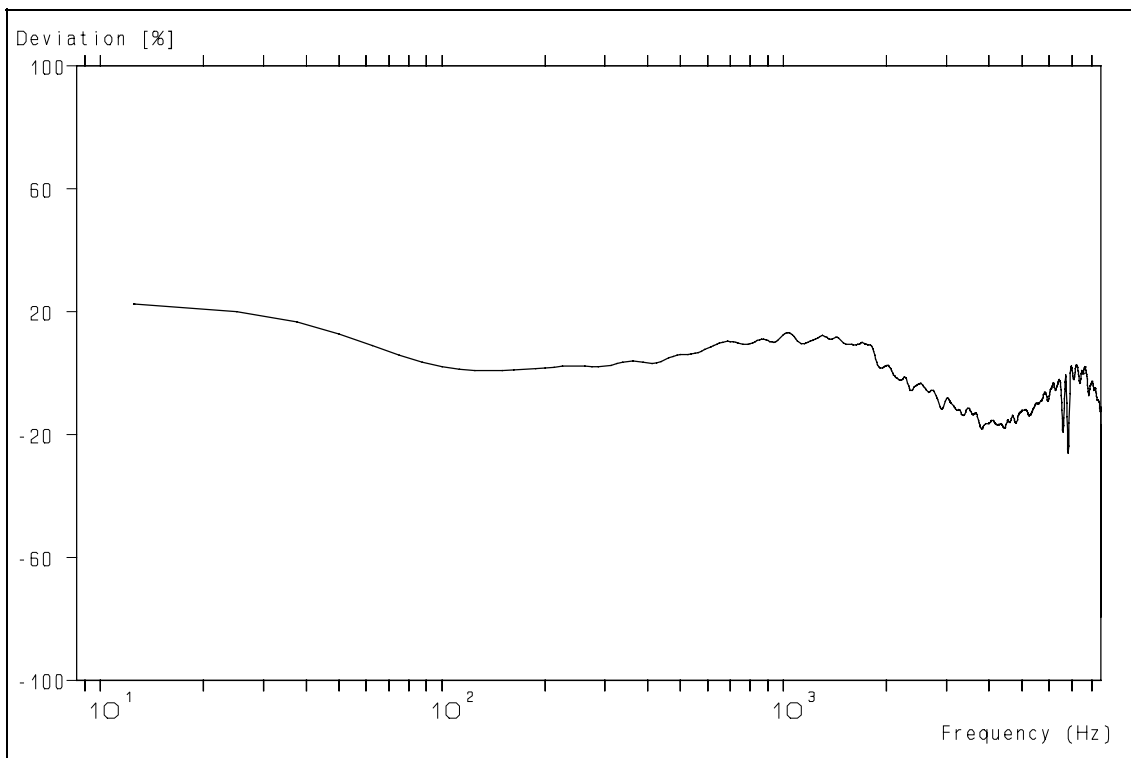


**Figure 11.27:** The deviation between the Power Spectrum of the  $v$ -component of the HWA data and the Power Spectrum, derived from the fitted ACF of fig. 11.25.

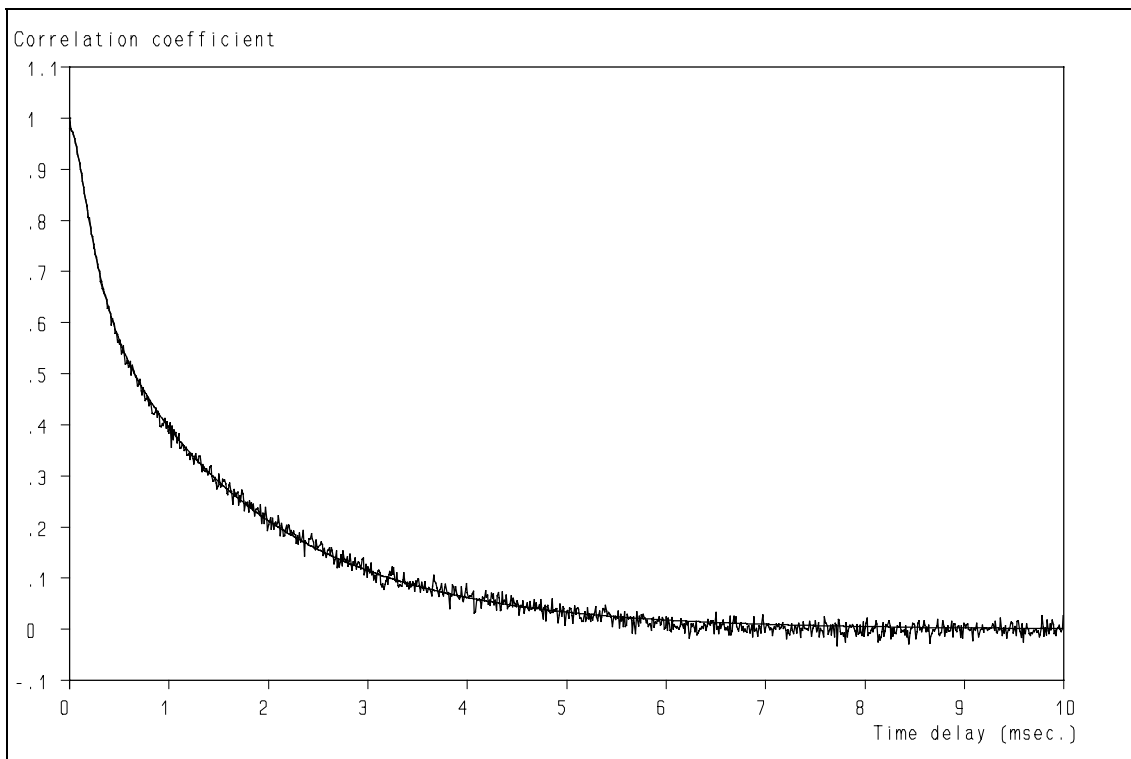


**Figure 11.28:** The ACF of the "LDA-like" HWA data ( $w$ -component) and the fitted ACF.

*Retrieval of turbulence and turbulence properties from LDA data with noise*

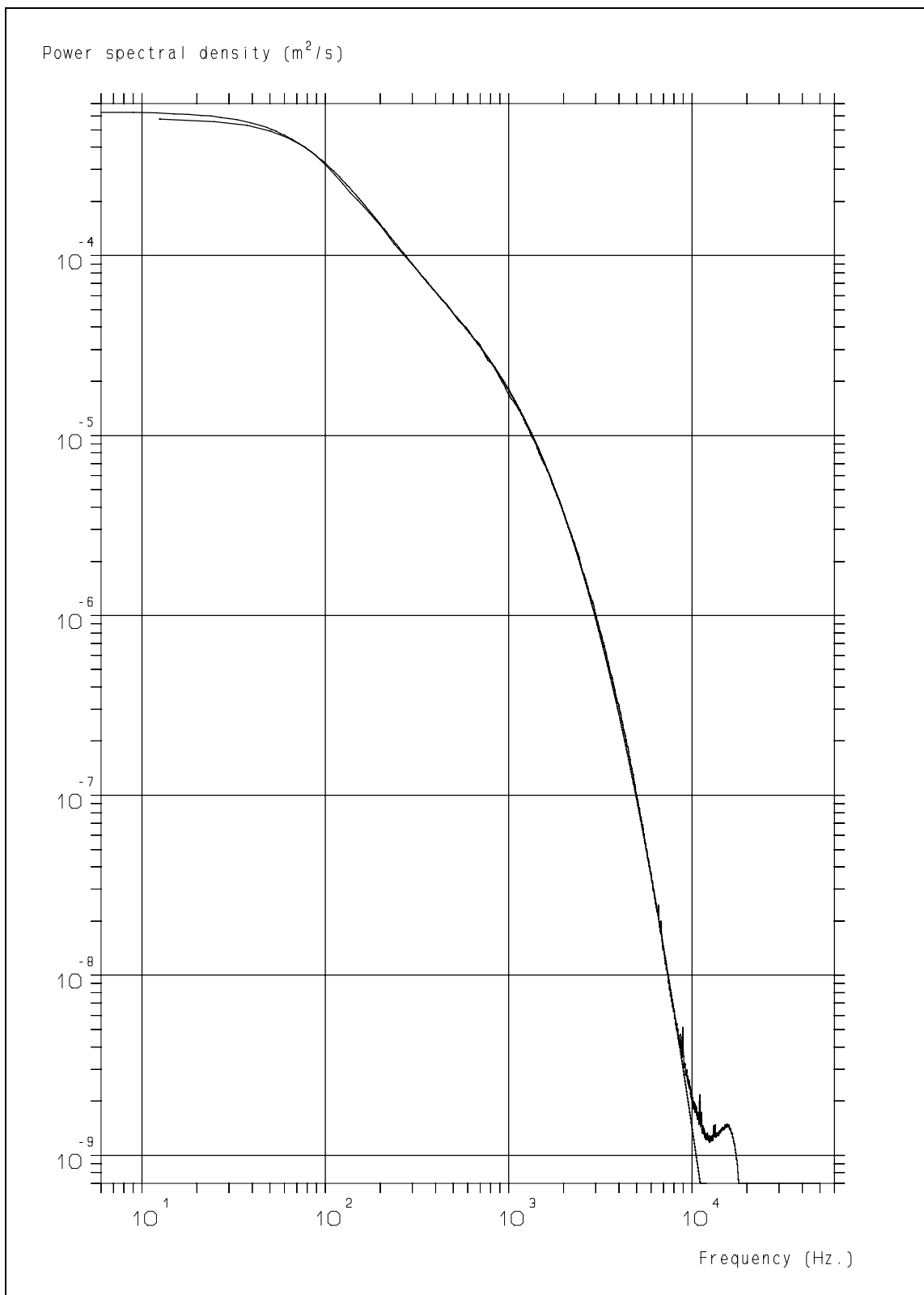


**Figure 11.29:** The Power Spectrum of the  $w$ -component of the HWA data and the Power Spectrum derived from the fitted ACF of fig. 11.28. The data-rate of the simulated LDA data is only 3.3 kHz!

### 11. Estimation of Turbulence PSD by Curve-Fit to the Auto Correlation Function

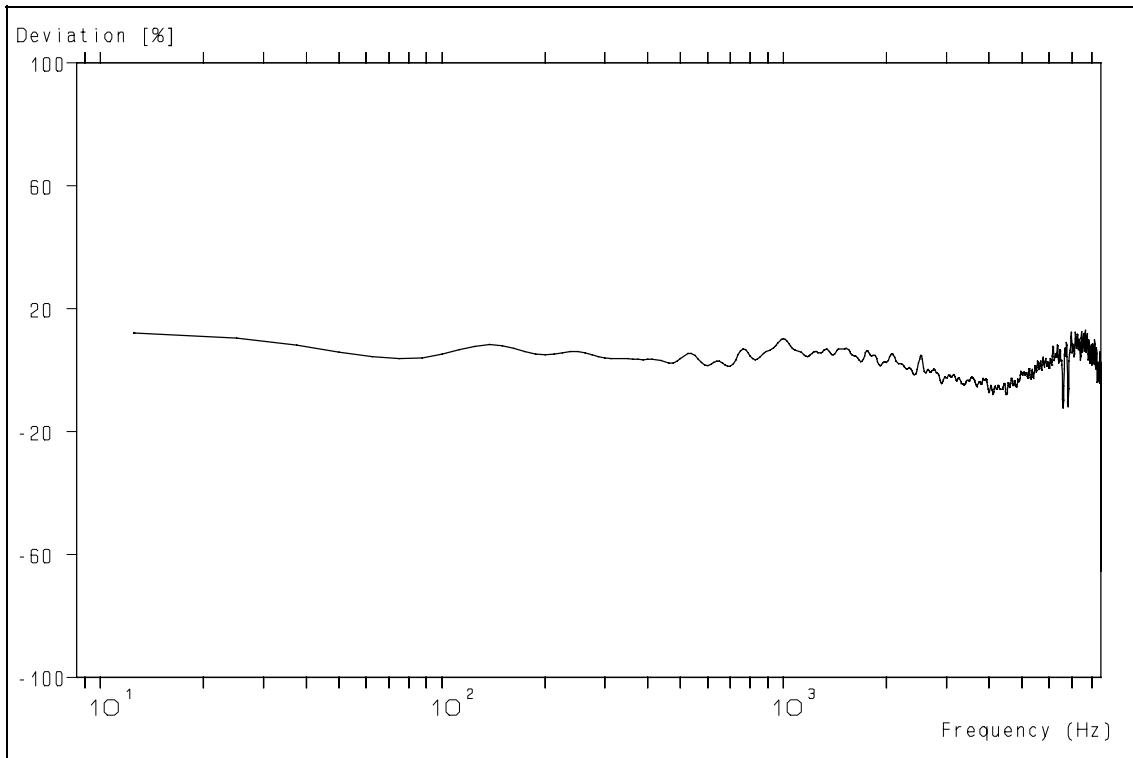


**Figure 11.30:** The deviation between the Power Spectrum of the  $w$ -component of the HWA data and the Power Spectrum, derived from the fitted ACF of fig. 11.28.

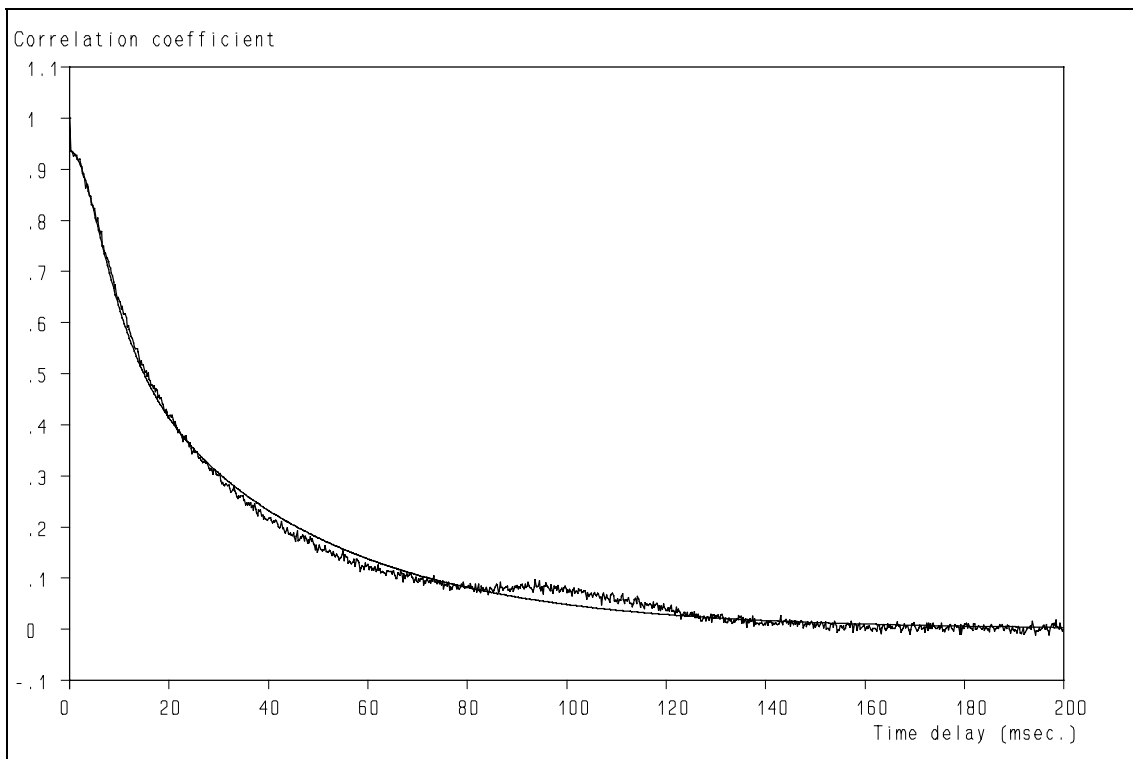


**Figure 11.31:** The ACF derived from the water pipe flow data-set and the fitted ACF.

*Retrieval of turbulence and turbulence properties from LDA data with noise*

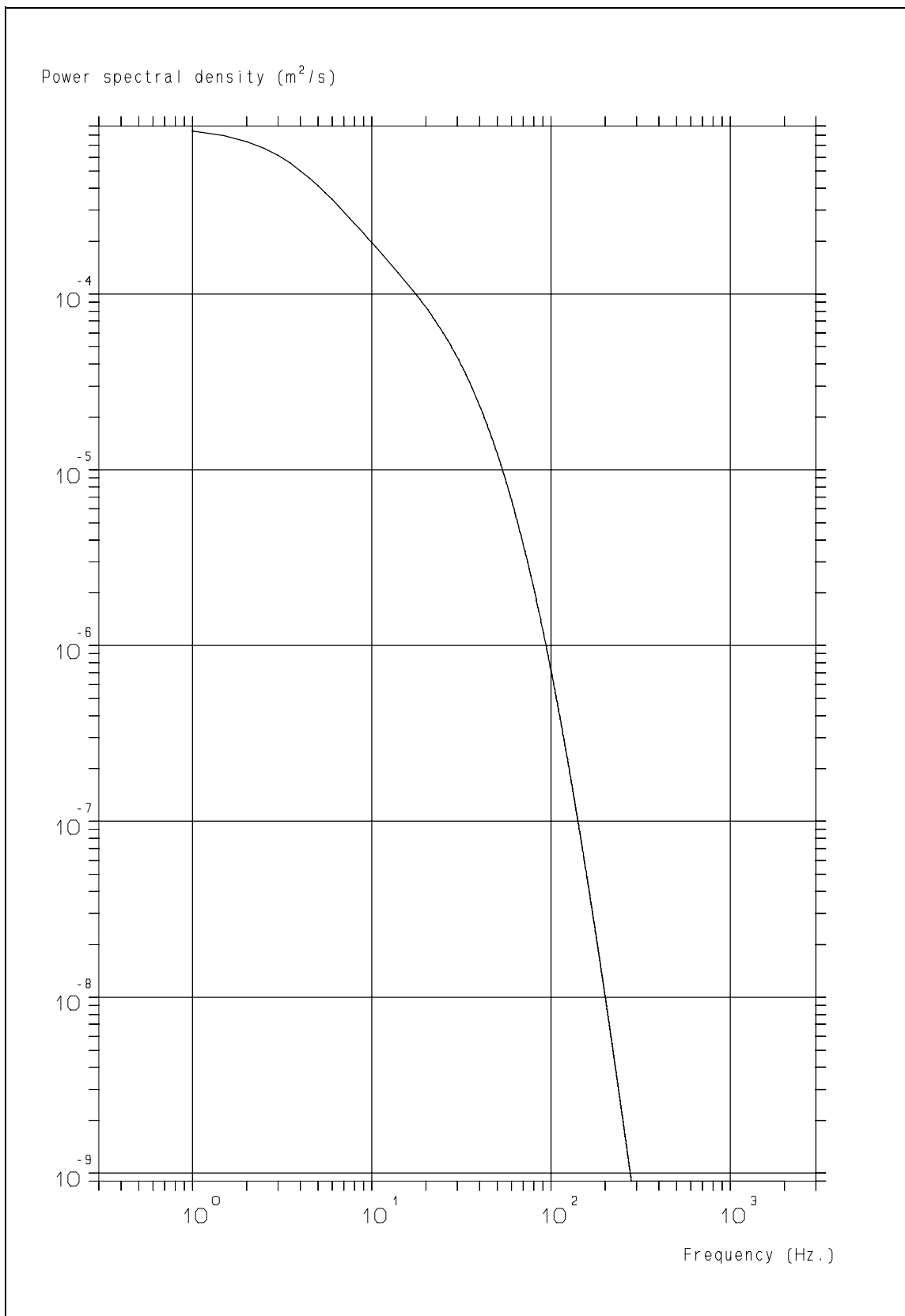


**Figure 11.32:** The Power Spectral Density derived from the fitted ACF of fig. 11.31.

### 11. Estimation of Turbulence PSD by Curve-Fit to the Auto Correlation Function

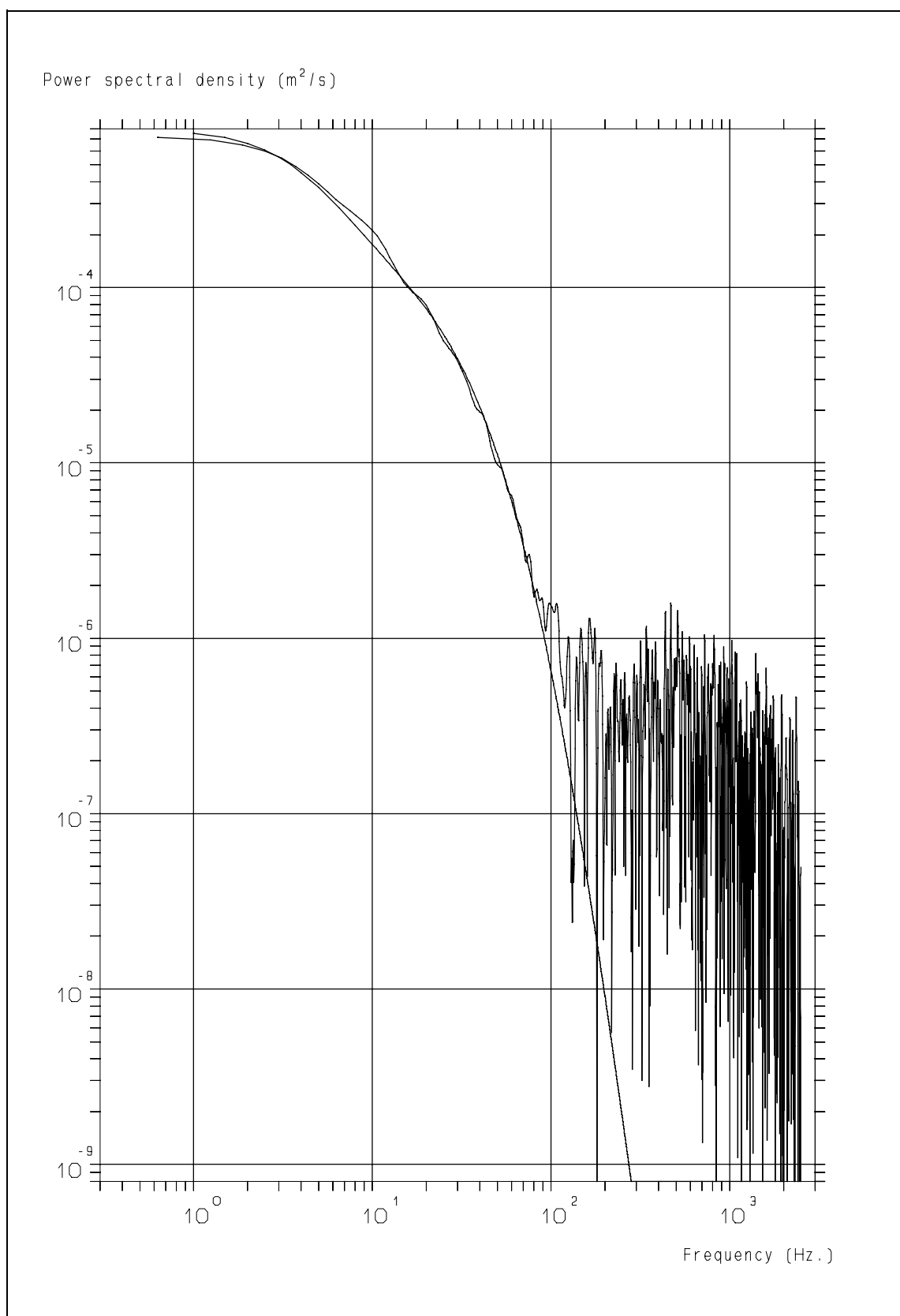


**Figure 11.33:** The Power Spectral Densities derived from the ACF's of fig. 11.31.

*Retrieval of turbulence and turbulence properties from LDA data with noise*

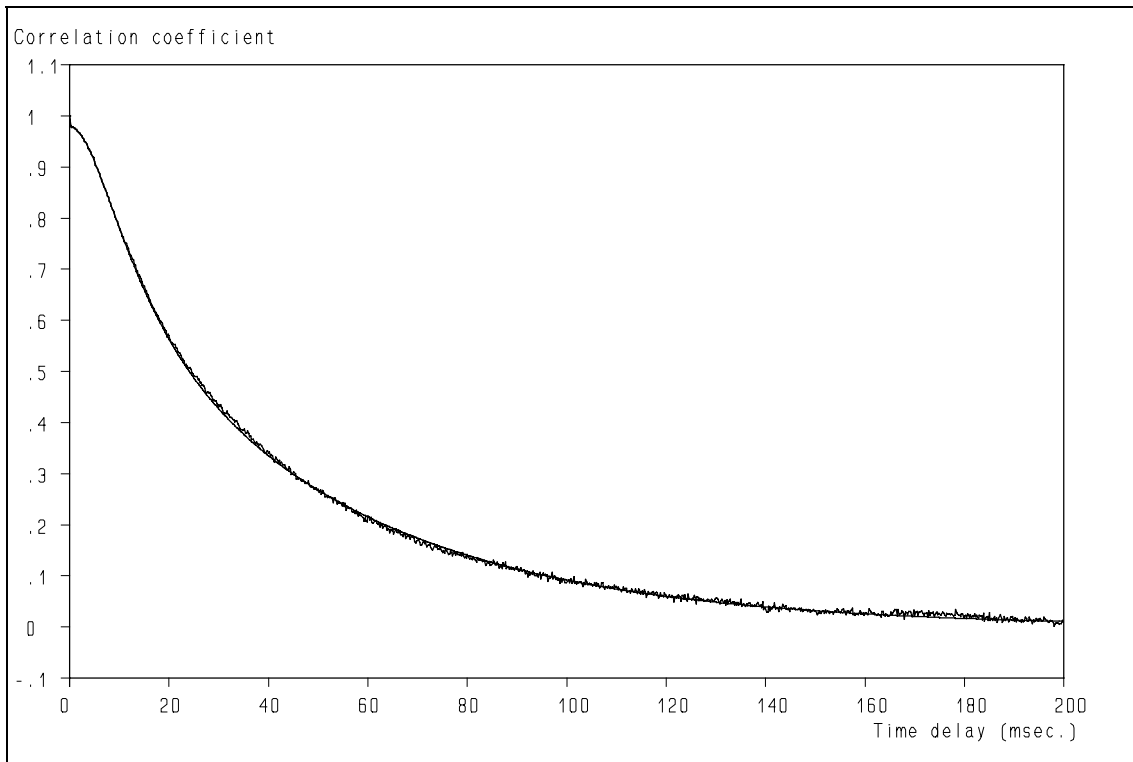


**Figure 11.34:** The ACF derived from the polymer solution pipe flow data-set and the fitted ACF.

### 11. Estimation of Turbulence PSD by Curve-Fit to the Auto Correlation Function

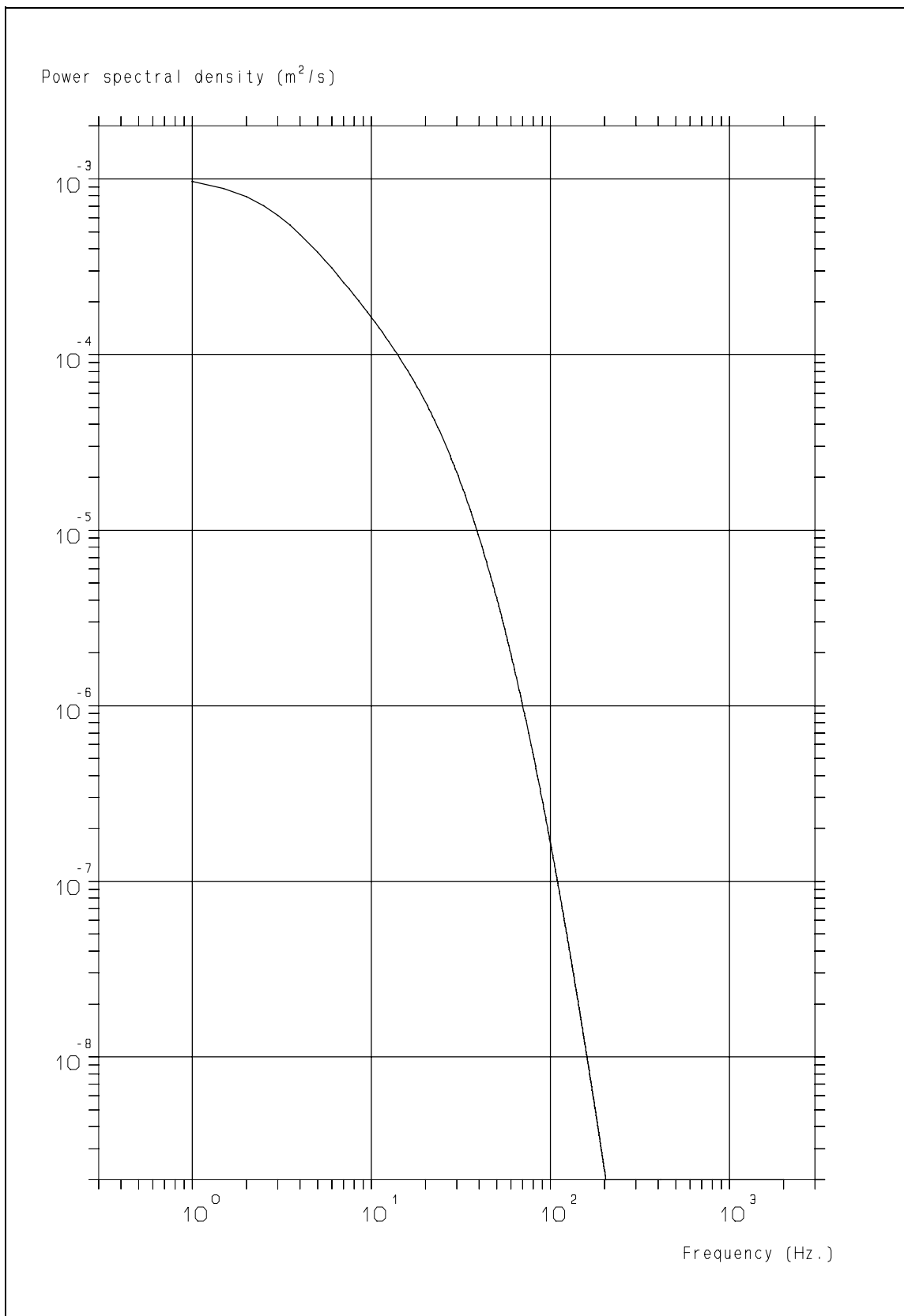


**Figure 11.35:** The Power Spectrum derived from the fitted ACF of fig. 11.34.

*Retrieval of turbulence and turbulence properties from LDA data with noise*

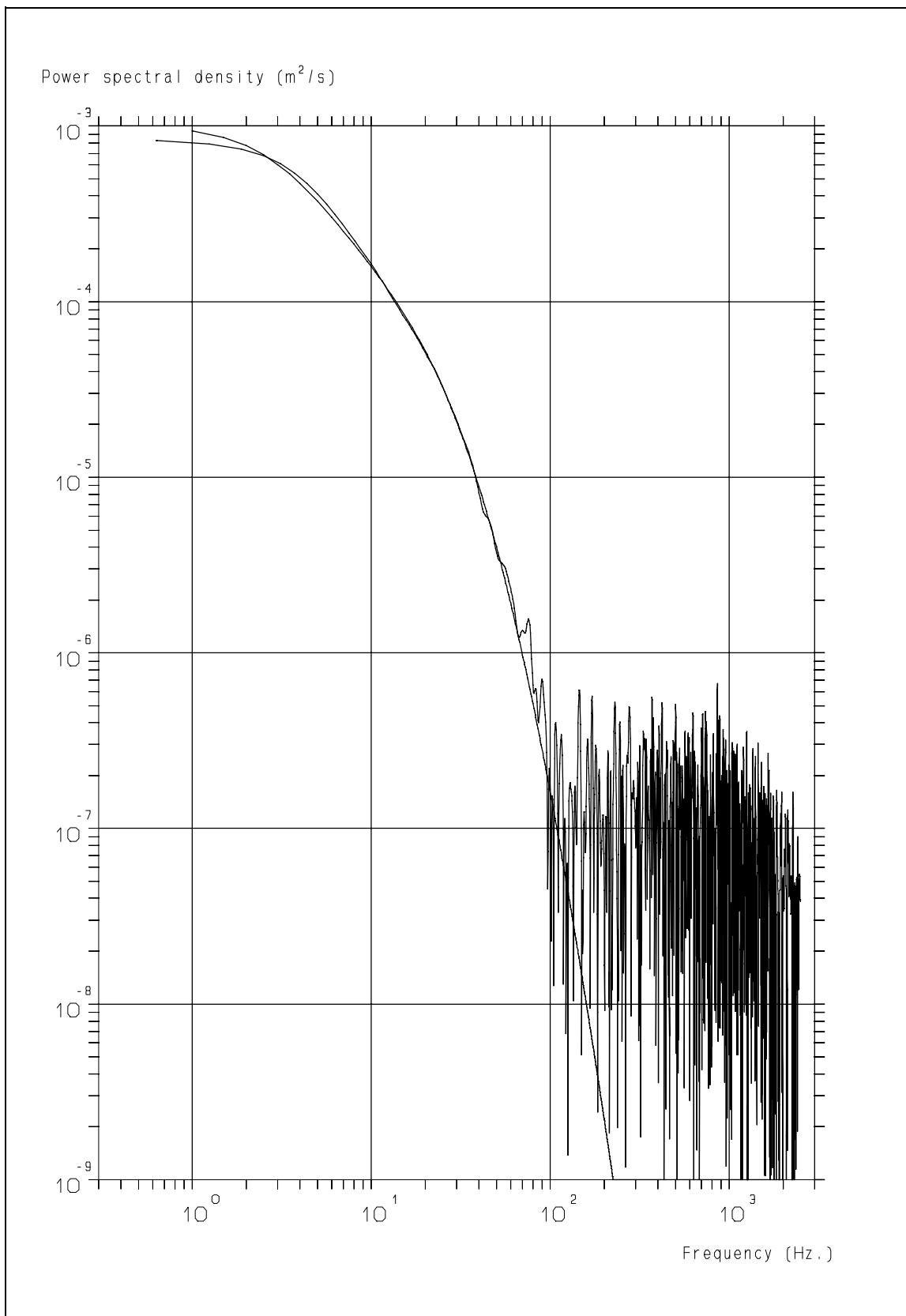


**Figure 11.36:** The Power Spectra derived from the ACF's of fig. 11.34.

## 11. Estimation of Turbulence PSD by Curve-Fit to the Auto Correlation Function

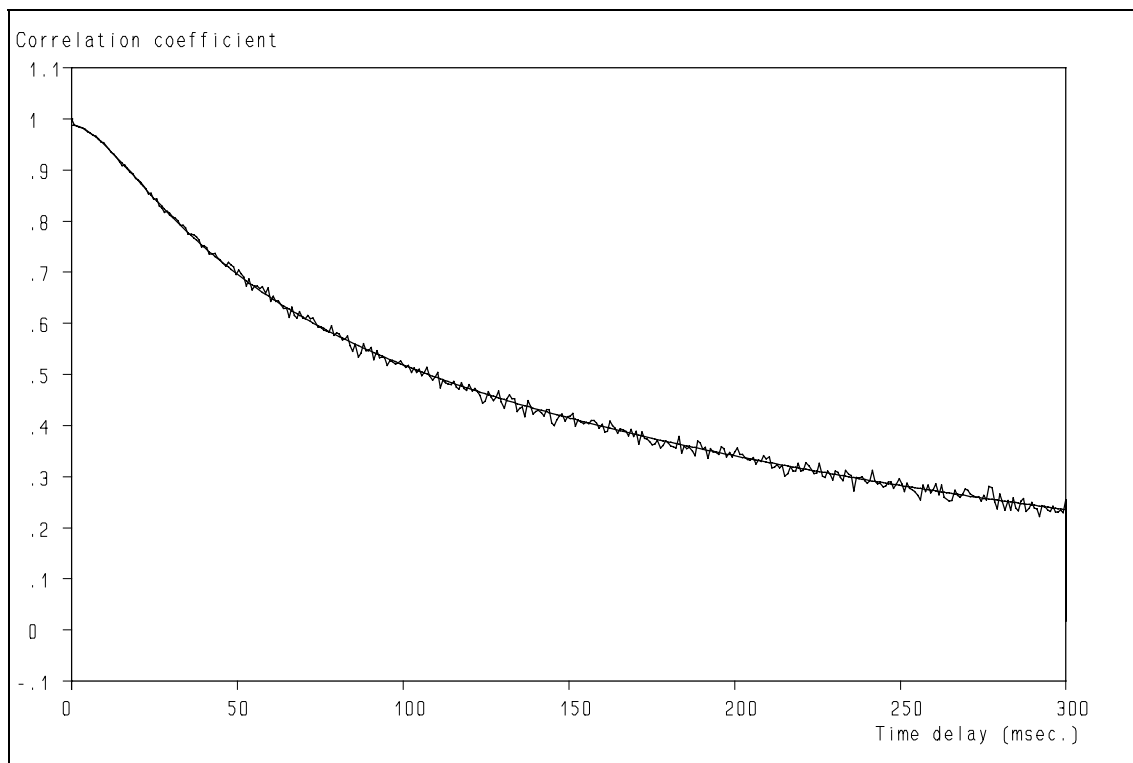


**Figure 11.37:** The ACF derived from the data-set of the  $u$ -component of the flow in the mixing layer and the fitted ACF.

*Retrieval of turbulence and turbulence properties from LDA data with noise*

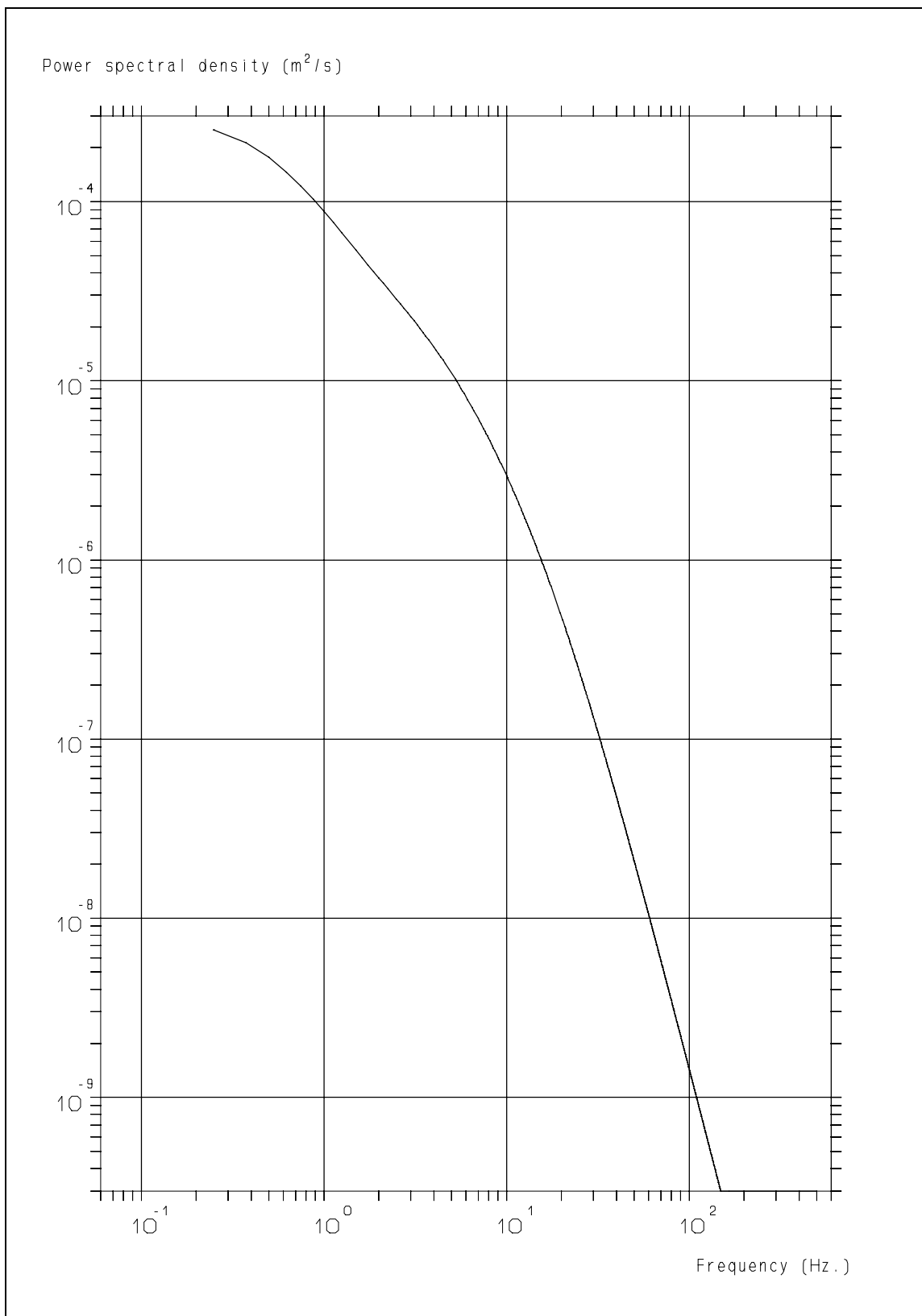


**Figure 11.38:** The Power Spectrum derived from the fitted ACF of fig. 11.37. Note that the data-rate of the original data is only 147 Hz!

### 11. Estimation of Turbulence PSD by Curve-Fit to the Auto Correlation Function

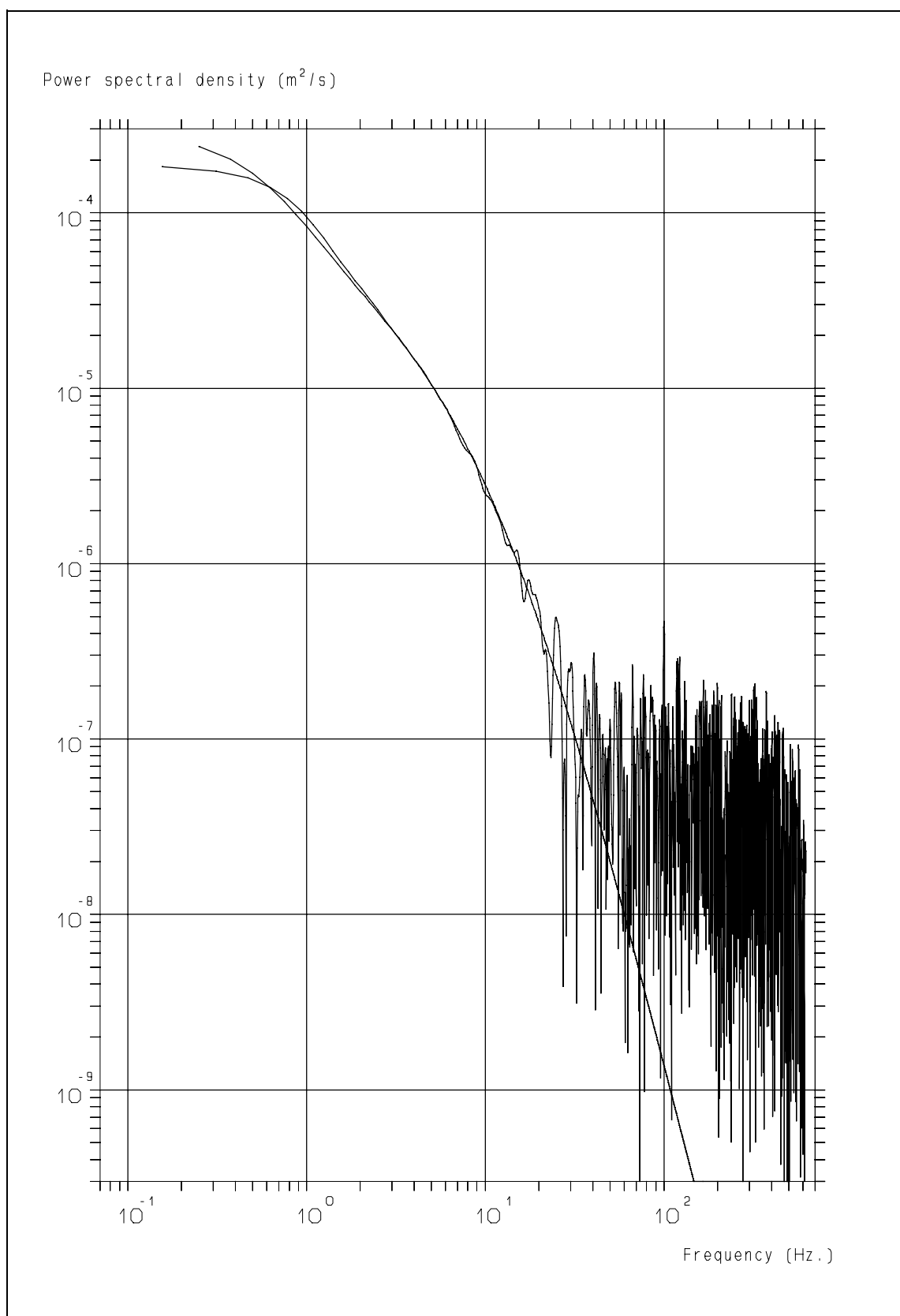


**Figure 11.39:** The Power Spectra derived from the ACF's of fig. 11.37.

*Retrieval of turbulence and turbulence properties from LDA data with noise*

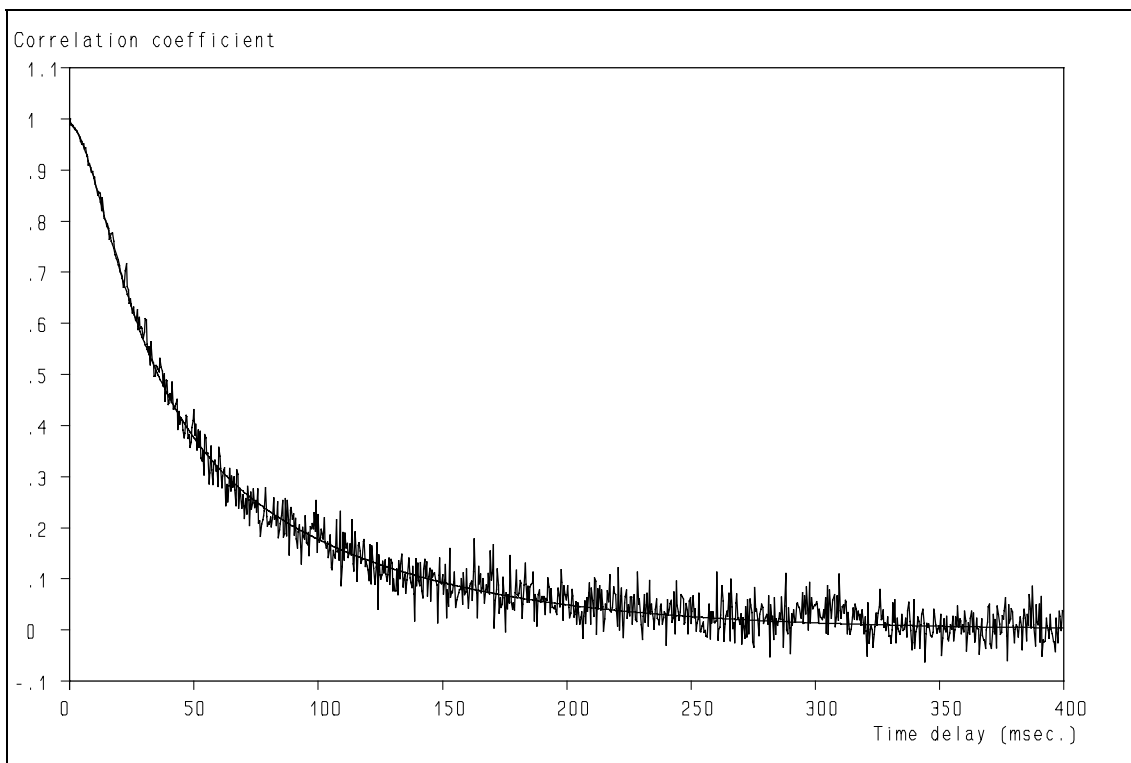


**Figure 11.40:** The ACF derived from the data-set of the  $v$ -component of the flow in the mixing layer and the fitted ACF.

### 11. Estimation of Turbulence PSD by Curve-Fit to the Auto Correlation Function

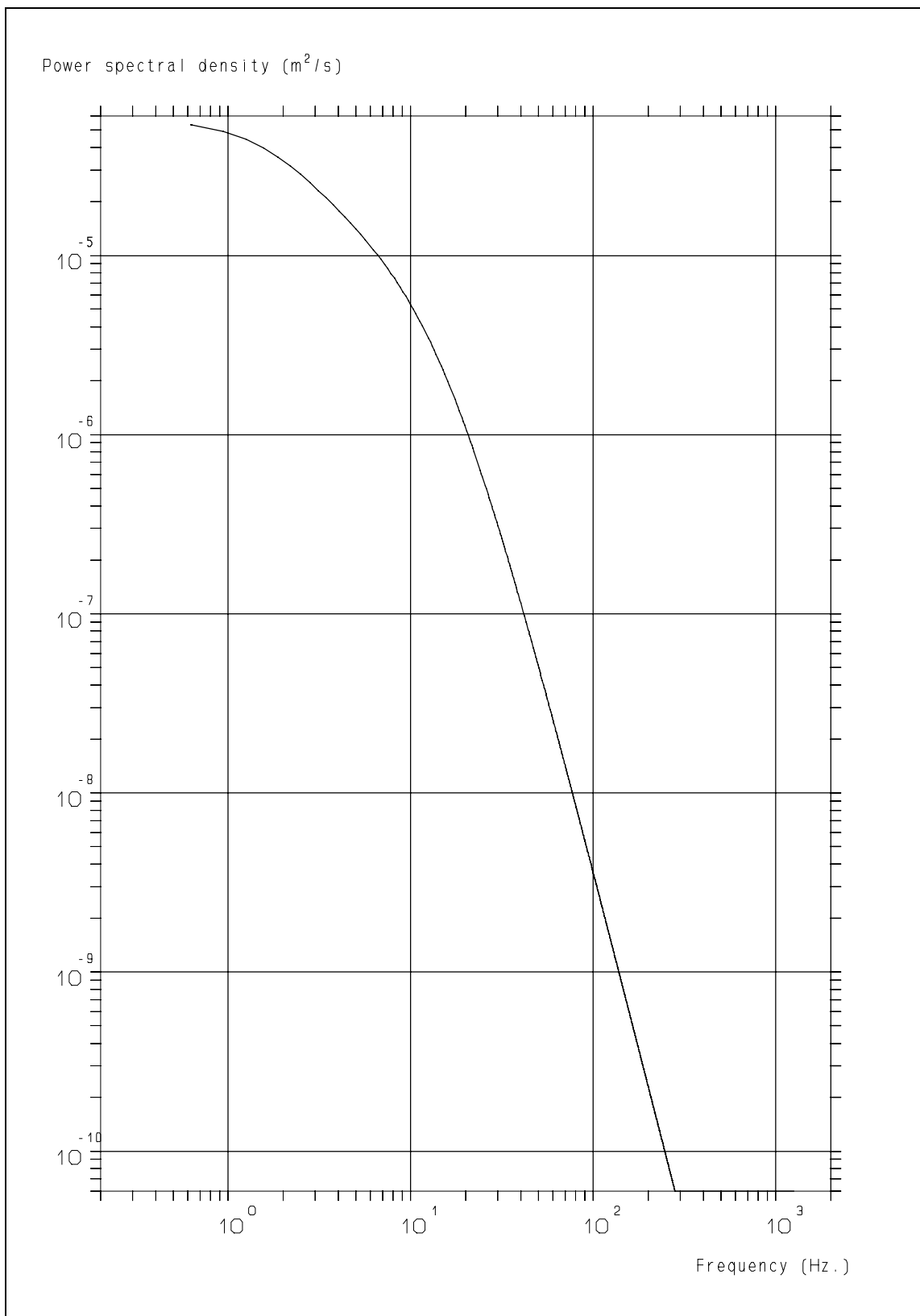


**Figure 11.41:** The Power Spectrum derived from the fitted ACF of fig. 11.40. Note that the data-rate of the original data is only 95 Hz!

*Retrieval of turbulence and turbulence properties from LDA data with noise*

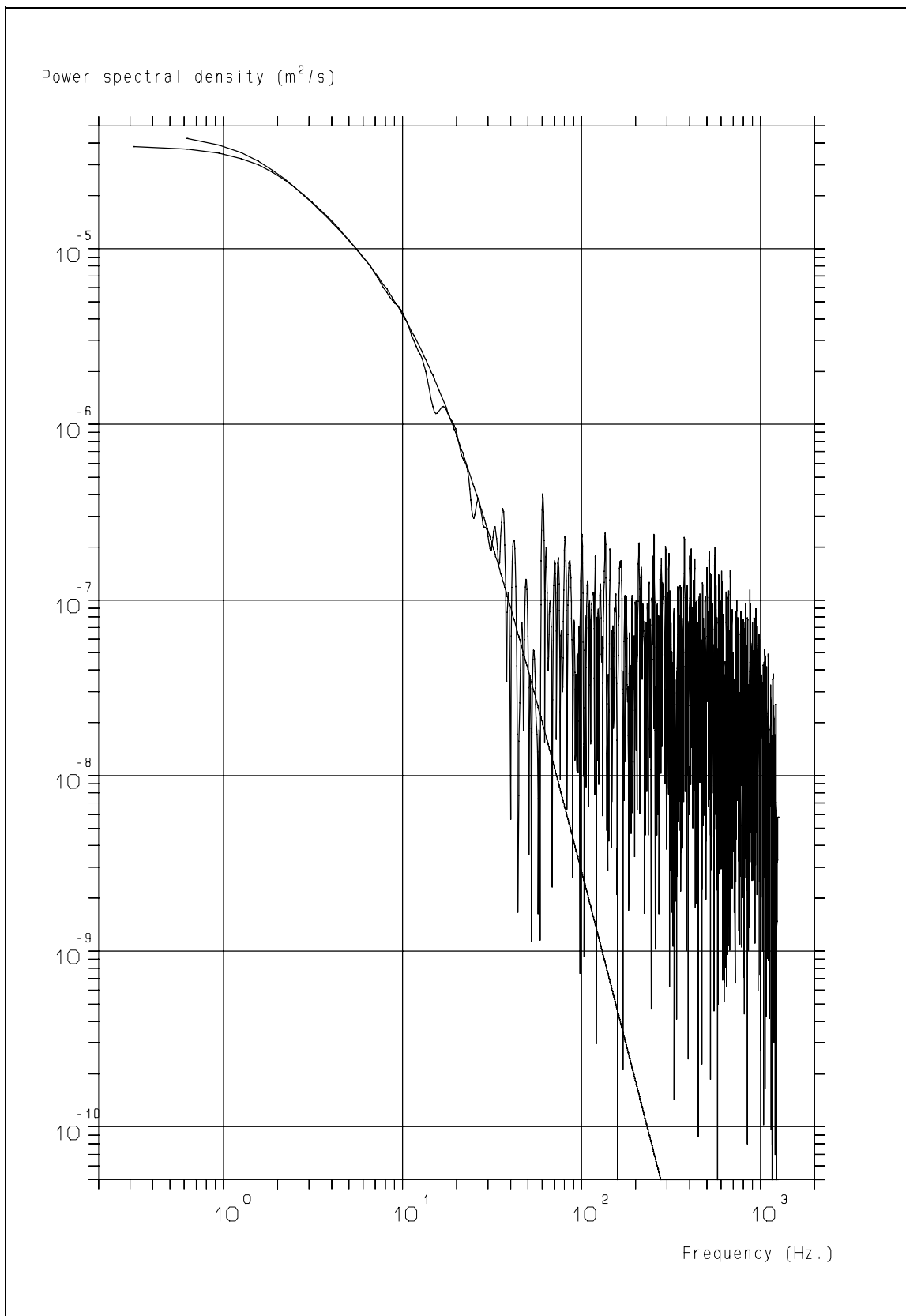


**Figure 11.42:** The Power Spectra derived from the ACF's of fig. 11.40.

## 11. Estimation of Turbulence PSD by Curve-Fit to the Auto Correlation Function

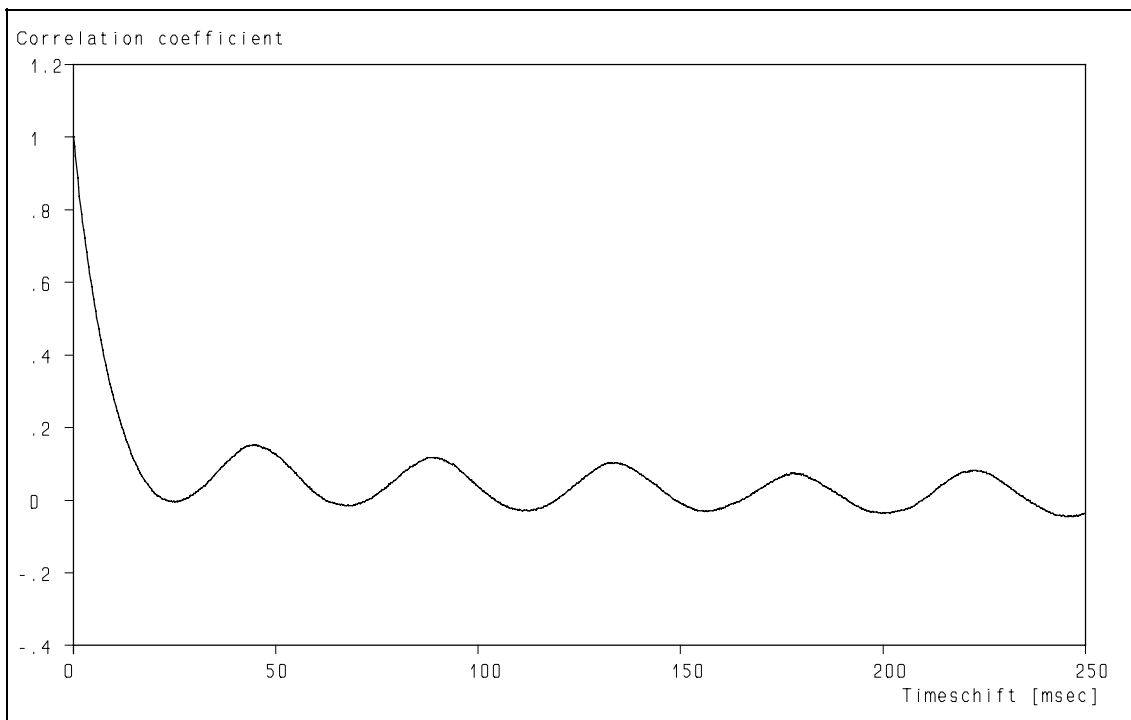


**Figure 11.43:** Slotted ACF, derived from the data-set of the flow in the jet of a stirrer including the periodic components.

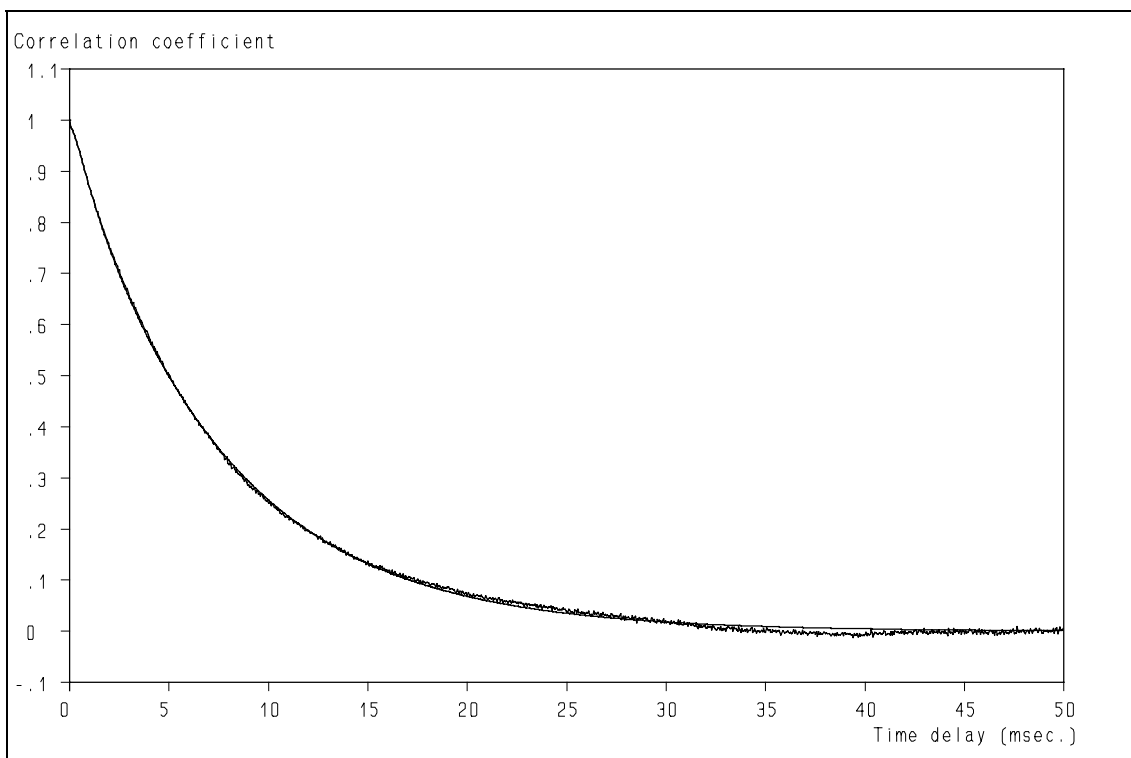


**Figure 11.44:** The ACF, derived from the data-set of the flow in the jet of a stirrer, after removal of the periodic components, and the fitted ACF.

*Retrieval of turbulence and turbulence properties from LDA data with noise*

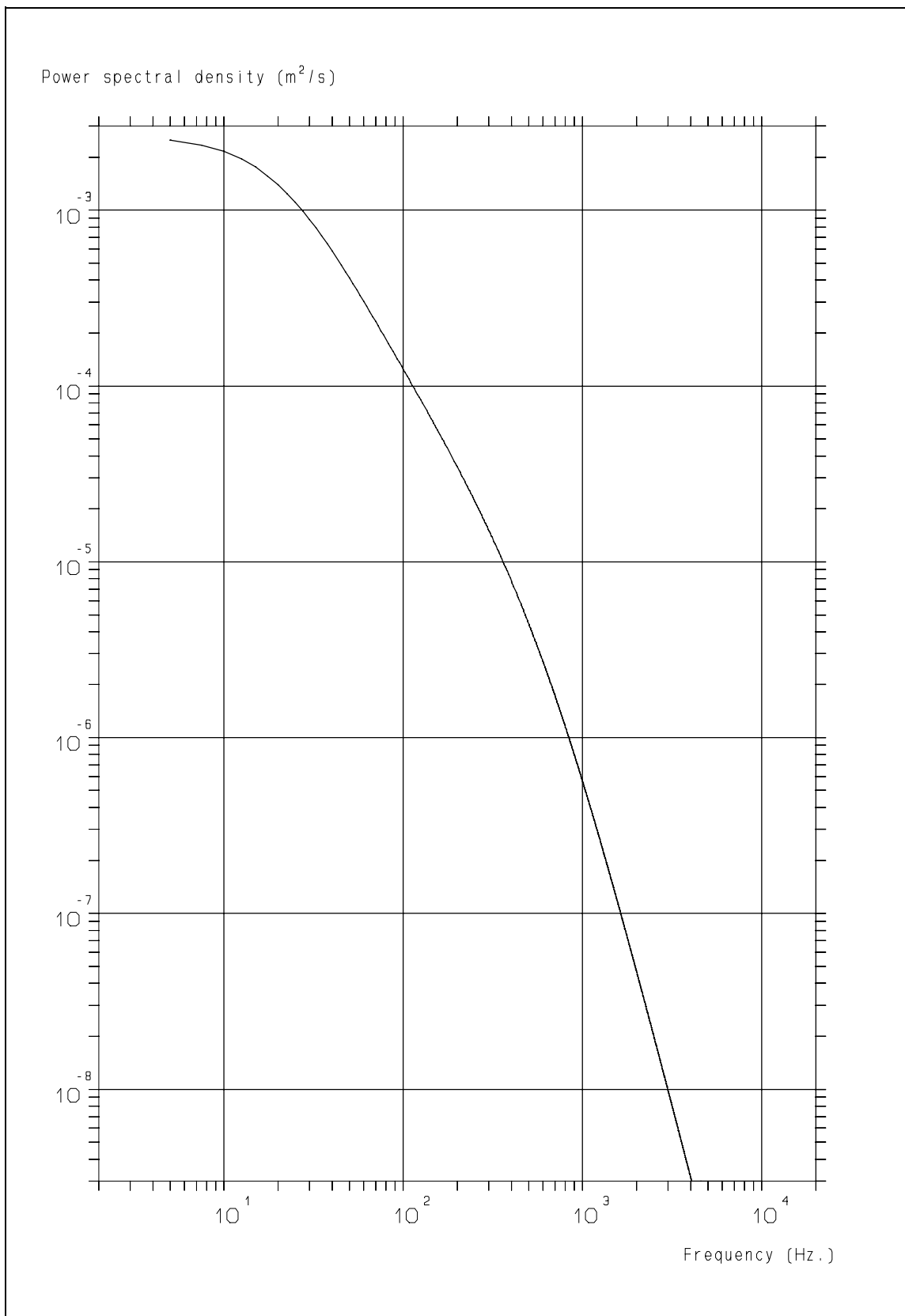


**Figure 11.45:** The Power Spectrum derived from the fitted ACF of fig. 11.44.

### 11. Estimation of Turbulence PSD by Curve-Fit to the Auto Correlation Function

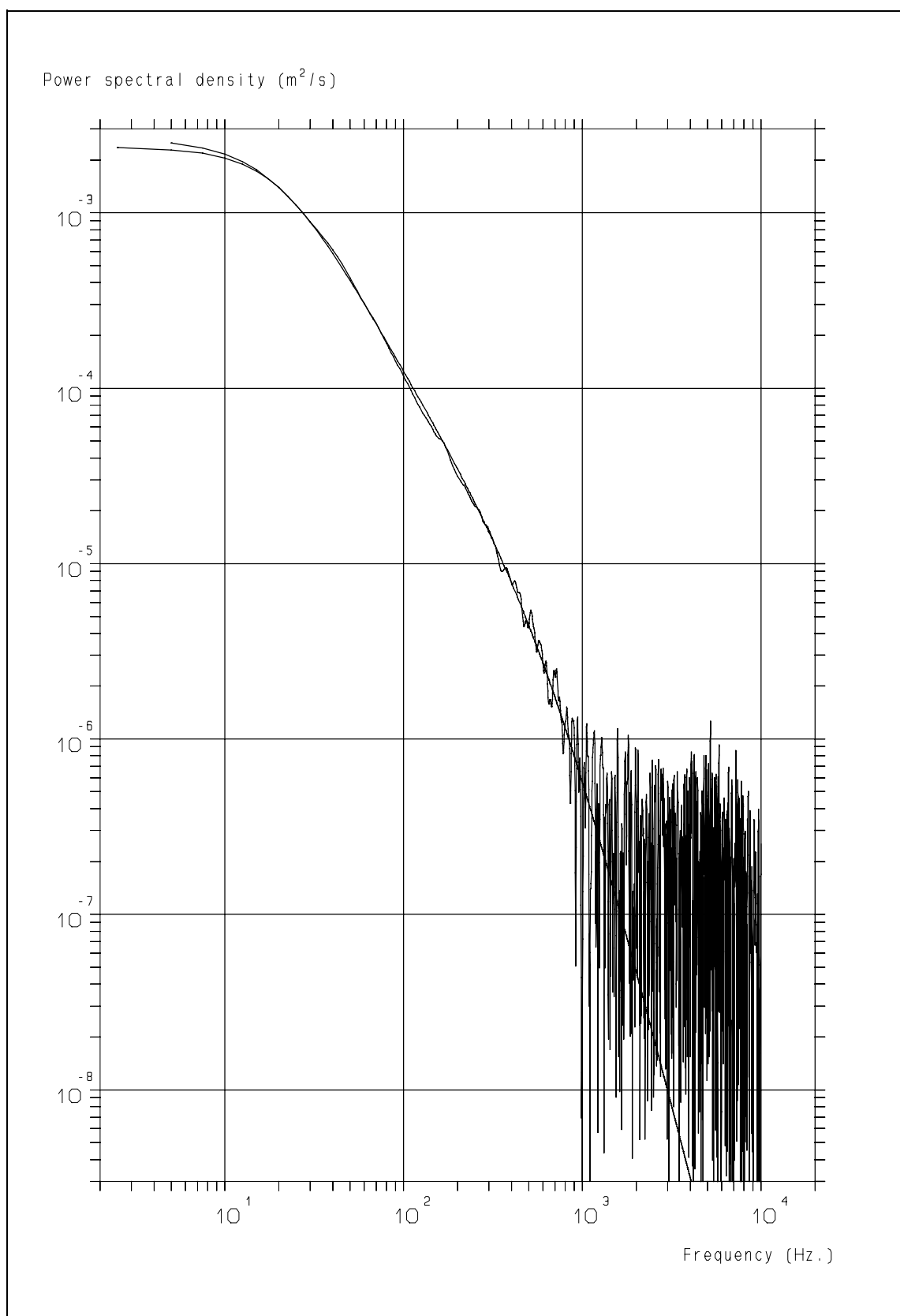


**Figure 11.46:** The Power Spectra derived from the ACF's of fig. 11.44.

*Retrieval of turbulence and turbulence properties from LDA data with noise*

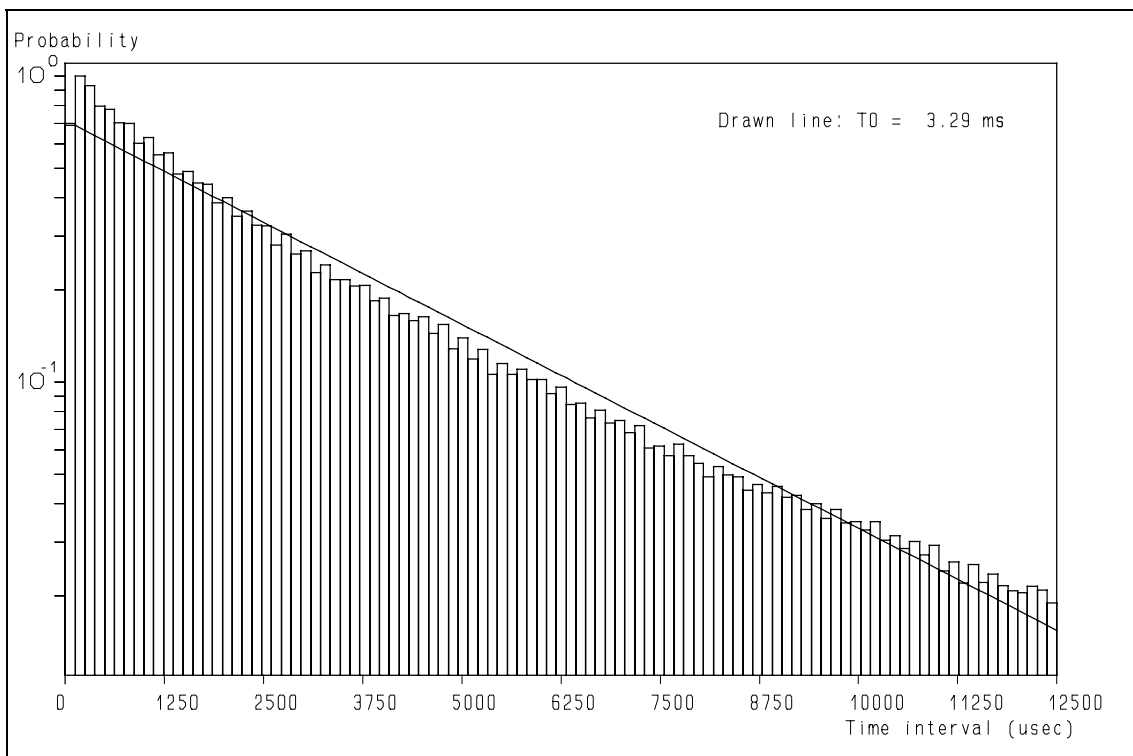


**Figure 11.47:** The time interval distribution of the data-set of the flow around the airfoil.

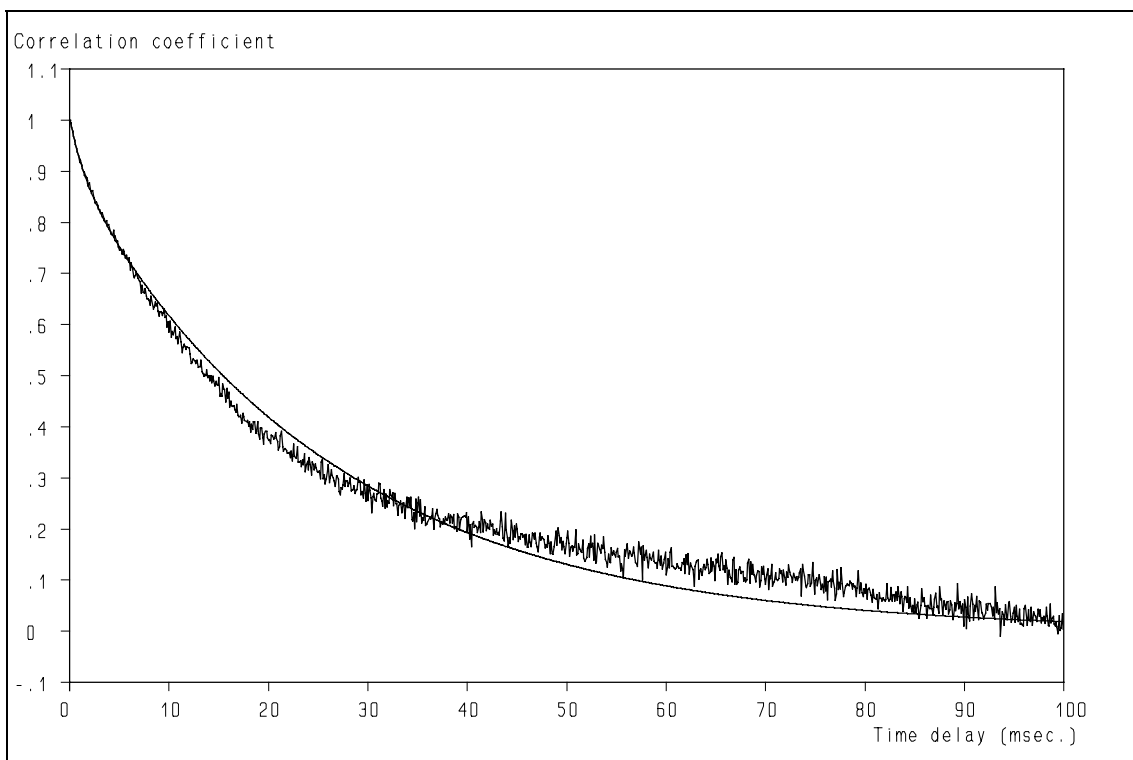


**Figure 11.48:** The ACF, derived from the data-set of the flow around the airfoil and the fitted ACF.

### 11. Estimation of Turbulence PSD by Curve-Fit to the Auto Correlation Function

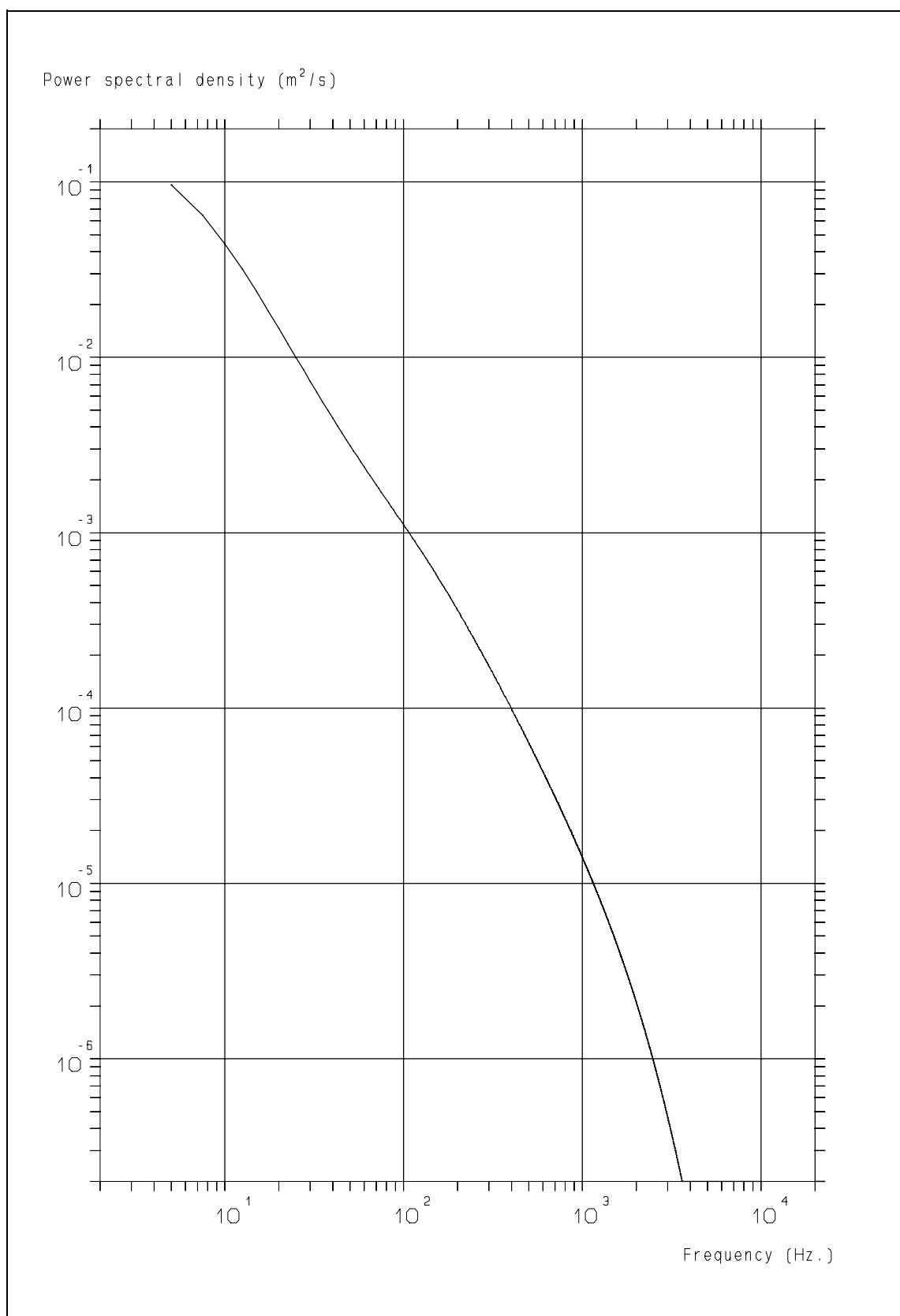


**Figure 11.49:** The Power Spectrum derived from the ACF of fig. 11.48.

*Retrieval of turbulence and turbulence properties from LDA data with noise*

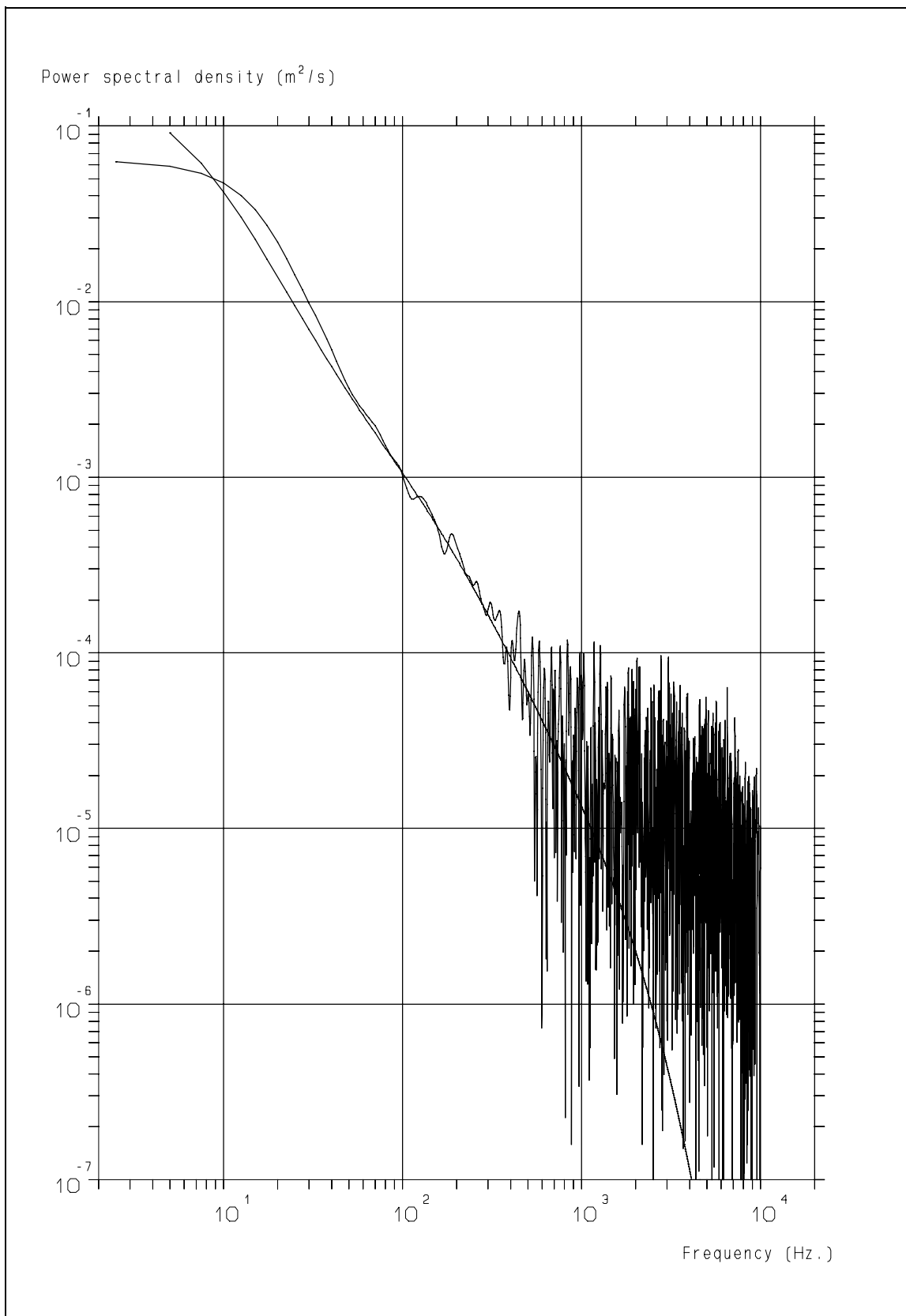


**Figure 11.50:** The Power Spectra derived from the ACF's of fig. 11.48.

## 11. Estimation of Turbulence PSD by Curve-Fit to the Auto Correlation Function

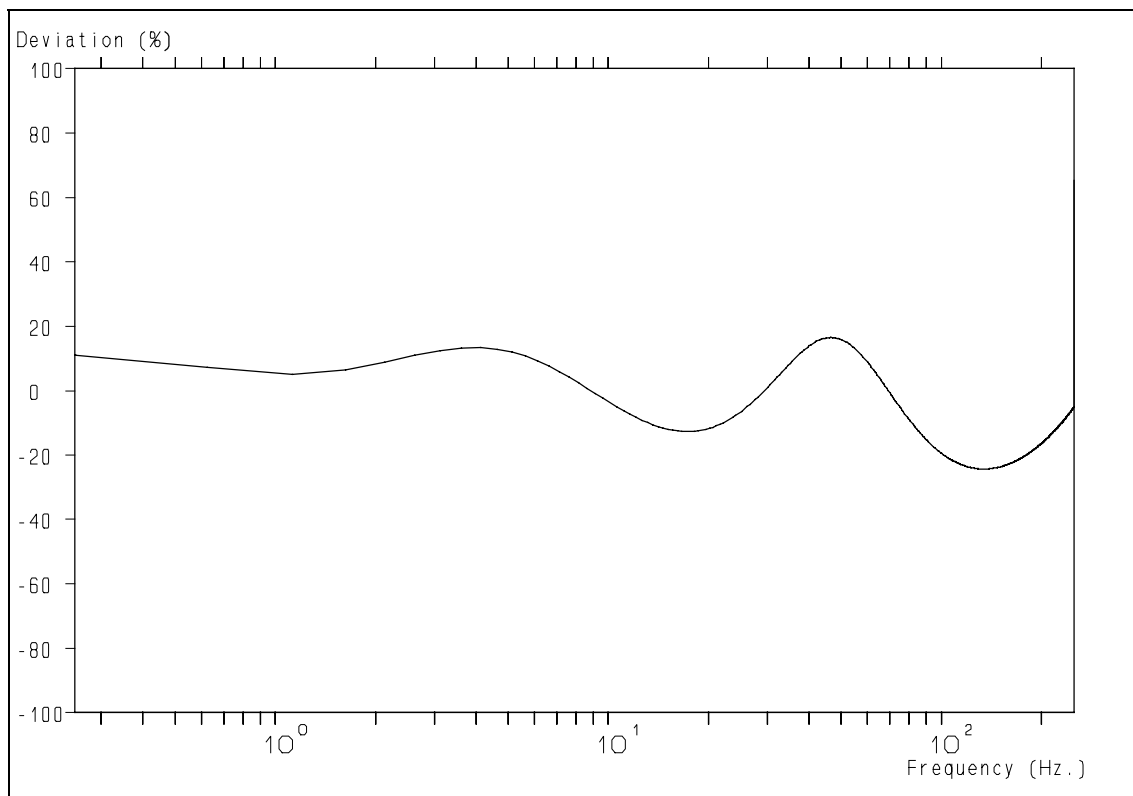


**Figure 11.51:** Deviation between the Bessem Power Spectrum and the Power Spectrum, derived from the curve-fit. Up to 250 Hz, 5 times the average data-rate, the error is within 25% of the actual value.

*Retrieval of turbulence and turbulence properties from LDA data with noise*

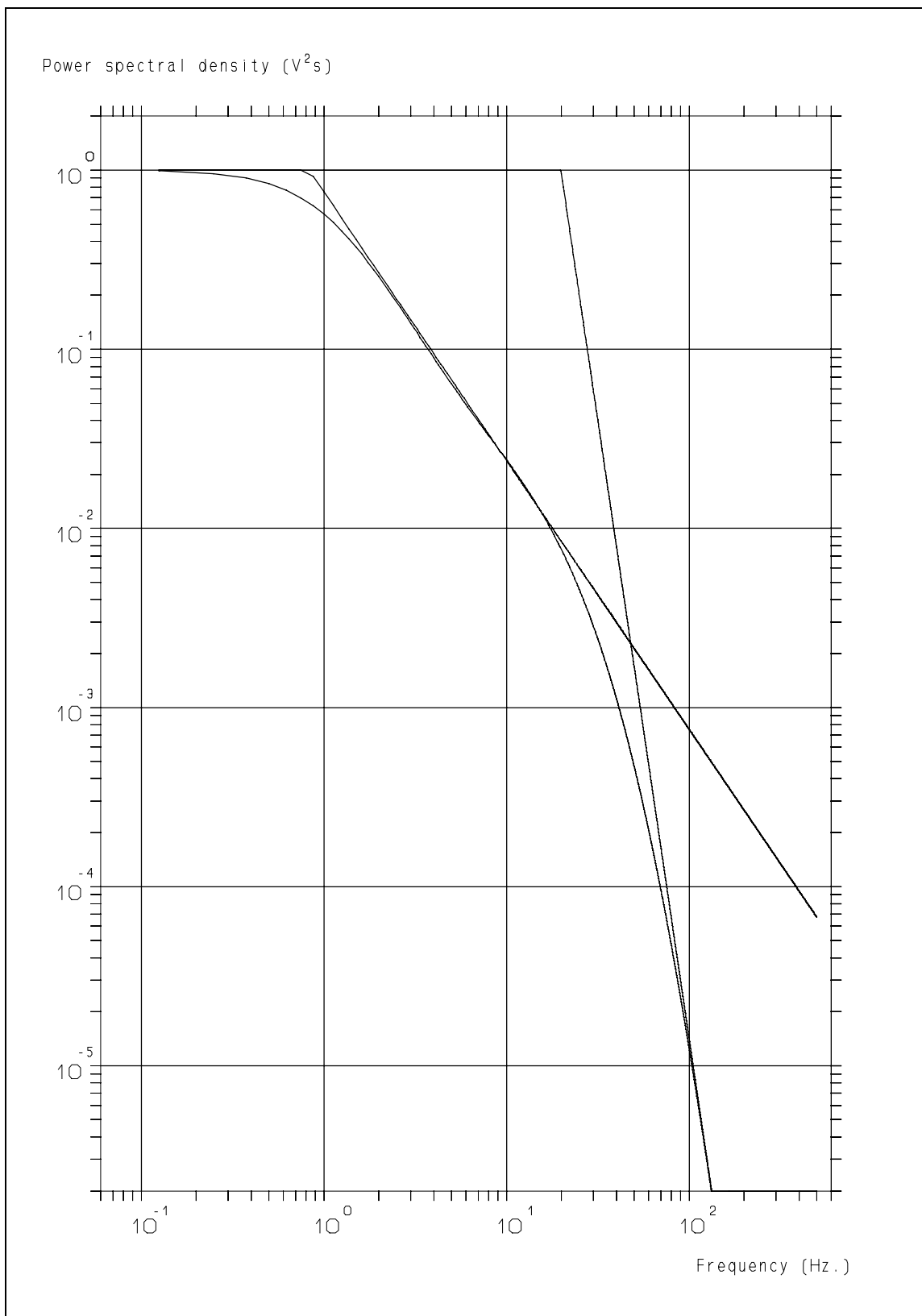


**Figure 11.52:** Estimation of the slopes of the Power Spectrum, derived from the fitted ACF of fig. 11.5.

## 11. Estimation of Turbulence PSD by Curve-Fit to the Auto Correlation Function

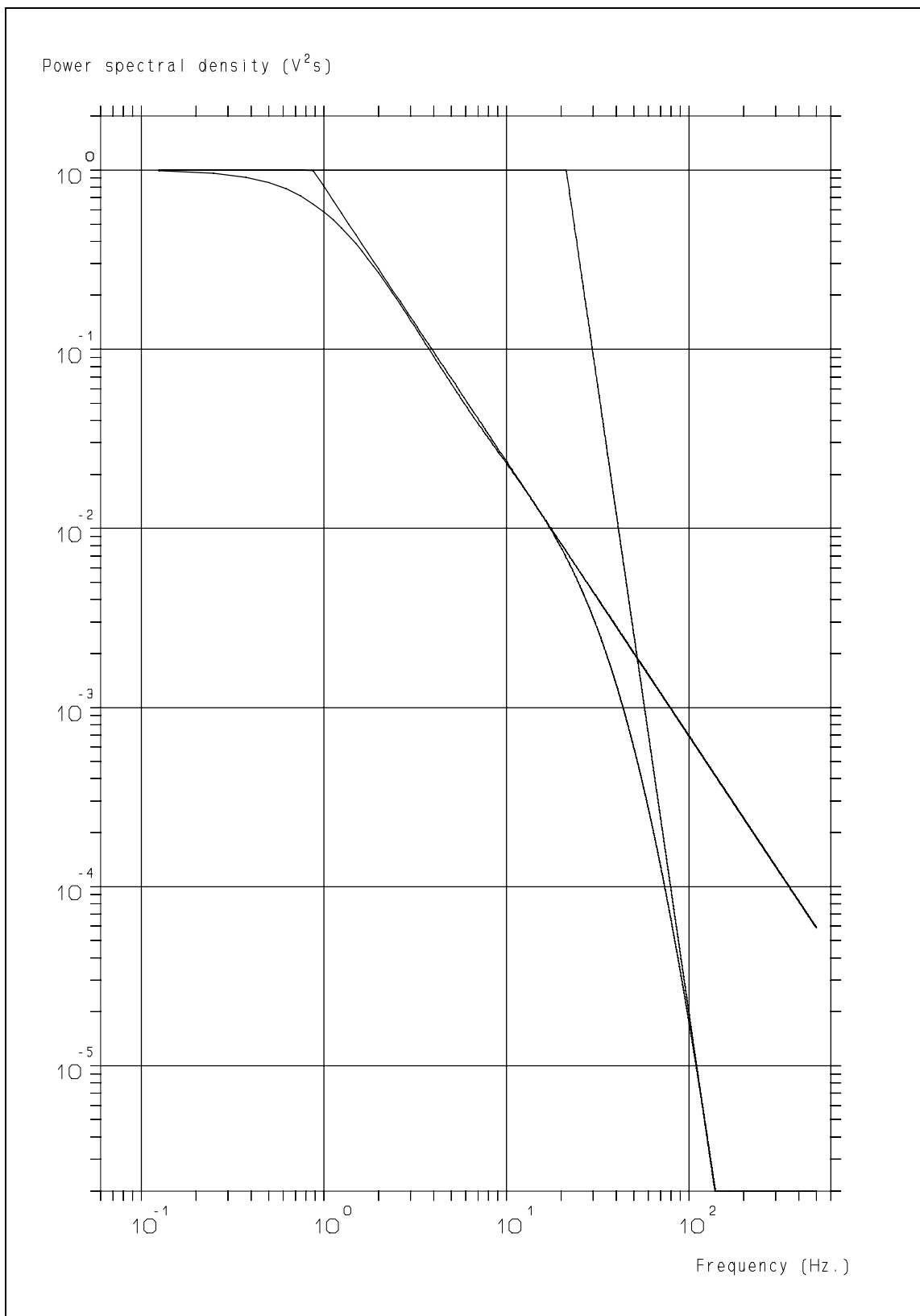


**Figure 11.53:** Estimation of the slopes of the Power Spectrum, derived from the fitted ACF of fig. 11.11.

# Chapter 12

## Extended reconstruction of turbulent velocity fluctuations

*All things are possible  
until they are proved impossible;  
and even the impossible  
may only be so as of now.*  
Pearl S. Buck

### 12.1 Introduction.

In the Chapters 6, 7 and 8 we have seen that velocity signal reconstruction is feasible when the data-rate is sufficiently high and the noise contribution is suppressed by using first-order Kalman reconstruction in combination with the pre-processing. However, even with this approach some residual noise remains present in the signal, which hampers its interpretation. To reduce this residual noise contribution further, use can be made of additional spectral information, obtained from the data itself. This spectral information can either be obtained using the cross-covariance technique as described in Chapter 9 or from the curve-fit technique as described in Chapter 11. How this information can be used for this extended velocity reconstruction will be discussed in the following sections. Subsequently it will be applied to simulated data, as *only* such data can be used for the determination of the quality of the reconstruction. This quality will be determined using a number of different techniques, some of which have been used in previous chapters.

The spectral estimate which will be used in this chapter is the spectral estimate, based on the cross covariance technique. If this is not available (e.g. because of a single channel measurement) one can simply substitute the spectral estimate based on the curve-fit technique. The only difference is that the cross-covariance technique requires two independent signals, which can -for the final reconstruction step- be averaged to reduce the noise level by a factor of  $\sqrt{2}$  as the noise contributions are not correlated.

However, some remarks need to be made at this point:

- The spectral estimator, obtained using the cross covariance technique, depends both on the original noise level and the noise suppression factor. The latter is determined by the amount of information available: the larger the amount of data, the larger the noise suppression factor is. This is illustrated in fig. 12.1 and 12.2, which show the decrease of the noise at the high frequency side of the spectrum with an increase in the amount of data. Therefore it is attractive to have both a high Signal-to-Noise ratio (SNR) of the original data in combination with a long measurement time. The latter also reduces the variance in the spectral estimates at lower frequencies (corresponding to larger eddies), because a larger number of integral time scales is used.
- The variance in the spectral estimates at the high frequency side of the spectrum is relatively high, compared to other parts of the spectrum. To use this for further reconstruction, a more continuous, smoothed, approximation will have to be used, as this variance is not a property of the turbulence, but an artifact of the data-processing.
- Note that the problem, mentioned above, does not occur when the curve-fit approach, as discussed in Chapter 11, is used, as this produces a smooth spectrum for all frequencies. Therefore a combination of both spectral estimators can also be an attractive alternative, which, however, is not evaluated in this thesis.

## 12.2 The Second-Order Kalman Reconstruction Filter.

Regarding the improvement, obtained with the first-order Kalman reconstruction technique, one might be tempted to think that a higher-order Kalman reconstruction filter would improve the results even further. The required parameters could be derived from the (low-noise) turbulence power spectral density (PSD). The next logical step would thus be a *second-order* Kalman reconstruction filter. Such a filter has been designed, based on the assumption that the accelerations decrease above the frequency where the slope in the PSD changes from  $-5/3$  to  $-7$  (50 Hz in the case of simulated turbulence according to the "Bessem" power spectrum). The spectrum of the *accelerations* is then approximately equal to a first-order low pass filter. Details can be found in Appendix D. The second-order Kalman reconstruction filter approaches the turbulence power spectrum better than the first-order version, as can be seen from fig. 12.3. Simulations have been performed using this second-order Kalman reconstruction filter in combination with the cross covariance technique.

### 12.2.1 Simulation & Results.

The data processing used is almost identical to the one shown on page 157 in Chapter 9, except that the first-order Kalman reconstruction filter has now been replaced by a second-order Kalman reconstruction filter, resulting in the scheme shown on page 243. When the filter gain of the second-order Kalman reconstruction filter is adjusted such that the Mean Squared Error (MSE, see Chapter 8) of the output signal is minimized, a power spectrum of the turbulence as in fig. 12.4 is obtained. For the higher frequencies, too much power of the signal has been removed resulting in a significant deviation of the computed power spectrum from the actual power spectrum. In the time domain, the second-order Kalman reconstruction filter is always capable of producing an MSE which is smaller than the MSE of the first-order Kalman reconstruction filter. However, the second-order Kalman reconstructed turbulence is therefore even more sensitive to underestimation of the contribution of the small eddies than it is with the use of the first-order version. See also the discussion on this subject in the Chapters 7 - 9.

### 12.2.2 Analysis.

The equations of the filter dynamics of the second-order Kalman reconstruction filter are:

$$\frac{d}{dt}v(t) = a(t) \quad [12.1]$$

$$\frac{d}{dt}a(t) = -\left(\frac{1}{\beta} + L\right)v(t) - \frac{\alpha}{\beta}a(t) + Lv^{obs}(t) \quad [12.2]$$

in which:

$v(t)$	= second-order Kalman reconstructed velocity	m/s
$a(t)$	= acceleration of $v(t)$	m/s <sup>2</sup>
$L$	= Kalman filter gain	1/s <sup>2</sup>
$\alpha$	= parameter related to the two cut-off frequencies of the turbulence power spectrum	s
$\beta$	= parameter related to the two cut-off frequencies of the turbulence power spectrum	s <sup>2</sup>

From the above mentioned equations for the filter dynamics we see that:

- The feedback of the observed (measured) velocity is only present in eq. [12.2].
- The filter gain is a scalar as in the case of the first-order Kalman reconstruction filter.

## 12. Extended reconstruction of turbulent velocity fluctuations

The transfer function  $G(j\omega)$  of the second-order Kalman reconstruction filter is:

$$G(j\omega) = \frac{L}{\frac{1}{\beta} + L - \omega^2 + j\omega \frac{\alpha}{\beta}} \quad [12.3]$$

and the transfer function  $S_G(j\omega)$  of the spectrum of the second-order Kalman reconstruction filter is:

$$S_G(\omega) = G(j\omega)G^*(j\omega) = \frac{L^2}{\left(\frac{1}{\beta} + L - \omega^2\right)^2 + \omega^2 \frac{\alpha^2}{\beta^2}} \quad [12.4]$$

which is approximately a second-order low-pass filter. This transfer function shows a resonance peak when the filter gain  $L$  is chosen such that the error function of the output of the Kalman filter and the "real" turbulence is minimized. This is why we think that the second-order Kalman reconstruction filter is less suited for the estimation of the turbulence power spectrum and thus neither for reconstruction purposes.

### 12.2.3 Discussion.

The second-order Kalman reconstruction filter reduces the noise more than the first-order Kalman filter. But it also suppresses the power of the turbulence signal for the higher frequencies more heavily when the filter gain is chosen such that the MSE has been minimized. We did not investigate the power spectra obtained using the cross covariance technique and the second-order Kalman reconstruction filter with a higher gain setting (in which case less signal is removed at the higher frequencies) any further.

The results of the second-order Kalman reconstruction filter were disappointing for the following reasons:

- The mathematical analysis of the second-order Kalman filter is complex and complicated. The danger of introducing errors is real.
- The model for the turbulence that is used is more extensive than the model in the first-order Kalman reconstruction filter but it is far from complete. Turbulence theories predict a decay of the PSD proportional to  $f^{-7}$  or an exponential decay (ref. 1, 2, 71 and 72) which still differs significantly from the decay proportional to  $f^{-4}$  which results from the second-order model. This problem will limit the accuracy of the reconstruction; perhaps a third-order turbulence model is more suitable.
- Optimisation of the MSE results in too much reduction of the high-frequency part of the spectrum and thus of the small eddies (see fig. 12.4). This hampers the study of this -for e.g. chemical engineering applications- very interesting part of the turbulent flow. It is not clear how to improve this in an objective and scientifically correct way. The risks that the result depends on experimenter experience or on "wishful thinking" are present. This needs to be avoided.
- Because of the above mentioned problems it is likely that further extension of the Kalman reconstruction filtering to orders higher than 2 (to model the turbulence better) will lead to severe mathematical problems. Also, the above reported results might be indicative that higher-order Kalman filters do not describe the properties of turbulence very well.

To circumvent the disadvantages of the second-order Kalman reconstruction filtering, a different approach has been evaluated, which has shown to give good results. This technique will be described in the next section.

### 12.3 The extended reconstruction filter.

A good estimate of the PSD of the turbulent velocity fluctuations can be obtained from the first-order Kalman reconstructed velocity signals using the cross covariance technique as has been shown in Chapter 9. Also, the first-order Kalman reconstructed velocity signals are a good estimate of the velocity fluctuations in time domain (ref. 87 and Chapter 7). However, the PSD is still different from the ideal as can be seen from fig. 12.5, which means that there is also room for improvement in time domain (ref. 89 and 90). This can be accomplished by the application of an extended reconstruction filter, which is to force the correct spectral characteristics on the first-order Kalman reconstructed velocity signal. This is feasible, because the correct spectral characteristics of the signal are known from the PSD estimate using the cross covariance technique whereas the PSD of the first-order Kalman reconstructed velocity signal can be obtained using e.g. the auto covariance function (ref. 89 and 90). However, because for the calculation of the cross covariance function two independent signals are required, it is attractive to use the *average* of these two signals as input signal for the extended reconstruction filter in stead of only one of these. The reason is that the noise contributions in the two signals are -in principle- uncorrelated, which means that the SNR of the *average* of these signals is  $\sqrt{2}$  higher than of each individual signal. This is confirmed by the calculation of the PSD of the average of these two signals as shown in fig. 12.6 compared to fig. 12.5. In practical situations it is not likely that the noises will be completely uncorrelated; for details see Chapter 3.

The required characteristic of the extended reconstruction filter is obtained by dividing the "low-noise" spectrum by the spectrum of fig. 12.6. Because we need the *amplitude* characteristic and the spectra present *power*, the square root of this ratio is to be used. To eliminate the variance at the high frequency side of the spectrum of fig. 12.2, a modelled filter has been used which is described by:

$$G(f) = \left( \frac{1 + \left(\frac{f}{f_1}\right)^m}{\left[1 + \left(\frac{f}{f_2}\right)^m\right] \cdot \left[1 + \left(\frac{f}{f_3}\right)^6\right]} \right)^{\frac{1}{2}} \quad [12.5]$$

in which:

$f_1 - f_3$  = characteristic frequencies Hz  
 $m$  = exponent

Fig. 12.7 shows the transmission of such a filter. The four parameters ( $f_1$ ,  $f_2$ ,  $f_3$  and  $m$ ) can be fitted to obtain the best approximation to the experimental result. This has been done manually up to now, but an automatic procedure is to be developed as a next step in the near future.

The actual filtering is done by convolving the average of the two first-order Kalman reconstructed velocity signals with the impulse response of the extended reconstruction filter. This impulse response can be obtained by Inverse Fourier Transformation of  $G(f)$ . To avoid phase errors and/or time shifts, the phase is set to zero for all frequencies. This is similar to the forward and backward predictions of the first-order Kalman reconstruction scheme. The resulting impulse response of the filter of fig. 12.7 is shown in fig. 12.8.

**N.B.** In all these discussions it should be taken into account that the random sampling acts as a low-pass filter when reconstruction is applied, the so-called particle rate filter (ref. 39, 63, 87 & 99 and Chapter 6). This does not really matter for the calculation of the *ratio* of the PSD's derived from the auto and cross covariance functions, but it should be taken into account for the extended reconstruction filter in order to correct automatically for the particle rate filtering. The resulting formula for the transfer function of the extended filter thus becomes:

## 12. Extended reconstruction of turbulent velocity fluctuations

$$G(f) = \left( \frac{\left[ 1 + \left( \frac{f}{f_1} \right)^m \right] \cdot \left[ 1 + (2\pi f t_0)^2 \right]}{\left[ 1 + \left( \frac{f}{f_2} \right)^m \right] \cdot \left[ 1 + \left( \frac{f}{f_3} \right)^6 \right]} \right)^{\frac{1}{2}} \quad [12.6]$$

in which  $t_0$  is the average time between two successive Doppler signals and the parameter of the exponential time-interval distribution (ref. 39, 63 and 87, see also Chapter 4 and 6). This results in the impulse response of fig. 12.9, in which the same parameters have been used as in fig. 12.7 and 12.8 and a  $t_0$  of 2 ms. (corresponding to a data-rate of 500 Hz.). After convolving the average of the two first-order Kalman reconstructed velocity signals with this impulse response, the reconstructed velocity signal has the correct spectral properties without any further assumptions for the properties of the flow *and* is corrected for the low-pass properties of the random sampling. It can therefore be regarded as a close to optimum estimation of the turbulent velocity fluctuations at any instant in time. The complete data-processing procedure for the second part is shown on page 252.

The correct behaviour of the extended reconstruction filter can be checked by calculation of the PSD of the reconstructed signal. This should be close to the PSD, obtained using the cross covariance technique. The result for this particular case is shown in fig. 12.10 and comparison with fig. 12.2 reveals that this is correct.

The average data-rate (which is  $1/t_0$ ) has its influence on the quality of the reconstruction and the noise level (see also Chapter 7 - 9). This is illustrated in fig. 12.11: the effective SNR of the input signal for the first-order Kalman reconstruction scheme depends on the data-rate: with increasing data-rate the noise suppression of the pre-processor is more effective, resulting in an increasing SNR. This is also reflected in the PSD's of fig. 12.12, 12.13 and 12.14 (data-rate 1000 Hz.), which are identical to fig. 12.2, 12.6 and 12.10 respectively (data-rate 500 Hz). This shows again the importance of a high data-rate.

### 12.4 Results.

The data-processing as outlined on page 252 is aimed primarily at the *temporal* reconstruction of the velocity signal. To illustrate the results of the different steps in the data-processing, the reconstructed signals are presented in time domain in a series of figures:

Fig. 12.15: Linear interpolation at 1 ms. intervals and only using the velocity estimate closest to the interval boundary. As a result, a large fraction of the velocity estimates remain unused because of the exponential time interval distribution (see ref. 105 and Chapter 8). The noise level is thus higher than necessary. Also note the sharp peaks due to the combination of a short interval in between two successive velocity estimates and a different noise contribution.

Fig. 12.16: Linear interpolation at 0.1 ms. intervals, followed by digital filtering and re-sampling at 1 ms. intervals increases the amount of velocity estimates that is used to almost 100% (see ref. 105 and Chapter 8). As a result, the noise level is lower compared to that of fig. 12.15.

Fig. 12.17: First-order Kalman reconstruction filtering removes the sharp accelerations of fig. 12.15 or 12.16 (see ref. 87 and Chapter 7). The result thus resembles the actual turbulent velocity fluctuations better.

## *Retrieval of turbulence and turbulence properties from LDA data with noise*

Fig. 12.18: Application of the extended reconstruction filter on the average of two first-order Kalman reconstructed velocity signals, based on independent measurements, produces the best temporal reconstruction possible at this moment.

Fig. 12.19: For comparison the actual input signal (the simulated turbulence) is shown simultaneously with the signal of fig. 12.18.

Fig. 12.20: A higher data-rate leads to a better reconstructed signal in agreement with theory (ref. 63, 87, 97 and 105 and Chapter 6 - 9).

These figures clearly show the improvement obtained after the different reconstruction steps. This is even more clearly illustrated by looking at the distribution of the accelerations.

Fig. 12.21: Distribution of the acceleration of the "Bessem" turbulence itself.

Fig. 12.22: Distribution of the acceleration of the raw data. Note that the horizontal scale is 4 times as wide as in fig. 12.21, but still a significant number of observations fall outside the range, as is illustrated by the high number of observations at the boundaries. These high values (in absolute sense) of the acceleration are caused by velocity estimations close to each other in time, but with a different noise contribution.

Fig. 12.23: Distribution of the accelerations after linear interpolation and re-sampling. Note that the scale is identical of the scale of fig. 12.21. Although the distribution is wider than that of fig. 12.21, the extreme values of fig. 12.22 have been removed. This is caused by the fact that the minimum distance in time is now one sampling interval and not arbitrarily low as in fig. 12.22.

Fig. 12.24: Distribution of the accelerations after re-sampling at a high data-rate and re-sampling after Gaussian anti-aliasing filtering. Note that the contributions at the boundaries have virtually disappeared compared to fig. 12.23. This illustrates the improvement of this approach compared to direct re-sampling (see ref. 105 and Chapter 8).

Fig. 12.25: Distribution of the accelerations after first-order Kalman reconstruction filtering. It comes already close to the distribution of fig. 12.21.

Fig. 12.26: Distribution of the accelerations after first-order Kalman reconstruction and extended reconstruction filtering. It is virtually identical to the distribution of fig. 12.21.

The effect of the extended reconstruction filtering and the data-rate is illustrated in table 12.1:

## 12. Extended reconstruction of turbulent velocity fluctuations

---

<u>Condition</u>	<u>MSE (x 10<sup>-5</sup>)</u>
1. Low (1 kHz) reconstruction-rate linear interpolation.	15.9292
2. High (10 kHz) reconstruction-rate linear interpolation.	10.4186
3. As 2. with Gaussian filter.	9.1148
4. First-order Kalman reconstruction (data-rate 500 Hz).	7.0037
5. As 4. and extended reconstruction filtering.	3.6940
6. As 5. (data-rate 1000 Hz).	2.0195

---

**Table 12.1:** Mean Squared Error Values.

These results show that the above described velocity signal reconstruction algorithm gives good estimates for the velocity as a function of time and the distribution of the accelerations. The required properties can be retrieved from the data itself and do not require assumptions or modelling of the flow or turbulence, except for the limitations of the accelerations, which is a part of the first-order Kalman reconstruction scheme. This avoids the risk of "self-fulfilling prophecies", which is an often mentioned pitfall of any velocity signal reconstruction technique. Although the data-processing consists of a number of different steps and is time-consuming, the result is a reconstructed velocity signal that is "state-of-the-art" and is *derived from the information contained in the data itself*. One should keep in mind that the amount of time involved in doing a good experiment is large and requires attention of the experimenter, whereas the data-processing can be fully automated and thus can run without any attention. In our view, therefore, the quality of the results is more important than the required processing time.

Although the results are satisfying and reproduce the turbulent velocity fluctuations well, one should always keep in mind that the quality of the results will *always* reflect the quality of the input data. This means that the better the quality of the input data, the better the quality of the output data. It is therefore necessary to optimise the *whole* laser-Doppler anemometry (LDA) system in order to obtain the best results. Important aspects have been discussed in Chapter 3 (see also ref. 63, 87, 97 and 105) and include the noise in the velocity estimates (SNR of Doppler signals and processor quality) and the data-rate (spatial resolution, tracer particle selection & concentration and detection configuration). Unfortunately, not all the parameters are unrelated and optimisation requires skill of the experimenter. However, in many cases a significant improvement can be obtained by looking at the system *in total*.

The data-processing is rather time consuming: to process a data-set of 10<sup>6</sup> samples takes roughly 15 hours on a 100 MHz Pentium PC. However, as all the parameters for the subsequent steps can be derived from the data itself, all the different steps can be automated. This means that the data-processing can be done during the night and in weekends, when the PC's are usually idle. It is not realistic to compare the actual measurement time with the data-processing time because the preparation of an experiment takes time as well. On top of that comes the continuing increase in processing power of computers, which will speed up the data-processing in the near future<sup>1</sup>. But if the data-processing would be the bottleneck, the cost of a PC is small compared to the cost of an LDA system (kfl. 5,- vs. kfl. 250,- and up) which would justify to add processing power to increase the capabilities of the LDA system.

To process the data on-line is not possible by the approach described in this report. However, if it would be required, the algorithms can be used in a *steady flow system* to operate on-line. A previous measurement can be used to determine the required parameters of the different processing steps and the actual data-processing can be done on-line using Digital Signal Processing (DSP) Integrated Circuits

---

<sup>1</sup> By the time that you read this a 100 MHz Pentium processor will probably be outdated!

## *Retrieval of turbulence and turbulence properties from LDA data with noise*

(IC's). This would require additional hardware and software to program the DSP's, but it is feasible in principle.

### **12.5 Concluding remarks and future work.**

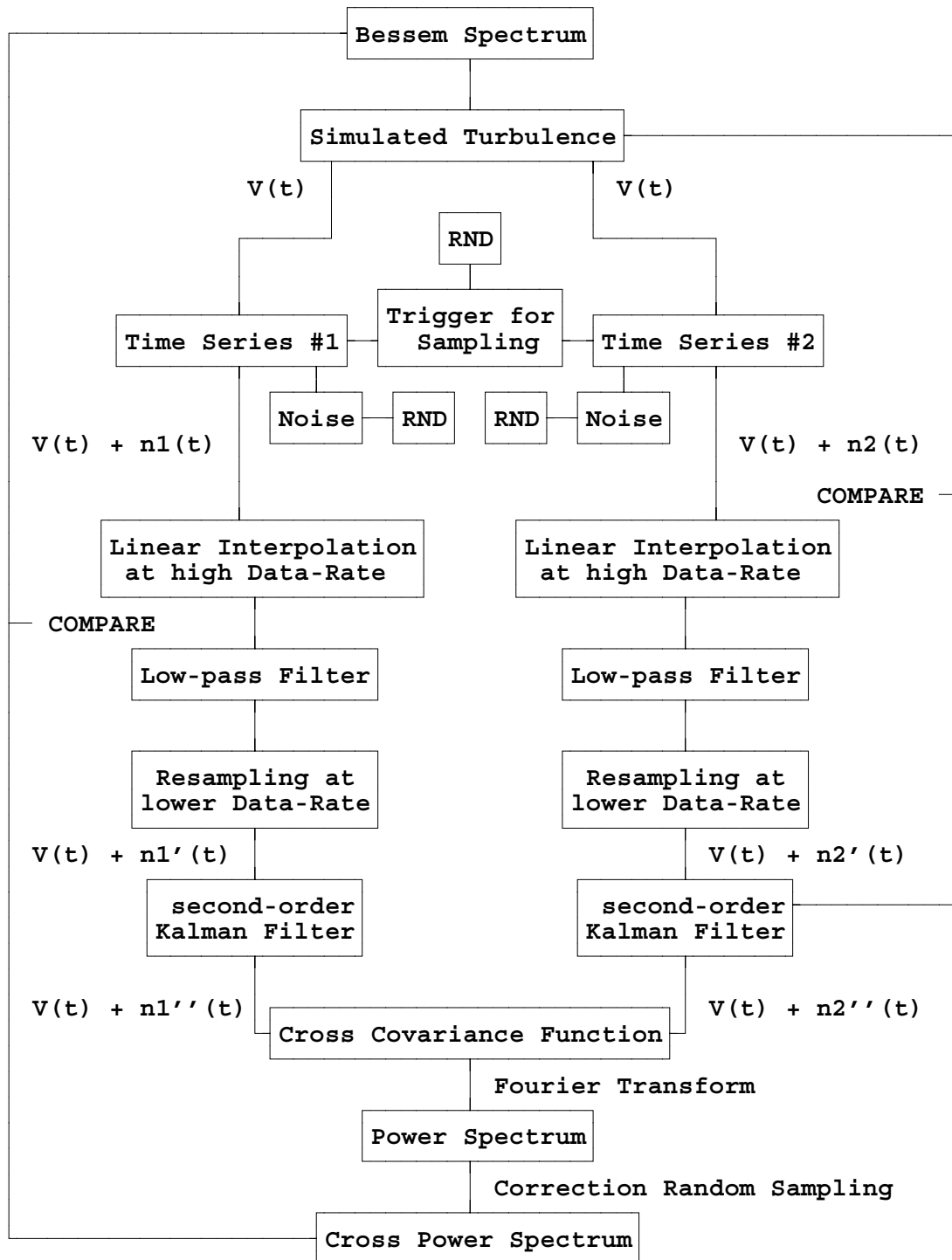
- A second-order Kalman reconstruction filter is feasible, but it is mathematically more difficult. However, a second-order Kalman reconstruction filter still requires assumptions, which are only a crude approximation of the properties of real turbulence. This limits the attractiveness of such an approach and is not in full accordance with the course of action chosen that as little as possible assumptions should be used for the velocity signal reconstruction algorithm.
- Processing of the first-order Kalman reconstructed velocity signal with an extended reconstruction filter, based on the auto- and cross-covariance functions, results in a reconstructed velocity which has spectral properties which are in agreement with the best possible estimate of the turbulence power spectrum. The Mean Squared Error values are then minimal and the distribution of the accelerations is in good agreement with the actual accelerations.
- Optimisation of the total LDA system remains essential to obtain high quality results. The important parameters are the SNR of the individual velocity estimates and the data-rate of the independent velocity estimates.

The work, reported in this chapter, has concentrated on the development of the data-processing algorithms. The design of the extended reconstruction filter has been done manually, but it can be automated. This would be the next logical step in the development. The final step would be to write a software package that would include all the data-processing as described in this thesis, including the design of the extended reconstruction filter.

An abridged version of the work, reported in this chapter, has been presented at the Lisbon conference of 1998 (ref. 116).

12. Extended reconstruction of turbulent velocity fluctuations

Data Processing I



*Retrieval of turbulence and turbulence properties from LDA data with noise*

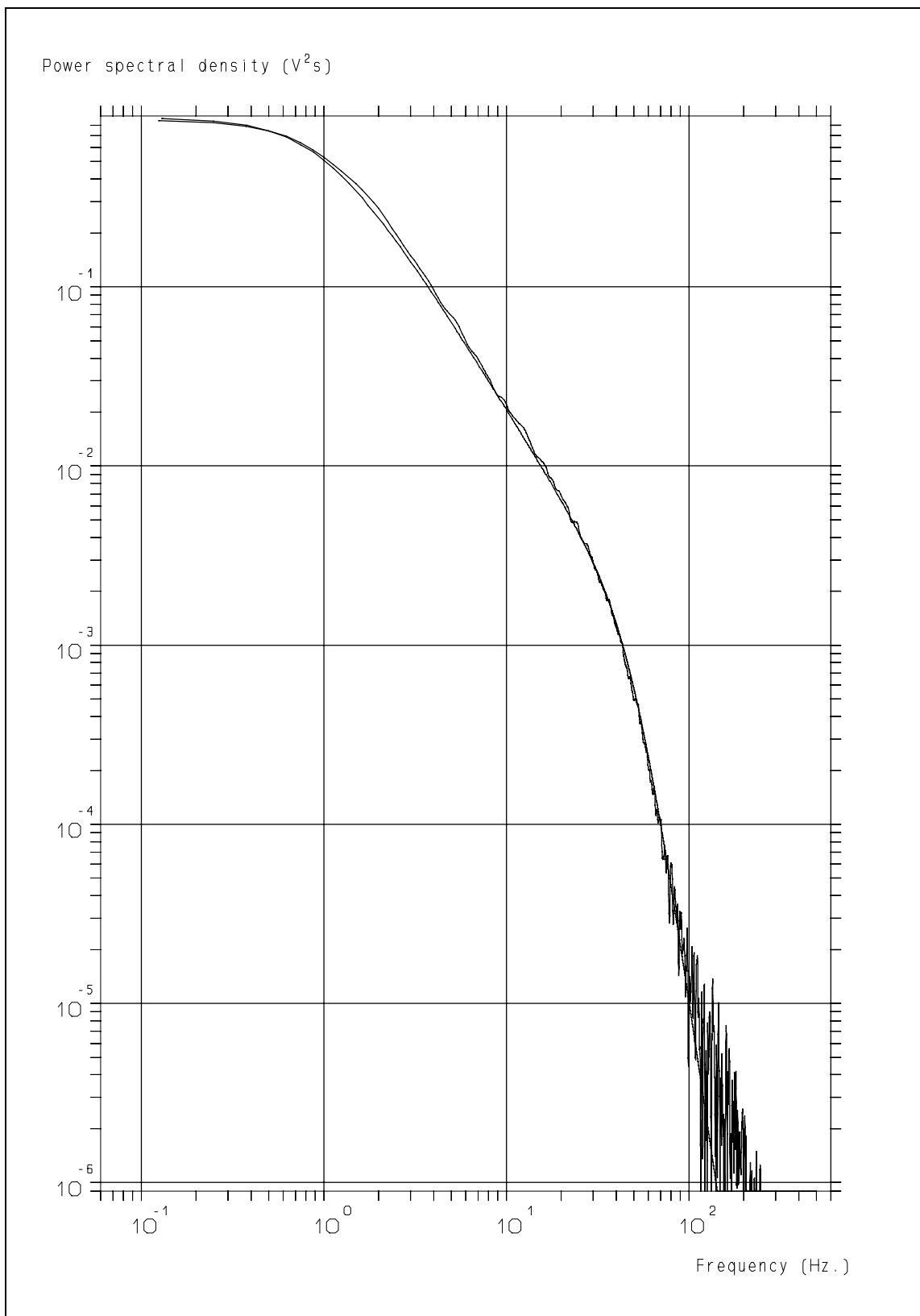


**Figure 12.1:** Power spectrum derived from the cross covariance function of first-order Kalman reconstructed turbulence ( $3 \cdot 10^5$  samples, wiggly at bottom) and the theoretical Bessem spectrum.

## 12. Extended reconstruction of turbulent velocity fluctuations

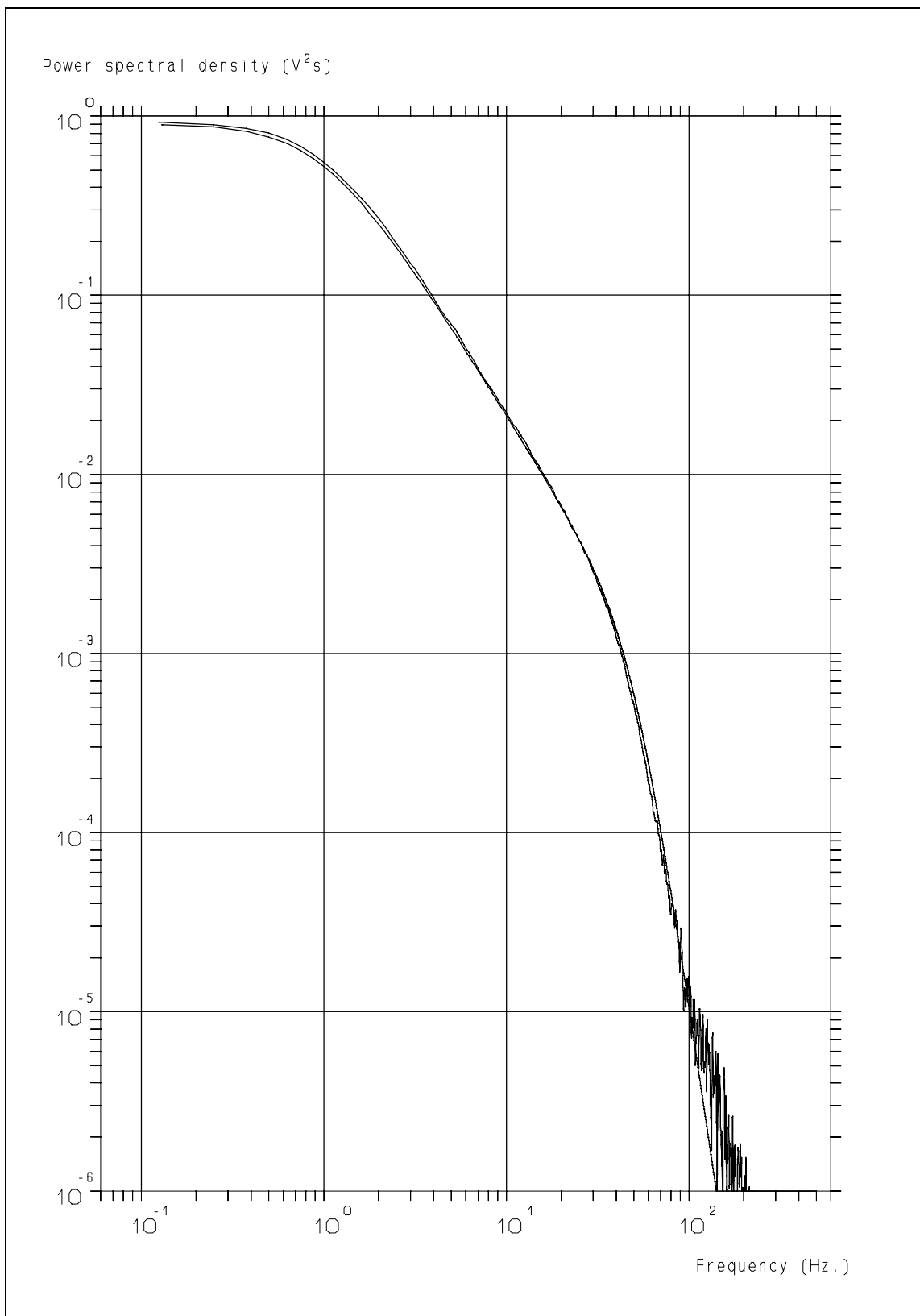


**Figure 12.2:** Power spectrum derived from the cross covariance function of first-order Kalman reconstructed turbulence ( $10^6$  samples, wiggly at bottom) and the theoretical Bessem spectrum.

*Retrieval of turbulence and turbulence properties from LDA data with noise*

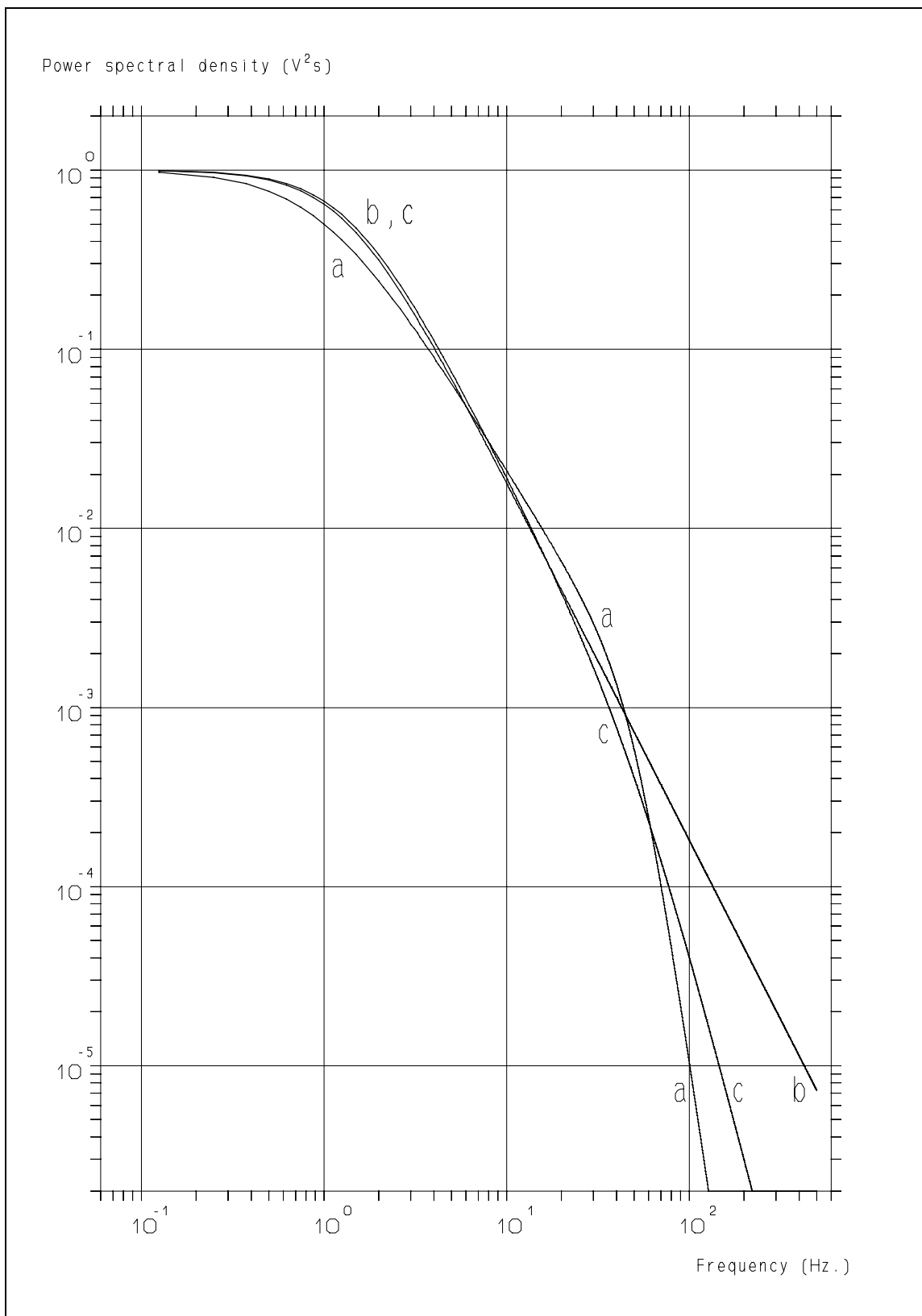


**Figure 12.3:** Spectra of "Bessem" turbulence (trace a), first-order (trace b) and second-order (trace c) Kalman reconstruction filters.

## 12. Extended reconstruction of turbulent velocity fluctuations

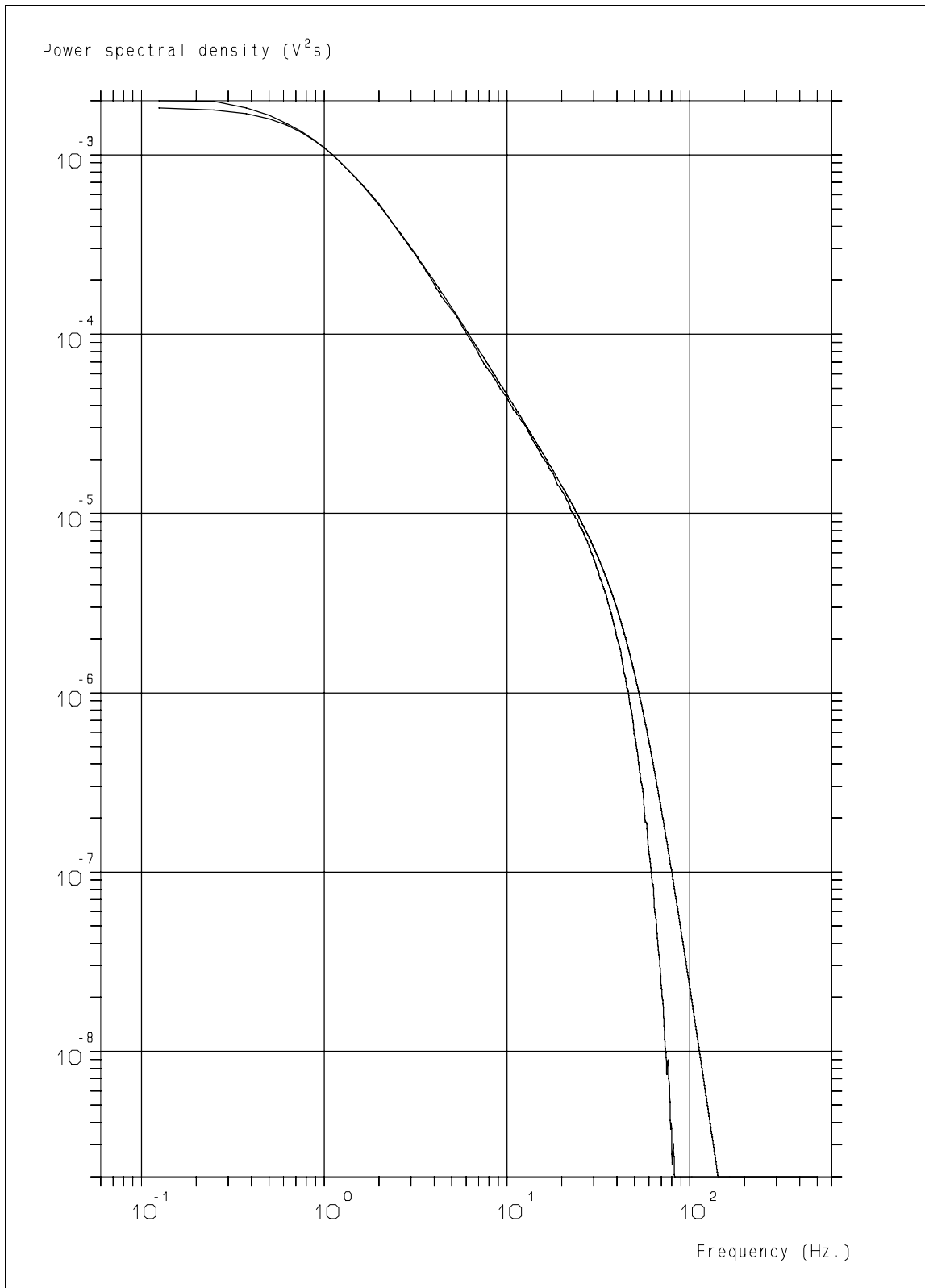


**Figure 12.4:** Power spectrum obtained using the optimum filter gain of the second-order Kalman reconstruction filter and the cross covariance technique (lower trace) and the theoretical Bessem spectrum.

*Retrieval of turbulence and turbulence properties from LDA data with noise*

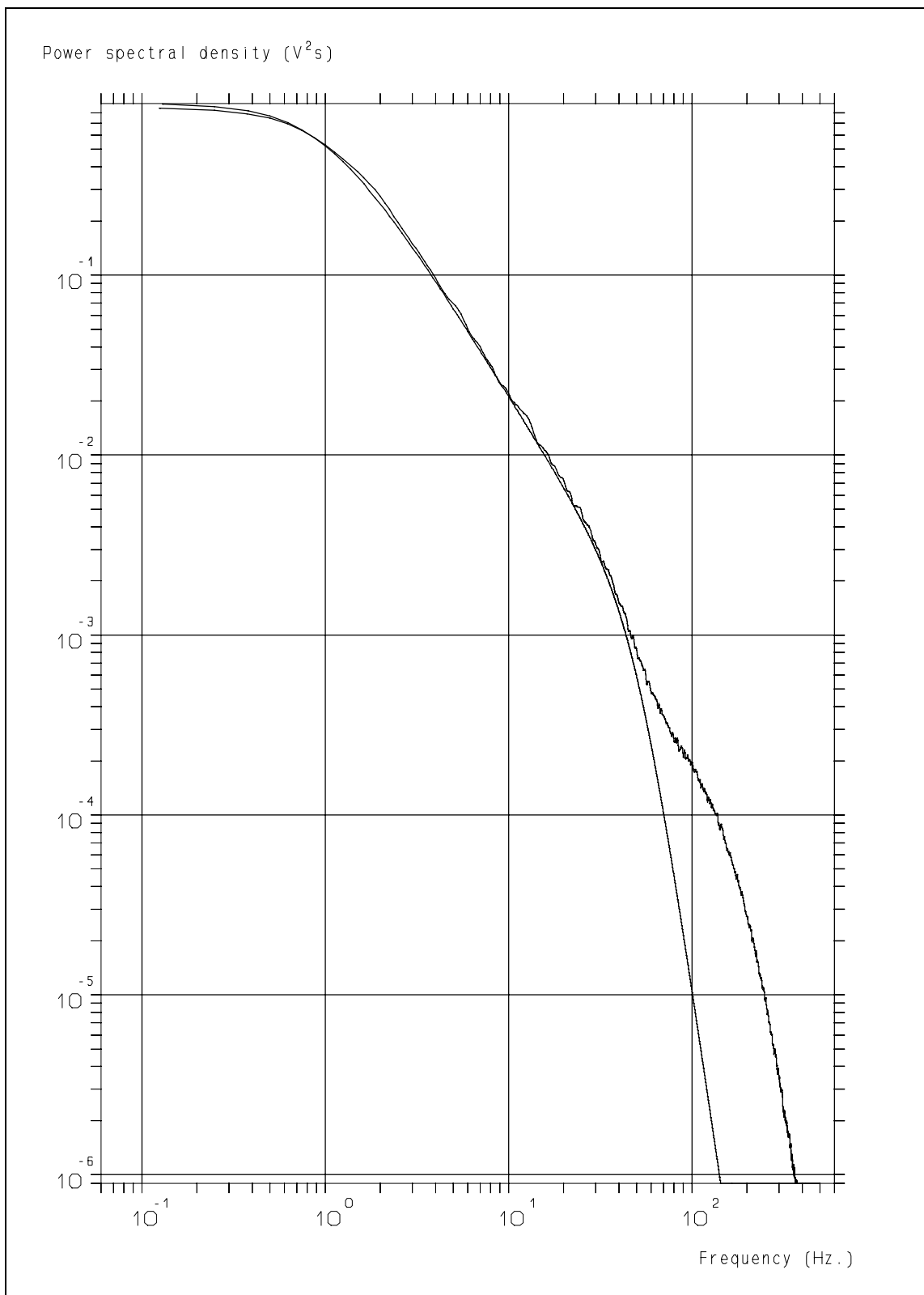


**Figure 12.5:** Power spectrum derived from the auto covariance function of first-order Kalman reconstructed turbulence (upper trace,  $3 \cdot 10^5$  samples, data-rate = 500 Hz) and the theoretical Bessem spectrum.

## 12. Extended reconstruction of turbulent velocity fluctuations

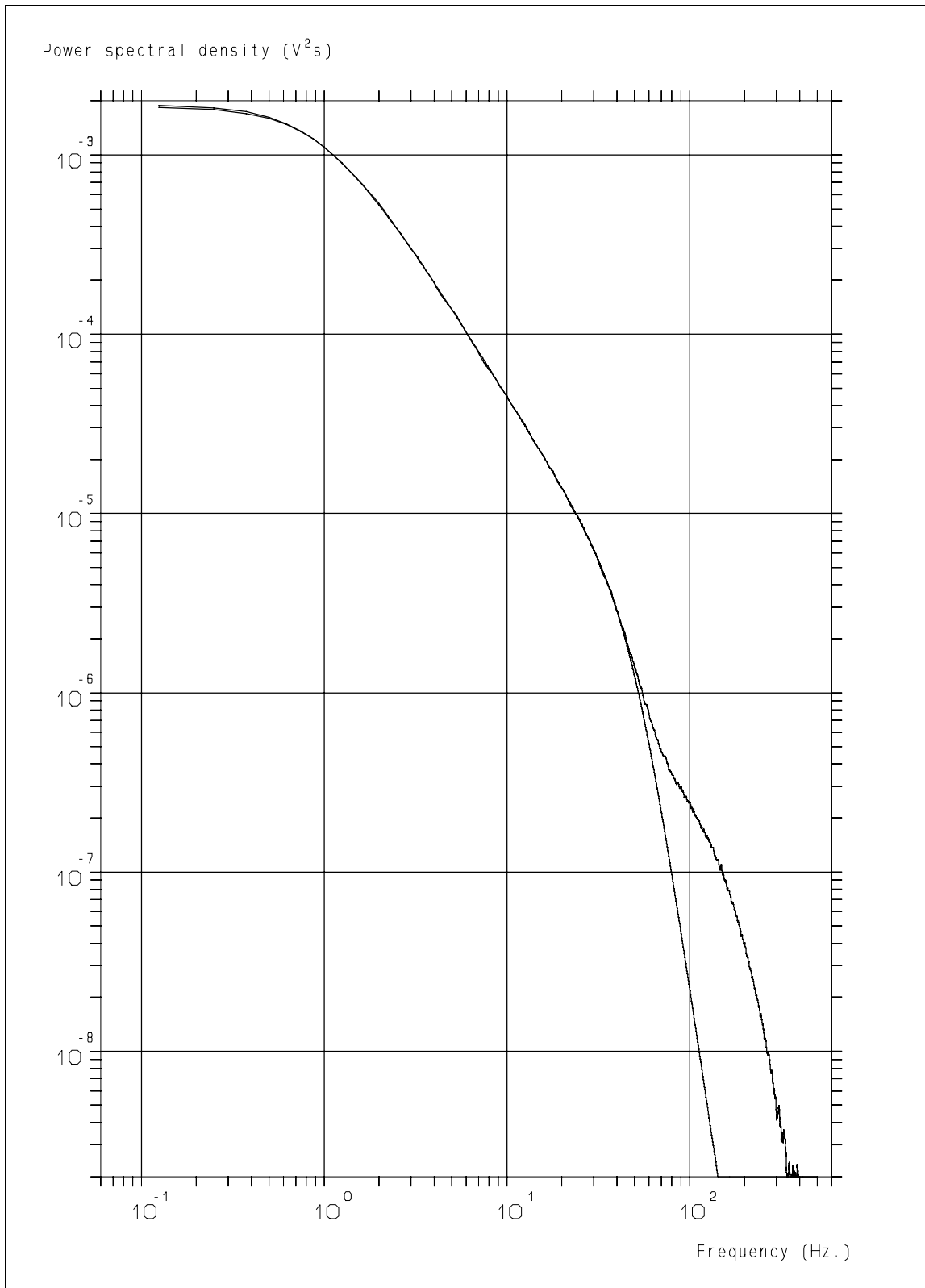


**Figure 12.6:** Power spectrum derived from the AVF of the *average* of two first-order Kalman reconstructed velocity traces (upper trace, data-rate = 500 Hz; compare with fig, 12.5) and the theoretical Bessem spectrum.

*Retrieval of turbulence and turbulence properties from LDA data with noise*

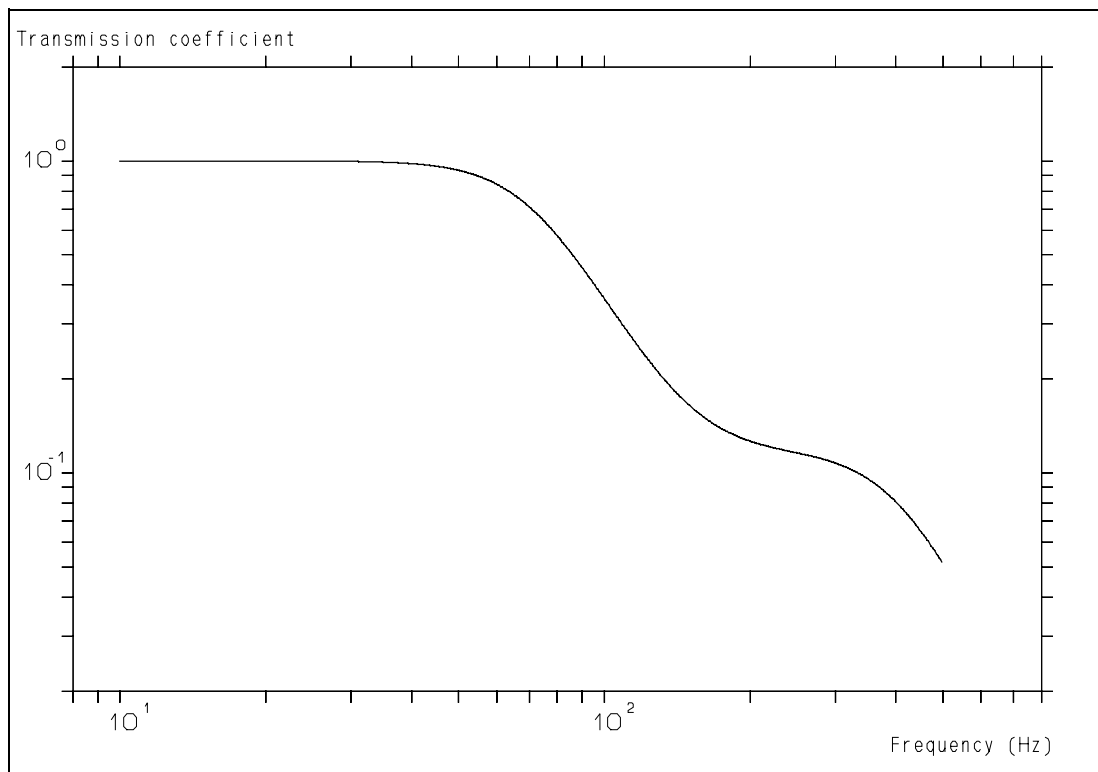


**Figure 12.7:** Characteristic of an extended reconstruction filter.  $f_1 = 151$  Hz,  $f_2 = 70$  Hz,  $f_3 = 395$  Hz and  $m = 5.6$

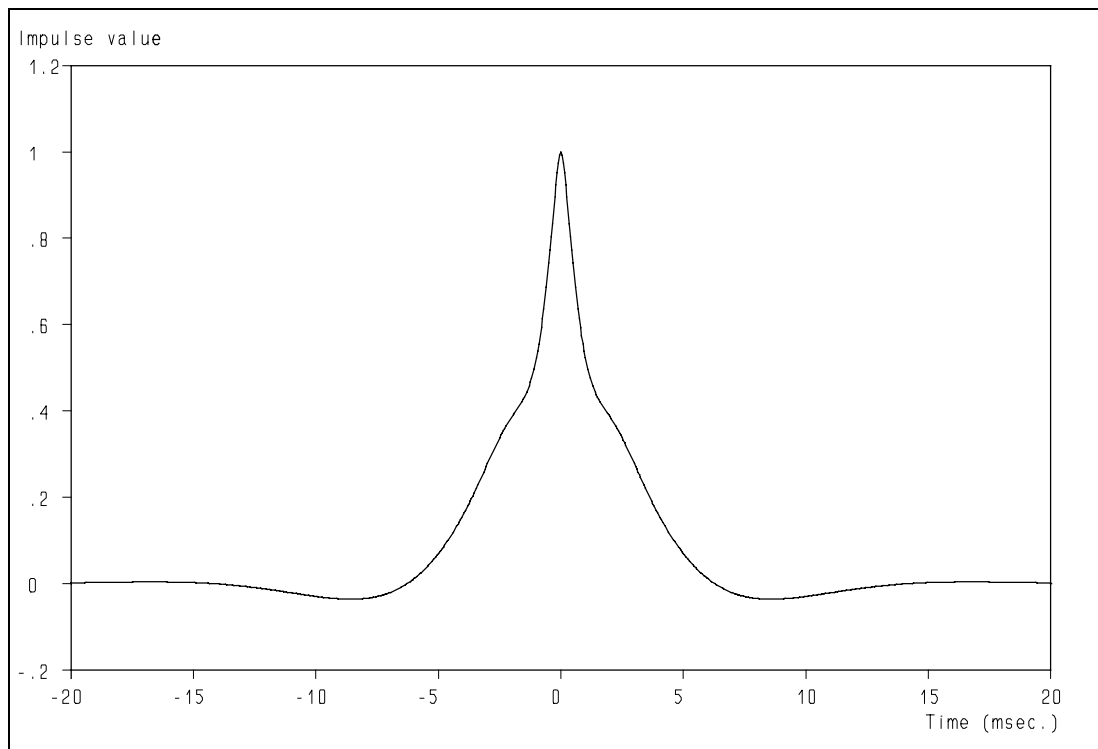


**Figure 12.8:** Impulse response of the extended reconstruction filter of fig. 12.7.

12. Extended reconstruction of turbulent velocity fluctuations

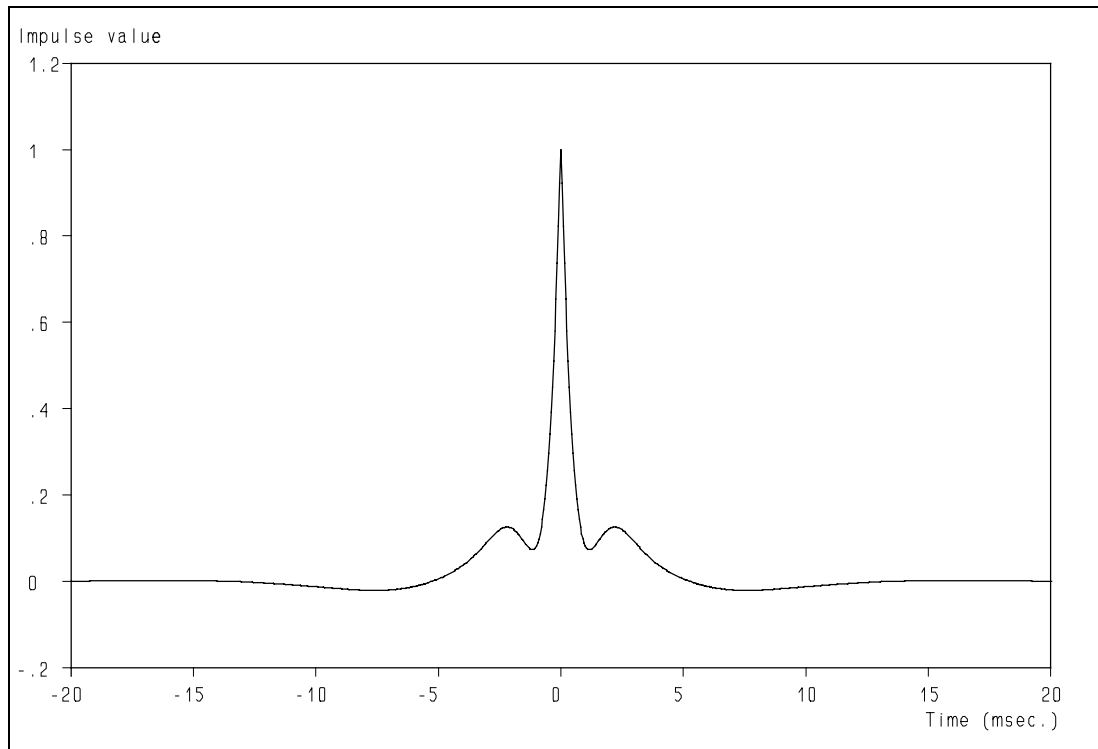
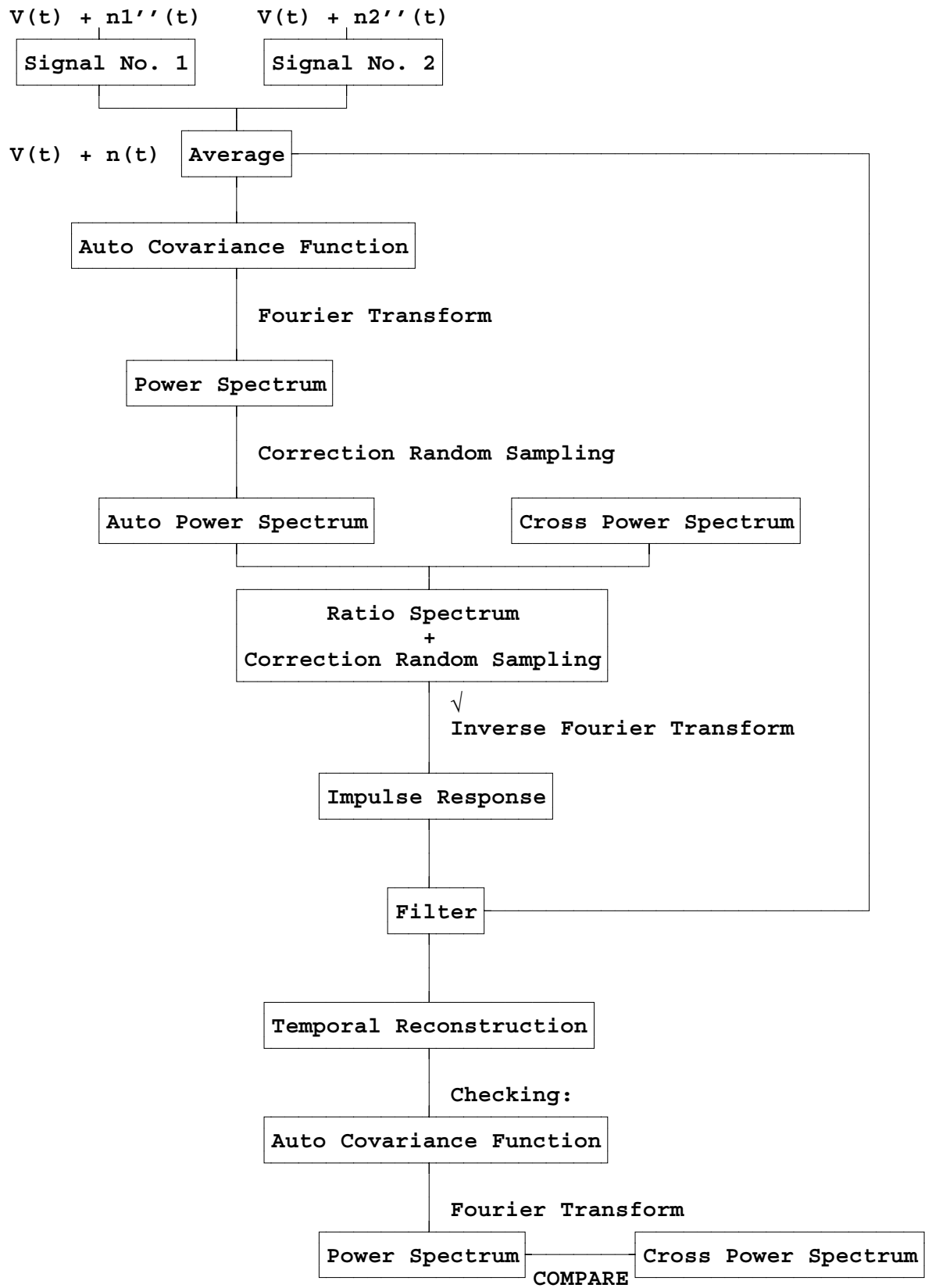


**Figure 12.9:** As fig. 12.8, but after correction for the particle rate filtering.

### Data Processing II



## 12. Extended reconstruction of turbulent velocity fluctuations

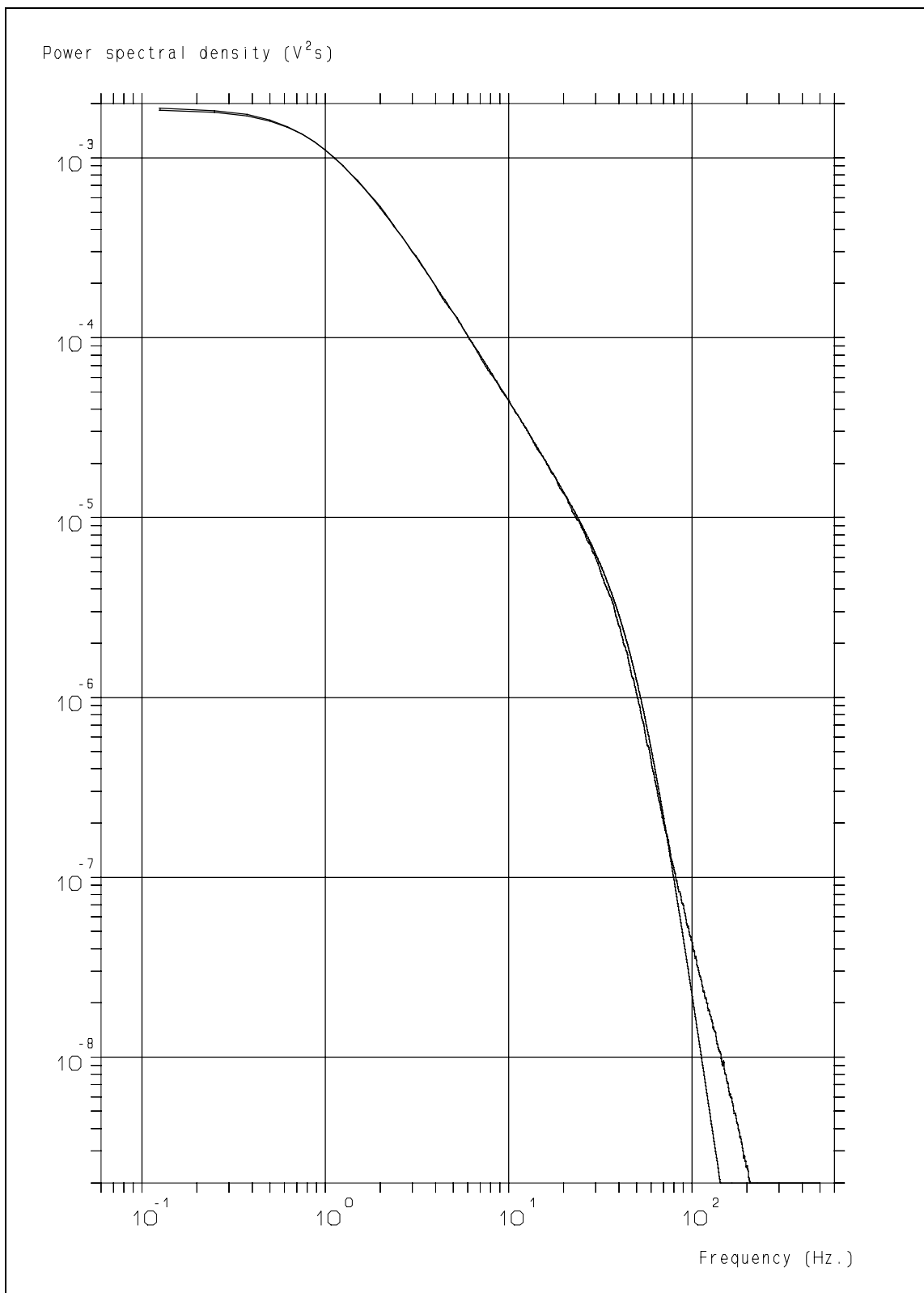


**Figure 12.10:** Power spectrum derived from the AVF of the filtered version of the average of two Kalman reconstructed velocity traces (upper trace, data-rate = 500 Hz) and the theoretical Bessem spectrum.

*Retrieval of turbulence and turbulence properties from LDA data with noise*

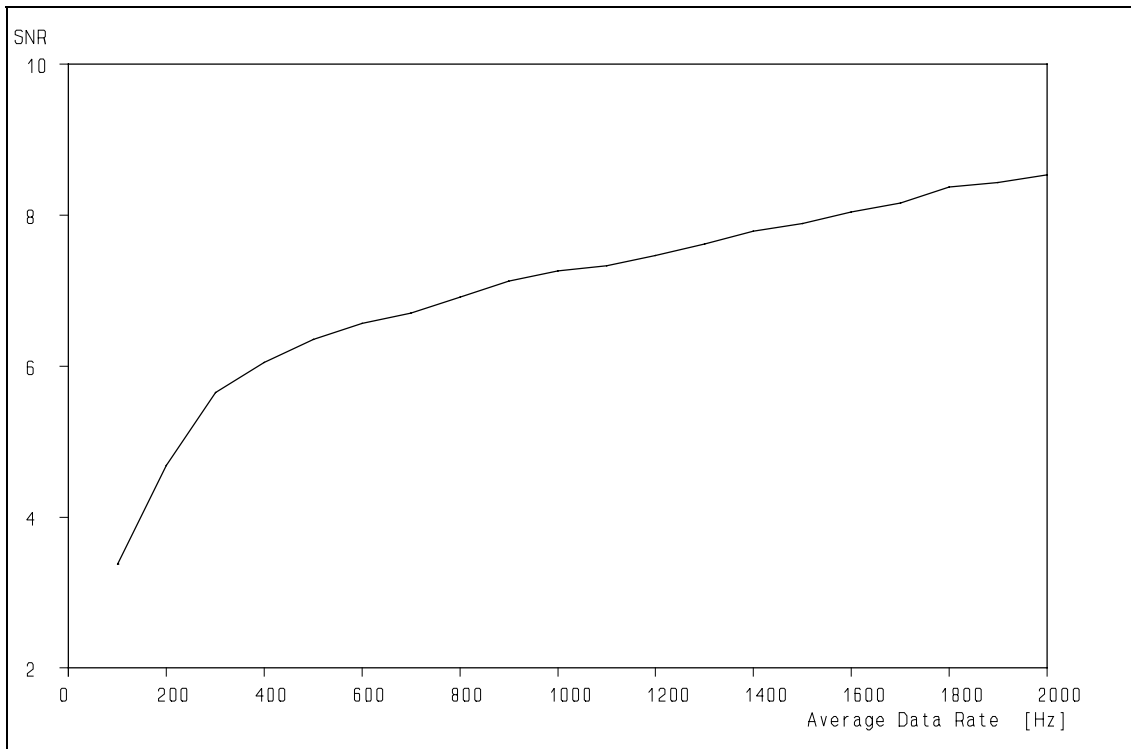


**Figure 12.11:** The input signal for the Kalman reconstruction filter has an SNR which depends on the average data-rate due to the noise reduction properties of the pre-processor, described in Chapter 8.

## 12. Extended reconstruction of turbulent velocity fluctuations

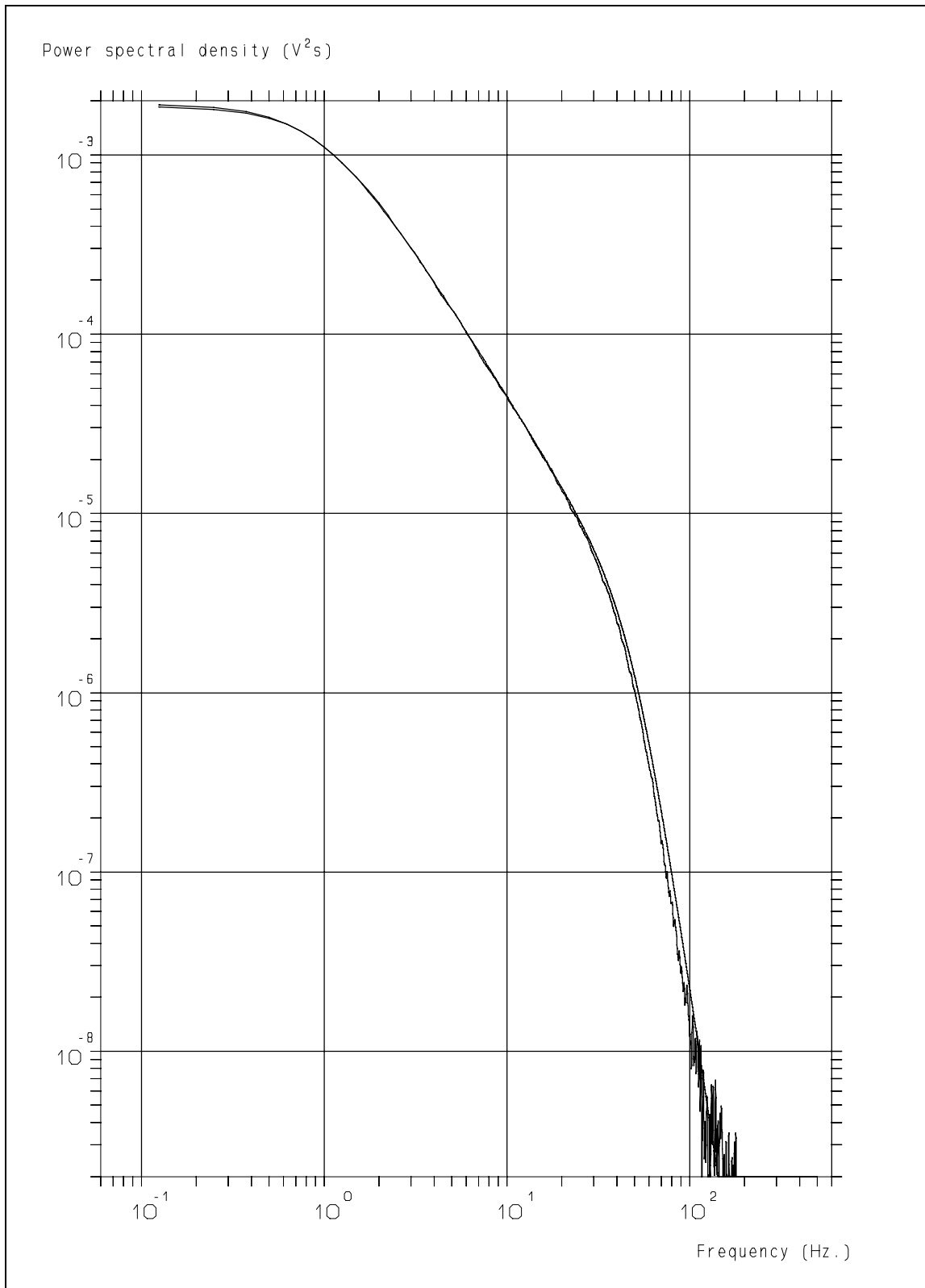


**Figure 12.12:** Power spectrum derived from the cross covariance function of two Kalman reconstructed velocity traces (data-rate = 1 kHz, wiggly at bottom) and the theoretical Bessem spectrum.

*Retrieval of turbulence and turbulence properties from LDA data with noise*

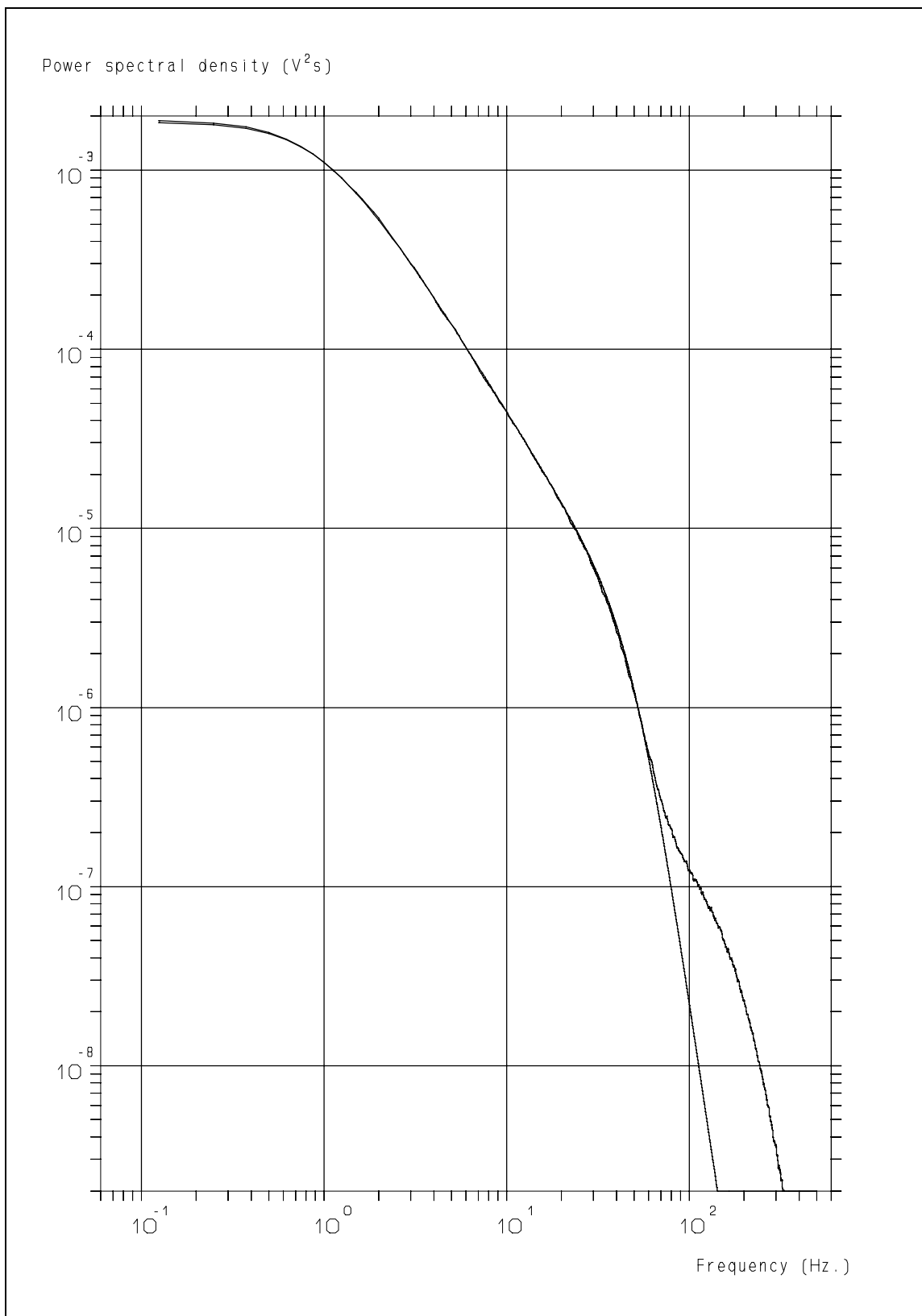


**Figure 12.13:** Power spectrum derived from the AVF of the average of two Kalman reconstructed velocity traces (upper trace, data-rate = 1 kHz) and the theoretical Bessem spectrum.

## 12. Extended reconstruction of turbulent velocity fluctuations

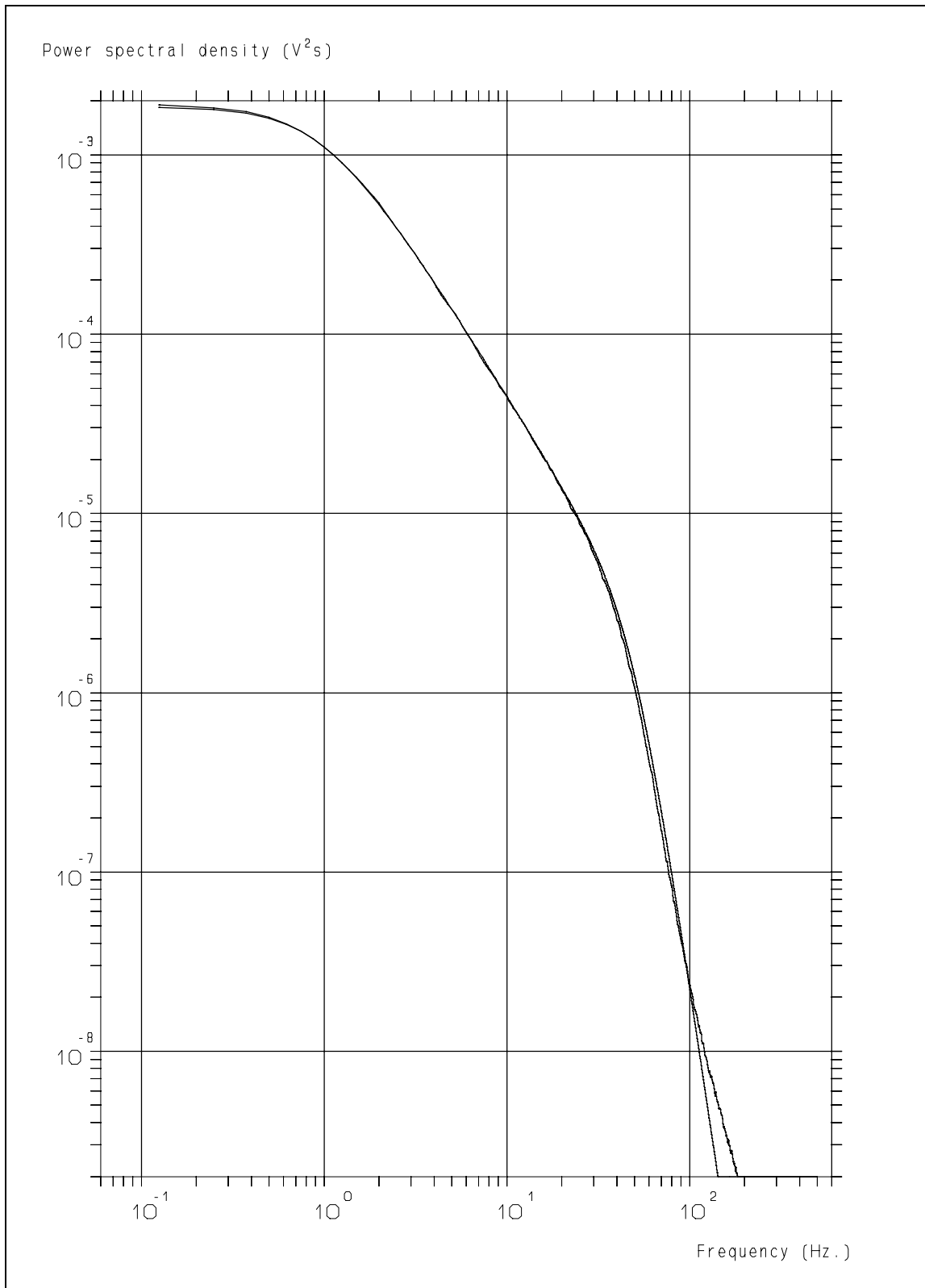


**Figure 12.14:** Power spectrum derived from the AVF of the filtered version of the average of two Kalman reconstructed velocity traces (upper trace, data-rate = 1 kHz) and the theoretical Bessem spectrum.

*Retrieval of turbulence and turbulence properties from LDA data with noise*

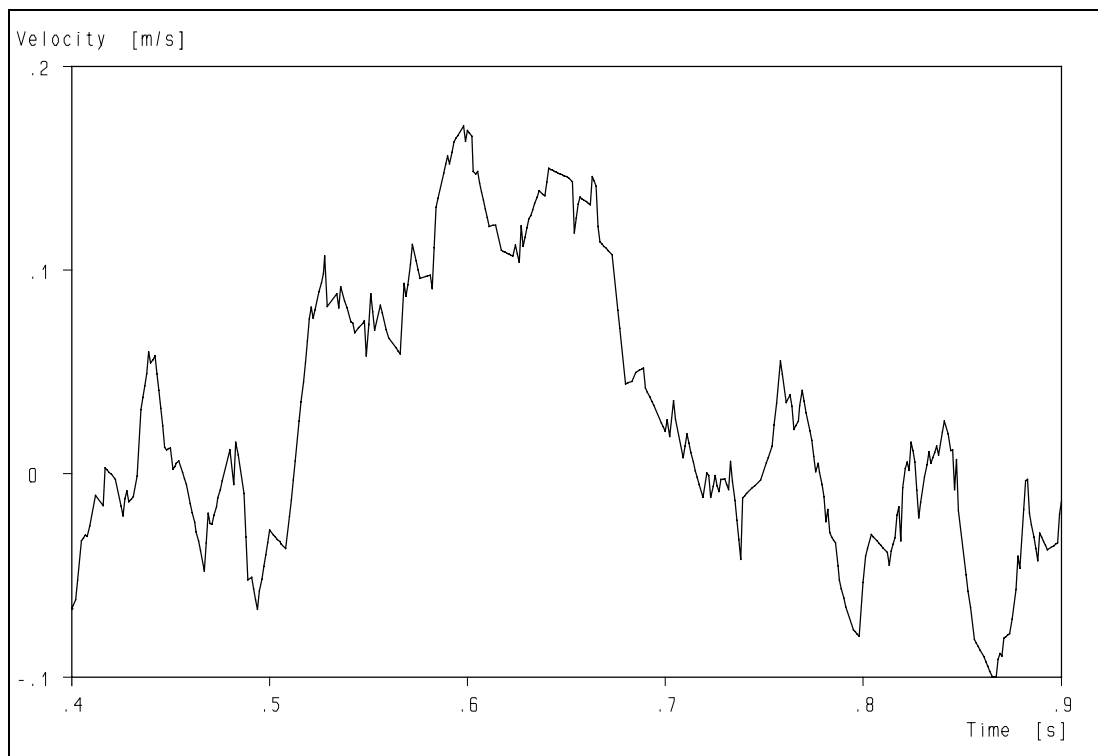


**Figure 12.15:** Velocity trace after linear interpolation at 1 kHz.

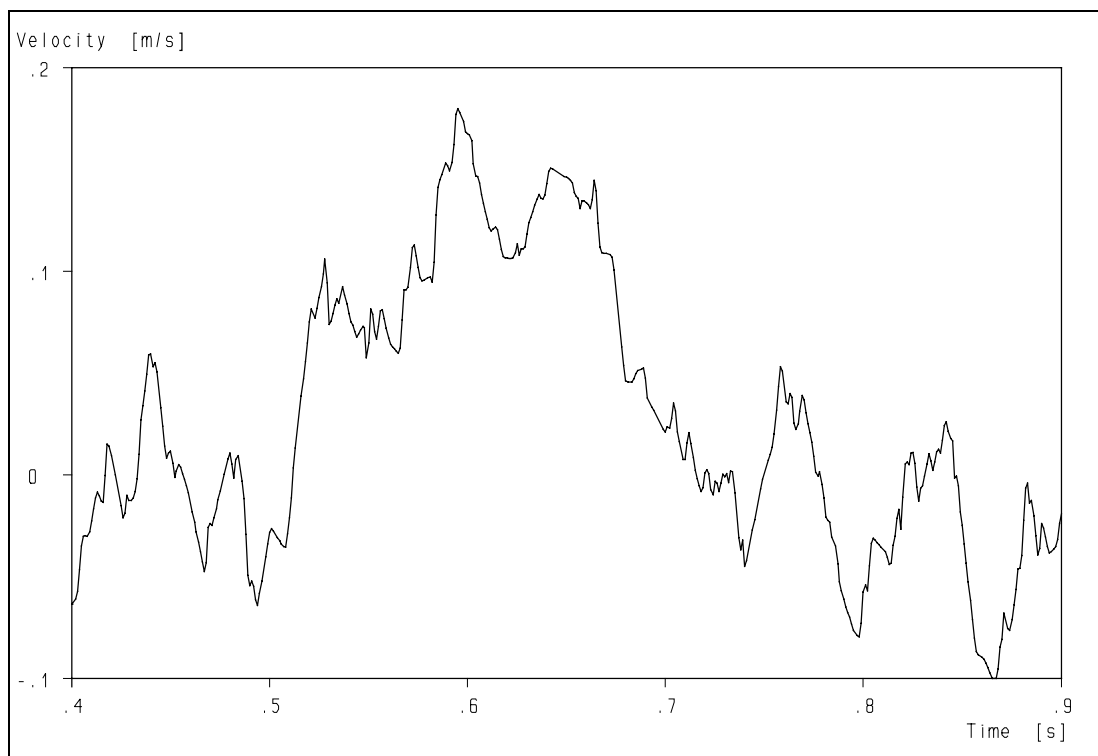


**Figure 12.16:** Velocity trace after linear interpolation at 10 kHz and using a Gaussian anti-aliasing filter, as described in Chapter 8.

## 12. Extended reconstruction of turbulent velocity fluctuations

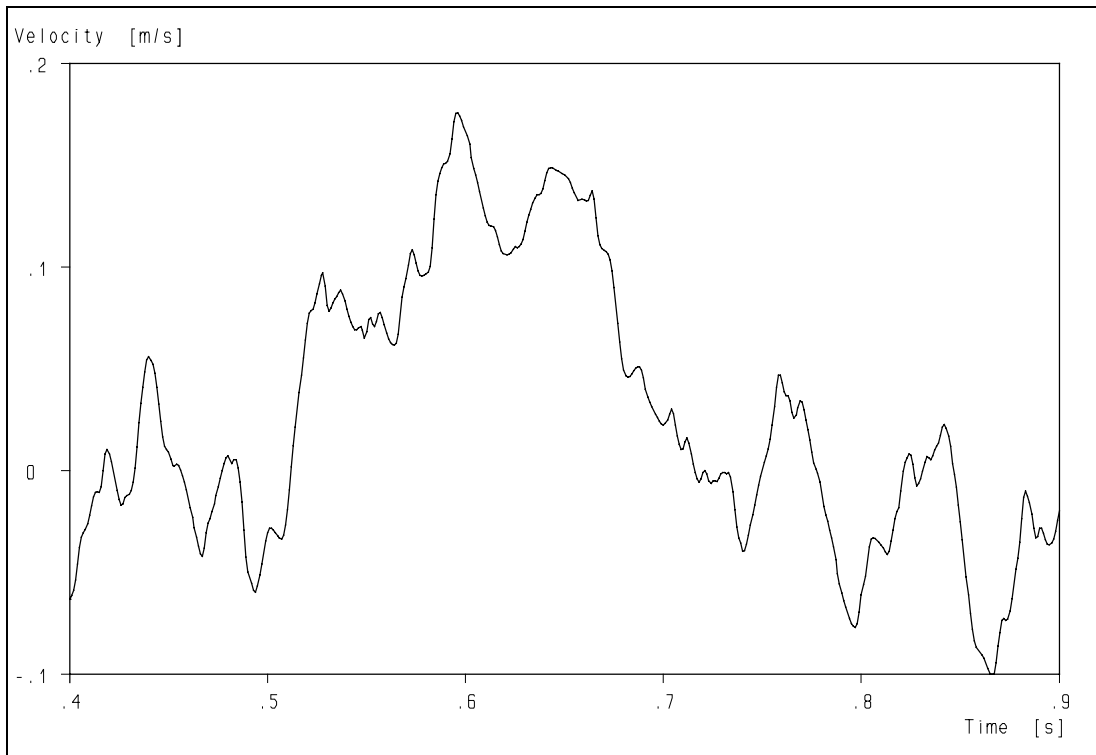


**Figure 12.17:** Velocity trace after first-order Kalman reconstruction.

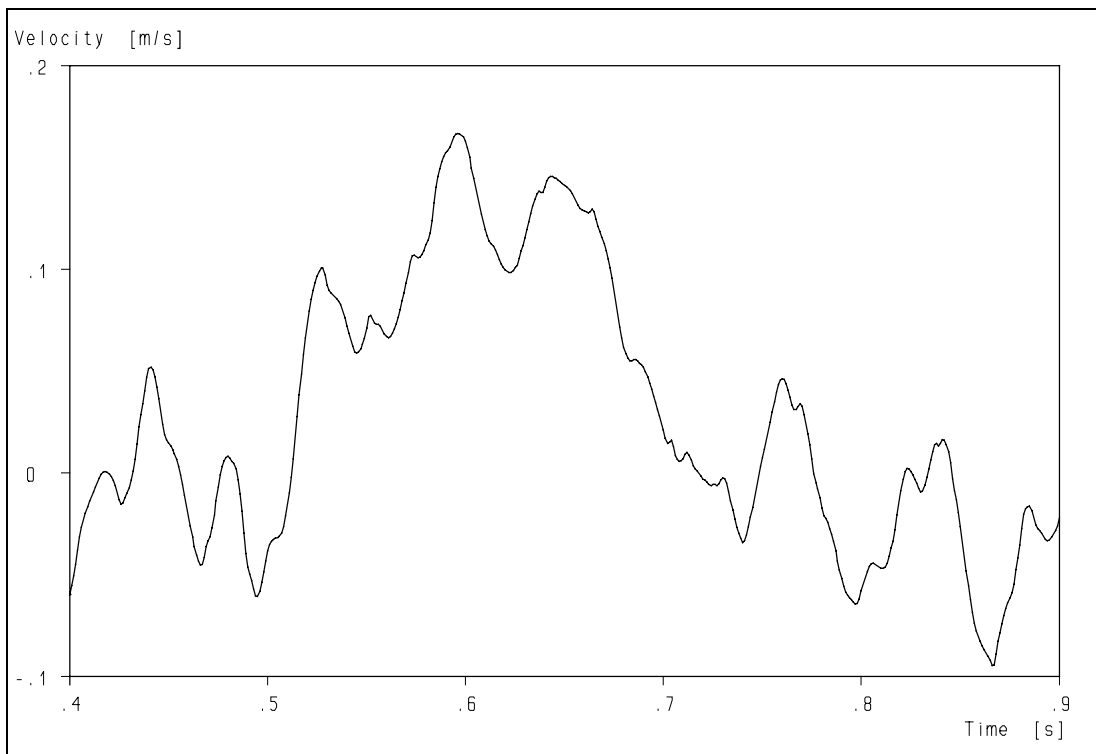


**Figure 12.18:** Extended reconstruction filtering applied to the average of two first-order Kalman reconstructed velocity traces.

*Retrieval of turbulence and turbulence properties from LDA data with noise*

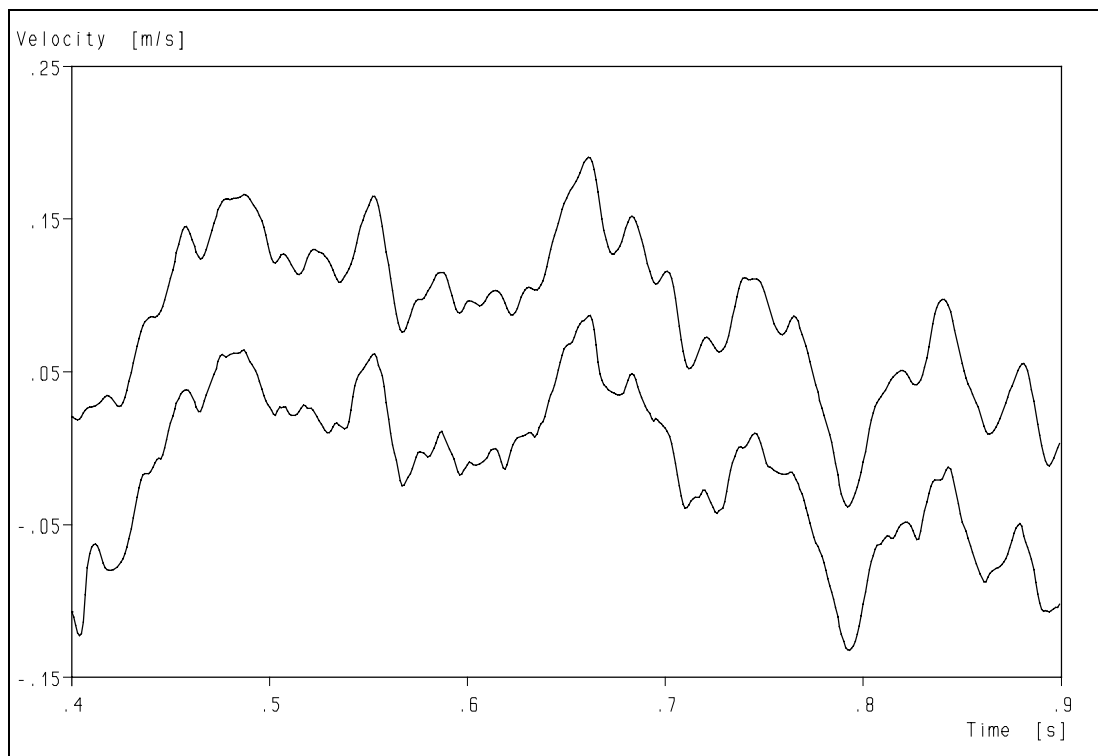


**Figure 12.19:** Simulated turbulence (upper curve) and reconstructed turbulence (lower curve); data-rate = 500 Hz.

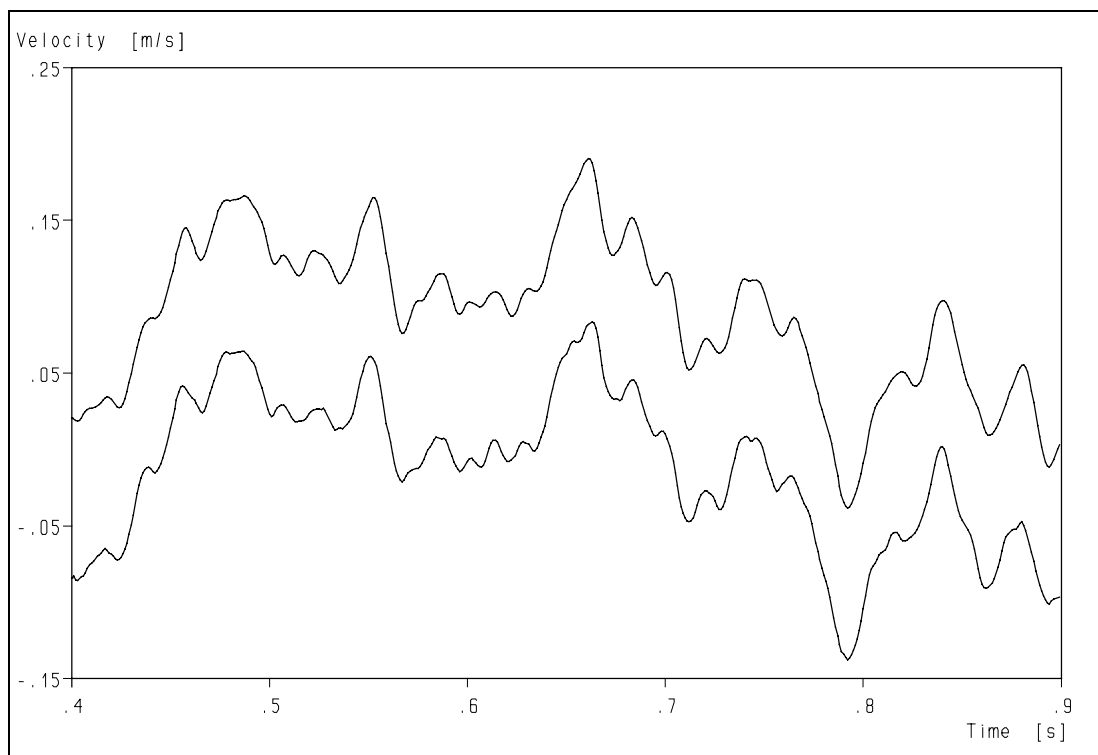


**Figure 12.20:** Simulated turbulence (upper curve) and reconstructed turbulence (lower curve); data-rate = 1 kHz.

## 12. Extended reconstruction of turbulent velocity fluctuations

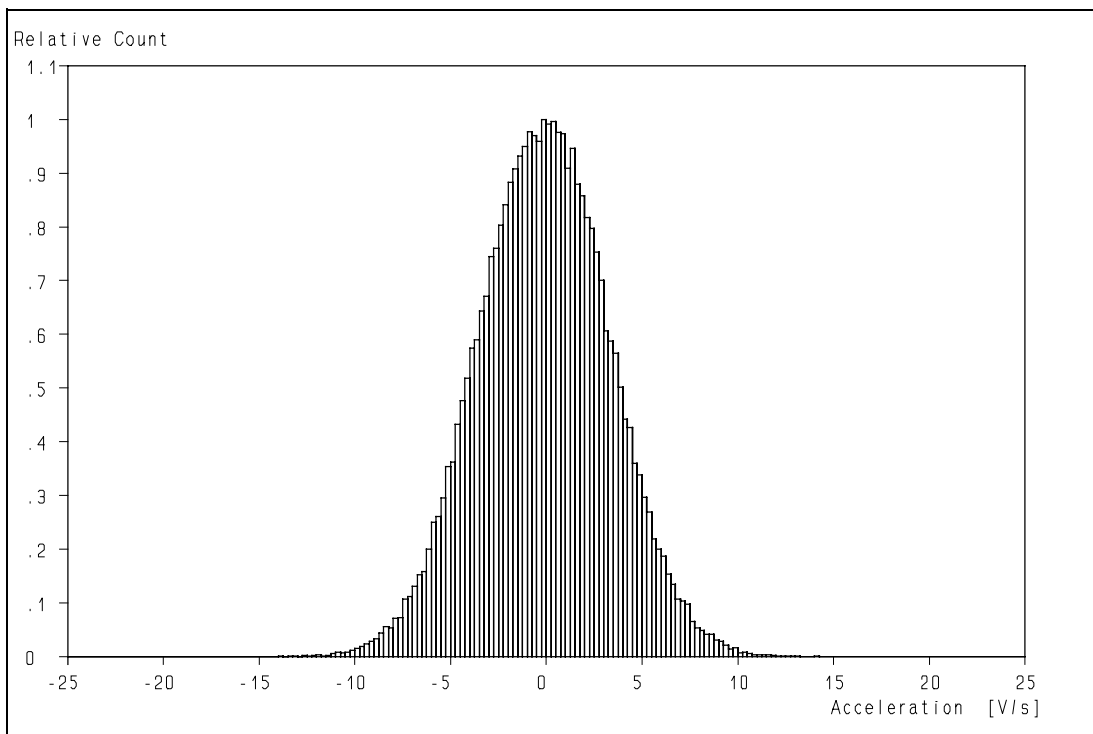


**Figure 12.21:** Histogram of the accelerations derived from the simulated turbulence.

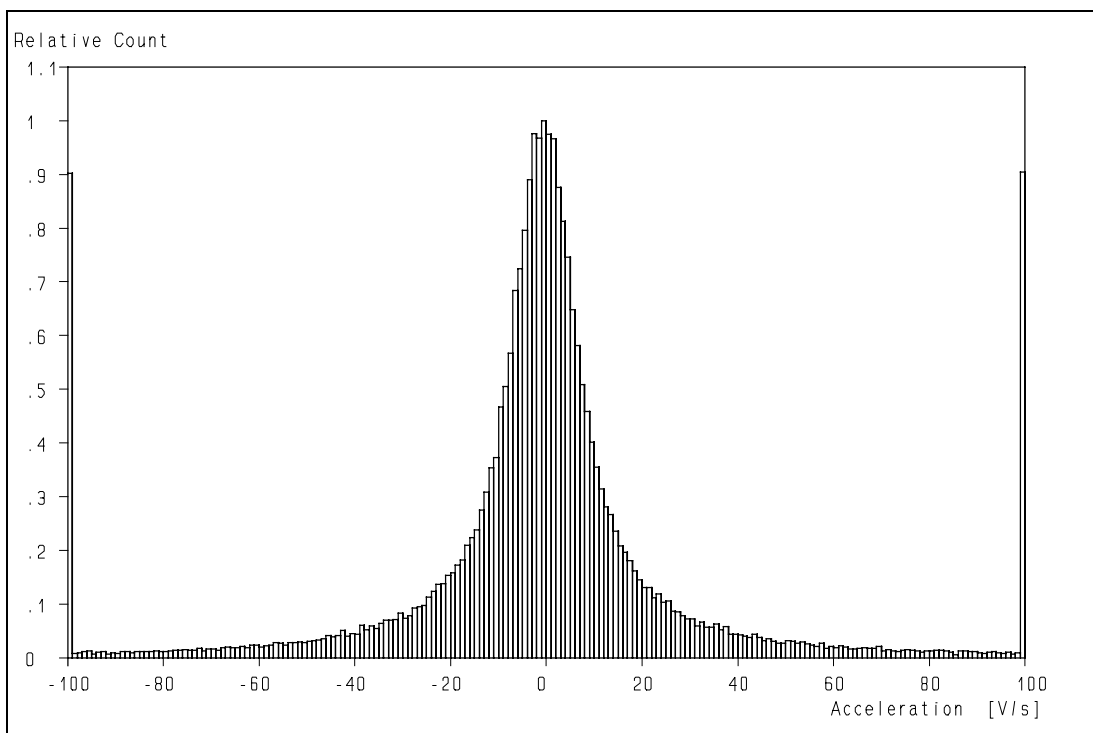


**Figure 12.22:** Histogram of the accelerations derived from the randomly sampled turbulence. Note the horizontal scale compared to fig. 12.21!

*Retrieval of turbulence and turbulence properties from LDA data with noise*

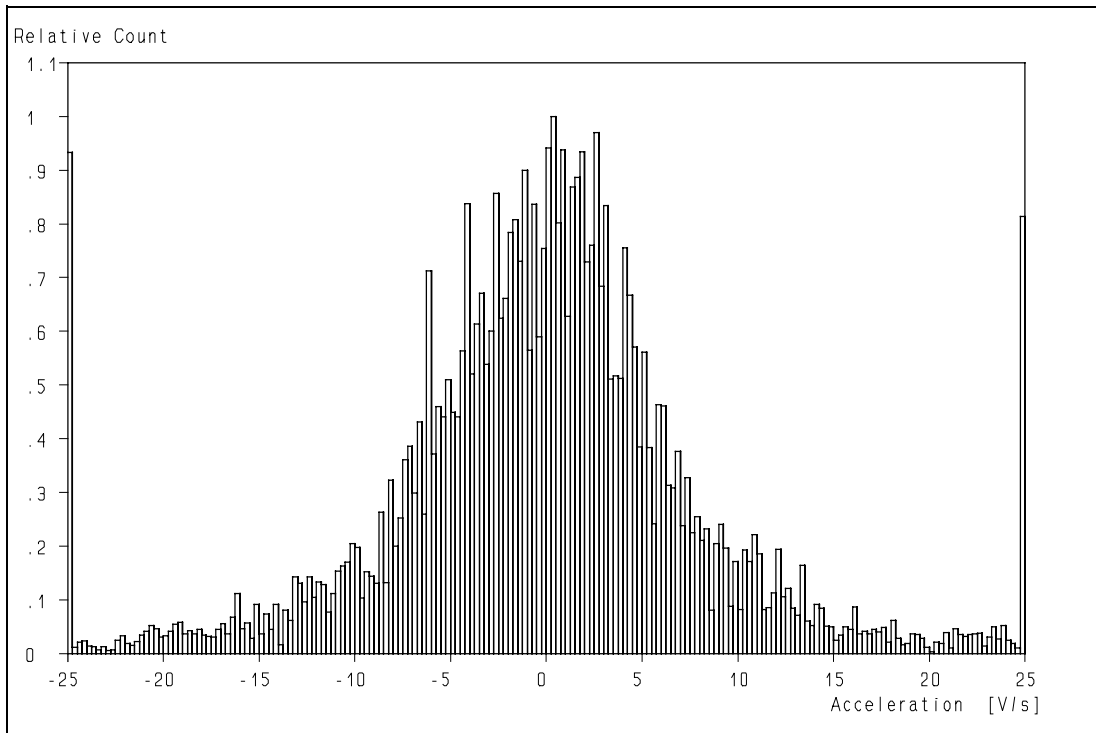


**Figure 12.23:** Histogram of the accelerations derived from the interpolated turbulence.

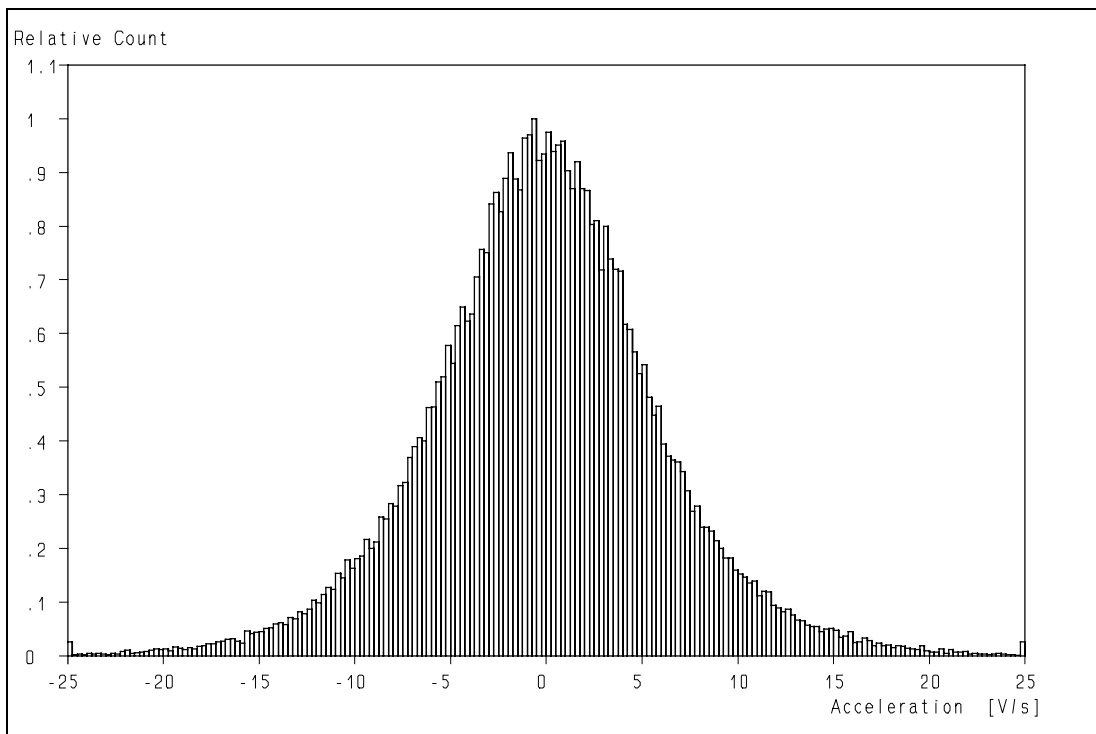


**Figure 12.24:** Histogram of the accelerations derived from the first-order reconstructed turbulence.

## 12. Extended reconstruction of turbulent velocity fluctuations

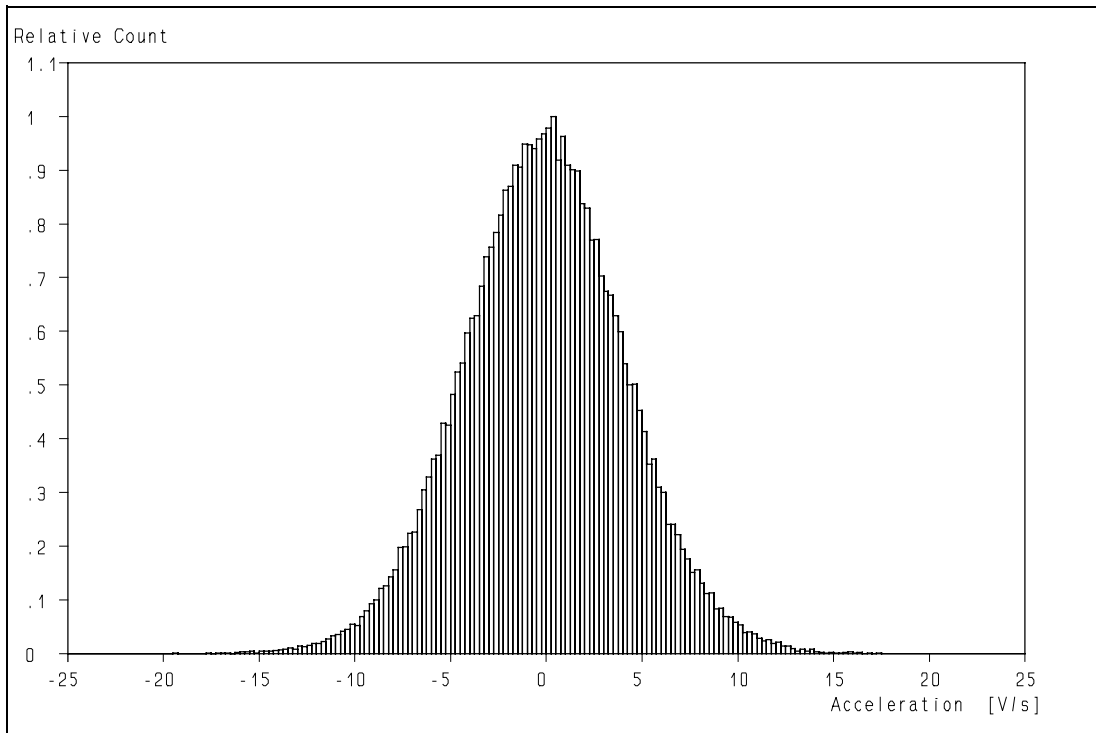


**Figure 12.25:** Histogram of the accelerations derived from the first-order Kalman reconstructed turbulence.

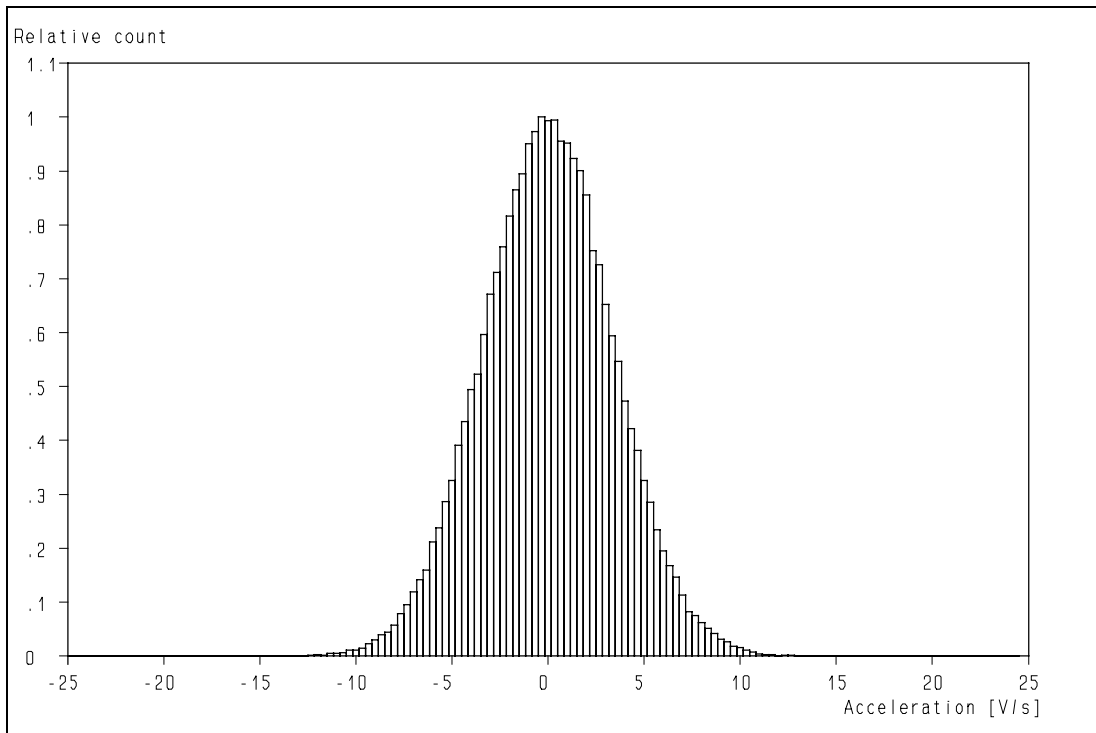


**Figure 12.26:** Histogram of the accelerations derived from the first-order Kalman and extended reconstruction filtering.

# Chapter 13

## Conclusions

*Real life is, to most man,  
a perpetual compromise  
between the ideal and the possible.*  
Bertrand Russell

Based on the results, presented in this thesis, several conclusions can be drawn:

1. Noise is inevitable in Laser-Doppler Anemometry (LDA). Although optimisation is possible (or rather required), there will still be a noise contribution to the individual velocity estimators. Any data-processing technique has to take this into account in order to obtain the required turbulence properties correctly.
2. The noise in the Doppler signal is basically responsible for the noise contribution to the individual velocity estimators, both in the value of the velocity *and* the arrival time. Especially the latter is often disregarded, but plays an essential part in the data-acquisition.
3. Monte-Carlo simulations are an essential tool in analyzing and understanding the different error (noise) sources in Laser-Doppler Anemometry. Especially the possibility to separate different effects is advantageous. It is also essential for the development and verification of novel data-processing techniques because only with simulated signals the input and output data can be compared directly.
4. Diagnostic tools are used too little for determining the quality of the raw LDA data. This leads to erroneous conclusions, drawn from inferior data-sets. Also, these diagnostic tools can help novices in the field of LDA measurements to improve their results and to optimise the measurement chain. Including information on the diagnostics of the LDA data in publications would enable readers to make an assessment of the quality of the data and thus of the results presented.
5. The Wavelet Transform proves to give better estimates of both the velocity and the arrival time of the Doppler signal than any of the other Doppler signal processing techniques in use today. It seems likely that the Wavelet Transform gives optimum estimators under the given conditions, but this has not (yet) been proven. In the worst case, the estimators will be close to this optimum.
6. For the purpose of velocity signal reconstruction, the data-rate should be at least equal to or higher than  $2\pi$  times the highest frequency present in the turbulence due to the particle rate filtering. This is caused by the creation of correlation by the reconstruction. While this value holds for S&H and first-order reconstruction which limit the correlation to the adjacent data point, other schemes which use more data-points simultaneously might require a higher data-rate.
7. The cross-covariance technique does not only reduce the noise level in the turbulence power spectrum, but also gives the correct estimator for this spectrum. The availability of two independent signals is also attractive for the extended velocity signal reconstruction, as the averaging of the two signals increases the Signal-to-Noise ratio by a factor of  $\sqrt{2}$ .
8. The use of all the information, available in the raw LDA data, improves the quality of the estimators derived from it. This can be achieved by the combination of a high re-sampling rate with the digital low-pass filtering for velocity signal reconstruction and by estimation of the auto correlation function

## *Retrieval of turbulence and turbulence properties from LDA data with noise*

by use of the slotting technique. With both techniques the error in the arrival time is of importance as this also determines the accuracy of the derived estimators.

9. The estimator for the auto correlation function on the basis of the slotting technique with Local Normalisation enables the retrieval of information on the small eddies below the noise level. Although there is no basic data-rate requirement (as for velocity signal reconstruction), a very low data-rate results in a low number of products per slot, thus increasing the variance in the estimator.
10. The approximation of the turbulence power spectrum by an analytical spectrum that can be described by a small (6) amount of parameters, enables estimation of the turbulence power spectrum below the noise level over a dynamic range of 6 decades with an error smaller than  $\pm 25\%$ . This is achieved by fitting the corresponding auto correlation function to the auto correlation function, obtained using the slotting technique with Local Normalisation. Because the data-rate criterion is circumvented, the spectrum can be estimated up to several times the data-rate and up to 10 - 15 times the particle rate cut-off frequency. This approach has created a practical solution for a problem that has been around since the beginning of LDA measurements. The value of this approach has been confirmed in a "benchmark" comparison with other techniques.
11. Velocity signal reconstruction is an attractive option for the use of LDA in more fundamental turbulence research. This can be achieved by using known properties of turbulence in combination with the specific properties of LDA data and "noise-free" turbulence power spectra. To obtain this, the only assumption that needed to be made was that the accelerations are finite. All the other information that is required can be retrieved from the LDA data itself. Because of the attractive properties of LDA (non-intrusive, no limitation to turbulence intensity, linearity and complete separation of the velocity components) it should be used more in complex flow fields for this purpose.
12. Although the novel data-processing techniques, described in this thesis, enable to retrieve more information than has been possible previously, these techniques still rely on the data they use as input. The quality of the results thus depends on the quality of the input data. Hence, one should strive for the highest possible quality of these data by optimisation of the whole measurement chain, from the light source via the light scattering in the measurement volume to and including the Doppler signal processor. This requires extensive operator experience and insight into the different mechanisms as many noise sources lay hidden in the complex data-generation and processing chain.
13. The data-rate is of great importance for the retrieval of the turbulence properties of the flow under investigation. When the slotting technique is applied, the variance of the correlation coefficient in the individual slots is directly related to the data-rate. When velocity signal reconstruction is applied, the data-rate determines the highest frequencies that can be reconstructed, determines the level of the "noise floor" in the power spectra (and thus the level of obscuration of smaller eddies) and determines the amount of turbulence energy, that is converted into noise. The low data-rates obtained with the use of modern LDA systems, are for the largest part responsible for the inferior results compared to the LDA systems in use in the years between 1973 and 1980.

*We conquer by continuing.....*  
George Matheson

# APPENDIX A

## Experimental evidence for the existence of velocity bias.

The one-dimensional velocity bias that has been introduced in some of the simulations, e.g. to determine the properties of the slotting algorithm with Local Normalisation, was severe. One-dimensional velocity bias does not occur in practice because all turbulent flows are three-dimensional. Therefore, it is likely to expect that in real measurement data velocity bias does occur, but to a lesser extent than has been used in the simulations. Most researchers agree upon the occurrence of velocity bias. However, some -though they are outnumbered- doubt its existence. So velocity bias is still a controversial topic in Laser-Doppler Anemometry. The discussions mainly concentrate on the *amount* of velocity bias and whether a correction is justified or not.

Besides velocity bias due to the spatial distribution of the tracer particles, other sources of velocity bias occur in LDA:

- Faster moving particles produce a shorter Doppler signal, reducing the possibility that the signals are detected and validated, which implies a bias towards *lower* velocities. This may partially counteract the effects from velocity bias.
- Faster moving particles also scatter less photons and thus both the amplitude and the quality of the Doppler signals is lower. This reduces the percentage that is detected and validated. Hence, this effect might also partially compensate for the effect of velocity bias.
- Usually higher velocities correspond to higher Doppler frequencies. In general all photodetectors will have a decreasing response with increasing frequency (low-pass filtering), thus reducing the Doppler signal strength and so reducing the percentage that is detected and validated. Hence, this effect enhances the partial compensation mentioned above.
- Turbulence is a three dimensional motion. The transport of the tracer particles is determined by all three components of the velocity vector. Hence all three components have to be measured simultaneously to calculate the transport velocity.
- At low data rates the bias will gradually be disconnected from the turbulence: the velocity fluctuations between two different sample times become averaged, because the distance between those sample points is larger than the size of the separate eddies. This is not the case for the average velocity itself.

The percentage of velocity bias is a measure of the correlation between the data-rate and the instantaneous velocity, 100% bias denotes a complete correlation, which could only occur in a one-dimensional flow without any counteracting effects as described above. In 1984 Adams (ref. 117) developed a simple method for bias detection.

The velocity range is divided in a number of bins. By plotting the interarrival time per velocity range an indication of the degree of correlation can be estimated. If the interarrival time decreases with increasing velocity, velocity bias occurs. Absil (ref. 67) showed that this method can only be used for high data densities,  $\Gamma/t_0 > 10$  in which  $1/t_0$  is the average data-rate and  $\Gamma$  is the integral time scale.

The Adams method will be used to demonstrate the occurrence -and thus the existence- of bias. We have analyzed a data-set measured in the jet of a stirrer in a mixing vessel. The turbulence intensity in such flows is high (> 50 %), thus there is a high probability of detecting velocity bias. The characteristic time  $t_0$  of the complete data set is 0.23 ms., as can be seen from the time interval distribution shown in fig. A.1, and the integral time scale is 7.30 ms. Fig. A.2 (lower trace) shows the auto correlation function (ACF) of this data-set when using the slotting technique with Local Normalisation. In the fig. A.3 - A.8 the time interval distributions are presented at different velocity

## Retrieval of turbulence and turbulence properties from LDA data with noise

ranges. The first bins of these distributions are empty because every processor has a dead time, i.e. time required to process a Doppler signal.

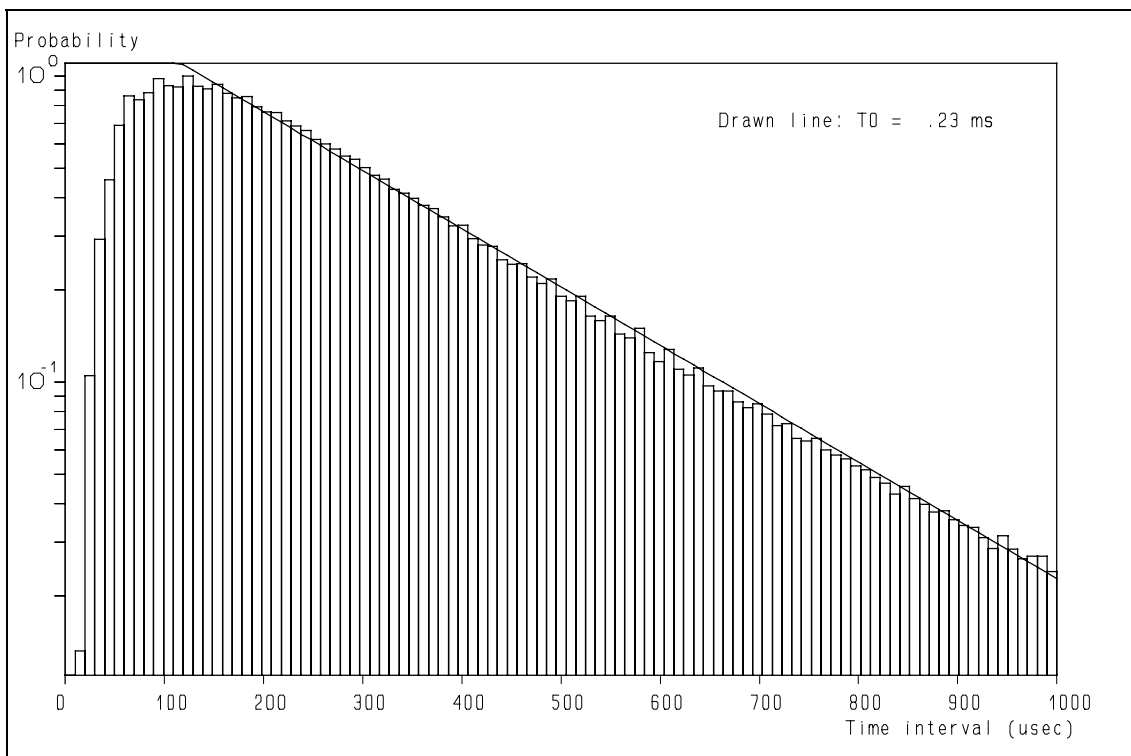
The results presented in table A.1 clearly show that velocity bias occurs, but as the data-rate is not proportional to the velocity range, at least some of the above mentioned compensating effects must occur as well. However, these measurement data clearly demonstrate that bias is a real phenomenon, and therefore corrections are required.

Fig. nr.	Velocity range [m/s]	$t_0$ [ms]
A.3	> 1.25	0.18
A.4	1.00 - 1.25	0.18
A.5	0.75 - 1.00	0.19
A.6	0.50 - 0.75	0.22
A.7	0.25 - 0.50	0.27
A.8	< 0.25	0.32

**Table A.1:** Characteristic time  $t_0$  at different velocity ranges.

Another demonstration of velocity bias can be obtained by analysis of the number of products in each slot. As has been shown in Chapter 4 on preliminary diagnostic testing of experimental data-sets, the number of products is *independent* of the time shift of the slot in the absence of velocity bias. This is in agreement with our simulations and experimental observations, as is illustrated in fig. A.9, which shows the number of products in each slot without bias and in fig. A.10, which shows the same for the experimental data-set under study.

Velocity bias thus occurs and can be demonstrated in experimental data-sets. The complexity of the phenomenon is, however, a severe problem for the determination of the required corrections. This has to be determined for each data-set separately by application of e.g. the methods used in this Appendix.



**Figure A.1:** Time interval distribution of the measured data file using all samples, independent of the velocity.

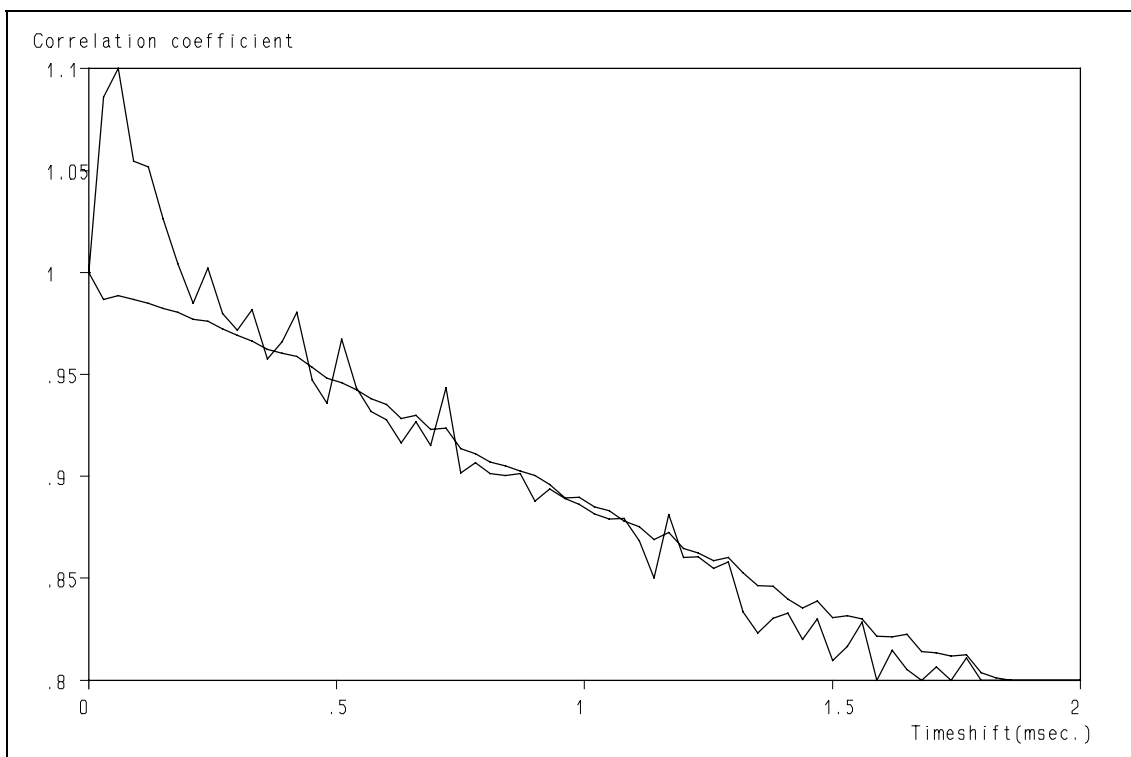


**Figure A.2:** Auto correlation functions of the experimental data-sets. The lower trace is obtained using the local normalisation.

Retrieval of turbulence and turbulence properties from LDA data with noise

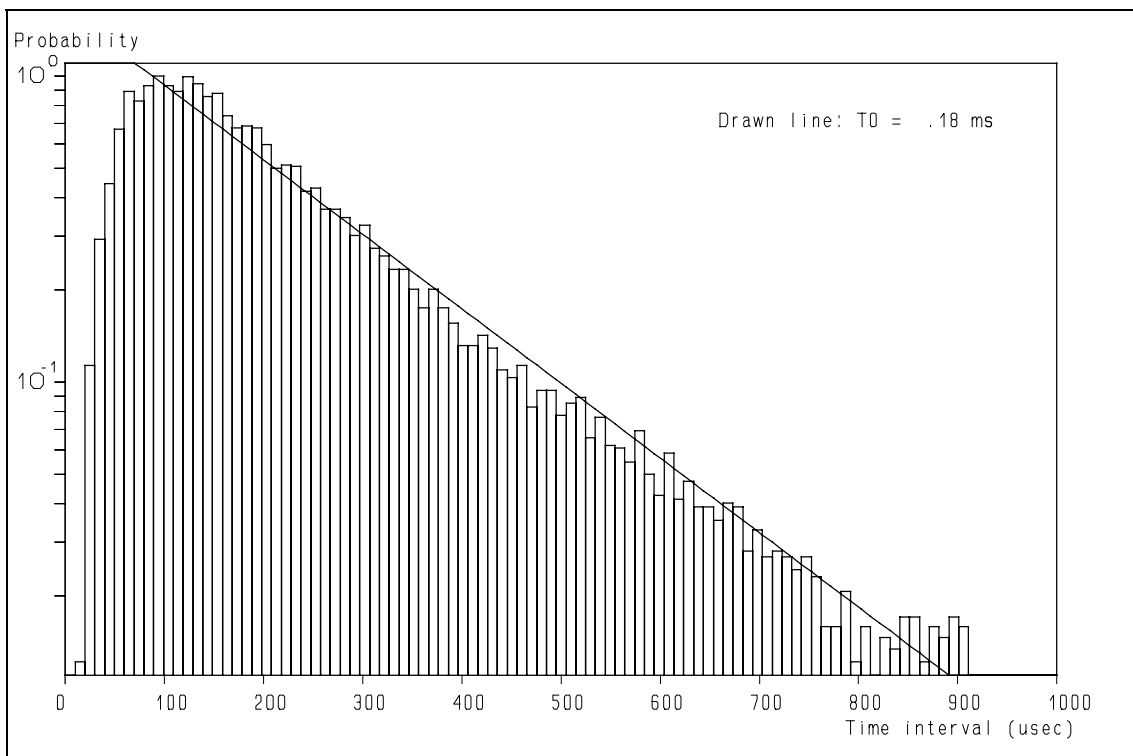


Figure A.3: Time interval distribution using samples with velocities  $> 1.25$  m/s.

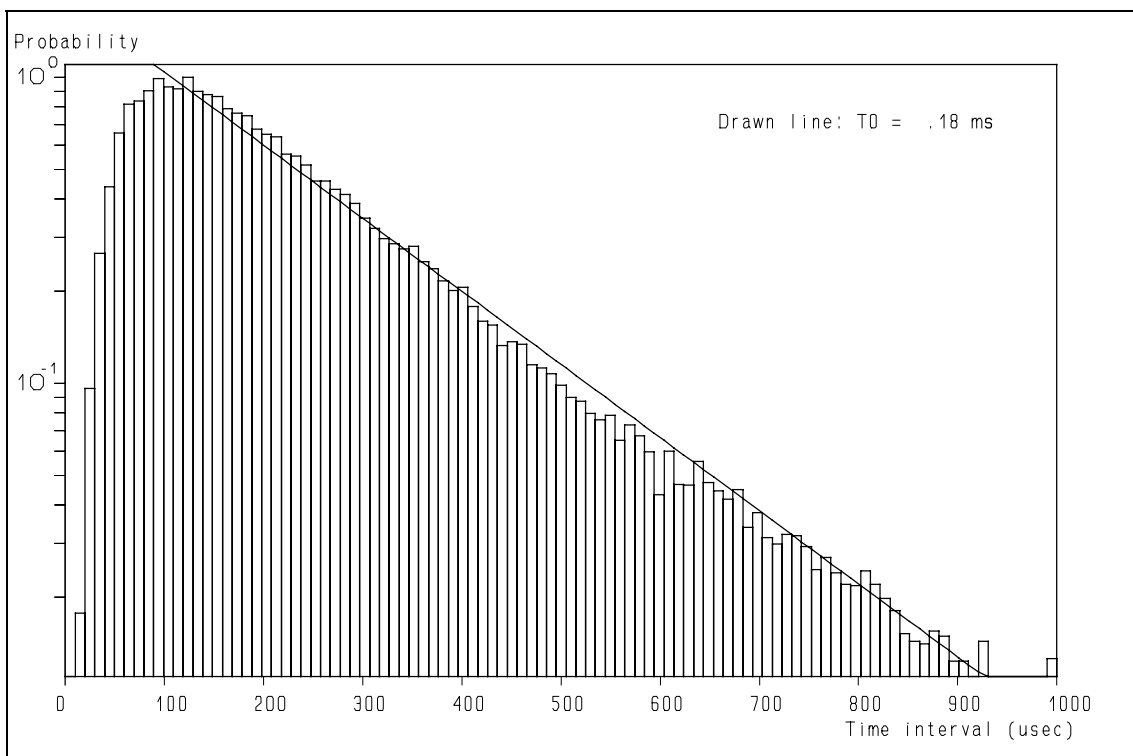
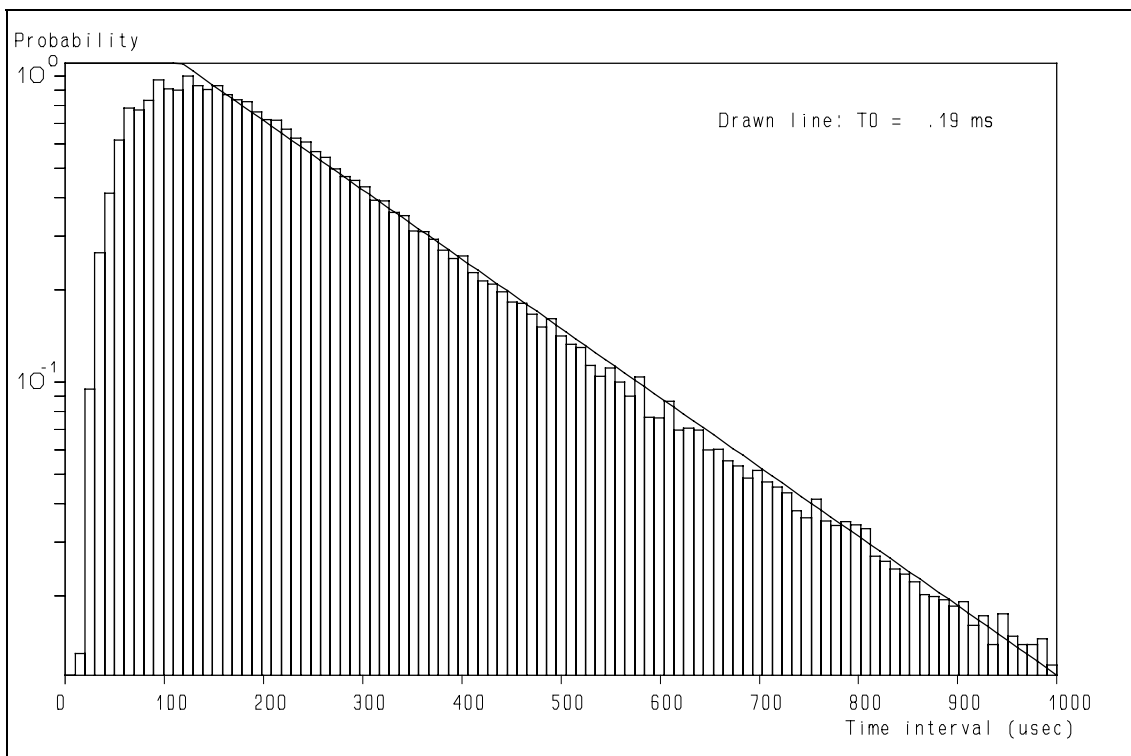
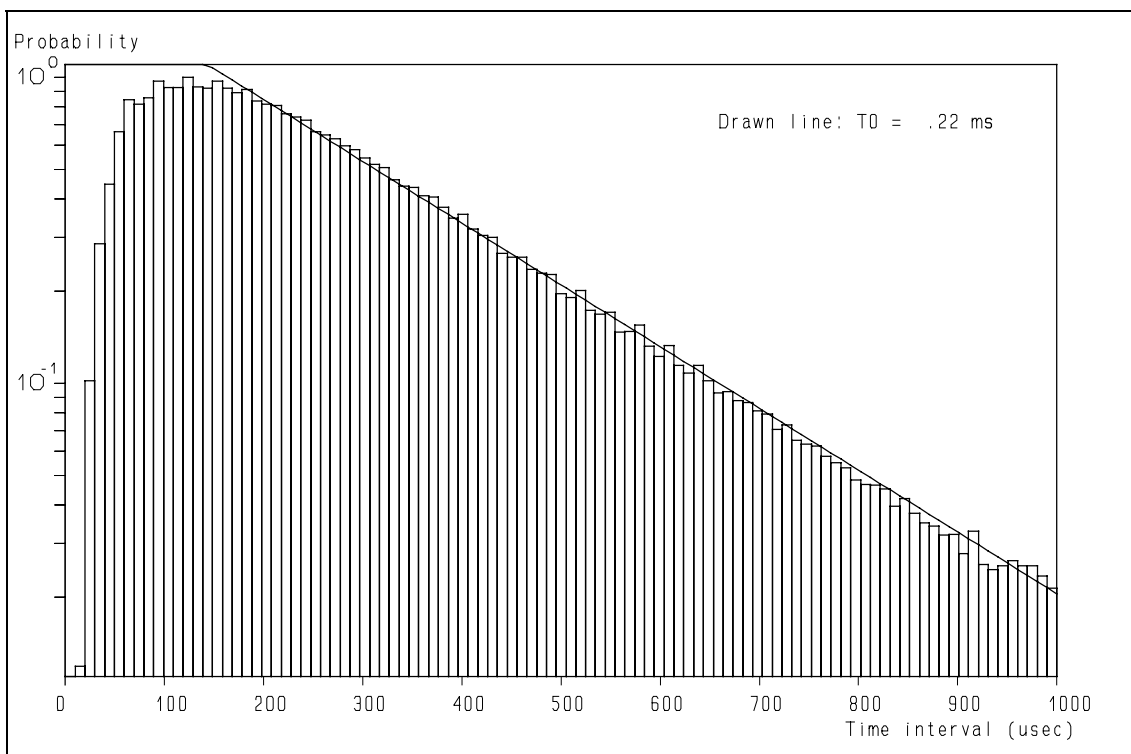


Figure A.4: Time interval distribution using samples with  $1 < u < 1.25$  m/s.



**Figure A.5:** Time interval distribution using samples with  $0.75 < u < 1$  m/s.



**Figure A.6:** Time interval distribution using samples with  $0.5 < u < 0.75$  m/s.

Retrieval of turbulence and turbulence properties from LDA data with noise

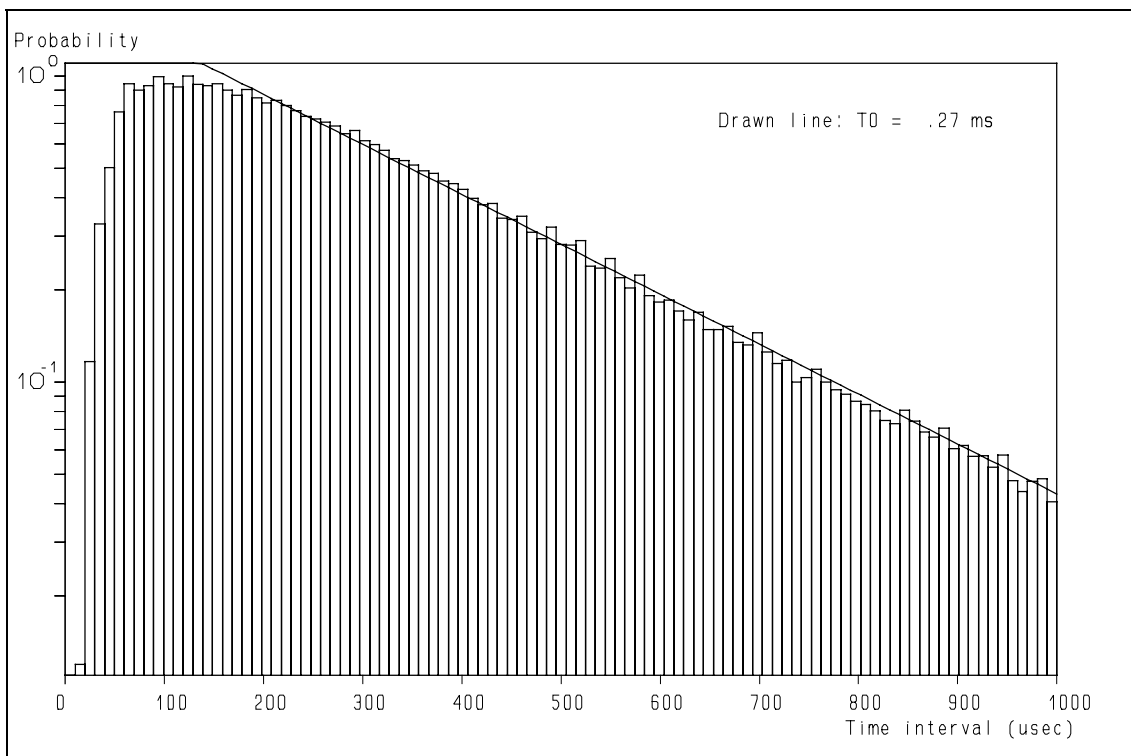


Figure A.7: Time interval distribution using samples with  $0.25 < u < 0.5$  m/s.

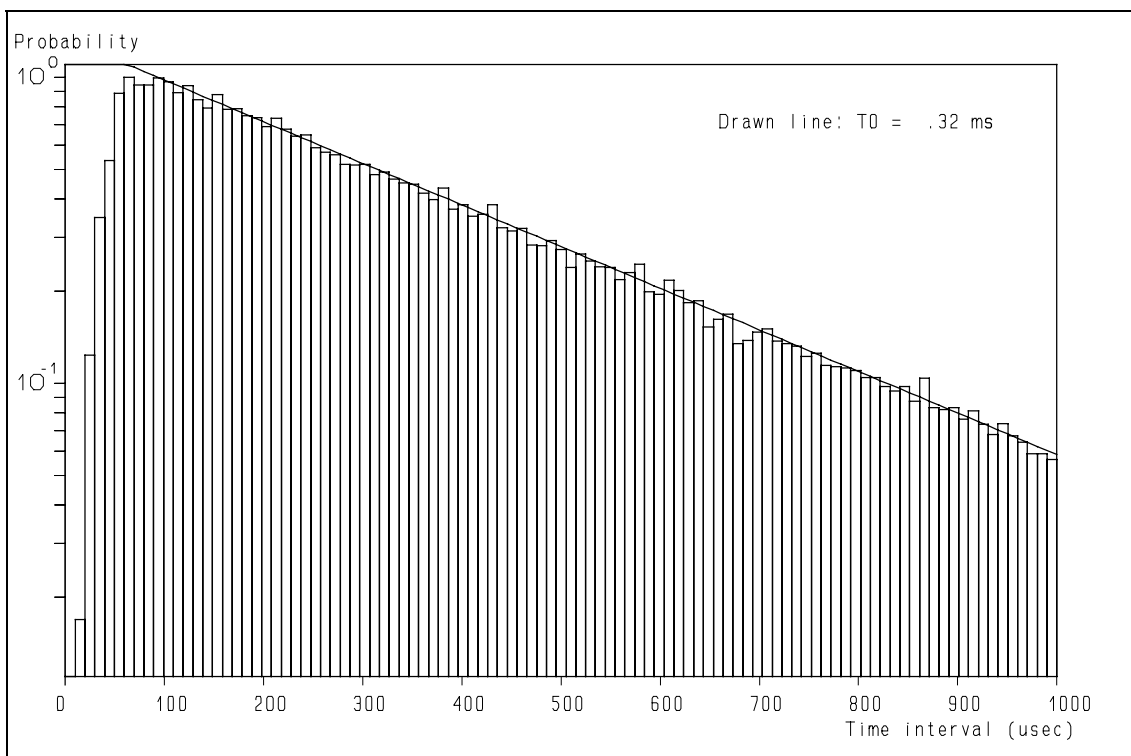
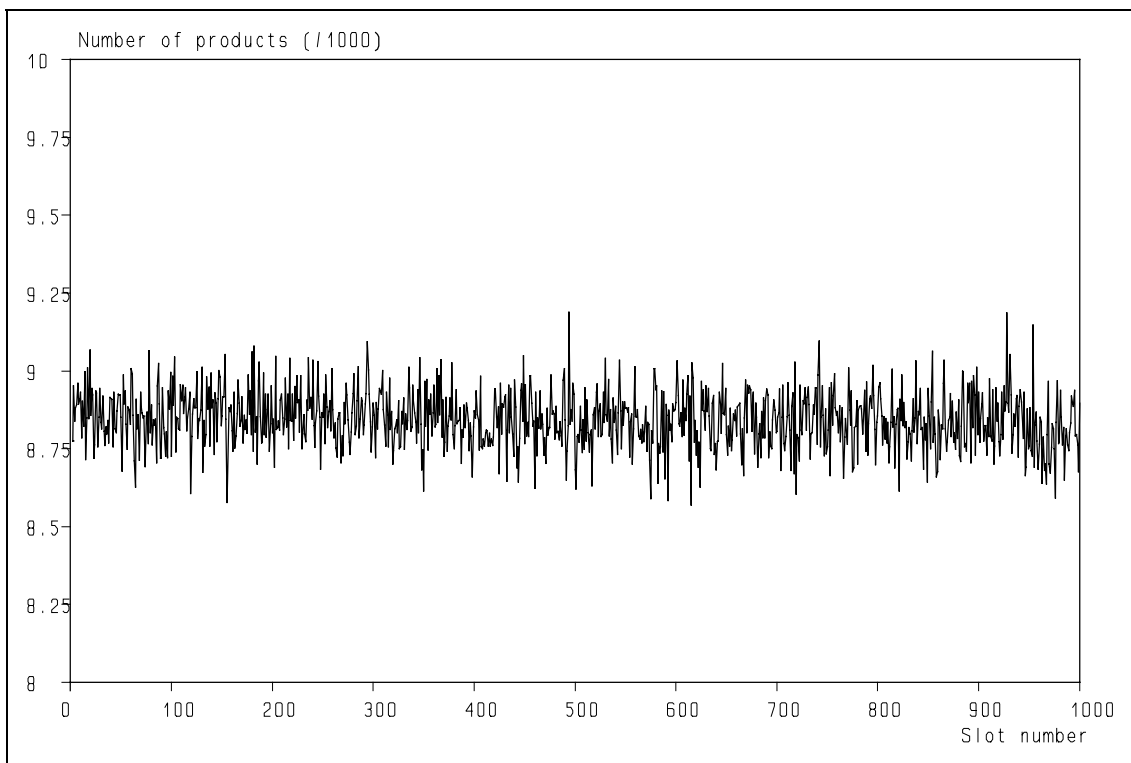
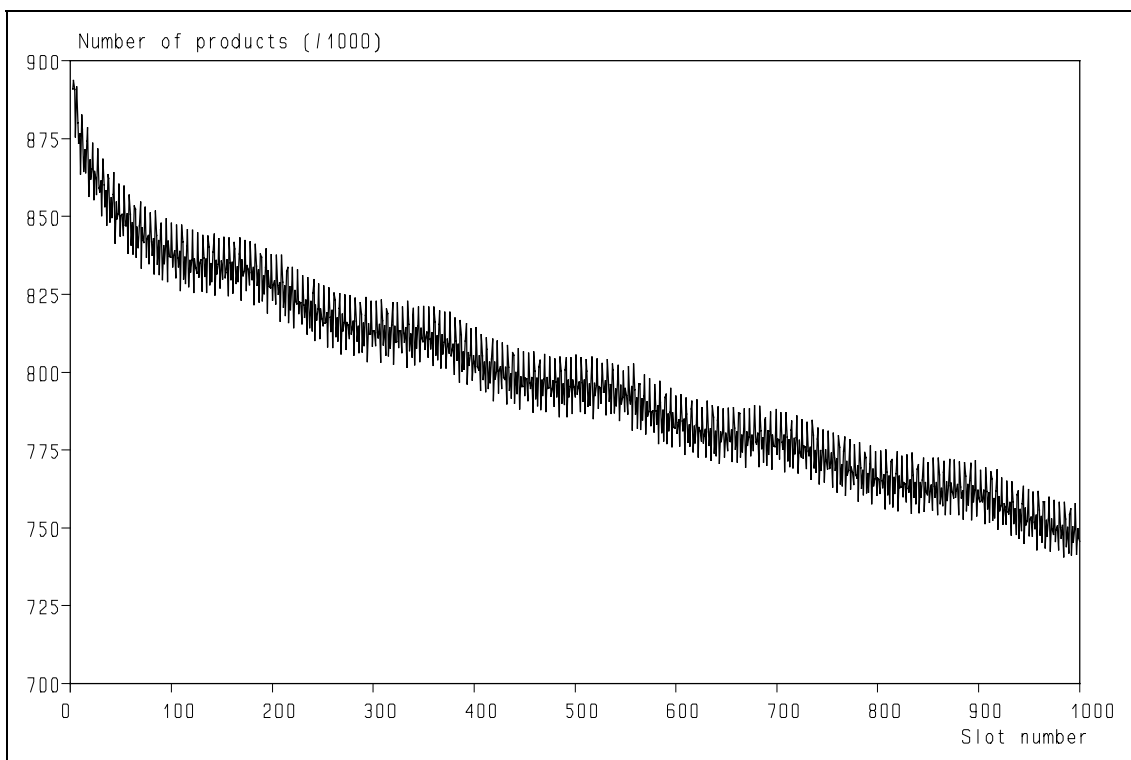


Figure A.8: Time interval distribution using samples with velocities  $< 0.25$  m/s.



**Figure A.9:** Number of products as a function of the slot number without velocity bias.



**Figure A.10:** Number of products as a function of slot number of the auto correlation function of fig. A.2. The decrease clearly indicates velocity bias.

*Retrieval of turbulence and turbulence properties from LDA data with noise*

## APPENDIX B

### The slope of the Auto Correlation Function.

From literature (ref. 1) it is known that the first derivative of the auto correlation function (ACF) of turbulent velocity fluctuations at  $\tau = 0$ ,  $\rho'_{uu}(0)$  must be zero. As consequence, the corresponding power spectra develop a slope of -4 dec./dec. or steeper for higher frequencies. This can be demonstrated by developing the auto correlation function by a Taylors' series for small time lags.

For small  $\tau$  values the auto correlation function  $\rho_{gg}(\tau)$  of a time function  $g(t)$  can be written as

$$\rho_{gg}(\tau) = 1 + \sum_{n=1}^{\infty} c_n |\tau|^n \quad n \in \mathbb{N} \quad [\text{B.1}]$$

$\rho'_{gg}(0) = 0$  implies that  $c_1$  is zero. The second derivative  $d^2 \rho_{gg}(\tau)/d\tau^2$  of eq. [B.1] thus becomes:

$$\rho''_{gg}(\tau) = \sum_{n=2}^{\infty} n \cdot n-1 \cdot c_n |\tau|^{n-2} \quad n \in \mathbb{N} \quad [\text{B.2}]$$

The first and second term in eq. [B.2] result in a slope of -2 dec./dec. of the power spectrum  $S_{(p)}$  at high frequencies, whereas the higher powers of  $\tau$  each decrease the slope by another -2 dec./dec.

Papoulis (ref. 89 and 90) showed that if the auto correlation function and the power spectrum of a differentiable function  $g(t)$  is given by resp.  $\rho_{gg}(\tau)$  and  $S_{gg}(f)$ , the auto correlation function  $\rho_{g'g'}(\tau)$  and the power spectrum  $S_{g'g'}(f)$  of its derivative  $dg(t)/dt$  are given by:

$$\rho_{g'g'}(\tau) = -\frac{d^2 \rho(\tau)}{d\tau^2} = \rho''_{gg}(\tau) \quad [\text{B.3}]$$

$$S_{g'g'}(f) \propto f^2 S_{gg}(f) \quad [\text{B.4}]$$

by combining eq. [B.3] with eq. [B.4] we obtain:

$$-\rho''_{gg}(\tau) \Leftrightarrow f^2 S_{gg}(f) \quad [\text{B.5}]$$

From eq. [B.5] and the power spectrum of eq. [B.2] follows that  $-f^2 S_{gg}(f)$  has a slope of -2 when  $f \rightarrow \infty$ . This implies that  $S_{gg}(f)$  has a slope of -4 at  $f \rightarrow \infty$  if  $\rho'_{gg}(0) = 0$ . Because the Fourier Transform is reversible, this also implies that if  $\rho'_{gg}(0) = 0$ ,  $S_{gg}(f)$  has a slope of a -4 or steeper.

*Retrieval of turbulence and turbulence properties from LDA data with noise*

## APPENDIX C

### The Derivation of the Analytical Auto Correlation Function.

#### C.1 Introduction.

In this appendix the mathematical approach is presented to transform the analytical Power Spectrum into an analytical Auto Correlation Function. Only the broad steps are reflected here in order to keep the derivation clear.

The general equation of the approximate Power Spectrum  $S(f)$  is given by:

$$S_a(f) = S_a(0) [1 + (f/f_0)^2] \prod_{k=1}^n \frac{1}{1 + (f/f_k)^2} \quad k \in \mathbb{N} \quad [\text{C.1}]$$

in which:

$S_a(0)$  = power of the spectrum at  $f = 0$  Hz m<sup>2</sup>/s or V<sup>2</sup>s  
 $f$  = frequency Hz  
 $f_k$  = characteristic frequency,  $k = 0 - 5$  Hz

This function has  $(n + 1)$  degrees of freedom. In electrotechnical terms the approximation is made up of one phase advance network and  $(n - 1)$  low-pass filters.

#### C.2 Theory.

The Power Spectrum  $S(f)$  of a function  $f(t)$  is defined as the Fourier transform of its Auto Covariance Function (AVF),  $R(\tau)$ . This is the averaged product of the values of  $f$  at two different times,  $f(t)$  and  $f(t')$  and  $\tau = t' - t$ , the time difference. The Auto Correlation Function (ACF),  $\rho(\tau)$  is the Auto Covariance Function divided by the mean square of  $f(t)$ . Because we are working with steady systems, the ACF as well as the AVF provide no information about the origin of time but they depend only on the time difference  $\tau$ . The Auto Covariance function is the Inverse Fourier Transform (IFT) of the Power Spectrum.

With the Fourier integral

$$R(\tau) = \int_{-\infty}^{\infty} S(f) \cdot e^{j 2\pi f \tau} df \quad \leftrightarrow \quad S(f) = \int_{-\infty}^{\infty} R(\tau) \cdot e^{-j 2\pi f \tau} d\tau \quad [\text{C.2}]$$

$S(f)$  is real and even. Because of this  $R(\tau)$  is also real and even. Eq. [C.2] can therefore be written as

$$R(\tau) = \int_{-\infty}^{\infty} S(f) \cdot \cos(2\pi f \tau) df \quad \leftrightarrow \quad S(f) = \int_{-\infty}^{\infty} R(\tau) \cdot \cos(2\pi f \tau) d\tau \quad [\text{C.3}]$$

Evaluating the IFT of eq. [C.1] will give the analytical description of the AVF. This transformation can be done by the residues approach of complex function theory.

## Retrieval of turbulence and turbulence properties from LDA data with noise

### Theorem:

If a function  $g(f)$  is a rational function whose denominator is of a degree which is at least two greater than the degree of the numerator and which is finite for all (real) values of  $f$ , then

$$\int_{-\infty}^{\infty} \cos(2\pi x f) \cdot g(f) df = 2\pi j \sum_k \text{Res} [e^{j 2\pi |x|z} \cdot g(z) | z=a_k] \quad (m \geq 0) \quad [\text{C.4}]$$

where the points  $a_k$  are the poles of  $g(z)$  of order  $m$  in the upper half-plane. For details see ref. 118.

Suppose  $g(f)$  can be represented as the numerator  $N(f)$  divided by the denominator  $D(f)$ :

$$g(f) = \frac{N(f)}{D(f)} \quad [\text{C.5}]$$

If in the case of a single pole where  $N(a_k)$  is finite and non-zero for all values of  $k$ , we may use L'Hopital's rule and evaluate for the residues of eq. [C.4]:

$$m=1: \quad \text{Res}(z) = \frac{N(z)}{D'(z)} \quad [\text{C.6}]$$

in which:

$D'(z)$  = the derivative of  $D(z)$  to  $z$ .

Combining eq. [C.5] and eq. [C.6] yields:

$$\int_{-\infty}^{\infty} e^{j 2\pi \tau f} \cdot S(f) df = 2\pi j \sum_k [e^{j 2\pi |\tau|z} \cdot \frac{N(z)}{D'(z)} | z=a_k] \quad (m \geq 0) \quad [\text{C.7}]$$

### C.3 Application of the theory.

The numerator and the denominator of the approximate Power Spectrum are given by

$$N_a(f) = S_a(0) [1 + (f/f_0)^2] \quad D_a(f) = \prod_{k=1}^n [1 + (f/f_k)^2] \quad [\text{C.8}]$$

The poles  $a_k$  of  $S_a(f)$  occur where the denominator  $D(f)$  vanishes.

The poles of eq. [C.1] in the upper half-plane are:

$$D(f) = 0 \quad \rightarrow \quad a_k = j f_k \quad \{k=1 \dots n | k \in \mathbb{N}\} \quad [\text{C.9}]$$

Substituting

$$\tau_k = \frac{1}{f_k} \rightarrow a_k = -\frac{1}{j\tau_k} \quad \{k=1\dots n | k \in \mathbb{N}\} \quad [\text{C.10}]$$

we obtain the result

$$\int_0^{\infty} e^{j2\pi f\tau} \cdot S(f) df = 2\pi j \sum_{k=1}^n [e^{j2\pi|\tau|z} \cdot \frac{N(z)}{D'(z)} \Big|_{z=-\frac{1}{j\tau_k}}] \quad (m \geq 0) \quad [\text{C.11}]$$

Combining eq. [C.1] and eq. [C.11] gives:

$$R_a(\tau) = S_a(0) \pi \sum_{k=1}^n \left[ e^{\frac{-2\pi|\tau|}{\tau_k}} \left( 1 - \frac{\tau_0^2}{\tau_k^2} \right) \frac{1}{\tau_k} \prod_{l=1 | l \neq k}^n \left( \frac{\tau_k^2}{\tau_k^2 - \tau_l^2} \right) \right] \quad [\text{C.12}]$$

The dimensionless Auto Correlation Function is the Auto Covariance Function divided by the Mean Square, equal to  $R_a(0)$ :

$$\rho_a(\tau) = \frac{S_a(0)}{R_a(0)} \pi \sum_{k=1}^n \left[ e^{\frac{-2\pi|\tau|}{\tau_k}} \left( 1 - \frac{\tau_0^2}{\tau_k^2} \right) \frac{1}{\tau_k} \prod_{l=1 | l \neq k}^n \left( \frac{\tau_k^2}{\tau_k^2 - \tau_l^2} \right) \right] \quad [\text{C.13}]$$

#### C.4 Verification.

This Auto Correlation Function should have some typical properties:

- Its first derivative to  $\tau$  at  $\tau = 0$  must be zero because the slope becomes steeper than -4 dec./dec. for frequencies above a starting frequency (see Appendix B).
- $\rho(\tau) = \rho(-\tau)$  holds for every Auto Correlation Function.

The analytical Auto Correlation Function obtained by inverse Fourier transformation satisfies these characteristics.

*Retrieval of turbulence and turbulence properties from LDA data with noise*

## APPENDIX D

### Derivation of the Second-Order Kalman Reconstruction Filter.

#### D.1 Introduction.

The first-order Kalman filter has been designed for processing of the velocity data in a turbulent flow under the assumption that the turbulence generating accelerations are described by a Gaussian white noise signal (ref. 87 and Chapter 7). This assumption is not realistic, as the turbulence theories predict a decrease of the accelerations with increasing wavenumber (or frequency) above the eddy size where the dissipation of the turbulent kinetic energy becomes important. Therefore extension of this simple model is attractive.

#### D.2 Improved turbulence model.

The following dynamic model for the evolution of the velocity  $v(t)$  over time  $t \geq t_{begin}$  of the fluid is being used:

$$v(t) + \alpha \frac{d}{dt} v(t) + \beta \frac{d^2}{dt^2} v(t) = \xi(t) \quad [\text{D.1}]$$

in which:

- $v(t)$  = turbulent velocity (component) m/s
- $\alpha$  = parameter related to the cut-off frequencies in the power spectrum for the second-order Kalman reconstruction filter s
- $\beta$  = parameter related to the cut-off frequencies in the power spectrum for the second-order Kalman reconstruction filter s<sup>2</sup>
- $\xi(t)$  = turbulence generating white noise signal with intensity  $\sigma^2$  m/s

The term  $\alpha dv(t)/dt$  is the frictional term of the differential equation with  $\alpha \geq 0$ . The term  $\beta d^2v(t)/dt^2$  introduces additional friction for the higher frequencies with  $\beta \geq 0$ . In general, the poles of the (complex) transfer function of this second-order differential equation are either real or complex depending on the specific values of the parameters  $\alpha$  and  $\beta$ . The coefficients  $\alpha$  and  $\beta$  can be chosen such that the modelled velocity does not oscillate (complex poles) but is damped (negative real poles).

For a damped system, the parameters  $\alpha$  and  $\beta$  satisfy the following equations:

$$\alpha = \tau_1 + \tau_2 ; \quad \beta = \tau_1 \tau_2 ; \quad \tau_1 = \frac{1}{\lambda} ; \quad \tau_2 = \frac{1}{\mu} ; \quad \lambda = 2\pi\lambda' ; \quad \mu = 2\pi\mu' \quad [\text{D.2}]$$

in which:

- $\tau_1, \tau_2$  = time constants of the dynamic system s
- $\mu > \lambda$ .

The consequence of this extension is that the additional limitation in the acceleration of  $v(t)$  comes from the extension of the dynamic model for the velocity  $v(t)$ . The power spectrum of  $v(t)$  is modelled as a cascade of two first-order low-pass filters having cut-off frequencies  $\lambda'$  and  $\mu'$ . On a log-log scale the slope of the power spectrum is zero for frequencies below  $\lambda'$ , -2 for frequencies between  $\lambda'$  and  $\mu'$

## Retrieval of turbulence and turbulence properties from LDA data with noise

and -4 for frequencies higher than  $\mu'$ . This power spectrum resembles the "Bessem" spectrum more closely than the spectrum of the model of the first-order Kalman filter as can be seen from fig. 12.3

This turbulence model is indeed an extension of the turbulence model of the first-order Kalman model as becomes clear when the second cut-off frequency  $\mu'$  approaches infinity. In that case,  $\tau_2 = 0$  and as a result  $\alpha = \tau_1$  and  $\beta = 0$  leading to the following equation for the velocity  $v(t)$ :

$$v(t) + \frac{1}{\lambda} \frac{d}{dt} v(t) = \xi(t) \quad [\text{D.3}]$$

which is nothing but the model on which the first-order Kalman filter has been based (see Chapter 7).

The second-order differential equation describing our model can be written as a set of two first-order differential equations using the identity:

$$\frac{d}{dt} v(t) = a(t) \quad [\text{D.4}]$$

in which:

$a(t)$  = the acceleration m/s<sup>2</sup>

Differentiating the acceleration gives:

$$\frac{d}{dt} a(t) = \frac{d^2}{dt^2} v(t) = \frac{\xi(t) - v(t) - \alpha \frac{d}{dt} v(t)}{\beta} \quad [\text{D.5}]$$

Combining eq. [D.4] and eq. [D.5] results in:

$$\frac{d}{dt} a(t) = \frac{\xi(t) - v(t) - \alpha a(t)}{\beta} \quad [\text{D.6}]$$

The velocity  $v(t)$  can be measured either with a constant data rate or at randomly distributed time intervals, yielding:

$$v_k^{obs} = v(t_k) + \eta_k ; \quad k = 0, 1, 2, \dots \quad [\text{D.7}]$$

in which:

$\eta$  = Gaussian-distributed white noise with variance  $\rho^2$  m/s  
i.e.

$$\eta_k = \mathbb{N}(\mathbf{0}, \rho^2) \quad [\text{D.7}^a]$$

and

$$E[\eta_k \eta_l] = \mathbf{0} \quad \forall k \neq l \quad [\text{D.7}^b]$$

### D.3 Design of the Second-Order Kalman Filter.

The dynamic model of the second-order Kalman filter can be written in matrix notation:

$$\frac{d}{dt} \underline{x}(t) = \mathbf{A} \underline{x}(t) + \underline{n}(t) \quad [\text{D.8}]$$

in which:

$\mathbf{A}$  = the 2 x 2 system matrix:

$$\mathbf{A} = \begin{pmatrix} 0 & 1 \\ -\frac{1}{\beta} & -\frac{\alpha}{\beta} \end{pmatrix} \quad [\text{D.8}^a]$$

$\underline{x}(t)$  is the dynamic state vector of the system:

$$\underline{x}(t) = \begin{pmatrix} v(t) \\ a(t) \end{pmatrix} \quad [\text{D.8}^b]$$

and  $\underline{n}(t)$  is the vector containing the external driving "noises", i.e.:

$$\underline{n}(t) = \begin{pmatrix} 0 \\ \xi(t) \end{pmatrix} \quad [\text{D.8}^c]$$

The observation equation of the system is given by:

$$\underline{y} = \mathbf{C} \underline{x} + \underline{\eta} \quad [\text{D.9}]$$

in which:

$\underline{y}$  = the vector containing the measured quantities of the system.

We have scalar measurements, so:

$$\underline{y}(t) = v^{obs}(t), \quad \mathbf{C} = (1 \ 0) \quad [\text{D.10}^a]$$

in which:

$v^{obs}(t)$  = measured velocity m/s

and

$$\underline{\eta} = \eta \quad [\text{D.10}^b]$$

The optimum prediction (or estimation) of the system can be obtained from the filter dynamics

$$\frac{d}{dt} \hat{\underline{x}}(t) = \mathbf{A} \hat{\underline{x}}(t) + \mathbf{L} \underline{e}(t); \quad \underline{e}(t) = \underline{y}(t) - \mathbf{C} \hat{\underline{x}}(t) \quad [\text{D.11}]$$

in which:

$\mathbf{L}$  = filter gain

### Retrieval of turbulence and turbulence properties from LDA data with noise

We are looking for a filter gain  $\mathbf{L}$  for which the prediction is the most accurate. This optimum (static) filter gain  $\mathbf{L}$  can be calculated from

$$\mathbf{L} = \mathbf{\Lambda} \mathbf{C}' \mathbf{\Pi}^{-1} \quad [\text{D.12}]$$

in which:

$\mathbf{\Lambda}$  = the (positive definite) matrix which is the solution to a Riccati equation

$$\mathbf{\Lambda} \mathbf{A} + \mathbf{A}' \mathbf{\Lambda} - \mathbf{\Lambda} \mathbf{C}' \mathbf{\Pi}^{-1} \mathbf{C} \mathbf{\Lambda} + \mathbf{\Sigma} = \mathbf{0} \quad [\text{D.13}]$$

in which:

$\mathbf{\Sigma}$  = the covariance matrices of the external driving noise  $\underline{n}$

$\mathbf{\Pi}$  = the covariance matrices of the measurement noise  $\underline{\eta}$

In this case,

$$\mathbf{\Pi} = \rho^2 \quad [\text{D.13}^a]$$

and

$$\mathbf{\Sigma} = \begin{pmatrix} 0 & 0 \\ 0 & \frac{\sigma^2}{\beta^2} \end{pmatrix} \quad [\text{D.13}^b]$$

The matrix  $\mathbf{\Lambda}$  is symmetric, so its elements can be parametrized

$$\mathbf{\Lambda} = \begin{pmatrix} a & b \\ b & c \end{pmatrix} \quad [\text{D.14}]$$

with the condition that  $a$ ,  $b$  and  $c$  are real numbers and  $a \geq 0$  and  $c \geq 0$ .

Solving the Riccati equation gives us three equations from which the elements of the matrix  $\mathbf{\Lambda}$  can be obtained :

$$-\frac{2b}{\beta} - \frac{a^2}{\rho^2} = 0 \quad [\text{D.15}^a]$$

$$a - \frac{\alpha}{\beta} b - \frac{c}{\beta} - \frac{ab}{\rho^2} = 0 \quad [\text{D.15}^b]$$

$$2b - 2\frac{\alpha}{\beta} c - \frac{b^2}{\rho^2} + \frac{\sigma^2}{\beta^2} = 0 \quad [\text{D.15}^c]$$

Expressing  $a$  as a function of  $b$  and  $c$  as a function of  $b$  gives us two expressions for  $b$ :

$$\frac{1}{2\alpha\rho^2}b^2 - \frac{\sqrt{\frac{2}{\beta}}}{\rho}b\sqrt{b} - \frac{\alpha^2+\beta}{\alpha\beta}b + \rho\sqrt{\frac{-2}{\beta}}\sqrt{b} - \frac{\sigma^2}{2\alpha\beta} = 0 \quad [\text{D.16}^{\text{a}}]$$

$$\frac{1}{2\alpha\rho^2}b^2 + \frac{\sqrt{\frac{2}{\beta}}}{\rho}b\sqrt{b} - \frac{\alpha^2+\beta}{\alpha\beta}b - \rho\sqrt{\frac{-2}{\beta}}\sqrt{b} - \frac{\sigma^2}{2\alpha\beta} = 0 \quad [\text{D.16}^{\text{b}}]$$

We know that  $\beta \geq 0$  and the substitution  $p = \sqrt{b}$  gives the following equations:

$$\frac{1}{2\alpha\rho^2}p^4 - j\frac{\sqrt{\frac{2}{\beta}}}{\rho}p^3 - \frac{\alpha^2+\beta}{\alpha\beta}p^2 + j\rho\sqrt{\frac{2}{\beta}}p - \frac{\sigma^2}{2\alpha\beta} = 0 \quad [\text{D.17}^{\text{a}}]$$

$$\frac{1}{2\alpha\rho^2}p^4 + j\frac{\sqrt{\frac{2}{\beta}}}{\rho}p^3 - \frac{\alpha^2+\beta}{\alpha\beta}p^2 - j\rho\sqrt{\frac{2}{\beta}}p - \frac{\sigma^2}{2\alpha\beta} = 0 \quad [\text{D.17}^{\text{b}}]$$

which is not easy to solve. Expressing  $a$  and  $b$  as a function of  $c$  does not make the equations any simpler. When  $b$  and  $c$  are expressed as a function of  $a$ , the equation for  $a$  reads:

$$\frac{\beta^2}{8\rho^6\alpha}a^4 + \frac{\beta}{2\rho^4}a^3 + \frac{\alpha^2 + \beta}{2\rho^2\alpha}a^2 + a - \frac{\sigma^2}{2\alpha\beta^2} = 0 \quad [\text{D.18}]$$

having the following four solutions:

$$a_1 = \frac{-\alpha\rho^2 - \sqrt{\alpha^2\rho^4 - 2\beta(\rho^4 - \sqrt{\beta^2\rho^8 + \rho^6\sigma^2})}}{\beta} \quad [\text{D.19}^{\text{a}}]$$

$$a_2 = \frac{-\alpha\rho^2 + \sqrt{\alpha^2\rho^4 - 2\beta(\rho^4 - \sqrt{\beta^2\rho^8 + \rho^6\sigma^2})}}{\beta} \quad [\text{D.19}^{\text{b}}]$$

$$a_3 = \frac{-\alpha\rho^2 - \sqrt{\alpha^2\rho^4 - 2\beta(\rho^4 + \sqrt{\beta^2\rho^8 + \rho^6\sigma^2})}}{\beta} \quad [\text{D.19}^{\text{c}}]$$

*Retrieval of turbulence and turbulence properties from LDA data with noise*

$$a_4 = \frac{-\alpha\rho^2 + \sqrt{\alpha^2\rho^4 - 2\beta(\rho^4 + \sqrt{\beta^2\rho^8 + \rho^6\sigma^2})}}{\beta} \quad [\text{D.19}^d]$$

Only the second solution ( $a_2$ ) is always real and positive for  $\alpha \geq 0$ ,  $\beta \geq 0$ ,  $\rho \geq 0$  and  $\sigma \geq 0$  and is thus the solution we are looking for.

Once we know the solution of  $a$ , we can solve  $b$  and  $c$  as well:

$$b = -\beta \frac{a^2}{2\rho^2} \quad [\text{D.19}^e]$$

and

$$c = \frac{\beta}{\alpha} \left( b - \frac{b^2}{2\rho^2} + \frac{\sigma^2}{2} \right) \quad [\text{D.19}^f]$$

from which it can be shown that  $b$  is negative and  $c$  is positive.

The optimum filter gain  $L$  is a vector which is a function of the parameters  $a$  and  $b$  only:

$$L = \begin{pmatrix} \frac{a}{\rho^2} \\ b \\ \frac{b}{\rho^2} \end{pmatrix} = \begin{pmatrix} L_1 \\ L_2 \end{pmatrix} \quad [\text{D.20}]$$

We now regard the filter gain  $L$  as the parameter which we can vary to tune the filtering of the second-order Kalman filter.

Substitution of the filter gains  $L_1$  and  $L_2$  in the equation for the predictions gives us the following set of coupled differential equations for the filter dynamics:

$$\frac{d}{dt} \hat{v}(t) = -L_1 \hat{v}(t) + \hat{a}(t) + L_1 v^{obs}(t) \quad [\text{D.21}^a]$$

$$\frac{d}{dt} \hat{a}(t) = -\left(\frac{1}{\beta} + L_2\right) \hat{v}(t) - \frac{\alpha}{\beta} \hat{a}(t) + L_2 v^{obs}(t) \quad [\text{D.21}^b]$$

subject to

$$\hat{v}(t_0) = v_0^{obs} ; \hat{a}(t_0) = 0 \quad [\text{D.21}^c]$$

We are dealing with a linear system in which the expectation value of the derivative of the velocity equals the expectation value of the acceleration, so we may write:

$$\frac{d}{dt} \hat{v}(t) = \hat{a}(t) \quad [\text{D.22}^a]$$

from which follows that the first filter gain  $L_1$  must be zero leading to the following equations for the filter dynamics:

$$\frac{d}{dt} \hat{v}(t) = \hat{a}(t) \quad [\text{D.22}^a]$$

$$\frac{d}{dt} \hat{a}(t) = -\left(\frac{1}{\beta} + L_2\right) \hat{v}(t) - \frac{\alpha}{\beta} \hat{a}(t) + L_2 v^{obs}(t) \quad [\text{D.22}^b]$$

These equations can be written as a set of two coupled differential equations (for a matrix  $\mathbf{A}$  and a vector  $\underline{b}$ )

$$\frac{d}{dt} \hat{\mathbf{x}}(t) = \mathbf{A} \hat{\mathbf{x}}(t) + \underline{b} v^{obs}(t) \quad [\text{D.23}]$$

with initial condition

$$\hat{\mathbf{x}}(t_0) = \begin{pmatrix} v_0^{obs} \\ 0 \end{pmatrix}. \quad [\text{D.23}^a]$$

In this case the matrix  $\mathbf{A}$  reads

$$\mathbf{A} = \begin{pmatrix} 0 & 1 \\ -\left(\frac{1}{\beta} + L_2\right) & -\frac{\alpha}{\beta} \end{pmatrix} \quad [\text{D.24}^a]$$

and vector  $\underline{b}$  equals

$$\underline{b} = \begin{pmatrix} 0 \\ L_2 \end{pmatrix} \quad [\text{D.24}^b]$$

If only discrete-time measurements of the velocities  $v_k^{obs}$  are available, reconstruction of the measured samples between subsequent time instants is necessary for the Kalman filter needs continuous-time measurements to generate optimum estimates at any time. When the data rate of the time series (after having applied some sort of signal reconstruction to the measured samples) is constant, the following procedure is still valid. We choose for a first-order interpolation between the samples, i.e. for  $k = 0, 1, 2, 3, \dots$

*Retrieval of turbulence and turbulence properties from LDA data with noise*

$$v^{obs}(t) = \alpha_k t + \beta_k \quad (t_k \leq t \leq t_{k+1}) \quad [\text{D.25}]$$

in which:

$$\alpha_k = \frac{V_{k+1}^{obs} - V_k^{obs}}{t_{k+1} - t_k} \quad [\text{D.25}^a]$$

and

$$\beta_k = \frac{t_k V_{k+1}^{obs} - t_{k+1} V_k^{obs}}{t_k - t_{k+1}}. \quad [\text{D.25}^b]$$

For  $k = 0, 1, 2, 3, \dots$ , and  $t_k \leq t \leq t_{k+1}$ , the equations for the filter dynamics can be written as

$$\frac{d}{dt} \hat{\mathbf{x}} = \mathbf{A} \hat{\mathbf{x}}(t) + \mathbf{b} (\alpha_k t + \beta_k) \quad [\text{D.26}]$$

with initial condition

$$\hat{\mathbf{x}}(t_k) = \hat{\mathbf{x}}_{t_k}. \quad [\text{D.26}^a]$$

The (forward) solution  $\hat{\mathbf{x}}(t)$  can be recursively obtained from

$$\hat{\mathbf{x}}(t) = \underline{\mathbf{c}}(t_k) \exp(\mathbf{A} (t - t_k)) - \underline{\mathbf{d}}(t) \quad [\text{D.27}]$$

in which:

$$\underline{\mathbf{c}}(t_k) = \hat{\mathbf{x}}_{t_k} + (\mathbf{I}_d (\alpha_k t_k + \beta_k) + \alpha_k \mathbf{A}^{-1}) \mathbf{A}^{-1} \mathbf{b} \quad [\text{D.27}^a]$$

and

$$\underline{\mathbf{d}}(t) = (\mathbf{I}_d (\alpha_k t + \beta_k) + \alpha_k \mathbf{A}^{-1}) \mathbf{A}^{-1} \mathbf{b}. \quad [\text{D.27}^b]$$

The coefficients of matrix  $\mathbf{A}$  and vector  $\underline{\mathbf{b}}$  are given by the parameters  $\lambda$ ,  $\mu$  and  $L_2$  so the optimum prediction as provided by the equations of the filter dynamics can be solved according to the solution given above.

The backward filtered prediction  $v^p(t)$  can be obtained by processing the data in reverse time order using the initial velocity

$$\hat{\mathbf{x}}(t_N) = \begin{pmatrix} v_N^{obs} \\ \mathbf{0} \end{pmatrix}. \quad [\text{D.28}]$$

The overall bidirectional prediction is the average of the forward and backward predictions

$$v^{pr}(t) = \frac{v^f(t) + v^b(t)}{2} \quad [\text{D.29}]$$

and can be taken as the optimal and phase-lag free estimation of the turbulence based on the available measurements.

#### D.4 Determination of the Turbulence Model Parameters.

A value for the filter gain has to be chosen in order to use the second-order Kalman reconstruction filter. This can be done either by an trial and error procedure in which the Mean Square Error is minimized using a simulation or the optimum filter gain is computed from the equations as provided by the Kalman theory. The optimum filter gain depends on four parameters, these are:

- $\lambda'$  : the first cut-off frequency of the power spectrum of the turbulence Hz
- $\mu'$  : the second cut-off frequency of the power spectrum of the turbulence Hz
- $\sigma^2$  : the variance of the driving noise term of the turbulence model  $\text{m}^2/\text{s}^2$
- $\rho^2$  : the variance of the measurement noise  $\text{m}^2/\text{s}^2$

The first two parameters  $\lambda'$  and  $\mu'$  can be retrieved from the power spectrum of the turbulence on a log-log scale. The determination of the last parameter  $\rho^2$  is also possible and can be retrieved from the slotted auto covariance function (ref. 63, 87 and 102).

The last parameter we need to know is the variance of driving white noise signal of the turbulence  $\sigma^2$  which can be derived from the variance of the velocity  $\sigma_v^2$ . The turbulence model reads:

$$v(t) + (\tau_1 + \tau_2) \frac{d}{dt} v(t) + \tau_1 \tau_2 \frac{d^2}{dt^2} v(t) = \xi(t) \quad [\text{D.30}]$$

in which:

$v(t)$  = velocity m/s

$\xi(t)$  = the driving white noise signal m/s

The transfer function  $G(j\omega)$  of the model is:

$$G(j\omega) = \frac{1}{1 - \tau_1 \tau_2 \omega^2 + j(\tau_1 + \tau_2)\omega} \quad [\text{D.31}]$$

from which the spectrum  $S(\omega)$  can be calculated:

Retrieval of turbulence and turbulence properties from LDA data with noise

$$S(\omega) = S_0 G(j\omega) G(j\omega)^* = \frac{4 (\tau_1 + \tau_2) \sigma^2}{1 + (\tau_1^2 + \tau_2^2) \omega^2 + \tau_1^2 \tau_2^2 \omega^4} \quad [\text{D.32}]$$

According to Parseval, the total power (mean square) contained in this spectrum ( $P_S$ ) is:

$$P_S = \frac{1}{2\pi} \int_{-\infty}^{\infty} S(\omega) d\omega = \frac{1}{2\pi} \int_{-\infty}^{\infty} \frac{4 (\tau_1 + \tau_2) \sigma^2}{1 + (\tau_1^2 + \tau_2^2) \omega^2 + \tau_1^2 \tau_2^2 \omega^4} d\omega = \quad [\text{D.33}^a]$$

$$= \frac{4 (\tau_1 + \tau_2) (\tau_1 - \tau_2) \sigma^2}{2(\tau_1^2 - \tau_2^2)} = 2\sigma^2 \quad [\text{D.33}^b]$$

Now, the mean square of the acceleration be calculated from the mean square of the (measured) velocity:

$$P_S = 2\sigma^2 = \sigma_v^2 \Rightarrow \sigma^2 = \frac{\sigma_v^2}{2} \quad [\text{D.34}]$$

## References.

1. J.O. Hinze, "Turbulence", Mc. Graw-Hill, New York, 2<sup>nd</sup> ed. (1975).
2. H. Tennekes and J.L. Lumley, "A First Course in Turbulence", The MIT Press, Cambridge (1983).
3. J.M. Burgers, "The motion of a fluid in the boundary layer along a plane smooth surface", Proc. 1<sup>st</sup> Intern. Congress Appl. Mech. Delft (1924).
4. J.M. Burgers, "Experiments on the fluctuations of the velocity in a current of air", Proc. Roy. Acad. Amsterdam, Vol. 29 (1926), pp. 547- 558.
5. J.M. Burgers, "Experimental investigation of the airflow in the boundary layer along a smooth surface", Journal of Applied Physics (Moskau), Vol. 4 (1927), pp. 8-20.
6. J.M. Burgers, "Hitzdrahtmessungen. Handb. der Experimentalphysik", Akad. Verlagsges. Leipzig Vol. 4 (1931), Part 1, pp. 636-667.
7. C.G. Lomas, "Fundamentals of Hot Wire Anemometry", Cambridge University Press (1986).
8. H.H. Bruun, "Hot-Wire Anemometry", Oxford University Press (1995).
9. F. Durst, A. Melling and J.H. Whitelaw, "Principles and Practice of Laser-Doppler Anemometry", Academic Press (1976).
10. B. Ruck and B. Pavlovski, "Limited Accuracy of Turbulence Measurement in Laser Doppler Anemometry", Proceedings of the Fifth International Conference on Laser Anemometry: Advances and Applications, Veldhoven (Netherlands) 23 - 27 August 1993, pp. 25 - 35.
11. J.C. Erdmann and R.I. Gellert, "Particle Arrival Statistics in Laser Anemometry of Turbulent flow", Applied Physics Letters, Vol. 29 (1976), pp. 408 - 411.
12. P.-J. Klijn, "Drag Reduction Phenomena in Turbulent Pipe Flow", Ph-D Thesis, University of Amsterdam (Netherlands), November 1979.
13. H.R.E. van Maanen and J.M.H. Fortuin, "Experimental Determination of the Random Lump-Age Distribution in the Boundary Layer of Turbulent Pipe Flow using Laser-Doppler Anemometry", Chemical Engineering Science, Vol. 38 (1983), pp. 399 - 423.
14. H. Tijms, "Stochastic Modelling and Analysis", Wiley & Sons, New York (1986).
15. H.C. van der Hulst, "Light Scattering by Small Particles", Dover Publications Inc., New York (1957, 1981).
16. J. Jensen, "A Survey of Methods for Measuring Correlation Functions", Disa Information no. 10 (1970), pp. 10 - 14.
17. R. Thompson, "Spectral Estimation of Irregularly Spaced Data", IEEE Transactions on Geoscience electronics, Vol. GE - 9, no. 2 (April 1971), pp. 107 - 110.
18. E. Masry, "Random Sampling and Reconstruction of Spectra", Information and Control, Vol. 19 (1971), pp. 275 - 288.
19. W.K. George and J.L. Lumley, "The Laser Velocimeter and its Applications to the Measurement of Turbulence", Journal of Fluid Mechanics, Vol. 60 (1973), pt. 2, pp. 321 - 362.
20. M. Whiffen and D. Meadows, "Two-axis, Single Particle Laser Velocimeter System for Turbulence Spectral Analysis", Proceedings of the second international workshop on laser velocimetry, Purdue University, West Lafayette, Ind. (U.S.A.), March 1974, pp. 1 - 15.
21. D. Smith and D. Meadows, "Power Spectra from Random-Time Samples for Turbulence Measurements with a Laser Velocimeter", Proceedings of the second international workshop on laser velocimetry, Purdue University, West Lafayette, Ind. (U.S.A.), March 1974, pp. 27 - 46.
22. W. Mayo, "A Discussion of Limitations and Extensions of Power Spectrum Estimation with Burst-Counter LDV Systems", Proceedings of the second international workshop on laser velocimetry, Purdue University, West Lafayette, Ind. (U.S.A.), March 1974, pp. 90 - 104.
23. W. Mayo, M. Shay and S. Riter, "Digital Estimation of Turbulence Power Spectra From Burst Counter LDV Data", Proceedings of the second international workshop on laser velocimetry, Purdue University, March 1974, West Lafayette, Ind. (U.S.A.), pp. 16 - 26.

## *Retrieval of turbulence and turbulence properties from LDA data with noise*

24. M. Gaster and J.B. Roberts, "Spectral Analysis of Randomly Sampled Signals", *J. Inst. Maths. Applics.*, Vol. 15 (1975), pp. 195 - 216.
25. W. Hösel and W. Rodi, "A Highly Accurate Method for Digital Processing of Laser-Doppler Velocimeter Signals", *Technisches Messen - ATM*, Vol. 45, no. 2 (Feb. 1978), pp. 43 - 48.
26. J. Roberts and M. Gaster, "Rapid Estimation of Spectra from Irregularly Sampled Records", *Proceedings of the IEEE*, Vol. 125, no. 2 (1978) pp. 92 - 96.
27. E. Masry, "Poisson Sampling and Spectral Estimation of Continuous-Time Processes", *IEEE Transactions on Information Theory*, Vol. IT-24, no. 2 (March 1978), pp. 173 - 183.
28. W. George, P. Beuther and J. Lumley, "Processing of Random Signals", *Proceedings of the Dynamic Flow Conference (1978)*, pp. 757 - 800.
29. W. Mayo, "Spectrum Measurements with Laser Velocimeters", *Proceedings of the Dynamic Flow Conference (1978)*, pp. 851 - 868.
30. I. Grant, "Periodic Sampling in Laser Anemometry", *Journal of Physics E (Scientific Instruments)*, Vol. 13, no. 5 (May 1980), pp. 571 - 574.
31. J. Roberts and M. Gaster, "On the Estimation of Spectra from Randomly Sampled Signals: a Method of Reducing Variability", *Proceedings of the Royal Society, London*, Vol. 371 (1980), pp. 235 - 258.
32. J. Roberts, J. Downie and M. Gaster, "Spectral Analysis of Signals from a LDA Operating in the Burst Mode", *Journal of Physics E: Sci. Instr.*, Vol. 13 (1980), pp. 977 - 981.
33. L. Lourenço, D. Olivari and M.L. Riethmuller, "LDA Data Processing: Theoretical and Experimental Optimization of LDV Data Acquisition and Handling", *Proceedings of the International Symposium on Applications of Laser-Doppler Anemometry to Fluid Mechanics, Lisbon (Portugal), 1982*, paper 17.3.
34. W. Bell, "Spectral Analysis Algorithms for the Laser Velocimeter: A Comparative Study", *AIAA Journal*, Vol. 21, no. 5 (1983), pp. 714 - 719.
35. D. Srikantaiah and H. Coleman, "Turbulence Spectra from Individual Realization LV data", *Experiments in Fluids*, Vol. 3 (1985), pp. 35 - 44.
36. J.B. Roberts and D.B.S. Ajmani, "Spectral Analysis of Randomly Sampled Signals using a Correlation Based Slotting Technique", *IEE Proceedings F (Communications, Radar and Signal processing)*, Vol. 133, no. 2 (April 1986), pp. 153 - 162.
37. R. Edwards and P. Kolodzy, "Computation of the Autocorrelation Function of Velocity Fluctuations using a Laser Anemometer in Sparsely Seeded Flows", *Proceedings of the International Symposium on Applications of LDA to Fluid Mechanics, Lisbon (Portugal), 1986*, pp. 103 - 112.
38. W. Bell, "Spectral Analysis of LV Data with the Slotted Correlation Method", *AIAA Journal*, Vol. 24 (1986).
39. R.J. Adrian and C.S. Yao, "Power Spectra of Fluid Velocities Measured by Laser-Doppler Velocimetry", *Experiments in Fluids*, Vol. 5 (1987), pp. 17 - 28.
40. D.B.S. Ajmani and J.B. Roberts, "Improved Spectral Estimation for Irregularly Spaced Data using Digital Filters", *Mechanical Systems and Signal Processing*, Vol. 4(1) (1990), pp. 77 - 94.
41. S. Gupta, P.K. Rajan and S.A. Patil, "Spectral Estimation of Nonuniformly Sampled Data using an Interpolation Technique", *IEEE International Symposium on Circuits and Systems, New Orleans, LA (U.S.A.), 1 - 3 May 1990*.
42. L.H.J. Absil, W. Steenbergen and D.M. Passchier, "Time and Spatial Correlation Measurements in the Turbulent Wake of a Circular Cylinder using Laser Doppler Anemometry", *Applied Scientific Research*, Vol. 47, no. 3 (July 1990), pp. 247 - 271.
43. C. McDonnell and J.A. Fitzpatrick, "Spectral Analysis of Turbulent Flows from LDA Measurements", *Proceedings of the 6<sup>th</sup> Int. Symp. on Applications of Laser Techniques to Fluid Mechanics, Lisbon (Portugal), July 20 - 23, 1992*.
44. M. Benak, M. Sturm and C.D. Tropea, "Correlation Estimators for Two-Point Laser-Doppler Anemometry", *Proceedings of the Fifth International Conference on Laser Anemometry, Advances and Applications, Veldhoven (Netherlands), 23 - 27 August 1993*, pp. 613 - 623.

## References

45. J. Adrian, J.A.C. Humphrey and J.H. Whitelaw, "Frequency Measurement Errors due to Noise in LDV Signals", Proceedings of the LDA-Symposium Copenhagen (Denmark), 1975, pp. 287 - 312.
46. W. Hösel and W. Rodi, "Errors Occurring in LDA-Measurements with Counter Signal Processing", Proceedings of the LDA-Symposium Copenhagen (Denmark), 1975, pp. 251 - 258.
47. Z. Zhang and J. Wu, "On Principal Noise of the Laser Doppler Velocimeter", Experiments in Fluids, Vol. 5 (1987), pp. 193 - 196.
48. L. Lading and R.V. Edwards, "Laser Velocimeters: Lower Limits to Uncertainty", Applied optics, Vol. 32, no. 21 (21 July 1993), pp. 3855 - 3866.
49. S. Gerosa and G.P. Romano, "Effect of Noise in Laser Doppler Anemometry", Mechanical Systems and Signal Processing, Vol. 8, no. 2 (1994), pp. 229 - 242.
50. H.R.E. van Maanen, K. van der Molen and J. Blom, "Reduction of Ambiguity Noise in Laser-Doppler Velocimetry by a Cross Correlation Technique", Proceedings of the LDA-Symposium Copenhagen (Denmark), 1975, pp. 81 - 89.
51. J.F. Meyers and J.W. Stoughton, "Frequency Domain Laser Velocimeter Signal Processor", Proceedings of the 3<sup>rd</sup> Int. Symp. on Applications of Laser Anemometry to Fluid Mechanics, Lisbon (Portugal), July 7 - 9, 1988.
52. Y. Fukuoka, E. Okada and H. Minamitani, "A Burst Spectrum Analyzer for Two-Dimensional Doppler Signals", Electronics and Communications in Japan, Part 2 (Electronics), Vol. 73, no. 2 (Feb. 1990), pp. 60 - 65.
53. T. Nakajima and Y. Ikeda, "Theoretical Evaluation of Burst Digital Correlation Method for LDV Signal Processing", Meas. Sci. Technol., Vol. 1 (1990), pp. 767 - 774.
54. K.A. Kusters, "The Influence of Turbulence on Aggregation of Small Particles in Agitated vessels", Ph.D. Thesis, Eindhoven University of Technology (Netherlands), 1991.
55. D. Matovic and C. Tropea, "Spectral Peak Interpolation with Application to LDA Signal Processing", Measurement Science and Technology, Vol. 2 (1991), pp. 1100 - 1106.
56. Chr. Caspersen, "The Enhanced Burst Spectrum Analyzer", DANTEC Information (June 1992) pp. 17 - 20.
57. K.M. Ibrahim and W.D. Bachalo, "The Significance of the Fourier Analysis in Signal Detection and Processing in Laser Doppler Applications", Proceedings of the 6<sup>th</sup> Int. Symp. on Applications of Laser Techniques to Fluid Mechanics, Lisbon (Portugal), July 20 - 23, 1992.
58. L.M. Jenson, "LDV Digital Signal Processor Based on Autocorrelation", Proceedings of the 6<sup>th</sup> Int. Symp. on Applications of Laser Techniques to Fluid Mechanics, Lisbon (Portugal), July 20 - 23, 1992.
59. E. Ritterbach, J. Höttges and H. Els, "Optical Improvement of LDV-measurement in Pipe Flow", Second International Conference on Laser Anemometry, Advances and Applications, Strathclyde (UK), 21 - 23 September 1987, Paper 18.
60. J.M. Bessem and H.R.E. van Maanen, "Optimization of Digital Storage of Random Analogue Data", Meas. Sci. Technol., Vol. 5 (1994), pp. 1331 - 1338.
61. J. Czarske, F. Hock and H. Müller, "Minimierung der Messunsicherheit von Laser-Doppler-Anemometern, Techn. Messen 61 (1994), 168-182 (in German).
62. Y.C. Chao and J.H. Leu, "A Fractal Reconstruction Method for LDV Spectral Analysis", Experiments in Fluids, Vol. 13 (1992), pp. 91 - 97.
63. R. Booij and J.M. Bessem (editors), Report on Workshop "User's Needs for Laser Doppler Anemometry", Supplement to the Proceedings of the Fifth International Conference on Laser Anemometry, Veldhoven (Netherlands) 23 - 27 August 1993, pp. 13 - 50.
64. K. van der Molen and H.R.E. van Maanen, "Measurement of Turbulence Power Spectra in Agitated Vessels of Different Size with a Laser-Doppler Velocimeter", Chemie Ingenieur Technik, Vol. 48-8 (August '76), pp. 733 - 734.
65. K. van der Molen and H.R.E. van Maanen, "Measurement of Turbulence Power Spectra in Agitated Vessels of Different Size with a Laser-Doppler Velocimeter", Proceedings of the Fourth Biennial Symposium on Turbulence in Liquids, University of Missouri-Rolla (U.S.A.), September 1975, pp. 138 - 147.

## *Retrieval of turbulence and turbulence properties from LDA data with noise*

66. K. van der Molen and H.R.E. van Maanen, "Laser-Doppler Measurements of the Turbulent Flow in Stirred Vessels to Establish Scaling Rules", *Chemical Engineering Science*, Vol. 33 (1978), pp. 1161 - 1168.
67. L.H.J. Absil, "Analysis of the Laser Doppler Measurement Technique for Applications in Turbulent Flows", Ph.D. Thesis, Delft University of Technology (Netherlands), 1995.
68. E. Müller, H. Nobach and C. Tropea, "Efficient Estimation of Power Spectral Density from Laser Doppler Anemometer Data", *Proceedings of the 7<sup>th</sup> International Conference "Laser Anemometry: Advances and Applications"*, Karlsruhe (Germany), 8 - 11 September 1997, paper 12.1.
69. J.S. Bendat and A.G. Piersol, "Random Data, Analysis and Measurement Procedures", John Wiley & Sons, New York (1986).
70. J.M. Bessem and H.R.E. van Maanen, "A Procedure for Minimum Distortion and Minimum Storage Needs for Digitised Random Analog Data", *Proceedings of the 5<sup>th</sup> International Conference on Laser Anemometry, Advances and Applications*, Veldhoven (Netherlands), 23 - 27 August 1993.
71. P.D.M. Spelt, "The Motion of Bubbles in a Turbulent Flow", Ph.D. Thesis, University of Twente (Netherlands), 1996.
72. A.N. Kolmogoroff, "The Local Structure of Turbulence in Incompressible Viscous Fluid for Very Large Reynolds Numbers", *Dokl. Akad. Nauk. SSSR*, Vol. 30, (transl. in *Proc. R. Soc. London*, Vol. 434, 9-13), (1941).
73. M.J. Tummers, D.M. Passchier and P.A. Aswatha Narayana, "LDA Measurements of Time- and Spatial Correlation Functions in and Adverse Pressure Gradient Wake", *Proc. of ASME/JSME Fluids Engng. and Laser Anemometry Conference*, Hilton Head Island, SC (U.S.A.), August 1995, FED Vol. 229, pp. 347 - 355.
74. P. Bradshaw, "An Introduction to Turbulence and its Measurements", Pergamon Press, London (1971).
75. K.N. Helland, C.W. Van Atta, and G.R. Stegen, "Spectral Energy Transfer in High Reynolds Number Turbulence", *J. Fluid Mech.*, Vol. 79 (1977), pp. 337 - 359.
76. V.L. Kononenko, "Optical Mechanisms of Doppler Line Splitting from a Single Large Particle", *Proceedings of the 7<sup>th</sup> International Conference "Laser Anemometry: Advances and Applications"*, Karlsruhe (Germany), 8 - 11 September 1997, paper 11.2.
77. F. Durst and J. Sender, "Photodetectors for laser-Doppler measurements", *Experiments in Fluids*, Vol. 9 (1990), pp. 13 - 16.
78. D. Dopheide and G. Taux, "Accurate Frequency Measurements of Noise-Added Doppler Signals by Means of Transient Recorders and LDA counters Using a Laser Diode LDA Simulator", *Proceedings of the Second International Symposium on Applications of Laser Techniques to Fluid Mechanics*, Lisbon (Portugal), July 1984, paper 4.3.
79. K.A. Shinpaugh, R.L. Simpson, A.L. Wicks, S.M. Ha and J.L. Fleming, "Signal Processing Technique for Low Signal-to-Noise Ratio Laser Doppler Velocimetry Signals", *Experiments in Fluids*, Vol. 12 (1992), pp. 319 - 328.
80. P. Lehmann and A. Schöne, "Estimation of the Signal-to-Noise Ratio of Laser-Doppler Signals", *Proceedings of the 7<sup>th</sup> International Conference "Laser Anemometry: Advances and Applications"*, Karlsruhe (Germany), 8 - 11 September 1997, pp. 99 - 106.
81. G.D. Tsakiris, "Resolution of a Spectrum Analyzer under Dynamic Operating Conditions", *Rev. Sci. Instrum.*, Vol 48 (November 1977), pp. 1414 - 1419.
82. R.V. Edwards, "Characteristics of Laser Anemometer Signals and Frequency Demodulators for Highly Seeded Flows", *Proceedings of the Fourth Biennial Symposium on Turbulence in Liquids*, University of Missouri-Rolla (U.S.A.), September 1975, pp. 122 - 138.
83. J.R. Baker and C. Wigley, "Design, Evaluation and Application of a Filter Bank Signal Processor", *Proceedings of the LDA-Symposium Copenhagen (Denmark)*, 1975, pp. 350 - 364.
84. J.C.F. Wang, "Measurement Accuracy of Flow Velocity via a Digital-Frequency-Counter Laser Velocimeter Processor", *Proceedings of the LDA-Symposium Copenhagen (Denmark)*, 1975, pp. 150 - 176.

## References

85. C. Fog, "A Photon-Statistical Correlator for LDA-Application", Proceedings of the LDA-Symposium Copenhagen (Denmark), 1975, pp. 336 - 350.
86. R. Booij, "Measuring with the Dantec Flow Velocity Analyzer", Report no. 5-92, Delft University of Technology (Netherlands), Department of Civil Engineering (1992).
87. H.R.E. van Maanen and H.J.A.F. Tulleken, "Application of Kalman Reconstruction to Laser-Doppler Anemometry Data for Estimation of Turbulent Velocity Fluctuations", Proceedings of the Seventh International Symposium on Applications of Laser Techniques to Fluid Mechanics, Lisbon (Portugal), 11 - 14 July 1994, paper 23.1.
88. P. Lehmann and E. H. Schombacher, "Features of a Combined FFT and Hilbert Transform for Phase Doppler Signal Processing", Meas. Sci. Technol. 8 (1997), pp. 409 - 421.
89. A. Papoulis, "The Fourier Integral and its Applications", McGraw-Hill Book Company, New York (1962).
90. A. Papoulis, "Signal Analysis", McGraw-Hill Book Company, New York (1984).
91. V. Čížek, "Discrete Fourier Transforms and their Application", Adam Hilger Ltd., Bristol (1986).
92. H.R.E. van Maanen, "Temporal Decay: A Useful Tool for the Characterisation of Resolution of Audio Systems? ", Proceedings of the 94<sup>th</sup> Convention of the Audio Engineering Society, Berlin (Germany), 16 - 19 March 1993, preprint # 3480 (C1-8).
93. O. Rioul and M. Vetterli, "Wavelets and Signal Processing", IEEE Signal Processing Magazine, October 1991, pp. 14 - 38.
94. D.T.L. Lee and A. Yamamoto, "Wavelet Analysis: Theory and Applications", Hewlett-Packard Journal, December 1994, pp. 44 - 54.
95. H.R.E. van Maanen and F.J. Nijenboer, "Application of the Wavelet Transform to Laser-Doppler Signal Processors", Proc. of the 8<sup>th</sup> Int. Symposium on Applications of Laser Techniques to Fluid Mechanics, Lisbon (Portugal), July 8 - 11 1996, paper no. 31.4.
96. T.S. Durrani, C. Greated and T.H. Wilmshurst, "An Analysis of Simulators and Tracking Systems for Laser-Doppler Velocimeters", Opto-electronics, Vol. 5 (1973), pp. 71 - 89.
97. A. Høst-Madsen and Chr. Caspersen, "The Limitations in High Frequency Turbulence Spectrum Estimation using the Laser Doppler Anemometer", Proceedings of the Seventh International Symposium on Applications of Laser Techniques to Fluid Mechanics, Lisbon (Portugal), 11 - 14 July 1994, paper 11.2.
98. R.F. Blackwelder and R.E. Kaplan, "On the Wall Structure of the Turbulent Boundary Layer", Journal of Fluid Mechanics, Vol. 76 (14 July 1976), pp. 89 - 112.
99. E. Müller, H. Nobach and C. Tropea, "LDA Signal Reconstruction: Application to Moment and Spectral Estimation", Proceedings of the Seventh International Symposium on Applications of Laser Techniques to Fluid Mechanics, Lisbon (Portugal), 11 - 14 July 1994, paper 23.2.
100. H. Kwakernaak and R. Sivan, "Linear Optimum Control Systems", Wiley Interscience, New York (1972).
101. N.D. Singpurwalla and R.J. Meinhold, "Understanding the Kalman Filter", the American Statistician, Vol. 37 (1985), pp. 123 - 127.
102. H.R.E. van Maanen and M.J. Tummers, "Estimation of the Auto Correlation Function of Turbulent Velocity Fluctuations using the Slotting Technique with Local Normalisation", Proc. of the 8<sup>th</sup> Int. Symposium on Applications of Laser Techniques to Fluid Mechanics, Lisbon (Portugal), 8 - 11 July 1996, paper no. 36.4.
103. L.H. Benedict and R.D. Gould, "Experiences Using Kalman Reconstruction for Enhanced Power Spectrum Estimates", Proc. of ASME/JSME Fluids Engng. and Laser Anemometry Conference, Hilton Head Island, SC (U.S.A.), August 1995, FED Vol. 229, pp. 1 - 8.
104. G. P. Romano, "The Measurement of Structure Functions with Laser Doppler Anemometry", Proceedings of the Ninth International Symposium on Applications of Laser Techniques to Fluid Mechanics, Lisbon (Portugal), July 13 - 16, 1998, paper 32.5
105. H.R.E. van Maanen, "A Novel Re-Sampling Technique for Randomly Sampled LDA Data", Proceedings of the 7<sup>th</sup> International Conference "Laser Anemometry: Advances and Applications", Karlsruhe (Germany), 8 - 11 September 1997, paper 12.3.
106. H. Nobach, E. Müller and C. Tropea, "Efficient Estimation of Power Spectral Density from Laser Doppler Anemometer Data", Experiments in Fluids, Vol. 24 (1998), pp. 449 - 509.

*Retrieval of turbulence and turbulence properties from LDA data with noise*

107. E. Müller, H. Nobach and C. Tropea, "Model Parameter Estimation from LDA Data at Low Particle Densities", Proc. of ASME/JSME Fluids Engng. and Laser Anemometry Conference, Hilton Head Island, SC (U.S.A.), August 1995, FED Vol. 229, pp. 417 - 424.
108. E. Müller, H. Nobach and C. Tropea, "Model Parameter Estimation from Non-Equidistant Sampled Data Sets at Low Data Rates", Measurement Science and Technology, Vol. 9 (March 1998), pp. 435 - 441.
109. H.R.E. Van Maanen and A. Oldenziel, "Estimation of Turbulence Power Spectra from Randomly Sampled Data by Curve-Fit to the Autocorrelation Function Applied to Laser-Doppler Anemometry", Measurement Science and Technology, Vol. 9 (March 1998), pp. 458 - 467.
110. P.R. Adby and M.A.H. Dempster, "Introduction to Optimization Methods", Chapman and Hall, London (1974).
111. A. Coghe and G.E. Cossali, "Effect of validation procedure on step noise amplitude in LDV spectra evaluation", Experiments in Fluids, Vol. 24 (1998), no. 5 - 6, pp. 382 - 388.
112. M.J. Tummers, L.H.J. Absil and D.M. Passchier, "An Experimental Investigation of Velocity Bias in a Turbulent Flow", Proc. 6<sup>th</sup> Int. Symp. on Appl. of Laser Techniques to Fluid Mech. Lisbon (Portugal), 1992, paper # 5.4.
113. C. Tropea and L.H. Benedict, "Benchmark Tests for the Estimation of Power Spectra from LDA Signals", Proceedings of the Ninth International Symposium on Applications of Laser Techniques to Fluid Mechanics, Lisbon (Portugal), July 13 - 16, 1998, paper 32.6
114. H.R.E. van Maanen, H. Nobach and L.H. Benedict, "Improved Estimator for the Slotted Autocorrelation function of Randomly Sampled LDA data", Measurement Science and Technology, Vol. 10 (January 1999), pp. L4 - L7.
115. R.E.G. Poorte, "On the Motion of Bubbles in Active Grid Generated Turbulent Flows", Ph.D. Thesis, University of Twente (Netherlands), 1998.
116. H.R.E. van Maanen and F.J. Nijenboer, "Improved Reconstruction of Turbulent Velocity Fluctuations from Laser-Doppler Anemometry Data", Proceedings of the Ninth International Symposium on Applications of Laser Techniques to Fluid Mechanics, Lisbon (Portugal), July 13 - 16, 1998, paper 32.2
117. E.W. Adams, "Experiments on the Structure of Turbulent Reattaching Flow, Appendix A: An Examination of Velocity Bias in Highly Turbulent Separated and Reattaching Flow", Report MD-443, Stanford University, Dept. of Mech. Eng. (1984).
118. F.B. Hildebrand, "Advanced Calculus for Applications", Prentice-Hall Int., Englewood Cliffs, New Jersey (1976).

## List of Symbols

$A_0$	=	maximum amplitude of Doppler signal	V
$\mathbf{A}$	=	system matrix of first-order Kalman reconstruction filter	
$\mathbf{A}$	=	2 x 2 matrix of the system, to be described by second-order Kalman reconstruction filter.	
$\mathbf{A}'$	=	transpose of $\mathbf{A}$ ; $A'_{ij} = A_{ji}$	
$a$	=	acceleration	m/s <sup>2</sup>
$a$	=	scaling factor	
$a_k$	=	poles in complex plane	
$\hat{a}$	=	predicted acceleration	m/s <sup>2</sup>
$B_w$	=	bandwidth (of noise signal)	Hz
$\underline{b}$	=	vector in coupled differential equation of second-order Kalman reconstruction filter	
$\mathbf{C}$	=	observation matrix of the system, to be described by first- or second-order Kalman reconstruction filter	
$\mathbf{C}'$	=	transpose of $\mathbf{C}$ ; $C'_{ij} = C_{ji}$	
$C(\Delta t)$	=	cumulative probability distribution	
$c_n$	=	coefficient in Taylor series expansion of auto correlation function	
$D(f)$	=	denominator of the function $f$	
$E$	=	expectation value of	
$e$	=	error value	
$\underline{e}(t)$	=	error value (vector)	
$f$	=	frequency	Hz
$f_{1,2}$	=	characteristic frequency of Bessem Power Spectrum	Hz
$f_b$	=	blade passing frequency	Hz
$f_d(t)$	=	Doppler signal	V
$f_d(\omega)$	=	spectrum of Doppler signal	Vs
$f_i$	=	characteristic frequency in $G$ , $i = 1 - 3$ , or in $S_a$ , $i = 0 - 5$	Hz
$f_i(t)$	=	measurement signal # $i$ ( $i = 1, 2$ ), including noise	m/s
$f_s$	=	sampling frequency of periodically sampled signal	Hz
$G$	=	transfer function (of extended reconstruction filter)	
$g_{per}(\tau)$	=	periodic function for compensation of periodic contributions to ACF	
$I(T)$	=	probability that the time interval between two Doppler-bursts $\leq T$ seconds	
$j$	=	imaginary operator	
$k$	=	spatial wavenumber	1/m
$L$	=	integral length scale in Von Kármán - Pao Power Spectrum	m
$L$	=	first-order Kalman reconstruction filter gain	1/s
$L$	=	second-order Kalman reconstruction filter gain	1/s <sup>2</sup>
$\mathbf{L}$	=	first- or second-order Kalman reconstruction filter gain	
$m$	=	exponent in $G$	
$m$	=	mass	kg
$N$	=	total number of observations	
$N_{acf}$	=	number of auto correlation function estimates	
$N(f)$	=	numerator of the function $f$	
$N_f(\omega)$	=	noise floor in (Doppler) spectrum	V <sup>2</sup> s <sup>2</sup>
$N_{k\Delta\tau}$	=	number of products in slot # $k$	
$N_p$	=	number of products in slot of auto correlation function	
$N_t$	=	total number of velocity observations in the data-set	
$n_i$	=	noise contribution to signal # $i$	m/s or V
$n(t)$	=	noise signal	m/s or V
$\underline{n}(t)$	=	external driving "noises" of the system, to be described by second-order Kalman reconstruction filter	m/s
$P$	=	probability distribution of	
$P(\Delta t)$	=	time interval distribution	1/s

## Retrieval of turbulence and turbulence properties from LDA data with noise

$P_S$	= total power in spectrum $S$	$m^2/s^2$ or $V^2$
$Res(f)$	= residues of the function $f$	
$R_{ff}(\tau)$	= auto covariance function of $f$	$m^2/s^2$ or $V^2$
$R_{fg}(\tau)$	= cross covariance function of $f$ and $g$	$m^2/s^2$ or $V^2$
$R(N)$	= set of numbers which is the sum of $N$ random numbers with homogeneous distribution in $[-0.5, +0.5]$	
$S(f)$	= power spectral density	$m^2/s$ or $V^2s$
$S_a(f)$	= analytical power spectral density	$m^2/s$ or $V^2s$
$S_G(\omega)$	= spectral transfer function	
$s$	= time $< t$	s
$T$	= integration time	s
$T_m$	= total measurement time	s
$T_\lambda$	= Taylor timescale	s
$t$	= time	s
$t'$	= $t - t_s$	s
$t_0$	= characteristic time of exponential time interval distribution ( $1/t_0$ = average data-rate of LDA data)	s
$t_a$	= arrival time	s
$t_k$	= time of realisation of observation $v_k^{obs}$	s
$t_s$	= shift in time	s
$U$	= average velocity of the $u$ -component of the velocity vector	m/s
$u(t)$	= turbulent velocity (component)	m/s
$\underline{u}(t)$	= (turbulent) velocity vector	m/s
$\tilde{u}(t)$	= turbulent velocity (component)	m/s
$u'(t)$	= fluctuating part of the turbulent velocity (component)	m/s
$\bar{u}$	= time average of the turbulent velocity (component)	m/s
$V$	= average velocity of the $v$ -component of the velocity vector	m/s
$v(t)$	= turbulent velocity (component)	m/s
$v'(t)$	= fluctuating part of the turbulent velocity (component)	m/s
$v_k^{obs}$	= velocity observation # $k$	m/s
$v^{pr}$	= predicted velocity	m/s
$\hat{v}$	= reconstructed velocity	m/s
$W$	= average velocity of the $w$ -component of the velocity vector	m/s
$w(t)$	= turbulent velocity (component)	m/s
$w'(t)$	= fluctuating part of the turbulent velocity (component)	m/s
$w_i$	= weight factor of parameter $i$	
$x$	= position in direction of $U$ component	m
$\underline{x}(t)$	= dynamic state vector of the system, to be described by first- or second-order Kalman reconstruction filter.	
$\hat{x}$	= optimal prediction of $\underline{x}(t)$	m/s
$x_i(t)$	= basic vector functions of wavelet space; $i = 1, 2$	
$\underline{y}$	= measurement vector of the system, to be described by first- or second-order Kalman reconstruction filter.	
$z$	= dummy variable	
$\alpha$	= first-order Kalman reconstruction filter parameter	
$\alpha$	= parameter related to the cut-off frequencies in the power spectrum for the second-order Kalman reconstruction filter	s
$\alpha_k$	= Kolmogoroff constant in Von Kármán - Pao Power Spectrum	

## List of Symbols

$\alpha_k$	= abbreviation for interpolated velocity observation calculation	m/s <sup>2</sup>
$\beta$	= first-order Kalman reconstruction filter parameter	
$\beta$	= parameter related to the cut-off frequencies in the power spectrum for the second-order Kalman reconstruction filter	s <sup>2</sup>
$\beta_k$	= Kolmogoroff constant in Von Kármán - Pao Power Spectrum	
$\beta_k$	= abbreviation for interpolated velocity observation calculation	m/s
$\Gamma$	= integral timescale	s
$\gamma$	= abbreviation for $L + \lambda$ in first-order Kalman reconstruction filter derivation	1/s
$\Delta t$	= time interval, sampling interval, slot width, $1/f_s$	s
$\Delta \tau$	= slot width	s
$\delta$	= optimal filter gain of first-order Kalman reconstruction filter	1/s
$\delta(\tau)$	= Dirac delta function	
$\varepsilon$	= dissipation rate per unit mass	m <sup>2</sup> /s <sup>3</sup>
$\zeta(t)$	= $\xi(t) \cdot m$	kgm/s
$\eta$	= Gaussian distributed white noise	m/s or V
$\eta_k$	= Kolmogoroff length scale	m
$\eta_{k,l}$	= noise contribution to velocity observation	m/s
$\underline{\eta}(t)$	= measurement noise vector	
$\kappa$	= wave number	1/m
$\Lambda$	= solution (matrix) to Ricatti equation	
$\lambda$	= wave length, eddy size	m
$\lambda$	= characteristic radial frequency of first- or second-order Kalman reconstruction filter	rad/s
$\lambda_T$	= Taylor micro timescale	s
$\lambda^*$	= $\lambda \cdot m$	kg/s
$\mu$	= characteristic radial frequency of second-order Kalman reconstruction filter	rad/s
$\nu$	= kinematic viscosity	m <sup>2</sup> /s
$\xi$	= white noise signal	
$\xi(t)$	= turbulence generating white noise signal with intensity $\sigma^2$	m/s <sup>2</sup> or m/s
$\underline{\xi}$	= stochastic driving vector	
$\Pi$	= covariance matrix of measurement noise	
$\rho$	= RMS value of $\eta_{k,l}$	m/s
$\rho^2$	= variance of measurement noise	m <sup>2</sup> /s <sup>2</sup>
$\rho(\tau)$	= auto correlation function	
$\Sigma$	= covariance matrix of external driving "noises"	
$\Sigma$	= $\sigma^2$	m <sup>2</sup> /s <sup>4</sup>
$\sigma$	= standard deviation	
$\sigma^2$	= intensity of turbulence generating white noise signal	m <sup>2</sup> /s <sup>4</sup>
$\sigma_n$	= RMS value of noise contribution	m/s
$\sigma_t$	= sigma of Gaussian envelope of wavelet or of Doppler signal	s
$\sigma_t$	= sigma of Gaussian impulse response of digital anti-aliasing filter	s
$\sigma_t$	= contribution of turbulent velocity fluctuations to the auto correlation function at $\tau = 0$ .	
$\sigma_t$	= RMS value of turbulent velocity fluctuations	m/s
$\sigma_v$	= RMS value of fluctuating part of the velocity (component)	m/s
$\tau$	= time shift	s
$\tau_a$	= damping of harmonic $a$	s
$\tau_i$	= time constant; $i = 1$ or $2$	s
$\tau_k$	= Kolmogoroff time scale	s
$\tau_k$	= parameter in analytical auto correlation and covariance function ( $= 1/f_k$ ); $k = 0 - 5$	s
$\tau'$	= dimensionless time shift $\tau/t_0$	
$\omega$	= radial frequency	rad/s
$\omega_0$	= radial frequency of wavelet or of Doppler signal	rad/s
$\omega'$	= dimensionless radial frequency $\omega t_0$	

## List of Abbreviations

AC	=	Alternating Current
ACF	=	Auto Correlation Function
A/D	=	Analog-to-Digital Conversion
ADC	=	Analog-to-Digital Converter
AVF	=	Auto Covariance Function
DC	=	Direct Current
DOS	=	Disk Operating System
DSP	=	Digital Signal Processing
FFT	=	Fast Fourier Transform
FT	=	Fourier Transform
HWA	=	Hot Wire Anemometry
IC	=	Integrated Circuit
IFT	=	Inverse Fourier Transform
LDA	=	Laser-Doppler Anemometry
LOG	=	Logarithm
MS	=	Mean Square
MS	=	MicroSoft
MSE	=	Mean Square Error
PC	=	Personal Computer
PSD	=	Power Spectral Density
Res	=	Residue
RMS	=	Root Mean Square
RND	=	RaNDom number with homogeneous distribution between [0,1]
RNG	=	Random Number Generator
SNR	=	Signal-to-Noise Ratio
S&H	=	Sample-and-Hold
WMS	=	Weighted Mean Square
WMSE	=	Weighted Mean Square Error
WT	=	Wavelet Transform

## Acknowledgements

*Skill is fine,  
and genius is splendid,  
but the right contacts  
are more valuable than either.*  
Sir Archibald McIndoe

"Science travels on a gravel road" is one of my favourite expressions. And nobody can travel that road without the guidance, help and support of others. Therefore I would like to thank a number of people who have -in one way or another- contributed to the realisation of the work, reported in this thesis. I know that the list is in no way complete and thus I want to start to thank everybody who has made me the man I am and especially those who have had the difficult task to teach me everything I know today, be it in science or in any other subject. Without you all this would never have materialised.

Next on the list are two men who -unfortunately- have already passed away, both too soon (in their middle 40's) as far as I am concerned. The first of these is Jan Blom, who was my first boss at the Shell Laboratory in Amsterdam and who introduced Laser-Doppler Anemometry to this Laboratory. I still see him outlining the basic principles to me at the blackboard in the beginning of '69. In those days Laser-Doppler Anemometry was hardly more than a toy, but the developments went fast -I am happy to say that we could contribute to these- and culminated in the Copenhagen conference of '75. We also had a presentation there on the cross correlation technique, that in a more extensive form is part of this thesis (see Chapter 9). I am honoured that both our names are connected through this presentation. The second of these men is Ton Nieberg, who was my partner and friend-for-life, and who always supported me in my work. In the summer of '97, a few month before his untimely death, he raised the question whether it would not be time for me to write a thesis. You hold the results in your hands.....

Next I want to thank my promoter, Gijs Ooms, for his outstanding work, not only during the preparation of this thesis, but also for the inspiring discussions we have had through the years. I will never forget that he instigated the work on coherent structures in boundary layers, which resulted in the experimental work for my masters' degree. It is interesting to realise that this work has been done using Laser-Doppler Anemometry too. I have been using a lot of experience on data-processing that I have gained from this investigation for the development of the novel techniques, described in this thesis.

I am greatly indebted to my co-promoter, Cameron Tropea, who has studied the work extensively and has come up with excellent comments and inspiring remarks, thus significantly contributing to the value of this work. He also pointed at several aspects, which have gained more emphasis than original, thus increasing the value even more. I also am very grateful for the precise comments of Prof. Giampolo Romano, who made valuable comments on the concept and found errors that had been overlooked by others.

It is impossible to do research and development without funding and therefore I would like to thank Gert Colenbrander, Peter Veenstra and Henk Molenaar for the money and the intriguing measurement problems they have supplied through the years to stimulate this work and the trust they have put in me. It has not always been clear that in the end useful results would be obtained, but they have been willing to take that risk. Also I would like to thank Caspar Verhaagen for the lobbying to get the funds organised every year. Whenever some "massaging" was required, I could count on him.

"Genius is one percent inspiration and ninety nine percent transpiration" is a famous expression of Thomas Alva Edison. If you are not a genius, this ratio is even worse, so the only way I could get this all done without drowning in my own sweat was to call for help from students. I have been very

## *Retrieval of turbulence and turbulence properties from LDA data with noise*

fortunate to be helped by five outstanding students, all from the University of Twente, being Arnoud Jippes, Quirijn von Geldern, Frank Nijenboer, Arjan Oldenziel and Edwin Drost. They have taken large chunks of the work and without their help this thesis would not be here. I would also like to thank them for their pleasant way of cooperation during their stay at the Laboratory in Amsterdam. I will never forget the extensive discussions we had on the progress of the work, but also the animated lunches and coffee breaks. I learned a lot during their stay.

Being a simple physicist, mathematics is a difficult subject. Fortunately, I had the privilege to ask two expert mathematicians for help: Herbert Tulleken and Gerard Beynon. Sometimes they thought that they did more for my students than I did and they were not that wrong. Without their extensive support, several tough mathematical nuts would not have been cracked. Especially the second-order Kalman reconstruction filter and the analytical Inverse Fourier Transformation of the modelled power spectrum require deep knowledge of difficult and complex mathematics, which I have not available.

"Two know more than one" is banging on an open door. But it proved again so true in the fruitful discussions we have had in the working party of the Dutch Association for Laser Anemometry on velocity signal reconstruction. So I would like to thank in particular Hans Bessem, Rob Booij and Mark Tummers for their essential contributions to the discussions, which have been very stimulating and fruitful. These people have also been active in the organisation of international conferences, which bring together experts from all over the world. I would like to thank them, Prof. K. Krishna Prasad, Herman Godefroy, Hans de Groot, Frits de Mul and E. Nijhof for the opportunity they have given me to unleash the discussion on users' needs for Laser Anemometry at the Veldhoven conference in '93, which has given an impulse to further development of Laser-Doppler Anemometry and set the scene for the work reported in this thesis.

At these international conferences one has the opportunity to discuss the latest developments with other experts. Such discussions are very fruitful and I would like to thank especially Cameron Tropea, Lance Benedict, Holger Nobach and Thomans Haedrich for their inspiring and challenging discussions on these topics. I especially appreciate their attitude that one can have different views and opinions, but still have a beer (and a good time) afterwards. That is how it always should be.

The verification of the results of the developed algorithms could only be done by the use of real (measured) data-sets. I know that measuring flows with LDA is hard work and therefore I would like to thank especially Jan Tukker, Mark Tummers, Jaap den Toonder and Anders Høst-Madsen for supplying me with the well-measured data-sets which make the results so much more convincing.

"Neither do man light a candle and put it under a bushel, but on the candlestick" is an old and wise saying from the Bible. However, one should be given the opportunity to put it on this candlestick. Therefore I would like to thank Dick Passchier for giving me the opportunity to contribute more than once to the post-doc Laser-Doppler Anemometry course and to convey part of my knowledge. I have experienced it as a privilege and enjoyed doing it. Too bad for the soar throat the next day..... But if you ask me again, I would do it without hesitation.

I hope that people that are not specifically mentioned in these acknowledgements will understand that I had to make a selection. I hope they realise that whenever they had a discussion with me on this subject, they will have influenced me and my view and therefore a part of them resides somewhere in this thesis. Thank you all for that.

## Curriculum Vitae

*God, grant me the serenity to accept  
the things I cannot change,  
the courage to change the things I can,  
and the wisdom to know the difference.*  
Reinhold Niebuhr

Hans Rudi Eduard van Maanen was born in Arnhem ("a bridge too far"), Netherlands on February 8<sup>th</sup> 1951. He went to elementary and secondary school (H.B.S.-b) there and then (1968) moved to Amsterdam where he started working at the Shell Laboratories. After a 5 months training period he became the assistant of Jan Blom in the department FP (Fundamental Physics) and worked on the study of turbulence in pipe flow and the development of Laser-Doppler Anemometry, which was still in its infancy. One of the results was presented by him at the conference in Copenhagen (1975, ref. 50). After that he was the assistant of Klaas van der Molen and he used the Laser-Doppler Anemometer for experimental investigation of the scaling rules for stirred vessels, which resulted in a publication in a.o. Chemical Engineering Science (ref. 66). Following that investigation he applied Laser-Doppler Anemometry at different experimental set-ups at the Laboratory in Amsterdam for e.g. the simulation of the atmospheric boundary layer in the wind tunnel (using the Photon Correlation Technique) and the dispersion of oil droplets in sea water. A major effort has been, however, the study of the coherent structures in the boundary layer of pipe flow.

Hans realised that his secondary school knowledge would not be sufficient for the rest of his life, so he started a study, during the evening hours, in 1969, which would educate him as a second grade teacher in Physics and Chemistry. Not that he wanted to be that, but the study was organised by, and run parallel with the studies at, the University of Amsterdam. He finished this study at the end of 1972 and subsequently continued with his bachelors' degree in Physics and Chemistry with Mathematics. He finished that with honours in 1978 and then ran into the problem how to get his Masters' degree? This was solved by the kind cooperation of the Shell Laboratory, the faculty of Physics and the faculty of Chemistry of the University of Amsterdam, who allowed Hans to do his experimental work on the coherent structures in turbulent boundary layers at the Shell Laboratory, be coached by Prof. J.M.H. Fortuin of the faculty of Chemistry, but still get his Masters' degree from the faculty of Physics. In this way he was able to get his Masters' degree in Physics with Mathematics and Information Science, again with honours, in 1982. The work on the coherent structures was presented at two different conferences and was also published in Chemical Engineering Science (ref. 13).

Hans worked on data-processing of the data from the two-phase flow loop in Bacton after his Masters' exam and his experience with the use of desktop computers in experiments was used more generally when he was appointed as group leader for the automation of experiments at the Laboratory in Amsterdam. But his heart lay more with research, so he was transferred to the Measurement Science department where he worked until his transfer to Rijswijk Laboratory in 1997. During this stay in the Measurement Science department, the problems with the novel Laser Doppler Anemometry systems surfaced and this ultimately resulted in the work, reported in this thesis. His current work is in the Rijswijk Laboratory on Production Measurement, which involves multi-phase metering of gas, condensate and water.

Hans lived together with Ton Nieberg from the spring of 1979 to the fall of 1997 when Ton suddenly and unexpectedly passed away when Hans was not at home. They had planned to get married when this would become possible with the change of the law on January 1<sup>st</sup> 1998 and had set the date on July 24<sup>th</sup> 1998 because the relatives from Canada would be in Holland. It was not to be.....

*There is only one way....Onward!*  
Isaac Asimov